THE PHYSICAL REVIEW

VOLUME 68

THE PHYSICAL REVIEW

A journal of experimental and theoretical physics established by E. L. Nichols in 1893

Published by the American Institute of Physics for the

AMERICAN PHYSICAL SOCIETY

Officers

President

J. H. Van Vleck
Harvard University
Cambridge, Massachusetts

Vice-President

Enrico Fermi
Institute for Nuclear Studies
University of Chicago
Chicago 37, Illinois

Secretary

K. K. Darrow
Bell Telephone Laboratories
Office:
Columbia University
New York 27, New York

Treasurer

G. B. Pegram
Columbia University
New York 27, New York

Local Secretary
for the Pacific Coast

J. Kaplan
University of California at Los Angeles
Los Angeles, California

Managing Editor

S. A. Goudsmit
Brookhaven National Laboratory
Upton, Long Island
New York

BOARD OF EDITORS

Editor

S. A. Goudsmit

Assistant Editor

S. Pasternack

Associate Editors

Harvey Brooks	M. Goldhaber	W. P. Allis
R. F. Christy	R. Hofstadter	F. G. Brickwedde
C. L. Critchfield	A. W. Lawson	W. B. Fretter
M. Deutsch	A. Pais	Conyers Herring
T. H. Johnson	R. Serber	H. W. Lewis
Bruno Rossi	C. H. Townes	Arnold Nordsieck

Manuscripts for publication should be submitted to S. A. Goudsmit, Brookhaven National Laboratory, Upton, Long Island, New York. The authors' institutions are requested to pay a publication charge of $15 per page which, if honored, entitles them to 100 free reprints. Instructions will be sent with galley proofs.

Proof and all correspondence concerning papers in the process of publication should be addressed to the Publication Manager, American Institute of Physics, 57 East 55 Street, New York 22, New York.

Subscription Price

United States and Canada.....$30.00
Elsewhere.....$37.50

Back Numbers[1]

Yearly back number rate when complete year is available
Prior to 1949: $25.00
Thereafter: $33.00
Single copies $3.00 each, prior to July, 1929;
$1.50 each, July, 1929–December, 1941;
$3.00 each, January, 1942–December, 1945;
$1.50 each, thereafter.
General index, 1893–1920: $4.00.

Subscriptions, renewals, and orders for back numbers should be addressed to the American Institute of Physics, 57 East 55 Street, New York 22, New York.

Changes of address in the case of members of the American Physical Society should be addressed to the Treasurer; in the case of other subscribers to the American Institute of Physics.

[1] Per Gates, Librarian of Physics Department, Cornell University, Ithaca, New York.

The Physical Review is published semi-monthly at Prince and Lemon Streets, Lancaster, Pennsylvania.

Entered as second-class matter August 29, 1947, at the Post Office at Lancaster, Pennsylvania, under the Act of March 3, 1879.

Acceptance for mailing at special rate of postage provided for in subsection (d-2), section 34.40, P. L. & R. of 1948, authorized January 29, 1949.

THE
PHYSICAL REVIEW

A journal of experimental and theoretical physics established by E. L. Nichols in 1893

SECOND SERIES, VOL. 88, NO. 6 DECEMBER 15, 1952

Wave Functions and Energy Levels for Cu^+ as Found by the Slater Approximation to the Hartree-Fock Equations*

GEORGE W. PRATT, JR.
Massachusetts Institute of Technology, Cambridge, Massachusetts

(Received August 25, 1952)

Results of a self-consistent field calculation using the Slater method are given for Cu^+. Wave functions, energies, total radial charge density, $2(2l+1)\cdot(1-Z_{nl})$ functions for the $3p$ and $3d$ electrons, and the $2Z_p(r)$ functions are listed. The corresponding results for the Hartree-Fock method, and in some cases the Hartree method, are given for comparison of the various calculations. The method of integrating the radial wave equation and a method for shortening the self-consistent calculation are included.

INTRODUCTION

THE quantum-mechanical many-body problem as treated by the Hartree method[1] is, for many purposes, somewhat oversimplified. The more accurate Hartree-Fock method,[2] which correctly includes the Pauli principle within the framework of the one-electron approximation, is so complicated to carry out that it has found only a rather restricted use. Slater[3] has shown that a considerable simplification of the Fock equations can be achieved if one uses an average exchange charge density and from this computes an average exchange potential energy. The purpose of this work was to examine the accuracy of Slater's method by applying it to Cu^+ which has been investigated by both the Hartree[4] and the Hartree-Fock method.[5]

The average exchange charge density as given by Slater for an atomic system containing an equal number of electrons of each spin is

$$\rho_{ex}=\frac{-e\sum_{j=1}^{N}\sum_{k=1}^{N}u_j^*(x_1)u_k^*(x_2)u_k(x_1)u_j(x_2)}{\sum_{j=1}^{N}u_j^*(x_2)u_j(x_1)}, \quad (1)$$

where u_j are orthonormal one-electron functions and the x_i refer to spatial and spin coordinates. In terms of this function the Fock equations are

$$H_1u_i(x_1)+\left\{\sum_{k=1}^{N}e^2\int\frac{u_k^*(x_2)u_k(x_2)}{r_{12}}dx_2\right\}u_i(x_1)-\left\{\sum_{k=1}^{N}e^2\int\frac{u_i^*(x_1)u_k^*(x_2)u_k(x_1)u_i(x_2)/r_{12}}{\sum_{i=1}^{N}u_i^*(x_1)u_i(x_1)}dx_2\right\}u_i(x_1)=E_iu_i(x_1), \quad (2)$$

where H_1 is the kinetic energy and the electrostatic energy coming from the electron-nucleus interaction of an electron at X_1. The result of the averaging has been to reduce the Fock equations to the eigenvalue type and to make the exchange term the same for all electrons. It is to be remembered that the Slater method only applies when the total many electron wave function is written as a single determinant.

The Fock equations are still rather complicated to apply, even using the averaged exchange term. In order to further simplify the application of these equations, Slater has used a free electron gas model to calculate the average exchange energy. When this is done, we are enabled to write the Fock equations in the case in which there are an equal number of electrons of each spin, as

$$H_1u_i(x_1)+\left[\sum_{k=1}^{N}e^2\int\frac{u_k^*(x_2)u_k(x_2)}{r_{12}}dx_2-3e^2\left\{\frac{3}{8\pi}\sum_{k=1}^{N}u_k^*(x_1)u_k(x_1)\right\}^{\frac{1}{3}}\right]u_i(x_1)=E_iu_i(x_1). \quad (3)$$

* Part of a thesis submitted in partial fulfillment of the requirements for the degree of Doctor of Philosophy in Physics in the Graduate School of the Massachusetts Institute of Technology. This work was supported by the ONR.

[1] D. R. Hartree, Proc. Cambridge Phil. Soc. **24**, 89, 111 (1927).
[2] V. Fock, Z. Physik. **61**, 126 (1930).
[3] J. C. Slater, Phys. Rev. **81**, 385 (1951); see also R. Sternheimer, Phys. Rev. **78**, 235 (1950).
[4] D. R. Hartree, Proc. Roy. Soc. (London) **A141**, 282 (1933).
[5] D. R. Hartree and W. Hartree, Proc. Roy. Soc. (London) **A157**, 490 (1936).

TABLE I. Trial eigenvalues for $P_{2p}(r)$ for Cu^+ and its corresponding behavior for large r.

E (at. units)	Behavior[a]
−69.489	Wave function went negative at $r=0.890$, slope 0.418
−69.494	Wave function went negative at $r=0.960$, slope 0.246
−69.495	Wave function went negative at $r=1.020$, slope 0.174
−69.496	Wave function had minimum at $r=1.120$, min 0.008956
−69.4955	Wave function went negative at $r=1.080$, slope 0.108
−69.4957	Wave function had minimum at $r=1.240$, min 0.003677

[a] The correct wave function should approach zero through positive values and become zero at about $r=1.30$.

For the case of unbalanced spins only slight modifications of the averaging procedure are required if we use a single determinant as the total wave function. In this case the Fock equations can be expressed as

$$H_1u_i(x_1)+\left[\sum_{k=1}^{N}e^2\int\frac{u_k^*(x_2)u_k(x_2)}{r_{12}}dx_2 - 3e^2\left\{\frac{3}{4\pi}\left(\frac{N_\pm}{N}\right)\sum_{k=1}^{N}u_k(x_1)u_k(x_1)\right\}^{\frac{1}{3}}\right]u_i(x_1) = E_iu_i(x_1), \quad (4)$$

where $N_\pm/N$ represents the fraction of electrons of a given spin at a radius r from the nucleus.

The local electron density $\sum_k u_k^*(x)u_k(x)$ can be related through Poisson's equation to the potential set up by the nucleus and all of the electrons. Denoting this potential by $2Z_p/r$, we can express the averaged exchange energy as

$$-\frac{6}{r}\left\{\frac{3}{32\pi^2}\right\}^{\frac{1}{3}}\left\{r^2\frac{d^2Z_p}{dr^2}\right\}^{\frac{1}{3}} \quad (5)$$

in atomic units. It is often very useful to write the $2Z_p(r)$ function and the exchange energy in terms of the radial wave functions $P_{nl}(r)$ where $u_{nl}(x)=[P_{nl}(r)/r]\cdot Y_{l,m}(\theta,\varphi)$. Assuming a spherically symmetric charge distribution, one finds for $2Z_p(r)$ the expression

$$2Z_p(r)=2Z-2\sum_{nl}2(2l+1)\times\left\{\int_0^r P_{nl}^2dr'+r\int_r^\infty\frac{P_{nl}^2}{r'}dr'\right\}, \quad (6)$$

where Z is the atomic number. For the exchange potential energy times r we have

$$z(r)=+6\left(\frac{3}{32\pi^2}\right)^{\frac{1}{3}}\left(r^2\frac{d^2Z_p}{dr^2}\right)^{\frac{1}{3}} =+6\left\{\frac{3}{32\pi^2}\sum_{nl}2(2l+1)rP_{nl}^2(r)\right\}^{\frac{1}{3}}. \quad (7)$$

The radial wave equation may be written as

$$\frac{d^2P_{nl}}{dr^2}+\left[E_{nl}+\frac{2Z_p}{r}+\frac{z(r)}{r}-\frac{l(l+1)}{r^2}\right]P_{nl}=0. \quad (8)$$

This equation leads to the definition of a new function $W(r)$, which is $W(r)=2Z_p(r)+z(r)$. In the actual calculations it was decided to use $W(r)$ to determine the degree of self-consistency.

METHOD OF SOLUTION

Having obtained the radial equation to be solved, let us investigate the method of its solution. This equation must be integrated numerically with trial values of the energy E_{nl}. Because of the fact that it often requires ten or more guesses of E_{nl} before a satisfactory value is found, a rapid and accurate integration method is highly desirable. In customary methods of numerical integration, one makes an estimate of a forward point, or a number of forward points, and then proceeds to improve these points by some sort of iterative scheme. These approaches are cumbersome to use on automatic equipment, especially I.B.M. machines, because of the complex machine programs required and the consequent reduction of the speed of solution. The Noumerov method[6] appears to be the answer to many of these difficulties. The essence of this method is to make a change of dependent variable so that one may find advance points with no iteration required but still have a very small truncation error.

Let the radial one-electron Schrödinger equation be written as

$$d^2P/dr^2=g(r)\cdot P(r), \quad (9)$$

where $g(r)$ is

$$g(r)=-[E+W(r)/r-l(l+1)/r^2]. \quad (10)$$

We now expand P about the point $r=r_n$ in a Taylor's series:

$$P_{n+1}=P_n+hP_n'+\frac{h^2}{2!}P_n''+\frac{h^3}{3!}P_n'''+\frac{h^4}{4!}P_n^{iv}+\cdots, \quad (11)$$

where h is $r_{n+1}-r_n$. Differentiating twice, one finds the expansion for d^2P/dr^2 to be

$$P_{n+1}''=P_n''+hP_n'''+\frac{h^2}{2!}P_n^{iv}+\frac{h^3}{3!}P_n^{v}+\cdots. \quad (12)$$

Let us define a new dependent variable $y(r)$ as

$$y_n(r)=P_n(r)-(h^2/12)P_n''(r). \quad (13)$$

We can write the Taylor's series expansion of $y(r)$ about r_n as

$$y_{n+1}=P_n+hP_n'+\frac{5h^2}{12}P_n''+\frac{h^3}{12}P_n''' -\frac{h^5}{180}P_n^{v}-\frac{h^6}{480}P_n^{vi}+\cdots. \quad (14)$$

[6] B. Noumerov, Publ. Observ. Astrophys. Cent. Russie **11** (Moscu, 1923); Monthly Not. Roy. Astron. Soc. **84**, 592 (1924).

To obtain y_{n-1} one merely changes the sign of h in the above expression. Thus the second difference in y at r_n is

$$\delta^2 y_n = y_{n+1} - 2y_n + y_{n-1} = h^2 P_n'' - (h^6/240) P_n^{vi}. \quad (15)$$

Therefore, if one neglects the sixth and higher order terms, we find the very simple relationship

$$\delta^2 y_n = h^2 P_n''. \quad (16)$$

Combining the definition of $y(r)$ with the original differential equation, we see that $y_n(r)$ can be written

$$y_n = P_n - (h^2/12) P_n'' = P_n(1 - g_n h^2/12). \quad (17)$$

We can also express the second difference in y as

$$\delta^2 y_n = h^2 P_n'' = h^2 g_n P_n,$$

which leads to the final expression

$$\delta^2 y_n = \left\{ \frac{h^2 g_n}{1 - g_n h^2/12} \right\} y_n. \quad (19)$$

If we define u_n as

$$u_n = \frac{g_n h^2/12}{1 - (g_n h^2/12)}, \quad (20)$$

our final form is

$$\delta^2 y_n = 12 u_n y_n. \quad (21)$$

The simplicity of solution of this equation is immediately apparent. The truncation error is controlled by the term $(h^6/240)P^{vi}$, so that by keeping h small this source of error can be readily controlled without using so small an h that the length of calculation becomes troublesome. In this work on Cu^+, h was taken as 0.005 from the origin to $r=0.800$. The interval was 0.010 between $r=0.800$ and 0.900; 0.020 between $r=0.900$ and 1.400; 0.040 between $r=1.400$ and 2.440; 0.080 between $r=2.44$ and 2.60; 0.160 between $r=2.60$ and 4.20; 0.320 for all larger values of r.

By choosing the intervals in the above manner the range of $h=0.005$ covered the values of r in which all wave functions passed through their maxima and minima. The $3d$ wave function had the outermost maximum of all wave functions, and this occurred at approximately $r=0.480$. Therefore, larger intervals were used in the range of r in which all functions were approaching zero with relatively small slopes.

TABLE II. Radial charge due to the $2p$ wave function corresponding to an eigenvalue of -69.4957.

r (at. units)	$\int_0^r P_{2p}^2 dr$
0.600	0.996929
0.700	0.999496
0.800	0.999856
0.900	0.999989
1.000	0.999998
1.240	1.000000

TABLE III. Comparison of initial and calculated $W(r)$ functions for the first and second cycles.

r	$W^{(0)}$	$W^{(1)}$	$W^{(2)}$	$W^{(3)}$
0.000	58.000	58.000	58.000	58.000
0.090	42.727	42.246	42.353	42.862
0.300	25.240	24.206	24.459	25.849
0.700	11.547	10.649	10.877	12.612
1.400	4.940	4.727	4.779	5.818
2.600	3.051	3.008	3.002	3.611
	First cycle		Second cycle	

The radial equation was integrated outward by the Noumerov method on the I.B.M. 602-A calculating punch computer[7] with trial values of the energy until a "best" eigenvalue was found. The exact eigenvalue will be the one for which the wave function goes to zero with zero slope for sufficiently large r. As the exact eigenvalue is never realized in practice, one must select some standard for an acceptable energy. The criterion used in this work was that the wave function should go through zero at large r with a slope of not more than ± 0.05. As an example of the kind of results obtained, Table I gives some trial eigenvalues for the $2p$ wave function of Cu^+ and the behavior of the wave function at large r. The value 69.4957 was selected as the final value of the energy. The charge within a sphere of radius r corresponding to this wave function are shown in Table II. The purpose of determining an energy value to so many figures is only to insure that the corresponding charge density will behave smoothly in the region where the wave function is going to zero.

Having determined all wave functions and energies, one proceeds to recompute the common potential $W(r)/r$ and the $2Z_p$ function. If the initial and final $W(r)$ functions do not agree to within some standard set for the calculation, another cycle must be undertaken. One cannot use the $W(r)$ resulting from previous cycle as the initial function for the next cycle, because the self-consistent procedure is not necessarily convergent. Let us denote the initial $W(r)$ for the first cycle as $W^{(0)}$. This function was obtained from the results of Hartree and Hartree's work on Cu^+ as calculated with exchange.[5] The final $W(r)$ as found from the wave functions resulting from the first cycle is denoted by $W^{(1)}$. The initial data for the second cycle will be labeled $W^{(2)}$, and this function was selected intermediate between $W^{(0)}$ and $W^{(1)}$ as follows:

$$W^{(2)} = W^{(0)} + \tfrac{3}{4}(W^{(1)} - W^{(0)}).$$

The method of selection of $W^{(2)}$ used here was merely a rough guess made with the hope of attaining a rapid convergence. It turned out that the factor $\frac{3}{4}$ was rather poor and should have been about 0.40. The function resulting from the second cycle $W^{(3)}$ is shown in Table III. It is clear that the self-consistent process is diverging at the end of the second cycle. One would

[7] N. A. Lindburger, Proc. Endicott Forum on Sci. Comp. (1948) (unpublished).

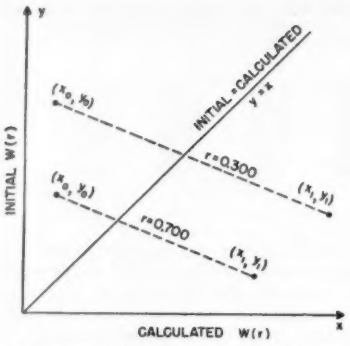

FIG. 1. The graphical estimation of a new $W(r)$ function.

expect that $W^{(3)}$ would lie between $W^{(1)}$ and $W^{(2)}$ if the method were converging.

The following approach was used to correct this divergent character. One can make a plot having the initial value of $W(r)$ for some given r along the ordinate. The derived value of $W(r)$ for that cycle at the same r is plotted along the abscissa. Using the results of the first and second cycles, two points at each value of r can be obtained:

$$(x_0, y_0) = (W^{(1)}, W^{(0)}),$$
$$(x_1, y_1) = (W^{(3)}, W^{(2)}).$$

A line is drawn connecting these points. The intersection of this line with the 45° line determines the new estimate of $W(r)$ at the given value of r. The function so obtained will be denoted by $W^{(4)}$, and it was used as the initial data for the third cycle. This method is illustrated in Fig. 1. The intersection can be obtained analytically as

$$W^{(4)} = \frac{W^{(0)}\{W^{(3)}-W^{(1)}\} - W^{(1)}\{W^{(2)}-W^{(0)}\}}{\{W^{(3)}-W^{(1)}\} - \{W^{(2)}-W^{(0)}\}}. \quad (22)$$

TABLE IV. A comparison of the initial and final $W(r)$ functions for the second and third cycles.

r	$W^{(2)}$	$W^{(0)}$	dw	$W^{(4)}$	$W^{(3)}$	dw
0.02	53.841	53.969	−0.13	53.989	53.890	0.008
0.10	41.108	41.639	−0.53	41.282	41.242	0.04
0.20	31.252	32.265	−1.02	31.599	31.470	0.13
0.26	26.917	28.171	−1.25	27.332	27.181	0.15
0.32	23.351	24.794	−1.44	23.805	23.652	0.15
0.40	19.557	21.180	−1.62	20.003	19.889	0.11
0.50	15.906	17.660	−1.75	16.396	16.246	0.15
0.65	11.903	13.667	−1.77	12.364	12.217	0.14
0.75	9.989	11.675	−1.68	10.406	10.275	0.12
0.90	7.938	9.459	−1.52	8.246	8.193	0.06
1.14	5.963	7.213	−1.25	6.187	6.187	0.00
1.38	4.849	5.901	−1.05	4.987	5.062	−0.07
1.68	...	...	...	4.135	4.248	−0.11
1.72	3.994	4.820	−0.83	...	...	...
2.44	3.116	3.754	−0.63	3.159	3.271	−0.11
3.24	2.666	3.178	−0.51	2.708	2.768	−0.06
	Second cycle			Third cycle		

The function $W^{(4)}$ was calculated by applying this relation at each point $r_{2n}=r_0+2nh$, and Lagrangian interpolation was used to find the values at $r_{2n+1}=r_0+(2n+1)h$.

The result of this method was most satisfactory in that the function $W^{(3)}$ as derived from the third cycle was in very close agreement with $W^{(4)}$. The degree of self-consistency achieved in the third cycle was within the standards set by Hartree. The success of the graphical interpolation is evident from the results shown in Table IV.

RESULTS

The final results of the third cycle of calculations are shown in Tables V through XV. Included in these data are the normalized radial wave functions $P_{nl}(r)$ as found by the Hartree-Fock method[5] and the Slater approximation for Cu^+. The total radial charge density is given for the Hartree,[4] Hartree-Fock, and Slater

TABLE V. The 1s radial wave function P_{1s} as determined by the Hartree-Fock method and by the Slater approximation.

r	Hartree-Fock	Slater	r	Hartree-Fock	Slater
0.000	0.000	0.000	0.120	1.211	1.206
0.005	1.328	1.327	0.140	0.809	0.804
0.010	2.299	2.294	0.160	0.530	0.526
0.015	2.985	2.980	0.180	0.344	0.340
0.020	3.445	3.438	0.200	0.221	0.217
0.025	3.729	3.721	0.220	0.141	0.137
0.030	3.876	3.867	0.240	0.089	0.086
0.035	3.918	3.909	0.260	0.056	0.054
0.040	3.881	3.871	0.280	0.036	0.033
			0.300	0.023	0.020
0.050	3.645	3.636			
0.060	3.290	3.281	0.350	0.007	0.004
0.070	2.890	2.880	0.400	0.002	0.000
0.080	2.488	2.479	0.450	0.001	0.000
0.090	2.110	2.103	0.500	0.000	0.000
0.100	1.769	1.762	0.550	0.000	0.000
			0.600	0.000	0.000

methods. In order to see the differences between the Slater and Hartree-Fock solutions to Cu^+ in more detail, a table is included showing the charge outside a sphere of radius r due to the 3p and 3d electrons, as found by both methods. The inner electrons of Cu^+ behave so much like Hartree-Fock electrons that similar tables are not given for them. A table is included showing the electronic energies as determined by the Hartree, Hartree-Fock, and Slater methods. This is accompanied by a table of uncertainties in the energies found in this work. Finally a table is given, showing the $2Z_p(r)$ function resulting from the third cycle and as derived from the Hartree-Fock work on Cu^+.

DISCUSSION

Let us inquire about the degree of self-consistency achieved in the work on Cu^+. The criterion for self-consistency that Hartree and many others have employed is to demand that the initial and calculated

radial charge functions $Z_{nl}(r)$, which are given as $\int_0^r P_{nl}(r)^2 dr$, must agree to within a certain tolerance. This is usually of the order of $0.02/2(2l+1)$. Because of the methods used to find a new estimate of $W(r)$ for each cycle, initial $Z_{nl}(r)$ functions were not available to compare with those functions obtained at the end of the cycle in the present calculation. It is possible however, to deduce approximately the deviations in the $Z_{nl}(r)$ functions from the differences between the initial and final $W(r)$ functions. If the relation

$$2(2l+1)Z_{nl}(r)_{\text{final}} = 2(2l+1)Z_{nl}(r)_{\text{initial}} + d$$

is assumed for all r and nl, where d is the deviation averaged over all nl and over all r for a cycle, then one can readily show that

$$2Z_p(r)_{\text{final}} = 2Z_p(r)_{\text{initial}} - d\sum_{nl} 2. \tag{23}$$

TABLE VI. The $2s$ radial wave function P_{2s} as determined by the Hartree-Fock method and by the Slater approximation.

r	Hartree-Fock	Slater	r	Hartree-Fock	Slater
0.000	0.000	0.000	0.200	−2.168	−2.170
0.005	0.407	0.409	0.220	−2.134	−2.134
0.010	0.700	0.702	0.240	−2.050	−2.049
0.015	0.896	0.898	0.260	−1.932	−1.930
0.020	1.011	1.013	0.280	−1.795	−1.791
0.025	1.061	1.062	0.300	−1.646	−1.642
0.030	1.057	1.058			
0.035	1.009	1.009	0.350	−1.270	−1.267
0.040	0.926	0.926	0.400	−0.940	−0.936
			0.450	−0.674	−0.672
0.050	0.686	0.683	0.500	−0.474	−0.472
0.060	0.384	0.379	0.550	−0.328	−0.326
0.070	0.054	0.048	0.600	−0.225	−0.222
0.080	−0.280	−0.287			
0.090	−0.602	−0.609	0.700	−0.104	−0.100
0.100	−0.900	−0.908	0.800	−0.048	−0.044
			0.900	−0.022	−0.018
0.120	−1.403	−1.411	1.000	−0.011	−0.006
0.140	−1.770	−1.777	1.100	−0.004	−0.001
0.160	−2.007	−2.013	1.200	−0.002	0.000
0.180	−2.132	−2.136	1.300	−0.001	0.000

For Cu^+ this becomes

$$2Z_p(r)_{\text{final}} = 2Z_p(r)_{\text{initial}} - 12d. \tag{24}$$

$W(r)$ is given as

$$W(r) = 2Z_p + z(r), \tag{25}$$

and we shall neglect the deviation in $z(r)$ in a cycle. Then the deviation in $2Z_p$ will be regarded as the same as that in $W(r)$, although it is probably less. If we set $12d$ equal to the maximum difference in the third cycle, which from Table IV is seen to be -0.15, then the maximum value of the averaged d is -0.0125. This value of d is of the same order of magnitude as that used by Hartree which is usually $d=0.02$.

One can get a better physical picture of the significance of this degree of consistency by computing the initial $W(r)/r$ function for the fourth cycle and taking the difference between this function, denoted as $W(r)^{(4)}/r$, and the final potential of the third cycle

TABLE VII. The $2p$ radial wave function, P_{2p}, as determined by Hartree-Fock method and by the Slater approximation.

r	Hartree-Fock	Slater	r	Hartree-Fock	Slater
0.000	0.000	0.000	0.220	1.934	1.933
0.005	0.016	0.016	0.240	1.808	1.804
0.010	0.061	0.060	0.260	1.670	1.665
0.015	0.128	0.126	0.280	1.528	1.520
0.020	0.213	0.208	0.300	1.386	1.377
0.025	0.310	0.303			
0.030	0.416	0.409	0.350	1.055	1.045
0.035	0.528	0.523	0.400	0.778	0.769
0.040	0.644	0.640	0.450	0.561	0.553
			0.500	0.398	0.392
0.050	0.877	0.877	0.550	0.279	0.274
0.060	1.103	1.106	0.600	0.195	0.189
0.070	1.312	1.318			
0.080	1.500	1.508	0.700	0.093	0.089
0.090	1.663	1.673	0.800	0.045	0.041
0.100	1.801	1.812	0.900	0.022	0.019
			1.000	0.011	0.008
0.120	2.002	2.013	1.100	0.005	0.004
0.140	2.111	2.121	1.200	0.002	0.003
0.160	2.142	2.150	1.300	0.001	0.000
0.180	2.113	2.119	1.400	0.000	0.000
0.200	2.040	2.042			

$W(r)^{(3)}/r$ as a perturbing potential. This has been done and the average value has been computed with respect to the $3d$ wave function. The $3d$ function was selected because it is the most sensitive of all the wave functions of Cu^+ and because the $3d$ eigenvalue incurred the largest changes from one cycle to another. The average value of the difference over the $3d$ wave function was found to be about 0.05. Therefore, it may be estimated that the $3d$ eigenvalue reported should not differ from

TABLE VIII. The $3s$ radial wave function, P_{3s}, as determined by Hartree-Fock method and by the Slater approximation.

r	Hartree-Fock	Slater	r	Hartree-Fock	Slater
0.000	0.000	0.000	0.350	0.438	0.401
0.005	0.152	0.156	0.400	0.757	0.724
0.010	0.261	0.267	0.450	1.001	0.974
0.015	0.334	0.341	0.500	1.170	1.148
0.020	0.376	0.384	0.550	1.268	1.254
0.025	0.393	0.401	0.600	1.311	1.302
0.030	0.389	0.400			
0.035	0.368	0.383	0.700	1.275	1.276
0.040	0.334	0.353	0.800	1.147	1.154
			0.900	0.983	0.994
0.050	0.238	0.263	1.000	0.817	0.828
0.060	0.119	0.147	1.100	0.663	0.675
0.070	−0.010	−0.020	1.200	0.531	0.542
0.080	−0.139	−0.109	1.300	0.420	0.429
0.090	−0.260	−0.234	1.400	0.329	0.337
0.100	−0.370	−0.345			
			1.600	0.198	0.204
0.120	−0.544	−0.527	1.800	0.117	0.121
0.140	−0.651	−0.644	2.000	0.069	0.070
0.160	−0.692	−0.695	2.200	0.040	0.040
0.180	−0.677	−0.688	2.400	0.023	0.021
0.200	−0.614	−0.632	2.600	0.014	0.009
0.220	−0.515	−0.539	2.800	0.008	0.001
0.240	−0.390	−0.419	3.000	0.004	0.000
0.260	−0.247	−0.279	3.200	0.002	0.000
0.280	−0.094	−0.129	3.400	0.001	0.000
0.300	0.062	0.026	3.600	0.000	0.000

TABLE IX. The $3p$ radial wave function P_{3p} as determined by the Hartree-Fock method and by the Slater approximation.

r	Hartree-Fock	Slater	r	Hartree-Fock	Slater
0.000	0.000	0.000	0.400	−0.804	−0.837
0.005	0.006	0.006	0.450	−0.993	−1.024
0.010	0.022	0.023	0.500	−1.123	−1.149
0.015	0.047	0.047	0.550	−1.200	−1.221
0.020	0.078	0.078	0.600	−1.235	−1.250
0.025	0.113	0.114			
0.030	−0.152	0.153	0.700	−1.212	−1.216
0.035	0.193	0.196	0.800	−1.115	−1.109
0.040	0.234	0.239	0.900	−0.986	−0.992
			1.000	−0.848	−0.831
0.050	0.317	0.325	1.100	−0.717	−0.697
0.060	0.395	0.406	1.200	−0.598	−0.577
0.070	0.465	0.478	1.300	−0.494	−0.474
0.080	0.524	0.540	1.400	−0.405	−0.386
0.090	0.572	0.589			
0.100	0.601	0.625	1.600	−0.269	−0.252
			1.800	−0.176	−0.162
0.120	0.642	0.659	2.000	−0.114	−0.103
0.140	0.632	0.646	2.200	−0.073	−0.065
0.160	0.583	0.592	2.400	−0.047	−0.041
0.180	0.503	0.508	2.600	−0.030	−0.026
0.200	0.400	0.399	2.800	−0.019	−0.018
0.220	0.281	0.274	3.000	−0.012	−0.008
0.240	0.152	0.139	3.200	−0.007	−0.005
0.260	0.018	0.001	3.400	−0.004	−0.003
0.280	−0.116	−0.140	3.600	−0.002	−0.001
0.300	−0.249	−0.276	3.800	−0.001	
			4.000		
0.350	−0.554	−0.586			

TABLE X. The $3d$ radial wave function P_{3p} as determined by the Hartree-Fock method and by the Slater approximation.

r	Hartree-Fock	Slater	r	Hartree-Fock	Slater
0.000	0.000	0.000	0.600	0.991	1.032
0.005	0.000	0.000			
0.010	0.000	0.000	0.700	0.978	1.004
0.015	0.001	0.001	0.800	0.937	0.949
0.020	0.002	0.002	0.900	0.882	0.882
0.025	0.003	0.003	1.000	0.821	0.811
0.030	0.005	0.006	1.100	0.759	0.740
0.035	0.008	0.008	1.200	0.698	0.673
0.040	0.011	0.012	1.300	0.639	0.610
			1.400	0.585	0.552
0.050	0.019	0.022			
0.060	0.030	0.035	1.600	0.488	0.450
0.070	0.044	0.050	1.800	0.406	0.367
0.080	0.061	0.069	2.000	0.337	0.298
0.090	0.080	0.090	2.200	0.279	0.242
0.100	0.101	0.114	2.400	0.231	0.197
			2.600	0.191	0.160
0.120	0.149	0.168	2.800	0.158	0.130
0.140	0.203	0.228	3.000	0.130	0.105
0.160	0.261	0.292	3.200	0.107	0.085
0.180	0.321	0.359	3.400	0.088	0.068
0.200	0.382	0.425	3.600	0.072	0.055
0.220	0.442	0.491	3.800	0.059	0.044
0.240	0.501	0.554	4.000	0.049	0.035
0.260	0.557	0.614			
0.280	0.610	0.670	4.500	0.029	0.019
0.300	0.660	0.723	5.000	0.018	0.008
			5.500	0.010	0.002
0.350	0.770	0.834	6.000	0.006	0.000
0.400	0.855	0.918			
0.450	0.917	0.977	7.000	0.002	0.000
0.500	0.958	1.013	8.000	0.001	0.000
0.550	0.981	1.030			

the actual value corresponding to the Slater method by more than 0.05.

By considering the differences between the initial function $W(r)^{(2)}$ for the second cycle and the initial function $W(r)^{(4)}$ for the third cycle, and the differences in the energies found for these cycles, one can make rough estimates of the uncertainties in the energies reported for the third cycle. The $W^{(3)}$, $W^{(4)}$ difference is of the same nature as the $W^{(4)}$, $W^{(6)}$ difference, but is approximately ten times as large. Therefore, one might expect a change in the energies corresponding to a fourth cycle to be about one-tenth of the change in the eigenvalues from the second to third cycle. For example, the $3d$ energy for the second cycle was -0.855 and for the third cycle it was -1.353, a change of about 0.50. According to the above, one might expect the change in the $3d$ energy for a fourth cycle to be about one-tenth of this difference or about 0.05 which is just what the perturbation arguments have indicated. In Table XIV are given the electronic energies and their corresponding uncertainties so determined. These uncertainties are to be interpreted as follows: The actual energy of a given level as determined by the Slater method will be more positive than the reported value by approximately the stated uncertainty.

Let us now examine the behavior of the common potential $W(r)/r$ which results from the free electron gas model of the exchange charge density. This quantity is given as

$$W(r)/r=[2Z_p+z(r)]/r$$
$$=\frac{2Z}{r}-\frac{2}{r}\sum_{nl}2(2l+1)\left\{\int_0^r P_{nl}^2dr+r\int_r^\infty\frac{P_{nl}^2}{r'}dr'\right\}$$
$$+\frac{6}{r}\left\{\frac{3}{32\pi^2}\sum_{nl}2(2l+1)rP_{nl}^2\right\}^{\frac{1}{3}}, \quad (26)$$

where Z is the atomic number. For large r, $W(r)/r$ approaches $2C/r$, where C is the net charge on the atom or ion being considered. This implies that an electron located outside the charge cloud of a singly ionized atom would move in a potential field of $2/r$ in atomic units. This is quite wrong, for such an electron experiences the field set up by the nuclear charge and $n-1$ electrons. Therefore, such an electron moves in a field which varies as $4/r$. This incorrect behavior arises because the exchange term as found by the free electron approximation goes to zero at large r. We recall that the exchange term not only represents the interaction of an electron with its exchange charge density but also corrects for the fact that an electron does not act on itself.

In the case of Cu^+ one would expect the incorrect behavior of the potential to have the greatest effect on the $3d$ states as they are the most extended. If one examines the table of total radial charge density, Table XI, it is apparent that very little charge lies outside a sphere of radius 1.68. Also the $3d$ electrons spend 92

percent of the time inside a sphere of this radius. One can conclude that almost the entire character of the $3d$ wave function will be determined by the physical properties of the ion which depend on values of r less than 1.68. The quantity $W(r)/r$ at $r=1.68$ is 4.25 and, therefore, only about 8 percent of the time do the outermost electrons move in a potential field which is less than $4/r$. One may surmise, therefore, that the incorrect asymptotic behavior of the total potential function will have only a small effect on the eigenfunctions and corresponding eigenvalues. This appears to be borne out by the results of the calculation.

TABLE XI. The total radial charge density in atomic units, $U(r)=\sum_{nl}2(2l+1)P_{nl}(r)^2$, for the Hartree, Hartree-Fock, and the Slater methods.

r	Hartree	Hartree-Fock	Slater	r	Hartree	Hartree-Fock	Slater
0.000	0.00	0.00	0.00	0.500	19.22	20.89	22.184
0.005	3.9	3.9	3.9	0.550	20.53	22.17	23.365
0.010	11.7	11.7	11.7	0.600	21.16	22.74	23.737
0.015	19.7	19.7	19.7				
0.020	26.3	26.3	26.42	0.700	20.45	21.70	22.266
0.025	31.0	31.0	31.05	0.800	18.02	18.89	19.053
0.030	33.7	33.7	33.74	0.900	15.02	15.54	15.422
0.035	34.9	34.9	34.93	1.000	12.17	12.39	12.086
0.040	34.8	34.8	34.90	1.100	9.72	9.72	9.307
				1.200	7.75	7.57	7.114
0.050	32.7	32.8	32.91	1.300	6.21	5.91	5.434
0.060	30.0	30.2	30.30	1.400	5.01	4.62	4.166
0.070	28.1	28.3	28.51				
0.080	27.4	27.7	27.99	1.600	3.37	2.89	2.490
0.090	27.9	28.3	28.69	1.800	2.35	1.86	1.531
0.100	29.4	29.9	30.30	2.000	1.69	1.21	0.963
				2.200	1.24	0.81	0.617
0.120	33.61	34.20	34.655	2.400	0.91	0.55	0.399
0.140	33.61	34.20	34.655	2.600	0.67	0.37	0.261
0.140	37.35	37.96	38.445	2.800	0.50	0.25	0.171
0.160	39.32	39.83	40.328	3.000	0.37	0.17	0.111
0.180	39.23	39.59	40.073	3.200	0.28	0.11	0.072
0.200	37.36	37.62	38.085	3.400	0.20	0.08	0.046
0.220	34.35	34.53	35.009	3.600	0.15	0.05	0.030
0.240	30.81	30.97	31.480	3.800	0.11	0.03	0.019
0.260	27.24	27.43	29.004	4.000	0.08	0.02	0.012
0.280	23.98	24.26	24.930				
0.300	21.26	21.67	22.451	4.500	0.03	0.00	0.004
				5.000	0.01	0.00	0.001
0.350	17.19	18.04	19.106	5.500	0.00	0.00	0.000
0.400	16.48	17.72	18.992	6.000	0.00	0.00	0.000
0.450	17.61	19.13	20.470	6.500	0.00	0.00	0.000

CONCLUSIONS

It is evident from the results presented that the Slater method is a rather accurate approximation of the Hartree-Fock solution to Cu^+. The energies found by the Slater method lie closer to the Hartree than Hartree-Fock values. Only the $1s$ and $3d$ levels show much real difference from the Hartree eigenvalues. The $1s$ energy as found by the Slater method is -649.53, more positive than the Hartree value of -658. This difference is most likely due to the failure of the exchange term to correct for the interaction of the $1s$ electrons with themselves, because the $1s$ electrons are concentrated in a region where the charge density due to the other electrons is quite small. The Slater $3d$ energy of -1.353 is somewhat of an improvement over the Hartree value of -1.195. This result indicates that Slater's exchange correction has not been a source of large error due to its incorrect behavior at large r.

TABLE XII. The charge outside a sphere of radius r due to the $3p$ electrons of Cu^+. This is given as $6(1-Z_{3p})$, and $Z_{3p}(r)$ is $\int_0^r P_{3p}(r)^2dr$.

r	Hartree-Fock	Slater	r	Hartree-Fock	Slater
0.000	6.000	6.000	0.300	5.693	5.679
0.005	6.000	6.000			
0.010	6.000	6.000	0.350	5.641	5.620
0.015	6.000	6.000	0.400	5.500	5.464
0.020	6.000	6.000	0.450	5.254	5.201
0.025	6.000	6.000	0.500	4.945	4.843
0.030	5.999	5.999	0.550	4.507	4.419
0.035	5.998	5.998	0.600	4.061	3.958
0.040	5.997	5.997			
			0.700	3.150	3.033
0.050	5.992	5.992	0.800	2.331	2.216
0.060	5.984	5.984	0.900	1.666	1.564
0.070	5.975	5.972	1.000	1.161	0.999
0.080	5.959	5.956	1.100	0.794	0.725
0.090	5.941	5.937	1.200	0.535	0.482
0.100	5.920	5.915	1.300	0.356	0.317
			1.400	0.235	0.208
0.120	5.873	5.865			
0.140	5.823	5.813	1.600	0.100	0.085
0.160	5.779	5.767	1.800	0.042	0.035
0.180	5.743	5.730	2.000	0.017	0.014
0.200	5.718	5.705	2.200	0.007	0.005
0.220	5.704	5.692	2.400	0.003	0.002
0.240	5.698	5.686	2.600	0.001	0.001
0.260	5.697	5.685	2.800	0.000	0.000
0.280	5.697	5.685	3.000	0.000	0.000

TABLE XIII. The charge outside a sphere of radius r due to the $3d$ electrons of Cu. This is given as $10(1-Z_{3d})$, and $Z_{3d}(r)$ is $\int_0^r P_{3d}(r)^2dr$.

r	Hartree-Fock	Slater	r	Hartree-Fock	Slater
0.000	10.000	10.000	0.350	9.39	9.27
0.005	10.000	10.000	0.400	9.06	8.88
0.010	10.000	10.000	0.450	8.67	8.43
0.015	10.000	10.000	0.500	8.23	7.94
0.020	10.000	10.000	0.550	7.76	7.41
0.025	10.000	10.000	0.600	7.27	6.88
0.030	10.000	10.000			
0.035	10.000	10.000	0.700	6.29	5.84
0.040	10.000	10.000	0.800	5.37	4.88
			0.900	4.54	4.04
0.050	10.000	10.000	1.000	3.82	3.20
0.060	10.000	10.000	1.100	3.19	2.73
0.070	10.000	10.000	1.200	2.66	2.27
0.080	10.000	10.000	1.300	2.21	1.82
0.090	10.000	10.000	1.400	1.84	1.50
0.100	10.000	10.000			
			1.600	1.27	0.98
0.120	9.99	9.99	1.800	0.87	0.65
0.140	9.99	9.99	2.000	0.59	0.42
0.160	9.98	9.97	2.200	0.41	0.28
0.180	9.96	9.95	2.400	0.28	0.18
0.200	9.93	9.92	2.600	0.19	0.12
0.220	9.90	9.88	2.800	0.13	0.10
0.240	9.86	9.82	3.000	0.09	0.06
0.260	9.80	9.76	3.200	0.06	0.03
0.280	9.73	9.67	3.400	0.04	0.02
0.300	9.65	9.56	3.600	0.02	0.01
			3.800	0.01	0.01
			4.000	0.01	0.00

TABLE XIV. The electronic energy levels as determined by the Hartree, Slater, and Hartree-Fock methods for Cu^+ together with the uncertainties in the values found for the Slater method. The unit of energy is the ionization energy of the hydrogen atom, $e^2/2a_0$.

nl	Hartree	Hartree-Fock	Slater	Uncertainty
$1s$	−658	−658.4	−649.5	0.1
$2s$	−78.45	−82.30	−78.92	0.16
$2p$	−69.86	−71.83	−69.50	0.13
$3s$	−8.986	−10.651	−8.822	0.03
$3p$	−6.078	−7.279	−6.279	0.06
$3d$	−1.195	−1.613	−1.353	0.05

From the table of total radial charge density one notes two points. First, the total radial charge density as found by the Slater method is more concentrated about the nucleus than the corresponding Hartree-Fock density, while the Hartree function is more spread out than the Hartree-Fock. Second, the values of this quantity found by the Slater method are more accurate than the Hartree method for large r.

A comparison of the Slater and Hartree-Fock radial wave functions for Cu^+ shows that the $1s$, $2s$, $2p$, and $3s$ functions are nearly the same. The $3p$ and $3d$ wave functions are more pulled in by the Slater method, but are generally within 5 percent of the Hartree-Fock values.

In the case of Cu^+ the total wave function can be written as a single determinant. The Slater approximation of the Fock equations only applies when the total wave function can be expressed in this manner. The simplification of the more general Fock equations and the consequences of incorrectly expressing a total wave function as a single determinant are questions which remain to be investigated.

As a general appraisal of the Slater method as applied to Cu^+ it can be said that it yields wave functions which are an improvement over the Hartree functions. The electronic energy levels are about equal to the Hartree results with poorer values for the innermost electrons and better values for the outermost electrons. The purpose of the Slater method is, of course, to make the task of finding fairly reliable eigenfunctions and eigenvalues easier than that of the Hartree-Fock method in those cases where such a simplification is applicable. In view of the fact that the Slater method requires less work than the Hartree method and is a slight improvement over that method, it appears that the Slater method merits thorough consideration when one is investigating atomic structure. One can also conclude from these results that the Slater method should be of considerable use in the investigation of crystal problems.

TABLE XV. The $2Z_p(r)$ function as determined by the Hartree-Fock method and as found by the Slater method. The product of r times $2Z_p(r)$ is the total electrostatic potential of the atom at a distance r from the nucleus.

r	Hartree-Fock	Slater	r	Hartree-Fock	Slater
0.000	58.00	58.000	0.450	16.00	15.288
0.010	55.35	55.322	0.500	14.13	13.412
0.020	52.92	52.863	0.550	12.47	11.759
0.030	50.75	50.662	0.600	11.01	10.317
0.040	48.80	48.686			
0.050	47.02	46.885	0.700	8.65	8.007
0.060	45.38	45.217	0.800	6.91	6.334
0.070	43.84	43.651	0.900	5.64	5.139
0.080	42.38	42.167	1.000	4.72	4.270
0.090	40.99	40.753	1.100	4.05	3.684
0.100	39.66	39.403	1.200	3.56	3.245
			1.300	3.19	2.935
0.120	37.18	36.886	1.400	2.91	2.740
0.140	34.94	34.597			
0.160	32.91	32.528	1.600	2.55	2.409
0.180	31.07	30.660	1.800	2.34	2.247
0.200	29.42	28.970	2.000	2.21	2.144
0.220	27.91	27.433	2.200	2.13	2.088
0.240	26.54	26.023	2.400	2.08	2.053
0.260	25.26	24.719	2.600	2.05	2.032
0.280	24.07	23.501	2.800	2.03	2.021
0.300	22.95	22.354	3.000	2.02	2.012
			3.200	2.01	2.006
0.350	20.38	19.733	3.400	2.00	2.004
0.400	18.08	17.391			

The author wishes to express his gratitude to the members of the Solid State and Molecular Theory Group at Massachusetts Institute of Technology for their criticisms and assistance in this work. The author wishes also to acknowledge the constant help and advice of the director of the group, Professor John C. Slater.

Production of π^0 Mesons by γ-Rays on Hydrogen*

A. SILVERMAN AND M. STEARNS†
Cornell University, Ithaca, New York
(Received August 27, 1952)

The production of π^0 mesons in the reaction

$$\gamma+p\rightarrow\pi^0+p$$

is investigated as a function of the incident γ-ray energy in the region from 200 Mev to 300 Mev. For the π^0 emitted at approximately 90° laboratory angle, the differential cross section can be represented by

$$(d\sigma_{\pi^0}/d\Omega)_{\pi/2}=C(K-145)^{1.9\pm0.4},$$

where K = energy of incident γ-ray in Mev. The approximate threshold for the reaction is 145 Mev.

The ratio of the cross section at 60° laboratory angle to that at 90° laboratory angle, for γ-rays between 250 Mev and 300 Mev, is 1.45 ± 0.25.

INTRODUCTION

THE first observation of the production of π_0 mesons by high energy γ-rays was made by Steinberger, Panofsky, and Steller[1,2] at Berkeley. In this experiment they detected the π^0 by observing coincidences between the two decay γ-rays. The measurements they made were the coincidence counting rates as a function of the angle between the γ-ray counters for various angles between the beam direction and the plane of the counters. In this way they were able to establish the decay of the π^0 into two γ-rays and the cross section for their production, which turned out to be of the same order as the production cross section for charged mesons. It is also possible to obtain some information, by this technique, on the energy of the π^0, since the counting rate as a function of the angle between the two counters depends upon the energy distribution of the π^0's. They were thus able to construct a rough picture of the production cross section as a function of the primary γ-ray energy. The present experiment was undertaken in an attempt to obtain more directly the information on the excitation function for the production of π^0's by γ-rays on hydrogen.

The reaction studied was the following: $\gamma+p=\pi^0+p'$, where γ is an incident γ-ray, p the target proton, and p' the recoil proton. Since we are dealing with a two-body collision, γ, π^0, and p' are coplanar. Thus, assuming the direction of the γ-ray beam known, there are five dynamical variables involved in the collision: the energy of the γ-ray, the energy and angle of the π^0, and the energy and angle of the recoil proton. Since the conservation laws provide three relationships among the five variables, measuring any two completely specifies all of them. In this experiment we choose to measure the energy and angle of the recoil proton.

* Work supported by contract with the ONR.
† Now at Carnegie Institute of Technology, Pittsburgh, Pennsylvania.
[1] Steinberger, Panofsky, and Steller, Phys. Rev. 78, 494 (1950).
[2] Steinberger, Panofsky, and Steller, Phys. Rev. 86, 180 (1952).

EXPERIMENTAL

Experimental Arrangement

The experimental arrangement is shown schematically in Fig. 1. All of the shielding and collimation has been omitted for the sake of clarity. The γ-ray beam is the bremsstrahlung radiation from the 315-Mev Cornell synchrotron. The reaction is observed by detecting coincidences between the recoil protons and one of the decay γ-rays from the π^0 meson. The γ-ray counter is a telescope of three stilbene crystals arranged as follows: As seen from the target there is an anticoincidence crystal, converter, and two crystals in coincidence. This is identical with the γ-ray detector described in references 1 and 2. The proton counter is a cylindrical NaI crystal (0.75 in. thick, 1.50 in. in diameter, mounted on a 5819 RCA phototube) in which the protons expend all of their energy. The pulse height is thus a measure of the proton energy. The pulse height was measured in a five-channel analyzer. The electronics was arranged so that the proton pulse height was measured only when a coincidence between the γ-ray and proton counters was registered.

The target used was a 0.23-g/cm² slab of polyethylene $(CH_2)_n$. The carbon background was determined using a carbon target whose stopping power for protons was equal to that of the polyethylene target.

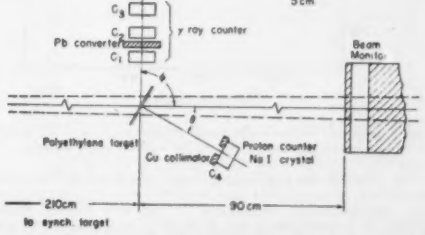

FIG. 1. Experimental arrangement.

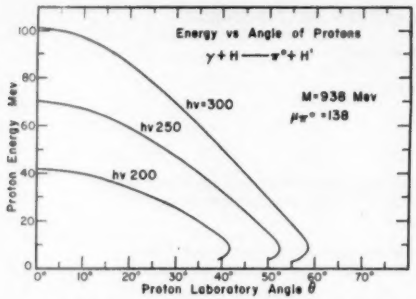

FIG. 2. Recoil proton angle *vs* proton energy for various γ-ray energies.

Choice of Angles for the Proton and γ-Ray Detectors

Figure 2 shows a graph of the energy of the recoil proton *vs* laboratory angle for various γ-ray energies. It is seen that the protons are confined to angles less than 60° to the beam direction for all energies up to 315 Mev. In this experiment measurements were made with the proton counter set at 30° and 45° to the beam direction.[3] By observing all protons with energy greater than 20 Mev, we were able to detect protons arising from γ-rays in the interval 200 Mev–315 Mev at 30°, and 250 Mev–315 Mev at 45°. The lower limit of 20 Mev for the proton energy was determined primarily by the desire to keep the chance coincidences down to a few percent. There are, however, several other reasons which make it undesirable to decrease this energy substantially. First, the target is about 15 Mev thick so that the resolution becomes bad very rapidly for proton energies below 15 Mev. Second, the double-valued character of the E_p *vs* θ curve (Fig. 2) make the interpretation ambiguous for low energy proton recoils.

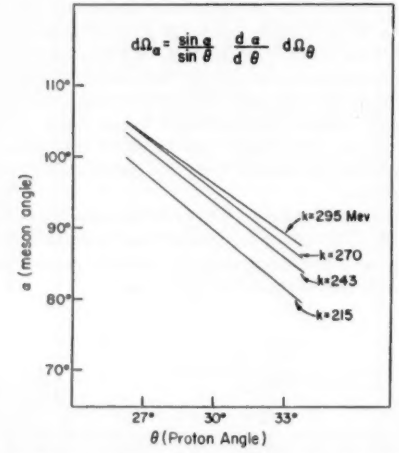

FIG. 3. Relation between the recoil proton angle and the meson angle in the laboratory system for various γ-ray energies

The direction in which the γ-ray counter is placed is dictated by the position of the proton counter. Consider a π° meson with velocity β. The probability per steradian, $p(\phi)$, of one of the decay γ-rays emerging at an angle ϕ with respect ot the π° is

$$p(\phi)=2(1-\beta^2)/[4\pi(1-\beta\cos\phi)^2].$$

This has clearly a maximum for $\phi=0$. Thus, for maximum detection efficiency, the γ-ray detector should be placed in the direction in which the π° is traveling. In Fig. 3 is shown the angle of the π° in the laboratory as a function of the proton laboratory angle for various γ-ray energies. The case shown is for the proton counter set as 30° with an aperture of ±3°. One sees that the π° angle varies only very slowly with γ-ray energy for a fixed proton angle; and for the proton at 30°, the π° emerges at close to 90°. With the proton at 45°, the π° angle is approximately 60° for all γ-ray energies between 250 Mev and 315 Mev.

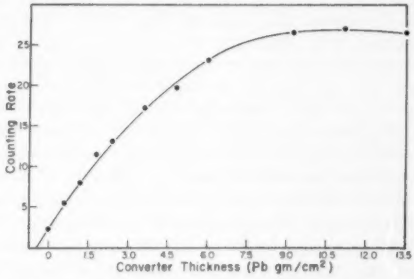

FIG. 4. The curve shows the relative efficiency of the γ-ray counter as a function of converter thickness for 170-Mev γ-rays. The absolute efficiency is obtained by fitting the thin converter data to a curve of form $1-e^{-\mu x}$, where μ=absorption coefficient for 170-Mev γ-rays on Pb.

The energy scale for the proton pulses was determined in a manner similar to that described by Keck.[4] This method consists essentially in measuring the maximum size pulses protons are able to produce in the crystal. These protons have a range just equal to the thickness of the crystal, and consequently their energy can be determined from the range-energy relations. This was checked by observing the photopeak of the ThC″ 2.6-Mev γ-ray. The two results agreed to within ten percent. The calibration provided by the protons was

[3] In principle, the technique is useful for measuring the angular distribution of the protons (and hence the π°'s). In practice, however, difficulties are encountered in the very forward angles because of electron pile up and at angles greater than 50° because here the proton energies become small and the range of γ-ray energies available is reduced (see Fig. 2).

[4] J. C. Keck, Phys. Rev. 85, 410 (1952).

used, since it does not involve the large extrapolation from 2.6 Mev to the energy region used in the experiment (20 Mev to 70 Mev).

The efficiency of the γ-ray detector is of considerable importance, particularly for obtaining the absolute cross section. Because of the Doppler shift, the γ-ray energies vary from about 150 Mev to 200 Mev. The variation of the pair production cross section over this energy range is about 5 percent. The efficiency is therefor approximately constant over this region. To get the absolute efficiency, the telescope was calibrated using the 170-Mev γ-ray available at this laboratory.[5,6] Figure 4 shows the counting rate at this energy as a function of converter thickness. Interpolating the results of DeWire *et al.*,[7] we obtain an absorption coefficient of 0.102 cm^2/g for 170-Mev γ-rays on lead. The converter thickness used was 10 g/cm^2. From Fig. 4, we calculate the efficiency to be 55 percent. A previous estimate,[8] based on the Monte Carlo calculations of Wilson[9] and related cloud chamber experiments by Shapiro[10] gave a result of 65 percent for the efficiency. The results quoted in the following sections will use the experimental value of 55 percent.

Auxiliary Experiments

In this section we shall present the results of several auxiliary experiments that were done to check that the coincidences observed were the result of photoproduction of neutral mesons.

(a) Table I shows the relative counting rates for the polyethylene and carbon targets with and without converter. One sees that the carbon background is approximately 20 percent and is independent of converter.[11] The 34 percent residual counting rate with the polyethylene target and no converter is due largely to the carbon background. About $\frac{1}{3}$ of this rate can be attributed to the efficiency of the γ-ray detector with zero converter since the efficiency with zero converter is about 5 percent due to conversion in the crystals themselves (see Fig. 4).

(b) The maximum proton energy at 30° (Fig. 2), corresponding to 315-Mev γ-rays, is about 72 Mev; and at 45° it is 45 Mev. Furthermore, the maximum backward angle is about 60°. Figure 5 shows the energy distribution of the observed protons at 30°, 45°, and 75°. Histograms A and B have arrows indicating the expected proton energy for 310-Mev γ-rays at 30° and 45°. It is clear that the maximum proton energy varies as expected as the proton angle is changed. Furthermore, at 75°, an angle forbidden to the recoil proton, the counting rate is zero.

TABLE I. Relative counting rates for the poly and carbon targets with and without converter.

Target	Counting rate
Poly	1.00
No target	0.00
Carbon	0.22±0.02
Poly (no converter)	0.34±0.07
Carbon (no converter)	0.24±0.06

(c) The counting rate was observed with the γ-ray counter rotated 180° about an axis parallel to the beam. The efficiency of the γ-ray counter is then reduced because of two factors: (1) the probability of one of the decay γ-rays striking the detector is reduced by a factor of $(1-\beta/1+\beta)^2 \cong 1/30$; (2) the energy of the γ-ray at 180° to the π^0 direction has been greatly reduced. The observed rate was 0.02±0.02 of the initial rate.

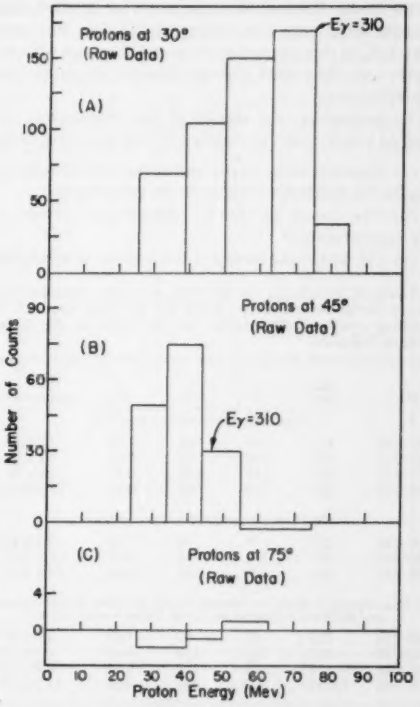

FIG. 5. Histograms showing the number of counts in each energy interval. (A) shows results obtained with the proton counter set at 30°; (B) at 45°; and (C) at 75°.

[5] J. W. Weil and B. D. McDaniel, Phys. Rev. **86**, 582 (1952).
[6] D. Luckey and J. W. Weil, Phys. Rev. **85**, 1060 (1952).
[7] DeWire, Ashkin, and Beach, Phys. Rev. **83**, 505 (1951).
[8] A. Silverman and M. Sterns, Phys. Rev. **83**, 853 (1951).
[9] R. R. Wilson, Phys. Rev. **86**, 261 (1952).
[10] A. Shapiro (private communication).
[11] C. Greifinger and J. Levinger (private communication) have estimated the efficiency per proton in carbon for producing proton-photon coincidences that would be detected by the present apparatus. They take into account (1) the probability that both the π^0 and proton escape from nucleus, (2) the effect of initial motion of proton, and (3) the effect of the potential well. They estimate the efficiency to be 5 percent within a factor of 3. The present experiment sets an upper limit of approximately 3 percent for this efficiency. This low efficiency could also be understood quite simply, assuming that several nucleons share the recoil energy.

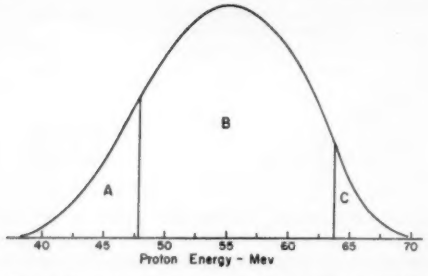

FIG. 6. Resolution curve of the proton counter for 270-Mev γ-rays. See text for discussion of various effects involved in determination of this curve.

(d) Data were taken with a 40-Mev absorber (one that absorbs protons of energy $\leqslant 40$ Mev) placed directly in front of the proton counter. The absorber and crystal together were 87 Mev thick. It was found that the energy spectrum shifted downward relative to that measured with no absorber by just the amount expected for protons. This also provided a check on the energy calibration of the proton counter. With the absorber in place, only protons from γ-rays in the region 255–310 Mev were detected. In this interval there were 377 counts with absorber and 354 counts without absorber for equal integrated beams.

To summarize, the results of the experiments described above, provide evidence for the following facts:

(a) Approximately 80 percent of the coincidences are due to the hydrogen content in the polyethylene.

(b) The counts are due to coincidences between γ-rays and protons.[12]

(c) The maximum energy of the protons as a function of the proton angle varies as expected for the reaction $\gamma+p=\pi^{\circ}+p'$.

(d) The counting rate as a function of the angle of the γ-ray counter, for fixed proton counter angle, also varies as expected for the above reaction.

TABLE II. Results for the 30° runs. K = γ-ray energy; n = observed No. of counts; n(corr) is the No. of counts corrected for "spilling over"; I(rel) = relative No. of γ-rays in the energy interval indicated.

K (Mev)	K_{av} (Mev)	n	n (corr)	I (rel)	$(d\sigma/d\Omega)_{90^{\circ}}$ cm²/steradian
(a) Four-channel analysis (no absorber)					
200–230	215	70	63	1.00	3.2×10^{-30}
230–255	243	106	97	0.61	6.1×10^{-30}
255–279	267	150	164	0.57	9.9×10^{-30}
279–310	295	204	206	0.50	12.3×10^{-30}
(b) Three-channel analysis (no absorber)					
200–230	215	70	64	1.00	3.5×10^{-30}
230–264	247	151	146	0.95	6.5×10^{-30}
264–310	290	309	320	0.85	12.4×10^{-30}
(c) Four-channel analysis (no absorber in the two lower energy channels, and 40-Mev Cu absorber in the two higher energy channels)					
200–230	215	67	60	1.00	2.9×10^{-30}
230–255	243	103	110	0.65	6.1×10^{-30}
255–285	270	200	188	0.70	8.9×10^{-30}
285–310	295	177	189	0.39	14.2×10^{-30}

[12] These cannot be Compton scattered protons because the angular correlation is wrong.

ANALYSIS OF DATA

Resolving Power of the Proton Detector

The resolving power of the apparatus is determined by three principal features. That is, given a monochromatic γ-ray beam, there are three factors which contribute to the spread in the energy measured for the recoil proton. They are (a) the angular resolution of the proton counter (by far the most important cause of spread), (b) the target thickness, and (c) the resolution of the NaI crystal. The first effect was calculated taking into account the angular aperture of the proton counter and the finite size of the beam. The resolution of the NaI counter was estimated in two ways. First, from the curvature in the high energy tail of the integral number-bias curve taken during the calibration and, second, from the photopeak of the 2.6-Mev ThC″ γ-ray. The result was approximately 15 percent width at half-maximum. The results are not sensitive to this number since its effect is not large. The net resolving power of the proton counter was obtained from the fold of these three effects. Figure 6 shows the resolution curve for a 270 Mev γ-ray. The angular aperture of the proton counter in all cases was $\pm3^{\circ}$. One sees that the resolution curve is quite broad. The major contribution to the width, as previously mentioned, is due to the angular aperture, but because the counting rate is sufficiently small (about one count per minute) it is undesirable to reduce the aperture much. The broadness of the resolution curve limits the fineness with which one can divide the spectrum. For all the analysis the spectrum was divided into three or four intervals. The areas marked B in Fig. 6 shows the limits of the third interval for a four-channel division of the spectrum. It is clear that some of the counts "spill over" into the second interval (A) and the fourth interval (C). In the calculation of the cross sections, the "spilling over" was corrected for.

Calculation of the Differential Cross Sections

The formula used for the calculation of the differential cross section is

$$\frac{d\sigma}{d\Omega_{\pi^{\circ}}dK}=\frac{1}{PNI}\frac{\Delta n}{\Delta\Omega_{\pi^{\circ}}},$$

where P = probability of detecting one of the γ-rays, N = number of hydrogen atoms per cm², I = number of incident γ-rays with energy between K and $K+dK$, and Δn = number of counts observed in this interval.

The solid angle $d\Omega_{\pi^{\circ}}$ is the meson solid angle. This can be caluclated from the known solid angle subtended by the proton counter.

The probability P for detecting one of the γ-rays is given by

$$P=\frac{2(1-\beta_{\pi^0}{}^2)\epsilon}{4\pi(1-\beta_{\pi^0}\cos\phi)^2}d\Omega_\gamma,$$

where β_{π^0} = velocity of the π^0, ϕ = angle between direction of γ-ray counter and velocity vector of the π^0, $d\Omega_\gamma$ = the solid angle subtended by the γ-ray counter, and ϵ = the efficiency of detecting the γ-ray which was measured to be 0.55. (See section on experimental arrangement.)

The number of γ-rays per unit energy interval I is different than a pure bremsstrahlung spectrum for two reasons: (a) the energy loss in the internal target (40-mil wolfram), and (b) the synchrotron beam is spread out over 2.5 milliseconds. Rather than try to calculate the effect of these corrections, the spectrum was measured with a pair spectrometer[7] under the conditions actually used. The spectrum differed from the bremsstrahlung spectrum primarily at the upper end where the beam spread has its maximum effect.

RESULTS

The results for the 30° runs are shown in Table II. The column headings are as follows: K = energy of γ-ray; n = observed number of counts; n(corr) is number of counts corrected for the "spilling over" from one channel into another because of the finite resolution; I(rel) = relative number of γ-rays in the energy interval indicated. Table II(a) is a four-channel analysis of the data taken with no absorber. Table II(b) is a three-channel analysis of the same data. Table II(c) is a mixture of these same data and data taken with the 40-Mev Cu absorber which could only be taken for incident γ-ray energies greater than 255 Mev. The Cu absorber data appear exclusively in the two higher energy channels of Table II(c), while the two lower energy channels use the same raw data used in Table II(a), normalized, however, to the number of monitor readings taken with the Cu absorber and to slightly different channel widths. The differential cross sections for neutral meson production at 95°±10° in the laboratory system are plotted in Fig. 7. The indicated errors are estimated instrumental errors as well as statistical errors. The high energy point is most uncertain because it involves the spectrum of the beam at the end point and the precise upper limit to the beam energy. The absolute cross section is estimated to have an error of about 30 percent arising primarily from uncertainties in measuring the integrated beam and in measuring the efficiency of the γ-ray detector. Figure 8 shows the log of the cross section *vs* the log of the energy above threshold (145 Mev) for the combined absorber and no absorber data.

Fitting the data with a straight line, one finds a slope equal to 1.9 as determined by a least squares calculation.

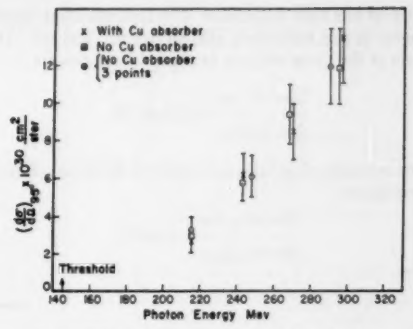

FIG. 7. Differential cross section for π^0 production *vs* photon energy.

Thus, the cross section can be written as

$$(d\sigma_{\pi^0}/d\Omega)_{95^\circ}=C(K-145)^{1.9\pm0.4},$$

where K = energy of the incident γ-ray.

The data taken with the proton counter at 45° involved γ-rays in the energy interval 255 Mev to 310 Mev. No attempt was made to obtain an excitation function in this region since at most one could obtain only two points. It is clear from the raw data [Fig. 5(b)] that the results are qualitatively similar to that at 30° for the same γ-ray interval. The ratio of the average cross section for γ-rays in the relevant

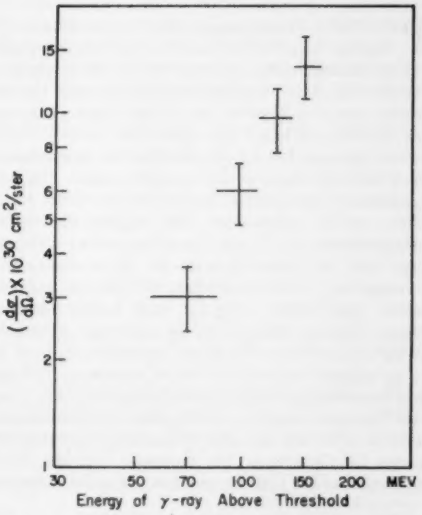

FIG. 8. Log of differential cross section for π^0 production *vs* log of photon energy. Assuming a straight line fit to the data, the slope of the line is 1.9±0.4 as determined by a least squares calculation.

interval has been calculated. The corresponding meson angles in the laboratory system are 95° and 60°. The ratio of the cross sections at these two angles are

$$\frac{(d\sigma/d\Omega_{\pi^0})_{60°}}{(d\sigma/d\Omega_{\pi^0})_{95°}}=1.45\pm0.25.$$

The corresponding ratio and angles in the center-of-mass system are

$$\frac{(d\sigma/d\Omega_{\pi^0})_{75°}}{(d\sigma/d\Omega_{\pi^0})_{110°}}=1.0\pm0.2.$$

The results of the excitation function and the absolute cross sections are in reasonable agreement with the results of Panofsky, Steinberger, and Steller.[2] They do not quote results on the angular distribution for a hydrogen target so that no comparison can be made.

The authors wish to express their gratitude to Professor J. W. DeWire for measuring the spectrum of the spread out beam, to Professor B. D. McDaniel for his assistance in measuring the efficiency of the γ-ray counter, and finally to Professor R. R. Wilson for his continued interest and guidance throughout the course of the experiment.

PHYSICAL REVIEW VOLUME 88, NUMBER 6 DECEMBER 15, 1952

Production of π^0 Mesons in Hydrogen and Deuterium by High Energy γ-Rays*

G. COCCONI AND A. SILVERMAN
Cornell University, Ithaca, New York

(Received August 27, 1952)

The angular distribution of the π^0's and the dependence of the cross sections on the energy of the γ-rays have been studied for the reactions

$$\gamma+P\rightarrow\pi^0+P,$$
$$\gamma+P\rightarrow\pi^0+D(P,N).$$

For the first reaction, the angular distribution in the center-of-mass system has the form $a+b\sin^2\theta$, with $a/b\simeq1$, and the cross section is proportional to approximately the square of the excess energy of the γ-rays above the threshold; $\sigma_D/\sigma_H\simeq2$ at all energies and angles.

INTRODUCTION

PREVIOUS investigations of π^0 production by γ-rays have used detection techniques involving coincidence measurements between two of the products of the reaction, i.e., coincidences either between the two decay γ-rays[1] or between one of the decay γ-rays and the recoiling nucleon.[2] The difficulties involved in the latter technique for angular distribution measurements have been discussed in the preceding paper. The measurement of coincidences between the two decay γ-rays offers certain advantages for angular distribution measurements, but it has the rather serious disadvantage that the counting rates are quite small. As a consequence, the measurements on hydrogen and deuterium, particularly using the usual subtraction technique, become difficult to do with any reasonable statistical accuracy. We have, consequently, been led to investigate the production of π^0 mesons on hydrogen and deuterium by detecting only one of the decay γ-rays and thus increasing the counting rates by approximately a factor of 50 over the rates obtained by detecting both γ-rays in coincidence. The increased counting rate is purchased at the cost of some loss in angular definition, since the decay γ-ray does not necessarily preserve the direction of the π^0. However, this disadvantage turns out to be not too serious because, as shown later, the γ-ray angular distribution reproduces quite faithfully the π^0 distribution for the energies with which we are concerned.

APPARATUS

The experimental arrangement is shown in Fig. 1. The targets used were of cylindrical shape, 2 in. in diameter, 2 in. long, and made of H_2O, D_2O, $(CH_2)_n$, and C. The results for H and D were obtained with the subtraction method. The measurements consisted in recording the coincidences $(B+C-A)$ between crystals B and C with crystal A in anticoincidence (hereafter called threefold coincidences) and coincidences $(B+C+D-A)$ between crystals B, C, and D again with crystal A in anticoincidence (hereafter called fourfold coincidences) at various angles θ and for various maximum energies of the bremsstrahlung γ-ray beam of the Cornell sychrotron. An aluminum absorber $2\frac{1}{4}$ in. thick was placed between the third and fourth crystal in order to make the fourfold coincidences insensitive to low energy γ-rays. The efficiencies of the threefold and fourfold coincidences as a function of γ-ray energy for a Pb converter 7 g/cm² thick are shown in Fig. 2. They were measured for γ-ray energies of 190, 140, and 100

* This work was supported in part by the ONR.
[1] Panofsky, Steinberger, and Steller, Phys. Rev. 86, 180 (1952).
[2] A. Silverman and M. Stearns, preceding paper [Phys. Rev. 88, 1225 (1952)].

Mev, using the monochromatic γ-ray beam available at this laboratory.[3] The efficiency of the threefold coincidences was also calculated using the Monte Carlo method of Wilson.[4] The experimental results are consistently lower by about 10 percent than the calculated ones. This is at least in part due to the fact that in the calculations the scattering was neglected. The efficiencies used in the analysis of the results are shown by the dotted curves in Fig. 2.

The evidence that the coincidences recorded were due to γ-rays arising from the decay of neutral mesons consists of the following observations:

(a) The dependence of the coincidence rates on the thickness and the material of the converters indicates that more than 90 percent of all counts were due to γ-rays.

(b) The counting rates decreased by more than a factor of 100 as the maximum beam energy was reduced from 310 Mev to 150 Mev.

(c) Assuming that all the counts arise from decay of π^0 mesons, one obtains a cross section for π^0 production on hydrogen of 1.5×10^{-28} cm^2, which is in good agreement with previous results.[1,2]

(d) The excitation function (see Fig. 4) measured on hydrogen is in reasonable agreement with previous results for π^0 production by γ-rays.[2]

(e) The γ-rays responsible for the fourfold coincidences have energies greater than about 80 Mev, the approximate threshold for this detector (see Fig. 2).

We believe that the above evidence is sufficient to establish that most of the coincidences recorded were due to decay γ-rays from neutral mesons. As far as we know, the only other process that could give rise to γ-rays scattered by H and D with properties similar to the ones listed before is Compton scattering. We have tried to measure the Compton scattering cross section of hydrogen at the π^0 threshold (150 Mev) and at 90° from the beam, and we found $d\sigma/d\Omega \leqslant 10^{-31}$ cm^2 steradian^{-1}. Thus, unless the cross section increases very rapidly with γ-ray energy so as to become several hundred times larger than the Thompson cross section, this process will contribute no appreciable background to our measurements.[5]

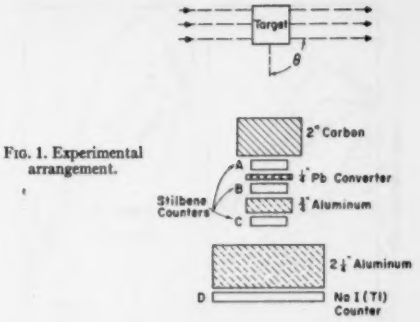

FIG. 1. Experimental arrangement.

DISCUSSION OF THE RESULTS

1. Hydrogen

Before analyzing the experimental data, it is necessary to discuss the relation between the π^0 angular distribution and the angular distribution of their decay γ-rays. Let us suppose that, for a primary γ-ray of energy ω, the cross section in the center-of-mass system for the reaction

$$\gamma+P\rightarrow\pi^0+P,$$

is given by the expression

$$d\sigma_{\pi^0}/d\Omega=A+B\cos^2\tilde{\theta},$$

where $\tilde{\theta}$ represents the angle in the center-of-mass system at which the π^0 is emitted. Let E and θ be the energy and the angle in the laboratory system of a decay γ-ray arising from the disintegration of the π^0. If $N(E,\theta)dEd\Omega$ is the intensity of the decay γ-rays with energy E and angle θ in the intervals dE and $d\Omega$, then

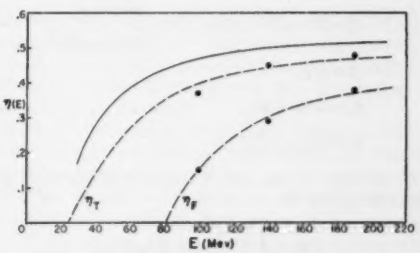

FIG. 2. Efficiency $\eta(E)$ of the threefold and fourfold coincidences as a function of the energy E of the γ-rays. The solid line describes the results obtained with the Monte Carlo method. The circles represent the measured efficiencies. The dotted lines correspond to the expressions,

$$\eta_T(E)=0.47\left[1-\exp\left(-\frac{E-25}{40}\right)\right]$$

and

$$\eta_P(E)=0.40\left[1-\exp\left(-\frac{E-81}{43}\right)\right],$$

used in the calculation.

[3] J. W. Weil and B. D. McDaniel, Phys. Rev. **86**, 582 (1952). A note describing these and other measurements performed in this laboratory on the efficiency of various γ-ray detectors will be published soon.

[4] R. R. Wilson, Phys. Rev. **86**, 261 (1952).

[5] It is, of course, possible that the Compton scattering has a resonance at some energy corresponding to a nucleon isobar level, and so its cross section is a very steep function of the energy. However, even in this case, the γ-ray emission must compete with meson emission and one would expect the meson widths to be larger than the γ-width approximately in the ratio of the mesic to the electric coupling constants.

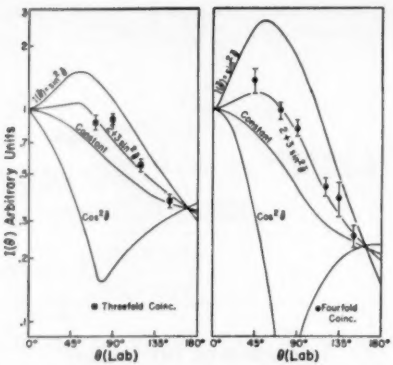

FIG. 3. Intensity $I(\theta)$ of threefold and fourfold coincidences as a function of the angle θ in the laboratory system. The curves show the expected $I(\theta)$ for various angular distributions of the π^0 in the center-of-mass system, for the reaction $\gamma+P\rightarrow\pi^0+P$. (Energy of the γ-rays = 280 Mev.) The curves have been normalized to unity at 0°. The ordinates of the experimental points have been multiplied by a constant in order to give the best fit to the $2+3\sin^2\tilde{\theta}$ distribution.

one can show that $N(\theta,E)$ is given by[6]

$$N(\theta,E)=\frac{1}{q\gamma_c(1-\beta_c\cos\theta)}\left\{A+\frac{B\sin^2\theta}{2\gamma_c^2(1-\beta_c\cos\theta)^2}\right.$$
$$\left.+\tfrac{3}{2}B\left[\frac{1}{\tilde{\beta}}-\frac{\mu^2}{2q\gamma_c(1-\beta_c\cos\theta)E}\right]^2\left[\left(\frac{\cos\theta-\beta_c}{1-\beta_c\cos\theta}\right)^2-\frac{1}{3}\right]\right\},$$

where

$M=$ mass of the nucleon,

$\mu=$ mass of the meson,

$$q=(\epsilon^2-\mu^2)^{\frac{1}{2}} \quad \text{with} \quad \epsilon=\frac{2M\omega+\mu^2}{2(2M\omega+M^2)^{\frac{1}{2}}},$$

$$\tilde{\beta}=q/\epsilon,$$

$$\beta_c=\omega/(\omega+M),$$

$$\gamma_c=1/(1-\beta_c^2)^{\frac{1}{2}}.$$

The intensity of the γ-rays observed at the angle θ is therefore given by

$$I(\theta)=\int_{E_{\min}}^{E_{\max}}N(\theta,E)\eta(E)dE,$$

where

$$E_{\min}=(1-\tilde{\beta})\frac{\epsilon}{2\gamma_c(1-\beta_c\cos\theta)}$$

and

$$E_{\max}=(1+\tilde{\beta})\frac{\epsilon}{2\gamma_c(1-\beta_c\cos\theta)}$$

[6] We are indebted to Dr. A. Borsellino for the derivation of this formula.

are, respectively, the minimum and the maximum energy of the photons emitted at θ, and $\eta(E)$ represents the efficiency of the detector for recording γ-rays of energy E; the expressions used for $\eta(E)$ are those given in the caption of Fig. 2. The solid curves in Fig. 3 are the calculated $I(\theta)$ for both the threefold and fourfold coincidences for $\omega=280$ Mev and for the following π^0 angular distributions:

$$d\sigma_{\pi^0}/d\Omega=\text{constant},$$
$$=\sin^2\tilde{\theta},$$
$$=\cos^2\tilde{\theta},$$
$$=2+3\sin^2\tilde{\theta}.$$

The value of 280 Mev chosen for the energy of the primary γ-ray represents the "average" γ-ray energy involved in this experiment.[7] It is perhaps worth while observing that the results do not depend critically on the value of ω, since a variation in ω affects them primarily through the value of the velocity of the π^0 in the center-of-mass system ($\tilde{\beta}$), and this velocity varies slowly with ω.

The results for the threefold coincidences are essentially independent of the efficiency factor $\eta(E)$, since $\eta(E)$ is nearly constant over a large part of the relevant spectrum. One sees that, as stated in the introduction, the angular distribution of the decay γ-rays is quite similar to that of the π^0 for the case calculated, where $\tilde{\beta}=0.807$. Actually the two distributions become identical for $\tilde{\beta}=1$.

The experimental results for the angular distribution measurements are shown in Fig. 3. They are consistent with an angular distribution of the π^0's in the center-of-mass system of the following type:

$$d\sigma_{\pi^0}/d\Omega=a+b\sin^2\tilde{\theta}, \quad \text{with } a/b\simeq 1.$$

In particular, the distribution $2+3\sin^2\tilde{\theta}$ fits the data quite well. This result was predicted by Brueckner and Watson[8] for a meson-nucleon state of angular momentum $J=\frac{3}{2}$ with isotopic spin $I=\frac{3}{2}$ or $\frac{1}{2}$. The same model gives quite good agreement with the experimental

TABLE I. Ratios σ_D/σ_H and σ_C/σ_H of the cross sections in deuterium carbon, and hydrogen, for production of π^0's by γ-rays.

Maximum energy of primary γ-rays (Mev)	θ (lab system)	σ_D/σ_H	σ_C/σ_H
310	45°	1.76±0.20	11.0±1.2
310	70°	2.03±0.17	10.0±0.7
310	90°	1.91±0.09	9.5±0.5
310	120°		9.2±1.0
310	135°	1.53±0.17	9.0±1.6
310	150°		11.1±1.4
273	90°	2.11±0.20	14.4±1.3
237	90°	1.88±0.37	21.6±3.0

[7] By "average" γ-ray energy we mean an energy such that half of the coincidences are due to γ-rays with energies lower than it.
[8] K. A. Brueckner and K. M. Watson, Phys. Rev. 86, 923 (1952).

excitation function and the ratio of the π^+ to π^0 cross sections.

Kaplon[9] and Francis and Marshak,[10] using psuedoscalar theory in the weak coupling approximation including a Pauli term to describe the nucleon magnetic moment, obtained results for the π^+/π^0 cross section ratio and for the excitation function which are in fair agreement with the experiments. However, their calculated angular distribution seems to be in definite contradiction with the above results.

Figure 4 shows the results for the yield of π^0's as a function of the maximum energy of the bremsstrahlung beam. The solid curves are the expected yields under the assumption that $\sigma_{\pi^0}=K(\omega-\omega_0)^n$, where ω_0 is the threshold energy. The different curves are calculated for $n=1$, 2, and 3.

One sees that, for hydrogen, n is about 2.5. This result is in fair agreement with the result of reference 2 in which $n=1.9\pm0.4$.

2. Deuterium

In column 3 of Table I are given the ratios of the deuterium to hydrogen cross sections for various energies and angles. Within the accuracy of the measurements, $\sigma_D\simeq 2\sigma_H$ independent of energy and angle. This result indicates that neutron and proton cross sections are quite similar and consequently that the strengths of the π^0 coupling to the proton and to the neutron are not very different. However, a quantitative measure of this coupling is not obtainable from the ratio σ_D/σ_H. The π^0 production cross section from deuterium cannot be considered as the simple sum of the cross sections from the proton and the neutron since interference effects can be present. On the other hand, the fact that the experimental ratio σ_D/σ_H is found to be largely independent of energy and angle, leads one to infer that the interference does not contribute much at the energies where our measurements were performed.

3. Carbon

During the course of obtaining the results for hydrogen, the subtraction process provided some information on carbon. The yield curve for carbon is shown in Fig. 4. The production of π^0's by γ-rays on carbon appears to be a more slowly varying function of the γ-ray energy than for hydrogen. If the cross section *versus* γ-ray energy curve for hydrogen at energies above 300 Mev is less steep than for smaller energies, then the motion of the nucleons in carbon would tend to produce the

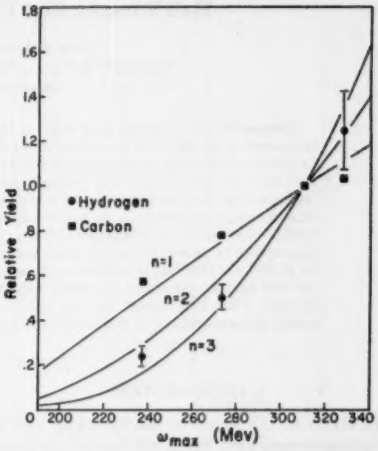

FIG. 4. Excitation curves for H and C deduced from the coincicences observed at 90° from the beam and assuming a distribution of the π^0's in the center-of-mass system proportional to $2+3\sin^2\theta$. The calculated curves, referred to a constant energy content in the γ-ray beam, are obtained from the expression

$$\text{yield}=\frac{K}{\omega_{max}}\int_{\omega_0}^{\omega_{max}}[(\omega-\omega_0)^n/\omega]d\omega.$$

The curves and the experimental points are normalized at 310 Mev.

observed effect. Another possible explanation involves the existence of charge exchange reactions in the carbon nucleus, according to the following schemes:

$$\gamma+N\rightarrow\pi^-+P, \qquad \pi^-+P\rightarrow\pi^0+N$$

and

$$\gamma+P\rightarrow\pi^+ +N, \qquad \pi^+ +N\rightarrow\pi^0+P.$$

However, since the energy dependence of the charge exchange reactions is not well known, and the effect of the motion of the nucleons is difficult to evaluate, a definite conclusion as to whether this explanation is adequate cannot be made.

In the last column of Table I are shown the ratios of the carbon to hydrogen cross sections at various energies and angles.

We are grateful to Professor A. Borsellino for the calculation of the angular distribution, to Professor B. D. McDaniel for his participation in making the efficiency measurements, and to Professor R. R. Wilson for making available to us some of the results of his Monte Carlo calculations.

[9] M. F. Kaplon, Phys. Rev. **83**, 712 (1951).
[10] N. C. Francis and R. F. Marshak, Phys. Rev. **85**, 496 (1952).

Hall Effect in Zinc Crystals at Low Temperatures*

JOHN K. LOGAN † AND JULES A. MARCUS
Department of Physics, Northwestern University, Evanston, Illinois
(Received September 3, 1952)

An experimental study has been made of the Hall effect in single crystals of zinc. For each crystal, one component of the Hall field was measured for a fixed crystallographic orientation of the current density, but for various orientations of the magnetic field in the plane perpendicular to the current density. At 77°K, the Hall field is a linear function of magnetic field which can be characterized by two coefficients. The first coefficient, for the interaction between the magnetic field component parallel to the hexagonal axis and current density component in the hexagonal plane, has a value of about 2×10^{-12} ohm cm/gauss. The second coefficient measures the interaction between the magnetic field component in the hexagonal plane and the current density component perpendicular to this field component. Its value is about 0.2×10^{-12} ohm cm/gauss At 20.4°K, the Hall field is nonlinear with magnetic field. For some orientations, the measured component of the Hall field increased with increasing magnetic field. In other cases, the opposite behavior was observed. Between 5 and 10 kilogauss, the Hall effect is of the same order of magnitude at 20.4°K as at 77°K. No correlation was apparent between Hall effect and either susceptibility or magnetoresistance.

I. INTRODUCTION

STUDIES of the magnetic susceptibility and magnetoresistance have indicated that at low temperatures the electronic structure of zinc may be noticeably affected by an applied magnetic field of a few thousand gauss.[1–5] If the de Haas-van Alphen effect and the irregularity in magnetoresistance can be attributed to the variation with magnetic field of the density of states near the Fermi energy, then it might be expected that the dependence of Hall effect upon magnetic field would be related to the susceptibility or magnetoresistance. There is experimental evidence that this may be true for bismuth.[6,7] To examine this possibility further an experimental study has been made of the Hall effect in zinc single crystals.

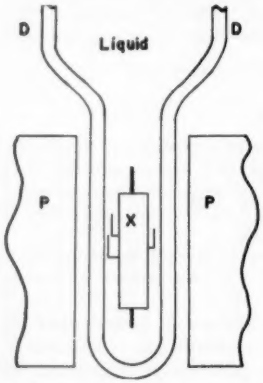

FIG. 1. Schematic arrangement of crystal X, Dewar D, and magnet P. Current leads are indicated by the heavier lines, potential leads, by the lighter.

In discussing galvano-magnetic effects in anisotropic media, it is necessary to adopt clear definitions to distinguish between the Hall effect and the magnetic change of resistance. For most isotropic substances at room temperature, the relation between electric field $\mathbf{E}$ and current density $\mathbf{J}$ can be written

$$\mathbf{E}=\rho\mathbf{J}+R\mathbf{B}\times\mathbf{J}, \tag{1}$$

where ρ is the resistivity, and R the Hall coefficient characteristic of the material. If the magnetic field $\mathbf{B}$ is zero, the electric field is parallel to the current density. The effect of the magnetic field is to add to the ohmic field $\rho\mathbf{J}$, a Hall field $R\mathbf{B}\times\mathbf{J}$, perpendicular to both magnetic field and current density.

In defining the Hall field for cases to which Eq. (1) does not apply, some, but not all, of the properties of $R\mathbf{B}\times\mathbf{J}$ can be retained. A choice must be made of the most "characteristic" properties. Thus, the Hall field *might* be defined as $\mathbf{E}(\mathbf{B})-\mathbf{E}(\mathbf{B}=0)$. With this convention, the Hall field is not necessarily perpendicular to either $\mathbf{B}$ or $\mathbf{J}$, nor does it necessarily change sign if $\mathbf{B}$ is changed to $-\mathbf{B}$. Most conventions agree that the Hall field vanishes if $\mathbf{B}=0$.

We have chosen to define the ohmic field as $\frac{1}{2}[\mathbf{E}(\mathbf{B})+\mathbf{E}(-\mathbf{B})]$ and the Hall field as $\frac{1}{2}[\mathbf{E}(\mathbf{B})-\mathbf{E}(-\mathbf{B})]$. Thus, the Hall field reverses its direction on reversing the magnetic field, while the ohmic field does not. Neither field changes its magnitude in this process. If $\mathbf{B}=0$, the Hall field is zero. These properties are mathematical consequences of our definition. They are also properties of the Hall field of Eq. (1).

Another definition which is sometimes used is based on the special experimental situation in which two potential probes are attached to a conductor so as to be on an equipotential surface in the absence of a magnetic field.

* Part of a dissertation submitted to the Graduate School of Northwestern University by John K. Logan in partial fulfillment of the requirements for the degree of Doctor of Philosophy.
† AEC Predoctoral Fellow, now at Naval Research Laboratory, Washington, D. C.
[1] J. A. Marcus, Phys. Rev. **76**, 413 (1949).
[2] L. Mackinnon, Proc. Phys. Soc. (London) **B62**, 170 (1949).
[3] Lazarev, Nakhimovich, and Parfenova, J. Exptl. Theoret. Phys. (U.S.S.R.) **9**, 1169, 1182 (1939).
[4] Lazarev, Nakhimovich, and Parfenova, Compt. rend. acad. sci. U.R.S.S. **24**, 855 (1939).
[5] N. M. Nachimovich, J. Phys. (U.S.S.R.) **6**, 111 (1942).
[6] A. N. Gerritsen and W. J. de Haas, Physica **7**, 802 (1940).
[7] Gerritsen, de Haas, and van der Star, Physica **9**, 241 (1942).

If a magnetic field is turned on along the direction perpendicular to the current direction and the line between the potential contacts, any potential difference between the probes is called a Hall voltage. For an anisotropic substance in which the ohmic field is a noticeable function of magnetic field strength, this convention may lead to a discussion of the "quadratic" Hall effect which does not reverse sign on reversing the magnetic field. On the basis of our definitions, such a quadratic effect would be considered as magnetoresistance rather than Hall effect.

The justification of our choice is based on a calculation by Casimir,[8] in which it is shown that, for the general case of an anisotropic material, if the vectors are resolved into components in any convenient rectangular coordinate system,

$$E_i=\sum_j \rho_{ij} J_j+(\mathbf{r}\times\mathbf{J})_i, \qquad (2)$$

where the ρ_{ij} are functions of $\mathbf{B}$ such that $\rho_{ij}(\mathbf{B})=\rho_{ij}(-\mathbf{B})$, while $\mathbf{r}(\mathbf{B})=-\mathbf{r}(-\mathbf{B})$. The vector $\mathbf{r}$ is called the Hall vector. It is seen from Eq. (2) that the Hall field is perpendicular to $\mathbf{J}$.

In the derivation of Eq. (2), Casimir omits the interaction of thermal current and temperature gradient with electric current and potential gradient. Because of this interaction, the Hall effect and magnetoresistive effect depend upon the thermal boundary conditions. A number of experimental investigations have shown that, for metals, when the magnetic field is perpendicular to the elctric current, the electric field component parallel to the current density is not changed by reversing the magnetic field.[9] This fact has been confirmed on our sample B (20.4°K, 8000 gauss) to within an experimental accuracy of about 0.2 percent. In making these measurements, the magnet was rotated through 360°, taking data every 15°. As a result, we consider that under experimental conditions the Hall field, defined in this way, is perpendicular to the current density, and can be described by a Hall vector in the manner of Eq. (2), without specifying in detail the thermal current or temperature gradient. It is this physical property, which is indicated by both calculation and experiment, that makes our definition seem the most appropriate.

II. EXPERIMENTAL TECHNIQUES

The crystals used in these experiments were grown under vacuum by the Bridgman technique from New Jersey Zinc Company S. P. Zinc.[10] They were 0.030 inch by 0.21 inch in cross section, and from 1 to 2 inches in length. The glass forms used were prepared by shrinking Pyrex glass tubing onto a stainless steel mandrel. Prior to making each form, the mandrel was coated with soot in a candle flame and dipped in a solvent such as CCl_4 to compact the coating. Since the purpose of the soot is to prevent the glass from sticking to the steel, this process was repeated, if necessary, to thoroughly coat the mandrel. The mandrel was then sealed into a length of glass tubing at a reduced pressure and the glass shrunk into the steel by heating in a gas-compressed air flame. When cool, the mandrel usually could be removed easily from the rectangular section.

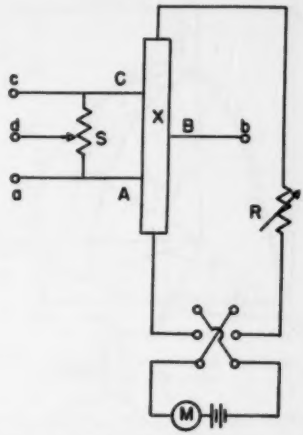

FIG. 2. Electric circuit. Voltage *bd* was measured by a Rubicon Type D microvolt potentiometer.

Prior to use, each crystal was lightly etched and the orientation of the crystal axes determined relative to its geometric shape. Each crystal was mounted in a plastic holder so as to minimize bending of the sample but allow for thermal expansion. To one edge, two potential leads of 0.003-inch copper wire were spot welded. These leads were about 5 mm apart. A third potential lead was welded to the opposite edge, approximately halfway between the other two. Current leads were soldered to the ends of the sample.

The relation of the crystal, Dewar, and magnet is given schematically in Fig. 1. The magnet could be rotated about an axis in the plane of the figure so as to change the direction of the magnetic field. The axis of the Dewar and the current through the crystal were parallel to this axis of rotation. Four-inch pole pieces and a gap of one inch were used. The magnet was calibrated with a search coil and ballistic galvanometer which had been standardized in fields determined by a proton resonance fluxmeter. The magnet calibration was accurate to about 100 gauss. Magnet current was supplied by storage batteries. Both the magnet and control resistors were water-cooled.

The electric circuit is given in Fig. 2. The current through the sample was provided by a storage battery and monitored by an ammeter. For most measurements, this was 3 amp.

Voltages were measured with a Rubicon Type D

[8] H. B. G. Casimir, Revs. Modern Phys. **17**, 343 (1945).

[9] See, for example, H. B. G. Casimir and A. N. Gerritsen, Physica **8**, 1107 (1941); D. Shoenberg, Proc. Cambridge Phil. Soc. **31**, 271 (1935).

[10] P. W. Bridgman, Proc. Am. Acad. Arts Sci. **60**, 305 (1925).

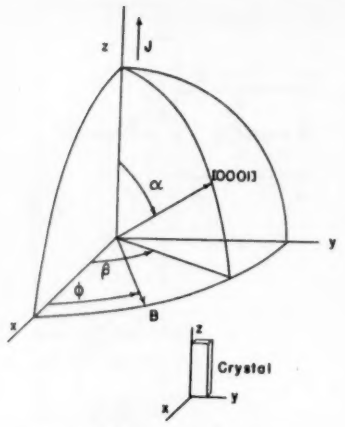

FIG. 3. Laboratory coordinate system.

microvolt potentiometer, using a Leeds and Northrup galvanometer (sensitivity 0.05 μv/mm at one meter). For convenience an auxiliary lens was used to project the image of the illuminator hairline on a screen. This system provided a magnification of four or five so that galvanometer deflections corresponding to 0.01 μv could be easily observed.

For crystals A and B, measurements were made to 0.01 μv. The final measurements on these crystals were reproducible to about this voltage. For crystal C the potentiometer was read to 0.002 μv because of the smallness of the emf's. After fitting a sinusoidal curve to the data at 77°K for this crystal, the rms deviation of observations from the curve was 6.5×10^{-3} μv compared with a peak-to-peak amplitude of 0.121 μv. To obtain this accuracy, it was necessary to insulate the potentiometer circuit carefully, particularly the potentiometer battery and the observer.

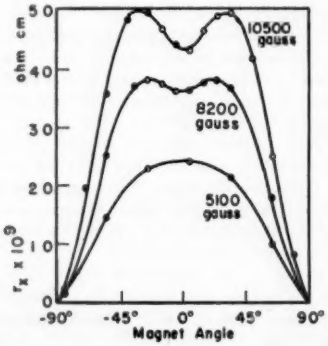

FIG. 4. Crystal A. r_x as a function of magnet azimuth at 20.4°K.

The noise level in the system varied greatly from experiment to experiment, ranging from about 0.005 μv to 0.05 μv. During the last experiments it was discovered that an erratic resistor contact in the magnet control circuit was responsible for the worst of the noise.

The potential difference between any pair of points *a, b, c, d* could be measured by use of a Leeds and Northrup thermocouple switch enclosed in a sheet metal box. Whatever extraneous voltage this switch introduced caused no trouble, although the switch position was not changed during a series of measurements. For Hall effect measurements, the voltage *bd* was measured. The other voltages were measured principally when changing samples. In the magnetoresistance measurements referred to earlier, the voltage *ac* was observed.

The input selector switch of the potentiometer was connected as a reversing switch, so that voltages of either polarity could be measured. Thermal emf's in this switch were less than 0.005 μv usually.

In principle, only two potential leads on opposite sides of the crystal are necessary in determining the Hall field. By measurements in fields of $\mathbf{B}$ and $-\mathbf{B}$, the observed voltages can be separated into an ohmic potential difference and a Hall voltage. For greatest accuracy, the zero field voltage should be comparable with or less than the Hall voltage. In practice, it is difficult to make such an adjustment of the potential leads. Consequently the circuit of Fig. 2 was used. A copper slide wire S of 60 ohms was connected between potential leads A and C, and the contact adjusted to make the voltage *bd* small in the absence of a magnetic field.

TABLE I. Hall coefficients at 77°K.

	$R_1\times10^{12}$ ohm-cm/gauss	$R_2\times10^{12}$ ohm-cm/gauss
Crystal A	2.5	...
Crystal B	1.8	0.21
Crystal C	0.1	0.19
Noskov	1.86	0.16
	2.01	0.19

To correct for thermal emf's in the potential leads, voltage *bd* was measured for the same value of current flowing in both senses through the crystal. The voltage due to the current was assumed to be one-half the algebraic difference of the measured values. Results obtained by this analysis were consistent for large variations in the thermal voltages.

Before taking data, the magnet current was usually set at a predetermined value and allowed to stabilize. Only minor adjustments in the control resistors were then necessary. For the most part, measurements were made for magnet orientations spaced at 15° intervals, the magnet being rotated continuously in one direction throughout 360°. Data for magnet settings 180° apart

were then combined so as to eliminate thermal emf's and ohmic potential difference.

The ohmic voltage was not analyzed, nor were magnetoresistance data consistently taken.

III. ANALYSIS OF MEASUREMENTS

Kohler has investigated the limitations imposed by crystal symmetry upon the Hall coefficients R_{mn} for the case in which the Hall vector can be written $r_m=\sum_n R_{mn}B_n$.[11] If, for zinc, we take the 3 direction along the hexagonal axis and the 1 and 2 directions along mutually perpendicular lines in the hexagonal plane, the Hall vector components are

$$r_1=R_2B_1, \quad r_2=R_2B_2, \quad r_3=R_1B_3. \tag{3}$$

For analysis of our experimental data, it is convenient to introduce the coordinate system of Fig. 3. The z axis is chosen parallel to the current density. The yz plane is taken parallel to the broad surface of the crystal. It is assumed that the potential contacts on the crystal edges lie in this plane so that the y component of the Hall field is determined by measurement. If the spherical coordinates of the hexagonal axis are α and β, the y component

TABLE II. Coordinates of [0001] and [$2\bar{1}\bar{1}0$] axes.

	α	β	α'	β'
Crystal A	90°	0°	....	....
Crystal B	32°	−16°	118°	14.5°
Crystal C	8.5°	−40°	95°	0.5°

of the Hall field is

$$F_y=-J\{[R_2a_1^2+(R_2b_2^2+R_1b_1^2)a_2^2]B_x +[(R_1-R_2)a_2^2b_1b_2]B_y+[(R_1-R_2)a_1a_2b_2]B_z\}, \tag{4}$$

where $a_1=\cos\alpha$, $a_2=\sin\alpha$, $b_1=\cos\beta$, $b_2=\sin\beta$. If $B_z=0$, F_y is a sinusoidal function of ϕ, the azimuth of the magnetic field. Knowing values of F_y for $\phi=0°$ and $\phi=90°$, it is possible to determine both R_1 and R_2.

If the Hall field is not linear with magnetic field, the effect can be characterized more directly by giving the Hall vector as a function of ϕ and of the magnetic field strength rather than in terms of field dependent Hall "coefficients." In these experiments, only r_x was determined.

IV. RESULTS

To analyze the data at 77°K, a sinusoidal curve was fitted to the data by the method of least squares[12] and F_y calculated for $\phi=0°$ and $\phi=90°$. These values of Hall field were then used to evaluate R_1 and R_2 on the basis of Eq. (4). The results are given in Table I. The extreme values observed by Noskov[13] are also indicated.

[11] M. Kohler, Ann. Physik **20**, 878 (1934).

[12] This procedure was adopted for convenience. We do not otherwise justify its use.

[13] M. M. Noskov, J. Exptl. Theoret. Phys. (U.S.S.R.) **8**, 717 (1938).

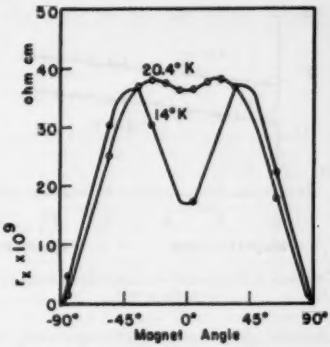

FIG. 5. Crystal A. r_x as a function of magnet azimuth at 8200 gauss.

Measured values of α and β are listed in Table II. Similar spherical coordinates, α' and β', for the [$2\bar{1}\bar{1}0$] axis are also tabulated.

For crystal C, the calculation of R_1 was strongly dependent upon $F_y(\phi=90°)$. If the value used were in error by a factor of −20, the value of R_1 would be about 2×10^{-13} ohm-cm/gauss. Such a change in $F_y(\phi=90°)$ would decrease R_2 to 0.17×10^{-12} ohm-cm/gauss. It is not unreasonable that $F_y(\phi=90°)$ might be in error by so large a factor. Assuming values of 2×10^{-13} and 0.2

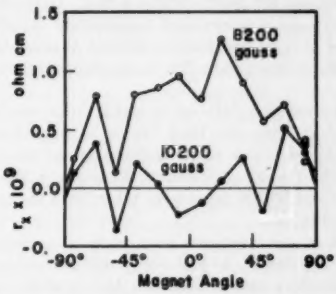

FIG. 6. Crystal C. r_x as a function of magnet azimuth at 20.4°K.

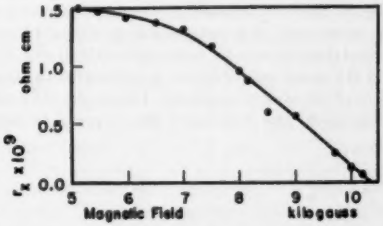

FIG. 7. Crystal C. r_x as a function of magnetic field strength $\phi=-22°$, 20.4°K. The points at 8200 gauss and 10,200 gauss are from the rotation diagrams of Fig. 6.

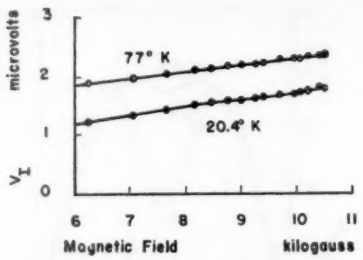

FIG. 8. Crystal A. Voltage bd as a function of magnetic field strength. $\phi=0°$.

$\times 10^{-2}$ ohm-cm/gauss for the Hall coefficients, the Hall potential difference across the thickness of this crystal for $\phi=90°$ can be estimated as about thirty times the potential difference across the width of the crystal. Accordingly, the discrepancy in this value of R_1 can be explained by assuming that the potential contacts did not lie in the yz plane.

Values of r_z at liquid hydrogen temperatures are given in Figs. 4 through 7. For crystal A, the data at 20.4°K are symmetric about $\phi=0°$. The curve at 14°K has been drawn accordingly.

For crystal B, plots of r_z *vs* ϕ at 20.4°K, 8200 and 10,200 gauss, are nonsinusoidal and somewhat skewed. They do not exhibit as pronounced a variation with field as those for either crystal A or C. Data taken at 14°K indicate a pronounced temperature dependence. Because of poor temperature control, these data were not sufficiently reproducible to be quantitatively significant.

Of the rotation data on crystal C little can be said other than that the Hall vector is nonlinear with magnetic field. The reproducibility of the data is indicated by the sets of points at 83°. In Fig. 7, the points at 8200 and 10,200 gauss were taken from the rotation data of Fig. 6.

A set of measurements were made on crystal A for $\phi=0°$, $T=20.4$°K, to look for a relationship between the Hall effect and de Haas-van Alphen effect, i.e., the field dependence of magnetic susceptibility.[1,2] The observed voltages, corrected for thermal emf's, are plotted in Fig. 8. Since corresponding measurements were not made at $\phi=180°$, it is not possible to separate the observed voltage into ohmic potential and Hall emf. From Fig. 4 the ohmic potential can be estimated as about 5 percent of the observed voltage. The results of Lazarev, Nakhimovich, and Parfenova[3] for a crystal of similar orientation indicate that $\Delta R/R_{H=0}$ increases nearly linearly with magnetic field by about 14 percent per kilogauss. As a consequence, it is unlikely that there are any oscillations in r_z for this orientation of crystal A in excess of 2 percent of r_z.

For comparison, corresponding measurements are given for 77°K. For a fixed field strength, the difference in voltage between these two sets of data is almost exactly equal to the ohmic potential difference in the measurements at 77°K.

Lazarev, Nakhimovich, and Parfenova[3,4] have reported magnetoresistance measurements on a single crystal of zinc for which, in terms of our coordinate system, $\alpha=88°$, $\beta=0°$. The magnetic field was in the xy plane. At 4.2°K, they observed an anomaly in the resistance for fields between 8000 and 10,000 gauss at $\phi=0°$. For $\phi=5°$, the anomaly was no longer observed, nor was it evident at 20.4°K, $\phi=0°$. Since crystals of several orientations were examined in their experiments and no further anomaly reported, the inference is that no other anomaly was evident in the data.

Gerritsen and de Haas,[6] and Gerritsen, de Haas, and van der Star[7] have studied the Hall effect in bismuth crystals and observed a qualitative correlation with the de Haas-van Alphen effect. No such correlation is apparent for the case of zinc. On the contrary, with the magnetic field parallel to the hexagonal axis, the Hall vector seems to be linear with magnetic field, whereas the susceptibility oscillates. When the magnetic field is perpendicular to the hexagonal axis, the susceptibility is not strongly dependent on magnetic field, while the Hall vector is nonlinear.

During this research Borovik[14] reported measurements on Hall effect on one zinc crystal for $\phi=0°$ and various field strengths. Since his sample was of different crystallographic orientation than any of ours, no direct comparison is possible. There does not seem to be any discrepancy between his results and ours.

In summary, these experiments show that at 20°K, the Hall effect is of the same order of magnitude as at 77°K. While the Hall vector for the latter case is a linear vector function of magnetic field, for the former it is not. The nature of this nonlinearity depends upon the crystallographic orientation of the magnetic field. Finally, no relationship was observed between Hall effect and either magnetoresistance or de Haas-van Alphen effect. Further experiments are planned in which a more systematic investigation will be made of both Hall effect and magnetoresistance.

[14] E. S. Borovik, Doklady Akad. Nauk S.S.S.R. **70**, 601 (1950).

Production of Charged π-Mesons in H, D, C, Cu, and Pb by 381-Mev Protons*

M. M. Block,† S. Passman,‡ and W. W. Havens, Jr.
Columbia University, New York, New York

(Received September 10, 1952)

The differential cross section for the production of charged π-mesons at 90° from a 381-Mev proton beam has been measured in H, D, C, Cu, and Pb. Nuclear emulsions, imbedded in a tapered copper absorber, placed 90° below the internal circulating proton beam of the Nevis cyclotron detected mesons of both signs, from 0 to 125 Mev. The beam was monitored by means of the C^{11} activity produced in the target to determine the absolute cross section. The hydrogen and deuterium results were obtained by subtracting the carbon cross section from polyethylene and deuterated paraffin, respectively. Assuming the reaction in H is $p+p\rightarrow\pi^++d$ with a $\cos^2\theta$ angular distribution, the total cross section for H at 381 Mev is calculated from the 90° value to be $(7.3\pm2.3)\times10^{-28}$ cm². The spectra for heavy nuclei are calculated with the assumptions that meson production occurs through nucleon-nucleon collisions and that the meson receives the maximum available energy in the c.m. system. Good agreement with the experimental results is found for matrix elements proportional to meson momentum. The π^+ production cross section increases with a dependence slower than $A^{\frac{1}{3}}$, whereas the π^- increases approximately as $A^{\frac{1}{3}}$. This asymmetry is also found in the large π^+/π^- ratio of 10 in carbon and about 25 in deuterium.

I. INTRODUCTION

A FUNDAMENTAL experiment related to understanding the role of π-mesons in nuclear forces is the study of meson production in various targets bombarded by a beam of high energy protons. The Berkeley group,[1] using the 184-inch synchrocyclotron, has investigated the production process in hydrogen as a function of meson emission angle at 340-Mev proton energy. They have also measured the 90° production cross section for carbon[2] and lead[3] at the same proton energy. Using the 385-Mev Columbia Nevis cyclotron we have extended this study of meson production to higher energies and to include additional elements. The elements investigated were hydrogen, deuterium, carbon, copper, and lead.

The hydrogen reaction involves the elementary nucleon-nucleon collision $p+p\rightarrow\pi^++(n+p)$ or (d). The next simplest nucleus, deuterium, is very loosely bound, and the two nucleons are expected to interact independently with the incident proton. The nucleon-nucleon reactions in deuterium leading to charged meson production are

$$(a)\quad p+p\rightarrow\pi^++p+n \quad\text{or}\quad p+p\rightarrow\pi^++d;$$
$$(b)\quad p+n\rightarrow\pi^++n+n;$$
$$(c)\quad p+n\rightarrow\pi^-+p+p.$$

The deuterium production cross section compared to the hydrogen cross section gives a measure of the relative magnitudes of the $(p$-$n)$ and $(p$-$p)$ interactions entering into π^+ meson production (reactions a and b). A comparison of the π^- and the π^+ cross section in deuterium will yield information about the relative magnitudes of the $(p$-$n)$ interaction entering into reaction (c) and the $(p$-$n)$ and $(p$-$p)$ interactions or reactions (a) and (b). The use of carbon, copper, and lead targets allows an investigation of meson production as a function of target atomic weight.

II. EXPERIMENTAL ARRANGEMENT

The mesons were produced by bombarding the target material to be studied with the internal circulating proton beam of the Nevis cyclotron. Charged mesons produced in the downward direction, at 90° to the beam, were detected in a nuclear emulsion imbedded in a tapered copper absorber placed 2½ in. below the target.

The geometry of the experimental arrangement in relation to the cyclotron is shown in Fig. 1. The target holder, target, absorber block, and photographic plate were all mounted on a probe, the details of which are shown in Fig. 2. This arrangement enabled the target and plate to be changed after each exposure by withdrawing the probe through a vacuum lock. The position of the probe was such that the target was at a radius of 73.5 in., corresponding to a beam energy of 381 Mev, as determined from the magnetic field strength.

Ilford C-2 200-micron nuclear emulsions were chosen as detectors to make possible positive identification of mesons in regions of high background. The characteristic small-angle scattering and rapid grain density variation of a slow meson in the C-2 emulsion make the identification relatively simple for a trained observer, even with an extremely high background. The C-2 sensitivity was chosen because it has a maximum cutoff of about 10 Mev for π-mesons and 65 Mev for protons, thus eliminating high energy proton tracks from the background.

The nuclear emulsion technique has the important advantage of permitting a determination of the sign of

* This research was supported jointly by the ONR and AEC. Publication was assisted by the Ernest Kempton Adams Fund for Physical Research of Columbia University, New York, New York.

† Now at Duke University, Durham, North Carolina.

‡ Now at Hughes Research and Development Laboratories, Culver City, California.

[1] F. Cartwright, Ph.D. thesis, University of California Radiation Laboratory Report UCRL-1278, 1951 (unpublished); V. Peterson, Phys. Rev. **80**, 136 (1950); Peterson, Iloff, and Sherman, Phys. Rev. **81**, 647 (1951).

[2] C. Richman and H. A. Wilcox, Phys. Rev. **78**, 496 (1950).

[3] M. Weissbluth, University of California Radiation Laboratory Report UCRL-568, 1950 (unpublished).

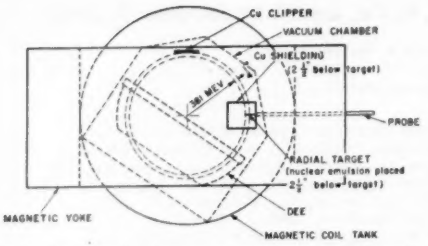

FIG. 1. Floor plan of Nevis cyclotron showing experimental arrangement for proton bombardment of radial target.

the charge and the type of meson detected, as well as the direction of incidence. Consequently, a separation of the π^+ and π^- mesons can be made.

The nuclear emulsions were imbedded inside a copper absorber block inclined at 10 degrees to the direction of the impinging mesons. Mesons of different energies traverse successively greater distances of absorber before they come to rest in the emulsion. Thus, the position of a meson ending in the plate is a measure of the distance it has traveled in the absorber, and hence of its energy. This method gives an energy detection interval from 0 to 125 Mev on one photographic plate, enabling a complete positive and negative spectrum to be obtained from a single exposure.

An experiment of this nature requires rectilinear trajectories from target to detector for mesons of all energies. To achieve this in a cyclotron, where the strong magnetic field causes mesons to travel in helical orbits whose radii of curvature vary with meson energy, the detector is placed directly below the target. In this position, mesons traveling straight down (90° from the proton beam) are moving parallel to the magnetic field lines and are unaffected by the field. To shield against unwanted helical trajectories, which correspond to other angles of emission from the target, a large shielding block of copper (14 in.×14 in.×5 in.) was placed around the absorber. The shielding block limits the meson trajectories arriving at the absorber plate to a bundle of mesons, containing all energies produced in the reaction, which travel in straight-line paths from the target to the plate.

The angular resolution of the apparatus was ±5°, so that the measurements included mesons emitted at (90°±5°) from the proton beam.

In the initial exposures, the target was in a vertical position and supported from above, as shown in Fig. 2. The vertical geometry has the advantage of utilizing the entire proton flux and giving relatively low background in the plates. The background tracks were almost exclusively limited to protons originating in the target or recoil protons due to neutrons emitted from the target.

The internal proton beam has a mean vertical amplitude between ¼ in. and ½ in. Hence, mesons formed at the upper edge of the target had to traverse approximately ¼ in. to ½ in. of target material before they could arrive at the detector. For light elements, this is not a serious energy resolution factor at high meson energies (above about 30 Mev), and does not appreciably affect the spectrum of an element like carbon. However, for hydrogen where the maximum energy of the mesons emitted at 90° in the laboratory system is 24 Mev, this effect considerably distorts the spectrum.

In order to improve the energy resolution, successive exposures were made with a target (thin in vertical dimensions) placed radially as shown in Fig. 1. In order to define the proton beam energy, a copper "clipper" was placed ¼ in. radially behind the target but displaced 90° in azimuth from the target, so that the neutrons emitted by the clipper could not strike the emulsion. However, this method introduced a severe, randomly oriented, proton background which obscured the low energy meson regions, making this technique unsuitable for hydrogen. The deuterium, copper, and lead spectra, which extend to much higher meson energies, were successfully obtained with this arrangement.

III. DETERMINATION OF CROSS SECTIONS

Let N be the number of mesons of energy E, detected in the corresponding region S of nuclear emulsion. Then, if $(d^2\sigma)/d\omega dE)$ is the differential cross section for meson production per target nucleus per unit solid angle and per unit energy interval at an energy E and an angle θ, it can readily be shown that

$$\frac{d^2\sigma}{d\omega dE}=\frac{A}{I\rho Ld}\times\frac{N}{S}\times\frac{r^2}{t[dE/dR]_E}, \tag{1}$$

where I=number of protons striking target, d=thickness of target, t=thickness of emulsion, L=Avogadro's number, ρ=density of target material, A=atomic weight of target, S=area of emulsion in which N mesons are found, $[dE/dR]_E$=rate of energy loss in emulsion at energy E of creation, and r=distance from target to region S in emulsion.

Now, the yield Y of C^{11} (in targets in which carbon is present) via the reaction $C^{12}(p,pn)C^{11}$ is given by

$$Y=\sigma_c(I\rho Ld/A), \tag{2}$$

where σ_c, the cross section for this reaction, has been studied at Berkeley as a function of incident proton energy. Thus we may eliminate various parameters in Eq. (1), such as I, the number of protons incident upon the target, by a knowledge of Y, which may be obtained from an absolute monitoring of the positron decay of the C^{11}, as described below; thus, we obtain

$$\frac{d^2\sigma}{d\omega dE}=\frac{\sigma_c}{Y}\times\frac{N}{S}\times\frac{r^2}{t[dE/dR]_E}. \tag{3}$$

The evaluation of each of the terms involved in Eq. (3) is discussed below.

The C^{11} cross section σ_s at 381 Mev was found by extrapolating the known linear behavior at lower energies[4] to 381 Mev. The cross section value used was 0.036 ± 0.003 barn.

The number of C^{11} atoms formed in the target is inferred from the C^{11} positron annihilation radiation measured by inserting the target or monitoring foil (for the case of noncarbon containing targets) shortly after exposure, in a lead shield containing an end-windowed Geiger tube separated from the target by $\frac{1}{8}$ in. thick aluminum converter. Calibration of geometry and counter efficiency was made with the aid of a solution of Cu^{64} whose β-activity was compared to that of a RaD+E source calibrated by the Bureau of Standards. From the decay scheme of Cu^{64} and its branching ratio,[5] the number of positron decays per unit volume of solution was computed.

A known volume of this Cu^{64} solution was coated over a polyethylene target, approximating the activity distribution in a bombarded target; and from the number of positron annihilation counts observed, the absolute calibration of the monitoring system was obtained.

The monitored counting rate, which was always consistent with the known 20.5-minute half-life of C^{11}, was extrapolated back to the time the cyclotron was turned off and corrected for the short exposure time, leading to evaluation of the parameter Y.

The ratio N/S, the number of mesons per unit emulsion area ending in a region of the emulsion r cm from the target, was obtained by the usual meson scanning procedure. For this process a binocular microscope having a precision stage motion from which the position on the plate could be determined to within 0.01 cm was employed. High resolution oil immersion objectives were used.

The number of π^+ and π^- mesons ending in the C-2 emulsion is derived using the well-known phenomenological classification of meson endings into π, ρ, σ_1, and true σ-stars. The number of π^+ mesons is given directly by the number of π-μ events plus the number of σ_1 mesons, which are interpreted principally as π-μ events in which the μ-meson leaves the emulsion before traversing its full 600-μ range. The number of π^-, or star-producing mesons, must be corrected for the zero prong stars which would otherwise be classified as ρ-mesons. The number of π^- mesons is given by 1.37 times the number of observed σ-stars.[6]

The $\pi^\pm$ mesons were highly collimated, with less than 1 percent coming from directions other than that of the target.

In order to improve statistics and at the same time check on observer detection efficiency, plates were exposed in "sandwich." In all cases, results from separate plates scanned by different observers agreed within the statistical limits. As a further check, scanned plates were interchanged between two observers, and the areas were independently rescanned.

From the mean coordinates of the scanned region, the range of the π-mesons in the absorber was computed. The energy of the mesons was determined from available range-energy tables.[7]

The number of mesons observed in the plates in an energy interval dE and a solid angle interval $d\omega$ differs from the number of mesons produced in this energy and angular interval for several reasons. The largest correction is due to mesons being lost through interaction with the nuclei of the copper absorber block. Recent experimental evidence has shown that the $\pi^\pm$ meson interaction cross section is geometrical.[8] The interaction mean free path used for copper was 11.7 cm. This gives a correction of almost 50 percent for a 100-Mev meson.

Small angle Coulomb scattering in the absorber will cause mesons that would normally arrive at the plate to be scattered out. However, since the experiment is carried out with "poor geometry," to the first approximation, as many mesons scatter into the plate as would scatter out.

The third correction is due to π-mesons decaying in flight before they reach the emulsion. The correction is complicated by the fact that the mesons spend part of their time-of-flight in the copper, where they continuously lose energy and thus change their velocity. Since the absorber is only 2.5 in. from the target, the correction is very small ($\sim$2 percent) and can be neglected in view of the known meson mean lives.

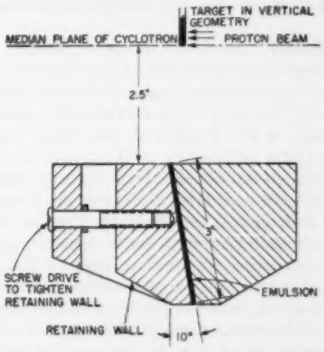

FIG. 2. Plan of probe head, containing nuclear emulsion and shielding material, which is inserted into the cyclotron.

[4] Aamodt, Peterson, and Phillips, University of California Radiation Laboratory Report UCRL-526, 1949).
[5] C. S. Cook and L. M. Langer, Phys. Rev. 73, 601 (1948).
[6] F. L. Adelman and S. B. Jones, Phys. Rev. 75, 1468 (1949).
[7] H. Bethe, Brookhaven National Laboratory Report T-7, 1949 (unpublished).
[8] Bernardini, Booth, Lederman, and Tinlot, Phys. Rev. 80, 924 (1950); H. Bradner and B. Rankin, Phys. Rev. 80, 916 (1950); Chedester, Isaacs, Sachs, and Steinberger, Phys. Rev. 82, 958 (1951); L. Lederman (private communication).

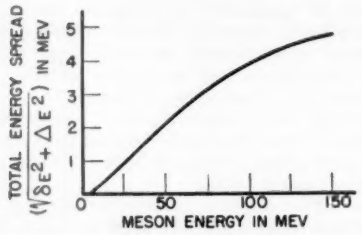

FIG. 3. Energy resolution of the apparatus *vs* meson energy.

The thickness of the emulsion after development was measured microscopically to within 1 micron. To correct for the shrinkage of the emulsion, a shrinkage factor was determined by measuring the emulsion thicknesses of test plates before development with a strain gauge and measuring them after development with a microscope. The thickness before development was measured to within 5 percent.

The rate of meson energy loss in emulsion, $[dE/dR]_E$, was calculated from an experimental range-energy curve for protons in Ilford C-2 emulsion,[9] and it was converted to mesons by using a ratio $(M_P)/(M_\pi)=6.65$. The resulting analytic range-energy relation used was $R=41.8E^{1.722}$, with E in Mev and R in microns.

IV. ENERGY RESOLUTION

The energy resolution in this experiment can be divided into the energy spread of the bombarding proton beam and the energy resolution of the detector.

Since the proton beam is an internal circulating beam, it is subject to energy degradation due to radial oscillations of the ions and multiple traversals of the targets.

The energy resolutions of the apparatus can be divided into two separate effects: (1) The finite vertical amplitude of the proton beam of the cyclotron which is between $\frac{1}{4}$ in. and $\frac{1}{2}$ in., so that mesons formed at the upper edge of the target had to traverse $\sim\frac{1}{4}$ in. of target material before they could arrive at the detector block. This gives a resolution that is energy dependent, being much poorer at lower meson energies. Above about 30 Mev this effect is negligible. (2) The detector itself has a finite resolution width due to range straggling and multiple scattering. The nuclear emulsion imbedded in the absorber measures the meson density as a function of depth of penetration of absorber. The projected path length of the meson (straight-line trajectory through the absorber) is taken to be the range of the meson; the energy is determined from a range-energy graph. Thus, in order to obtain the energy resolution, the distribution in range of absorber of a monoenergetic beam of mesons must be investigated.

Straggling introduces a range spread due to a statistical fluctuation of the number of collisions and energy loss per collision of particles traversing the absorber. The distribution is Gaussian, and its half-width is a function of meson energy.

Multiple scattering causes a particle's path to deviate from a straight line into a curved trajectory. This gives rise to a distribution in projected depth for a beam of monoenergetic particles. Since the effects of range straggling and multiple scattering are statistically independent, the two widths are added in quadrature to give the resultant resolution of the detector. A plot of resultant resolution *versus* meson energy is shown in Fig. 3. For meson energies lower than about 30 Mev, the meson energy spread due to the detector is seen to be negligible. Thus, a sensitive measure of the energy spread in the beam would be to find a reaction giving monoenergetic mesons of lower than 30 Mev for a monoenergetic proton beam and to measure the energy distribution of the detected mesons. In practice, the production of mesons in hydrogen provides such a line source of mesons of 24 Mev at 90 degrees to a 381-Mev proton. Since all energy spreads are due to factors which degrade the beam energy, one would expect to find a fairly sharp upper energy cutoff and a low energy smear due to the beam spread. However, in addition to the proton beam spread, the mesons also lose energy in the target. If we assume that the beam height is $\frac{1}{2}$ in., from the half-width of the hydrogen spectrum presented later (Fig. 6), the spread in beam energy resulting from multiple traversals and radial oscillation can be computed. This calculation gives a proton beam spread of the order of 10 Mev.

V. RESULTS

A. Carbon

A carbon target 0.3 g/cm² was placed in the vertical geometry described previously and exposed for 2.5 minutes in an average beam current of approximately 5×10^{-10} ampere. Figure 4 shows the 90° differential cross section $(d^2\sigma^+)/(d\omega dE)$ for the production of π^+ mesons, based on 550 π–μ decays.

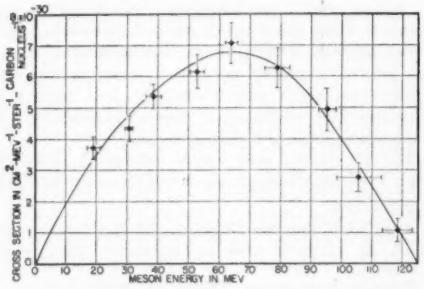

FIG. 4. Experimental results for the differential cross section for production of π^+ mesons in carbon at 90°±5° from a 381-Mev proton beam.

[9] Bradner, Smith, Barkas, and Bishop, Phys. Rev. 77, 462 (1950).

Figure 5 shows the 90° differential cross section $(d^2\sigma^-)/(d\omega dE)$ for π^- mesons. This spectrum consists of 29 observed meson-produced stars found in the identical areas scanned for positives.

The π^+ cross section, integrated over meson energy, is $(d\sigma^+)/(d\omega)=(5.3\pm1.1)\times10^{-28}$ cm² steradian^{-1}, and the corresponding negative cross section is $(d\sigma^-)/(d\omega)=(4.2\pm1.0)\times10^{-29}$ cm² steradian^{-1}.

The positive spectrum has a peak of 7×10^{-30} cm² steradian^{-1} Mev^{-1} at about 70 Mev.

The negative cross section has a peak of about 10×10^{-31} cm² steradian^{-1} Mev^{-1} in the neighborhood of 40 Mev. The statistics are not good enough to permit an accurate determination of shape, but the peak appears to be at a lower energy than the positive spectrum peak and the cutoff is also lower than that of the positive spectrum.

The energy resolution indicated is the energy spread due to the width of the regions scanned in the plate. The uncertainties indicated in the spectral data are statistical probable errors involved in the counting of mesons. The uncertainty in the differential cross sections $(d\sigma)/(d\omega)$ involves, in addition, the uncertainty in the absolute calibration, including the C^{11} monitoring and plate thickness measurements.

B. Hydrogen

The hydrogen cross section was obtained by a subtraction technique using a polyethylene target $(CH_2)_n$. Since Eq. (3) gives the cross section per (CH_2) group, the hydrogen meson production cross section is obtained by subtracting the carbon cross section, previously obtained, and halving the difference. Fortunately, the differential cross section for hydrogen is relatively large so that the subtraction errors are small.

A 0.23-g/cm² polyethylene target was exposed under the same conditions as the carbon target and in the same vertical geometry. The 90° meson energy spectrum from hydrogen, consisting of 250 π–μ decays, is shown in Fig. 6, where the statistical uncertainty indicated includes the errors incurred in subtraction.

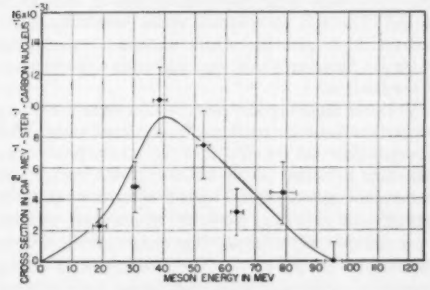

FIG. 5. Experimental results for the differential cross section for the production of π^- mesons in carbon at 90°±5° from a 381-Mev proton beam.

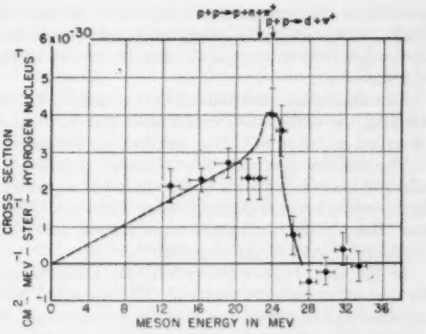

FIG. 6. Experimental results for the differential cross section for the production of π^+ mesons in hydrogen at 90°±5° from a 381-Mev proton beam.

The results for hydrogen show a pronounced maximum at 24 Mev and a sharp cutoff just above this energy.

The possible reactions leading to the production of π^+ mesons in hydrogen are $p+p\rightarrow\pi^++p+n$ or π^++d. In the latter case the mesons are produced in a line spectrum at the maximum energy available in the nucleon-nucleon collision. For the case of a 381-Mev proton striking a proton at rest and forming a π^+ meson and a deuteron, the maximum energy the meson would receive at 90° in the laboratory system would be 24 Mev. This curve is therefore consistent with the results at Berkeley,[6] which showed that the meson energy spectrum is mainly concentrated about the maximum energy constant with deuteron formation.

The curve cuts off sharply because the maximum energy the meson can receive is slightly above 24 Mev for the highest energy proton in the machine, and therefore, the poor resolution will not affect this cutoff. The curve falls off much less sharply on the low energy side because all the effects of the resolution, previously discussed, would tend to decrease the energy of the mesons.

Although the shape of the spectrum is distorted because of the poor resolution, the area under the curve should not be appreciably affected. Integration over the spectrum gives the cross section for production of mesons in hydrogen at 90°, $(d\sigma)/(d\omega)=(5.0\times1.2)\times10^{-29}$ cm² steradian^{-1}.

The results of angular distribution measurements at Berkeley[1] indicate that the mesons are emitted with a $\cos^2\theta$ distribution in the center-of-mass systems of the colliding nucleons. Using this angular distribution, the total cross section is found to be $\sigma=(7.3\pm2.3)\times10^{-28}$ cm² at 381 Mev.

C. Deuterium

A deuterated paraffin target, 60 mils thick, was prepared and mounted in the radial geometry. The com-

position of the paraffin was C_nD_{2n} (>96 percent) and C_nH_{2n} (<4 percent).[10] Consequently, for the process of meson production, the paraffin can be treated as pure C_nD_{2n}.

The deuterium contribution was obtained by subtracting the carbon differential cross section from the observed spectrum of C_nD_{2n}, and halving this result.

The positive spectrum $(d^2\sigma^+)/(d\omega dE)$, consisting of 174 π–μ decays, is shown in Fig. 7. It has a maximum in the region between 30 and 50 Mev of about 4.5×10^{-30} cm² Mev⁻¹. The integrated cross section $(d\sigma^+)/(d\omega) = (2.9\pm1.2)\times10^{-28}$ cm² steradian⁻¹.

In the same regions scanned for the positives, only $6\pi^-$ meson stars were observed. The statistical errors are too large to permit the drawing of a spectrum, but an estimate of the total 90° negative cross section $(d\sigma^-)/(d\omega)$ is about 1.1×10^{-29} cm² steradian⁻¹ D nucleus⁻¹.

D. Copper

A 1.4 $_{\text{c}}$ cm² copper target was covered by a 13-mil polyethylene foil and exposed in the radial geometry.

The π^+ spectrum, of 157 π–μ decays, is shown in Fig. 8. The integrated cross section at 90°, $(d\sigma^+)/(d\omega) = (7.0\pm1.7)\times10^{-28}$ cm² steradian⁻¹. The total number of 11 π^- mesons observed was too small to permit the drawing of a spectrum, but an estimate of the integrated cross section at 90° is $d\sigma/d\omega = (1.6\pm0.7)\times10^{-28}$ cm² steradian⁻¹.

E. Lead

A 1.75 g/cm² lead target covered by a 13-mil polyethylene foil was exposed in the radial geometry for approximately 5 minutes in a beam current $\sim10^{-10}$ amperes.

The π^+ spectrum, consisting of 173 π–μ decays, is shown in Fig. 9. The spectrum has a maximum at about

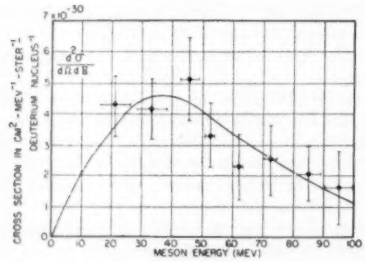

FIG. 7. Experimental results for the differential cross section for the production of π^+ mesons in deuterium at 90°±5° from a 381-Mev proton beam.

[10] The deuterated paraffin was prepared by the Texas Oil Company, which gave a composition of 97.2 percent deuterium. A spectroscopic analysis of the particular batch used in the experiment was made by Professor T. I. Taylor of the Columbia University Chemistry Department, and he found a composition of 96 percent deuterium.

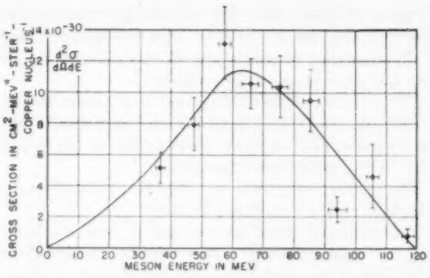

FIG. 8. Experimental results for the differential cross section for the production of π^+ mesons in copper at 90°±5° from a 381-Mev proton beam.

70 Mev of 2.6×10^{-29} cm² steradian⁻¹ Mev⁻¹. The integrated cross section at 90° is $(d\sigma^+)/(d\omega) = (15\pm3.7)\times10^{-28}$ cm² steradian⁻¹.

In the identical region scanned for negatives, only 14 meson-produced stars were observed. The statistical errors are too large to give a reasonable spectral shape, so the results are not shown. An estimate of the integrated negative cross section at 90° is $(d\sigma^-)/(d\omega) = (3.5\pm1.7)\times10^{-28}$ cm² steradian⁻¹.

The experimental variation of π^+ production as a function of A is shown in Fig. 10(a). The positive meson cross section $(d\sigma)/(d\omega)$ at 90° increases much slower than the A variation that would be expected if each nucleon were to contribute equally or the $A^{\frac{2}{3}}$ variation if only nucleons in the surface were to contribute. The cross section for π^- protons *vs* A is shown in Fig. 10(b). In this case the cross section increases much more rapidly with A than for positive mesons.

VI. ANALYSIS OF MESON PRODUCTION

In order to calculate meson production cross sections in the heavy elements, the following basic assumptions are made:

(1) Meson production in a heavy nucleus occurs only through nucleon-nucleon collisions, i.e., the bombarding proton interacts with only one nucleon of the target nucleus. The only contribution of the remainder of the nucleons is to give the struck nucleon a momentum which is characteristic of the momentum distribution of the nucleus.

(2) In the meson production reaction there is a strong interaction between nucleons in the final state. This strong interaction requires that the meson receive the maximum available energy consistent with energy and momentum conservation. This is in accordance with the experimental results at Berkeley[1] which show that for a p-p collision meson production occurs principally via the reaction $p+p\rightarrow\pi^++d$. The assumption of strong interaction in the final state does not necessarily imply deuteron formation, since even an unbound final state in which the neutron and proton interact strongly will

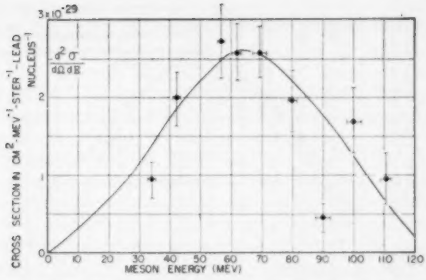

FIG. 9. Experimental results for the differential cross section for the production of π^+ mesons in lead at 90°±5° from a 381-Mev proton beam.

give the meson close to the maximum available energy and result in a high energy peak. This assumption considerably simplifies the analysis, since the kinematical reaction is now that of a two-body problem instead of that of the three-body problem. This assumption also automatically permits the Pauli principle to be satisfied for the case of meson production at 90°, as the final state nucleons will have a large energy in the laboratory system and will therefore be above any of filled momentum states of the heavy nucleus.

(3) There is no interaction between the escaping meson and the nucleus. The differential cross section for production of mesons in a nucleon-nucleon collision is given by

$$d\sigma/d\omega=(2\pi/\hbar)(|H_{AB}|^2/v_r)\rho, \tag{4}$$

where H_{AB} is the matrix element that connects the initial state of two nucleons to the final state of two nucleons (or deuteron) plus a π-meson, ρ is the number of final states per unit energy interval, and v_r is the relative velocity of the two initial nucleons.

The matrix elements can be calculated by means of meson theory,[11] using the different interaction operators characteristics of the various types of meson fields. However, results based on meson theory are frequently in serious disagreement with experiment. For this reason, it seems safer, though less fundamental, to analyze the results phenomenologically, as did Watson and Brueckner.[12] Extending their treatment of meson production near threshold, a partial wave analysis is made which leads to six types of matrix elements that have the following energy and angular dependence in the c.m. system: (AI) constant; (AII) constant $\cos(\theta)$; (BI) $T_m^{\frac{1}{2}}$; (BII) $T_m^{\frac{1}{2}}\cos\theta$; (CI) T_m; and (CII) $T_m\cos\theta$, where T_m is the maximum available energy in the c.m. system consistent with deuteron formation and θ in the angle of emission of the meson in this system.

The energy dependence of the density of final states when combined with the relative velocity factor has been shown to be approximately equal to $\sqrt{T_m}$[13] for the case of deuteron formation. If the energy and angle of emission of the meson in the c.m. system are known, then the energy of the colliding nucleons is completely specified. Thus, the differential production cross section for two colliding nucleons of energy E_g in the c.m. system can be calculated.

In order to determine the meson production cross section in a heavy nucleus the momentum distribution of the target nucleus must also be considered. The Fermi degenerate gas model was used in this calculation for this is the simplest model and is applicable to all nuclei of sufficiently high atomic weight.

The 90° laboratory differential cross section as a function of meson energy is calculated as follows. A meson energy at 90° in the laboratory system is selected. The corresponding meson energy T_m and angle θ in the c.m. system having energy E is calculated. The appropriate cross section is computed using T_m and θ and is multiplied by the probability of having a system with a c.m. energy E_g. The result is converted into a laboratory cross section and then integrated over all values of E_g consistent with kinematics. This results in a point by point numerical evaluation of the meson spectrum.

In view of the approximate nature of this calculation, in attempting to describe only the general characteristics of meson production in a heavy nucleus the momentum component of the target nucleon perpendicular to the direction of motion of the incident protons is neglected,

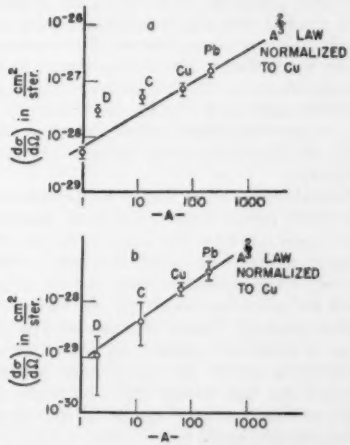

FIG. 10. (a) The differential π^+ production cross section at 90° to a 381-Mev proton beam is plotted *vs* the mass number A of the target. (b) The π^- production cross section at 90° to a 381-Mev proton beam is plotted *vs* the mass number A of the target.

[11] K. Brueckner, Phys. Rev. **82**, 598 (1951).
[12] K. Watson and K. Brueckner, Phys. Rev. **83**, 1 (1951).
[13] K. Brueckner, University of California Radiation Laboratory Report UCRL-630, 1950 (unpublished).

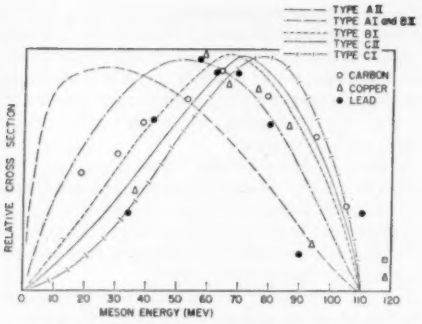

FIG. 11. The theoretical curves for the differential production cross section for the different matrix elements are compared to the experimental results for carbon, copper, and lead. The theoretical curves are arbitrarily normalized to the experimental curves to give the experimentally integrated cross section at 90°. The curves for the type AI and BII matrix elements are so similar that an average of both has been plotted.

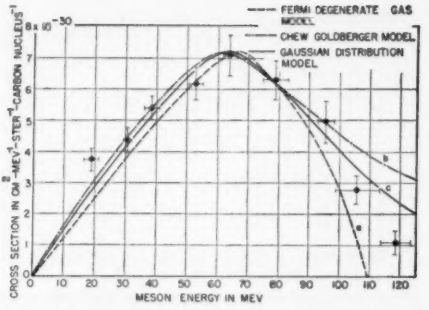

FIG. 12. The theoretical curves for the production of π^+ meson for three different nuclear models are compared with the experimental data for carbon; curve a is for a Fermi degenerate gas distribution with a 22-Mev cutoff, curve b is for the Chew-Goldberger model, curve c is for a Gaussian distribution with an average energy of 19.3 Mev.

since this has a relatively small influence on the calculated spectrum.

Utilizing matrix elements of types AI, AII, BI, BII, CI, CII combined with the energy dependence of the density of states and the probability factor for having a c.m. energy E_θ, computations have been made for a proton-bombarding energy of 385 Mev. The results of these calculations compared to the 90° experimental carbon, copper, and lead π^+ cross section data at 381 Mev are shown in Fig. 11.

The curves calculated from the matrix elements of type AI and BII were almost indistinguishable; therefore, only one curve was plotted. The curves were arbitrarily normalized to give the experimentally determined cross section at 90°. This arbitrary normalization obviates the need for correcting the production spectrum for meson reabsorption within the struck nucleus, providing this interaction is not strongly dependent on meson energy.

The calculations for the energy independent matrix element (AII) predict a maximum in the spectrum at too low a meson energy. The results with the AI and BII matrix elements are much too high at the low energy end of the meson spectrum, and the CI matrix elements are much too low at the low energy end of the meson spectrum. Matrix elements of type BI and CII give a better fit regarding the correct maximum of the spectrum and the low energy shape, but they do not explain the high energy tail. The results of the calculations have also been applied to deuterium and were reported previously.[14]

As a test of the sensitivity of these calculations to the assumption of a particular nuclear model, the calculations were repeated using the Chew-Goldberger[15] momentum distribution deduced from the pick-up effect and the Gaussian distribution having an average of 19.3 Mev, which also seems to fit the pick-up effect data.[16]

The results for the Fermi, Chew-Goldberger, and Gaussian distributions utilizing matrix element BI, arbitrarily normalized to fit the experimental data at 65 Mev, are shown in Fig. 12.

Recent evidence[15,16] indicates that the Chew-Goldberger distribution overemphasizes the high momentum tail and that the Gaussian distribution gives a better fit. This is confirmed in our calculations. The calculations fit the spectrum at the low energies and predict the correct maximum. They also give a high energy tail which is greater than the experimental results. This is to be expected since the matrix elements for all meson energies were assumed to vary as $T_m^{\frac{1}{2}}$. This relation holds only in the neighborhood of threshold, and the variation should be less rapid with increasing meson energy, an effect which would decrease the cross section for the production of very high energy mesons. Also, the recoil of the final nucleus has not been taken into account in the calculation. The neglect of this effect would raise the high energy end over its true value.

Since positive and negative mesons were treated symmetrically, the calculations should apply equally for negative mesons. However, the π^- spectra are *not* explained by the theory, as the maximum of the spectrum occurs at a lower meson energy than predicted. In addition, the absolute value of $(d\sigma^-)/(d\omega)$ is an order of magnitude below that of the corresponding π^+ cross section, whereas the assumption of equal *n-p* and *p-p* forces requires an *a priori* ratio $\pi^+/\pi^-=3$ for carbon. The large experimental π^+/π^- ratio ($\sim$25) in deuterium, which has been analyzed previously,[14] indicates that the main contribution to positive pions comes

[14] Passman, Block, and Havens, Phys. Rev. **85**, 370 (1952).
[15] G. Chew and M. Goldberger, Phys. Rev. **77**, 470 (1950).
[16] E. M. Henley and G. H. Huddlestone, Phys. Rev. **82**, 954 (1951).

from the reaction in deuterium: $p+p\rightarrow\pi^{+}+d$. However, the calculated ratios of the 90° π^{+} deuterium to the 90° π^{+} hydrogen cross sections are far too low (matrix elements CI, CII, BI, and BII predict a ratio of 2.2, 1.7, 1.6 and 1.2, respectively, whereas the experimental ratio is 5.6 ± 2.3). This effect is difficult to understand, since it implies that a more energy-dependent excitation function than the $T_m^{\frac{1}{2}}$ or T_m matrix element dependence is required. This is not required, however, to explain the spectral shapes of the heavy elements. An alternative explanation, namely, that the two nucleons in deuterium do not act as independent particles in the process of meson formation, is also difficult to explain, since one might expect that, if the deuterium nucleus as a whole were to interact, a "tritium" peak (reaction $p+d\rightarrow t+\pi^{+}$) might be appreciable. Furthermore, the spectral shapes of the heavy elements were correctly predicted with the assumptions of independent nucleons. Certainly, in a deuterium nucleus where the binding is weak the assumption of independence should be better. Thus, one might suspect that negative mesons are produced by a different process from positive mesons.

The authors wish to express their gratitude to Dr. Chien Shiung Wu for materially aiding us in the absolute β-ray measurements and to Professor T. I. Taylor for making the mass spectrographic analysis of the deuterated paraffin.

The assistance of the Nevis cyclotron staff and the Nuclear Emulsions group is gratefully acknowledged. In particular, we wish to thank Mr. Saul Basri and Mr. Robert Feldmann for aiding in the scanning of the data.

Miss Anne Lapham of Duke University aided us in some of the calculations.

PHYSICAL REVIEW VOLUME 88, NUMBER 6 DECEMBER 15, 1952

Excitation Function for Charged π-Meson Production in Hydrogen and Carbon by 345- to 380-Mev Protons*

S. Passman,† M. M. Block,‡ and W. W. Havens, Jr.
Columbia University, New York, New York

(Received September 10, 1952)

The 90° differential cross section for charged meson production in hydrogen and carbon is measured for incident proton energies 345 to 380 Mev. For hydrogen, the 90° π^{+} meson production energy spectra occur as peaks in the energy region predicted from the kinematics of the reaction $p+p\rightarrow\pi^{+}+d$. Ratios of these 90° π^{+} differential cross sections are $(d\sigma)/(d\omega)$ at 380 Mev: $(d\sigma)/(d\omega)$ at 365 Mev: $(d\sigma)/(d\omega)$ at 345 Mev = 2.6:1.6:1 with a statistical uncertainty of 15 percent. For carbon the π^{+} meson production spectra show an increase in the energy of the maximum of the broad distributions, with increasing incident proton energy. The $(\pi^{+})/(\pi^{-})$ ratio in carbon is found to be in the range $(10\pm3):1$ for all three proton energies studies. Qualitative agreement with these carbon π^{+} meson spectra is obtained from a phenomenological analysis based upon the assumptions of nucleon-nucleon collisions in which the target has a Gaussian momentum distribution.

INTRODUCTION

THE reaction $(p-p,\pi^{+})$ has been studied in great detail at Berkeley[1] with both liquid hydrogen targets and polyethylene-carbon subtraction techniques in conjunction with the external 340-Mev proton beam. The resulting π^{+} meson energy spectrum was observed as a clustering of the mesons about the maximum energy permitted by conservation laws, which indicates a strong nucleon-nucleon interaction in the final state of the reaction. Therefore, in the case of a triplet final spin state there is a strong possibility of deuteron formation. From the angular distribution of π^{+} mesons produced in $p-p$ collisions, Whitehead and Richman[2] conclude that the π^{+} production in the center-of-mass system has a $(0.07\pm0.07+\cos^{2}\theta)$ angular dependence.

Because of the difficulties associated with the quantum theoretical perturbation calculations of nucleon-nucleon meson production, one finds it more reliable if not as fundamental to apply the phenomenological theory of Watson and Brueckner.[3] In their method, the previously discussed qualitative features of the experimental results follow from the principles of conservation of parity and angular momentum together with an application of the exclusion principle, all contingent upon the pseudoscalar nature of the π^{+} meson. An important test for this theory is the dependence of the nucleon-nucleon meson production cross section upon the incident proton energy, since the energy dependence of the transition operator for this process is directly related to the type of meson-nucleon interaction assumed.

Experiments concerning the production spectra of charged mesons in carbon and the heavy elements[4]

* This work was supported jointly by the ONR and AEC. Publication was assisted by the Ernest Kempton Adams Fund for Physical Research of Columbia University, New York, New York.

† Now at Hughes Research and Development Laboratories, Culver City, California.

‡ Now at Duke University, Durham, North Carolina.

[1] Peterson, Illoff, and Sherman, Phys. Rev. **81**, 647 (1951); Cartwright, Richman, Whitehead, and Wilcox, Phys. Rev. **78**, 823 (1950); **81**, 652 (1951).

[2] Marian Whitehead and Chaim Richman, Phys. Rev. **83**, 97 (1951).

[3] K. Watson and K. Brueckner, Phys. Rev. **83**, 1 (1951).

[4] Richman, Weissbluth, and Wilcox, Phys. Rev. **85**, 161 (1952); Block, Passman, and Havens, Phys. Rev. **83**, 167 (1951).

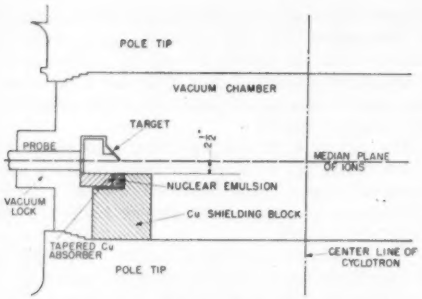

FIG. 1. Cross section view of cyclotron vacuum chamber.

indicate broad single maxima distributions, believed due to the effect of the momentum distribution of the bound target nucleons. Used in this way, the meson probes nuclear structure characterized by internal momenta distributions, just as in the nucleon-nucleon case the meson probes nuclear forces at very close distances.

Theoretical analyses of these heavy element meson production spectra,[5] based upon the impulse approximation, while giving a qualitative explanation of the shape of the observed distributions, have been handicapped because of lack of information concerning the nucleon-nucleon meson production excitation function as well as the paucity of information on the high momentum nucleon states present in the target nucleus. The variation in the cross section of meson production in carbon with increased incident proton energy should give additional information regarding these questions.

EXPERIMENTAL METHOD

The experimental technique, employing nuclear emulsions as detectors for measuring absolute meson production cross sections from targets bombarded by the internal circulating proton beam of the Nevis cyclotron, is basically the same as was reported in the previous paper on the variation of meson production with the atomic number Z and atomic weight A of the target material for 381-Mev protons.[6]

In order to increase the energy resolution for the measurement of the hydrogen meson spectra, the target holder was redesigned so that the thin target is inclined at 45° to the vertical as shown in Fig. 1, rather than the vertical position used in the earlier work. This allows mesons traveling in the downward direction toward the detector to traverse only the thin ~40-mil dimension of the polyethylene target with a consequent small energy loss in the target. To localize the active meson-producing region of the target, a 5 in.×5 in.×1 in. copper beam "clipper" was placed at the same radial distance as the target, slightly (¼ in.) above the median plane of the circulating protons but displaced 90° in azimuth, in order to exclude neutrons, produced in the clipper, from the emulsion region. By this method, proton irradiation was successfully limited to the leading ¼ in. of the targets, directly in the median plane, as measured by a monitoring of the C^{11} activity induced in the carbon and polyethylene targets. The copper clipper also serves to prevent a significant degradation of the proton beam energy through multiple traversals of the target, since scattering of the proton beam in the target may send the protons into the clipper region where they are absorbed, stopped, or outscattered.

For the excitation function measurements the energy of the incident proton beam was varied by radially displacing the probe, on which the target and detector are mounted in a permanent relative geometry, to new $H\rho$ values in the vacuum chamber.

Exposures were made at proton energies of 345, 365, and 380 Mev. The upper limit of these proton energies was due to the characteristics of the Nevis cyclotron which had an $n=0.2$ point, where the well-known beam blow-up takes place, at a radial distance corresponding to 381-Mev proton energy. Proton energies below 345 Mev lead to π^+ production from hydrogen at extremely low 90° emission energies, where background difficulties make it impossible to detect mesons using the present photographic technique.

The requirement of bombarding targets by the internal proton beam of the cyclotron involves the problem of incident beam energy degradation due to radial oscillations of the circulating protons as well as multiple traversals of the target. By using the copper clipper, it was hoped to reduce this beam degradation by the removal of some of these protons scattered from the target. Estimates of the remaining beam energy spread can best be made with the help of the meson spectra obtained from hydrogen.

The hydrogen spectrum is expected to occur as a peak at the energy predicted from kinematics of the reaction $p+p\rightarrow\pi^++d$, with a much smaller low energy tail due to the reaction leading to an unbound $N-P$ final state. The observed spread of this peak is a measure of the energy and angular resolution of the detector as well as the spread in incident proton beam energy. From the experimental hydrogen π^+ spectra (shown in Fig. 2) together with estimates of the detector energy and angular resolution, and meson energy loss in traversing the target, in conjunction with the variation in meson energy with emission angle and proton energy, it is

TABLE I. Summary of 90° differential cross sections for meson production, integrated over meson energy, $(d\sigma)/(d\omega)_{90°}$, in cm^2 $sterad^{-1}$.

Element	At 380-Mev incident proton energy	At 365-Mev proton energy	At 345-Mev
Hydrogen	$(7.5\pm1.8)\times10^{-29}$	$(4.6\pm1.2)\times10^{-29}$	$(2.9\pm0.7)\times10^{-29}$
Carbon	$(6.7\pm1.5)\times10^{-28}$	$(6.4\pm1.4)\times10^{-28}$	$(4.7\pm1.3)\times10^{-28}$

[5] Ernest M. Henley, Phys. Rev. **85**, 204 (1952); Passman, Block, and Havens, Phys. Rev. **83**, 167 (1951).

[6] Block, Passman, and Havens, preceding article [Phys. Rev. **88**, 1239 (1952)].

estimated that the spread in incident proton energy is approximately 10 Mev. As discussed later, these sharply peaked meson spectra produced in hydrogen are observed to occur in the meson energy region predicted from kinematics of the reaction $p+p\rightarrow\pi^{+}+d$, corresponding to an incident proton energy approximately the same as calculated from the $(H\rho)$ value at the target position. Since any uniform spread in incident proton energy extending considerably below this $H\rho$ value would result in a displacement of the meson spectrum peak to lower meson energies, contrary to observation, it is inferred that proton energies corresponding to the proper $H\rho$ value at the target position strongly predominate in the beam energy distribution.

The method of calculation of the absolute differential cross section for meson production, from a knowledge of the areal density of π^{+} meson endings observed along the inclined Ilford *C*-2 nuclear emulsion, is described in detail in the previous paper.

An accurate monitoring of the incident proton flux is accomplished by an absolute measurement of the target's C^{11} positron activity after bombardment. The excitation function for this reaction, $C^{12}(p,pn)C^{11}$, has been measured by Aamodt *et al.*[7]

The meson production cross sections are corrected for a geometrical nuclear interaction cross section to account for absorption and scattering in the tapered copper absorber.

MESON PRODUCTION IN HYDROGEN

A. Results

The 90° differential cross sections for π^{+} meson production in hydrogen at incident proton energies of 345, 365, and 380 Mev were obtained by a subtraction technique involving thin polyethylene $(CH_2)_n$ and carbon targets. The feasibility of this subtraction method rests upon the experimental fact that the 90° π^{+} spectrum from hydrogen occurs as a sharp peak in the low energy region where the carbon differential cross section is relatively quite small.

The polyethylene targets were 0.23 g/cm² wide in the proton beam direction and only 0.09 g/cm² thick. Mesons of 20-Mev kinetic energy traveling downward through the target toward the detector region (see Fig. 1) will lose less than 1 Mev, on the average, by ionization loss in the target, while the high energy incident protons have a negligible energy loss in traversing the thin targets.

Results for the hydrogen 90° differential cross sections $d^2\sigma/d\omega dE$ at the above proton energies are plotted in Fig. 2 as a function of meson energy. These meson spectra are observed to have peaks at meson energies consistent with energy and the momentum conservation laws for the reaction $p+p\rightarrow\pi^{+}+d$, as indicated by arrows drawn in the figures.

[7] Aamodt, Peterson, and Phillips, University of California Radiation Laboratory Report 526, 1949 (unpublished).

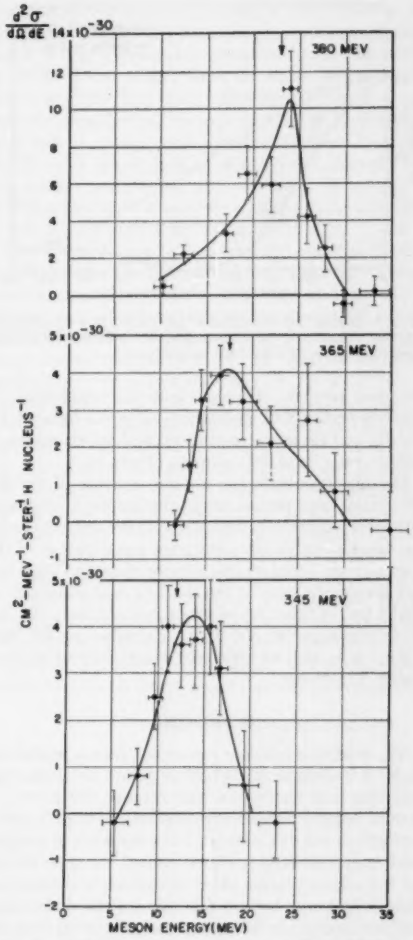

FIG. 2. π^{+} differential cross section in hydrogen at (90°±1.5°) to the proton beam for 345-Mev, 365-Mev, and 380-Mev proton energy.

The statistical uncertainties indicated in the data are the standard deviations of the counting including the errors due to subtraction. The hydrogen spectra are based on the following numbers of observed $\pi-\mu$ decays: 150 events for the H spectrum at 345 Mev, 250 for 365 Mev, and 180 for 380 Mev.

Values for the 90° π^{+} differential cross sections in hydrogen, integrated over meson energy $d\sigma/d\omega$, are given in Table I. These values are obtained by a histogram of the meson energy spectra, and the statistical uncertainties given are for the absolute values of

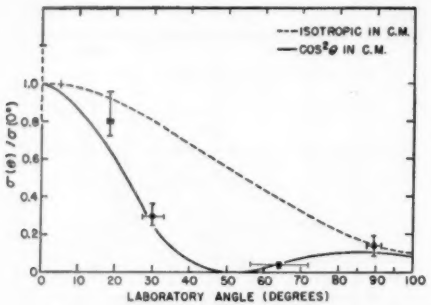

FIG. 3. Angular dependence of π^+ production in $p-p$ collisions, from V. Peterson *et al.*, University of California Radiation Laboratory Report UCRL-1405 (unpublished).

the cross sections. These include the uncertainty in absolute proton flux monitoring using the induced C^{11} activity and the measurements of emulsion thickness, as well as statistics of the counting of mesons.

The uncertainty in the relative increase of the 90° differential cross section for π^+ production in hydrogen with increasing proton energy should involve principally the uncertainty of the histogram computation of the cross section, based on the number of mesons detected. Any systematic error in the absolute calibration will be minimized in these ratios which are $(d\sigma/d\omega)_{90°}$ at 380 Mev: $(d\sigma/d\omega)_{90°}$ at 365 Mev: $(d\sigma/d\omega)_{90°}$ at 345 Mev $=2.6:1.6:1$, with an estimated uncertainty of approximately 15 percent.

B. Analysis

The available evidence concerning meson production in $p-p$ collisions at 340 Mev points to production occurring principally via the reaction $p+p\rightarrow\pi+d$,[8] with an angular dependence proportional to $(0.07\pm0.07+\cos^2\theta)^2$ in the c.m. system. From the work of Durbin, Loar, and Steinberger, who measured the cross section for the inverse process of π^+ absorption in deuterium,[9] there is reason to believe that this angular distribution remains constant in the proton energy interval from 340 to 380 Mev. However, their estimate of the isotropic contribution to the cross section is closer to 0.16 ± 0.08 rather than the 0.07 ± 0.07 given by Whitehead and Richman.

A comparison of our value of the 90° π^+ differential cross section for 345-Mev protons with work done at Berkeley at 340 Mev at other angles is given in Fig. 3. This figure, from an article by Peterson, Illoff, and Sherman,[10] shows the 340-Mev differential cross section $d\sigma/d\omega$, for π^+ mesons produced in hydrogen at 18°, 30°, and 60°, to the proton beam, normalized to Cartwright's measurement at 0°. We have appended our value for $d\sigma/d\omega$ at 90° and 345 Mev. If one assumes the reaction $p+p\rightarrow\pi^++d$, with the resulting line spectrum of mesons in the c.m. system, then from a transformation of the solid angle factor between c.m. and laboratory systems, one can easily derive the dependence of $d\sigma/d\omega$ upon laboratory angle of emission for various assumptions about the c.m. angular dependence. Curves indicating isotropic and $\cos^2\theta$ c.m. angular dependence are shown in Fig. 3. The agreement with experiment is seen to be quite good for the $\cos^2\theta$ assumption.

If one analyzes the 90° π^+ differential cross sections at the incident proton energies of 345, 365, and 380 Mev by assuming the reaction $p+p$ yields π^++d, together with a $\cos^2\theta$ angular distribution in the c.m. system, as indicated from the above discussion, then one can calculate the total π^+ cross sections in hydrogen by means of the solid angle transformation factor between laboratory and c.m. systems at these proton energies. The values of the resulting absolute total cross sections σ_{tot} are 10.6×10^{-28} cm² at an incident proton energy of 380 Mev, 6.1×10^{-28} cm² at 365 Mev, and 3.5×10^{-28} cm² at 345 Mev. The statistical uncertainty in these absolute cross sections is ~25 percent.

In comparing the excitation function for meson production in hydrogen with theoretical predictions, the significant quantity is the *relative* increase in the meson production total cross section with increasing proton energy. Consequently, the excitation function for the total cross section for π^+ meson production in hydrogen, σ_{tot}, relative to the value of σ_{tot} at 345 Mev is plotted in Fig. 4. This curve is arbitrarily normalized to an absolute value of 3.5×10^{-28} cm² at 345 Mev. By way of comparison, the point at 340 Mev represents the combined Berkeley results for σ_{tot} as quoted by Peterson *et al.*[1] In Fig. 4, the statistical uncertainties in σ_{tot} relative to the 345-Mev cross section measurement are indicated together with the data. These cross section ratios, σ_{tot} (380 Mev): σ_{tot} (365 Mev): σ_{tot} (345 Mev) $=2.95:1.7:1$, with a statistical uncertainty of approximately 20 percent, are very little affected by small isotropic contributions to the angular dependence of the cross section.

An attempt to fit the experimental excitation function for meson production in hydrogen with a simple power law, such as $(T_{max})^n$, where T_{max} is the maximum c.m. meson energy available in the collision, indicates that the assumption of $n=2$, as shown by the solid curve (B) in Fig. 4, is in fairly good agreement with the data.

The inverse process concerning π^+ absorption in deuterium yielding two fast protons, $\pi^++d\rightarrow p+p$, has been studied by Durbin, Loar, and Steinberger[11] for meson energies between 25 and 53 Mev in the center-of-mass system. This is equivalent to the kinematical situation for the process $p+p\rightarrow\pi^++d$ for incident

[8] F. Cartwright, thesis, University of California, 1951 (unpublished).
[9] Durbin, Loar, and Steinberger, Phys. Rev. **83**, 646 (1951); and H. Loar (private communication).
[10] Peterson, Illoff, and Sherman, University of California Radiation Laboratory Report 1405 (unpublished).
[11] Durbin, Loar, and Steinberger, Phys. Rev. **84**, 581 (1951).

proton energies 350–410 Mev. From detailed balancing considerations, Cheston[12] has shown that these two inverse processes are connected through the relation

$$\sigma_{\substack{\text{total}\\(\pi^++d)}} = \sigma_{\substack{\text{total}\\(p+p)}} \times \frac{2}{3(2S+1)} \times \frac{p^2}{q^2},$$

(S=meson spin), where p and q are the proton and meson momenta, respectively, in the c.m. system of the reacting particles. From our work on the excitation function of the $p+p\rightarrow\pi^++d$ process, we can therefore predict an increase in the total cross section for $\pi^++d\rightarrow p+p$ of 1.95±20 percent in the meson energy interval 24–39 Mev (corresponding to proton energies 345–380 Mev for the inverse process), in good agreement with the value obtained directly for this process by Durbin *et al.*, namely, 1.9±15 percent.

Brueckner[13] has calculated the cross section for meson production in a nucleon-nucleon collision on the basis of third-order perturbation theory using the methods of Feynman and Dyson applied to meson theory. Only for pseudoscalar theory with pseudovector coupling does the calculation give a nonisotropic angular dependence. The formation of a deuteron is included in this calculation by the incorporation of the deuteron wave function, evaluated at the origin, as an additional factor in the matrix element for the process. The predicted dependence of the $p+p\rightarrow\pi^++d$ meson production process on incident proton energy varies near threshold as the $\frac{3}{2}$ power of the meson's kinetic energy in the center-of-mass system, $(T_{\max})^{\frac{3}{2}}$, for the case of *PS* theory with *PV* coupling. Including the contribution of the unbound final $n-p$ state in the proportion estimated by Brueckner, amounting to $\frac{1}{3}$ of the cross section for the bound state at 350 Mev, yields the over-all energy dependence of the $(p-p, \pi^+)$ production process shown by the dotted curve (A) in Fig. 4. This theoretical excitation function, which is arbitrarily normalized to a value of 3×10^{-28} cm^2 at 340 Mev, is seen to be significantly below the observed experimental energy dependence in the region of high proton energies.

Because of the inherent difficulties involved in the application of quantum theoretical-perturbation methods to a process involving such strong interaction constants as meson production, the phenomenological theory of Watson and Bruechner[14] has been used. This phenomenological theory, which has been successful in interpreting the 0°, 340 Mev $(p-p, \pi^+)$ spectrum of Cartwright,[8] predicts a variation of this $(p-p, \pi^+)$ total cross section with increasing proton energy, for the case of a transition operator proportional to the first power of the meson momentum, that is essentially the same as the results previously given from Brueckner's work. For the assumption of a triplet final $n-p$ spin state, including the large contribution due to deuteron formation, the predicted π^+ meson production excitation function of Watson and Brueckner is given by curve A, Fig. 4, arbitrarily normalized to a cross section of 3×10^{-28} cm^2 at 340 Mev, the value quoted by the above authors. This energy dependence, which clearly rises less sharply than the experimental excitation function, can be brought into agreement by requiring that the factor $\Gamma^2(\hat{p})$, defined by Watson and Brueckner as the nucleon momentum $(\hat{p})$ dependent factor in the matrix elements (but assumed constant in their results), should have a dependence of the order of $\hat{p}^4$.

Chew *et al.*[15] have recently pointed out that Watson and Brueckner's treatment does not separate the meson-nucleon interaction from the interaction between the two nucleons. These authors proceed to separate out the effects of nuclear binding in initial and final states of the $p+p\rightarrow\pi^++d$ reaction, in the spirit of explicitly evaluating the transition operator factor $\Gamma^2(\hat{p})$ of Watson and Brueckner. These calculations lead to additional factors in the production cross section, proportional to the Fourier amplitude of the deuteron or diproton wave function which are then multiplied by the meson-nucleon matrix elements and kinematical factors to yield the over-all energy dependence of the reaction. These Fourier amplitudes probably decrease fairly rapidly with increasing incident proton momentum, $\sim(1/\hat{p}^5)$, so that the required *meson-nucleon* interaction must rise even more sharply with energy than was previously estimated, in order to explain the steep experimental excitation function for the over-all production process. Durbin, Loar, and Steinberger[11] speculate that this steep energy dependence is probably

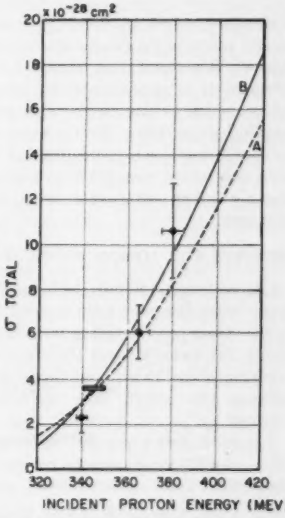

FIG. 4. Variation of the total cross section for meson production in $p-p$ collisions with increasing incident proton energy.

[12] W. Cheston, Phys. Rev. **83**, 1118 (1951).
[13] Keith A. Brueckner, Phys. Rev. **82**, 598 (1951).
[14] K. Watson and K. Brueckner, see reference 2.
[15] Chew, Goldberger, Steinberger, and Yang, Phys. Rev. **84**, 581 (1951).

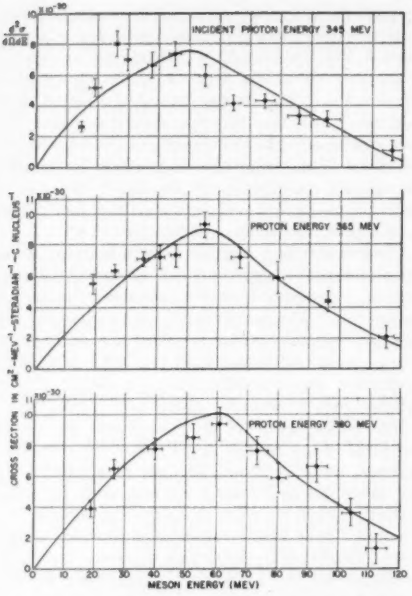
INCIDENT PROTON ENERGY 345 MEV
PROTON ENERGY 365 MEV
PROTON ENERGY 380 MEV
CROSS SECTION IN CM²-MEV⁻¹-STERADIAN⁻¹-C NUCLEUS⁻¹
MESON ENERGY (MEV)

FIG. 5. π^+ meson differential production cross sections in carbon at (90°±5°) to the proton beam for 345-Mev, 365-Mev, and 380-Mev proton energy. The curves represent theoretical 90° meson spectra from carbon using a Gaussian target nucleon momentum distribution together with a $(T_{max})^2$ empirical nucleon-nucleon meson production excitation function.

of the same origin as the sharp excitation function in neutral photomeson production. To explain this latter process, Brueckner and Case[16] have suggested the influence of a resonance interaction with a nucleon isobar, which is one of the characteristics of strong coupling meson theory. Such a meson-nucleon resonance interaction has also been proposed by Brueckner,[17] to explain the recent experimental evidence[18] for a large, strongly energy dependent π^+ scattering process in hydrogen.

RESULTS FOR MESON PRODUCTION IN CARBON

Carbon targets, 50 mils thick and 75 mils or 0.3 g/cm² in the beam direction, were exposed to the proton beam at $H\rho$ values corresponding to incident proton energies of 345, 365, and 380 Mev. The duration of the exposures averaged about 15 sec, and the incident beam currents striking the target were approximately 0.6×10^{-8} amperes.

Figure 5 shows the 90° differential cross sections $(d^2\sigma)/(d\omega dE)$, for π^+ mesons produced in carbon at the above-mentioned three proton energies. These π^+ spectra are based upon 350 $\pi-\mu$ events for the 345-Mev cross section, 550 $\pi-\mu$ events for the 365-Mev cross section, and 300 $\pi-\mu$ events for the 380-Mev cross section. The absolute value of the 380-Mev cross section is somewhat higher than that reported in the previous paper, although it is within the statistical uncertainties stated, which correspond only to the probable error in counting mesons. The absolute cross section involves the calibration using the C^{11} activity which will introduce an additional error. However, the uncertainty in the relative increase should not involve this absolute calibration.

The meson spectra from carbon are seen to occur as broad single maxima distributions. The shift of the energy of the maximum of the curve from ~45 Mev for a proton energy of 345 Mev, to ~55 Mev at 365 Mev, and to ~62 Mev at 380 Mev, is noteworthy.

To obtain the 90° π^+ differential cross sections integrated over meson energy $(d\sigma^+)/(d\omega)$ the above data are histogrammed, yielding the values given on line 2 of Table I. The uncertainties given include the estimate of the precision of the absolute calibration as well as the statistics of counting. From this table it is seen that the relative increase in the 90° π^+ carbon cross section is less than the increase in the hydrogen cross section in this same incident proton energy interval.

With regard to the production of π^- mesons in carbon the significant experimental fact is that the negatives are produced in much less quantity than the positives, for all three proton energies studied. In the identical regions scanned for π^+ mesons included in the previous distributions, only 23 π^- mesons were found for the 345-Mev spectrum, 21 π^- for 365 Mev, and 29 π^- for 380 Mev.

Because of these limited statistics, only qualitative statements may be made concerning the production of negatives in carbon. The spectrum of π^- mesons appears to shift to lower energies than the corresponding π^+ spectrum at the same proton energy. That is, the energy of the maximum of the curve of the π^- distribution occurs at a lower meson energy than that of the π^+ distribution, and the meson spectrum cut-off energy is also lower for the case of π^- mesons (~90 Mev). The ratios of the π^+ to π^- 90° cross sections for carbon, integrated over meson energy, were within the range $(10\pm3):1$ for all three proton energies studied.

This observed π^+/π^- ratio in carbon is considerably greater than the *a priori* expected ratio of $(A+Z)/(A-Z)=3$, which would be found if the protons and neutrons in the carbon nucleus had equal cross sections for meson production and if the $(p-n, \pi^+)$ reaction had the same probability as $(p-n, \pi^-)$.

Analysis of the still larger π^+/π^- ratio observed for meson production in deuterium by protons[19] indicates that the strong interaction in the final state of the $(p-p, \pi^+)$ reaction may account for this charge assymmetry in meson production.

[16] K. A. Brueckner and K. M. Case, Phys. Rev. **83**, 1141 (1951).
[17] Keith A. Brueckner, Phys. Rev. **86**, 106 (1952).
[18] Anderson, Fermi, Long, and Nagle, Phys. Rev. **85**, 936 (1952).
[19] Passman, Block, and Havens, Phys. Rev. **85**, 370 (1952).

A large π^+/π^- production ratio of the order of 15 was recently observed by Dudziak[20] for mesons produced in carbon at 0° to the Berkeley 340-Mev proton beam. However, Richman and Wilcox in an early experiment on meson production[21] found a π^+/π^- ratio of 5.1 ± 1.0 in carbon at 90° to this same proton beam. The discrepancy between this value and that of the present work occurs principally in the π^+ production, where we find a differential cross section at 345 Mev that is approximately twice as large as that reported by Richman and Wilcox, namely, $(2.3\pm0.5)\times10^{-28}$ cm^2 sterad^{-1}, although the statistical uncertainty in the ratio of these absolute cross sections is ~35 percent. Good agreement with regard to the spectral shape of the energy distributions is found; both experiments indicate a sharp rise in the cross section at low energies, the maximum occurring at an energy of approximately 45 Mev and tailing off at higher energies, although the cross section is still not zero at the maximum energy observed, 120 Mev.

PHENOMOLOGICAL CALCULATION OF π^+ MESON PRODUCTION IN CARBON

Calculation of the production of π^+ mesons in carbon is done in the same manner as in the previous paper using the following assumption:

(a) Meson production in carbon occurs through nucleon-nucleon interactions.

(b) The momentum distribution of target nucleons before collision is Gaussian, falling to $1/e$ of its maximum value at a nucleon energy of ~14 Mev, as suggested by the work of Cladis[22] on the energy spectrum of protons scattered from carbon.

(c) The nucleon-nucleon meson production process has the following properties:

(1) a $\cos^2\theta$ angular dependence in the c.m. system;

(2) a strong final state nucleon interaction which requires the emitted meson to receive all the available kinetic energy T_{max} in the c.m. system;

(3) the excitation function is proportional to $(T_{max})^2$ (see Fig. 4).

Results of the calculations at 345, 365, and 380 Mev are plotted together with the experimental data in Fig. 5 and show fairly good agreement with regard to (a) the general shape of the meson spectra, (b) the shift of the meson spectrum peak energy to higher meson energies with increasing proton bombardment energy, and (c) the presence of the high meson energy tail in the distribution, probably due to the high momentum states in the carbon nucleus.

Although the theoretical curves are independently normalized in this figure, the calculations do predict an increase in this 90° differential cross section of ~1.5 in the energy interval 345 to 380 Mev, in good agreement with the experimental increase (see Table I).

A further application of this calculation is to the ratio of 90° π^+ production cross sections in carbon and hydrogen. Based on the above calculation, using a normalized target momentum distribution and the experimental meson production excitation function, it is found that the expected efficiency of a nucleon in carbon for meson production is approximately twice that of a free nucleon at rest. This effect is due to the strong excitation function for π^+ production which weights the collisions in which the target nucleon approaches the incident nucleon, with a consequent increase in the available c.m. meson energy, more than those collisions in which the target nucleon's motion is in the other direction. For the *experimental* ratio of the carbon and hydrogen 90° π^+ cross sections we find ratios of (10–12):1 in the proton energy interval studied. Correcting for meson reabsorption in the target nucleus, from the work of Brueckner, Serber, and Watson,[23] we would expect these production cross sections to stand in the ratio of 18:1. In view of the efficiency factor of 2 for component nucleons of the carbon nucleus, owing to their relative motion, this observed ratio of π^+ production in carbon to hydrogen can be understood if the $(p-n, \pi^+)$ production process has $\frac{1}{2}$ the probability of the $(p-p, \pi^+)$ process, in agreement with *a priori* considerations of the production process, since either proton in the latter case may give rise to the positive meson. While this conclusion is in agreement with analysis of meson production in deuterium,[24] where the large π^+ production cross section requires an appreciable contribution from the $p-n$ reaction, it makes it difficult to understand the observed large positive to negative ratio in carbon and deuterium, since this hypothesis would require an assymmetry in the $(p-n, \pi^+)$ and $(p-n, \pi^-)$ production processes. This asymmetry appears to be contrary to notions of charge independence of nuclear forces at low energy.

We gratefully acknowledge the assistance of the Nevis cyclotron staff and the Nuclear Emulsions group. Dr. Chien-Shiung Wu kindly aided us in the original absolute calibration of our monitoring apparatus. Mrs. Marjorie Boehlert and Mr. Saul Basri aided us in scanning the photographic plates.

[20] Walter F. Dudziak, Phys. Rev. **86**, 602 (1952) and private communication.
[21] C. Richman and H. A. Wilcox, Phys. Rev. **78**, 496 (1950).
[22] John B. Cladis, Ph.D. thesis, University of California, 1952 (unpublished).
[23] Brueckner, Serber, and Watson, Phys. Rev. **84**, 258 (1951).
[24] Passman, Block, and Havens, Phys. Rev. **85**, 370 (1952).

The Reaction Energies of $Ne^{21}(d, \alpha)F^{19}$ and $Ne^{21}(d, p)Ne^{22}$ from Magnetic Analysis*

CURT MILEIKOWSKY† AND WARD WHALING
Kellogg Radiation Laboratory, California Institute of Technology, Pasadena, California
(Received August 15, 1952)

Separated isotopic targets of Ne^{21}, which were produced at the Nobel Institute of Physics, have been used to measure the Q-values of the reactions (1) $Ne^{21}(d, \alpha)F^{19}$, and (2) $Ne^{21}(d, p)Ne^{22}$. A double focusing magnetic spectrograph was used to compare the energy of the protons and alpha-particles from these reactions with the alpha-particles from ThC and ThC′. The angle of observation and the deuteron bombarding energy were chosen so that the particles being studied and the alpha-line used for energy calibration lay nearly side by side on the photographic plate used as a detector. The Q-values measured are 6.432 ± 0.010 Mev for reaction (1) and 8.137 ± 0.011 Mev for reaction (2). From these Q-values and the mass of F^{19} the atomic masses of Ne^{21} and Ne^{22} are obtained. Other alpha-groups from reaction (1) correspond to transitions to states in F^{19} at 0.113 ± 0.008 Mev and 0.192 ± 0.012 Mev above the ground state. Additional particle groups from N and Na contamination on the targets have been observed: The Q-values measured are 8.613 ± 0.011 Mev for $N^{14}(d, p)N^{15}$ and 4.723 ± 0.008 for $Na^{23}(d, p)Na^{24}$.

I. INTRODUCTION

THE Q-values measured with the precision afforded by magnetic analysis provide a very accurate measure of mass differences. A sufficient number of mass differences have been measured to determine the masses of most of the light nuclei up through F^{19} directly in terms of O^{16}. In the past year these accurate Q-values measurements have been extended by Buechner's group at the Massachusetts Institute of Technology to include many of the nuclei between Ne and P. However, there has not yet been reported any precise measurement of the mass difference between F and Ne which would make it possible to relate the masses of these heavier nuclei to O^{16}. This paper describes a measurement of the $Ne^{21}(d, p)Ne^{22}$ and $Ne^{21}(d, \alpha)F^{19}$ Q-values which determine the masses of Ne^{21} and Ne^{22} in terms of O^{16}. Together with the measurements of the MIT group, these Q-values may be used to determine the masses of many of the heavier nuclei by means of nuclear transmutation energies.

II. APPARATUS

The isotopic targets of Ne^{21} were prepared in the 1.6-meter isotope separator of the Nobel Institute[1] by bombarding silver disks, 0.8 inch in diameter by 0.125-inch thick, with Ne^{21} ions at an energy of about 50 kev. These targets are thus very thin for protons, deuterons, and alpha-particles of a few Mev. The Ne^{21} bombardments were sufficient to saturate the targets. Since the neon is absorbed in the silver surface and escapes readily if the silver is heated,[2] the target was mounted in close thermal contact with a block of copper which was maintained at room temperature during the deuteron bombardment, and the deuteron beam on the target was kept below 0.3 microampere to prevent local heating.

TABLE I. Sources of experimental error and their contribution to the probable error in the $Ne^{21}(d, \alpha)F^{19}$ Q-value.

Source of error	Probable error in Q kev
Statistical error in E_2 ($\pm\frac{1}{4}$ width at half-maximum)	7
Energy of ThC alpha-particles	4
Surface layer correction ($\pm\frac{1}{4}$ layer thickness)	1
Displacement of beam spot relative to ThC source (±0.5 mm)	5
Deuteron bombarding energy (±0.2 percent)	3.5
Angle of observation ($\pm0.2°$)	2
Net probable error in $Q=10$ kev	

The energy of the incident deuterons from the 3.0-Mev Van de Graaff generator of the Kellogg Radiation Laboratory was measured with a 90° electrostatic analyzer. The analyzer was calibrated against the $Al^{27}(p, \gamma)Si^{28}$ resonance at 0.9933 Mev,[3] and the linearity of the analyzer was checked by observing this same resonance with the H^+ and HH^+ ions. The electrostatic analyzer calibration was checked frequently during the course of the experiment. At each run the target was bombarded with 1000–1600 microcoulombs of D^+ ions.

The energy of the emitted particles was measured with the 16-inch double focusing magnetic spectrograph. The full solid angle of 0.007 steradian was utilized. Ilford emulsions, 100 microns thick, were placed in the focal plane of the spectrograph to detect the particle groups. A weak ThC−ThC′ alpha-source was placed 6 mm from the target spot as measured along the axial direction of the spectrograph so that the spectrum of particles from the alpha-source appeared on the photographic plate displaced axially 5 mm from the spectrum of particles emitted from the target. The angle of observation, $150.2\pm0.2°$, and the bombarding energies were chosen so that the alpha-calibration line lay very near the line whose energy was to be measured. The plate was exposed simultaneously to the calibration alphas and the reaction products, and thus any drift in

* Assisted by the joint program of the ONR and AEC and by the Swedish Atomic Committee.
† On leave from the Nobel Institute of Physics, Stockholm, Sweden.
[1] Bergstrom, Thulin, Svartholm, and Sieghahn, Ark. Fys. 1, 281 (1949).
[2] C. Mileikowsky and R. Pauli, Ark. Fys. 4, 299 (1952).
[3] Herb, Snowden, and Sala, Phys. Rev. 75, 246 (1949).

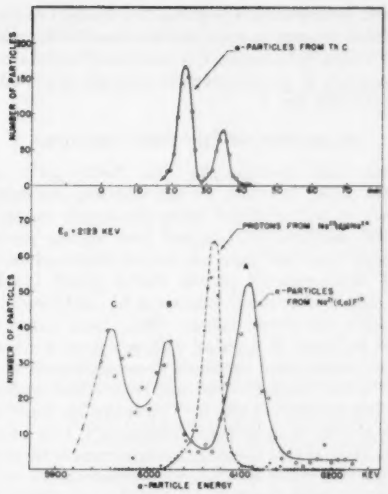

FIG. 1. Alpha-spectrum from $Ne^{21}(d,\alpha)F^{19}$. The group marked *A* corresponds to transitions to the ground state of F^{19}; groups *B* and *C* are attributed to transitions to states in F^{19} at 113±8 kev and 192±12 kev above the ground state. The dot-dashed part of peak *C* is obtained from plates exposed at a lower magnetic field. The ThC lines which were used to calibrate the energy scale are shown in the upper figure, plotted against the radial displacement from the end of the photographic plate. The energy scale is different for protons and alphas; $E_{\text{proton}}=0.9931E_\alpha$. The dotted curve shows the protons from the reaction $Na^{23}(d,p)Na^{24}$.

the magnetic field during an exposure would appear in the width of the calibration alpha-line. The magnetic field was monitored continuously during an exposure with a fluxmeter of the type that has been described previously.[4] The method of preparing the alpha-sources and the method of measuring the angle of observation have also been described.[5]

III. RESULTS

A. $Ne^{21}(d,\alpha)F^{19}$

The spectrum observed at a bombarding energy of 2.129 Mev is shown in Fig. 1. The upper curve shows the two alpha-calibration lines from ThC. The energies assigned to these two alpha-lines are 6.038±0.003 Mev and 6.078±0.003 Mev calculated from Briggs'[6] measurement of $H\rho$ for RaC and the Cavendish measurements[7] of the ratios of the velocity of the thorium alpha-particles to the velocity of the RaC alpha-particles. A 4-kev correction in this calculated energy has been included for the penetration of the recoil ThB nucleus into the target backing. The group of alpha-particles marked *A* is from the $Ne^{21}(d,\alpha)F^{19}$ reaction and has an energy of 6.106 Mev which is obtained by a linear extrapolation of the momentum scale set by the calibration alpha-lines.

The target surfaces were slightly discolored, and it would appear that during the course of the Ne^{21} bombardment carbon also was deposited on the surface. Thus the observed energy must be corrected for the energy loss of the alpha-particles in this contamination layer on the surface of the target. The thickness of this layer was measured by observing the energy of deuterons scattered from the face of the target and comparing this energy with the energy of deuterons scattered from a clean evaporated silver surface. In this measurement the photographic plate was replaced by collecting slits and a scintillation counter, and the magnetic field was varied to observe the spectrum. Figure 2 shows these two spectra, from which it appears that the layer on the surface is 3.6 kev thick, for deuterons of 873 kev. The two steps are displaced by twice this amount since the deuterons pass through the layer twice. The 6-Mev alpha-particles would lose 5.9 kev in passing through this layer. Two Ne^{21} targets were used in the present work, one with a contamination layer of 3.6 kev for 873-kev deuterons, one with a layer of 11 kev. By comparing the energy of the $Ne^{21}(d,\alpha)F^{19}$ alpha-particles from the two targets, it was found that the Ne^{21} was distributed throughout the contamination layer, as would be expected if the contamination were laid down during the Ne^{21} bombardment in the isotope separator. Hence the energy of the emitted alpha-particles has been corrected for penetration through only one-half of the surface layer. Four measurements of this alpha-particle energy were made, and the corresponding *Q*-value is 6.432±0.010 Mev; relativistic effects have been included in the calculation of the *Q*-value, and nuclear masses have been used. The contributions to the probable error are summarized in Table I.

Two other lines marked *B* and *C* appear in our ex-

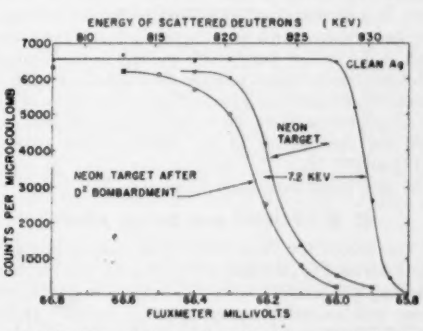

FIG. 2 Spectrum of deuterons scattered from clean silver and from the neon target before and after 1000-microcoulomb deuteron bombardment. The incident deuteron energy is 873 kev.

[4] C. C. Lauritsen and T. Lauritsen, Rev. Sci. Instr. **19**, 916 (1948).
[5] W. Whaling and C. W. Li, Phys. Rev. **81**, 150 (1950).
[6] G. H. Briggs, Proc. Roy. Soc. (London) **A157**, 183 (1936).
[7] W. B. Lewis and B. U. Bowden, Proc. Roy. Soc. (London) **A145**, 235 (1934).

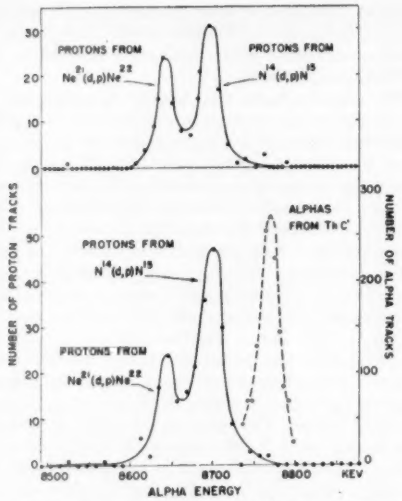

FIG. 3. The proton spectrum from $Ne^{21}(d, p)Ne^{22}$ and $N^{14}(d, p)N^{15}$, at a deuteron bombarding energy of 1.354 Mev. The upper and lower curves were obtained with two different targets. The dotted curve shows the alpha-line from ThC′ used to calibrate the energy scale for the lower curve. The energy scale is different for proton and alphas, $E_{proton}=0.9931E_{\alpha}$.

posures. The variation of their energy with changes in the deuteron bombarding energy indicates a target nucleus of mass 21±4, and we attribute these lines to the $Ne^{21}(d, \alpha)F^{19}$ reaction leading to states in F^{19} at 113±8 kev and 192±12 kev above the ground state. These levels have not been reported earlier.

B. $Ne^{21}(d, p)Ne^{22}$

The spectrum of protons observed at a bombarding energy of 1.354 Mev is shown in Fig. 3. The protons from the $Ne^{21}(d, p)Ne^{22}$ reaction have very nearly the same energy as the protons from the $N^{14}(d, p)N^{15}$ reaction. In a plate exposed at 1.850-Mev deuteron energy, the two proton groups were not resolved, but the variation of the proton energy with changes in the incident deuteron energy makes possible the resolution and identification of the proton groups. Taking the energy of the ThC′ calibration alpha-line to be 8.772±0.003 Mev, we find for the Q-value of the $Ne^{21}(d, p)Ne^{22}$ reaction 8.137±0.011 Mev. This value is lower than the value 8.34 Mev found from range measurements.[8]

C. $N^{14}(d, p)N^{15}$ and $Na^{23}(d, p)Na^{24}$

The proton line from $N^{14}(d, p)N^{15}$ shown in Fig. 3 has been used to calculate the Q-value for this reaction, yielding 8.613±0.011 Mev. This value is in good agreement with an earlier measurement by the MIT group[9] of 8.615±0.009 Mev. The proton line in Fig. 1 has been identified as coming from the reaction $Na^{23}(d, p)Na^{24}$ and yields a Q-value for this reaction of 4.723±0.008 Mev, again in good agreement with the MIT value, 4.731±0.009 Mev.[9]

IV. MASSES OF THE NEON ISOTOPES

From our Q-values for the $Ne^{21}(d, \alpha)F^{19}$ and $Ne^{21}(d, p)Ne^{22}$ reactions we can calculate the atomic masses of Ne^{21} and Ne^{22} using the atomic masses of H^1, D^2, He^4, and F^{19} obtained from nuclear reaction energies,[10] and Ne^{20} mass can then be obtained from the MIT measurement[11] of the $Ne^{20}(d, p)Ne^{21}$ Q-value. We assume that the Q-values can be used directly to calculate the *atomic* masses. These mass values are listed in Table II together with recent mass spectroscopic values based on Ewald's[12] measurements of the $D_2O^{16}-Ne^{20}$, $D_2HO^{16}-Ne^{21}$, and $D_3O^{16}-Ne^{22}$ doublets; the first doublet has also been measured by Nier[13] who finds a value in agreement with Ewald's. It is evident from Table II that there is good agreement between the nuclear and mass spectroscopic measurements of the masses of Ne^{20} and Ne^{22}; for Ne^{21}, however, there is a discrepancy of 109 μMU. The agreement between the nuclear and mass spectroscopic values for Ne^{20} and Ne^{22} may be interpreted as lending mass spectroscopic support to our mass of Ne^{21}, since the nuclear transmutation mass values for Ne^{20} and Ne^{22} are obtained directly from the nuclear transmutation mass of Ne^{21}.

With the value of the $Ne^{21}(d, p)Ne^{22}$ Q-value we are able to check the consistency of the following cycle of nuclear reactions: $Ne^{21}(d, p)Ne^{22}$, $Ne^{22}(d, p)Ne^{23}$, $Q=2.964$ ±0.007 Mev;[9] $Ne^{23}(\beta)Na^{23}$, $Q=4.21\pm0.015$ Mev;[14] and $Na^{23}(d, \alpha)Ne^{21}$, $Q=6.902\pm0.010$ Mev.[9] The cycle so formed fails to close by 178 kev, which is far more than the quoted errors would allow. If all the measurements are correct, it would appear that one of the measured transitions may not go to the ground state. In view of the fact that the earlier range measurement of the $Ne^{21}(d, p)Ne^{22}$ Q-value gave a result which would close the cycle, we emphasize that we have examined the region of the spectrum where the protons corresponding to the higher Q-value would fall and find none. Further evidence that the protons we observe correspond to the ground state transition lies in the agreement with

TABLE II. Masses of the neon isotopes, in atomic mass units.

From nuclear data	19.998	773±27	21.000	502±25	21.998	356±28
From mass spectroscopy	19.998	771±12	21.000	393±22	21.998	329±19

[8] J. Ambrosen and K. M. Bisgaard, Nature **165**, 888 (1950).
[9] Strait, Van Patter, Buechner, and Sperduto, Phys. Rev. **81**, 747 (1951).
[10] Li, Whaling, Fowler, and Lauritsen, Phys. Rev. **81**, 512 (1951).
[11] Van Patter, Sperduto, Endt, Buechner, and Enge, Phys. Rev. **85**, 142 (1952).
[12] H. Ewald, Z. Naturforsch. **6A**, 293 (1951).
[13] A. O. Nier, Phys. Rev. **81**, 624 (1951).
[14] H. Brown and V. Perez-Mendez, Phys. Rev. **78**, 812 (1950).

Ewald's value for the mass of Ne^{22}, and in the agreement with Middleton's range measurement[15] of the energy of the alpha-particles from $Ne^{22}(d,\alpha)F^{20}$.

[15] R. Middleton and C. T. Tai, Proc. Phys. Soc. (London) **A64**, 801 (1951).

We are grateful to Civ. Ing. S. Thulin, Nobel Institute of Physics, for preparing the targets, to Professor W. W. Buechner for valuable advice on his experience with neon targets, and to Mr. H. H. Woodbury of this laboratory for assistance in exposing the plates.

PHYSICAL REVIEW VOLUME 88, NUMBER 6 DECEMBER 15, 1952

The Beta-Decay of F^{20}†

DAVID E. ALBURGER
Brookhaven National Laboratory, Upton, New York
(Received July 25, 1952)

The beta-decay of F^{19} has been investigated with a lens spectrometer using sources activated by the $F^{19}(d,p)F^{20}$ reaction. A simple beta-ray spectrum of allowed shape is observed having an end-point energy of 5.406±0.017 Mev. Beta-emission is followed by a 1.631±0.006 Mev gamma-ray from an excited state of Ne^{20}. The gamma-ray energy was checked by comparing with the Sb^{124} gamma-ray, measured as 1.692±0.005 Mev, and by failure to observe photoneutrons from Be. Beta-ray branching to the ground state of Ne^{20}, if present, has a relative intensity of less than 1 percent. The total F^{20} disintegration energy, 7.038±0.018 Mev, is used together with other nuclear data to derive a Ne^{20} mass which is independent of mass spectrographic measurements. The result, $Ne^{20} = 19.998794 \pm 0.000026$ amu, is in agreement with mass spectrographic values.

INTRODUCTION

UP to the present the scale of accurate atomic mass values[1,2] based solely on nuclear measurements has extended only up to F^{20}. Isotopes in the mass region from Ne^{20} to sulfur are interconnected by beta-decay energies and reaction Q-values which have errors of less than 20 kev. However, this group of elements has been linked to O^{16} only through mass spectrographic work owing to the lack of accurate nuclear data connecting the isotopes of fluorine and neon.

Several ways of bridging this gap by means of nuclear measurements are apparent. One such method is the determination of the ground state Q-value of the $Ne^{21}(d,\alpha)F^{19}$ reaction, a problem which might not be expected to be easy because of the relatively low abundance of Ne^{21} in ordinary neon and the difficulty of making a suitable target.

A second possibility consists of determining the total disintegration energy of F^{20}. It is known[3] that this isotope decays to Ne^{20} by emission of hard beta-rays with a half-life of 12 seconds and that most of the beta-rays are in coincidence with 1.6-Mev gamma-rays corresponding to a level in Ne^{20}. Evidence has been found for complexity of the beta- and gamma-ray spectra. Jelley has reported[3] a single beta-ray group of endpoint energy 5.03±0.05 Mev and two gamma-rays of 1.63±0.02 Mev and 2.45±0.06 Mev having an intensity ratio of 8.4 to 1. On the other hand, Littauer has found[4] a weak gamma of 1.0±0.1 Mev in addition to the one of 1.63 Mev. He also reports that the main beta-component has a 5.33±0.05 Mev end point and that 3.5 percent of the beta-decays proceed to the ground state of Ne^{20} and have an end-point energy of 6.74±0.1 Mev. The value 6.66±0.05 Mev given by Jelley as the total F^{20} disintegration energy disagrees beyond the stated errors with 6.96±0.05 Mev obtained from Littauer's data. In either case the probable error is too large to use the result in establishing a mass scale involving only measurements having errors of less than 20 kev.

Because of the desire to obtain a more accurate total disintegration energy and at the same time to examine the possible complexities in the beta- and gamma-ray spectra it was felt that an investigation of the F^{20} beta-decay should be made.

GAMMA-RAY MEASUREMENTS

A lens spectrometer employing ring focus was used to study the gamma-ray spectrum from sources of F^{20} produced by the $F^{19}(d,p)F^{20}$ reaction. A 1.8-Mev deuteron beam at a current of 5 μamp was furnished by the Brookhaven electrostatic accelerator and was allowed to strike a thick CaF_2 target located in a brass cup at the normal source position of the spectrometer. Photoelectric converters consisting of uranium foil were attached to the cup whose walls were thick enough to stop the energetic beta-rays. The spectrometer was located 17 feet from the magnetic analyzer of the accelerator and the beam was brought through an extension tube.

In the first tests in which the spectrometer and accelerator vacuum systems were connected together it was found that N^{13} activity, produced by deuteron bom-

† Under contract with the AEC.
[1] Li, Whaling, Fowler, and Lauritsen, Phys. Rev. **83**, 512 (1951).
[2] D. M. Van Patter, Massachusetts Institute of Technology Technical Report No. 57 (1952) (unpublished).
[3] J. V. Jelley, Phil. Mag. **41**, 1199 (1950).
[4] R. M. Littauer, Phil. Mag. **41**, 1214 (1950).

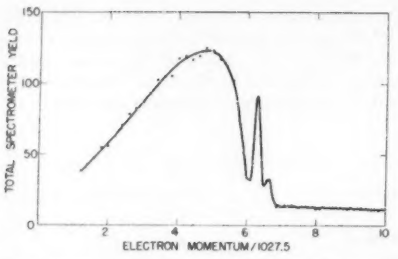

FIG. 1. Spectrum of Compton and photoelectrons due to F^{20} gamma-radiation. A 40-mg/cm² U converter was used.

bardment of carbon-containing deposits on the defining apertures, diffused to the detector end of the spectrometer chamber and caused a high and variable background. When the vacuum systems were separated, the background was low and the data were reproducible within the statistical errors.

Because of the short half-life of the F^{20} activity a monitoring technique was used to normalize the spectrometer yield. The monitor was a gamma-ray Geiger counter located near the source end of the instrument, while the spectrometer detector was an end-window Victoreen counter. The monitor was shielded by lead on all sides except in the direction of the source. The procedure for taking data consisted of irradiating the target for 12-15 seconds, shutting off the beam by turning down the accelerator voltage, and recording the spectrometer yield occurring during a fixed number of monitor counts. Only one point was taken for each irradiation and the actual length of the counting interval was generally about 20 seconds. During the target bombardment the voltages on the monitor and spectrometer counter tubes were reduced below threshold in order to avoid the extremely high counting rates due to prompt gamma-rays.

Figure 1 is a curve of total spectrometer yield *versus* momentum taken with a 40 mg/cm² thick uranium converter at 3 percent spectrometer resolution. The spectrum has the normal shape expected of a single gamma-ray line and gives no indication of other photoelectron peaks or Compton electron groups being present. The region above 1.6 Mev was examined with particular care in an effort to locate photoelectrons due to the 2.45-Mev gamma-ray reported[3] by Jelley.

The energy of the F^{20} gamma-ray was determined by comparing the photoelectric peaks from a 23.8-mg/cm² uranium converter with those produced by the 1.332± 0.001-Mev gamma-ray[5] of Co^{60}. In all such measurements the resolution baffle settings were kept fixed and the position of the converter was reproduced as closely as possible. By using data such as that shown in Fig. 2, the F^{20} energy was determined (1) from the *K*-line peak position, assumed to be shifted by half the energy thickness of the converter, and (2) directly from the high energy extrapolated edge of the *K*-line according to the technique developed[6] by Hornyak, Lauritsen, and Rasmussen. The average of all such determinations of the F^{20} gamma-ray energy is 1.631±0.006 Mev in agreement with the previous but less accurate measurements.[3,4]

Wattenberg has reported[7] that photoneutrons are produced in Be by F^{20} gamma-rays corresponding to an intensity greater than 10 percent per beta-ray. Since the $Be^9(\gamma,n)Be^8$ threshhold is now established as 1.666±0.002 Mev by the measurement[8] of Mobley and Laubenstein, it would appear that the present result, which indicates that the F^{20} gamma-ray energy is definitely below the $Be(\gamma,n)$ threshhold, represents a discrepancy with the data of Wattenberg.

In order to obtain a check on the F^{20} gamma-ray, a comparison measurement was made on the 1.7-Mev gamma-ray of Sb^{124}. This has been reported as having an energy of 1.708±1 percent according to Kern, Zaffarano, and Mitchell,[9] and Cook and Langer[10] and 1.69± 0.02 Mev according to Feister and Curtiss.[11]

The photoelectron spectrum of the 1.7-Mev gamma-ray obtained with a 0.2-mC source of Sb^{124} and the same converter and spectrometer geometry as for Co^{60} and F^{20} is included in Fig. 2. The decreasing yield at the right is part of the Compton spectrum of the weak 2.1-Mev gamma-ray.[9,10] The best average value for the energy, obtained from the peak and from the extrapolated end point of the *K* line, is 1.692±0.005 Mev.

The close proximity in energy of the Sb^{124} and F^{20} gamma-rays allows these independent values to be compared by measuring the momentum separation of the conversion lines. This was done by matching the

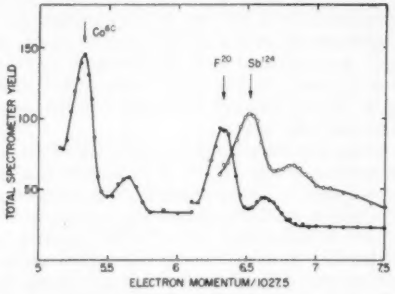

FIG. 2. A comparison of the relative momenta of photoelectron lines from a 23.8-mg/cm² U converter due to the gamma-rays of Co^{60}, F^{20}, and Sb^{124}.

[5] Lind, Brown, and DuMond, Phys. Rev. **76**, 591 (1949).

[6] Hornyak, Lauritsen, and Rasmussen, Phys. Rev. **76**, 731 (1949).

[7] A. Wattenberg, Phys. Rev. **71**, 497 (1947).

[8] R. C. Mobley and R. A. Laubenstein, Phys. Rev. **80**, 309 (1950).

[9] Kern, Zaffarano, and Mitchell, Phys. Rev. **73**, 1142 (1948).

[10] C. S. Cook and L. M. Langer, Phys. Rev. **73**, 1149 (1948).

[11] I. Feister and L. F. Curtiss, J. Research Natl. Bur. Standards **40**, 315 (1948).

two curves over the entire photoelectron spectrum after normalizing to the same amplitude. The energy difference $Sb^{124}-F^{20}$ was found to be 60 kev in agreement with the 61-kev difference according to the direct determinations.

The measured value of the Sb^{124} gamma-ray would mean that an energy of 26±5 kev is available above the $Be^9(\gamma,n)Be^8$ threshhold corresponding to a photoneutron energy of 23±5 kev when the recoil of the Be^8 nucleus is taken into account. Hanson has measured[12] the Sb-Be photoneutron spectrum by examining proton recoils in a proportional counter. He obtained an average neutron energy of 24±3 kev in favorable agreement with the earlier values of Wattenberg, and of Hughes and Eggler,[13] which were 24±15 kev and 35± 10 kev, respectively. Hanson's measurement gives an excellent check on the Sb^{124} gamma-ray energy found here and adds further weight to the validity of the F^{20} value.

Finally, in collaboration with M. McKeown a search was made for Be photoneutrons resulting from the gamma-rays of F^{20}. The accelerator target was surrounded by Be and paraffin blocks, and a slow neutron BF_3 detector was placed in this structure. When the 0.2-mC Sb^{124} source was inserted near the fluorine target position, the photoneutron detector yield was about 2400 counts per minute. A gamma-ray counter was used to compare the strength of the Sb^{124} source with the average gamma-ray strength of the F^{20} activity. Irradiations of the target produced F^{20} sources having an average strength of about 2 mC during a 10-sec period immediately following bombardment.

A very weak short-lived photoneutron activity of 10-30 sec half-life was observed above background but the strength was too small to permit a determination of the half-life. If this yield is taken as an upper limit and if the source strength is normalized according to the data on Sb^{124}, then it may be shown that the F^{20} gamma-ray intensity capable of producing photoneutrons in Be corresponds to less than ¼ percent per beta-ray. The small yield actually observed could be due to bremsstrahlung or to target impurities. This result would rule out the presence of the 2.45-Mev gamma-ray reported[3] by Jelley.

The photoneutrons assigned to F^{20} by Wattenberg were probably due to the gamma-rays of N^{16}, an activity produced by fast pile neutrons according to the $F^{19}(n,\alpha)N^{16}$ re-action. McKeown has re-examined[14] this case using fluorine sources irradiated in the Brookhaven reactor. A strong photoneutron yield from Be was observed but showed only a single decay period of 7.5 seconds which is the known half-life of N^{16}.

[12] A. O. Hanson, Phys. Rev. **75**, 1794 (1949).
[13] D. J. Hughes and C. Eggler, Phys. Rev. **72**, 902 (1947).
[14] The author is indebted to Mr. McKeown for permission to quote his results.

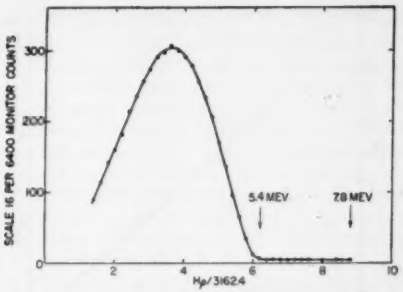

FIG. 3. Total spectrum of F^{20} beta-rays and scattered radiation *versus* momentum, after subtraction of a small room background.

BETA-RAY SPECTRUM

Examination of the F^{20} beta-spectrum was made with the lens spectrometer using BaF_2 targets 1–2 mg/cm² thick deposited on 0.05-mil nickel foil (160 kev thick for deuterons). The accelerator beam was first passed through a baffle system, then a central region of the target 8 mm in diameter, and finally into a Faraday cup for current measurement. The BaF_2 was deposited on the spectrometer side of the nickel supporting foil and its location was the same as that occupied by the uranium converter used in calibration measurements. In order to isolate the spectrometer vacuum chamber from the accelerator, thereby eliminating the diffusion of N^{13} activity, a gasketed section having a 0.05-mil nickel window was included in the beam tube baffle system. The two nickel foils thus reduced the beam from an initial energy of 1.9 Mev to about 1.6 Mev by the time the target material was reached. A deutron current of a few tenths μamp was sufficient to produce a usable F^{20} activity.

In all of the F^{20} beta-ray work the spectrometer resolution was 2.7 percent. Calibration of the instrument was carried out with 10-mC sources of Na^{24} prepared by irradiation of Na_2CO_3 in the reactor. A uranium converter 23.8 mg/cm² thick and 8 mm in diameter was attached to the source capsule and the position of the *K* photoelectron line due to the hard gamma-ray was determined. The binding energy of the *K* shell electrons in U was taken[15] as 115.6 kev and the peak shift due to the converter thickness was assumed to be 12.0 kev. The gamma-ray energy value, 2.753_8±0.001 Mev, recently reported[16] by Hedgran and Lind served as the calibration standard. To insure an accurate extrapolation above the calibration point, the coil current at each regulator setting was checked by measuring the voltage drop across the current shunt with a Leeds and Northrup type *K* potentiometer. The stability of the current was better than one part in 2000.

The procedure for monitoring the source strength

[15] Y. Cauchois, J. phys. et radium **13**, 113 (1952).
[16] A. Hedgrah and D. A. Lind, Ark. Fys. **13**, 178 (1952).

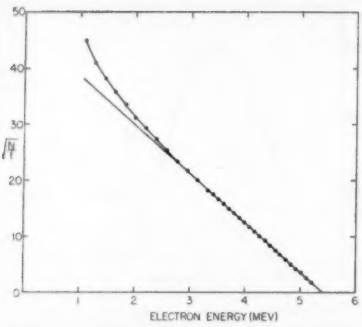

FIG. 4. Kurie plot of the F^{20} beta-ray spectrum.

and taking data was similar to that followed in the gamma-ray measurements already described. In Fig. 3 the curve of spectrometer yield *versus* momentum, after subtraction of a small room background, represents the average data of eight sets of interlaced points. Room background was determined at each point by allowing the F^{20} activity to decay for 10 half-lives and then observing the number of counts occurring in the same length of time as the corresponding counting interval. The magnitude of the room background was generally about $\frac{1}{3}$ as great as the yield shown in Fig. 3 beyond the spectrum endpoint.

The curve above 5.4 Mev is constant within statistics up to 7.8 Mev and is mainly due to scattered gamma- and beta-rays. A beta-ray group having an end point near 7 Mev and a relative intensity of as much as 1 percent would not be consistent with the data. This result is at variance with the 3.5 percent branch to the ground state of Ne^{20} found[4] by Littauer.

A Kurie plot of one of the more detailed runs on the F^{20} beta-spectrum, made after subtraction of the scattered background, is shown in Fig. 4. The calculations were carried out with the help of Fermi function tables prepared[17] by I. Feister and in every case the end point was determined by a least squares straight line fit to the uppermost 20 points. Two secondary values obtained by least squares straight line fits to the upper and lower 10 points of this group were also made, and the resulting end points always agreed with that obtained from all 20 points to within 5 kev. The accurate linearity of the Kurie plot in the upper half of the spectrum is evident from these calculations. The deviation from linearity at lower energies is probably reasonable in view of the source and backing thicknesses used.

The end-point energies obtained from the various runs, each of which was independently calibrated, occurred within a range of 11 kev. The best average value for the end-point energy is found to be 5.406± 0.017 Mev, where the assigned error is largely due to the location of the calibration peak. Errors in the correction for the peak shift due to converter thickness, the Na^{24} gamma-ray energy, linearity of the current regulator, and the determination of the end-point energy value were smaller than the calibration error but were included in estimating the over-all probable error.

[17] I. Feister (private communication).

DISCUSSION

The total F^{20} disintegration energy is found by adding to the sum of the beta- and gamma-ray values determined above the recoil energy imparted to the Ne^{20} nucleus as a result of beta-ray emission. The maximum recoil amounts to 940 ev, and to allow for this a 1-kev correction has been added although it is small compared with the assigned error. The F^{20} decay energy is therefore 7.038±0.018 Mev, where the probable errors of the beta- and gamma-ray measurements have been combined in the usual way.

The result may be used together with other nuclear data to derive a mass value for Ne^{20} which is related to O^{16} by means of nuclear disintegration and decay processes and is therefore independent of mass spectrographic measurements. The mass of F^{19}, 19.004456± (15) amu, quoted by Li *et al.* in their analysis[1] of light element masses as the best fit value according to nuclear reactions, has been taken as the base in calculating the Ne^{20} mass. The Q-value of the $F^{19}(d,p)F^{20}$ reaction, given[18] by Strait *et al.* as 4.373±0.007 Mev, may be combined with Li *et al.*'s F^{19}, giving a mass[19] of 20.006352± (17) amu for F^{20}. When the mass equivalent of the F^{20} disintegration energy found in the present work is subtracted from F^{20} the mass of Ne^{20} is found to be 19.998794±(26) amu. The relationship 1 amu = 931.152 Mev was used to convert the F^{20} disintegration energy to mass units.

It is of interest to compare this result with the most recent mass spectrographic values of Ne^{20}. The data with the highest quoted accuracy are those of Ewald,[20] who reports that Ne^{20} has a mass of 19.998771±(12) amu, while Nier's value[21] is 19.998835±(43) amu. In both cases the Ne^{20} mass was derived by measuring the separation between D_2O and Ne^{20}. Ewald's mass difference for this doublet is 30.688±0.010 mMU which agrees with that of Nier, 30.721±0.039 mMU, well within the combined errors. However, the mass defect of the deuterium atom used in calculating the Ne^{20} mass was different in the two cases. The mass defect of D measured by Ewald is 14.732±0.004 mMU which is in good agreement with the nuclear reaction value[1] 14.735±0.006 mMU, while Nier's measurement gives 14.778±0.008 mMU. Thus, in the calculation of Ne^{20}

[18] Strait, Van Patter, Buechner, and Sperduto, Phys. Rev. **81**, 747 (1951).

[19] This mass is the same as quoted by Li *et al.*, but the calculated error is 0.002 mMU smaller.

[20] H. Ewald, Z. Natursforsch. **6a**, 293 (1951).

[21] A. O. Nier, Phys. Rev. **81**, 624 (1951).

from D_2O-Ne^{20} a discrepancy of 0.092 mMU occurs between Ewald's and Nier's results just from the D mass defect used. If one were to correct Nier's data by using the nuclear reaction (or Ewald's) mass defect for D then his value of Ne^{20} would be 19.998749±(43) amu. Whether this correction is made or not, the Ne^{20} mass based on the present work agrees with both Ewald and Nier well within the combined probable errors.

The mass of F^{19} measured by Ewald, namely, 19.004414 ±(17) amu, and Li *et al.*'s value of 19.004456±(15) amu from nuclear data do not agree as well as in the Ne^{20} case, since the difference of 0.042 mMU is larger than the sum of the errors. Also, the F^{20} disintegration energy derived from Ewald's values for F^{19} and Ne^{20} and the Q-value of the $F^{19}(d,p)F^{20}$ reaction is 7.019±0.021 Mev, which is lower than the measured value but agrees within the errors. In summary, it appears that Ewald's mass value of Ne^{20} is in satisfactory agreement with nuclear data while his mass of F^{19} may be slightly low.

The F^{20} disintegration energy may be combined with the 4.529±0.007 Mev Q-value of the $Ne^{20}(d,p)Ne^{21}$ reaction,[22] the previously quoted Q of the $F^{19}(d,p)F^{20}$ reaction, and other data relating the d, p, and α masses to predict a ground state Q-value of 6.451±0.022 Mev for the $Ne^{21}(d,\alpha)F^{19}$ reaction. A direct experimental determination of this Q-value would be very worth while.

The linearity of the F^{20} beta-ray Kurie plot and the logft value of 5.0, calculated from Moszkowski's curves,[23] show that the transition is allowed according to Nordheim's classification.[24] The accurate linearity exhibited by the least squares analyses previously mentioned is a further argument against the presence of a level in Ne^{20} at 2.45 Mev excited to an extent reported[3] by Jelley. The ground state of the even-even nucleus Ne^{20} doubtlessly has zero spin and even parity, while the first excited state at 1.6 Mev probably has spin 2 and even parity according to the empirical rule[25] of Goldhaber and Sunyar. It would appear that F^{20} should have a spin of 2 or 3 and even parity based on the above assumptions and the lack of transitions to the ground state of Ne^{20}. Using the 1 percent upper limit of intensity previously quoted a transition to the ground state would have a log ft greater than 7.5 and would therefore be at least first forbidden.[24]

In either case a spin of 2 or 3 and even parity for F^{20} would fit the shell model picture. The odd proton should be $s_{\frac{1}{2}}$ and the odd neutron $(d_{5/2})^5{}_{5/2 \text{ or } 3/2}$. These could combine to give spin 2 or 3 and in all cases the parity would be even.

In connection with the attempts to observe photoneutrons from Be due to F^{20} gamma-radiation an interesting feature was pointed out[26] by Goldhaber. The energy of the F^{20} gamma-ray, according to the present measurement, occupies the unique position of lying below the $Be^9(\gamma,n)Be^8$ threshhold but above the threshhold for the direct breakup of Be^9 into two alpha-particles and a neutron. The threshhold energies of these two processes are known from other information to be about 90 kev apart. The small upper limit of photoneutron yield established in this work shows that the cross section for the three-particle reaction in the neighborhood of 60 kev above threshhold is less than 10^{-30} cm^2.

The author is indebted to M. McKeown for collaborating in the photoneutron measurements and to M. Goldhaber and H. Motz for helpful discussions of the results.

[22] Van patter, Sperduto, Endt, Buechner, and Enge, Phys. Rev. **85**, 142 (1952).
[23] S. A. Moszkowski, Phys. Rev. **82**, 35 (1951).
[24] L. W. Nordheim, Phys. Rev. **78**, 294 (1950).
[25] M. Goldhaber and A. W. Sunyar, Phys. Rev. **83**, 906 (1951).
[26] M. Goldhaber (private communication).

The Disintegration Scheme of V^{48}†

PAUL L. ROGGENKAMP, CHARLES H. PRUETT, AND ROGER G. WILKINSON
Indiana University, Bloomington, Indiana

(Received August 28, 1952)

The disintegration scheme involved in the decay of 16-day V^{48} to Ti^{48} has been established by scintillation studies, and spins and parities have been assigned to the levels. The angular correlation of the well-known cascade gamma-ray pair with energies of 0.99 and 1.32 Mev has been measured. The corresponding levels are found to have spins 0–2–4. The positron spectrum has been measured with a magnetic beta-ray spectrometer and shows evidence for positron emission to a level in Ti^{48}, 22.2 Mev above the ground state. The positron group involved in the decay to the 2.31-Mev level of Ti^{48} is found to have an end point of 0.69 Mev.

INTRODUCTION

THE general features of the decay of 16-day V^{48} are well known. The disintegration by K-capture and positron emission to an excited state of Ti^{48} is followed by the emission of two cascade γ-rays of energies 1.32 and 0.99 Mev.[1–3] In addition, a third γ-ray of energy 2.22 Mev is present in 1–5 percent of the disintegrations.[4–6] The recent scintillation spectrometer work of Miller[5] and Ticho *et al.*[6] exclude the assignment of this γ-ray as the cross-over transition. Miller has found that the de-excitation of Ti^{48} following the β-decay of Sc^{48} is accompanied by the 1.32- and 0.99-Mev γ-rays only. The 2.22-Mev γ-ray, if present at all in the Sc^{48} decay, is estimated to have an intensity not more than 10^{-3} of the intensity of the 1.32-Mev γ-ray. In the V^{48} decay, on the other hand, the intensity of the 2.22-Mev radiation is found to be approximately 2 percent of the 1.32-Mev γ-ray. This view is supported by the careful energy measurements of Ticho *et al.* They find that the high energy γ-ray is about 90 kev less in energy than the sum of the 0.99- and 1.32-Mev energies. Moreover, as has been pointed out by Miller, no possible spin assignment of the excited levels can account for a cross-over having the lifetime ($<10^{-7}$ sec) and intensity of the 2.22-Mev γ-ray.

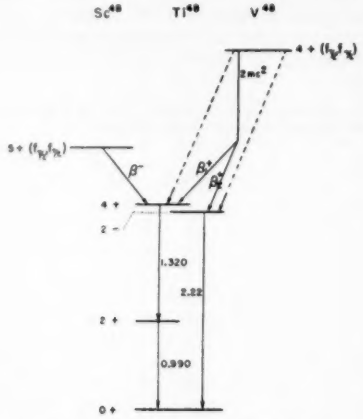

FIG. 1. Disintegration scheme of V^{48}.

In this paper, the results of further experiments which clarify the decay scheme of V^{48} are presented. The level system, shown in Fig. 1, has been verified by coincidence scintillation spectrometry. The directional correlation of the cascade γ-rays has been measured and fairly definite spin assignments made for the corresponding levels. Finally, the positron and negatron spectrum have been re-investigated with a magnetic beta-ray spectrometer, in order to obtain more information concerning the level at 2.22 Mev.

EQUIPMENT

The same apparatus is used for coincidence spectrometry measurements and angular correlation studies. For coincidence studies the source is placed midway between two $\frac{3}{4}$-in. cubical NaI(Tl) crystals $\frac{1}{2}$ in. off the line joining their centers. The crystals are mounted in air-tight Lucite holders filled with vacuum-dehydrated mineral oil. The crystal containers are mounted on selected RCA 5819 photomultiplier tubes. Light-tight aluminum housings enclose the photomultiplier tubes. The distance between the two counters can be varied from 2.5 in. to 8 in. No "sum" lines are observed under these conditions. Lead shielding between the counters minimizes crystal-to-crystal scattering.

The electronic circuits are for the most part conventional. The high voltage for the 5819's is furnished by an electronically stabilized supply, the output of which is continually monitored with a potentiometer. The voltage applied to the tubes is maintained constant to within ± 0.1 percent for the duration of a run. Thermal drifts are minimized by maintaining the room temperature constant to within two degrees. Cathode follower preamplifiers are mounted adjacent to the 5819 tube sockets to allow the use of leads less than 5 cm long. The pulses from the cathode followers are amplified by Atomic Instruments Model 204-B linear

† Supported by the joint program of the ONR and AEC.

[1] W. C. Peacock and M. Deutsch, Phys. Rev. **69**, 306 (1946).
[2] Good, Peaslee, and Deutsch, Phys. Rev. **69**, 313 (1946).
[3] Robinson, Ter-Pogossian, and Cook, Phys. Rev. **75**, 1099 (1949).
[4] R. G. Fluharty and M. Deutsch, Phys. Rev. **76**, 182 (1949).
[5] Maurice M. Miller, Phys. Rev. **88**, 516 (1952).
[6] Ticho, Green, and Richardson, Phys. Rev. **86**, 422 (1952).

amplifiers which are operated with 0.2 μsec rise times. Pulses out of the two amplifiers are fed into fast single channel differential pulse-height selectors which are modifications of the circuit described by Roulston.[7] This circuit has a dead-time of about 1 μsec and is especially useful in coincidence work in which high singles counting rates are encountered. The usual disadvantages of a circuit containing no elaborate pulse shaping devices, "window amplifiers" etc., are present. However, the attendant variation of effective slit width with pulse-height setting and slit width instability in time is more than offset by the speed of the circuit, since large slit widths are generally used. The outputs of the two single channel discriminators are mixed in a coincidence circuit which uses a delay line pulse shaper to obtain a resolving time of 0.15 μsec. Delayed coincidence studies are accomplished by inserting a variable delay line in either channel.

For angular correlation measurements, one of the counters can be positioned on a circle at angles from 85° to 275° with respect to the second (fixed) counter. The source, in this case, is placed on the axis of rotation. The instrument is designed to allow accurate repositioning at any angle and possesses practically no geometrical asymmetry. Asymmetries in counting rates due to stray magnetic fields are minimized by the use of Mumetal shields. The source-to-crystal distance can be varied continuously from 1.5 in. to 4.5 in. For the $\frac{3}{4}$-in. crystals used, these limits correspond to angular resolutions of 9° and 25° as determined from annihilation radiation coincidence measurements.

Since only pulse heights in desired ranges are accepted in each channel the correlation between two selected γ-rays may be studied with little or no interference from scattering or other undesired γ-rays. Lead shields are placed between the counters only in certain special instances in which multiple scattering may be a problem.

The beta-ray experiments were carried out with a small 180° shaped field spectrometer having a resolution of about 1.5 percent and a transmission of about 1.5 percent. Although the basic radius of curvature of the instrument is only 7.5 cm, scattering effects are kept to a minimum by the focusing action and by the large dimensions of the vacuum chamber.

SOURCES

The V^{48} used in these experiments was produced by $Sc^{48}(\alpha, n)V^{48}$ in the Indiana University cyclotron. The Sc was removed by repeated *HF* precipitation and centrifugation. Impurities such as Cu and Ga were removed by *HS* precipitation and ether extraction. Sources reasonably free of carrier were finally obtained by electrodeposition from a dilute and slightly basic solution. While no V carrier was added, a small amount of foreign material, probably iron, plated out with the V^{48}. Sources for the coincidence spectrometry were prepared by placing one small drop of vanadium chloride in a cylindrical Lucite cup. Over-all source dimensions were of the order of 2 mm for most measurements. The beta-ray spectrometer sources were made in the conventional manner.

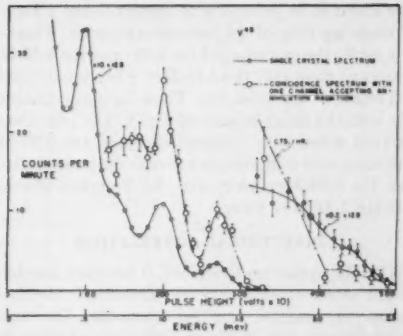

FIG. 2. Single channel and coincidence spectra of the γ-rays of V^{48}. The prominent peaks are due to γ-rays at 0.511 Mev (annihilation radiation), 0.99 Mev, and 1.32 Mev. The curves at the right are an expanded plot in the region of the 2.22-Mev γ-ray. The energy scale is obtained by calibration with Cs^{137}.

COINCIDENCE SPECTROMETRY

The single crystal spectrum and a coincidence spectrum are shown in Fig. 2. Prominent photoelectron peaks in the single crystal spectrum correspond to the 0.511-Mev annihilation radiation and the well-known γ-rays of energies 0.99 and 1.32 Mev. In addition, a weak line corresponding to the high energy γ-ray is found at 2.2 Mev. By rough estimate (the usual corrections applied) the 2.22-Mev γ-ray is found to have about 2 percent the intensity of the 1.32-Mev γ-ray. The coincidence spectrum shown in Fig. 2 was obtained by setting one channel to accept the annihilation photopeak while scanning the remainder of the spectrum with the other channel. The curve represents the coincidence rate between the two channels, corrected for chance coincidences, *versus* discriminator setting of the variable channel. The energy scale was obtained by calibration with the Cs^{137} photoelectron peak. The true-to-chance coincidence ratio ranged from 10 for the 0.99-Mev peak to 2 for the 2.22-Mev peak. The coincidence spectrum clearly shows that all three γ-rays are in coincidence with the annihilation radiation and hence with the positrons.

The results of other coincidence measurements are as follows. With the fixed channel adjusted to accept the 0.99 peak, coincidence spectrum peaks were observed at 0.99 and 1.32 Mev, but none at 2.22 Mev. When the fixed channel was set on the 2.22-Mev peak, no coincidences above chance were recorded at 0.99 or 1.32 Mev. In all of the experiments the coincidences

[7] K. I. Roulston, Nucleonics **7**, 27 (1950).

were found to be prompt with respect to the 1.5×10^{-7} sec resolving time of the coincidence circuit. These results verify the cascading of the 0.99- and the 1.32-Mev γ-rays and show that the 2.22-Mev γ-ray is not coupled with either of the other two. These facts are consistent only with the decay scheme of Fig. 1. The coincidences observed when both channels accepted the 0.99-Mev peak are due to coincidences between the photoelectrons from the 0.99-Mev γ-ray and the Compton electrons from the 1.32-Mev γ-ray.

DIRECTIONAL CORRELATION

With the apparatus described, it becomes possible in certain cases to extend $\gamma-\gamma$ directional correlation studies to positron emitting elements. The strong angular correlation of the annihilation radiation ordinarily present is not troublesome in this case since the γ-rays involved, 0.99 and 1.32 Mev, give rise to photoelectron peaks which are well beyond the annihilation radiation peak. The amplifier gains were adjusted so that the pulse heights due to the γ-rays were approximately the same in each channel. Figure 3 shows a typical singles spectrum as obtained in either channel with a 1.5-volt slit. In order to enhance the true-to-chance coincidence ratio, coincidence counts were taken with slits wide enough (13.5 volts) to accept the photoelectrons of both γ-rays and with the discriminators set high enough to exclude annihilation radiation. Coincidence counting rates in the three runs taken ranged from 15 to 30 counts per minute with corresponding true-to-chance ratios from 12 to 5. Total counts of about 5000 were recorded in each run at the intermediate settings and approximately 10,000 counts at 90° and 180°. An angular resolution of 20° was used. Correction for this effect was less than the expected statistical fluctuation. The results are shown in Fig. 4. The measured asymmetry coefficient $[n(180)-n(90)]/n(90)$ is 0.171 ± 0.02. The solid curve in Fig. 4 is a plot of the theoretical correlation function to be expected for spin assignments 0–2–4. As a check on the performance of the equipment, the well-known[8] correlation of Co^{60} was determined with the 13.5-volt slits. The expected correlation was found, the asymmetry coefficient being 0.147 ± 0.02. In addition, the contribution of the annihilation radiation was checked by repeating the experiment with Cu^{64}, with the discriminator settings and slit width the same as for the case of V^{48}. For sources of Cu^{64} comparable in intensity with the V^{48} sources, no effect was found. It seems reasonable to conclude that the spins of the levels involved in the cascade γ-rays emission are 0–2–4.

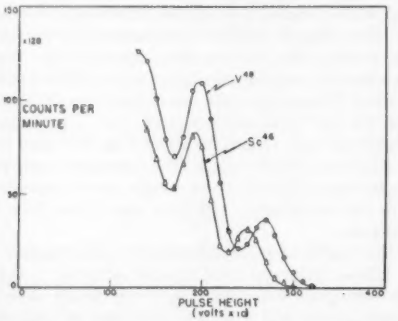

FIG. 3. Single channel spectra of the 0.89- and 1.12-Mev γ-rays of Sc^{46} and the 0.99- and 1.32-Mev γ-rays of V^{48} obtained with the same spectrometer conditions. The discriminator slit width was 1.5 volts.

MAGNETIC SPECTROMETER MEASUREMENTS

It seemed advisable, in view of the coincidence spectrometry results, to re-investigate the positron and electron spectra of V^{48}. A careful search was made for internal conversion lines in the region 70 to 120 kev. Since no lines were found, it is quite probable that there is no transition from the 2.31-Mev level to the 2.22-Mev level. Sources were too weak to study the photoelectrons of the 2.22-Mev γ-ray.

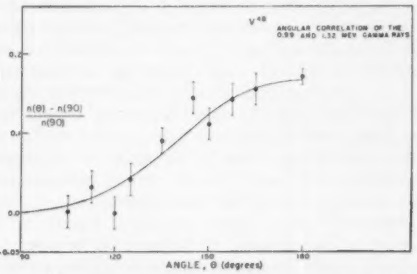

FIG. 4. The directional correlation of the 0.99 and 1.32-Mev γ-rays of V^{48}. The solid curve represents the theoretical correlation function $W(\theta)=1+0.125\cos^2\theta+0.042\cos^4\theta$.

Figure 5 shows a Fermi plot of the positron spectrum taken with a source 0.3 mg/cm² thick. In addition to the main group having an end point at 0.69 ± 0.01 Mev, there is evidence for a second group with an end point at approximately 0.82 Mev and 5 percent intensity. While the presence of this group seems fairly definite, it must be emphasized that the estimated intensity and end point may be quite in error. The small uncertainties in the background generally present in positron measurements are in this instance not negligible. Although careful background measurements were made at each point, errors are still large and accurate determination of the intensity and endpoint cannot be made until much stronger sources are available. It should be pointed out that every point was followed through nearly two half-lives and found to decay with a 16-day half-life. The departure from the straight line in the

[8] E. L. Brady and M. Deutsch, Phys. Rev. 78, 558 (1950).

neighborhood of 250 kev is somewhat surprising with the source thickness used, and it is possible that the spectrum possesses a shape other than allowed. This matter requires further study.

DISCUSSION

The foregoing results are summarized in the decay scheme presented in Fig. 1. The data pertinent to the discussion of the beta-rays and positrons involved in the decay to Ti^{48} are listed in Table I.

The values of the spins and parities $(0+, 2+, 4+)$ of the levels involved in the angular correlation make possible a quite consistent assignment of the remaining levels. An upper limit of 3 is already available to the spin of the 2.22-Mev level since the transition from this level is prompt with respect to 10^{-7} sec. According to the shell model the ground states of Sc^{48} and V^{48} are characterized by $(f_{7/2}f_{7/2})$ for the odd neutron and odd proton. Nordheim's[9] rules for such nuclei call for high spin and even parity for these levels. Therefore, a beta-ray or positron transition to the first excited state of Ti^{48} would involve no parity change, and the spins of the ground states of Sc^{48} and V^{48} must be at least 4 to account for the absence of these transitions. On the other hand, the transitions β^- and β_1^+ are characterized as allowed by their ft-values and the parity changes involved, so that the ground-state spins of Sc^{48} and V^{48} cannot be greater than 5. With the spins of these states thus limited to 4+ or 5+, the occurrence of the 2.22-Mev level in the V^{48} decay, and its absence in the Sc^{48} decay, can only be explained by assigning 5+ to the Sc^{48} ground state and 4+ to V^{48}. As a consequence of this, the spin and parity of the 2.22-Mev level must be 2− if it is to be populated in a measurable amount.

TABLE I. Data concerning the beta-rays and positrons involved in the decay to Ti^{48}.

	Intensity	Energy Mev	log ft	K/β^+
$\beta^-(Sc^{48})$	100%	0.64	5.4	
$\beta_1^+(V^{48})$	95%	0.69	6.1	0.7
$\beta_2^+(V^{48})$	~5%	~0.80	>7.4	>0.7(?)

The fact that no γ-transition was found between the 2.31- and 2.22-Mev level is in accord with these assignments. Furthermore, this transition is not expected since the 2.22-Mev γ-ray is not seen in the Sc^{48} decay. It is possible that the transition from the 2.22-Mev level to the first excited state exists. Its existence would be difficult to detect in the presence of the much stronger 1.32-Mev γ-ray. The intensity measurements, although subject to large errors, suggest that the 2.22-Mev γ-ray is not intense enough to account for all of the positrons, β_2^+. Furthermore, the coincidence studies (Fig. 2) suggest that K_2/β_2^+ is as large, or larger than K_1/β_1^+. A quantitative estimate of these ratios is not possible because of the large multiple scattering corrections. If the transition from the 2.22-Mev level to the 0.99-Mev level does occur, it does so in less than 3 percent of the disintegrations.

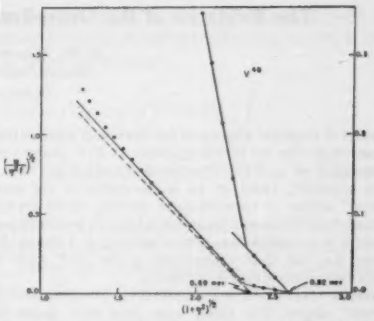

FIG. 5. Fermi plot of the beta-rays of V^{48} taken with a 180° shaped field spectrometer. The curve at the right is an expanded plot of the end-point region. The dotted line represents the Fermi plot of the main group of positrons.

Recently, it has been proposed[10,11] that the decay of Sc^{48} to Ti^{48} involves the excitation of a level one Mev above the 2.31-Mev level. It is certain from this work that such a level does not exist in the decay of V^{48} to Ti^{48}. This would mean that the photopeak of the 0.99-Mev γ-ray shown in Fig. 3 is actually due to two γ-rays. A comparison with the Sc^{46} photopeak is shown in Fig. 3. The curves were obtained under identical conditions. When account is taken of the small difference in energies of the higher energy γ-rays of Sc^{46} and V^{48}, the intensity ratios in the two cases are the same. It must be concluded that the 0.99 and 1.32 γ-rays of the V^{48} decay are of equal intensity if the γ-rays of Sc^{46} are of equal intensity as is generally established.

The authors wish to thank Dr. Milo B. Sampson and the cyclotron staff for the bombardments and Mr. Arthur Lessor for his assistance with the chemistry.

[9] L. W. Nordheim, Revs. Modern Phys. **23**, 322 (1951).

[10] D. Kurath, Phys. Rev. **87**, 528 (1952).

[11] Hammermesh, Hummel, Goodman, and Engelkemeir, Phys. Rev. **87**, 528 (1952).

The Evidence of the Once-Forbidden Spectra for the Law of β-Decay

H. M. MAHMOUD AND E. J. KONOPINSKI
Indiana University, Bloomington, Indiana
(Received August 20, 1952)

A series of empirical arguments has developed which leave two alternatives for the law of β-interaction: an *STP* (scalar+tensor pseudoscalar) or a *VTP* (*V*=vector) combination. We offer a new argument, based on an interpretation of the reported "allowed" shapes of once-forbidden spectra, which favors the *STP* over the *VTP* form. This new development may be important because it is a possible last step in arriving at a unique law of β-decay (i.e., all three components of the *STP* form would become both admissible and necessary).

A critical stage in the new argument is the explanation of the "allowed" shapes. The theory may yield such shapes if the Coulomb potential energy at the nucleus is sufficiently larger than the kinetic energy with which electron and neutrino are emitted. That condition happens to be best fulfilled just for the cases in which the "allowed" shapes are the most accurately observed. However, the dominance of the Coulomb effect cannot be a sufficient condition except with the *STP* or *VA* forms of β-interaction. Other forms make deviations from the allowed shape possible even when the Coulomb energy is supposed indefinitely large.

The last type of deviation has the same origin as the well-known Fierz interference in allowed spectra. The absence of the latter effect has been widely quoted but apparently never heretofore examined in detail. It is important in one of the series of arguments mentioned above. Hence, we investigate the empirical limits on Fierz-type deviations not only in once-forbidden but also in allowed spectra.

1. INTRODUCTION

THE Fermi theory of β-decay is not completely definite, even though it has dealt successfully with much that is known concerning β-processes. The definite part of the theory consists of criteria which are equally well satisfied by several specific formulations. The alternatives can be exhaustively enumerated in more ways than one. The customary way leads to a β-interaction expressed as an arbitrary linear combination of five "forms"; the scalar form, symbolized by *S*; the polar vector, *V*; the tensor, *T*; the axial vector, *A*; and the pseudoscalar, *P*. There has been a continuous effort to find and interpret experimental evidence that some definite combination of the five forms is the correct one.

The following points are currently regarded as having been established by the evidence:

I. The *T or A* forms must be part of the correct law of β-interaction. The main evidence is of two kinds. Only the *T*, or the *A*, form yields Gamow-Teller selection rules, which are needed for understanding the short lives of many β-transitions with a unit spin change. Only these two forms yield the "unique" spectrum shapes, found for *n*-times forbidden transitions in which the spin changes by $n+1$ units.

II. The *S or* the *V* form must also be included. The chief evidence for this is the short life found for β-transitions between nuclear states of zero spin, during the decay[1] of C^{10} and O^{14}. Forms other than the *S* or *V* lead to much smaller decay probabilities for these cases, relative to other transitions.

III. The *P* form is needed to explain the singular RaE spectrum, according to the analysis of Petschek and Marshak.[2] Actually, the *P* form is needed in combination with the *T* for this.

Each of the above arguments requires the inclusion of some component form without precluding the presence of other forms. The following argument seems to be the only generally recognized empirical one which tends to eliminate some of the possible combinations.

IV. It is usually regarded as evident that not both the *T* and *A* forms, nor both the *S* and *V* forms, can be parts of the β-coupling. If they are, then the spectra of allowed β-emission should be expected to deviate from the "allowed" (essentially statistical[3]) shape, through the operation of the so-called "Fierz interference." However, no unquestionable deviations have ever been found.[4]

Perhaps the weakest of the above arguments is **III**; points for and against it are put forward in Sec. 5. However, even if one accepts this one together with all the other arguments, they still do not lead to a unique law of β-interaction. They are equally consistent with either an *STP* or a *VTP* combination. We shall introduce here a possible method for deciding between those final two possibilities. Like **III**, and perhaps also **IV**, our new argument (**V**) needs further confirmation before it will become completely acceptable, but at present it points to the *STP* combination as the correct one. This development would be important because one will have finally arrived at a unique law of β-decay. The law would be unique in the sense that each of its component forms would be necessary, and also the only ones admissible. Formerly, it was not entirely clear that β-decay data alone would ever be able to lead to a unique law.

The argument **V** now offered is in one respect an extension of **IV**. A Fierz type of interference can be identified in the theory of once-forbidden spectra as

[1] Sherr, Muether, and White, Phys. Rev. **75**, 282 (1949); R. Sherr and J. Gerhart, Phys. Rev. **86**, 619 (1952).
[2] A. Petschek and R. Marshak, Phys. Rev. **85**, 698 (1952).
[3] What is generally called the "allowed shape" (linear Kurie plot) is here called the "statistical shape" because we consider at least the possibility that allowed spectra deviate from linearity on Kurie plots.
[4] C. S. Wu, Revs. Modern Phys. **22**, 386 (1950).

well as for allowed transitions. Whereas for the latter the Fierz interference arises only from SV and TA combinations, in the once-forbidden cases it also arises from SA, VT, and AP combinations. That such interference should not be admitted for once-forbidden spectra seems to be supported by evidence of the same kind as for allowed spectra: All the normal once-forbidden spectra are reported to have the statistical shape. (The one "abnormal" example, RaE, needs separate consideration, Sec. 5.)

An important preliminary to argument V is an explanation of how a once-forbidden spectrum may have a statistical shape even in the absence of Fierz interference. The various effects which can arise are differentiated in Sec. 2. The condition for a statistical shape then becomes expressible as: a large Coulomb energy, Ze^2/R, at nuclear radius R, as compared to the kinetic energy which the electron and neutrino finally obtain. This condition is best fulfilled just for the observed cases in which the statistical shape is best confirmed. Whether the condition is sufficiently well fulfilled for all cases reported to have the allowed shape is not easily settled because of the essential occurrence of nuclear matrix elements which can be only crudely estimated. Hence, in Sec. 2 we take the standpoint that the statistical shape is experimentally established and follow out its implications. The result is our argument V.

The importance of the experimental detectability of Fierz interference for both arguments IV and V leads us to make a critical examination of the data: in Sec. 3, the allowed transitions and in Sec. 4, the once-forbidden cases. The empirical limits put on the Fierz type of effect, in both kinds of spectra, are about equally narrow. However, because of the greater complication of the once-forbidden theory, the interpretation there is not as straightforward as it is for the allowed transitions. It becomes clear that measurements of once-forbidden spectra which show positive deviations from the statistical shape (low Z, high energy) are needed to check on our explanation of the cases of no deviation, before argument V can be regarded as established on the same footing as IV.

2. THE SIGNIFICANCE OF ONCE-FORBIDDEN SPECTRA WITH STATISTICAL SHAPES

We use notation in which the β-interaction energy density is

$$\Sigma_X G_X X + \text{Herm. conj.} \qquad (1)$$

with $X=S$, V, T, A, or P. Each of these five symbols stands for one of the interaction forms of the list (6a–e) of Konopinski.[5] Each G_X is a Fermi coupling constant, measuring the magnitude of interaction of form X which might be present in the correct law.

We present the theoretically expected spectra in terms of a "shape factor,"[6] C_n, which multiplies the well-known statistical factor to give the spectrum characteristic of the degree of forbiddenness, $n(=0, 1, 2\cdots)$. For allowed transitions,[7]

$$C_0=[G_S^2+\kappa^2 G_V^2 \pm (2\kappa/W)G_S G_V]\left|\int \beta\right|^2 + [G_T^2+\lambda^2 G_A^2 \pm (2\lambda/W)G_T G_A]\left|\int \beta\sigma\right|^2. \qquad (2)$$

The upper sign refers to positron, the lower to negatron, emission. Of course, the intrinsic signs of $G_S G_V$ and $G_T G_A$, as well as their magnitudes, are to be treated as unknown. The real[8] parameters κ and λ are defined by

$$\int 1 = -\kappa \int \beta \quad \text{and} \quad \int \sigma = -\lambda \int \beta\sigma, \qquad (3)$$

which are nuclear matrix elements to be found in reference 5. W is the electron energy, inclusive of rest mass, in units of mc^2.

The terms $\sim 1/W$ in (2) are the well-known Fierz interference terms. Their presence would cause allowed spectra to deviate systematically from a statistical shape. The apparent absence of such deviations is the basis of argument IV of the introduction. We proceed to show that interference effects of the same type can be identified in the theory of once-forbidden spectra.

The latter was worked out by Uhlenbeck and Konopinski[6] for each of the five interaction forms separately. Recently, Smith[9] and Pursey[10] calculated the contributions from the interference between the various forms. The resulting shape factor C_1, if written with the same generality as C_0 in (2), would require too formidable an expression for convenience. We therefore take several steps to simplify its exposition.

First, we restrict the name "once-forbidden" here to just the transitions having spin changes $\Delta I=0$ or ± 1, together with parity change. The $\Delta I=\pm 2$ transitions are well understood, as indicated in argument I of the introduction, and need no discussion here.

Second, we accept argument IV,[11] so that we need consider as possible alternatives for the β-law only the four arbitrary combinations: STP, SAP, VTP, or VAP.

Third, we separate the shape factor into three parts:

$$C_1=C_1^{(0)}+C_1^{(1)}+C_1^{(2)}. \qquad (4)$$

$C_1^{(0)}$ is to consist of the terms which contribute to $I_i=0\to I_f=0$ transitions. Then the S and V forms do not contribute to $C_1^{(0)}$ at all, and only $C_1^{(0)}(TP)$ and $C_1^{(0)}(AP)$ will be needed [(12) and (13)]. $C_1^{(1)}$ is to consist of terms which contribute to $\Delta I=\pm 1$ but not to $\Delta I=\pm 2$ (or $0\to 0$) transitions. The P interaction

[5] E. J. Konopinski, Revs. Modern Phys. **15**, 209 (1943).
[6] Called "correction factor" in the paper of E. J. Konopinski and G. E. Uhlenbeck, Phys. Rev. **60**, 308 (1941).
[7] M. Fierz, Z. Physik **104**, 553 (1937). The largest contribution of the P form is $G_P^2|\int \beta\gamma_5|^2$; it requires a nuclear parity change and so is classed as once-forbidden, rather than allowed.
[8] C. Longmire and A. Messiah, Phys. Rev. **83**, 464 (1951).
[9] A. Smith, Phys. Rev. **82**, 955 (1951).
[10] D. Pursey, Phil. Mag. **42**, 1193 (1951).
[11] Evidence for it is examined critically in Sec. 3.

TABLE I. Once-forbidden transitions.

	ΔI[a]	W_0	$\alpha Z/R(W_0-1)$	Ref.
Pm^{147}	5/2→7/2	1.415	49.5	b
W^{185}	3/2→5/2	1.84	27.5	c
Pr^{143}	5/2→7/2	2.82	11.8	c
Rb^{86}	?	2.44	11.0	d
Au^{198}	?	2.88	13.7	c
Ba^{139}	?	5.5	4.6	f
RaE	0→0(?)	3.29	11.5	

[a] See reference 13.
[b] See reference 14.
[c] See reference 15.
[d] See reference 16.
[e] See reference 17.
[f] See reference 18.

makes no contribution to $C_1^{(1)}$ since its only matrix element[7] is $\int\beta\gamma_5$, which vanishes unless $\Delta I=0$. The $C_1^{(2)}$ is the complete shape factor for the $\Delta I=\pm 2$ transitions which we have dismissed; however, $C_1^{(2)}$ also contributes to $\Delta I=0, \pm 1$ transition, although not to $0\to 0$, $1\leftrightarrow 0$ or $\frac{1}{2}\to\frac{1}{2}$ cases. As indicated in argument **I**, $C_1^{(2)}$ arises from T or A interactions only.

Fourth, we introduce certain real[8] parameters, x_i, y_i, z_i, which help simplify the notation for the nuclear matrix elements which occur. The latter are defined in references 5 and 6. Here we define x_i by means of

$$\begin{aligned}
\int\beta\mathbf{r} &= -ix_1(G_T/G_S)\int\beta\boldsymbol{\sigma}\times\mathbf{r},\\
\int\mathbf{r} &= -ix_2(G_A/G_V)\int\boldsymbol{\sigma}\times\mathbf{r},\\
\int\beta\mathbf{r} &= ix_3(G_A/G_S)\int\boldsymbol{\sigma}\times\mathbf{r},\\
\int\mathbf{r} &= ix_4(G_T/G_V)\int\beta\boldsymbol{\sigma}\times\mathbf{r}.
\end{aligned}\tag{5}$$

Next, the y_i are defined by

$$\begin{aligned}
\int\beta\boldsymbol{\alpha} &= y_1(\alpha|Z|/2R)\int\beta\boldsymbol{\sigma}\times\mathbf{r},\\
\int\boldsymbol{\alpha} &= y_2(\alpha|Z|/2R)(G_A/G_V)\int\boldsymbol{\sigma}\times\mathbf{r},\\
\int\boldsymbol{\alpha} &= -y_4(\alpha|Z|/2R)(G_T/G_V)\int\beta\boldsymbol{\sigma}\times\mathbf{r}.
\end{aligned}\tag{6}$$

Here, Z is the nuclear charge and R the nuclear radius in units of $\hbar/mc$. Finally, the z_i are defined by

$$\begin{aligned}
\int\gamma_5 &= iz_1(\alpha|Z|/2R)\int\boldsymbol{\sigma}\cdot\mathbf{r},\\
\int\beta\gamma_5 &= -iz_2(\alpha|Z|/2R)(G_A/G_P)\int\boldsymbol{\sigma}\cdot\mathbf{r},\\
\int\beta\gamma_5 &= iz_3(\alpha|Z|/2R)(G_T/G_P)\int\beta\boldsymbol{\sigma}\cdot\mathbf{r}.
\end{aligned}\tag{7}$$

Attempts[10,12] have been made to evaluate these matrix elements from simplified nuclear models. These estimates give x_i, y_i, z_i the order of magnitude unity when all $G_X/G_{X'}\to 1$ (except $z_2, z'\to 0$, see below).

Fifth, we present the shape factor here only in the approximation $(\alpha Z)^2\ll 1$. This is more than adequate for our purposes. We have actually used the precise expressions to be found in references 6, 9, and 10 for checking various of the smaller effects. The corresponding increase in accuracy is, however, largely illusory, because of uncertainties in nuclear matrix elements, in the nuclear radius, and in the finite nucleus and screening effects.

We are now ready to give $C_1^{(1)}$ for the $ST(P)$ and $VA(P)$ interactions. For both, one can use the single, positive-definite expression:

$$\begin{aligned}
C_1^{(1)} = G_{A(T)}{}^2\Big|\int(\beta)\boldsymbol{\sigma}\times\mathbf{r}\Big|^2\Big\{\Big[\frac{\alpha Z}{2R}(1+x_i-y_i)\\
+(1+x_i)\frac{p^2}{3W}\mp(1-x_i)\frac{q}{3}\Big]^2+\Big(\frac{1+x_i}{3}\frac{p}{W}\Big)^2\\
+\frac{(1-2x_i)^2}{18}p^2+\frac{(1+2x_i)^2}{18}q^2\Big\}.
\end{aligned}\tag{8}$$

The upper sign applies to the VA combination, the lower to ST. Further, one may change to the case of positron emission by changing the sign of y_i. $i=2$ and 1, respectively, for VA and ST. p and q are electron and neutrino momenta, respectively, in units of mc. $q=W_0-W$ if W_0 is the spectrum end-point value of the electron energy W.

Expression (8) makes clear an important result: The main Coulomb effect on the electron, $\sim(\alpha Z/2R)^2$, is *energy-independent*. Dependence on energy here means on the kinetic energy with which the electron emerges, and naturally the Coulomb potential energy is independent of that.

As contrast, we immediately present $C_1^{(2)}$, which constitutes the entire shape factor for the $\Delta I=\pm 2$ transitions:

$$C_1^{(2)} = G_{T,A}{}^2\Sigma|B_{ij}|^2(p^2+q^2)/12.\tag{9}$$

B_{ij} is another nuclear matrix element defined in reference 6. This expression yields the distinctive shapes referred to in argument **I** and arises only from the T or A forms of interaction. Here, the large possible angular momentum change $|\Delta I|$ makes the role of orbital angular momenta important. As a consequence, energy-dependent centrifugal effects dominate, rather than such Coulomb effects as were described in the preceding paragraph. The energy-dependent terms of (8) are largely centrifugal effects like those of (9).

Not all the constant terms of (8) arise from the Coulomb effect on the electron. The matrix elements

[13] T. Ahrens and E. Feenberg, Phys. Rev. **86**, 64 (1952).

$f(\beta)\alpha$ and $f(\beta)\gamma_5$ of (6) and (7) contribute to the once-forbidden shape factors in the same way as do the $f(\beta)$ and $f(\beta)\sigma$ to the allowed shape factor (2), i.e., with constant terms. However, as the estimates of (6) and (7) mentioned above indicate, here also the Coulomb energy is a measure of the size of the contribution. This results in the combination of Coulomb terms actually shown in (8). Hence, the size of all the energy-independent contributions to the shape factor can be said to be measured by the Coulomb energy at the nuclear radius, $\alpha Z/R$.

The existence of the constant terms has particular significance in view of the fact that all the measured once-forbidden spectra are reported to have the statistical shape (except RaE, Sec. 5). Thus, the experiments appear to demand an energy-independent shape factor, C_1.

One can now see that it is important for all the observed cases, that the Coulomb energy should dominate over the electron-neutrino kinetic energies: $\alpha Z/R \gg W_0-1$. The uncertain parameters x_i, y_i cannot take on values which would tend to cancel the Coulomb terms. The only alternative would be for the kinetic energy terms to preserve a precarious balance against each other. Such a balance should in principle vary from case to case and frequently fail, giving deviations such as have not so far been observed. It is fortunate for the theory that in all the cases for which the statistical shape is reported, the condition $\alpha Z/R \gg W_0-1$ is fulfilled. This is shown in Table I[13-16] for the once-forbidden cases in which the spectra are best measured (i.e., unobscured by concurrent transitions).

Supporting evidence for our interpretation that it is the dominance by the Coulomb terms $\sim(\alpha Z/2R)^2$ which is responsible for the statistical shapes comes from the $\Delta I=\pm 2$ transitions. A notable fact about these distinctive transitions is their long comparative half-lives ($\langle \log ft\rangle_{Av}\approx 9$) as against those for $\Delta I=\pm 1$ ($\langle \log ft\rangle_{Av}\approx 7$). The main part of this difference must be due to the absence of the large Coulomb contribution $\sim(\alpha Z/2R)^2$ in (9). This implies that if the Coulomb term were suppressed in (8), e.g., by adverse x_i, y_i values, then the $\Delta I=\pm 1$ half-lives would become as long as the $\Delta I=\pm 2$ ones, contrary to what is actually observed.

Not only (8), but all the possible $\Delta I=0$, ± 1 shape factors contain the Coulomb terms $\sim(\alpha Z/2R)^2$. For the $SA(P)$ and $VT(P)$ combinations, we write $C_1^{(1)}$ keeping only these usually dominant terms:

$$C_1^{(1)}(SA)\approx G_A^2\left|\int \boldsymbol{\sigma}\times\mathbf{r}\right|^2(\alpha Z/2R)^2 \times[1+x_3^2-2x_3/W], \quad (10)$$

$$C_1^{(1)}(VT)\approx G_T^2\left|\int \beta\boldsymbol{\sigma}\times\mathbf{r}\right|^2(\alpha Z/2R)^2[(1-y_1)^2 +(x_4-y_4)^2-2(1-y_1)(x_4-y_4)/W]. \quad (11)$$

The striking fact about these expressions is that they predict deviations from the statistical shape even for large Coulomb energies. Yet we depend on the latter to account for the occurrence of statistical shapes among once-forbidden spectra.

The energy-dependent terms of (10) and (11) are $\sim 1/W$ and arise from the calculations in the same way as do the Fierz interference terms in the allowed shape factor C_0 of (2). Thus, an argument develops against the inclusion of SA and VT combinations in the β-law which is of the same kind as argument **IV** against SV and TA combinations.

There remains to be considered the shape factors $C_1^{(0)}$ which form a part of the total shape factor (4) for $\Delta I=0$ transitions and constitute the entire shape factor for $0\to 0$ transitions. For either the $(S)TP$ or $(V)TP$ forms of the β-law,

$$C_1^{(0)}(TP)=G_T^2\left|\int \beta\boldsymbol{\sigma}\cdot\mathbf{r}\right|^2\left\{\left[\frac{\alpha Z}{2R}(1-z_3) +\frac{1}{3}\left(\frac{p^2}{W}-q\right)\right]^2+\left(\frac{p}{3W}\right)^2\right\}. \quad (12)$$

Clearly, this leads again to the statistical shape in the usual case of $\alpha Z/R \gg W_0-1$. However, the $(S)AP$ or $(V)AP$ forms yield

$$C_1^{(0)}(AP)\approx G_A^2\left|\int \boldsymbol{\sigma}\cdot\mathbf{r}\right|^2(\alpha Z/2R)^2[(1-z_1)^2 +z_2^2+2z_2(1-z_1)/W], \quad (13)$$

when $\alpha Z/R \gg W_0-1$. Here, the Fierz type of deviation occurs again.

The complete roster of possible once-forbidden shape factors, (8) to (13), has led to the following conclusions. The reported statistical shapes (energy-independent shape factors) seem best explainable, according to either an STP or VA form of β-law, as due to the normal dominance of the Coulomb energy. The VTP or SAP forms are probably incorrect because even for large Coulomb energies they, in general, predict deviations from the statistical shape, of a Fierz type.

Two considerations tend to keep this argument from being completely conclusive, at least for the present. These apply to some degree also to the widely accepted argument **IV**, which has a similar basis in allowed spectra. They are:

(a) The uncertain quantities x_i, y_i, z_i may have such values, in all the cases observed so far, that the Fierz interferences would be unobservable.

(b) Although the spectra are reported to have sta-

[13] Mayer, Moszkowski, and Nordheim, Revs. Modern Phys. **23**, 315 (1951).
[14] Langer, Motz, and Price, Phys. Rev. **77**, 798 (1950).
[15] L. M. Langer (private communication); see also F. B. Shull, Phys. Rev. **74**, 917 (1948).
[16] H. R. Muether and S. L. Ridgway, Phys. Rev. **80**, 750 (1950).
[17] L. M. Langer and H. C. Price, Phys. Rev. **76**, 641 (1949).
[18] L. R. Shepherd and S. M. Hill, Nature **162**, 566 (1948).

tistical shapes, the experiments might have been too inaccurate to detect Fierz deviations.

The adequacy of the experiments is discussed in detail in Sec. 3, for allowed spectra, and in Sec. 4, for once-forbidden spectra.

As regards point (a), one may point out at once that it is unlikely for the matrix elements, in all the cases observed, to take on just such values as would hide the effects of Fierz interference. In principle, the matrix elements may vary markedly, relative to each other, from case to case. Certainly, the objection (a) will become difficult to believe if the reports of statistical shapes of greater accuracy continue to accumulate.

For a less vague consideration of the objection (a), we may rely on the estimates of the nuclear matrix elements due to Pursey[10] and to Ahrens and Feenberg.[12] One has

$$\kappa \approx 1 \quad \text{and} \quad \lambda \approx 1 \tag{14}$$

for the parameters in C_0, (2). This results immediately from the nonrelativistic approximation for the Dirac $\beta (\approx -1)$. That approximation is invalid if β does not commute with other operators occurring in the matrix element.

We quote the estimates for the ratios involved in (5), (6), and (7) in terms of the quantities ξ_i, η_i, ζ_i defined exactly like x_i, y_i, z_i except that the G's are omitted, i.e.,

$$x_i \to \xi_i, \quad y_i \to \eta_i, \quad z_i \to \zeta_i \quad \text{as} \quad G_X/G_X \to 1. \tag{15}$$

Further, we restrict the quotations for ξ_i, η_i to those applicable to the first three, better-defined cases in Table I:

$$\xi_1 \approx \xi_2 \approx \xi_3 \approx \xi_4 \approx 1, \tag{16}$$

$$\eta_1 \approx \eta_2 \approx \eta_4 \approx \Lambda, \tag{17}$$

where Λ is a quantity defined by Ahrens and Feenberg. These authors find $\Lambda \approx 1$ for such cases as ours. On the other hand, Pursey gives $\Lambda \approx 2$. The discrepancy stems from different assumptions as to the nuclear model. The estimates (16) are probably more reliable than the others since they follow from kinematical considerations whereas Λ requires more presumptions about the nuclear Hamiltonian.

Further, Ahrens and Feenberg give

$$\zeta_1 \approx 1, \tag{18}$$

while Feenberg and Primakoff[12] estimate

$$\zeta_2 \approx \zeta_3 \approx 0, \tag{19}$$

TABLE II. Allowed spectra.

	Rad'n.	ΔI	W_0	Ref.
N^{12}	β^+	0	3.44	a
S^{35}	β^-	0	1.33	b
Cu^{64}	β^-	1	2.119	c
Cu^{64}	β^+	1	2.285	c

[a] See reference 19.
[b] See reference 20.
[c] See reference 21.

being of the order of m/M, the ratio of electron to nucleon mass. According to the last result, the P form will not contribute at all unless G_P has an unlikely high value.

If one accepts the estimates just reviewed, one sees that objection (a) does not hold for C_0 and for $C_1^{(1)}(SA)$. Thus, sufficiently accurate experiments should reveal the presence of Fierz interference if the SV, TA, or SA combinations occur in the correct law. The apparent absence of an observable Fierz deviation confirms argument **IV** and, further, also our new argument insofar as it is directed against the SA combination.

The consequence of the estimates for the VT combination (11) depends on whether $\Lambda \approx 1$ or $\Lambda \approx 2$. If $\Lambda \approx 1$, not only is the Fierz interference in the $C_1^{(1)}(VT)$ shape suppressed but *all* the Coulomb terms $\sim(\alpha Z/2R)^2$. Hence, a VT law would predict for $\Delta I = \pm 1$ transitions a distinctly nonstatistical shape very similar to the $\Delta I = \pm 2$ shapes; moreover, the half-lives of the $\Delta I = \pm 1$ and $\Delta I = \pm 2$ transitions would be expected to be about the same. Thus, Feenberg's evaluation ($\Lambda \approx 1$) would make the argument against the VT combination very strong.

On the other hand, Pursey's estimate of $\Lambda \approx 2$ would make the Fierz interference in the VT combination observable. If one accepts only the more reliable estimate $\xi_4 \approx 1$ for the first three cases of Table I, then (11) becomes

$$C_1^{(1)}(VT) \approx \left| \int \beta \sigma \times \mathbf{r} \right|^2 (\alpha Z/2R)^2 (1-\Lambda)^2 \times [G_T^2 + G_V^2 - 2G_T G_V/W]. \tag{20}$$

Thus, if the constant terms here are appreciable at all ($\Lambda \neq 1$) then a Fierz deviation should be present unless $G_V G_T \to 0$.

Finally, accepting the estimates (19) as valid destroys our argument as directed against the AP combination (13). If the P form does not contribute at all, naturally its effects become unobservable and objection (a) holds. However, the RaE case, discussed in Sec. 5, may indicate that occasionally at least the estimate (19) fails.

On the basis of the estimates of the nuclear matrix elements, therefore, argument **V** can be successfully directed only against including VT and SA forms in the β-law. This, together with argument **IV**, leaves only the STP and VAP possibilities.

3. FIERZ INTERFERENCE IN ALLOWED SPECTRA

The absence of Fierz deviations in allowed spectra is frequently quoted as a basis for argument **IV**, but no systematic examination seems to have been presented so far. We have special interest in the details because the sensitivity of current measurements to the Fierz effect also determines the effectiveness of argument **V**, which depends on the absence of the Fierz type of deviation in once-forbidden spectra [see objection (b) in Sec. 2].

The most convenient way to derive information from spectrum shapes is to examine their (Fermi-)Kurie plots. The ordinates of these are, in theory,

$$K_n=(W_0-W)C_n^{\frac{1}{2}}. \tag{21}$$

When the shape factor C_n is independent of the energy W, the spectrum has a statistical shape and the Kurie plot is linear $\sim(W_0-W)$. Kurie plots of experimental points have an arbitrary ordinate scale, being proportional to the square root of the source intensity. This fact, together with the fact that the plot itself is used to determine W_0, tends to make experimental Kurie plots insensitive to possible deviations from linearity. Nevertheless, the current accuracy of measurement does not seem to warrant more sensitive treatment.

If the Fierz type of effect should be present, then the Kurie plot should deviate from linearity, since it is now proportional to

$$K_n\sim(W_0-W)(1+2\varphi/W)^{\frac{1}{2}}, \tag{22}$$

where φ is some number for each spectrum, given in theory by some one of the shape factors like (2), (10), or (11). The report that the spectra yield linear Kurie plots implies $\varphi=0$, but some amount of deviation would have been undetected. Thus, we can only expect to set upper limits on $|\varphi|$ from the experiments. If these turn out to be substantially less than unity, their difference from zero will have been rendered unlikely. That conclusion has particular force when a small $|\varphi|$ implies some $|G_X/G_{X'}|$ is a small fraction. A theory with one Fermi constant much smaller than another strains credibility. The burden of proof is transferred to the point of view that the small component exists.

The observed spectra which have the best chance to reveal the presence of Fierz interference are those which are measured reliably down to a low electron energy. We therefore look at spectra which are not superposed with concurrent, lower energy, transitions. Table II seems to have the best measured examples.[19–21]

To provide an equal basis for judging the consistency with experiment of the theories with ($\varphi\neq0$) and without ($\varphi=0$) Fierz interference, we proceeded as follows. For each test, we chose a suitable (small) numerical value of φ. Then we compared the conventional experimental Kurie plot ($\varphi=0$) with a plot of the same points divided by $(1+2\varphi/W)^{\frac{1}{2}}$. The second type we refer to as a "Fierz plot." The latter, rather than the conventional plot, should be linear if actually the $\varphi\neq0$ is correct, as can be seen from (22). Of course, it turns out that both plots are nearly linear if $|\varphi|$ has been chosen small enough. We then located the straight lines which the experimental points of each plot ought to follow by using the points on the high energy side of the intensity maximum, the corresponding ones of the Kurie and of the Fierz plots. That part of every spectrum is always the most reliably measured. Finally we examined and evaluated the deviations from the constructed lines which are exhibited by the points not used in the constructions.

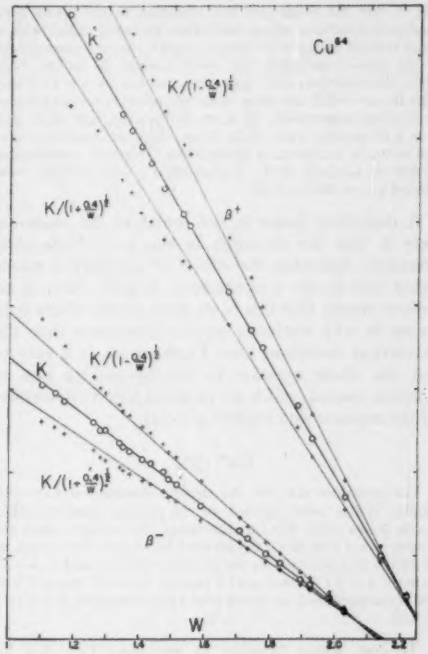

FIG. 1. Conventional Kurie (K) and Fierz ($K/(1+2\varphi/W)^{\frac{1}{2}}$ with $\varphi=\pm1/5$ plots for the Cu^{64} spectra.

The conventional Kurie plots usually showed roughly *random* deviations from linearity. We took the root-mean-square of the percentage deviations, ϵ, as a measure of the experimental accuracy. Then we found in each case that values of φ surpassing certain limits would yield Fierz plots which deviated *systematically* from linearity. We regarded the limiting φ's to have been reached when the systematic mean percentage deviation δ in the Fierz plot just exceeded the random deviation ϵ in the Kurie plot. This seemed quite a generous allowance for random error. Of course, we did not try infinite progressions of φ's. From a suitable enough initial choice it can be shown possible to perform a type of linear extrapolation to the limiting φ: We find $\delta-\delta_0\sim\varphi$ if δ_0 is the percentage deviation in the Kurie plot.

Cu^{64} (β^-)

Ten points with $W>1.5$ were used to determine the straight lines for the Kurie plot and two Fierz plots with $\varphi=\pm0.2$ in

[19] W. Hornyak and T. Lauritsen, Phys. Rev. **77**, 160 (1950).
[20] R. Albert and C. S. Wu, Phys. Rev. **74**, 847 (1949); Langer, Motz, and Price, Phys. Rev. **77**, 798 (1950).
[21] Langer, Moffat, and Price, Phys. Rev. **76**, 1725 (1949); C. Wu and R. Albert, Phys. Rev. **75**, 1107 (1949).

Fig. 1. For the Kurie plot the remaining twelve points were randomly distributed above and below the straight line with a mean relative deviation of $\delta_0 \approx 0.1$ percent; the root mean square of the relative deviations was $\epsilon = 0.9$ percent. As for the Fierz plots, the deviations were systematic, too low for $\varphi = +0.2$ and high for $\varphi = -0.2$, the mean value of their relative magnitudes amounting, respectively, to $\delta_+ = -2.0$ percent ($\varphi = +0.2$) and $\delta_- = +3.0$ percent ($\varphi = -0.2$). From these we concluded that the values of φ capable of giving Fierz deviations, undetectable within the accuracy of the measurements ($\epsilon = 0.9$ percent), were limited by $-0.06 < \varphi < 0.08$.

A disturbing factor in the course of the reasoning here is that the deviation in the $\varphi < 0$ Fierz plots resembles somewhat the effects of too thick a source being used in the measurement. Actually there is no serious danger that this is so; thick source effects tend to set in with distinctly greater abruptness than the theoretical deviations here. Furthermore, it is easy to put the whole question to rest by looking also at positron spectra, which are expected to have deviations of the opposite sign according to (2).

Cu^{64} (β^+)

The procedure used for the electron spectrum of Cu^{64} gave similar results when applied to the positron spectrum. Here seven points with $W > 1.6$ determined the straight lines, and eleven points with $W < 1.6$ were used to measure the deviations. With the notation used for the previous case we found $\delta_+ = -3.9$ percent, $\delta_- = 3.1$ percent, $\epsilon = 1.1$ percent, $\delta_0 = -0.7$ percent, with the consequent limit on unobserved Fierz deviations of $-0.1 < \varphi < 0.03$.

It now seems possible to say that $|\varphi| \lesssim 0.1$ for allowed transitions with $\Delta I = \pm 1$. In such cases, C_0 of (2) is simplified because $\int \beta = \int 1 = 0$. Then, theoretically,

$$\varphi = \pm \lambda G_T G_A / (G_T^2 + \lambda^2 G_A^2). \tag{23}$$

Hence, we can say $|\lambda G_A / G_T| \lesssim 0.1$ *or* $|G_T / \lambda G_A| \lesssim 0.1$. Considering that probably $\lambda \approx 1$, see (14), we have here the implication that one of the G's is less than 0.1 of the other. This is about as closely as the present experiments can prove that not both G_T and G_A differ from zero. The significant limits are

$$G_A^2/G_T^2 < 1 \text{ percent} \quad \textit{or} \quad G_T^2/G_A^2 < 1 \text{ percent}.$$

We hope to come to a similar conclusion about the pair G_S, G_V from the $\Delta I = 0$ experiments.

N^{13}

The measurement of the deviations of thirteen points with $W < 2.5$ from the straight line drawn through ten points with $W > 2.5$ gave $\delta_+ = -3.6$ percent; $\delta_- = 4.3$ percent, $\epsilon = 1.2$ percent, $\delta_0 = +0.5$ percent, and consequently $-0.04 < \varphi < 0.09$.

S^{35}

Six points with $W > 1.16$ and nine points with $W < 1.16$ were used giving $\delta_+ = -2.2$ percent, $\delta_- = 1.7$ percent, $\epsilon = 1.2$ percent, $\delta_0 = +0.4$ percent, from which $-0.12 < \varphi < 0.12$.

The N^{13} experiment seems good enough to conclude that $|\varphi| \lesssim 0.1$ for $\Delta I = 0$ transitions, also. Theoretically, see (2),

$$\varphi = \pm \kappa G_S G_V \Big/ \Big[G_S^2 + \kappa^2 G_V^2 + (\lambda^2) G_{T(A)}^2 \Big(\Big| \int \beta \sigma \Big|^2 \Big/ \Big| \int \beta \Big|^2 \Big) \Big] \tag{24}$$

depending on whether the near vanishing of (23) is taken to imply that G_T or G_A is to be neglected. For[22] N^{13}, $|\int \beta\sigma|^2 / |\int \beta|^2 \approx 1/3$. The Fierz interference is expected to be less detectable when $\Delta I = 0$ than it was for $\Delta I = \pm 1$. Nevertheless, it is clear that $|G_S/G_V|$ *or* $|G_V/G_S|$ must be substantially less than unity and presumably zero.

4. FIERZ-TYPE INTERFERENCE IN ONCE-FORBIDDEN SPECTRA

We wish to compare argument **V**, against SA and VT combinations, with the argument **IV**, against SV and TA combinations, by showing that the once-forbidden spectra limit the amount of the Fierz-type deviation as much as do the allowed spectra.

We probably must forego directing our argument also against AP combinations. Not only does the estimate (19) of $\int \beta\gamma_5$ make it possible that P effects are unobservable anyway, but also there seem to exist no suitable measurements to implement the argument for this case. Many spectra have been observed which are expected to have[13] $\Delta I = 0$ (Zr^{97}, Ag^{111}, Cd^{115}, In^{115m}, La^{141}, Dy^{165}, Er^{169}, Er^{171}, Ce^{144}, Pr^{144}). However, all these are overlaid with concurrent transitions or other obscuring effects. The unobscured portion of each spectrum is reported to have the statistical shape, but the obscurations may have hidden considerable Fierz interference.

Table I lists all the once-forbidden spectra which seem to be well-measured down to low energies. Only for the first three cases does the shell model define the spin change fairly well, as $\Delta I = 1$. For these reasons we confined our examination to Pm^{147}, W^{185}, and Pr^{143}.

Pm^{147}

Figure 2 shows the conventional Kurie plots and also the Fierz plots for $\varphi = \pm 1/5$. For each, the points with $W > 1.2$ were used to locate the presumptive straight lines. The deviations of the points with $W < 1.2$ were random for the Kurie plot ($\delta_0 = 0.2$ percent), having a root-mean-square percentage deviation, $\epsilon = 0.9$ percent. The $\varphi = +1/5$ plot has a systematic mean percentage deviation, $\delta_+ = -1.9$ percent. This reduces to -0.9 percent if $\varphi = 0.1$. The $\varphi = -1/5$ plot has a systematic mean deviation $\delta_- = +4.5$ percent. That reduces to $+0.9$ percent if $\varphi = -0.03$. We conclude $-0.03 < \varphi < 0.1$.

W^{185}

The results here were much the same as for Pm^{147}. The points near the end point showed some scattering; hence, they were not

[22] E. P. Wigner, Phys. Rev. **56**, 519 (1939).

relied on to determine the straight lines. It was necessary to use instead points more nearly at the middle of the spectrum. This naturally cut down the range in which the Fierz deviations could show themselves. In conclusion, it was then possible to say that $-0.09<\varphi<0.14$.

Pr^{143}

The accuracy here was found to be about the same as for W^{185}. The result was $-0.13<\varphi<0.09$.

Thus, with some indication of concurrence from W^{185} and Pr^{143}, the most stringent limits on the amount of Fierz interference is imposed by the particularly carefully measured Pm^{147} spectrum. From it we can conclude that $|\varphi|\lesssim 0.1$.

We interpret the result $|\varphi|\lesssim 0.1$ by supposing, in turn, that the Fierz interference arises from the SA combination as in (10), then from the VT combination, as in (11) or (20). According to (10) and (15),

$$|\varphi| = |x_3|/(1+x_3^2) = |\xi_3 G_S G_A|/(G_A^2+\xi_3^2 G_S^2).$$

We can put $\xi_3 \approx 1$ according to (16) without introducing more uncertainty than was done for argument **IV** when $\kappa \approx \lambda \approx 1$ was supposed. Then $|\varphi|\lesssim 0.1$ implies with the present interpretation:

$$G_A^2/G_S^2 \lesssim 1 \text{ percent} \quad or \quad G_S^2/G_A^2 \lesssim 1 \text{ percent}.$$

When the VT combination is being tested,

$$|\varphi| = |(1-\eta_1)(\xi_4-\eta_4)G_V G_T|/[(1-\eta_1)^2 G_T^2 + (\xi_4-\eta_4)^2 G_V^2]$$

according to (11) and (15). When (16) is used,

$$|\varphi| \approx |G_V G_T|/[G_T^2+G_V^2].$$

Hence, $|\varphi|\lesssim 0.1$ makes

$$G_V^2/G_T^2 \lesssim 1 \text{ percent} \quad or \quad G_T^2/G_V^2 \lesssim 1 \text{ percent}.$$

One must remember, however, that the terms under consideration here are multiplied with $(1-\eta_1)^2$, which may nearly vanish. It has already been pointed out, in Sec. 2, how this would only strengthen the case against the VT combination.

We have thus carried out argument **V** to the same kind of result as **IV**. Ratios of the type $G_X^2/G_{X'}^2$ were shown to be small enough for the presumption that they vanish to be likely. However, such a presumption is not necessary to complete argument **V**, as it was for argument **IV**. This is because we have an independent measure for the possible values of the ratios in question. One can show[24] that the comparative half-lives of H^3 (or the neutron) and He^6 can be consistent with each other only if

$$G_F^2/G_G^2 = 0.6 \text{ to } 2.4.$$

Here G_F may be G_S *or* G_V, whereas G_G is G_T *or* G_A. The subscripts F and G refer to "Fermi" and "Gamow-Teller" selection rules. One can see that the limits on the G's imposed by the absence of Fierz deviations make the SA and VT combinations inconsistent with the H^3, He^6 half-lives.

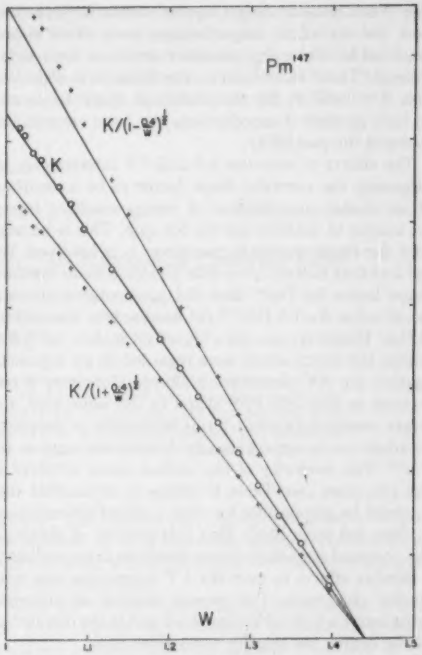

FIG. 2. Conventional Kurie (K) and Fierz plots ($\varphi=\pm 1/5$) for Pm^{147}.

So far argument **V** may seem at least as secure as argument **IV**. However, we have ignored the small energy-sensitive terms, aside from the constant ones $\sim(\alpha Z/2R)^2$, which enter all the shape factors C_1 and are specifically shown in (8). We have been relying heavily on the reports of the statistical shape as an empirical fact from which the negligibility of the energy-sensitive terms follows. From the theoretical side, the negligibility of these terms depends on the precise values adopted for the nuclear radius, for the G's and for the relative sizes of the nuclear matrix element (the parameters ξ_i, η_i, ζ_i). Thus, the possible disturbing effect of the terms in question is subject to considerable uncertainty. It is fortunate that the best limits on φ have been derived from the Pm^{147} case, which has a particularly low energy release W_0 and so should be the least disturbed.

The energy-sensitive terms might disturb the above conclusions in the following way. Contrary to those conclusions, the Fierz terms may actually be appreci-

[24] E. J. Konopinski and L. M. Langer, Annual Reviews of Nuclear Science, 2 (1952).

able. Their presence might not be evident in deviations from the statistical shape because their effect is just cancelled by the energy-sensitive terms we have so far ignored. There is, of course, the immediate objection that it is unlikely for the statistical shape to depend on such accidental cancellations. We have nevertheless explored the possibility.

The efforts to save the SA and VT interactions, by supposing the constant shape factor to be a resultant of accidental cancellations of energy-sensitive terms, are easiest to describe for the SA case. This is because only the single uncertain parameter x_3 is involved. We did find that indeed $x_3\approx+0.08$ yielded a more constant shape factor for Pm^{147} than did $x_3=0$ when a conventional value $R=1.5A^{\frac{1}{3}}10^{-13}$ cm was used for the nuclear radius. However, $x_3=\xi_3G_S/G_A=0.08$ makes $|\varphi|\lesssim 0.1$, within the limits which were regarded as an argument against the SA combination above. Moreover, if one wanted to save the Pr^{143} shape in the same way, the larger energy-dependent terms here make it necessary to adopt an x_3 approximately 3 times as large as for Pm^{147}. The similarity of the nuclear states involved in the two cases (see Table I) makes it implausible that ξ_3 could be responsible for such a threefold variation. It does not seem likely that this method of obtaining the observed statistical shapes should be taken seriously.

Similar efforts to save the VT interaction met with similar objections. The greater number of uncertain parameters which is here involved makes the description of the details too lengthy to be given here.

5 CONCLUDING DISCUSSION

The arguments **IV** and **V** by themselves leave only the alternatives STP and VAP with which to reproduce the observed statistical shapes of the once-forbidden spectra. These forms are supposed to do that by way of the large constant Coulomb terms in the shape factors (8). The energy-sensitive terms of (8) are supposed to be negligible, at least within the accuracy of the observations. The uncertain factors in all these terms make it impossible to prove that they indeed are so negligible; all that can be done at present is to show that it is possible that they are.

A typical situation arises when a detailed effort is made to fit $C_1^{(1)}(ST)$ of (8) to Pm^{147}. The only appreciable perturbation to the constant $(\alpha Z/2R)^2$ term is the addition to it of the terms

$$\frac{\alpha Z}{3R}\left\{\frac{G_T+\xi_1G_S}{G_T(1-\Lambda)+\xi_1G_S}\cdot\frac{p^2}{W}+\frac{G_T-\xi_1G_S}{G_T(1-\Lambda)+\xi_1G_S}q\right\}.$$

If we take $G_T=G_S$, $\xi_1=1$, $\Lambda=1$, and $R=1.5A^{\frac{1}{3}}\times10^{-13}$ cm, this causes $\sim+3$ percent mean deviation from the statistical shape. This deviation can be reversed if $\Lambda\to2$ and $G_T>G_S$ instead. Such conclusions were little changed when we used the more precise expressions of references 6 and 9, and when we considered finite nucleus and screening effects. One sees that there is little point in pursuing this study in view of the uncertainties involved. Probably such uncertainties will be best resolved when cases with $W_0-1\to\alpha Z/2R$ are found and measured. Certainly, deviative effects are better evaluated from definite deviations than through their apparent absence, as in the cases now available.

There is one case of definite deviation from the statistical shape which may be a once-forbidden transition: the singular RaE spectrum. This was analyzed by Petschek and Marshak,[2] who concluded that the shape could be reproduced only by $C_1^{(0)}(TP)$ and so must be a $0\to0$ transition. Rather than formula (12) they used its more precise equivalent,[25] to be found in references 6 and 9. In order to make the application successful, it was necessary to assume that

$$z_3=\zeta_3G_P/G_T\approx+1.$$

The main objection against the Marshak-Petschek treatment is Ahrens, Feenberg, and Primakoff's estimate (19) that $\zeta_3\to0$ and hence $z_3\to1$ is unlikely. This objection does indeed make the RaE analysis; hence argument **III**, doubtful. On the other hand, the RaE analysis may perhaps be regarded as empirical evidence that at least for some nuclear states the estimate $\zeta_3\to0(\equiv\int\beta\gamma_5\to0)$ may fail. The fact that the RaE case is the only one of its kind, even though deliberate searches[17] have been directed toward finding similar cases, perhaps adds plausibility to the occurrence of the failure as a singular instance.

There is an additional, qualitative piece of evidence which supports the Marshak-Petschek result. $z_3\approx1$ means that the deviation from a constant shape factor, in spite of $\alpha Z/R\gg(W_0-1)$ as seen in Table I, is achieved through the approximate cancellation of the large term $\sim(\alpha Z/2R)^2$ in (12). This has the consequence that the half-life of RaE is lengthened; a highly uncertain estimate is a lengthening by a factor of about $10^{2.8}$. Now, the study of comparative half-lives reveals that RaE does indeed have a life $\sim10^{2.5}$ times as long as that of otherwise similar nuclei. RaE has $\log ft\approx8$, and involves in its transition an 83rd proton and a 127th neutron. The Pb^{209} transition also converts a 127th neutron into an 83rd proton. It has $\log ft\approx5.6$. Hg^{205} and RaE″ involve 81st protons and 125th neutrons, one below magic numbers in each case. These nuclei have $\log ft=5.4$ and 5.5, respectively.

The Marshak-Petschek result provides the argument **III**, which is the only one favoring the STP over the VAP combination. Without it, our new argument **V** leaves both the latter alternatives, having only eliminated the SAP and VTP forms.

Our results contradict the Critchfield-Wigner[26] hy-

[25] They also find that the corrections for finite nuclear size are important.

[26] C. Critchfield, Phys. Rev. **63**, 417 (1943).

pothesis ($S-A-P$) and also the Tolhoek-DeGroot[27] symmetry principle. The latter leads one to expect either an SAP form or a VT form for the β-interaction. This may mean that the neutron and proton are not quite as equivalent during Fermi interaction as is presumed in the symmetry principle.

We wish to acknowledge the help of Professor A. C. G. Mitchell in making this work possible. This work was assisted by the joint program of the ONR and AEC.

[27] H. Tolhoek and W. DeGroot, Phys. Rev. **84**, 150 (1951).

PHYSICAL REVIEW VOLUME 88, NUMBER 6 DECEMBER 15, 1952

Variations in the Relative Abundances of the Isotopes of Common Lead

C. B. COLLINS, R. M. FARQUHAR, AND R. D. RUSSELL
Department of Physics, University of Toronto, Toronto, Canada
(Received July 18, 1952)

Mass spectrometer measurements of the relative isotopic abundances of samples of lead ores from Archean-type rocks showed larger variations than reported by Nier. The isotopic constitution of one lead was within the limits calculated by Holmes and by Bullard and Stanley. From the new measurements combined with existing data estimates of the time of formation of the earth's crust of 3.5 billion years and of a maximum time of formation of the elements of 5.5 billion years have been calculated. These values are in reasonable agreement with previous estimates.

NIER[1] reported the first, and still the only, thorough investigation of the variations of the isotopic constitution of ordinary and radiogenic leads. Several authors have since used Nier's data to calculate the time of solidification of the earth's crust (Holmes,[2] 3.35 billion years, Bullard and Stanley,[3] 3.29 billion years) and a limit on the time of formation of the elements (Alpher and Herman,[4] 5.3 billion years). All these estimates have been based upon extrapolations from the abundances of ordinary leads ranging in age from 25 to 1400 million years. More analyses of ordinary leads dated at 2000 million years or older have been needed to check these estimates. We have therefore analyzed a number of common lead samples, dating as many as possible from Nier's ages and from analyses of radiogenic leads in our own laboratory. Calculations of the age of the earth's crust and of a maximum age of the elements have been made, using the new measurements listed in Table I combined with Nier's data.[1]

The experimental work was carried out with a 180° direction-focusing Nier-type mass spectrometer with a resolution of about 1/300 of an atomic mass unit. Analyses were made using lead tetramethyl as previously reported by the authors[5,6] and by Dibeler and Mohler.[7] The isotopic lead abundances listed in Table I are believed to be accurate to within 1 percent on an absolute basis, although comparative measurements are good to 0.1 percent.

Since Pb^{204} is not believed to be of radiogenic origin, the total amount of this isotope is assumed to have remained constant from the time of formation of the elements to the present. The abundances of Pb^{206}, Pb^{207} and Pb^{208} are therefore given with respect to Pb^{204}.

A value of 5.5 ± 0.2 billion years for the maximum limit on the time of formation of the elements has been calculated from the data given in Table I combined with Nier's measurements of the isotopic constitution of common leads of known age. The method of calculation and the assumptions made were essentially the same as those of Alpher and Herman,[4] and all values of constants were the same except the half-life of U^{235}, which was taken as 7.07×10^8 years.[8]

Using Nier's data, Alpher and Herman reported a figure of 5.3 billion years. The average abundances of the lead isotopes at different times have been listed in Table II.

The calculated relative number of atoms of U, Th, and Pb in the earth's crust at the present time are U—1.00, Th—3.83, and Pb—7.35.

The isotopic abundances of those lead minerals (Table I) which could be assigned an age were combined with Nier's measurements[1] on other dated lead minerals and used to calculate a value for the age of the earth's crust after the method of Bullard and Stanley.[3] This method assumes that the isotopic constitution of lead

[1] A. O. Nier, J. Am. Chem. Soc. **60**, 1571 (1938); Phys. Rev. **55**, 150 (1939); Nier, Thompson, and Murphey, Phys. Rev. **60**, 112 (1941).
[2] A. Holmes, Nature **157**, 680 (1946); **159**, 127 (1947); **163**, 453 (1949).
[3] E. C. Bullard and J. P. Stanley, Suomen Geeodeetisen Laitoksen Julkaisuja, Veroffentlichungen des Finnischen Geodatischen Institutes, No. 36, 33 (1949).
[4] R. A. Alpher and R. C. Herman, Phys. Rev. **84**, 1111 (1951).
[5] Collins, Freeman, and Wilson, Phys. Rev. **82**, 966 (1951); C. B. Collins and J. R. Freeman, Trans. Roy. Soc. Canada **45**, Sec. IV, 23 (1951).
[6] Collins, Lang, Robinson, and Farquhar, Geol. Assoc. Canada (to be published).
[7] V. H. Dibeler and F. L. Mohler, J. Research Natl. Bur. Standards **47**, 337 (1951).
[8] Fleming, Ghiorso, and Cunningham, Phys. Rev. **82**, 967 (1951).

TABLE I. Isotopic abundances of "common" lead.

No.[a]	Source of lead locality	Isotopic abundances referred to $Pb^{204}=1.00$ 206	207	208	Age in 10^6 years
1	Bolivia galena	18.94	15.86	39.70	25[b]
2	Kengere, Belgian Congo	17.58	15.94	38.34	630[c]
3	Frontenac Co., Ontario, Canada	16.79	15.40	36.49	1000[c]
4	Matachewan, Ontario, Canada	15.83	15.41	34.88	
5	Negus Mine, Yellowknife, N.W.T., Canada	14.63	15.27	34.46	1850[d]
6	Sioux Lookout galena, Ontario, Canada	14.03	14.89	33.78	2480[e]
7	Rex property, Great Slave Lake, N.W.T., Canada	16.37	15.65	36.34	1850[d]
8	Rex property, Great Slave Lake, N.W.T., Canada	16.42	15.75	36.54	1850[d]
9	Horseshoe Island, Yellowknife, N.W.T., Canada	14.16	15.08	34.28	
10	Delhi Township, Ontario, Canada	16.07	15.47	35.17	
11	Garson Mine, Sudbury, Ontario, Canada	23.35	16.98	45.57	
12	Worthington Mine, Sudbury, Ontario, Canada	26.00	16.94	52.21	
13	Upper Canada Mine, Ontario, Canada	19.6	15.2	33.6	
14	Rosetta Mine, Barberton, Transvaal, South Africa	12.65	14.27	32.78	
15	Great Bear Lake, N.W.T., Canada	15.93	15.30	35.3	1400[e]
16	Ivigtut, Greenland	14.65	14.65	34.48	
17	Galena, Joplin, Missouri	22.35	16.15	41.8	

[a] Samples Nos. 1 to 14 were analyzed by the authors. Samples Nos. 15, 16, and 17, were analyzed by Nier *et al.* (see reference 1).
[b] Geological dating by J. T. Wilson.
[c] See references 6 and 1. Both authors agree on these ages.
[d] See reference 6.
[e] Nier's two isotopic ages (see reference 1) for the Huron claim have been changed slightly using the new half-life value for U^{235} (see reference 8) of 7.07×10^8 yr, to 2465 and 2580×10^6 yr. These values were averaged with Ahren's age [L. H. Ahrens, Geochim. Cosmochim. Acta. 1, 312 (1951)] obtained by the Rb–Sr method of 2400×10^6 yr. The average of 2480 has been applied to the Sioux Lookout galena which occurs in the same geological area.

was identical everywhere when the crust solidified, but has differed from place to place at any subsequent time. A least squares analysis is used to determine the time at which all lead had the same isotopic composition and to calculate its composition at that time. The values obtained were

$$t_0=(3.5\pm0.2)\times10^9 \text{ years, at which time}$$
$$Pb^{206}/Pb^{204}=11.33$$

and

$$Pb^{207}/Pb^{204}=13.55.$$

The value of 3.5 ± 0.2 billion years for the age of the earth's crust is higher than that of Holmes (3.35 ± 0.2 billion years) and of Bullard (3.29 ± 0.2 billion years),

TABLE II. Calculated average isotopic abundances of lead at different times.

Isotope	$t=5.5\times10^9$ yr	$t=3.5\times10^9$ yr	$t=0$ (present)
204	1.00	1.00	1.00
206	5.12	11.36	18.45
207	0.00	13.48	15.61
208	26.31	31.10	38.40

whose calculations were based entirely on Nier's data. The abundances of Pb^{206} and Pb^{207} relative to Pb^{204} listed above agree well with those in Table II from the mean abundance-time curves used for setting a limit on the age of the elements. This agreement indicates that the two independent methods of calculation are consistent with each other.

DISCUSSION

The calculations carried out by the authors have been based on a set of dated leads of known isotopic constitution. While the two calculations are different in principle, they both depend on the total effect of all the determinations, rather than on any individual one. Single samples such as Rosetta Mine, No. 14, cannot be dated from abundance-time curves such as those of Alpher and Herman,[4] who also pointed out this difficulty. These findings do not support the abundance-time scale for common lead reported by McCrady.[9] The same argument applies to samples Nos. 11 and 12. These discrepancies show that individual samples which have a high or low abundance of Pb^{204} are the result of differences in the relative amounts of Pb, U, and Th from place to place and from time to time, in certain cases. For most samples it is possible to apply a criterion based on the ratio of Pb^{207}/Pb^{206} to find whether the sample is anomalous.

The investigations whose results have been given briefly here will be reported more fully in another publication.

[9] E. McCrady, Trans. Am. Geophys. Union **33**, No. 2 (1952).

Angular Distribution Functions for High Energy Cosmic-Ray Particles

H. S. GREEN, H. MESSEL,* AND B. A. CHARTRES
University of Adelaide, Adelaide, South Australia
(Received August 18, 1952)

The main purpose of this paper is to provide theoretical data which should enable one (a) to distinguish between two different types of differential cross sections for nuclear collisions at high energies, equally compatible with present experimental indications, and (b) to differentiate between certain models of meson production.

The exact angular distribution function is determined on the basis of one type of differential cross section, for both mesons and nucleons, in high energy nucleon-nucleus collisions, and in any type of medium. For both types of cross section, formulas are derived for the general moment of the angular distribution.

Numerical results for the mean square angle of scattering of mesons and nucleons in collisions between a nucleon and a nucleus are presented graphically for both light and heavy nuclei.

1. INTRODUCTION

IT is possible to infer a good deal about the differential cross section for nucleon-nucleon collisions at ultra-relativistic energies by the analysis of cosmic-ray data. As two of the authors have shown,[1,2] the observed radial distribution of nucleons of a given energy about the axis of extensive air showers enforces the conclusion that the scattered particles in a high energy nucleon-nucleon collision must be very near to the forward and backward directions in the center-of-mass frame of reference. This conclusion is confirmed directly by the interpretation of the results of Branch.[3] Further conclusive evidence on this point can be drawn from the observations of McCusker, Messel, Millar, and Porter[4] on the spread of showers in water. Some qualitative considerations due to Heisenberg[5] indicate the same conclusion.

However, there is still some arbitrariness in the angular distribution of particles in the neighborhood of the forward and backward direction, which present experimental evidence does not seem able to resolve. The purpose of the present paper is to study two types of differential cross section, equally compatible with the experimental evidence now available, but with opposite characteristics for energies near to that of the primary. It is hoped that future experiments will be able to differentiate between these two types of cross section, and enable one to specify which is most nearly correct.

One of the two types of differential cross sections considered is that which we have determined previously;[1,6] it has the property that the mean square angle of scatter for both nucleon-nucleon and nucleon-nucleus collisions has a finite and rather large value for values of the secondary energy nearly equal to that of the primary. The other is suggested by a refinement of the conditions imposed by the relativistic transformation, and has the merit that it allows the angular distribution functions—both for nucleon-nucleus collisions and in a finite absorber such as the atmosphere—to be determined explicitly. Thus, the new cross section makes it unnecessary to resort to the reconstruction of the angular distribution function from its moments.[1] It is differentiated from the old cross section[1,6] by the fact that the mean square angle of scatter tends to zero for values of the secondary energy nearly equal to that of the primary.

Another important question on which the present considerations are intended to give information is the mechanism of meson production within the nucleus. We have determined the angular distribution functions for the mesons predicted by a special model for meson production which allows one meson to be created at each nucleon-nucleon encounter, but does not permit the mesons to interact again with the nucleons within the nucleus in which they were created. It is not necessary to specify the type of meson and it seems indeed unlikely that they could be π-mesons at the energy considered. On this model, the number and angular distributions of the nucleons are independent of whether the mesons are created singly or multiply in nucleon-nucleon encounters, though the distributions of the mesons are affected. As far as the number distribution of the nucleons and mesons is concerned, it has been shown[7] that the theoretical predictions are in accord with the experimental data, though the results are not very sensitive to the model assumed. It is hoped that the results for the angular distributions will provide a more critical test of the model proposed.

2. DIFFERENTIAL CROSS SECTION FOR NUCLEON-NUCLEON COLLISIONS

As has been shown previously by two of the authors,[8] the maximum angle $\cos^{-1}c_0$ through which a nucleon may be scattered in an inelastic collision with a second

* Now at the University of Sydney, Sydney, Australia.
[1] H. Messel and H. S. Green, Phys. Rev. **87**, 738 (1952).
[2] H. Messel and H. S. Green, Phys. Rev. **87**, 378 (1952).
[3] M. Branch, Phys. Rev. **84**, 147 (1951).
[4] McCusker, Messel, Millar, and Porter (to be published).
[5] W. Heisenberg, Report of the International Physics Conference, Copenhagen, June, 1952 (unpublished).
[6] B. A. Chartres and H. Messel, Phys. Rev. **87**, 748 (1952).
[7] Messel, Potts, and McCusker, Phil. Mag. **43**, 889 (1952).
[8] H. S. Green and H. Messel, Proc. Phys. Soc. (London) **A64**, 1083 (1951).

nucleon at rest is given by the formula

$$c_0=\bar{U}_0(U-1)/\bar{P}_0P, \tag{1}$$

where $\bar{P}_0$ and $\bar{U}_0$ are the momentum and energy of the primary nucleon in center-of-mass coordinates, and P and U are the momentum and energy of the scattered nucleon considered in the laboratory frame. (Energies and momenta are measured in proton mass units.) In our previous work, we have adopted $1-U^{-1}$ as a good approximation to the right-hand side of (1) for high energies; a more refined approximation is

$$c_0=1+U_0^{-1}-U^{-1}, \tag{2}$$

where $U_0=2\bar{U}_0^2-1$ is the primary nucleon energy in the laboratory frame. Generally, $U_0\gg U$, but when $U_0\approx U$, the approximation $c_0=1-U^{-1}$ is invalid.

Assuming a differential cross section of the type

$$W(U_0, U, c)dUdc=UF(U_0, U)y\{U(1-c)\}dUdc, \tag{3}$$

with

$$F(U_0, U)=20UU_0^{-5}(U_0-U)^3,$$

one obtains a total cross section:

$$F(U_0, U)dU\int_0^{1-U/U_0} y(x)dx. \tag{4}$$

If the function $y(x)$ is assumed to be of the form

$$y(x)=\beta e^{-\beta x}, \tag{5}$$

where β is very large, the upper limit to the integral in (4) is unimportant, even near $U=U_0$, since $F(U_0, U)$ itself must vanish there. However, it seems natural to choose the argument of the function $y(x)$ in such a way that the upper limit of the integral in (4) should be independent of the energy; thus,

$$\Omega(U_0, U, c)dUdc$$

$$=\frac{U_0U}{U_0-U}F(U_0, U)y\left\{\frac{U_0U(1-c)}{U_0-U}\right\}dUdc. \tag{6}$$

This formula differs very little from (3) except near $U=U_0$, where the replacement of U^{-1} by $U^{-1}-U_0^{-1}$ gives a more intense concentration of particles in the forward direction, and hence a smaller mean square angular deviation for a given value of β. An interesting feature of (6) is that the apparently more complicated argument of $y(x)$ does in fact allow us to obtain the angular distribution function explicitly for both nucleons and mesons in the nucleus and in a finite absorber, such as the atmosphere or lead, etc. The tedious procedure of reconstructing the distribution function from its moments, which is always possible,[1,6,9] is thereby avoided.

[9] H. Messel, *Progress in Cosmic Ray Physics* (North Holland Publishing Company, Amsterdam, 1953), Vol. II (to be published).

3. THE DIFFUSION EQUATION FOR HOMOGENEOUS NUCLEAR MATTER AND THE NUCLEUS

In previous papers,[1,6] the diffusion equation

$$C\frac{\partial\nu(U, C)}{\partial z}+\nu(U, C)$$

$$=2\int_U^\infty dU'\int_{c_0}^1 dc\int_0^{2\pi}\frac{d\omega}{2\pi}\nu(U', C')W(U', U, c), \tag{7}$$

$$C'=Cc+Ss\cos\omega, \quad S=(1-C^2)^{\frac{1}{2}}, \quad s=(1-c^2)^{\frac{1}{2}}, \tag{8}$$

was derived, wherein $\nu(U, C, z)dUdC$ is the probability of finding a nucleon at depth z (measured in interaction lengths in the direction of motion of the incident particle), with energy U, dU and direction of motion making an angle of cosine C, dC with that of the incident particle, in homogeneous nuclear matter.

With the assumed mechanism of meson production stated in Sec. 1, the analogous equation for the meson angular distribution function $\pi(U, C, z)$ is

$$C\frac{\partial\pi(U, C)}{\partial z}$$

$$=\int_U^\infty dU'\int_{c_0}^1 dc\int_0^{2\pi}\frac{d\omega}{2\pi}\nu(U', C')W(U', U, c). \tag{9}$$

It follows from (7) and (9) that

$$2C\partial\pi/\partial z=C\partial\nu/\partial z+\nu. \tag{10}$$

Integrating from 0 to z, one has

$$2C\pi(U, C, z)=C\nu(U, C, z)-\delta(1-C)\delta(U-U_0)$$

$$+\int_0^z\nu(U, C, z')dz', \tag{11}$$

where U_0 is the energy of the primary nucleon. To obtain results for the nucleus, one applies the averaging operator

$$\mathbf{N}(D_A)=\int_0^{D_A}\frac{2zdz}{D_A{}^2}$$

to (11), obtaining

$$2Cp(U, C)=Cn(U, C)-\delta(1-C)\delta(U-U_0)$$

$$+\int_0^{D_A}\nu(U, C, z)(1-z^2/D_A{}^2)dz, \tag{12}$$

where $p(U, C)$ and $n(U, C)$ are the angular distribution functions for the mesons and nucleons, respectively, scattered from the nucleus of atomic weight A.

The angular moments $n_{(k)}(U)$ derived from the function $n(U, C)$ have been given previously,[1,6,9] and it can be shown from (12) that the corresponding

angular moments $p_{(k)}(U)$ for the mesons, derived from $p(U, C)$ are obtained by replacing $\{1-h(v)\}$ by $\frac{1}{2}W(v)h(v)/\alpha(v)$ in all places in the formulas for $n_{(k)}(U)$ in our previous papers.[1,6,9] For example, the mean square angle of emission for scattered nucleons of energy greater than U is

$$\langle\theta^2\rangle_n = N_{(1)}(U)/N_{(0)}(U),$$
$$N_{(k)}(U) = \int_U^\infty n_{(k)}(U)dU, \tag{13}$$

$$N_{(0)}(U) = (2\pi i)^{-1}\int_{v_0-i\infty}^{v_0+i\infty}(U_0/U)^v\{1-h(v)\}dv/v,$$
$$N_{(1)}(U) = (2\pi i U_0)^{-1}\int_{v_0-i\infty}^{v_0+i\infty}(U_0/U)^v 2y_{(1)}W(v-1) \tag{14}$$
$$\times\{\alpha(v)-\alpha(v-1)\}^{-1}\{h(v)-h(v-1)\}dv/v.$$

So the corresponding formulas for the mesons are

$$\langle\theta^2\rangle_\pi = P_{(1)}(U)/P_{(0)}(U),\ P_{(k)}(U) = \int_U^\infty P_{(k)}(U)dU, \tag{15}$$

where

$$P_{(0)}(U) = (2\pi i)^{-1}\int_{v_0-i\infty}^{v_0+i\infty}(U_0/U)^v\{\tfrac{1}{2}W(v)h(v)/\alpha(v)\}dv/v,$$

$$P_{(1)}(U) = (2\pi i U_0)^{-1}\int_{v_0-i\infty}^{v_0+i\infty}\left(\frac{U_0}{U}\right)^v\frac{y_{(1)}W(v-1)}{\alpha(v)-\alpha(v-1)} \tag{16}$$
$$\times\left\{\frac{W(v-1)h(v-1)}{\alpha(v-1)}-\frac{W(v)h(v)}{\alpha(v)}\right\}\frac{dv}{v}.$$

The definitions of $y_{(1)}$, $W(v)$, $h(v)$, $\alpha(v)$ are unchanged.

So far the cross section considered has been that of (3). When (6) is adopted, the distribution functions $n(U, C)$ and $p(U, C)$ may be obtained explicitly, and the moments easily derived from them as desired.

Equation (7) is much simplified by the application of the transform defined by

$$\bar{\nu}(U, k) = \int_{-1}^{1} J_0(kT)\nu(U, C)dC, \tag{17}$$

where T is the tangent of the angle whose cosine C is. The inverse of this transform is

$$\nu(U, C) = C^{-3}\int_0^\infty J_0(kT)\bar{\nu}(U, k)kdk, \quad (C>0), \tag{18}$$

as may be shown by expressing the Bessel function by a Fourier integral. It is evident from our previous work[1,6,8] that the multiplier C on the left-hand side of (7) may legitimately be replaced by 1, the effect being to neglect terms of order U^{-1} compared with unity. The differential cross sections which we adopt are analytic functions of c which assume extremely small values for $c<c_0$; the error involved in replacing c_0 by -1 in (7) is thus completely negligible, unless one is interested in computing very high moments (of the order of $\beta\approx 100$) of the angular distribution function. For our present purpose, therefore, we replace c_0 by -1.

To obtain the transform of

$$R(U, C) = 2\int_U^\infty dU'\int_{-1}^{1}dc\int_0^{2\pi}\frac{d\omega}{2\pi}\nu(U', C')W(U', U, c),$$

one requires to evaluate the expression

$$\int_{-1}^{1}J_0(kT)\int_{-1}^{1}dc\int_0^{2\pi}\frac{d\omega}{2\pi}\nu(U', C')W(U', U, c)dC.$$

Interchange the integrations with respect to C and c, and change the angular variables C and ω to C' and λ, where

$$C = C'c+S's\cos\lambda. \tag{19}$$

The above integral then becomes

$$\int_{-1}^{1}dc\int_{-1}^{1}dC'\int_0^{2\pi}\frac{d\lambda}{2\pi}\nu(U', C')W(U', U, c)J_0(kT).$$

Let T, T', and t be the tangents of the angles whose cosines are C, C', and c, respectively; then, using the small angle approximation, one has

$$c = 1-\tfrac{1}{2}t^2, \quad T^2 = T'^2+t^2-2tT'\cos\lambda. \tag{20}$$

Since

$$\frac{1}{2\pi}\int_0^{2\pi}J_0\{k(T'^2+t^2-2tT'\cos\lambda)^{\frac{1}{2}}\}d\lambda = J_0(kT')J_0(kt), \tag{21}$$

one obtains

$$\int_{-1}^{1}J_0(kT)R(U, C)dC = 2\int_U^\infty dU'\bar{\nu}(U', k)\bar{W}(U', U, k), \tag{22}$$

where

$$\bar{W}(U', U, k) = \int_{-1}^{1}W(U', U, c)J_0(kt)dc. \tag{23}$$

If (3) is substituted in (23), one obtains

$$\bar{W}(U', U, k) = F(U', U)\exp[-k^2/(2\beta U)], \tag{24}$$

and the transform of (7) is

$$\frac{\partial\bar{\nu}(U)}{\partial z}+\bar{\nu}(U) = \exp[-k^2/(2\beta U)]\int_U^\infty F(U', U)\bar{\nu}(U')dU'. \tag{25}$$

This integral equation can be reduced to a fourth-

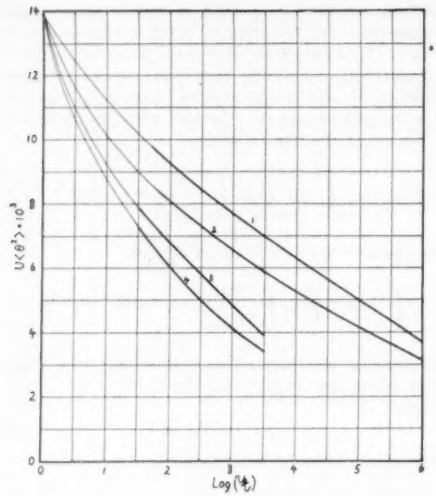

FIG. 1. Plot of $U\langle\theta^2\rangle\times10^3$ against the logarithm of the ratio of the primary energy U_0 and the energy U above which particles are emitted from a nucleus. Energies are measured in proton mass units. $\langle\theta^2\rangle$, defined by Eq. (13) for nucleons and by Eq. (15) for mesons, gives the mean square angle of emission in radians squared of particles resulting from a nucleon-nucleus collision. Curves 1 and 2 are for nucleons and mesons, respectively, and valid for the heavy nuclei silver and bromine. Curves 3 and 4 are for nucleons and mesons, respectively, and valid for the light nuclei carbon, oxygen, and nitrogen. The light portion of the curves represents extrapolation to the known value of $\langle\theta^2\rangle$ for $U\to U_0$. Results were obtained using the cross section (3) with $\beta=144$.

order differential equation, by taking the Laplace transform with respect to z of

$$\frac{\partial^4}{\partial U^4}\left\{\frac{\partial\bar{\mu}(U)}{\partial z}+\bar{\mu}(U)\right\}=120^{-4}\exp[-k^2/(2\beta U)]\bar{\mu}(U),$$
$$\bar{\mu}(U)=U^{-1}\bar{\nu}(U)\exp[k^2/(2\beta U)]. \tag{26}$$

This does not appear to be soluble in terms of elementary functions. If, however, one replaces $W(U', U, \epsilon)$ throughout by $\Omega(U', U, \epsilon)$, as defined in (6), then the transform of (7) becomes

$$\frac{\partial\bar{\nu}(U)}{\partial z}+\bar{\nu}(U)$$
$$=\int_U^\infty \exp\left\{-\frac{k^2}{2\beta}\left(\frac{1}{U}-\frac{1}{U'}\right)\right\}F(U', U)\bar{\nu}(U')dU', \tag{27}$$

or

$$\frac{\partial\bar{\omega}(U)}{\partial z}+\bar{\omega}(U)=\int_U^\infty F(U', U)\bar{\omega}(U')dU', \tag{28}$$

where

$$\bar{\omega}(U)=\exp\{k^2/(2\beta U)\}\bar{\nu}(U).$$

For $z=0$, one has

$$\bar{\omega}(U, k, z=0)=\exp[k^2/(2\beta U)]\delta(U_0-U). \tag{29}$$

The solution of (28), obtained by Mellin transforms, is therefore

$$\bar{\omega}(U)=\frac{U_0^{-1}}{2\pi i}\int_{v_0-i\infty}^{v_0+i\infty}\left(\frac{U_0}{U}\right)^{v+1}$$
$$\times\exp[k^2/(2\beta U_0)]e^{-\alpha(v)z}dv, \quad (v_0>0). \tag{30}$$

Hence,

$$\bar{\nu}(U)=\exp\left\{\frac{k^2}{2\beta}\left(\frac{1}{U_0}-\frac{1}{U}\right)\right\}\nu_{(0)}(U, z). \tag{31}$$

where $\nu_{(0)}(U, z)$ is the well-known differential average numbers integral. Taking the inverse transform defined by (18), one obtains

$$\nu(U, C)=\frac{\beta U_0 U}{U_0-U}\exp\left\{-\frac{\beta U U_0(1-C)}{U_0-U}\right\}\nu_{(0)}(U, z),$$
$$C>0. \tag{32}$$

It has thus been proved that the angular dependence of the differential cross section implied by (6) is hereditary with respect to nuclear collisions. If this cross section is correct, the angular distribution function corresponding to a single incident particle of given energy is obtained under all circumstances by multiplying the average number of nucleons at depth z by the same angular dependent factor. Thus, the mean square angle with the shower axis made by particles *with* (not *above*) a given energy depends only on that energy and the energy of the primary, and is independent of the number of intervening collisions.

To obtain the angular distribution function for the particles emerging from a nucleus, one applies the operator $\mathbf{N}(D_A)$ to $\nu(U, C)$; thus,

$$n(U, C)=\mathbf{N}(D_A)\nu(U, C)$$
$$=\frac{\beta U_0 U}{U_0-U}\exp\left\{-\frac{\beta U U_0(1-C)}{U_0-U}\right\}n_{(0)}(U), \tag{33}$$

where $n_{(0)}(U)$ is the differential average numbers integral,

$$n_{(0)}(U)=\frac{U_0^{-1}}{2\pi i}\int_{v_0-i\infty}^{v_0+i\infty}\left(\frac{U_0}{U}\right)^{v+1}\{1-h(v)\}dv. \tag{34}$$

Similarly, for the mesons,

$$p(U, C)=\frac{\beta U_0 U}{U_0-U}\exp\left\{-\frac{\beta U U_0(1-C)}{U_0-U}\right\}p_{(0)}(U), \tag{35}$$

where

$$p_{(0)}(U)=\frac{U_0^{-1}}{2\pi i}\int_{v_0-i\infty}^{v_0+i\infty}\left(\frac{U_0}{U}\right)^{v+1}\frac{W(v)h(v)}{2\alpha(v)}dv, \tag{36}$$

if the mechanism of meson production described in the introduction is correct. The confirmation of the theoretical distribution indicated by (35) would substantiate the hypotheses which were made.

The moments of the distribution function $n(U, C)$ given by (33) are

$$n_{(k)}(U)=2^k\int_{-1}^{1} n(U, C)(1-C)^k dC$$
$$=k!\left\{\frac{2(U_0-U)}{\beta U_0 U}\right\}^k n_{(0)}(U). \quad (37)$$

Hence, the moments of the distribution function $N(U, C)$ for particles with energy *greater than* U are

$$N_{(k)}(U)=\int_U^\infty n_{(k)}(U)dU$$
$$=\frac{k!2^k}{(\beta U)^k}\frac{1}{2\pi i}\int_{v_0-i\infty}^{v_0+i\infty}\left(\frac{U_0}{U}\right)^v\sum_{l=0}^{k}(-1)^{k-l}\binom{k}{l}$$
$$\times\{1-h(v-l+k)\}\frac{dv}{v+k}. \quad (38)$$

The equivalent formulas for the mesons are

$$p_{(k)}(U)=k!\left\{\frac{2(U_0-U)}{\beta U_0 U}\right\}^k p_{(0)}(U),$$

and

$$P_{(k)}(U)=\frac{k!2^k}{(\beta U)^k}\frac{1}{2\pi i}\int_{v_0-i\infty}^{v_0+i\infty}\left(\frac{U_0}{U}\right)^v\sum_{l=0}^{k}(-1)^{k-l}\binom{k}{l}$$
$$\times\frac{W(v-l+k)h(v-l+k)}{2\alpha(v-l+k)}\frac{dv}{v+k}. \quad (39)$$

4. THE DIFFUSION EQUATION FOR THE ATMOSPHERE AND OTHER MEDIA

The diffusion equation for the nucleons in media consisting of dispersed nuclei is identical in form with that for the nucleus:

$$C\frac{\partial\phi(U, C)}{\partial\theta}+\phi(U, C)$$
$$=\int_U^\infty dU'\int_{-1}^{1}dc\int_0^{2\pi}\frac{d\omega}{2\pi}\phi(U', C')n(U', U, c), \quad (40)$$

where $\phi(U, C)$ is the differential angular distribution function at depth θ, measured in interaction lengths, and $n(U', U, c)$ is the function $n(U, C)$ of the previous section corresponding to a primary of energy U'. The analysis of the previous section is equally applicable to (40), up to the analog of (25), after which some specific form of differential cross section has to be adopted. If (3) is regarded as applicable, it is possible to evaluate the moments of $\phi(U, C)$, and to reconstruct the function itself, as we have shown[1,9] previously. If (6) is used, however, then the function $\phi(U, C)$ can be obtained directly by following a method identical with that of the previous section. The result is

$$\phi(U, C, \theta)=\frac{\beta U_0 U}{U_0-U}\exp\left\{-\frac{\beta U U_0(1-C)}{U_0-U}\right\}\phi_{(0)}(U, \theta), \quad (41)$$

where $\phi_{(0)}(U, \theta)$ is the average numbers integral:

$$\phi_{(0)}(U, \theta)=\frac{U_0^{-1}}{2\pi i}\int_{v_0-i\infty}^{v_0+i\infty}\left(\frac{U_0}{U}\right)^{v+1}\exp\{-h(v)\theta)\}dv. \quad (42)$$

The moments of the distribution are

$$\phi_{(k)}(U, \theta)=k!\left\{\frac{2(U_0-U)}{\beta U_0 U}\right\}^k\phi_{(0)}(U, \theta). \quad (43)$$

For integral spectra, one has

$$\Phi_{(k)}(U, \theta)=\frac{k!2^k}{(\beta U)^k}\frac{1}{2\pi i}\int_{v_0-i\infty}^{v_0+i\infty}\left(\frac{U_0}{U}\right)^v\sum_{l=0}^{k}(-1)^{k-l}\binom{k}{l}$$
$$\times\exp\{-h(v-l+k)\theta\}\frac{dv}{v+k}. \quad (44)$$

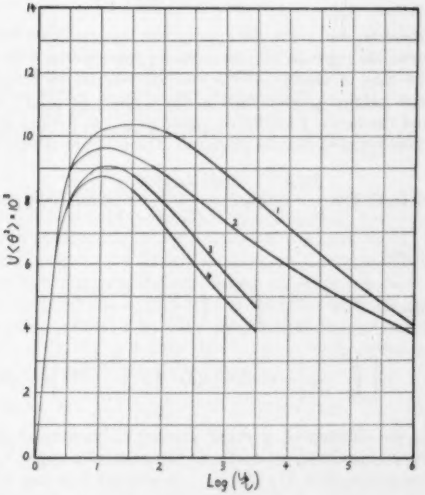

FIG. 2. Plot of $U\langle\theta^2\rangle\times10^3$ against the logarithm of the ratio of the primary energy U_0 and the energy U above which particles are emitted from a nucleus. Energies are measured in proton mass units. $\langle\theta^2\rangle$, defined by Eq. (13) for nucleons and by Eq. (15) for mesons gives the mean square angle of emission in radians squares of particles resulting from a nucleon-nucleus collision. Curves 1 and 2 are for nucleons and mesons, respectively, and valid for the heavy nuclei silver and bromine. Curves 3 and 4 are for nucleons and mesons, respectively, and valid for the light nuclei carbon, oxygen, and nitrogen. The light portion of the curves represents extrapolation to the known value of $\langle\theta^2\rangle$ for $U\to U_0$. Results were obtained using the new cross section (6) with $\beta=80$.

For the mesons in the atmosphere, the possibility of decay has to be taken into account. It is known, also, that π-mesons of low energy interact strongly with nuclei. However, at higher energies (>2 Bev) the experimental evidence is by no means conclusive on this point, and there are grounds[10,11] for supposing, as we have tentatively assumed for the nucleus, that at very high energies, the nuclear interaction of π-mesons may be neglected. Thus, we carry over our assumptions pertaining to mesons in the nucleus, into the theory for the atmosphere. They are true, of course, only at high energies, and hence ionization loss of energy for the charged mesons may be neglected with equal force.

It should be stressed that this theory for the mesons is very tentative, and is presented only for purposes of comparison with future experimental data.

The fundamental diffusion equation for either positively charged, negatively charged, or neutral mesons can be expressed in the following form:

$$C\frac{\partial m(U,C,\theta)}{\partial\theta}=\frac{1}{3}\int_U^\infty dU'\int_{-1}^1 dc\int_0^{2\pi}\frac{d\omega}{2\pi}\phi(U',C',\theta)\times p(U',U,c)+\frac{m_\pi c}{\tau\theta'(t)U}m(U,C,\theta). \quad (45)$$

where m_π and τ are the appropriate meson masses and mean life times in the c.m. system, respectively, $\theta'(t)$ is the rate of change of the nuclear interaction length with height (proportional to the density at height t), and the factor $\frac{1}{3}$ attributes equal weight to each of the three types of mesons produced. The solution of (45) is

$$m(U,C,\theta)=\frac{\beta U_0 U}{U_0-U}\exp\left\{\frac{\beta U U_0(1-C)}{U_0-U}\right\}m_{(0)}(U,\theta), \quad (46)$$

where

$$m_{(0)}(U,\theta)=\frac{(3U_0)^{-1}}{2\pi i}\int_{v_0-i\infty}^{v_0+i\infty}\left(\frac{U_0}{U}\right)^{v+1}\frac{W(v)h(v)}{2\alpha(v)}\times\left[\int_0^\theta\exp\left\{-h(v)\lambda+[t(\theta)-t(\lambda)]\frac{m_\pi c}{\tau U}\right\}d\lambda\right]dv \quad (47)$$

is the differential average number of mesons of the type considered at depth θ. For neutral π-mesons in the atmosphere, the lifetime τ is so small that one has

$$\int_0^\theta\exp\left\{-h(v)\lambda+[t(\theta)-t(\lambda)]\frac{m_\pi c}{\tau U}\right\}d\lambda=-\exp\{-h(v)\theta\}\tau U\theta'(t)/(m_\pi c), \quad (48)$$

for $U\ll 10^8$ Bev. For an isothermal atmosphere, the integral may also be evaluated exactly for both charged and neutral mesons in terms of the incomplete gamma-function.

In media of constant density, one has

$$t(\theta)-t(\lambda)=k(\lambda-\theta)/\delta_0, \quad (49)$$

where k is the interaction mean free path in g/cm^{-2}, and δ_0 is the density. Hence,

$$m_{(0)}(U,\theta)=\frac{(3U_0)^{-1}}{2\pi i}\int_{v_0-i\infty}^{v_0+i\infty}\left(\frac{U_0}{U}\right)^{v+1}\frac{W(v)h(v)}{2\alpha(v)}\times\left[\frac{\exp\{-h(v)\theta\}-\exp\{-km_\pi c(\delta_0 U)^{-1}\theta\}}{\{km_\pi c(\delta_0\tau U)^{-1}-h(v)\}}\right]dv. \quad (50)$$

The moments of the radial distribution of particles in extensive air showers are easily obtained for the new cross section Ω by substitution in the formula (70) of reference 1 the new values of the $n_{(k)}$, given by (37). The explicit determination of the radial distribution function presents difficulties not encountered in connection with the angular distribution function; there is some hope, however, that these difficulties may be overcome in the future.

If $f(\mathbf{p},\mathbf{r},t)$ is the angular-radial distribution function for the nucleons, and $m(\mathbf{p},\mathbf{r},t)$ that for the mesons, there exists the relation

$$\frac{1}{\theta'(t)}\left(\frac{\partial m}{\partial t}-\frac{p_1}{U}\frac{\partial m}{\partial r_1}-\frac{p_2}{U}\frac{\partial m}{\partial r_2}\right)-\frac{m_\pi c m}{\tau U\theta'(t)}=\frac{1}{3}\int_U^\infty dU'\int_{-1}^1 dc\int_0^{2\pi}\frac{d\omega}{2\pi}f(\mathbf{p}',\mathbf{r},t)p(U',U,c), \quad (51)$$

where $c=\mathbf{p}\cdot\mathbf{p}'/(U'U)$, $U'=|\mathbf{p}'|$, and $U=|\mathbf{p}|$. The solution of (51), which is physically obvious, is

$$m=\frac{1}{3}\int_\infty^t\exp\left\{\frac{m_\pi c}{U}(t-t')\right\}\int_U^\infty dU'\int_{-1}^1 dc\int_0^{2\pi}\frac{d\omega}{2\pi}\times f\{\mathbf{p}',\mathbf{r}+\mathbf{p}(t-t')/U,t'\}p(U',U,c)\theta'(t')dt'. \quad (52)$$

Thus the radial distribution of the mesons is obtainable in terms of that of the nucleons.

5. RESULTS AND DISCUSSION

To obtain explicit results from the preceding formulas, it is first necessary to fix the parameter β contained in the differential cross section. This can be accomplished most accurately by comparison of the calculated and observed mean square distance of the nucleons from the shower axis at sea level, in extensive air showers. In this way one obtains the values $\beta=144$ for the cross section (3), and $\beta=80$ for (6).

Using these values of β, we have determined the mean square angle of emission of nucleons and mesons of energy greater than a given value, for both light and heavy nuclei, and both types of cross section, in colli-

[10] Messel, Potts, and McCusker, Phil. Mag. **43**, 889 (1952).
[11] H. Messel and R. B. Potts, Phys. Rev. **87**, 757 (1952).

sions between a nucleon and a nucleus. Results are presented in Figs. 1 and 2.

We consider first the results for the cross section (3), and $\beta=144$. It can be shown rigorously that as U approaches U_0, the mean square angle approaches the value $2/\beta$. This is different from the very small value obtained by the evaluation of (13) and (14) by the method of steepest descents, which, as we have pointed out previously[12] does not give good results when U is comparable with U_0. The light portion of the lines in Figs. 1 and 2 represent extrapolations to meet the known values for $U=U_0-0$.

As expected, using the cross section defined by (6), one obtains results differing radically from those already considered only when $U\approx U_0$. With (6), the value of $\langle\theta^2\rangle$ approaches zero, instead of the large value $2/\beta$ resulting from the use of (3). Evidently suitable experiments should be able to decide between the two alternative cross sections.

The results for the mesons are very similar to those for the nucleons, but somewhat smaller, as one might expect on the model adopted. On any other model, the difference between the spread of the mesons and that of the nucleons would be less. This difference could, in principle, enable one to determine which of the various models[7] of meson production, so far considered in cascade theory, is most nearly correct.

On account of its hereditary property, the normalized angular distribution for scattered particles in nuclear collisions represented by (6) is preserved under all conditions throughout the atmosphere and is the same for the mesons as for the nucleons.

[12] H. Messel and H. S. Green, Proc. Phys. Soc. (London) **A65**, 245 (1952); Phys. Rev. **83**, 1279 (1951).

PHYSICAL REVIEW VOLUME 88, NUMBER 6 DECEMBER 15, 1952

The Stopping Power of K-Electrons*

M. C. WALSKE
Los Alamos Scientific Laboratory, University of California, Los Alamos, New Mexico

(Received August 27, 1952)

The stopping power of K-shell electrons for large incident particle energies is calculated in this paper, adding to and correcting previous work on the subject. A definition is given for the average ionization potential of an atom independent of the energy of the incident particle. An integral representation is derived for Bethe's term C_K which corrects the simple K-shell stopping number expression. Finally, asymptotic formulas, applicable at large incident particle energies, are given for use with any element.

I. INTRODUCTION

THE energy loss of charged particles passing through matter has been calculated by Bethe,[1,2] using the Born approximation. Provided the velocity, v, of the incident particle is much larger than the "velocity" of the atomic electrons, the energy loss per cm path length is

$$-\frac{dE}{dx}=\frac{4\pi e^4z^2}{mv^2}NB, \tag{1}$$

where $B=Z\ln(2mv^2/I)$. Here ez is the charge of the incident particle, m the electronic mass, N the number of stopping atoms per cm^3, Z the nuclear charge, and I the average excitation potential of the stopping atom. The quantity B is called the stopping number.

If v is not large compared to the "velocity" of some of the atomic electrons, and this will often be true for the inner electrons of heavier elements, (1) must be modified by calculating B for these electrons separately (and without the approximations that impose on (1) a lower limit for v)[3]. Bethe[2] has done this for the stopping number, B_K, of the K-electrons and has given curves of B_K *vs* η_K. η_K is a convenient variable given as the quotient of $mv^2/2$ by the "ideal" ionization potential, $Z_{K\,\mathrm{eff}}{}^2$ Ry of the K-shell. For large η_K Bethe gives an asymptotic formula of the form

$$B_K(\theta_K,\eta_K)=S_K(\theta_K)\ln\eta_K+T_K(\theta_K)-C_K(\theta_K,\eta_K), \tag{2}$$

where θ_K is the observed ionization potential[4] in units $Z_{K\,\mathrm{eff}}{}^2$ Ry. It is then possible to expand

$$C_K(\theta_K,\eta_K)=U_K(\theta_K)\eta_K{}^{-1}+V_K(\theta_K)\eta_K{}^{-2}+\cdots, \tag{3}$$

and Brown[5] has done this, obtaining the constant $U_K(\theta_K)$ for various θ_K. As pointed out by Walske and Bethe,[6] Brown's values need a correction. The details

* Part of this work is included in the author's doctoral thesis at Cornell University, 1951.

[1] H. Bethe, Ann. Physik **5**, 325 (1930).

[2] M. S. Livingston and H. A. Bethe, Revs. Modern Phys. **9**, 263 (1937). A detailed discussion of Bethe's stopping power theory is given in this reference.

[3] These approximations are the ones mentioned at the end of Sec. II.

[4] More accurately, the energy difference between ground state and lowest unoccupied state should be used.

[5] L. M. Brown, Phys. Rev. **79**, 297 (1950).

[6] M. C. Walske and H. A. Bethe, Phys. Rev. **83**, 457 (1951).

of this correction will be presented here, and $V_K(\theta_K)$ will be given. Furthermore, Brown determined the constants $S_K(\theta_K)$ and $T_K(\theta_K)$ in (2). There is a slight numerical error[7] in his values of $T_K(\theta_K)$, which will be corrected in this paper. This error also necessitates new curves for $C_K(\theta_K, \eta_K)$. The $B_K(\theta_K, \eta_K)$ curves as given in Brown's paper remain unchanged.

II. INTEGRAL REPRESENTATION OF $C_i(\theta_i, \eta_i)$

We shall define for any atomic shell, i, $C_i(\theta_i, \eta_i)$ by a formula similar to (2):

$$B_i(\theta_i, \eta_i) = S_i(\theta_i) \ln\eta_i + T_i(\theta_i) - C_i(\theta_i, \eta_i) \quad (i = K, L, M \cdots), \quad (4)$$

where θ_i is the observed ionization potential of the ith shell divided by the "ideal" ionization potential, $Z_{i\,\mathrm{eff}}^2$ Ry/n_i^2 (n_i is the principal quantum number of the ith shell), and $\eta_i = mv^2/2Z_{i\,\mathrm{eff}}^2$ Ry. It follows then that $B = \sum_i B_i(\theta_i, \eta_i)$ is the total stopping number of the atom. It can be shown[8] that $\sum_i S_i(\theta_i) = Z$, and so one may also write

$$B = Z \ln(2mv^2/I_{\mathrm{Ar}}) - \sum_i C_i(\theta_i, \eta_i),$$

where we define I_{Ar} by

$$Z \ln I_{\mathrm{Ar}} = \sum_i S_i(\theta_i) \ln(Z_{i\,\mathrm{eff}}^2 \,\mathrm{Ry}/\lambda_i(\theta_i) n_i^2),$$

with $\lambda_i(\theta_i)$ given by

$$T_i(\theta_i) = S_i(\theta_i) \ln[4n_i^2 \lambda_i(\theta_i)].$$

As shown in reference 8, $S_i(\theta_i)$ is equal to the number of i-electrons times $\frac{1}{2}$ of 1 plus the oscillator strength per i-shell electron. This formulation enables one to define a velocity-independent average ionization potential, and also displays clearly the form of the correction needed in (1) at low velocities of the incident particle.

Analogously to Bethe's formula for the K-shell,[2] we can write the exact expression for the stopping number for the ith shell in an integral form which is not limited by the velocity condition on (1):

$$B_i(\theta_i, \eta_i) = \int_{W_{\min} = \theta_i/n_i^2}^{\infty} W dW \int_{W^2/4\eta}^{\infty} \frac{dQ}{Q^2} |F_{W,i}(Q)|^2, \quad (5)$$

where W is the energy transferred to the atomic electron in units $Z_{i\,\mathrm{eff}}^2$ Ry, $Q = q^2 =$ (change in incident particle's momentum)$^2/2mZ_{i\,\mathrm{eff}}^2$ Ry, and $|F_{W,i}(Q)|^2$ is the sum of the squares of the matrix elements of $e^{iq\cdot s}$ between the various i-shell electron states and the states greater in energy by W.

[7] This error was also published in reference 6 where some of Brown's results were quoted. Also in reference 8 the quantity λ is slightly changed by the corrected $T_K(\theta_K)$.

Bethe, Brown, and Walske[8] have considered the expression[9]

$$x(\theta, \eta) = \int_0^{\infty} dW \int_{1/4\eta}^{4\eta} \frac{dQ}{Q} \phi_W(Q) - \int_{W_{\min}}^{\infty} dW \int_{1/4\eta}^{W^2/4\eta} \frac{dQ}{Q} \phi_W(0) - \lim_{Q_1 \to 0} \int_0^{W_{\min}} dW \left[\int_{1/4\eta}^{Q_1} \frac{dQ}{Q} \phi_W(0) + \int_{Q_1}^{\infty} \frac{dQ}{Q} \phi_W(Q) \right], \quad (6)$$

where $\phi_W(Q) = W|F_W(Q)|^2/Q$, and where the integral up to $W_{\min}$ denotes all transitions forbidden by the Pauli principle. They have shown that this expression behaves, for all η and for fixed θ, exactly as the sum of a logarithmic term in η and a term independent of η. We shall consider the difference between (5) and (6), and eventually we shall show that this difference goes to zero for large η, and so it is just the $-C(\theta, \eta)$ of (4). For the purpose of taking the difference of (5) and (6) it is convenient to rewrite (6), using in the first term the sum rule of Bethe (reference 1),[10]

$$\int_0^{\infty} dW \phi_W(Q) = n^2 = \int_0^{\infty} dW \phi_W(0). \quad (7)$$

Then we write the third term of (6) as

$$\int_{1/4\eta}^{4\eta} - \int_{Q_1}^{4\eta}.$$

The second of these expressions will be used as it stands; the first is combined with the first term in (6) as transformed by (7), and this result is in turn combined with the second term of (6). One may then take the limit on Q_1 and get

$$x(\theta, \eta) = \int_{W_{\min}}^{\infty} dW \int_{W^2/4\eta}^{4\eta} \frac{dQ}{Q} \phi_W(0) - \int_0^{W_{\min}} dW \int_0^{4\eta} \frac{dQ}{Q} [\phi_W(Q) - \phi_W(0)] - \int_0^{W_{\min}} dW \int_{4\eta}^{\infty} \frac{dQ}{Q} \phi_W(Q).$$

[8] Bethe, Brown, and Walske, Phys. Rev. **79**, 413 (1950).

[9] We now drop the i-shell subscripts.

[10] $\int_0^1 dW \phi_W(Q)$ is to be interpreted as $\sum_{\mathrm{all}\ n} \phi_n(Q)$, where $\phi_n(Q) = (E_n - E_0)|F_n(Q)|^2/Q$. The n^2 occurs in (7) from our taking the effect of the n_i^2 distinct electrons in a given shell into $|F_n(Q)|^2$ and $|F_W(Q)|^2$.

The difference of (5) and (6), $-C(\theta,\eta)$, is then

$$-C(\theta,\eta)=\int_{W_{\min}}^{\infty}dW\int_{4\eta}^{\infty}\frac{dQ}{Q}\phi_W(Q)+\int_0^{\infty}dW\int_{W^2/4\eta}^{4\eta}\frac{dQ}{Q}[\phi_W(Q)-\phi_W(0)]+\int_0^{W_{\min}}dW\int_0^{W^2/4\eta}\frac{dQ}{Q}[\phi_W(Q)-\phi_W(0)]+\int_0^{W_{\min}}dW\int_{4\eta}^{\infty}\frac{dQ}{Q}\phi_W(Q).$$

We may, to order η^{-4}, neglect the last integral above because for large Q and *fixed* W, $\phi_W(Q)\sim Q^{-5}$ [see Eq. (9) for the K-shell case]; therefore, the last integral goes as η^{-5} for large η. We shall now rewrite the second term above. We denote it by G so that we may write

$$G=\int_0^{4\eta}dW\int_{W^2/4\eta}^{4\eta}\frac{dQ}{Q}[\phi_W(Q)-\phi_W(0)]-\int_{4\eta}^{\infty}dW\int_{4\eta}^{W^2/4\eta}\frac{dQ}{Q}[\phi_W(Q)-\phi_W(0)].$$

(Note our reversal of the limits in the inner integral of the second term of G.) Reversing the order of integration, the first term of G is just

$$G_1=\int_0^{4\eta}\frac{dQ}{Q}\int_0^{(4\eta Q)^{\frac{1}{2}}}dW[\phi_W(Q)-\phi_W(0)]-\int_0^{4\eta}\frac{dQ}{Q}\int_0^{\infty}dW[\phi_W(Q)-\phi_W(0)],$$

since the inner integral of the second term vanishes by the sum rule (7). Combining,

$$G_1=-\int_0^{4\eta}\frac{dQ}{Q}\int_{(4\eta Q)^{\frac{1}{2}}}^{\infty}dW[\phi_W(Q)-\phi_W(0)],$$

and reversing the order of integrations once again,

$$G_1=-\int_0^{4\eta}dW\int_0^{W^2/4\eta}\frac{dQ}{Q}[\phi_W(Q)-\phi_W(0)]-\int_{4\eta}^{\infty}dW\int_0^{4\eta}\frac{dQ}{Q}[\phi_W(Q)-\phi_W(0)].$$

Inserting this result in G above, we have

$$G=-\int_0^{\infty}dW\int_0^{W^2/4\eta}\frac{dQ}{Q}[\phi_W(Q)-\phi_W(0)].$$

Thus, to order η^{-4} we may write

$$-C(\theta,\eta)=\int_{W_{\min}}^{\infty}dW\int_{4\eta}^{\infty}\frac{dQ}{Q}\phi_W(Q)-\int_{W_{\min}}^{\infty}dW\int_0^{W^2/4\eta}\frac{dQ}{Q}[\phi_W(Q)-\phi_W(0)]. \quad (8)$$

We now write out $\phi_{W,K}(Q)$ for the K-shell[11] explicitly (from reference 1) and study the properties of (8):

$$\phi_{W,K}(Q)=\frac{2^7W}{1-e^{-2\pi/k}}\times\frac{(Q+\frac{1}{2}k^2+\frac{1}{2})\exp\left[-\frac{2}{k}\tan^{-1}\left(\frac{2k}{Q-k^2+1}\right)\right]}{[(Q-k^2+1)^2+4k^2]^3}, \quad (9)$$

with $W=k^2+1$. If we consider fixed W, then in the first integral of (8) the integrand goes as Q^{-6}, and so the integral converges well. In the second integral a logarithmic divergence is avoided at small Q by the fact that $\phi_W(Q)-\phi_W(0)$ goes to zero for small Q. For large W and Q we have convergence through a cancellation of the first integral with the first term of the second integral.

Anticipating our results in expanding (8) in a power series in η^{-1} with no constant term, we may conclude that (8) is indeed the $-C(\theta,\eta)$ of (4). In addition, since $x(\theta,\eta)$ was obtained in reference 5 by rewriting $B(\theta,\eta)$ with a $Q_{\max}$ of 4η instead of the true $Q_{\max}$ of infinity and with the assumption $Q_{\min}\ll 1$ for all W, it follows that the error introduced by these two approximations is of order η^{-1}. Bethe has used this fact frequently in his stopping power theory where large η were being considered.

III. SEPARATION OF $C(\theta,\eta)$ INTO CONTRIBUTIONS FROM HIGH AND LOW MOMENTUM TRANSFERS

If in (8) we break off the W integration at $4\eta\alpha$, with α a constant such that $\frac{1}{2}<\alpha<1$, then to order η^{-4}:

$$-C(\theta,\eta)=C_1(\theta,\eta)+C_2(\eta), \quad (10)$$

where

$$C_1=\int_{W_{\min}}^{4\eta\alpha}dW\int_{4\eta}^{\infty}\frac{dQ}{Q}\phi_W(Q)-\int_{W_{\min}}^{4\eta\alpha}dW\int_0^{W^2/4\eta}\frac{dQ}{Q}[\phi_W(Q)-\phi_W(0)], \quad (10a)$$

and

$$C_2=\int_{4\eta\alpha}^{\infty}dW\int_{4\eta}^{\infty}\frac{dQ}{Q}\phi_W(Q)-\int_{4\eta\alpha}^{\infty}dW\int_0^{W^2/4\eta}\frac{dQ}{Q}[\phi_W(Q)-\phi_W(0)]. \quad (10b)$$

[11] W for the K-shell has been called ϵ elsewhere in the literature. The $\tan^{-1}$ in (9) is to be taken in the first and second quadrants.

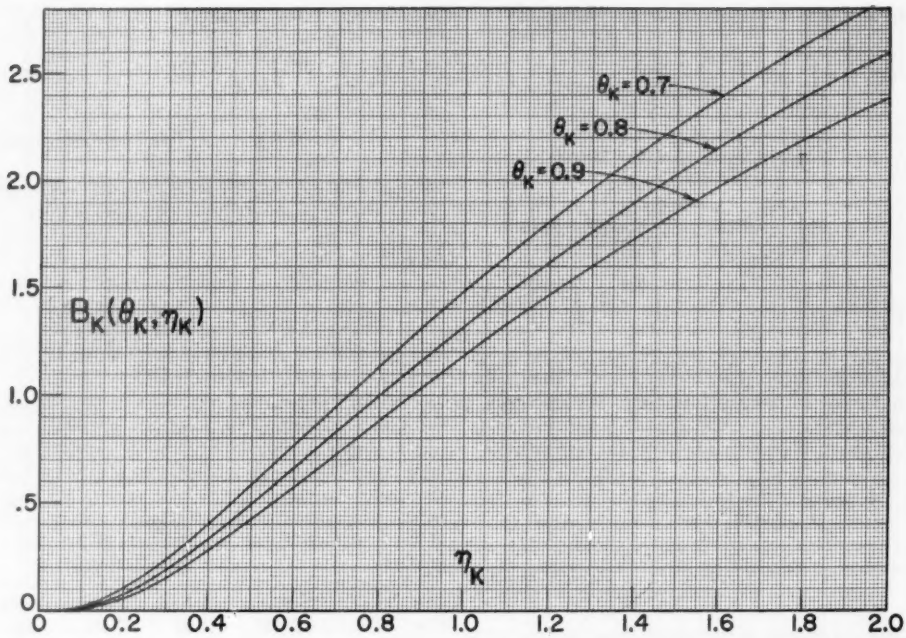

FIG. 1. $B_K(\theta_K, \eta_K)$, stopping number contribution of K-electrons.

First we consider C_1. Since the maximum of $\phi_W(Q)$ occurs at about $W=Q$ (see (9)), and since with our choice of α, $Q-W$ is at least of order η, the first term of C_1 contributes only to order η^{-5}. We may neglect it since we are ultimately interested in an expansion of $C(\theta, \eta)$ in the form (3) only to the term in η^{-2}. In the second term the main contribution arises from small Q, and for this reason we call C_1 the low momentum transfer contribution to $C(\theta, \eta)$. The integrand in the second term may be expanded in a power series in Q which converges inside the circle of convergence in the complex Q plane. The radius of this circle is the distance from the origin to the nearest singularity of the integrand which for the K-shell[12] [see (9)] occurs at $(Q-k^2+1)^2+4k^2=0$. Hence, the radius of the circle of convergence is $k^2+1=W$. Thus, the power series is convergent for real $Q<W$, but from the upper limit on the Q integration we see that the maximum Q is $W^2/4\eta$, which is at most at the maximum W just $(4\eta\alpha/4\eta)W = \alpha W < W$ since we have chosen $\frac{1}{2}<\alpha<1$. Thus, the expansion is quite valid here, and using it C_1 is correctly obtained to order η^{-4} from the second term of (10a).

Brown [reference 5, Eqs. (25) to (31)] has done this for $W_{\min}=0$[13] in the case of the K-shell obtaining the term in η^{-1}. However, in Brown's case the upper limit of the W integration is infinity rather than $4\eta\alpha$. Still his method gives C_1 (with $W_{\min}=0$) to order η^{-2} since one may easily show using (9) that the different $W_{\max}$ makes a difference only in order $\eta^{-5/2}$. If one extends Brown's work to the η^{-2} term, the net result for the

TABLE I. Comparison of computed and asymptotic $C_K(\theta_K, \eta_K)$.

	Computed values of $C_K(\theta_K, \eta_K)$			$C_K(\theta_K, \eta_K)$ from (19)		
	$\theta_K=0.7$	0.8	0.9	$\theta_K=0.7$	0.8	0.9
$\eta_K=10$	0.2407	0.2460	0.2472	0.2799	0.2852	0.2864
$\eta_K=20$	0.1153	0.1180	0.1186	0.1216	0.1243	0.1249

TABLE II. Stopping number contribution of K-electrons, $B_K(\theta_K, \eta_K)$.

η_K	$\theta_K=0.7$	$\theta_K=0.8$	$\theta_K=0.9$
1.5	2.249	2.031	1.857
1.75	2.573	2.337	2.142
2.0	2.851	2.595	2.385
2.5	3.366	3.077	2.841
3.5	4.122	3.782	3.508
5.0	4.931	4.537	4.221
10.0	6.406	5.900	5.496

[12] The same general conclusions to be drawn for the K-shell can be shown to hold for the L-shell, and undoubtedly hold for all shells.

[13] This is just the case of a hydrogen atom except that it is for 2 K-electrons.

K-shell is

$$C_{1,K}(W_{\min}=0,\eta_K) = -\eta_K^{-1}-(19/6)\eta_K^{-2} \text{ (to order } \eta_K^{-2}). \quad (11)$$

IV. EVALUATION OF $C_{2,K}(\theta_K, \eta_K)$, HIGH MOMENTUM TRANSFER CONTRIBUTION TO $C_K(\theta_K, \eta_K)$, TO ORDER η_K^{-2}

For the K-shell C_2 is explicitly [see (10b) and (9)]

$$C_{2,K}=2^7\int_{4\eta_0}^{\infty}\frac{WdW}{1-e^{-2\pi/k}} \times\left\{\int_{4\eta}^{\infty}\frac{dQ}{Q}\frac{(Q+\frac{1}{3}k^2+\frac{1}{3})\exp\left[-\frac{2}{k}\tan^{-1}\left(\frac{2k}{Q-k^2+1}\right)\right]}{[(Q-k^2+1)^2+4k^2]^3} -\int_0^{W^2/4\eta}\frac{dQ}{Q}\left[\frac{(Q+\frac{1}{3}k^2+\frac{1}{3})\exp\left[-\frac{2}{k}\tan^{-1}\left(\frac{2k}{Q-k^2+1}\right)\right]}{[(Q-k^2+1)^2+4k^2]^3} -\frac{1}{3}\frac{\exp\left(-\frac{4}{k}\tan^{-1}k\right)}{(k^2+1)^5}\right]\right\}.$$

Since the main contribution to $C_{2,K}$ arises from $Q\sim 4\eta$ which is large, we call $C_{2,K}$ the high momentum contribution to $C_K(\theta,\eta)$. In order to rewrite the two inside integrals with the same limits of integration we let $Q=y$ in the first, and $Q=W^2/y$ in the second. We make the further transformation $z=y-k^2+1$, and remembering that $W=k^2+1$, we obtain

$$C_{2,K}=\frac{2^7}{3}\int_{k_0}^{\infty}dk\frac{2k(k^2+1)}{1-e^{-2\pi/k}}\int_{a^2-k^2-1}^{\infty}\frac{dz}{z+k^2-1} \times\left[\frac{(3z+4k^2-2)\exp\left(-\frac{2}{k}\tan^{-1}\frac{2k}{z}\right)}{(z^2+4k^2)^3} -\frac{(z+4k^2+2)(z+k^2-1)^5\exp\left(\frac{2}{k}\tan^{-1}\frac{2k}{z}\right)}{(z^2+4k^2)^3} \cdot\frac{\exp\left(-\frac{4}{k}\tan^{-1}k\right)}{(k^2+1)^5}+\frac{\exp\left(-\frac{4}{k}\tan^{-1}k\right)}{(k^2+1)^5}\right], \quad (12)$$

where $k_0=(\alpha a^2-1)^{\frac{1}{2}}$, $a^2=4\eta$, and the $\tan^{-1}$ are in the first and second quadrants.

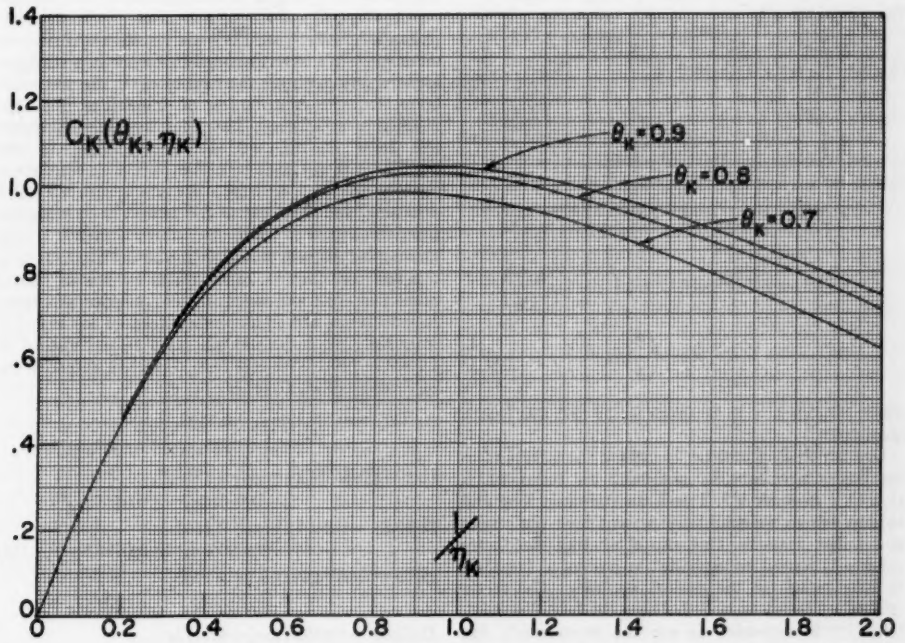

FIG. 2. $C_K(\theta_K, \eta_K)$, correction to K-electrons' stopping number contribution.

So far we have chosen α so that $\frac{1}{2}<\alpha<1$. It is now convenient to further restrict α so that the lower limit on the z integration, a^2-k^2+1, is never greater than k^2.[14] That is, we want $a^2-k^2+1\leq k^2$, or $k\geq[(a^2+1)/2]^{\frac{1}{2}}$. This will be true if $k_{\min}=k_0=[(a^2+1)/2]^{\frac{1}{2}}$. In terms of α this means $\alpha a^2-1=(a^2+1)/2$, or $\alpha=1/2+(3/2)a^{-2}=1/2+(3/8)\eta^{-1}$, which for reasonably large η is consistent with $\frac{1}{2}<\alpha<1$.

We shall now show that the contribution, say H, to $C_{2,K}$ from $k^2<z\leq\infty$ may be neglected without error to order η^{-2}. H is written exactly as (12) except that the z-limits are k^2 to infinity. Expanding the square bracket of (12) in powers of k^2/z, one sees that the last term in the bracket serves its purpose of canceling the logarithmic divergence arising in the second term at large z. The result is that the square bracket is $O(k^{-8}z^{-1})$, making the inside integral $O(k^{-10})$, and so to highest order

$$H=O\int_{k_0}^{\infty}k^4dk\int_{k^2}^{\infty}dzk^{-8}z^{-2}=O\int_{k_0}^{\infty}dkk^{-6}$$
$$=O(k_0^{-5})=O(\eta^{-5/2}).$$

Thus, since we are calculating to order η^{-2}, we may neglect H. Also, since the third term in the square bracket of (12) is only important as noted above in H, we may neglect it henceforth in $C_{2,K}$ to order η^{-2}. Thus, to order η^{-2},

$$C_{2,K}=\frac{2^7}{3}\int_{k_0}^{\infty}dkk(k^2+1)\operatorname{csch}\pi/k$$
$$\times\int_{a^2-k^2+1}^{k^2}dz\frac{1}{z+k^2-1}\cdot\frac{1}{(z^2+4k^2)^2}$$
$$\times\Big\{(4k^2+3z-2)\exp\Big(\frac{2}{k}\tan^{-1}\frac{z}{2k}\Big)$$
$$-(4k^2+z+2)(k^2+z-1)^5\exp\Big(-\frac{2}{k}\tan^{-1}\frac{z}{2k}\Big)$$
$$\times\exp\Big(\frac{4}{k}\tan^{-1}\frac{1}{k}\Big)\Big/(k^2+1)^5\Big\},$$

where $\tan^{-1}$ is now to be taken in the first and fourth quadrants.

One is now in a position to expand the integrand to the degree necessary for obtaining the terms which give $C_{2,K}$ to order η^{-2}. This is an extremely long and tedious job so we shall only present here the results and a few remarks. One can show that the factor $(z+k^2-1)^{-1}$ need be expanded in powers of $(z-1)/k^2$ to four terms for the desired accuracy. The factor $(z^2+4k^2)^{-2}$ is not expanded. Using the fact that $k\gg1$, $(k^2+1)^{-5}$ is expanded as are the exponentials and $\tan^{-1}1/k$, but $\tan^{-1}z/2k$ is not expanded. The result is that all the z integrals are elementary. The k integration can then not be done explicitly, but to order η^{-2} the η-dependence can be determined by breaking the k integration into appropriate ranges and separating leading terms. It is particularly noteworthy that the parameter k_0 does not affect the result directly. The terms involving k_0 cancel out, independent of the fact that $k_0=[(a^2+1)/2]^{\frac{1}{2}}$. This is as it should be since the precise choice of k_0 (or α) is only felt in order $\eta^{-5/2}$. Our result to order η^{-2} is

$$C_{2,K}=-\eta_K^{-1}-(25/6)\eta_K^{-2}. \tag{13}$$

Adding this to $C_{1,K}(W_{\min}=0,\eta_K)$ [see (11)] we get, to order η_K^{-2},

$$C(W_{\min}=0,\eta_K)=2\eta_K^{-1}+(22/3)\eta_K^{-2}. \tag{14}$$

V. ASYMPTOTIC FORMULAS FOR $B_K(\theta_K,\eta_K)$ TO ORDER η_K^{-2}

In order to calculate $C_K(\theta_K,\eta_K)$ for elements other than hydrogen we must subtract from (14) the contributions arising from transitions to hydrogen-like states which are forbidden in the heavier elements by the Pauli principle, i.e., occupied states. Brown (reference 5) has worked out in detail the method of doing this, and has applied it to obtain $C_K(\theta_K,\eta_K)$ to order η_K^{-1}. Except for his omission of the high momentum transfer contribution, $C_{2,K}$, and a numerical error in his determination of $T_K(\theta_K)$ [see (2)], his results are correct to order η_K^{-1}. We have extended this work in a straightforward way to obtain the term in η_K^{-2}. The procedure is to find the contribution of transitions from the K-shell to all discrete states for hydrogen, subtract this from $B_K(W_{\min}=0,\eta_K)$ corresponding to the $C_K(W_{\min}=0,\eta_K)$ given by (14) to obtain the continuum contribution in a hydrogen-like atom with no outer screening, and then add to the latter the contribution from transitions to continuum states with $W<1$ (and unoccupied discrete states) in the actual atom. It is in this last contribution, called $D_K(\theta)$ by Brown, that a numerical error was made in the η-independent term. In calculating the η-independent term of his Eq. (22) from his (20), he mistakenly used $1+n^{-2}$ instead of $1-n^{-2}$ in (20). With this term corrected, and with the η_K^{-2} term added, $D_K(\theta)$ is

$$\begin{aligned}
D_K(0.7) &=0.3783_1\ln\eta_K+0.3503_9\\
&\quad+0.0528_6\eta_K^{-1}+0.0133_6\eta_K^{-2},\\
D_K(0.75)&=0.28729\ln\eta_K+0.2945_2\\
&\quad+0.01910\eta_K^{-1}+0.01850\eta_K^{-2},\\
D_K(0.8) &=0.21072\ln\eta_K+0.2362_6\\
&\quad-0.00063\eta_K^{-1}+0.01887\eta_K^{-2},\\
D_K(0.85)&=0.14569\ln\eta_K+0.1769_0\\
&\quad-0.01008\eta_K^{-1}+0.01616\eta_K^{-2},\\
D_K(0.9) &=0.08996\ln\eta_K+0.1173_8\\
&\quad-0.01190\phi_K^{-1}+0.01161\eta_K^{-2}.
\end{aligned} \tag{15}$$

[14] Note that $z_{\min}=a^2-k^2+1$ is automatically greater than $-k^2$.

Brown's result for the contribution of the discrete states to B_K for hydrogen, extended to the η_K^{-2} term, is

$$0.56500 \ln\eta_K + 0.46869 + 0.11896\eta_K^{-1} + 0.00462\eta_K^{-2}, \quad (16)$$

and his result for $B_K(W_{\min}=0, \eta_K)$[15] as corrected by (14) is

$$B_K(W_{\min}=0, \eta_K) = 2\ln\eta_K + 2.57861 - 2\eta_K^{-1} - (22/3)\eta_K^{-2}. \quad (17)$$

Subtracting (16) from (17) we obtain the continuum contribution, E_K:

$$E_K = 1.43500 \ln\eta_K + 2.10992 - 2.11896\eta_K^{-1} - 7.33795\eta_K^{-2}. \quad (18)$$

Finally, adding (18) to (15) we get $B_K(\theta_K, \eta_K)$, the asymptotic formulas for the stopping number of the K-shell:

$$\begin{aligned}
B_K(0.7, \eta_K) &= 1.8133\ln\eta_K + 2.4603 - 2.0662\eta_K^{-1} - 7.3246\eta_K^{-2},\\
B_K(0.75, \eta_K) &= 1.7223\ln\eta_K + 2.4044 - 2.0999\eta_K^{-1} - 7.3194\eta_K^{-2},\\
B_K(0.8, \eta_K) &= 1.6457\ln\eta_K + 2.3462 - 2.1196\eta_K^{-1} - 7.3191\eta_K^{-2}, \quad (19)\\
B_K(0.85, \eta_K) &= 1.5807\ln\eta_K + 2.2868 - 2.1290\eta_K^{-1} - 7.3218\eta_K^{-2},\\
B_K(0.9, \eta_K) &= 1.5250\ln\eta_K + 2.2273 - 2.1309\eta_K^{-1} - 7.3263\eta_K^{-2}.
\end{aligned}$$

Of course, $C_K(\theta_K, \eta_K)$ to order η_K^{-2} is just the negative of the last two terms of (19).

As a check on the last two terms of (19), $C_K(\theta_K, \eta_K)$ has been evaluated numerically for $\eta_K = 10$ and 20 using the expression (8). A comparison with $C_K(\theta_K, \eta_K)$ as obtained from the last two terms of (19) is given in Table I. From this table one can see that the asymptotic terms for C_K are high by about 16 percent at $\eta_K = 10$ and by about 5.5 percent at $\eta_K = 20$ for all θ_K. If one adds to the asymptotic formula for B_K (or subtracts from C_K) a term $45\eta_K^{-3}$ these errors are reduced to about -2.4 percent and 0.6 percent, respectively, for all θ_K. This should therefore be done. That the θ_K-variation of C_K is given to greater accuracy by (19) than the full value of C_K can be seen by differencing the C_K's of different θ_K for the two sets of values in Table I.

For convenience we reprint in Fig. 1 curves of $B_K(\theta_K, \eta_K)$ for $\theta_K = 0.7$, 0.8, 0.9, and for $0 \leq \eta_K \leq 1.5$ which were calculated by the author from expression (5) and previously published by L. M. Brown in reference 5. In Table II we give a continuation of these calculations up to $\eta_K = 10$. These values are accurate to at least one percent. At $\eta_K = 10$ we have two completely independent calculations of B_K; one is to take the first two terms of (19) and to subtract the exact numerically calculated value of C_K from Table I, the other is the direct calculation of B_K reported in Table II. The values for the successive θ_K calculated via C_K are 6.401, 5.895, and 5.497, in excellent agreement with Table II. In Fig. 2 we have combined the values from Table II and the first two terms of (19) in order to plot $C_K(\theta_K, \eta_K)$ *vs* $1/\eta_K$. Near the origin on this graph we have relied upon the asymptotic formula and the exact calculations of C_K at $\eta_K = 10$ and 20. This curve is changed from the one in reference 5 by the correction to the constant term in (19).

It is a pleasure for the author to acknowledge his indebtedness to Professor H. A. Bethe for his friendly guidance and encouragement of this work.

[15] This is just twice the stopping number of a hydrogen atom since it is written for two K-electrons.

A Nuclear Resonance Modulation Correction*

M. M. PERLMAN AND M. BLOOM†
Radiation Laboratory, McGill University, Montreal, Canada

(Received August 11, 1952)

A theoretical modulation correction with experimental justification is derived. It is found that the experimentally measured value of the second moment is always larger than the true value by an amount $\frac{1}{2}Hm^2$ where Hm is the modulation amplitude. The correction holds even for amplitudes close to the line width and gives consistently good results when applied to the analysis of line shapes.

IT is well known that the effect of low temperatures on solids is to reduce the amount of molecular rotation present and hence to produce a correspondingly wider magnetic resonance signal. Indeed, this fact has been used in many investigations on the structure and internal properties of liquids and solids.

However, the wider the resonance line, the weaker it becomes. For detection purposes then, it becomes necessary to use comparatively large values of modulation amplitude in order to obtain an observable signal. As has been demonstrated,[1] this often results in experimentally measured values of the second moment of the absorption line being in error by as much as 20 percent. Because of the difficulties involved in obtaining an adequate signal and accurate and detailed plots of line shape, no experimental attempts have as yet been made to account quantitatively for this effect.

If one considers the function of the modulation as being mainly an averaging of the line shape over the range of modulation, one can derive a first-order theoretical correction using the following simple considerations:

We have

$$G(H)=\frac{1}{2Hm}\int_{H-Hm}^{H+Hm} g(H')dH'=\frac{F(H)}{2Hm}, \qquad (1)$$

where

$g(H)$ = true line shape function,

$G(H)$ = experimental line shape function,

for a modulation field of the form $Hm\sin wt$. We want

$$(\Delta H_2^2)_{\text{true}}=\frac{\int_{-\infty}^{\infty} H^2g(H)dH}{\int_{-\infty}^{\infty} g(H)dH}=\frac{A}{C}, \qquad (2)$$

where ΔH_2^2 denotes the second moment over the absorption line. We know

$$(\Delta H_2)^2_{\text{exp}}=\frac{\int_{-\infty}^{\infty} H^2G(H)dH}{\int_{-\infty}^{\infty} G(H)dH}=\frac{\int_{-\infty}^{\infty} H^2F(H)dH}{\int_{-\infty}^{\infty} F(H)dH}=\frac{X}{Y}. \qquad (3)$$

We expand $g(H')$ in a Taylor series in the neighborhood of H, i.e., we put

$$g(H')=g(H)+(H'-H)\left(\frac{dg}{dH'}\right)_H+\frac{(H'-H)^2}{2!}\left(\frac{d^2g}{dH'^2}\right)_H+\cdots. \qquad (4)$$

Substituting (4) into (3) and integrating, we obtain

$$(\Delta H_2)^2_{\text{exp}}=\frac{\int_{-\infty}^{\infty} H^2g(H)dH+\frac{Hm^2}{6}\int_{-\infty}^{\infty} H^2\left(\frac{d^2g}{dH'^2}\right)_H dH}{\int_{-\infty}^{\infty} g(H)dH+\frac{Hm^2}{6}\int_{-\infty}^{\infty}\left(\frac{d^2g}{dH'^2}\right)_H dH}=\frac{A+B}{C+D}=\frac{A}{C}\frac{1+B/A}{1+D/C}, \qquad (5)$$

neglecting derivatives of order 4 or greater;

$$\frac{A}{C}=(\Delta H_2^2)_{\text{true}}\simeq(\Delta H_2)^2_{\text{exp}}\left(1+\frac{D}{C}-\frac{B}{A}\right). \qquad (6)$$

For most lines $D/C\ll B/A$ (this may be shown experimentally), and $B/A\simeq\frac{1}{2}Hm^2Y/X$ (assume $g(H)=G(H)$ to first order and perform two partial integrations).

To first order, we have

$$(\Delta H_2^2)_{\text{exp}}=(\Delta H_2^2)_{\text{true}}+\tfrac{1}{2}Hm^2. \qquad (7)$$

The proton resonance in NH_4NO_3 at room temperature is ideally suited for a study of the effect of modulation on the second moment. The signal is strong, and the line width fairly narrow ($\sim$4 gauss), so that the effect on the second moment of a modulation amplitude of 2 gauss or more should be easily detectable. (For wider lines of $\sim$10 gauss, the statistics on the evaluation of the second moment are such that they mask the effect of amplitudes of less than about 3 gauss.)

Fourteen room temperature absorption curves were plotted and found suitable, two for each of $2Hm=1$, 3, 4.4, 5, 6, 8, and 10 gauss, where Hm is the modulation amplitude. The true second moment, that is, its value at zero modulation amplitude, was taken as 3.0 gauss.[2] The statistics on the second moment are in all cases better than ±3 percent.

The experimental results are plotted in Fig. 1. The solid line, drawn to fit the experimental points was

* This work was supported by a Fellowship from the Shell Oil Company of Canada.

† Now at University of Illinois, Urbana, Illinois.

[1] E. Andrew, J. Chem. Phys. **18**, 607 (1950).

found to follow the formula $(\Delta H_2^2)_{exp}=(\Delta H_2^2)_{true}+\frac{1}{2}Hm^2$, exactly as determined above. Thus, the experimentally measured value of the second moment is always larger than the true value.

In the Van Vleck[2] formula for the second moment the internuclear distances appear to the inverse sixth power. Thus, an error of 10–20 percent in the determination of the second moment results in an error of only 1–3 percent in the evaluation of the internuclear parameters. A further check on Eq. (7), however, is provided by an analysis of the compound KH_2PO_4, where the calculated second moment (assuming that the hydrogens lay midway along the O−H−O bond, and taking an O−H−O bond distance of 2.54A as determined from Raman spectra experiments) of the proton resonance is 3.3 gauss.[2] The average uncorrected experimental second moment on the basis of 6 runs at −183°C was found to be 4.8±0.4 gauss[2] (an error of ~45 percent). A modulation amplitude of 2 gauss was used, thus yielding a corrected second moment of 3.5±0.4 gauss[2] in agreement with the calculated result.

[2] J. H. Van Vleck, Phys. Rev. **74**, 1168 (1948).

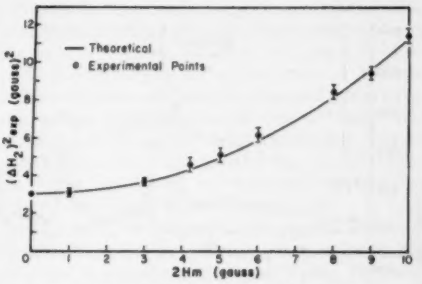

FIG. 1. The experimental modulation correction.

The experimentally observed line is the derivative of the true absorption line. When the modulation amplitude becomes nearly equal to the line width, small amounts of higher odd order derivatives are admixed. However, these effects are small, and a reasonably faithful first derivative may be obtained even in this region. In any case, the correction has been found to hold when the amplitude approaches the line width.

PHYSICAL REVIEW VOLUME 88, NUMBER 6 DECEMBER 15, 1952

Energy Levels in Light Nuclei*

J. C. ARTHUR,† A. J. ALLEN, R. S. BENDER, H. J. HAUSMAN,‡ AND C. J. MCDOLE§
University of Pittsburgh, Pittsburgh 13, Pennsylvania
(Received July 21, 1952)

Targets of beryllium, Nylon, lead fluoride, sulfur, and lead sulfide were bombarded with 8-Mev protons from the University of Pittsburgh cyclotron. Energy levels were observed in Be^9, C^{12}, N^{14}, O^{16}, F^{19}, and S^{32} by inelastic scattering at 150° from thin targets. Single levels were assigned in Be^9 and C^{12}; two levels were assigned in N^{14}; nine levels were assigned in F^{19}; and seven levels were assigned in S^{32}.

I. INTRODUCTION

THE present investigation was undertaken to look for additional low-lying levels in some light nuclei. Similar work has been done at this laboratory by Ely *et al.*,[1] Reilley *et al.*,[2] and Hausman *et al.*[3] The 8-Mev proton beam from the University of Pittsburgh cyclotron was used to bombard targets of beryllium, Nylon, fluorine, and sulfur. The incident and reaction particle momenta were analyzed magnetically. Inelastic scattering was used to determine energy levels in Be^9, C^{12}, N^{14}, O^{16}, F^{19}, and S^{32}.

II. APPARATUS

The apparatus used is essentially the same as that described previously.[4,5] It was modified by placing the detector inside the vacuum system to permit the observation of lower energy scattered particles. The target holder was remodeled to provide a means for calibration of the reaction particle analyzer without losing the vacuum.

A beam of 8-Mev protons from the cyclotron was focused by a sector magnet into a shielded scattering room. Within the scattering room the incident beam was analyzed magnetically by a 40° sector magnet and the spread in energy adjusted by appropriate slits. Charged reaction particles were momentum analyzed by a 60° sector magnet and detected by a scintillation counter using a ZnS crystal. Both analyzing magnets were calibrated with polonium alpha-particles using

* Work done in the Sarah Mellon Scaife Radiation Laboratory and assisted by the joint program of the ONR and AEC.
† Now at Project Lincoln, Massachusetts Institute of Technology, Cambridge, Massachusetts.
‡ Now at the Ohio State University, Columbus, Ohio.
§ AEC Predoctoral Fellow.
[1] Ely, Allen, Arthur, Bender, Hausman, and Reilley, Phys. Rev. **86**, 859 (1952).
[2] Reilley, Allen, Arthur, Bender, Ely, and Hausman, Phys. Rev. **86**, 857 (1952).
[3] Hausman, Allen, Arthur, Bender, and McDole, following paper [Phys. Rev. **88**, 1296 (1952)].
[4] Bender, Reilley, Allen, Ely, Arthur, and Hausman, Rev. Sci. Instr. **23**, 542 (1952).
[5] University of Pittsburgh Radiation Laboratory Precision Scattering Report No. 2, May (1952) (unpublished).

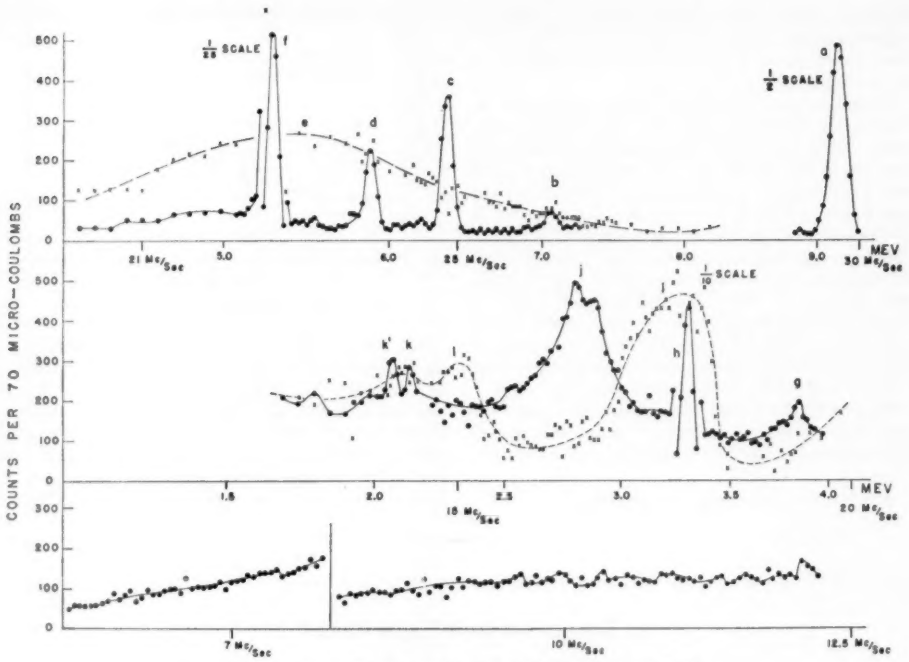

FIG. 1. Spectrum of charged particles scattered from beryllium at 150°.

$H\rho = 3.3159 \times 10^6$ gauss-cm[6]. Magnetic field strength measurements were made with proton resonance detectors. The analyzing magnets were carefully demagnetized before each run. The incident beam current was integrated to 70 microcoulombs (30 microcoulombs for one S^{32} bombardment) for each setting of the magnet which analyzed the scattered particles. The spread in incident energy was 0.04 Mev during the experiment with the beam incident perpendicularly on the target. At least two bombardments of each element were made using different targets where possible.

III. EXPERIMENTAL PROCEDURE AND DISCUSSION

A. Be^9+Proton

Beryllium targets of 0.2 mg/cm² and 0.3 mg/cm² were bombarded with protons and the reaction particles studied at 150° with respect to the incident beam. Figure 1 shows a plot of the number of counts per 70 microcoulombs of charge collected *vs* proton resonance frequency in Mc/sec at which reaction particles were detected. Peaks *b*, *c*, *d*, and *f* are due to elastic scattering from Al^{27}, O^{16}, C^{12}, and Be^9. Peak *h* is from the known excited level in Be^9 at 2.4 Mev. The average value of excitation energy obtained for this level from two runs is 2.44 Mev, which is to be compared with the values of 2.422±0.005 Mev determined by Van Patter *et al.*[6] and 2.433±0.005 Mev determined by Browne *et al.*[7] No new levels were found in Be^9 for an excitation energy of 6 Mev.

Peaks *a*, *e*, *g*, and *j* have been identified as deuterons from the reaction $Be^9(p,d)Be^8$ corresponding to the ground state and energy levels in Be^8 at 2.8, 4.0, and 5.1 Mev, respectively.

Peaks *i* and *l* are alpha-groups from the $Be^9(p,\alpha)Li^6$ reaction corresponding to the ground state and excited levels in Li^6 at 2.1 Mev (for a bibliography see Hornyak *et al.*,[8] hereafter referred to as HFML). The peaks *k* and *k*¹ are attributed to inelastic protons from the 4.4-Mev level in C^{12} which appears as a surface contaminant on the front and back of the target.

Peaks *e*, *i*, and *l* were obtained by subtraction of the readings taken with a foil in front of the detector from readings taken without a foil.

B. Nylon+Proton

Nylon targets of surface density 0.50 mg/cm² were bombarded by 8-Mev protons. The reaction particles

[6] Van Patter, Sperduto, Huang, Strait, and Buechner, Phys. Rev. **81**, 233 (1951).

[7] Browne, Williamson, Craig, and Donahue, Phys. Rev. **83**, 179 (1951).

[8] Hornyak, Lauritsen, Morrison, and Fowler, Revs. Modern Phys. **22**, 309 (1950).

were analyzed at 90° and 150°. Peaks *a*, *b*, c_1, and *c* of Fig. 2 are elastically scattered protons from O^{16}, N^{14}, C^{13}, and C^{12}, respectively. Peak *f* is the only excited state obtained in C^{12} for an excitation energy of 6.5 Mev. An excitation energy of 4.45 Mev was determined for this level. This is an average value obtained from four Nylon bombardments and nine other bombardments where carbon was a surface contaminant. The width of the peak is thought to be caused mainly by target thickness. A fresh target was used for the data yielding peak *f* Fig. 2 in an attempt to reduce the probability of target deterioration causing a widening of the peak. Many previous investigations of C^{12} have been made (see HFML, p. 325). The most accurately known value for this energy level is 4.438±0.014 Mev obtained by magnetic analysis.[8]

Three levels and possibly a fourth were found in N^{14} from the reaction $N^{14}(p,p')N^{14*}$. Peaks *d*, *e*, and *g* of Fig. 2 correspond to energy levels of 2.32, 3.96, 5.09 Mev. If e_1 were a peak in N^{14} the value of the energy level would be 3.76 Mev. Since a C^{13} elastic peak was observed it is possible that it is an energy level of this isotope.|| Its excitation energy in C^{13} would be 3.69 Mev. A level in C^{13} is known to exist at 3.677±0.005 Mev.[8] Previous investigations on N^{14} energy levels were made by Thomas and Lauritsen[9] giving values of 1.643±0.004, 2.318±0.008, 3.390±0.010, 3.9?, 5.056±0.025 Mev; by Burrows *et al.*[10] giving values of 3.95 and 5.06 Mev; and by Heydenburg *et al.*[11] giving levels at 2.35 and 3.95 Mev. Thomas and Lauritsen observed gamma-rays resulting from bombarding an enriched C^{13} target with deuterons. The gamma-ray energies which they assigned as energy levels in N^{14} at 1.6 Mev and 3.4 Mev have since beeen attributed to cascading gamma-rays (private communication with T. Lauritsen).

Peaks *h* and *i* are assigned to the oxygen doublet at 6.0 and 6.1 Mev. The best information about the doublet which can be calculated from the Nylon, PbS, and PbF_2 data (oxygen appeared as a contaminant on the last two targets) is a value of 0.087±0.010 Mev for the doublet separation. Previous measurements of these levels and their separation have been made by Chao *et al.*[12] They give values of 6.052, 6.136, and 0.084±0.006 Mev for the energy levels of the two peaks and their separation, respectively. Several other measurements of these levels have been made (see HFML, p. 343).

C. F^{19} + Proton

A target of PbF_2(1.20 mg/cm²) was evaporated on a go'd backing. With 8-Mev protons incident on the

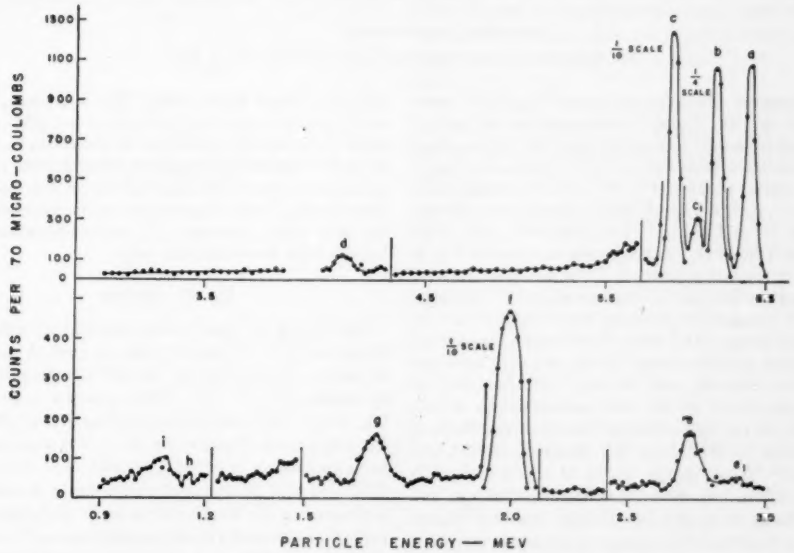

FIG. 2. Spectrum of charged particles scattered from Nylon at 150°.

|| *Note added in proof:* Further work indicates that this level is from C^{13}.

[9] R. G. Thomas and T. Lauritsen, Phys. Rev. **78**, 88 (1950).
[10] Burrows, Powell, and Rotblat, Proc. Roy. Soc. **A209**, 478 (1951).
[11] Heydenburg, Phillips, and Cowie, Phys. Rev. **85**, 742 (1952).
[12] Chao, Tollestrup, Fowler, and Lauritsen, Phys. Rev. **79**, 108 1950).

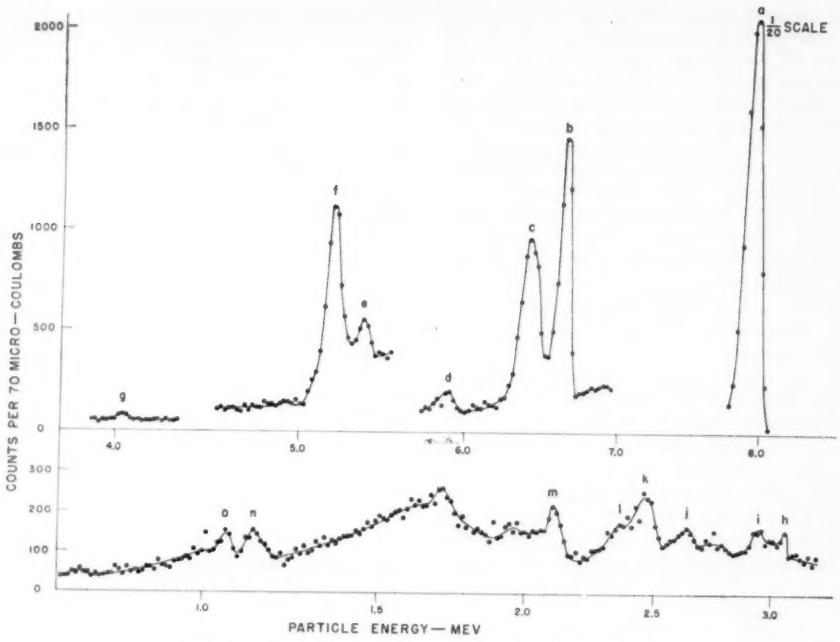

FIG. 3. Spectrum of charged particles scattered from fluorine at 150°.

target protons from the reaction $F^{19}(p,p')F^{19*}$ were observed at 150°. Figure 3 shows sections of each of two bombardments. Peak *a* is a group of protons elastically scattered from lead and gold. Peaks *b*, *c*, and *d* are the elastic peaks of F^{19}, O^{16}, and C^{12}, respectively. Peaks *e*, *f*, *g*, *h*, *i*, *j*, j_1, *k*, and *l* correspond to energy levels in F^{19} at 1.37, 1.59, 2.82, 3.94, 4.06, 4.41, 4.48, 4.59, and 4.76. Peak j_1 is not shown as a peak in Fig. 3. Peak *m* is the excited state in C^{12} at 4.4 Mev. Peaks *n* and *o* are the 6.0- and 6.1-Mev levels in O^{16}. No other levels of comparable intensity were observed for an excitation energy of 6.7 Mev. There were indications of seven other possible energy levels: one each at 4 and 4.3, three near 4.6, and two near 4.8 Mev, each of which reproduced on the two bombardments. A bibliography of previous investigations of energy levels of F^{19} is given by HFML, p. 353. Recently, Bullock and Sampson[13] found energy levels at 1.36±0.05, 2.76 ±0.05, 3.92±0.05 Mev; Heydenburg, Phillips, and Cowie[12] found levels at 1.53, 3.83 Mev, and Shull[14] found a level at 1.52 Mev. No attempt was made to study the reaction $F^{19}(p,\alpha)O^{16*}$. The spectrum shown in Fig. 3 is taken with the alpha-groups removed by placing aluminum foils in front of the detector. A broad peak appears between 1 and 2 Mev. This is a proton group which appeared on a bombardment of the gold backing made under similar conditions. It is thought to be due to (p,p') reactions in copper or silver known to exist in the gold in quantities less than 0.2 percent. All peaks shown in Fig. 3 were observed on two bombardments of the same target; however, the values above were calculated from the second run only.

D. S^{32}+Proton

The $S^{32}(p,p')S^{32}$ reaction was studied by bombarding targets of lead sulfide and sulfur on gold. A spectrum of the reaction particles in the 150° direction obtained by bombarding S^{32} with 8-Mev protons is shown in Fig. 4. *a*, *b*, and *c* are the elastic peaks of Au^{197}, S^{32}, and O^{16}, respectively. Peaks *e*, *f*, *g*, *h*, *i*, *j*, and *n* are assigned to excited levels in S^{32} at 2.25, 3.81, 4.32, 4.50, 4.74, 5.04, and 5.83 Mev, respectively. Peaks *k* and *l* are attributed to the 4.4-Mev level in C^{12} and result from carbon contaminants on the target surfaces. Four peaks (*d*, d_1, *m*, and *o*) were not used for calculations. In previous studies of S^{32} (see Alburger and Hafner[15]) excited levels were observed at 2.25 and 4.34 Mev.

[13] M. L. Bullock and M. B. Sampson, Phys. Rev. **84**, 967 (1951).
[14] F. B. Shull, Phys. Rev. **83**, 875 (1951).
[15] D. E. Alburger and E. M. Hafner, Revs. Modern Phys. **22**, 379 (1950).

IV. RESULTS AND ERRORS

Table I is a list of the elements studied and the energy levels obtained. In all (p,p') reactions, except F^{19}, where three figures are quoted an estimate of the probable error is 0.02 Mev (for F^{19} the estimated probable error is 0.03 Mev). The primary contribution to this probable error is due to an uncertainty in the calibration of the magnetic field strength of the reaction particle analyzer. This uncertainty arises from a nonlinearity between the ratio of the measured field strength to the fringing field strength and the measured field strength and also from hysteresis effects. There are indications, in general, that the levels are higher than previously published values of the same levels where the accuracy quoted is of the order of 0.01 Mev.

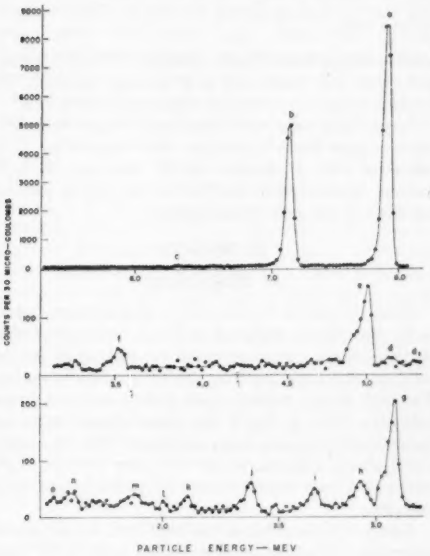

FIG. 4. Spectrum of charged particles scattered from sulfur at 150°.

TABLE I. Energy levels in Be^9, N^{14}, O^{16}, F^{19}, and S^{32}.

Element	Energy level (Mev)	Doublet separation (Mev)
Be^9	2.44	
C^{12}	4.45	
N^{14}	2.32	
	3.76?	
	3.96	
	5.09	
O^{16}	6.0	0.087
	6.1	
F^{19}	1.37	
	1.59	
	2.82	
	3.94	
	4.06	
	4.41	
	4.48	
	4.59	
	4.76	
S^{32}	2.25	
	3.81	
	4.32	
	4.50	
	4.74	
	5.04	
	5.83	

The authors wish to thank L. M. Diana, K. B. Rhodes, R. F. Weise, R. A. Barjon, Miss C. Gegauff, and E. M. Perkins for their many contributions to this project.

Energy Levels in Magnesium, Vanadium, Chromium, and Manganese*

H. J. HAUSMAN,† A. J. ALLEN, J. S. ARTHUR,‡ R. S. BENDER, AND C. J. MCDOLE§
University of Pittsburgh, Pittsburgh 13, Pennsylvania
(Received July 21, 1952)

Targets of Mg, V, Cr, and Mn have been bombarded by 8-Mev protons from the 47-in. cyclotron and the reaction particle observed at an angle of 150° to the incident beam. Three levels are assigned to Mg^{24}, seven to Mg^{25}, and two to Mg^{26}. Fourteen levels are reported for V^{51}, 15 for Cr, and 15 for Mn^{55}.

I. INTRODUCTION

MEASUREMENTS of the energy levels of stable nuclei in the region 10 to 30Z by means of inelastic charged particle reactions have been relatively neglected as compared to investigations on the light nuclei. Recently[1] an extensive program of instrumentation has been completed at the University of Pittsburgh for the study of nuclear reactions. This has permitted the use of an energy-analyzed beam of eight-Mev protons for precision determinations of nuclear energy levels. The present paper is a continuation of the studies of energy levels in the medium Z range as reported by Reilley *et al.*[2] and Ely *et al.*[3]

II. APPARATUS

The apparatus for the precision scattering project has been described elsewhere.[1] Briefly, the diverging beam of protons from the University of Pittsburgh 47-in. cyclotron is focused by a 14° sector magnet on a slit located in the center of an eight-foot shielding wall. The slit acts as a source for the beam-analyzing magnet which focusses the beam of particles at a point $1\frac{3}{4}$ in. in front of the target. The dispersion of the beam-analyzing magnet is 300 kev/in. for eight-Mev protons. Reaction particles are magnetically analyzed by a third magnet of high resolution. Charged particle groups are detected by a zinc sulfide fluorescent screen and an EMI 5311 photomultiplier tube. A set of remotely controlled absorption foils which can be positioned in front of the detector slit and scintillation screen are used to differentiate between charged particles of the same momentum.

Thin targets (approximately 10 kev) of magnesium, chromium, vanadium, and manganese were obtained by evaporation of the pure metals from conically shaped 30-mil tungsten filaments. Thicker targets used for general survey of the materials were evaporated from 5-mil tantalum boats except vanadium. Thin (18-microinch) gold foils were used as a backing material. No inelastic levels were observed from the gold backing.

Target thicknesses were measured by carefully weighing the target frame before and after evaporation. It is estimated that thicknesses can be measured to ±20 percent. Spectroscopic analysis of the targets showed less than $\frac{1}{10}$ percent contamination.

III. RESULTS

A. Magnesium

From the proton bombardment of aluminum, previously reported by Reilley *et al.*,[2] two unresolved alpha-particle groups were observed at an angle of 90° to the incident beam resulting from the $Al^{27}(p,\alpha)Mg^{24}$ reaction. The high energy alpha-particle group, assigned to the 1.38-Mev level in Mg^{24}, was superimposed upon an inelastic proton group from aluminum. The low energy alpha-group, assigned to the 4.14-Mev level in Mg^{24}, although of very weak intensity had indications of being complex.

A survey of the protons scattered from a thin natural magnesium target at an observation angle of 90° indicated four resolved proton groups: the magnesium elastic peak, a group corresponding to the 1.38-Mev level, and a resolved doublet at 4.14-Mev excitation. Since naturally occurring magnesium contains three isotopes, there existed the possibility that one of the proton groups assigned to the 4.14-Mev doublet in Mg^{24} could have arisen from an excited state in either Mg^{25} or Mg^{26}. It was decided to determine whether the apparent doublet exists in Mg^{24} at 4.14-Mev excitation by observing the alpha-particles from the proton bombardment of aluminum at an angle of 150° to the incident beam.

The reason for the choice of the observation angle of 150° was twofold. Calculations showed that the relative motion of the alpha-particle groups to that of neighboring proton groups from aluminum would be such as to eliminate any overlap. Also, the variation of energy of the scattered particles with angle is such as to improve the relative resolution of the alpha-groups.

With a 0.19-mg/cm² aluminum target, three resolved alpha-groups were found corresponding to the 1.38-Mev level in Mg^{24} and a doublet at 4.14 Mev. No alpha-particle group corresponding to the ground-state reaction was found. However, the momentum of the ground-

* Work done in the Sarah Mellon Scaife Radiation Laboratory and assisted by the joint program of the ONR and AEC.
† Now at the Ohio State University, Columbus, Ohio.
‡ Now at Project Lincoln, Massachusetts Institute of Technology, Cambridge, Massachusetts.
§ AEC Predoctoral Fellow.
[1] Bender, Reilley, Allen, Ely, Arthur, and Hausman, Rev. Sci. Instr. 23, 542 (1952).
[2] Reilley, Allen, Arthur, Bender, Ely, and Hausman, Phys. Rev. 86, 857 (1952).
[3] Ely, Allen, Arthur, Bender, Hausman, and Reilley, Phys. Rev. 86, 859 (1952).

state alpha-group was very near to that of the intense aluminum proton elastic peak. Because of the large relative difference in intensity, an upper limit was placed on that of the ground-state alpha-group. It was estimated as being no greater than 1/20 the intensity of the 1.38-Mev alpha-group.

A thick target 0.44 mg/cm² survey of the protons scattered from natural magnesium at the observation angle of 150° resolved 15 proton groups. Actual level assignments were made using a thin (0.1 mg/cm²) natural magnesium target and improved resolution. A spectrum of the proton groups scattered from a thin natural magnesium target is plotted in Fig. 1. Peaks *a*, *c*, and *d* are the elastic peaks of Mg, O, and C. Three of the proton groups, peaks *e*, *n*, and *o*, were assigned to levels in Mg^{24}, positive identification being made by the $Al^{27}(p,\alpha)Mg^{24}$ measurements. Inasmuch as the ground-state alpha-group from the above (p,α) reaction was not resolved, a Q value of 1.594 as reported by Van Patter[4] was used to calculate the excited levels in Mg^{24}. The values determined are 1.39, 4.12, 4.22, which are in good agreement with the assignments made by inelastic proton measurements.

Seven proton groups were tentatively assigned to excited states in Mg^{25}. The assignment of these levels was made by comparison with the levels reported by Endt *et al.*[5] from the $Al^{27}(d,\alpha)Mg^{25}$ reaction and from the $Mg^{24}(d,p)Mg^{25}$ reaction. The proton group corresponding to the 2.744 level reported has indications of being complex. It is probable that this group corresponds to the 2.736- and 2.799-Mev doublet in Mg^{25} reported by Endt *et al.*[5] Two groups have been assigned to Mg^{26} by comparing their energies with the reported[6] levels.

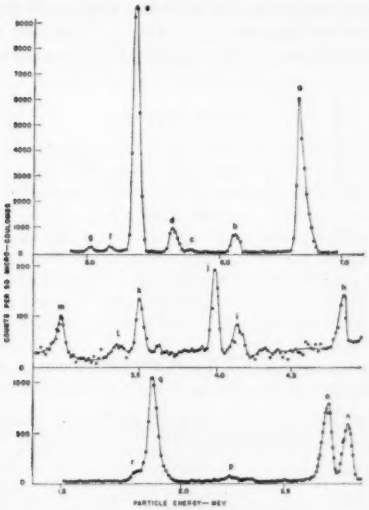

FIG. 1. Spectrum of charged particles scattered from magnesium at 150°.

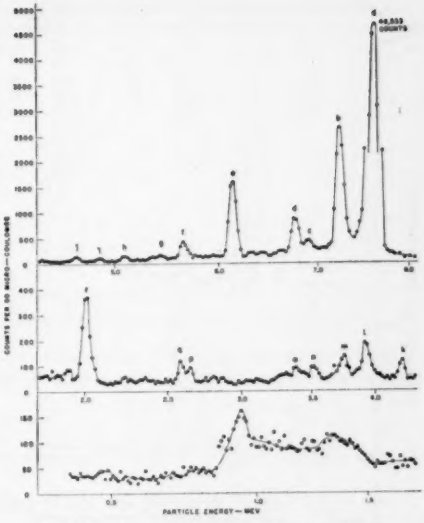

FIG. 2. Spectrum of charged particles scattered from vanadium at 150°.

B. Vanadium

A thin (less than 5 kev) target of vanadium was bombarded with 8-Mev protons and the reaction particles observed at an angle of 150° to the incident beam. Natural vanadium has two stable isotopes, V^{50} and V^{51}. The percentage of V^{50} in natural vanadium, 0.25 percent, is small enough that the likelihood of detecting inelastic proton groups from V^{50} is small. Consequently, all energy levels have been assigned to excited states in V^{51}.

Seventeen proton groups (see Fig. 2) were recorded. Calculations show peaks *a*, *b*, and *f* to be elastically scattered protons from gold, vanadium, and carbon, respectively. The proton group corresponding to peak *r* has been assigned to the 4.44-Mev level in carbon. Four energy levels have been previously recorded in V^{51}.[7] Two of the levels, 0.267 and 0.320 Mev, were determined from K capture in Cr^{51}; the 1.1- and 4.7-Mev levels were determined by $Ti^{48}(\alpha,p)V^{51}$ reaction. Peaks *c* and *e* can tentatively be assigned to the 0.320- and 1.1-Mev levels. There was no indication in the present experiment of the 0.267-Mev level. It is possible that the group corresponding to the 0.267-Mev level could be of such low

[4] D. M. Van Patter, Massachusetts Institute of Technology Technical Report No. 57, January (1952) (unpublished).
[5] Endt, Enge, Haffner, and Buechner (to be published).
[6] Endt, Haffner, and Van Patter, Phys. Rev. 86, 518 (1952).
[7] Way, Fano, Scott, and Thew, *Nuclear Data*, National Bureau of Standards. Circular 499 (1950).

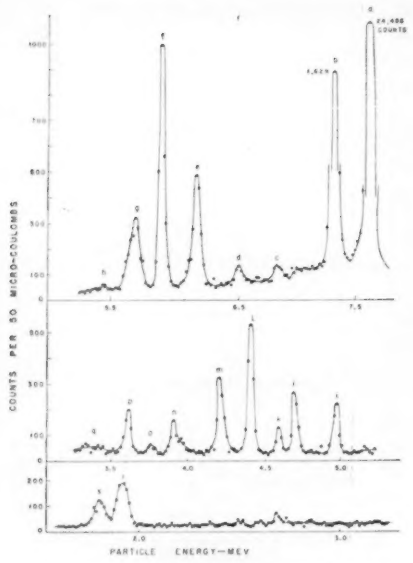

FIG. 3. Spectrum of charged particles scattered from chromium at 150°.

intensity as to be obscured by background. There is a low intensity doublet, peaks *p* and *q*, corresponding to excitation energies of 4.90 and 4.97 Mev, respectively, which can possibly be assigned to the 4.7-Mev level reported.

C. Chromium

The spectrum of scattered protons from a thin natural chromium target at an angle of 150° to the incident beam is shown in Fig. 3. Twenty-three proton groups were observed in the reaction, nineteen of which are shown from the thin target spectrum. Peaks *a*, *b*, *e*, and *g* are the elastically scattered protons from gold, chromium, oxygen, and carbon, respectively. Peaks *r* and *s* have been assigned to the 4.44-Mev level in carbon which was present on both the front and rear faces of the target. Particle groups *f*, *i*, and *l*, corresponding to excited states of 1.46, 2.43, and 3.01 Mev in Cr^{52} agree with the known levels[7] in Cr^{52} determined by the decay of Mn^{52}. There is a possible assignment of peak *d* to the 0.835-Mev level of Cr^{54} determined by Deutsch and Elliot[8] from the decay of Mn^{54} and the subsequent emission of an 0.835 gamma-ray.

Since natural chromium has five stable isotopes, absolute assignment of energy levels cannot be made at present. It is possible, however, that peaks *j*, *k*, *m*, *n*, and *p* are inelastic groups from Cr^{52}, the most abundant chromium isotope, due to their large relative intensities.

[8] M. Deutsch and L. G. Elliot, Phys. Rev. **65**, 211 (1944).

D. Manganese

Since manganese consists of only one stable isotope, the assignment of the groups shown in Fig. 4 is relatively simplified. The spectrum of manganese was obtained at an angle of 150° to the incident beam. Both thick and thin target spectrums were obtained and the energy levels quoted in Table I are an average of both runs. Peaks *a*, *b*, *e*, and *h* were determined to be the elastic groups for gold, manganese, oxygen, and carbon, respectively. Peak *t* has been assigned to the 4.44-Mev level in carbon. Peak *c* has been assigned to an excited state in Mn^{55}. The unresolved nature of the carbon elastic peak is assumed to be caused by layers of carbon deposited during successive evaporations in the preparation of the manganese target. Peak *u* has also been assigned to the 4.44-Mev level in carbon and probably arises because of the large carbon deposits on the back of the gold foil. Other than the above-mentioned groups, all peaks have been assigned to excited states in Mn^{55}. It is interesting to note that in the region of proton group energy of 2.0 to 4.0 Mev there appears to be a large number of low intensity unresolved groups. No attempt was made to resolve groups in this region as it was indicated that the experimental level widths are large compared to the level spacing.

IV. DISCUSSION

A detailed analysis of the spectral distributions of the emitted particle groups from the bombarded targets will not be discussed here. However, there are some general conclusions concerning these distributions which

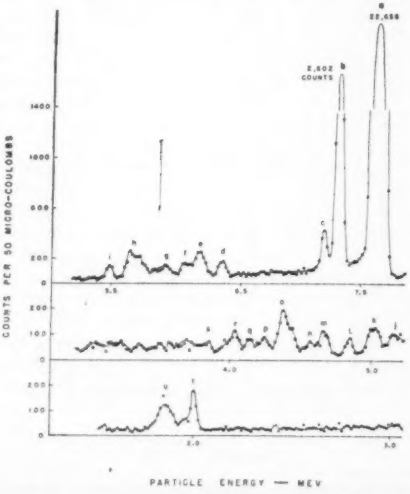

FIG. 4. Spectrum of charged particles scattered from manganese at 150°.

indicate qualitative agreement with the expected distributions predicted by the statistical models of the nucleus. The various statistical treatments for the heavier elements ($A>50$) predict a level spacing above a few Mev excitation energy which is very small compared to the natural widths of the levels.

On broad general lines it can be seen that the level densities of the residual nuclei, vanadium, chromium, and manganese, increase with increasing excitation of the residual nucleus. The general tendency of the intensity distributions of these three elements is a gradual decrease in the intensities of the groups as a function of increasing group energy. This is in qualitative agreement with the distributions predicted by Weisskopf and Ewing.[9]

TABLE I. Energy levels (probable error ±0.02 Mev).

Mg^{26}	Mg^{25}	Mg^{28}	Mg	V^{51}	Cr^{53}	Cr	Mn^{55}
1.38	0.61	1.83	3.54	0.33	1.45	0.48	0.13
4.13	1.62	2.96	4.71	0.48	2.43	0.81	1.00
4.24	1.98		5.03	1.16	2.99	2.69	1.30
	2.56			1.84		2.79	1.56
	2.76			2.22		3.20	1.91
	3.41			2.43		3.46	2.27
	3.91			2.65		3.51	2.42
				3.11		3.65	2.59
				3.41		3.80	2.77
				3.58		3.99	2.85
				3.83		4.07	3.05
				3.96		4.78	3.21
				4.90			3.31
				4.97			3.42
							3.64

The authors are indebted to Mr. L. M. Diana, Mr. K. B. Rhodes, Mr. R. F. Weise, Mr. E. M. Perkins, and Mr. R. A. Barjon for their collaboration in this project.

[9] V. F. Weisskopf and D. H. Ewing, Phys. Rev. **57**, 472 (1940).

PHYSICAL REVIEW VOLUME 88, NUMBER 6 DECEMBER 15, 1952

Nuclear Energy Levels in the Region of the 28-Neutron Shell*†

GEORGE F. PIEPER‡
Sloane Physics Laboratory, Yale University, New Haven, Connecticut
(Received August 21, 1952)

Energy levels of the titanium nuclei of mass numbers 47, 48, 49, 50, and 51 have been obtained by measuring the ranges of proton groups from the reactions Ti(d,p)Ti. With the use of enriched isotopes, it has been possible to assign thirty observed Q values to their proper reactions. Good agreement was found in most cases in which results of this study could be compared with the results of others.

The data have been analyzed in terms of the strong spin-orbit coupling shell model of nuclear structure. A study of the binding energy of each residual nucleus and the energy of its first excited state revealed definite evidence for the existence of a closed shell at 28 neutrons.

I. INTRODUCTION

OF the well-known magic numbers, the evidence for particular stability is poorest in the cases of 20 and 28. Mayer[1] did not expect the shells at 28 neutrons or protons to be strongly marked. Harvey[2] found a change in neutron binding energy of about 1 Mev, but the decrease apparently occurred between 29 and 30 neutrons, rather than between 28 and 29. Collins, Nier, and Johnson[3,4] have reported discontinuities in the binding energy surface at 20 and 28 neutrons and protons.

The known excited states of nuclei have been studied by Pollard[5] and by Scharff-Goldhaber[6] in attempts to observe regularities which might be attributed to shell structure. The most noticeable regularity which has been found is that the energy of the first excited state as a function of the number of protons or neutrons in the nucleus reaches a series of maximum values at closed shells. Figures 1 and 2 are plots of the first excited states which are known for light elements as functions of proton and neutron number. These plots show definite evidence for shell effects at 8 and 20 nucleons. Data of this sort are scare in the regions of the higher magic numbers.

The present investigation is concerned with the expected shell at 28 neutrons; a companion investigation[7] is concerned with the 28-proton shell. The element titanium is particularly suited for this problem since it has stable isotopes containing 24, 25, 26, 27, and 28 neutrons. Analysis of the proton groups from the series of reactions Ti(d,p)Ti allows the study of the binding energies and energy levels of a series of nuclei having a constant number of protons and a continuous series of neutron numbers, 25 through 29. Any effects on the

* Part of a dissertation presented to the faculty of the Graduate School of Yale University in partial fulfillment of the requirements for the degree of Doctor of Philosophy.
† Assisted by the joint program of the ONR and AEC.
‡ AEC Predoctoral Fellow.
[1] M. G. Mayer, Phys. Rev. **78**, 16 (1950).
[2] J. A. Harvey, Phys. Rev. **81**, 353 (1951).
[3] Collins, Nier, and Johnson, Phys. Rev. **87**, 236 (1952).
[4] Collins, Nier, and Johnson, Phys. Rev. **86**, 408 (1952).
[5] E. C. Pollard, Nucleonics **2**, No. 4, 1 (1948); Phys. Rev. **82**, 326 (1951); and ONR Progress Report, January 30, 1951 (unpublished).
[6] G. Scharff-Goldhaber, Phys. Rev. **87**, 218 (1952).
[7] D. C. Hoesterey, thesis, Yale University (1952) (unpublished).

binding energy or energy level pattern of the series of nuclei from the expected closing of the $1f_{7/2}$ shell at 28 neutrons would be expected to appear in this study, since the constancies of the mode of excitation and the proton number make it plausible to interpret any variation solely in terms of the neutron number.

Pertinent experimental information concerning the titanium nuclei is not plentiful. The masses of the stable nuclei have been measured by Collins, Nier, and Johnson.[4] Harvey[5] has reported Q values for the ground state (d,p) reactions on Ti^{46}, Ti^{47}, and Ti^{48}; these were obtained by measuring the ranges in aluminum of protons from a natural titanium target observed at 30° to an incident beam of 14-Mev deuterons. The Ti^{48} ground-state peak was identified by its intensity; the other Q values were assigned on the basis that lighter isotopes should have higher energy ground-state groups.

Energy levels are known from radioactivity studies for only two of the titanium nuclei. The excitation energies of Ti^{48} were first studied by Pollard,[8] using the reaction $Sc^{45}(\alpha,p)Ti^{48}$; levels were found at 1.1 ± 0.4 and 2.3 ± 0.4 Mev. The decay scheme of V^{48} has been investigated by Peacock and Deutsch,[9] by Robinson, Ter-Pogossian, and Cook,[10] and by Green, Ticho, and Richardson.[11] All of these experiments have yielded evidence for gamma-rays of 1.32 and 0.99 Mev, indicating that the positron transition of V^{48} leads to the second excited state of Ti^{48}, 2.31 Mev above the ground state. The first excited state may lie at either 0.99 or 1.32 Mev; both results are consistent with Pollard's value of 1.1 ± 0.4 Mev. The decay scheme of Sc^{48} has been studied by Peacock and Deutsch[9] and by Hamermesh *et al.*[12] The results of the latter group show evidence for three gamma-rays, one of energy 1.33 Mev and two of energy about 0.98 Mev. These results are consistent with the above interpretation of the positions of the excited states of Ti^{48} and indicate in addition that the third excited state lies in the region of 3.3 Mev.

The other titanium nucleus whose energy levels are are known is Ti^{46}. A number of investigations[13] indicate that the first excited state may be at either 0.89 or 1.12

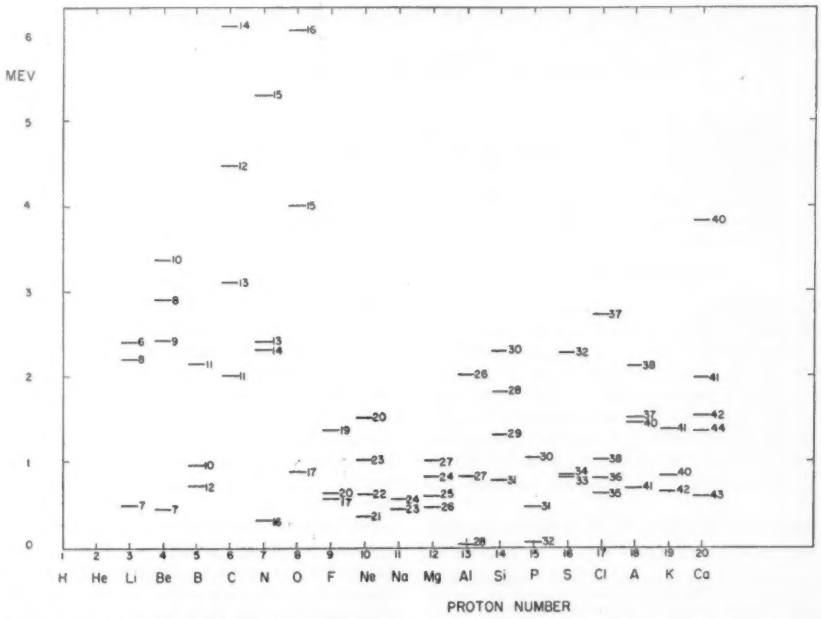

FIG. 1. First excited states in Mev as proton number up to $Z=20$. Mass numbers of nuclei are given beside level positions.

[8] E. C. Pollard, Phys. Rev. **54**, 411 (1938).
[9] W. C. Peacock and M. Deutsch, Phys. Rev. **69**, 306 (1946).
[10] Robinson, Ter-Pogossian, and Cook, Phys. Rev. **75**, 1099 (1949).
[11] Green, Ticho, and Richardson, Phys. Rev. **87**, 195 (1952) and Phys. Rev. **86**, 422 (1952).
[12] Hamermesh, Hummel, Goodman, and Engelkemeir, Phys. Rev. **87**, 528 (1952).
[13] C. L. Peacock and R. G. Wilkinson, Phys. Rev. **74**, 297 (1948); E. T. Jurney, Phys. Rev. **74**, 1049 (1948); F. T. Porter and C. S. Cook, Phys. Rev. **81**, 298 (1951).

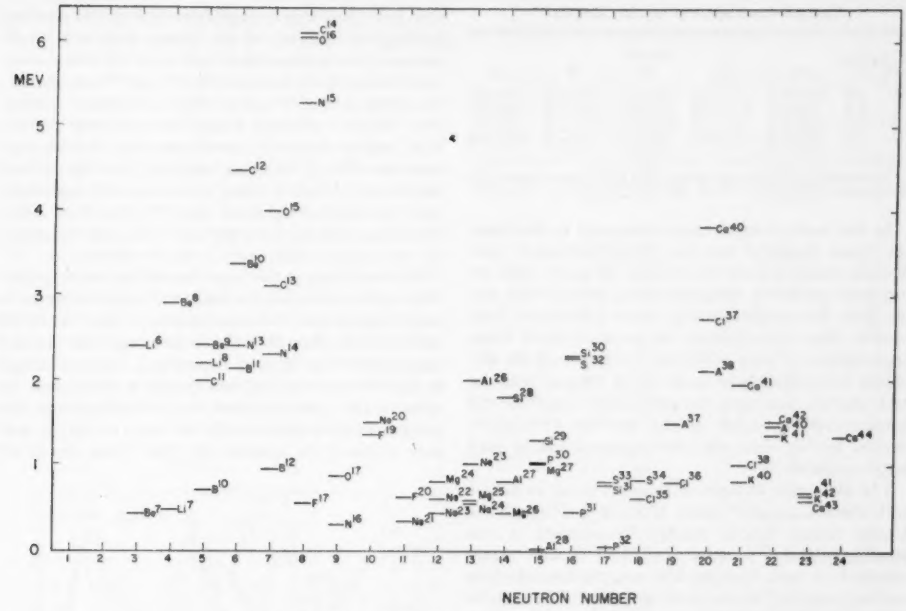

FIG. 2. First excited states in Mev *vs* neutron number up to $N=24$.

Mev, but the second excited state is definitely established at 2.01 Mev.

II. EXPERIMENTAL METHOD

The experimental procedure used in this work has been employed before.[14–16] The bombardments in which protons at 90° to the direction of the incident beam were measured were carried out in a chamber built by Martin.[16] The arrangement is shown in Fig. 3. A different chamber, one with a gold window thick enough to stop the beam, was used to measure protons at 0°. The electronic circuits associated with the proportional counter have been described elsewhere.[16–17]

The technique used was the peaked proportional counter method. Pulses from the counter are amplified and then put through a biased diode discriminator and into a blocking oscillator for shaping before recording. If the discriminator is adjusted so that the pulse from every proton passing through the counter is recorded, integral curves will be obtained when the proton yield for a fixed number of deuterons is plotted as a function of range.[18] If an appropriate discriminator adjustment is made so that only those pulses with amplitudes greater than a certain fixed value are recorded, the peak in the Bragg ionization curve may be used to restrict observation to a small interval of range; in this way nearly differential or "peaked" group spectra are obtained. High peaking corresponds to a small range interval and vice versa.

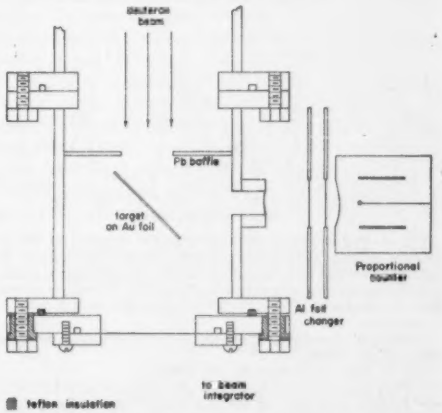

FIG. 3. Arrangement of apparatus for counting of protons at 90° to the direction of the incident beam.

[14] W. O. Bateson, Phys. Rev. **80**, 982 (1950); P. W. Davison, Phys. Rev. **75**, 757 (1949).
[15] B. B. Benson, Phys. Rev. **73**, 8 (1948).
[16] A. B. Martin, Phys. Rev. **71**, 127 (1947); **72**, 378 (1947).
[17] H. A. Schultz and E. C. Pollard, Rev. Sci. Instr. **19**, 617 (1948).
[18] M. S. Livingston and H. A. Bethe, Revs. Modern Phys. **9**, 245 (1937).

TABLE I. Composition of titanium samples.[a]

Per-cent	Natural Ti	Enriched 46	47	48	49	50
46	7.95	82.66±0.09	1.83±0.03	0.16±0.01	1.09±0.03	1.25±0.01
47	7.75	5.24±0.04	82.05±0.09	0.32±0.01	1.21±0.03	1.23±0.04
48	73.45	10.39±0.04	14.62±0.06	98.90±0.02	15.71±0.05	10.99±0.07
49	5.51	0.86±0.02	0.81±0.01	0.48±0.01	77.27±0.07	1.84±0.03
50	5.34	0.84±0.02	0.69±0.01	0.14±0.01	4.71±0.08	84.69±0.04

[a] The following impurities were also detected but in no case was the amount of the impurity greater than 0.08%: Al, Na, Si, Mg, Cu, Ca, Ag, Fe, Cd, Cr, Mn, and Sn.

In this work, integral curves were used to determine the mean ranges of the few groups sufficiently well isolated to allow such observation. In most cases the increased resolution obtainable from peaked data was required. The approximate Q values determined from peaked data (extrapolated range-extrapolated beam approximation) were corrected by means of an empirical correction curve based upon integral data for each reaction and upon the accurate Q value[19] for the ground-state transition in the reaction $O^{16}(d,p)O^{17}$, oxygen having been the chief contaminant in each target material.

The five stable isotopes of titanium occur in nature with the abundances[20] given in Table I. Through the United States Atomic Energy Commission, it was possible to obtain samples of titanium dioxide highly enriched in each isotope. The composition of these enriched samples[21] is also given in Table I. The samples were in the form of finely ground TiO_2 powder. Thin targets were constructed by painting on thin gold foils small amounts from suspensions of the TiO_2 samples in ethyl alcohol.

III. RESULTS

In view of the large amount of data obtained in this work, only a few curves of results can be shown. Figure 4 shows the proton groups observed at 90° in the reaction $Ti^{48}(d,p)Ti^{49}$ in a single cyclotron run at medium peaking. In addition to the groups from the 48–49 reaction, groups from the ground state and first excited state transitions in the reaction $O^{16}(d,p)O^{17}$ are evident. The group labeled B may be due to the ground state of the $C^{12}(d,p)C^{13}$ reaction. Carbon was probably present in all targets, since ethyl alcohol was used in their construction. The Q value as computed for the carbon reaction is 2.85±0.15 Mev, which is in fair agreement with the result of Buechner *et al.*,[22] 2.729±0.009 Mev. The assignment has been left uncertain since the group did not appear consistently in all the data.

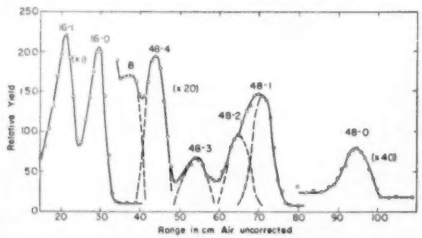

FIG. 4. Proton groups from $Ti^{48}(d,p)Ti^{49}$ observed at 90° at medium peaking. Each group is labeled by the mass number of the target nucleus and the number of the excited state to which it is attributed; lettered groups are unassigned. The dashed curves show the resolution of multiple groups into their components.

Ti[48] was chosen as the target for the first investigation of the series because of the high purity of the sample. It was advantageous to locate the groups from the 48–49 reaction first, since each of the other enriched samples contained Ti[48] as its chief impurity. It was convenient to be able to recognize these groups in later work. In some of the other reactions they interfered with the group spectrum under study to some extent; it was then necessary to subtract the yield from the 48–49 reaction to determine what was left from the desired reaction.

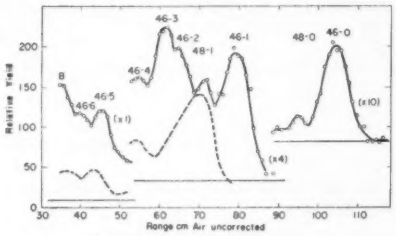

FIG. 5. Proton groups from $Ti^{46}(d,p)Ti^{47}$ observed at 90°. Dashed curve represents yield from competing reaction $Ti^{48}(d,p)Ti^{49}$. The labeling system is explained in Fig. 4.

The proton groups observed at 90° from a target of enriched Ti[46] are shown in Fig. 5, the result of a single cyclotron run at medium peaking. Just inside the group of longest range, there is a group of small yield whose extrapolated range agrees with that of 48–0, the ground-state group from the 48–49 reaction. It has been assumed that this group is 48–0. On the basis of this assignment, the dashed curve has been drawn in Fig. 5 to represent the yield from the 48–49 reaction. This curve was calculated from a run on Ti[48] made under similar peaking conditions as were used for the 46–47 data; the calculation was based on equalizing the yields of group 48–0 in the two cases. It is noteworthy that the largest maximum of the dashed curve corresponds quite well with one of the maxima of the solid curve. In view of the uncertainties involved in matching yields, due in particular to the critical de-

[19] Hornyak, Lauritsen, Morrison, and Fowler, Revs. Modern Phys. **22**, 291 (1950).

[20] A. O. Nier, Phys. Rev. **53**, 282 (1938).

[21] These samples were prepared by the Stable Isotopes Research and Production Division of the Oak Ridge National Laboratory by the method of electromagnetic separation and were analyzed in their laboratory.

[22] Buechner, Strait, Sperduto, and Malm, Phys. Rev. **76**, 1543 (1949).

pendence of yield on peaking, the agreement has been accepted, and the peak so labeled has been assigned to group 48–1. Extrapolated ranges of the inner groups were obtained from a curve of subtracted results, determined by taking the difference between the solid and dashed curves of Fig. 5. In all cases these ranges were in reasonably good agreement with those obtained from Fig. 5, neglecting the effects of the Ti^{48} contamination. This result is fortuitous; it means that the Q values for the inner groups are not strongly dependent on the accuracy with which the relative yields from Ti^{46} and Ti^{49} are known.

The same procedure of subtracting the 48–49 yield was used where necessary in the cases of the other three reactions. The only case in which almost no interference was encountered was that of $Ti^{50}(d,p)Ti^{51}$. Figure 6 shows the proton groups observed in this reaction at 90°. It is noteworthy that the first excited state group 50–1 lies very near the ground-state group 50–0; with no other isotope was this the case. The

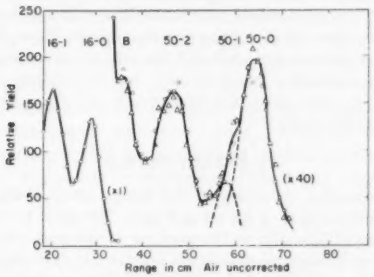

FIG. 6. Proton groups from $Ti^{50}(d,p)Ti^{51}$ observed at 90°. The dashed curves show the resolution of a multiple group into its components. The labeling system is explained in Fig. 4.

group 50–2 is too wide to be a single group and is almost certainly double. The indication is also strong that there is a large group from the 50–51 reaction in the region of the oxygen groups. Some indication of group 50–1 appeared in each of several runs made under various peaking conditions, but better resolution than that shown in Fig. 6 was impossible. Nor could the probable double structure of 50–2 be resolved. Data taken at low peaking showed the presence of a very weak group whose Q values agreed with that of 48–0; the subtraction of the yield from the 48–49 reaction from the yield from the Ti^{50} sample made no difference in the Q values of any of the Ti^{50} groups.

The results of the entire study are summarized in Table II. In cases of severe interference the Q values are only estimates or have large probable errors.

IV. COMPARISONS

The ground-state Q values for the series of reactions Ti(d,p)Ti can be compared to those calculated from the masses of Collins, Nier, and Johnson[4] (CNJ) and to

TABLE II. Energy levels of titanium nuclei.

Reaction	Q-Mev	Energy level—Mev		Relative yield at 90°
$Ti^{46}(d,p)Ti^{47}$	6.45±0.05	Ti^{47}	0	1
	5.05±0.08		1.40±0.08	3.4
	4.06±0.09		2.39±0.09	1.3
	3.81±0.09		2.64±0.09	3.2
	3.36±0.09		3.09±0.09	1.7
	2.75±0.09		3.70±0.09	5
	2.27±0.09		4.18±0.09	5
$Ti^{47}(d,p)Ti^{48}$	8.14±0.05	Ti^{48}	0	1
	6.81±0.09		1.33±0.09	1
	5.83±0.16		2.31±0.16	<5
	4.83±0.09		3.31±0.09	10
	3.64±0.12		4.50±0.12	15
	3.2		5.0	18
	2.9		5.3	25
$Ti^{48}(d,p)Ti^{49}$	5.81±0.04	Ti^{49}	0	1
	4.46±0.05		1.35±0.05	9
	4.11±0.07		1.70±0.07	6
	3.40±0.07		2.41±0.07	4
	2.70±0.05		3.11±0.05	12
$Ti^{49}(d,p)Ti^{50}$	8.62±0.05	Ti^{50}	0	1
	7.04±0.06		1.58±0.06	1
	5.6		3.0	<1
	4.48±0.06		4.14±0.06	24
	3.74±0.09		4.88±0.09	24
	3.23±0.10		5.39±0.10	19
	2.63±0.10		5.99±0.10	33
$Ti^{50}(d,p)Ti^{51}$	4.11±0.07	Ti^{51}	0	1.0
	3.50±0.12		0.61±0.12	0.3
	2.96±0.08		1.15±0.08	0.8
	2.5		1.6	

those reported by Harvey.[2] This comparison is made in Table III. The agreements in all cases are very good, except for the reaction $Ti^{47}(d,p)Ti^{48}$.

In the study of this one discrepancy, the following considerations are pertinent: (1) If the discrepancy is due to an error in the CNJ masses, then there must be at least two errors of the same magnitude since the Q values are computed from mass differences and the differences on either side of the one in question lead to Q values in good agreement with the measured ones. The possibility of a systematic error in the mass measurements would appear to be very slight, especially in view of the use of different substances for the doublet comparison in each case. (2) Since Harvey's experiments were carried out using natural titanium, it is possible that the Q value he attributed to the 47–48 reaction should in fact be assigned to the 49–50 reaction. It

TABLE III. Comparison of ground-state Q values.

Reaction	Ground-state Q value—Mev		
	Collins, Nier, and Johnson	Harvey	Pieper
$Ti^{46}(d,p)Ti^{47}$	6.41±0.10	6.51±0.10	6.45±0.05
$Ti^{47}(d,p)Ti^{48}$	9.40±0.11	8.82±0.4	8.14±0.05
$Ti^{48}(d,p)Ti^{49}$	5.75±0.07	5.92±0.05	5.81±0.04
$Ti^{49}(d,p)Ti^{50}$	8.66±0.06		8.62±0.05
$Ti^{50}(d,p)Ti^{51}$			4.11±0.07

IV. COMPARISONS

TABLE IV. Binding energies of titanium nuclei in Mev.

Mass number	Neutron number	Binding energy of last neutron	Total binding energy	Binding energy per particle
46	24		397.80±0.09	8.648±0.002
47	25	8.68±0.05	406.48±0.07	8.649±0.001
48	26	10.37±0.05	416.85±0.05	8.684±0.001
49	27	8.04±0.04	424.89±0.07	8.671±0.001
50	28	10.85±0.05	435.74±0.08	8.715±0.002
51	29	6.34±0.07	442.08±0.10	8.668±0.002

would be in good agreement with the other results, considering its rather large probable error. (3) Recently Harvey[23] has observed the inelastic scattering of 7.7-Mev protons from a number of targets, including natural titanium. The first excited level in the case of titanium occurred at 1.00±0.05 Mev and the second level at approximately 2.4 Mev. (4) In the present work the low yield made the detection of the group of Q value 8.14 Mev quite difficult. Although a search made at both 90° and 0° for a longer range proton group produced no result, the only conclusion which can be drawn is that any such longer range group must have a yield less than about 15 percent of the yield of the group of Q value 8.14 Mev.

The most reasonable conclusion from these considerations is that the true ground-state group in the reaction $Ti^{47}(d,p)Ti^{48}$ was not observed in the present study; the group assigned as 47–0 would then correspond to the first excited state transition. If this is the case, the energy level scheme would agree with that determined from the inelastic proton scattering work of Harvey; the ground-state Q value would be 9.13 Mev. Since this latter value is not in particularly good agreement with CNJ's value of 9.40 Mev, even this conclusion cannot be accepted without reservation. The radioactivity studies discussed earlier throw no light on this matter, since all the gamma-rays involved can be fitted with equal ease into the two schemes in which the group of Q value 8.14 Mev corresponds to the ground state or to the first excited state.

V. BINDING ENERGIES

From the well-established value for the binding energy of the deuteron,[24] 2.226±0.003 Mev, and the Q values measured in this work, the binding energy of the last neutron in each of the nuclei Ti^{47} through Ti^{51} can be calculated. In addition, if the mass value of one of the isotopes is assumed (e.g., that of Ti^{48}, which is the best known[4,25]), it is also possible to calculate from the present results the total binding energy and binding energy per particle of each of the nuclei Ti^{46} through Ti^{51}. It is of interest to examine all these values to determine whether there is any significant change in these binding energies as a result of the completion of the $1f_{7/2}$ shell at 28 neutrons. The information is given in Table IV.

The values of the binding energy of the last neutron show readily the odd-even effect, that nuclei containing even numbers of neutrons have higher neutron binding energies than those with odd neutron numbers. It is noteworthy also that the binding energy of the 29th neutron is 1.7 Mev less than that of the 27th neutron, while the difference between the binding energies of the 27th and 25th neutrons is only 0.6 Mev. The weak binding of the 29th neutron is a definite indication of the closing of the 28-neutron shell. The same feature is shown in the values of the binding energy per particle, although the odd-even effect is smoothed here. The difference in the two cases is essentially that the effect is attributed entirely to the last neutron in the one case and is spread among all the nucleons in the other. In either approach the change in binding with the addition of the 29th neutron is noticeable, although it is much smaller than the discontinuities observed in the regions of the higher magic numbers.[2] No use has been made of the semiempirical mass formula for comparison purposes, in view of its lack of accuracy in this region of the nuclide chart.[26]

VI. ENERGY LEVELS

A complete summary of the energy levels found in the present work is shown in Fig. 7. The most striking feature of this plot is the position of the first excited state as a function of neutron number; it rises slightly with the addition of the 27th and 28th neutrons and then drops sharply at 29. This behavior is in agreement with that previously noted at the lower magic numbers, although here the effect is not so marked.

Another way of plotting the results of these experiments is shown in Fig. 8, in which the neutron binding energy (Q plus 2.23 Mev) for each state is shown. It

FIG. 7. Energy levels of titanium nuclei. The long lines represent actual values of the energy levels; the short lines above and below are the probable limits of error. Solid lines in parentheses indicate that the existence of a level is known, but its accurate measurement was impossible. Excited states of Ti^{48}, as determined from radioactivity studies, are given as dotted lines; the parentheses in this case indicate that the first excited state may lie at either of the two values shown.

[23] J. A. Harvey, Phys. Rev. **88**, 162 (1952) and private communication.

[24] R. C. Mobley and R. A. Laubenstein, Phys. Rev. **80**, 309 (1950).

[25] H. E. Duckworth and R. S. Preston, Phys. Rev. **82**, 468 (1951); H. A. Bethe, *Elementary Nuclear Theory* (John Wiley and Sons, Inc., New York, 1947).

[26] E. Fermi, *Nuclear Physics* (University of Chicago Press, Chicago, Illinois, 1950), p. 8.

is noteworthy that the level pattern seems to show a series of regularities, in all states of binding energy less than about 7 Mev, in the states of even A nuclei, and in those of odd A nuclei. The ground state of Ti^{51} seems to have corresponding states in the other nuclei. Unfortunately, not much significance can be attached to these regularities at this stage.

The results of a recent study by Kinsey and Bartholomew[27] of the neutron capture gamma-rays from natural titanium (Ti^{48} contributes 95 percent of the total capture cross section) can be combined with the present results concerning excited states of Ti^{49}. Gamma-rays were observed corresponding to ten transitions; four of these were in good agreement with the four excited levels of Ti^{49} found in the present study. No gamma-ray was found corresponding to the ground-state transition, nor was any such ray expected since it would presumably involve electric octupole radiation. Figure 9 summarizes the situation.

Kinsey and Bartholomew's results indicate extremely strong transitions to the first two excited states of Ti^{49}. The relative intensities of the gamma-rays to the first and second excited states were 53 and 32, respectively; no other ray had a relative intensity greater than 5. The possibility that the first excited state is a $2p_{\frac{1}{2}}$ level is in accord with the strength of the transition, for the capture gamma-ray would then be electric dipole radiation. Breit[28] has suggested that the approximate ratio of 2 to 1 in the intensities of these two transitions

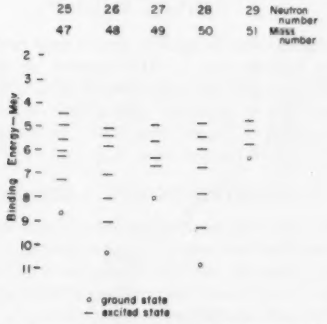

FIG. 8. Neutron binding energies of all observed states.

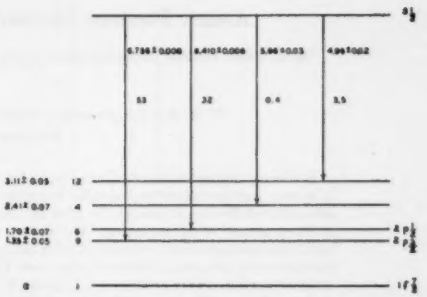

FIG. 9. Energy levels of Ti^{49}. The figures at the left are the energy levels in Mev and relative yields at 90° of proton groups determined by Pieper using the reaction $Ti^{48}(d,p)Ti^{49}$; those next to the arrows are the energies in Mev and relative intensities of the gamma-rays determined by Kinsey and Bartholomew from the reaction $Ti^{48}(n,\gamma)Ti^{49}$. Tentative level assignments are also given for some states.

might be interpreted as an argument that the second excited state is a $2p_{\frac{1}{2}}$ level. He points out that for dipole radiation and pure $s_{\frac{1}{2}}$ to p transitions, neglecting frequency differences, the theoretical ratio of 2 to 1 applies; since the two strongest lines have intensities in approximately this ratio, with the higher energy ray the stronger, and since the energy difference is nearly the same as for the ground-state doublet of Li^7, there appears to be reason for speculatively considering the first two excited states of Ti^{49} as forming a p-neutron doublet. Should these level assignments be correct, the splitting of the p doublet in Ti^{49} is 0.35 ± 0.09 Mev from the (d,p) work and 0.345 ± 0.008 Mev from Kinsey and Bartholomew's data. A situation which might be interpreted in a similar manner exists in the case of Ca^{41}, which has been studied by Sailor[29] and by Kinsey, Bartholomew, and Walker.[30] Here the splitting (if such exists) is 0.53 ± 0.05 Mev, while the intensity ratio is 83 to 11.

It is a pleasure for the writer to express his gratitude to Professor E. C. Pollard, who suggested this investigation and guided the work through all its stages, and to Professor G. Breit for many helpful discussions. Thanks are also extended to Dr. B. B. Kinsey and Dr. J. A. Harvey for making available some of their results before publication.

[27] B. B. Kinsey (private communication).
[28] G. Breit (private communication).
[29] V. L. Sailor, Phys. Rev. 75, 1836 (1949).
[30] Kinsey, Bartholomew, and Walker, Phys. Rev. 85, 1012 (1952).

Atomic Electron Ejection in Large-Angle Scattering*,†

M. E. EBEL, *Institute for Atomic Research and Department of Physics, Iowa State College, Ames, Iowa*

AND

W. F. FRY,‡ *Department of Physics, University of Chicago, Chicago, Illinois*

(Received August 8, 1952)

It is found that an electron in the kev range frequently accompanies the large-angle scattering of μ-mesons, π-mesons, and protons in photographic emulsions. For μ-mesons of energy between 1.6 and 4.1 Mev which are scattered through angles greater than 28°, there is observed an electron of energy greater than 10 kev in 21±6 percent of the scatterings. The electron energy distribution seems to follow an inverse 7/2 power law. These electrons are interpreted as being ejected as the result of the direct Coulomb action of the incident particle on the electrons of the scattering atom. The high probability of ejection arises from the fact that an incident particle which undergoes a large-angle scattering always passes through the region of greatest electron density. The probability of ejection is calculated from second-order perturbation theory using approximations valid at high energies. Although the approximations limit the usefulness of the result, the assumed mechanism seems adequate for the description of the phenomenon.

I. DESCRIPTION OF THE PHENOMENON

A STUDY of the tracks in photographic emulsions of μ-mesons, π-mesons, and protons which have been scattered through large angles reveals that frequently a low energy electron track appears to originate from the point of scattering. A typical example of a large-angle scattering of a μ-meson accompanied by such an electron is shown in Fig. 1. Electron tracks of range greater than about 1.5 microns were studied, which corresponds to an energy of about 10 kev. The number of the electrons ejected per unit energy interval decreases rapidly with increasing electron energy. There appears to be no correlation of the electron energy with the angle of scattering.

The probability that a 2-Mev μ-meson produces a δ-ray of energy greater than 10 kev in an atomic collision is very small ($\sim 10^{-6}$). However, in a large-angle scattering the probability is greatly increased because the impact parameter is necessarily small, and consequently the incident particle passes through a region of high electron density. In fact, if the angle of scattering is greater than 30°, the impact parameter is less than $e^2Z/(Mv^2\tan 15°)$, where M is the mass of the μ-meson and Z is the atomic number of the scattering atom. If the energy of the incident particle is greater than 1 Mev, the impact parameter is always much less than the radius of the innermost Bohr orbit of the scattering atom.

We can form a simple estimate of the probability of electron ejection in large-angle scattering by neglecting the momentum distribution of the electrons and using the Bohr formula for δ-ray production,

$$(2\pi e^4 Z_s^2/mv^2)(d\epsilon/\epsilon^2)N\Delta x, \tag{1}$$

where $Z_s e$ is the charge of the scattered particle, ϵ is the energy acquired by the electron, and $N\Delta x$ is the product of the electron density and distance traversed by the incident particle. We assume that the $2n^2$ electrons of the nth shell are uniformly distributed over a sphere of volume $(4\pi/3)(a_0n^2/Z)^3$, where a_0 is the radius of the first Bohr orbit of hydrogen. The product of the electron density and the distance traversed in passing through this shell $N\Delta x$ is approximately $3Z^2/(\pi a_0^2 n^2)$. Writing ϵ_n for the average binding energy of the electrons in this shell and using (1), we find for the probability that an electron be ejected in the energy range ϵ to $\epsilon+d\epsilon$:

$$p(\epsilon)d\epsilon \approx \frac{6e^4 z_s^2 z}{mv^2 a_0^2} \sum_n \frac{1}{n^2} \frac{d\epsilon}{(\epsilon_n+\epsilon)^2}. \tag{2}$$

This formula when integrated gives a total probability of about 2 percent that a 2-Mev μ-meson which undergoes a large-angle scattering from an atom with $Z=40$ eject an electron of energy greater than 10 kev. This value is low, and the deficiency is to be found in the initial motion of the electrons.

II. OBSERVATIONS WITH μ-MESONS

A study has been made of the phenomenon using slow μ-mesons. For these particles large-angle scatterings are relatively frequent and the interaction with nuclei is through the Coulomb field; nuclear interactions other than Coulomb interactions are negligible.

Electron sensitive G-5 plates of 400 microns in thickness were exposed behind absorbers to slow positive π-mesons from the 122-Mev π-meson channel of the University of Chicago cyclotron. The plates were searched for π–μ decays in which the μ-meson was subsequently scattered through an angle greater than 28° and the energy of the μ-meson was greater than 1.6 Mev at the point of scattering. A study was made of the μ-meson scatterings in which an electron track occurred with its origin within about a one-half micron along the μ-meson track from the scattering point.

From a total of 60 μ-meson scatterings, 13 have such

* Work performed in the Ames Laboratory of the AEC.
† Supported in part by a joint program of the ONR and AEC.
‡ AEC Postdoctoral Fellow. Present address: Department of Physics, University of Wisconsin, Madison, Wisconsin.

an electron track. The probability that a normal δ-ray occurs within one-half micron of the scattering point was determined experimentally and found to be about 3 percent. The electron energies were estimated from the ranges with the aid of the range-energy relationship of Zajac and Ross.[1] Electrons with energies greater than about 10 kev could be detected. Thus it was found that μ-mesons of energy between 1.6 and 4.1 Mev which are scattered through angles greater than 28° have a probability of 18 ± 6 percent of ejecting an electron of energy greater than about 10 kev.

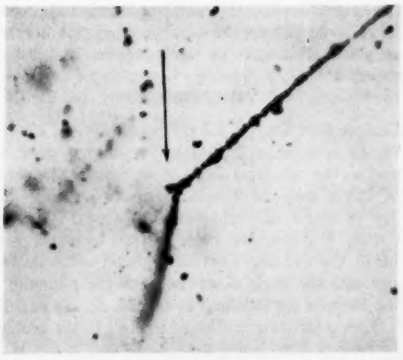
(b)

FIG. 1. A projection drawing of a π–μ–e decay and a μ-meson scattering is shown in part (a). A low energy electron track associated with the large-angle scattering of the μ-meson is shown in the photomicrograph (b). The low energy electron track accompanying the scattering is indicated by the arrow. The electron energy is about 18 kev.

[1] B. Zajac and M. Ross, Nature **164**, 311 (1949).

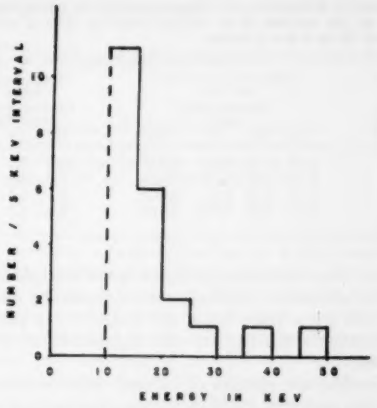

FIG. 2. The differential energy distribution of electrons from scattered μ-mesons is shown in the above histogram.

The energy distribution of the ejected electrons is shown in Fig. 2. This histogram contains the 13 scatterings mentioned above and an additional 9μ-meson scatterings having associated electrons. The distribution seems to follow roughly an inverse 7/2 power law.

A study was made of the relative probability of forward and backward ejection as compared to the direction of the incident μ-meson. In three cases the electron was ejected in the backward hemisphere, and in eight cases it was ejected in the forward hemisphere. In 13 cases it was not possible to determine the initial direction of the electron.

III. THEORETICAL CONSIDERATIONS

The differential probability $p(\epsilon)d\epsilon$ of electron ejection in large-angle scattering is the ratio of the transition probability for large-angle scattering with electron ejection to the total transition probability for large-angle scattering. Both transition probabilities are integrated over the solid angle of scattering. The first transition probability is calculated by means of a second-order time-dependent perturbation scheme. The perturbations are the Coulomb interactions of the incident particle and the atomic nucleus and of the incident particle and the atomic electrons.

Of the four terms comprising the total matrix element, one involves only interactions with the nucleus and is identically zero, one contains only interactions with electrons and is negligibly small, and the other two have both kinds of interactions and are equally important. By representing the states of the electronic system by Hartree-type wave functions, the ejection probability is reduced to a sum of probabilities for the initial one-electron states. By assuming that the energy of an

TABLE I. Differential and integral probabilities (multiplied by 100) for the ejection of an electron from an atom of atomic number 40 by a slow μ-meson.

Meson energy (Mev)	Differential probability (per 5 kev) Electron energy (kev) 25	50	75	100	Integral probability Minimum electron energy (kev) 25	50	75
1	3.67	0.62	0.21	0.022	10.0	2.4	0.6
2	2.38	0.41	0.14	0.015	7.0	1.8	0.4
3	1.82	0.32	0.11	0.012	5.3	1.4	0.3
4	1.51	0.27	0.092	0.010	4.2	1.1	0.2

ejected electron is large compared to the binding energy in the atom, it is permissible to represent the ejected electron by a plane wave. All states of the particle undergoing scattering are also represented by plane waves.

Consider the ejection of an electron from the one-electron state designated by the quantum numbers nlm. The two terms of the matrix element are

$$H_a=e^4Z_s^2Z\lim_{\eta\to 0}\sum_{\bar{k}'}\times\left\{\frac{(\bar{k}|1/r_a|\bar{k}')(\bar{k}\bar{\kappa}|1/(\bar{r}_s-\bar{r})|\bar{k}_0nlm)}{(\hbar^2/2M)(k'^2-k_0^2)+(\hbar/2M)(\kappa^2+\alpha^2)-i\eta\hbar}\right\},$$

$$H_b=e^4Z_s^2Z\lim_{\eta\to 0}\sum_{\bar{k}'}\times\left\{\frac{(\bar{k}\bar{\kappa}|1/(\bar{r}_s-\bar{r})|knlm)(\bar{k}'|1/r_a|\bar{k}_0)}{(\hbar/2M)(k'^2-k_0^2)-i\eta\hbar}\right\}. \quad (3)$$

In these expressions, $\hbar\bar{k}_c$ and $\hbar\bar{k}$ are the initial and final momenta of the scattered particle, respectively; $\hbar\bar{\kappa}$ is the momentum of the ejected electron; $-\hbar^2\alpha^2/2m$ is the initial energy of the electron; and $\bar{r}_s$ and $\bar{r}_a$ are position vectors of the scattering particle and electron, respectively. The η appears as the result of assuming that the perturbation builds up an $\exp\eta t$ and serves to define the integrals uniquely. For the evaluation of these quantities, the wave function for the initial state of the electron is transformed to momentum space. The sum over intermediate states of the product of integrals is then combined into one multiple integral.

In both H_a and H_b this integral reduces to an integral of the form

$$\int d\bar{\kappa}_0\varphi_{nlm}(\bar{\kappa}_0)\{|\bar{\kappa}_0-\bar{\kappa}|^2|\bar{k}+\bar{\kappa}-\bar{k}_0-\bar{\kappa}_0|^2\times[|\bar{k}_0+\bar{\kappa}_0-\bar{\kappa}|^2-k^2-i\eta\hbar]\}^{-1}, \quad (4)$$

where $\varphi_{nlm}(\bar{\kappa}_0)$ is the momentum wave function for the state nlm. It is seen that this integral contains a dependence on the angle of ejection of the electron. However, since the integral is difficult to evaluate, it is replaced by

$$\varphi_{nlm}(\bar{\kappa})|\bar{k}-\bar{k}_0|^{-2}\int d\bar{K}K^{-2}[|\bar{k}_0+\bar{K}|^2-k^2-i\eta\hbar]^{-1}. \quad (5)$$

In this approximation, which is best at high electron energies, the angular dependence is lost. The momentum wave functions are written as $\varphi_{nlm}(\bar{\kappa})=P_{nl}(\kappa)Y_{lm}$, where Y_{lm} is a normalized spherical harmonic.

After integrating over the angle of ejection and dividing by the probability of scattering, the probability for ejection becomes

$$p(\epsilon)d\epsilon=\frac{(2\epsilon/\epsilon_0)^{\frac{1}{2}}}{mv^2}\{\pi^2+16[\tanh^{-1}(k/k_0)]^2\}\times\sum_{nl}2(2l+1)a_0^{-2}|P_{nl}(\kappa)|^2d\epsilon, \quad (6)$$

where $\epsilon_0=27$ ev.

In the numerical evaluation of this formula, the $P_{nl}(\kappa)$ are taken to be

$$(-i)^l\alpha^{l+5/2}\left[\frac{2^{4l+5}(l+1)!l!}{\pi(2l+1)!}\right]^{\frac{1}{2}}\frac{\kappa^l}{(\kappa^2+\alpha^2)^{l+2}}, \quad (7)$$

where $\alpha=Z_{eff}/(na_0)$ and Z_{eff} is Slater's effective charge. It is readily seen that almost all the ejections come from the innermost electrons of the atom. Table I gives the differential and total probabilities for the ejection of an electron from an atom of atomic number 40 by an incident μ-meson of four different energies. Since the binding energy of a K-electron in such an atom is 20 kev, the condition that the energy of the ejected electron be large compared to the binding energy is not met below about 50 kev; hence the values for 25 kev have limited validity.

IV. DISCUSSION

We note that Eq. (6) for the probability of ejection of an electron in a large-angle scattering does not depend on the minimum angle of scattering. The choice of 28° in the μ-meson observations insures a high probability of single scattering as compared to multiple scattering. Furthermore, there appears to be no correlation of the electron ejection probability or electron energy with the angle of scattering of the μ-meson.

The authors are indebted to Dr. M. Schein and Dr. J. K. Knipp for their continued interest in the problem and for many stimulating discussions and to Dr. H. L. Anderson for the use of the facilities of the cyclotron.

Activation Cross Sections for 14-Mev Neutrons*

STUART G. FORBES†
University of California, Los Alamos Scientific Laboratory, Los Alamos, New Mexico
(Received August 18, 1952)

Cross sections for several nuclear reactions induced by 14-Mev neutrons were measured by the activation method. The number of activated atoms was determined by absolute beta-counting. Corrections for finite sample thicknesses were determined experimentally in every case. Cross sections for the following reactions were measured: $(n,2n)$ for Cu^{63}, Cu^{65}, Ag^{107}, and Ag^{109}; (n,p) for Al^{27}, P^{31}, Fe^{56}, and Cu^{65}; (n,α) for Al^{27}.

I. INTRODUCTION

IF a nuclear reaction leads to the formation of an unstable isotope, the resulting radioactivity provides a means for determining the reaction cross section. In particular, if there are beta-particles emitted from the product nucleus, they may be counted in order to determine the total number of active atoms present. The cross section for the formation of these active atoms can then be found from the neutron flux, sample weight, and the number of activated atoms. In cases involving K-capture, beta-counting may still be employed if a known fraction of the disintegrations involve beta-particle emission. Similarly the cross section for the production of isomers may be determined to obtain the cross section for the production of a particular isotope provided each isomer decays at least in part by beta-emission.

Activation methods have been applied to the measurement of reaction cross sections by Wäffler,[1] using neutrons from the D+Li and D+B reactions, and by Cohen,[2] using neutrons from the D+Be reaction. Fowler and Slye[3] investigated the $Cu^{63}(n,2n)$ reaction cross section near the threshold, using neutrons from the D+D reaction; and more recently Paul and Clarke[4] measured activation cross sections for forty elements using neutrons from the T+D reaction. The present activation experiments[5] utilized 14.1-Mev neutrons produced by bombarding a thick tritium-zirconium target with 125-kev deuterons.

II. METHOD

For a measurement of the cross section σ for the production of a particular radioactive isotope, one needs to know the neutron flux nv, the number of atoms N in the sample, and the equilibrium activity A of the sample. Then for a thin sample,

$$\sigma = A/(nvN).$$

By absolute beta-counting and from a knowledge of the bombarding and counting schedule, the half-life, and the decay scheme of the isotope under consideration, the equilibrium activity was found.

The neutron flux from the D+T source was determined by counting the alpha-particles produced by the reaction. Samples were located so as to receive neutrons emitted from the target at an angle of 90° with respect to the deuteron beam. By collision mechanics the number of neutrons per cm² incident on the sample was calculated from the number of alpha-particles entering a proportional counter at 135° to the deuteron beam. The angular distribution of the neutrons is known to be isotropic in the center-of-mass system at low bombarding energies.[6]

The number of atoms in each sample was calculated from the sample weight.

III. BETA-COUNTING

Two counters were used. One was a Tracerlab type TGC-2 end-window Geiger counter and the other was a side-window proportional counter using a flow filling of methane at atmospheric pressure. The samples for the end-window counter were supported below the window on an adjustable shelf which was used in three positions to provide different counting efficiencies. The samples for the side-window counter were placed directly on the counter window (0.5 mg/cm² rubber hydrochloride) to obtain a high counting efficiency. Tests were performed on the proportional counter in order to show that it possessed a well-defined sensitive volume inside of which beta-particles were detected with essentially 100 percent efficiency. This was shown both by analysis of the pulse-height distribution curve produced by beta-particles from RaE and by intercalibration with the Geiger counter at two beta-energies. The pulse-height distribution indicated that less than 1 percent of all the pulses fell below the bias setting of the scaling unit. The relative sensitivity of the counter was the same for the 1.17-Mev beta-particles from RaE as for the 0.51-Mev beta-particles from Cs^{137}.

Calibrations of the counters were obtained by counting RaDEF standards certified by the National Bureau of Standards. In order to use these standards a correction must be applied because of scattering by the thick backing on which they are supplied and for the

* Work done under the auspices of the AEC.
† Now at Phillips Petroleum Company, Idaho Falls, Idaho.
[1] H. Wäffler, Helv. Phys. Acta **23**, 239 (1950).
[2] B. L. Cohen, Phys. Rev. **81**, 184 (1951).
[3] J. L. Fowler and J. M. Slye, Jr., Phys. Rev. **77**, 787 (1950).
[4] E. B. Paul and R. L. Clarke, Phys. Rev. **86**, 605 (1952).
[5] S. G. Forbes, Ph.D. thesis, Oregon State College, June, 1951 (unpublished).
[6] D. L. Allen and M. J. Poole, Proc. Roy. Soc. (London) **A204**, 500 (1951).

scattering in the active deposit itself which is about 1 mg/cm² thick. The corrections to be applied cannot be readily determined experimentally, but Burtt[7] found that (for source-to-window distances greater than about 1 cm) a correction factor of 1.79 for the combined effects gave good agreement with standards prepared in the laboratory. Therefore, for the three Geiger-counter geometries in the present work, the disintegration rate quoted by the Bureau of Standards was used to obtain geometry factors G from the following relation:

$$1.79G \times \text{disintegrations/min} = \text{counts/min}.$$

Intercalibration of the one close (47 percent) proportional counter geometry with the Geiger-counter geometries was then accomplished by counting rate comparisons using a thin deposit of Cs^{137} on Zapon. The geometry factors thus obtained were in good agreement with the values calculated from geometry considerations. Since the counter sensitivities varied slightly with time, frequent checks on the geometry factors were made using the standards.

Background, coincidence loss, and window and air absorption corrections were applied to the observed counting rates. Scattering by the housing was assumed to be negligible. Backscattering was made negligible by using Zapon films of about 40 $\mu g/cm^2$ to support all samples. The samples were in the form of disks ½ inch in diameter in order to simulate closely the size of the RaDEF beta-standards.

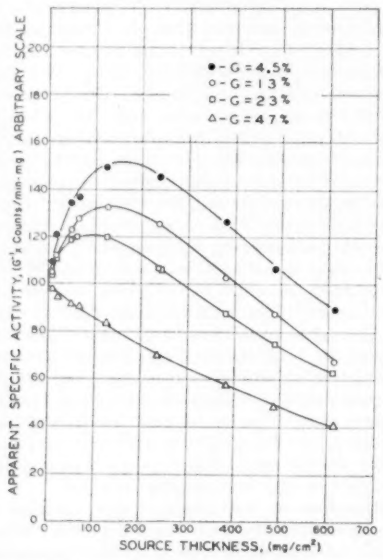

FIG. 1. Effect of sample thickness on apparent specific activities for Cu^{64} beta-rays in copper foils for the three Geiger-counter geometries of 4.5, 13, and 23 percent, and for the 47 percent proportional counter geometry.

[7] B. P. Burtt, Nucleonics **5**, No. 2 (1949).

Because of complications introduced by scattering effects, the self-absorption and scattering in the sample were determined experimentally in every case. This was done by measuring the apparent specific activity ($G^{-1} \times$ counts/min-mg) as a function of the source thickness (mg/cm²) and extrapolating to zero thickness to obtain the true specific activity which would be observed in the absence of scattering and absorption in the sample. Typical results of such an experimental determination are shown in Fig. 1 for four different counting geometries. These curves were obtained by giving a series of foils of different thicknesses equal bombardments with 14-Mev neutrons so that the true specific activities of all the foil were equal. Similar curves have been obtained by other observers.[8–10] The use of a thick sample support tends to flatten these curves somewhat but does not remove the necessity of extrapolation to zero sample thickness and the determination of the corresponding backscattering factor.

Curves similar to those shown in Fig. 1 were obtained experimentally in the 23 percent and 47 percent geometries for every beta-activity used in the cross-section determinations with one exception. The self-scattering of Ni^{65} beta-particles by the copper sample was assumed to be the same as that of Mn^{56} beta-rays scattered by iron. All the curves showed the same general shape, although the magnitude and location of the peaks for the 23 percent geometry varied considerably.

An attempt was made to simulate a thick foil by stacking several thin foils, but the experimental data consistently fell below that obtained from single layers and was considerably more erratic. Evidently poor contact between successive layers permitted sufficient "leakage" of the beta-particles emitted in the plane of the sample to reduce the fore-scattering appreciably.

In practice, the shape of the curves of activity *vs* sample thickness was determined by bombarding a series of foils simultaneously in the strongest neutron flux available in order to obtain reasonable counting statistics for the very thin foils. The absolute cross-section measurement could then be made by bombarding a relatively thick foil at a greater distance from the source in order to increase the precision of the flux determination.

IV. RESULTS

The values of the cross sections found from the measurements are listed in Table I. The isotopic cross sections were calculated on the basis of isotopic abundances and branching ratios for beta-decay as given by the National Bureau of Standards summary of nuclear

[8] Collie, Shaw, and Gale, Proc. Phys. Soc. (London) **A63**, 282 (1950).

[9] Solomon, Gould, and Anfinsen, Phys. Rev. **72**, 1097 (1947).

[10] K. D. George, National Research Council of Canada, Document CR TEC-309 (1946) (unpublished).

data.[11] A correction was made to the decay of Cu^{64} for 46 percent K-capture. No other K-capture corrections were made. The half-lives quoted in Table I are those used in the calculations. Deviations from published values are based on actual observations.

The cross section for the $Cu^{65}(n,p)Ni^{65}$ reaction was found by comparing the activity of the 2.56-hour Ni^{65} to the activity of the 12.8-hour Cu^{64}. The cross section for the (n,p) reaction is relatively small, so that it was necessary to follow special procedures in order to resolve the two activities. A relatively thick foil of 120 mg/cm^2 was used in order to attenuate the lower energy Cu^{64} beta-rays. The activation was made in the strongest flux available to improve the counting statistics, and the bombardment was limited to two hours in order to avoid saturation of the longer-lived Cu^{64}. The counting was done in the 47 percent geometry to avoid complications in estimating the self-scattering correction for the Ni^{65} beta-rays.

The ratio of the $Al(n,\alpha)$ and $Al(n,p)$ cross sections was found also by comparing the activities produced by a single bombardment. The resulting ratio was $\sigma(n,\alpha)/\sigma(n,p)=1.70$, which is in excellent agreement with the ratio obtained from the individual determinations.

V. DISCUSSION OF ERRORS

The largest error in many cases is introduced by the calibration of the counters with the RaDEF beta-standards. The standard error in the disintegration rates of the standards is given as 3 percent. An additional error of 2 to 3 percent is introduced by the necessity of making long extrapolations of the absorption curves in order to correct for absorption in the window and air. The error in the product of the backscattering and self-scattering factors is not known but is believed to be about 5 percent on the basis of the results obtained by Burtt. The estimated standard error in the counter calibration is therefore 6 percent. This could be reduced to 1 or 2 percent if accurately calibrated thin beta-ray standards free from alpha-radiation and mounted on thin backings were available.

Determination of the true specific activity from the extrapolation to zero sample thickness is another source of large error. For elements of low atomic number such as aluminum for which very thin foils are readily obtained, the extrapolation has about 2 percent uncertainty. In cases where the beta-energy is low or where the atomic number is high, the use of very thin foils is required in order to determine the shape of the initial portion of the curve. The effects of wrinkles in the foils or variations in the thickness become more prominent in this region, and the accuracy of the measurements is reduced.

[11] Way, Fano, Scott, and Thew, *Nuclear Data*, National Bureau of Standards Circular 499 (1950).

TABLE I. Reaction cross sections for 14.1-Mev neutrons.

Reaction	Half-life	Isotopic cross section (millibarns)	Estimated error (percent)
$Al^{27}(n,p)Mg^{27}$	9.6 min.	79	7
$Al^{27}(n,\alpha)Na^{24}$	15.0 hr	135	7
$P^{31}(n,p)Si^{31}$	170 min	91	10
$Fe^{56}(n,p)Mn^{56}$	2.59 hr	124	10
$Cu^{63}(n,2n)Cu^{62}$	9.9 min	510	7
$Cu^{65}(n,2n)Cu^{64}$	12.8 hr	970	8
$Cu^{65}(n,p)Ni^{65}$	2.56 hr	19	20
$Ag^{107}(n,2n)Ag^{106}$	24.5 min	560[a]	10
$Ag^{109}(n,2n)Ag^{108}$	2.3 min	1000	10

[a] Cross section for the production of the 24.5-min isomer only.

The standard error for the neutron flux is estimated as 2 percent. This value is based on the sentivity of the calculations to variations in the different parameters involved. At the low bombarding energies (125-kev deuterons) used, the corrections for the asymmetry in the angular distribution of the particles in the laboratory system of reference is not very great, and hence the calculations are not very sensitive to changes in the bombarding energy, the rate of deuteron energy loss in the thick target, or uncertainties in the variation of the D+T reaction cross section with energy. Errors in the distance between source and sample introduced by motion of the deuteron beam over the target will cancel out if several runs are averaged.

The purity of all samples used was known to be at least 99 percent; hence the number of atoms is subject to errors of less than 1 percent from this source.

It is unlikely that any of the observed activities are assigned to the wrong radioisotope, since such a wrong assignment would involve either an improbable reaction or the presence of an impurity with an extremely large cross section. Small amounts of an activity having a half-life similar to that under investigation would be difficult to detect, however, since no chemical separations were made.

Errors in the sample weights and statistical errors in the beta-counting were less than 1 percent in most cases.

The estimated error in Table I is the rms value of the standard errors directly involved in the measurements and does not include estimates of the uncertainties in the decay schemes.

The relative values of the cross sections should be more accurate than the absolute values since the counter calibration error does not enter. There will be 1 or 2 percent error remaining caused by fluctuations in the counter sensitivities even though these were checked periodically.

The author wishes to express his appreciation to Dr. E. R. Graves and to Dr. J. H. Coon for their interest and helpful suggestions during the course of this research and to the AEC whose graduate program made this work possible.

Coulomb and Nuclear Interactions of Cosmic-Ray Mesons and Protons in Lead*

W. L. WHITTEMORE AND R. P. SHUTT
Brookhaven National Laboratory, Upton, New York
(Received September 9, 1952)

A cloud-chamber experiment shows that positive and negative particles at sea level in the momentum range 0.3–3.1 Bev/c scatter in 5 cm of lead in the same manner. The experimental scattering distributions have a large-angle "tail" which agrees rather well with the theoretical distributions of Molière and of Snyder and Scott who assumed that the nucleus scatters like a point charge. These distributions should not be valid here because the charge distribution within the nucleus must be considered in detail for such energetic mesons. The recent calculation of Olbert specifically neglecting the scattering of particles which penetrate the nucleus predicts a much smaller probability for large-angle scattering than observed. A rough extrapolation of the calculations of Amaldi *et al.* to the case of lead shows that it is possible to explain perhaps 10 percent of the observed large-angle scattering as due to inelastic electric scattering within the nucleus, if the radius of the electric charge on a proton is taken to be 2×10^{-14} cm. Negative particles observed at 3.4-km altitude scatter in lead much the same as the sea-level particles. The scattering of positive particles observed at 3.4-km altitude indicates that protons in the momentum range 1–4.8 Bev/c suffer a small amount of nuclear scattering in lead corresponding to $(0.13\pm0.07)\sigma_g$, where σ_g is the geometrical cross section. All nuclear interactions combined give a total interaction cross section for lead of $(0.38\pm0.09)\sigma_g$. These surprisingly small cross sections are compared with other data from the literature.

I. INTRODUCTION

A CLOUD-CHAMBER experiment has been performed at sea level and at 3.4-km altitude to study the scattering of cosmic-ray mesons and protons in lead. The results of this investigation are presented in two parts. The first part, including Secs. III and IV, deals with the electrical scattering of mu-mesons. The second part (Secs. V to VII) deals with the interactions of protons in lead, including star production and meson production in addition to the nuclear scattering of protons.

The multiple Coulomb scattering of charged particles has been investigated theoretically by several authors.[1–5] The various results are generally in agreement in the region of highly multiple scattering and predict a distribution which is approximately Gaussian. However, some of the results differ for the region of plural and single scattering. The single scattering depends upon the assumptions made concerning the charge distribution within the nucleus. Molière[3] and Snyder and Scott[4] assumed a point charge which gives a differential distribution in $(p\beta\theta)$ for single scattering varying for large angles ($p\beta\theta>\sim3$ degree-Bev/c for the present investigation) about as $1/(p\beta\theta)^3$, where p is the momentum, $\beta=v/c$ (v and c are, respectively, the velocity of the incident particle and the velocity of light), and θ is the angle of scattering projected on a plane. On the other hand, Olbert[5] has assumed that the probability of scattering of fast particles through angles larger than $\theta_{\max}\approx\lambda\!\!\!^{-}/R$ is identically zero, where $\lambda\!\!\!^{-}=\hbar/p$ is the wavelength of the incident particle and $R=1.4\times10^{-13}A^{\frac{1}{3}}$ is the nuclear radius. A stands for the atomic mass number. The resulting distribution indicates a much reduced probability for large-angle scattering of particles of high energy. For the approximations used in all of the calculations as well as for the present observations, only angles $\theta<1$ radian are to be considered. Thus, for $\lambda\!\!\!^{-}>R$, Olbert assumes no cutoff within the angular range considered, and the different theories become identical.

The modification of the scattering due to the charge distribution inside the nucleus must be taken into account when $\lambda\!\!\!^{-}<R$. A calculation by Amaldi *et al.*[6] shows that the amount of elastic Coulomb scattering (coherent scattering) inside the nucleus is very small. In this respect, Olbert's assumption is valid. On the other hand, the calculation of Amaldi *et al.* for the effect of incoherent scattering within the nucleus indicates that Olbert's assumption may have to be modified, as will be shown later, for those particles which penetrate the nucleus.

The work of Hanson *et al.*[7] on the multiple scattering of 15.7-Mev electrons has shown that electrons scatter in gold according to the predictions of Molière's theory within the experimental accuracy of 2 percent, with the possible exception that Molière's theory predicts slightly fewer scatterings in the region of plural scattering. Since $\lambda\!\!\!^{-}>R$ for 15.7-Mev electrons Molière's distribution should here be valid for all angles. Very few data are available for the scattering of energetic mu-mesons capable of probing the nucleus. Previous experiments[8–10] on mesons, which gave simultaneous information on the

* Work done at Brookhaven National Laboratory under the auspices of the AEC.
[1] W. Bothe, *Handbuch der Physik* (Julius Springer, Berlin, 1933), Vol. 22, II, p. 1.
[2] E. J. Williams, Proc. Roy. Soc. (London) **169**, 531 (1939); S. Goudsmit and J. L. Saunderson, Phys. Rev. **57**, 24 (1940); **58**, 36 (1940).
[3] G. Molière, Z. Naturforsch. **3a**, 78 (1948).
[4] H. S. Snyder and W. T. Scott, Phys. Rev. **76**, 220 (1949); W. T. Scott, Phys. Rev. **85**, 245 (1952).
[5] S. Olbert, Phys. Rev. **87**, 319 (1952).
[6] Amaldi, Fidecaro, and Mariani, Nuovo cimento **VII**, 553 (1950).
[7] Hanson, Lanzl, Lyman, and Scott, Phys. Rev. **84**, 634 (1951).
[8] F. L. Code, Phys. Rev. **59**, 229 (1941).
[9] J. G. Wilson, Proc. Roy. Soc. (London) **A174**, 73 (1940).
[10] J. A. Vargus, Phys. Rev. **56**, 480 (1939).

momentum and scattering angle, have not provided sufficient information at the large angles to decide between the various theories. Amaldi and Fidecaro[11] have obtained experimental results for very large-angle scattering ($p\beta\theta > \sim 15$ degree Bev/c) revealing a small cross section (of the order of 2×10^{-30} cm^2/nucleon) for mesons with energies greater than 300 Mev, but since they dealt only with very large angles, their experiment did not provide details of the distribution at intermediate scattering angles. The purpose of the first part of the present experiment was to obtain sufficient data on the electrical scattering of mu-mesons in the region of plural and relatively small-angle single scattering to check the various theories.

The second part of this experiment concerns the interaction of protons with lead nuclei. The cosmic-ray flux at 3.4-km altitude is rather rich in protons, as previous results have indicated.[12,13] At this altitude protons form about 20 percent of the total penetrating component in the momentum range from 0.3 to 9.6 Bev/c. Thus protons constitute a large fraction of the positive penetrating component alone. Therefore, a cloud-chamber investigation of the interactions of particles with positive charge only should lead to measureable results.

Until quite recently only meager information was available on the interaction in lead of protons with momenta in the range 1–5 Bev/c. Anderson and Neddermeyer[14] performed an experiment at 4.3-km altitude with a cloud chamber in a magnetic field. The arrangement was such as to provide in principle the desired information. However, this experiment was performed before the various components of cosmic rays were known, and the results cannot be applied here. Other experiments[15–17] were performed later at mountain altitudes with cloud chambers containing various arrangements of metal plates, but these experiments did not include a magnetic field to measure the momentum or the sign of charge of the particles involved. Therefore, the effects due to protons alone could not be isolated except in the cases where multiple scattering measurements and relative ionization could be used to identify the protons. In these cases the energy was still largely undetermined. Thus it seemed of interest to make a study of the proton-interaction cross section, where the momentum of the proton would be measured directly. It is the purpose of the second part of this paper to give the results of the present experiment on the interaction of protons in lead and to discuss these in view of the recent results of others.

[11] E. Amaldi and G. Fidecaro, Nuovo cimento **VII**, 535 (1950).
[12] Miller, Henderson, Potter, and Todd, Phys. Rev. **84**, 981 (1951).
[13] W. L. Whittemore and R. P. Shutt, Phys. Rev. **86**, 940 (1952).
[14] C. D. Anderson and S. Neddermeyer, Phys. Rev. **50**, 263 (1936).
[15] W. E. Hazen, Phys. Rev. **63**, 213 (1943); **65**, 67 (1944).
[16] M. J. Dandin, Compt. rend. **218**, 830 (1944).
[17] W. M. Powell, Phys. Rev. **69**, 385 (1946).

II. APPARATUS

The experimental arrangement, designed specifically to measure simultaneously the momentum and scattering of cosmic-ray particles has been described briefly.[12] A few additional details will now be given. The apparatus is similar in principle to that used by Brode for mass measurements[18] and by Glazier *et al.*[19] for momentum measurements. Two cloud chambers were mounted one above and one below the air gap of a permanent magnet[20] providing a field of about 9000 gauss. Through the center of the lower chamber a lead plate, 5 cm thick, was mounted horizontally. A 1-cm plate was mounted below the 5-cm plate. An arrangement of Geiger counters connected in coincidence selected particles which traversed the air gap of the magnet as well as the two cloud chambers. It was possible, although very unlikely, that a meson not originally in the solid angle determined by the counter system could be scattered into it by the iron pole pieces. Fiducial wires were located in the cloud chambers in order to enable one to recognize events of this type. A system of mirrors allowed one camera to view both cloud chambers simultaneously along the axis of each. A second camera viewed both chambers in a similar fashion with a stereoscopic angle of 20°.

The circular expansion cloud chambers were of conventional design, 6 inches deep and 19 inches in diameter. The cylindrical walls of the chamber were made of $\frac{3}{32}$-inch Plexiglas coated on the inside with a thin solution of polystyrene dissolved in toluene. This thin coating prevented the alcohol vapor from destroying the surface of the walls. The pressure of argon and condensable vapor (a 50–50 mixture of water and ethyl alcohol) in the chamber when fully compressed was 1.4 atmospheres at sea level and 1.1 atmospheres at 3.4-km altitude. Fixed-volume expansions were made in the usual way by releasing air from behind a Neoprene diaphragm through a fast-acting valve.[20] The time of 0.008 sec between passage of a particle and completion of the expansion was sufficiently short to give tracks of less than one-millimeter width. After a 5-second delay following a fast expansion caused by an incident particle the chamber was recompressed. Thereafter three slow expansions taking about one second each followed at 15-second intervals. Finally, the chamber was allowed to recover in the compressed state for an additional 70 seconds, making the minimum total time between fast expansions two minutes.

Illumination for each chamber was provided by 2 fourteen-inch quartz flash tubes, 5-mm inside diameter, mounted in parabolic reflectors and placed on both sides of the chambers. Each flash tube was energized by a condenser bank of 120 microfarads charged to 2000

[18] R. B. Brode, Revs. Modern Phys. **21**, 37 (1949).
[19] Glazier, Hammermesh, and Safanov, Phys. Rev. **80**, 625 (1950).
[20] R. P. Shutt and W. L. Whittemore, Rev. Sci. Instr. **21**, 643 (1950); **22**, 73 (1951).

volts. The lead plates in the bottom cloud chamber were covered on both sides by polished ferrotype plates to improve the illumination in the region around the plates. The light delay after expansion was 0.05–0.10 sec. The photographs were made on 35-mm Linagraph Ortho perforated film, using a demagnification of about 15. The cameras located at the front and at the 20° position had apertures of $f/9$ and $f/11$, respectively.

The momentum p is given by $p=5.3/\theta_p$, when p is measured in units of Bev/c, and θ_p is the angle in degrees between the track in the top chamber and in the top half of the bottom chamber. This approximate expression for p is no longer valid when $\theta_p>20°$; but for the mesons under consideration $\theta_p<15°$. As described,[13] the scattering in the walls of the cloud chambers and interposed Geiger counters caused an error of less than one percent in the momentum measurement and was negligible compared to the distortions due to turbulence. The momentum p could be measured in the range 0.300 ± 0.006 to 11 ± 4 Bev/c. The lead plates in the bottom chamber were used for the study of the projected angle θ of scattering for particles whose momenta were measured. For each singly occurring particle the quantity $p\theta$ could be evaluated. The scattering theories show that the proper variable to study is $p\beta\theta$, not $p\theta$, which is determined by the above measurements. For mesons of the momenta under consideration, however, the value of β is very nearly unity, and therefore, the quantity $p\theta$ can actually be used to characterize the scattering. On the other hand, protons of the same momentum as the mesons under consideration have a value of β substantially less than unity, ranging down to 0.31 for protons with $p=0.30$ Bev/c. Therefore, a correction to the measured quantity $p\theta$ must be applied for protons.

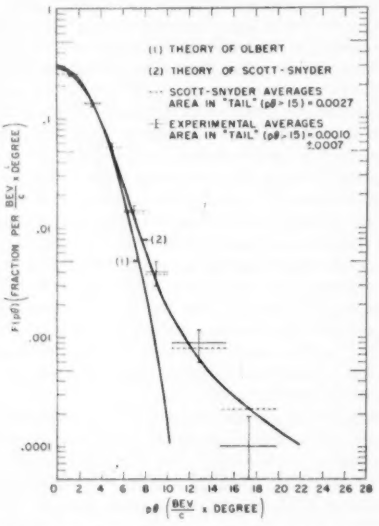
(1) THEORY OF OLBERT
(2) THEORY OF SCOTT-SNYDER
SCOTT-SNYDER AVERAGES AREA IN "TAIL" (pθ > 15) = 0.0027
EXPERIMENTAL AVERAGES AREA IN "TAIL" (pθ > 15) = 0.0010 ±0.0007
F(pθ) (FRACTION PER BEV/c x DEGREE)
pθ (BEV/c x DEGREE)
0 2 4 6 8 10 12 14 16 18 20 22 24 26 28
.1
.01
.001
.0001

FIG. 1. The differential distribution $F(p\theta)$ in projected scattering variable $p\theta$ below 5 cm of lead for *negative* mu-mesons with $0.30<p<3.1$ Bev/c observed at sea level. In all distributions only those particles were included which ionized at the minimum rate above and below the 5-cm plate.

III. RESULTS OF EXPERIMENT ON SCATTERING OF MU-MESONS IN LEAD

The differential distributions $F(p\theta)$ of scattering in 5 cm of lead of negative and positive mesons observed *at sea level* are given in Figs. 1 and 2, respectively. Mesons in the momentum range from 0.300 to 3.1 Bev/c have been included with the exception of positive particles in the range 0.70 to 1.0 Bev/c. The omission of the latter group from the data as well as the inclusion of only those particles which ionized at the minimum rate both above and below the 5-cm plate aids in the elimination of a contribution due to nuclear interactions of protons in a momentum range where protons may still be numerous.[21] Protons with $p<0.7$ Bev/c were stopped in the 5-cm plate by ionization losses. Protons with $p>1.0$ Bev/c could not have been stopped by ionization losses alone. It should be noted that except for somewhat larger statistical fluctuations the same distributions are exhibited individually for positive as well as for negative particles if the data are subdivided into groups with momenta in the ranges 0.3–1.0, 1.0–1.9, and 1.9–3.1 Bev/c. The distributions in both Fig. 1 and Fig. 2 are normalized so that the total area under each curve is unity.

Some of the scattering data were affected by errors in measuring θ_p and θ which tended to distort the distributions. The data included in Fig. 1 and Fig. 2 were affected only to a negligible extent by these errors; however, data for momenta >3.1 Bev/c which were not included were affected to a very important extent in the following manner. The scattering distribution can be represented approximately by a Gaussian curve except for a "tail," starting at $p\theta=7$ degree-Bev/c, which is small compared to the bulk of the scattering. This "tail" contains the large angles, compared to which the measuring errors are negligible. The measuring errors can also be represented by Gaussian curves having a root-mean-square width representing an average magnitude of the error. If σ_t is the root-mean-square width of the true scattering distribution and σ_e is the root-mean-square deviation of a large number of measurements of $p\theta$, caused by the various measuring errors, then the root-mean-square width σ_0 of the observed scattering distribution is given by $\sigma_0^2=\sigma_t^2+\sigma_e^2$. Thus the Gaussian curve with width σ_t broadens to a Gaussian curve with width σ_0 because of the measuring errors. The average measuring error for θ_p was taken to be about 0.3°. The error in the measurement of the projected angle of scattering below the 5-cm plate was taken to be 0.5°.

[21] M. G. Mylroi and J. G. Wilson, Proc. Phys. Soc. (London) **A64**, 404 (1951).

Therefore, σ_s increases with p, since $p \propto 1/\theta_p$, but is constant with θ. For mesons with $p<3.1$ Bev/c, the scattering data for the 5-cm plate were not appreciably affected by these errors, as a computation shows. For $p>3.1$ Bev/c, however, the effects of these errors became important, resulting in an observed scattering distribution about twice as broad as the true distribution for particles in the range $4.8<p<11.0$ Bev/c. For the 1-cm lead plate, the situation was much worse because the error in measuring the scattering angle below the 1-cm plate was at least 1.0°, due to the added turbulence and poor lighting in the bottom section as well as to the splitting of the tracks caused by electrostatic charges on the Plexiglas walls of the cloud chamber. Thus all of the scattering data from the 1-cm plate were affected in a significant and nonuniform manner by the various errors. Since it was preferred to use only those data for which the computations show that corrections were unimportant, only the data in Fig. 1 and Fig. 2 were used to exhibit the Coulomb scattering in lead.

A different type of error might affect the "tail" of the distributions given in Fig. 1 and Fig. 2. As mentioned above, the "tail" contains particles scattered into angles large compared to the measuring errors. Moreover, the momenta involved could also be measured with good accuracy. The only serious source of error for these events lay in the possibility that an incident particle not in the solid angle selected by the counter trays was scattered into the bottom counter and cloud chamber by the pole tips of the magnet in such a manner that the apparent momentum was considerably increased. This effect would have made the observed values of $p\theta$ too large and contributed falsely to a "tail." The observed "tail" was larger than the curve of Olbert (approximately Gaussian) by a number of events corresponding to 2.5 percent of the incident particles. A calculation shows that the number of mesons scattered in the pole tips could not have amounted to more than 0.15 percent of the incident flux. Furthermore, a detailed examination of the individual events forming the "tail," making use of the fiducial wires mentioned above, showed no case where a meson hit a magnet pole face. Therefore, the experimental distributions in Fig. 1 and Fig. 2 were not influenced significantly by measuring errors or instrumental uncertainty.

IV. DISCUSSION OF RESULTS ON MU-MESON SCATTERING

The theoretical distributions of Olbert (curve 1) and Snyder and Scott or Molière (curve 2) are shown also in Fig. 1 and Fig. 2, together with the experimental data. The theories of Molière and of Snyder and Scott are represented by the same distribution. The results of Olbert, however, are quite different. As discussed in Sec. I, the difference between the theories lies in the treatment of the electric charge distribution within the nucleus. Since λ is about 2×10^{-14} cm ($\ll R=8\times10^{-13}$ cm) for a meson with $p=1$ Bev/c, one sees that the theories of Molière and of Snyder and Scott cannot be applied here, since the nucleus can no longer be considered as a single point charge. Surprisingly enough, their theories agree rather well with the experimental results up to much larger values of $p\theta$ than expected. As pointed out in Sec. III, mesons with momenta in smaller intervals (e.g., 0.3–1.0, 1.0–1.9, 1.9–3.1 Bev/c) separately gave the same experimental distributions.

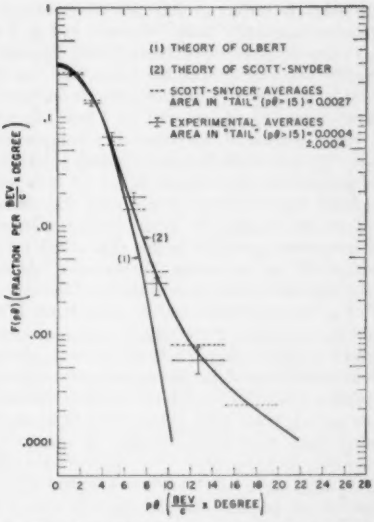
(1) THEORY OF OLBERT
(2) THEORY OF SCOTT-SNYDER
--- SCOTT-SNYDER AVERAGES AREA IN "TAIL" (pθ>15) = 0.0027
EXPERIMENTAL AVERAGES AREA IN "TAIL" (pθ>15) = 0.0004 ±0.0004
F(pθ) (FRACTION PER BEV/c x DEGREE)
1
.1
.01
.001
.0001
(2)
(1)
0 2 4 6 8 10 12 14 16 18 20 22 24 26 28
pθ (BEV/c x DEGREE)

FIG. 2. The differential distribution $F(p\theta)$ below 5 cm of lead for *positive* mu-mesons with $0.30<p<3.1$ Bev/c observed at sea level, omitting $0.70<p<1.0$ Bev/c.

The scattering distribution predicted by Olbert does not agree with the experimental results. In fact, even for values as small as $p\theta=7$, the distribution of Olbert, assuming no scattering within the nucleus, predicts a probability for scattering which is smaller than observed by a factor of two, and it becomes progressively smaller than observed for larger values of $p\theta$, reaching a value 10^3 times too small at $p\theta=15$, and 10^6 times too small at $p\theta=20$. The theory of Olbert could be brought into substantial agreement with the present results only by requiring that the electric charge of the whole lead nucleus is concentrated in a volume with radius of less than one sixth of the nuclear radius of 8×10^{-13} cm. Unless one attributes the observed excess scattering to the nuclear interaction of mu-mesons, one must conclude that the theory of Olbert has to be modified to include the effect of the distribution of charge within the nucleus.

The difference between Olbert's and the experimental distributions represents a "tail" containing about 2.5 percent of the total area under the curves. It must be

emphasized that neither protons nor electrons nor pi-mesons could cause the "tails" observed in Fig. 1 and Fig. 2. In the first place, since the scattering distribution of negative particles showed the same "tail" as that observed for the positive particles, protons could not be the cause. Moreover, protons with $p>1$ Bev/c form not more than 1 percent of the penetrating component at sea level.[21] Since the mean free path for nuclear scattering in lead for protons will be shown in Sec. VI to be about 1200 g/cm^2, the 5-cm lead plate caused only about 5 percent of the protons to suffer nuclear scattering. Therefore protons gave rise to less than $0.05\times1=0.05$ percent of all the scattering. Furthermore, electrons were not sufficiently numerous at sea level to cause this "tail." For the momentum region above 0.300 Bev/c, only about one percent of the ionizing tracks were due to electrons.[22] Cascade theory[23] indicates that of those electrons which existed in this momentum range only 5–10 percent should have produced a shower containing just *one* particle below 5 cm of lead. This indicates that not more than $0.1\times1=0.1$ percent of the incident particles were electrons which could have given a falsely identified large angle event. Furthermore, this expected number of one-particle electron showers agrees also with that which one can predict on the basis of the observed electron showers with two or more particles. The number of pi-mesons incident on the apparatus must be very small (<0.1 percent), since it is known that very few mu-mesons (and hence, pi-mesons) are produced below 3.4-km altitude[18] and also that few protons (~1 percent)[21] are incident at sea level with sufficient energy to produce energetic pi-mesons. Thus the effects of protons, electrons, and pi-mesons on the production of the "tail" are negligible at sea level.

It might be noted that, if the electrical scattering theory of Olbert were assumed to be strictly correct, the "tail" observed for mu-mesons would indicate a non-electrical interaction. The cross section one obtains by attributing to nuclear effects all large-angle scattering beyond that predicted by Olbert is about 10^{-25} cm^2 per lead nucleus. This is a value very similar to that obtained previously by many workers, who attributed to nuclear scattering the difference between the observed scattering and that predicted by the theory of Williams. In this regard, see Code,[8] Wilson,[9] Vargus,[10] Shutt,[24] Sinha,[25] and Sahiar.[26] The cross section obtained from the present experiment would be essentially the same whether Williams' or Olbert's theory is used. The present results are compatible with those of Amaldi *et al.*,[11] obtained by a different method for very large scattering angles only, if one attributes to the electron component the few particles we observed to be scattered through $p\theta>15$.

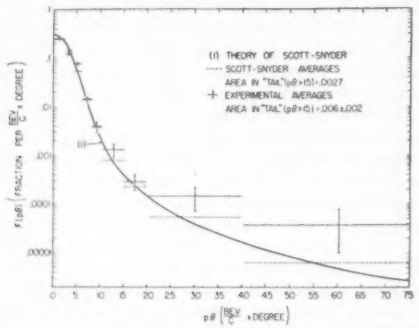

FIG. 3. The differential distribution $F(p\theta)$ below 5 cm of lead for *negative* particles observed at 3.4-km altitude with $1.0<p<4.8$ Bev/c.

To investigate whether the observed scattering for the larger values of $p\theta$ could be wholly due to electrical interactions within the nucleus, the theory by Amaldi *et al.*[6] has been used to estimate the effect of incoherent scattering resulting in excitation of the nucleus. While Amaldi's calculations apply only to light nuclei such as lithium and carbon, these calculations, nevertheless, should give an indication of the order of magnitude to be expected for this type of scattering in a heavy nucleus like lead, if a correction factor is introduced to take account of the Z dependence of the incoherent Coulomb scattering. A computation shows that incoherent scattering within the nucleus might account for 5 to 10 percent of the observed large-angle scattering if the radius of the charge distribution in the individual protons is taken as 2×10^{-14} cm, and for only about one percent if the radius is taken as 1.4×10^{-13} cm. This theory as applied to lead is too crude to allow any detailed conclusions. However, it seems unlikely that a detailed calculation carried out for lead specifically would yield a cross section larger by an order of magnitude. Hence, the large observed cross section may indicate some non-Coulomb interaction in addition to an electric charge distribution for single protons (as well as mu-mesons) much smaller than the size corresponding to the proton radius of 1.4×10^{-13} cm. We conclude that the present experiment is sufficient to indicate the need for a treatment of the contribution to scattering of an incident mu-meson by the individual protons within a lead nucleus.

V. NUCLEAR SCATTERING OF PROTONS OBSERVED AT 3.4-km ALTITUDE

The equipment described in Sec. II was operated at an altitude of 3.4 km in the same manner as at sea level. Since protons form a significant part of the penetrating component at 3.4 km, one would expect to observe not only the electrical scattering of the incident particles,

[22] E. J. Williams, Proc. Roy. Soc. (London) **A172**, 194 (1939).
[23] D. J. X. Montgomery, *Cosmic Ray Physics* (Princeton University Press, Princeton, 1949), p. 341.
[24] R. P. Shutt, Phys. Rev. **61**, 6 (1942).
[25] M. S. Sinha, Phys. Rev. **68**, 153 (1945).
[26] A. Sahiar, Proc. Indian Acad. Sci. **34**, 201 (1951).

but also nuclear scattering of protons and other events such as stars and meson production.

Figure 3 shows the differential distribution observed at 3.4-km altitude for negative particles with momenta in the range 1.0–4.8 Bev/c. It is in very good agreement with the sea-level data exhibited in Fig. 1 and Fig. 2, except that, for the larger angles where $p\theta > 15$, about 6.0 ± 4.2 times as many particles were observed at altitude as at sea level. This excess number forms about 0.5 percent of all the scattered particles. Although this small excess for large angles might be taken to indicate the nuclear scattering of pi-mesons in the natural cosmic-ray beam, it probably only indicates the presence of a considerable number of electrons in the incident beam at 3.4-km altitude,[27] some of which triggered the apparatus even though anticoincidence counters were used at the sides. As shown in Sec. IV, an energetic electron ($E > 1$ Bev) has less than a 10-percent chance to produce a one-particle shower below 5 cm of lead. This would imply that electrons may have formed 5 percent of the incident flux, if the additional large-angle scattering is due to electrons. Additional evidence of a rather large component of electrons occurring singly in the cloud chamber is provided by the fact that the intensity of electron showers with two or more particles observed at 3.4-km altitude was about 2 times the intensity observed at sea level in spite of the use of anticoincidence counters. An auxiliary experiment, making use of carbon placed above the apparatus in order to increase the number of pi-mesons observed, showed that pi-mesons scattered by nuclear interactions contributed less than 0.1 percent to the scattering distribution. Furthermore, a computation of the intensity of pi-mesons expected at 3.4-km altitude on the basis of the meson production spectrum of Sands[28] gives a value of about 0.25 percent of the penetrating component. The rather good agreement in the range $0 < p\theta < 15$ with the results obtained at sea level is taken as evidence that the negative particles observed here are mainly mu-mesons.

The positive particles at 3.4-km altitude scattered in quite a different manner from the negative particles at the same altitude. Figure 4 shows the scattering results obtained for positive particles alone in the momentum range from 1.0 to 4.8 Bev/c. The lower limit of 1.0 Bev/c was chosen to lie considerably above the upper limit of 0.7 Bev/c for absorption of protons by ionization losses in the 5-cm lead plate, so that both protons and mesons had to ionize at the minimum rate below the plate. Also protons with less momentum could have suffered sufficient Coulomb scattering in the lead to scatter out of the illuminated volume. The upper limit of 4.8 Bev/c was chosen because protons of larger momenta formed a very small part of the incident beam. The large range of momenta (1.0–4.8 Bev/c) was chosen to include enough protons to make the results significant.

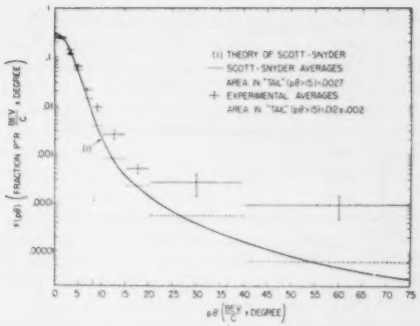

FIG. 4. The differential distribution $F_i(p\theta)$ below 5 cm of lead for *positive* particles observed at 3.4-km altitude with $1.0 < p < 4.8$ Bev/c. Approximately 27 percent of the incident positive particles were protons; the rest were mainly mu-mesons.

The scattering distributions for positive (Fig. 4) and negative (Fig. 3) particles differ in the following manner. In the first place, the area under the scattering distribution for $p\theta > 15$ for positive particles is 2.0 ± 0.7 times that for the negative particles. This fact alone might indicate only a fluctuation in the number of electrons. However, one should note that the distribution for negative particles agrees with the sea-level distributions everywhere except for $p\theta > 15$, whereas the distribution for positive particles deviates for values below $p\theta = 15$ as well as for larger values, as should be the case if protons were included. The deviation for values of $p\theta < 15$ nearly disappears when one makes a correction for the fact that the scattering distribution for protons included in Fig. 4 should be plotted as a function of $p\beta\theta$ instead of $p\theta$, since β for many of the protons included is considerably less than unity.

Using the data already presented in a previous publication,[13] one finds that 590 ± 60 protons[29] were incident on the apparatus accompanied in the same time interval by 1589 ± 40 positive and 1392 ± 37 negative particles, which penetrated the 5-cm lead plate. These particles were mainly mu-mesons except for a few electrons, as noted above. This information is included in Table I, where N_p stands for the number of protons; $N_\mu{}^+$, positive mu-mesons; $N_\mu{}^-$, negative mu-mesons.

The total experimental scattering distribution $F_i(p\theta)$ for positive particles can be expressed as the sum of several individual distributions:

$$F_i(p\theta) = n_\mu{}^+ F_{ei}(p\theta) + n_p(1-w)F_{ei}{}'(p\theta) + n_p w \int_{-\infty}^{+\infty} F_p(p\theta')F_{ei}{}'[p(\theta-\theta')]d(p\theta'), \quad (1)$$

[27] B. Rossi, Revs. Modern Phys. **20**, 537 (1948).
[28] M. Sands, Phys. Rev. **77**, 180 (1950).

[29] This number is about 10 percent less than the number calculated from the data of reference 13 because, of those particles whose momenta could be measured, 10 percent fell too near the edges of the scattering plate to provide reliable scattering data.

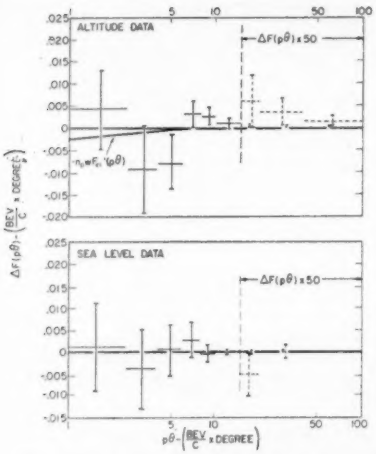

FIG. 5. The differential distribution of the difference $\Delta F(p\theta)$ between the total experimental scattering distribution for positive particles and that for negative particles. It is shown in the text that $\Delta F(p\theta)$ for $p\theta>10$ represents the nuclear scattering of protons. The data obtained at 3.4-km altitude show evidence for nuclear scattering, whereas the data obtained at sea level for mu-mesons do not.

where

$$\int_{-\infty}^{+\infty} F_t(p\theta)d(p\theta)=1, \quad n_\mu{}^+=N_\mu{}^+/(N_\mu{}^++N_p),$$

$$n_p=N_p/(N_\mu{}^++N_p).$$

$F_{el}(p\theta)$ is the differential electric scattering distribution of mu-mesons where β is essentially unity, $F_{el}'(p\theta)$ is the electrical scattering distribution of protons and depends on β, because many of the protons included are relatively slow, w is the fraction of the N_p protons which suffers nuclear scattering with a distribution given by $F_p(p\theta)$. w and $F_p(p\theta)$ are to be determined. Since the momentum distribution of protons is given,[13] one can determine the distribution $F_{el}'(p\theta)$ from the distribution $F_{el}(p\theta)$ by transforming from the variable $p\theta$ to $p\beta\theta$ and remembering that $F_{el}(p\beta\theta)$ is a universal function in all electrical scattering theories. In order to eliminate the effect of electrons from the results, the *experimental* distribution for negative particles (Fig. 3) has been used for $F_{el}(p\theta)$. The last term in the integral Eq. (1) gives the distribution of nuclear scattering modified by the ever-present scattering due to electrical interaction. It will be shown that the distribution of nuclear scattering in the laboratory frame of reference is much broader than the distribution for electrical scattering. Therefore, one can write

$$\int_{-\infty}^{+\infty} F_p(p\theta')F_{el}'[p(\theta-\theta')]d(p\theta')$$

$$\approx F_p(p\theta)\int_{-\infty}^{+\infty} F_{el}'[p(\theta-\theta')]d(p\theta')=F_p(p\theta),$$

since

$$\int_{-\infty}^{+\infty} F_{el}'[p(\theta-\theta')]d(p\theta')=1.$$

With this simplification one obtains from (1)

$$F_t(p\theta)-[n_\mu{}^+F_{el}(p\theta)+n_pF_{el}'(p\theta)]$$

$$=n_pw[F_p(p\theta)-F_{el}'(p\theta)]=\Delta F(p\theta). \quad (2)$$

Therefore, the difference between the total differential scattering distribution $F_t(p\theta)$ and the electrical scattering distribution $[n_\mu{}^+F_{el}(p\theta)+n_pF_{el}'(p\theta)]$ represented as $\Delta F(p\theta)$ does not give directly the nuclear scattering distribution for protons, but is decreased by the electrical scattering of the fractional n_pw protons that were scattered by nuclear interactions. However, the electrical scattering distribution decreases rapidly as $p\theta$ increases. For a sufficiently large value of $p\theta$ (10 for the present experiment) $F_{el}'(p\theta)$ can be neglected compared to $F_p(p\theta)$. For larger values of $p\theta$, $\Delta F(p\theta)$ gives the nuclear scattering directly. It should be mentioned that elastic diffraction scattering of protons is completely negligible for $p\theta>10$ for two reasons. In the first place, a computation has shown that this type of scattering decreases to a very small fraction of its maximum when $p\theta>6$. Furthermore, the cross section for this scattering, even for small angles, should be very small compared to electrical scattering because the nucleus is presumably not completely opaque (see discussion below).

Figure 5 gives the experimental values of $\Delta F(p\theta)$ for the data obtained at sea level and 3.4-km altitude. Since protons formed less than one percent of the penetrating component with $p>1.0$ Bev/c at sea level, one would expect that here $\Delta F(p\theta)$ should be identically zero for all values of $p\theta$. The data of Fig. 5 seem to be consistent with this view for the data obtained at sea level, except for statistical fluctuations. In particular, for $20<p\theta<40$, $\Delta F(p\theta)$ is identically zero and for $p\theta>40$ no particles of either sign of charge were observed. On the other hand, $\Delta F(p\theta)$ obtained at 3.4-km altitude has small but finite positive values for $10<p<80$. For the smaller values of $p\theta$ the effect of the electrical scattering of the mu-mesons and protons becomes very important and obscures the effect of nuclear scattering of the protons since the absolute error becomes relatively much larger. Also shown in Fig. 5 is the electrical distribution $-n_pwF_{el}'(p\theta)$ for protons. As pointed out above, for $p\theta>10$ the electrical scattering is negligible compared to the observed scattering.

The final net nuclear scattering is obtained by subtracting $\Delta F(p\theta)$ obtained at sea level from $\Delta F(p\theta)$ obtained at 3.4-km altitude. Subtracting the values obtained at sea level will tend to eliminate any instrumental errors. The resulting values have statistical significance only for $p\theta > 10$. An extrapolation must be made to account for the scattering between $p\theta = 0$ and $p\theta = 10$. Two extrapolations were performed assuming for the scattering in the center-of-mass system an isotropic distribution and a $\cos^2\theta$ distribution, respectively. Each extrapolation was joined to the experimental value at $p\theta = 10$, where $\Delta F(p\theta)$ represents the true nuclear scattering. For the isotropic distribution the total area under the curve corresponds to the nuclear scattering of 25 ± 12 out of $N_p = 590 \pm 60$ protons. For the $\cos^2\theta$ distribution, the area corresponds to 30 ± 15 out of 590 ± 60 protons. One sees that the precise nature of the scattering distribution is relatively unimportant with the present experimental error, since these two very different distributions yield similar results. We will assume that the average of these, 28 ± 14, is the best estimate of the number of protons which scatter by nuclear interaction in 5 cm of lead. The mean free path for nuclear scattering can be calculated in the usual manner from these data. In 5 cm of lead (57 g/cm^2), 590 ± 60 protons yield 28 ± 14 scattered protons. The mean free path for nuclear scattering in lead is $57 \times (590 \pm 60)/28 \pm 14 = 1200 \pm 600$ g/cm^2. Since the geometrical cross section σ_g for lead nuclei corresponds to 160 g/cm^2, we see that our scattering results imply a cross section for nuclear scattering of $\sigma_s = (0.13 \pm 0.07)\sigma_g$.

A fractional error in N_p produces a larger fractional error in σ_s which is not only inversely proportional to N_p but also depends on ΔF which itself depends sensitively on N_p (Eq. (2)). As an example, if N_p were actually 40 percent smaller than indicated by the present experiment,[13] one would obtain $\sigma_s = 0.31\sigma_g$. However, such a large error in N_p, which would be 4 times the statistical error given, appears to be quite unlikely.

VI. OTHER NUCLEAR INTERACTIONS OF PROTONS

In Sec. V we have derived from the data obtained at 3.4-km altitude a cross section for nuclear scattering. By examining the data for other evidence of nuclear interactions we can obtain a total interaction cross section. Nuclear stars have been classified by the symbols $N = 0$, $N = 1$, and $N \geqq 2$, referring to the lower limit of the number of densely ionizing prongs observed below the lead. 5-cm lead plate, since others may be absorbed in the lead. Protons with $p > 1.0$ Bev/c could only be stopped ($N = 0$) by some nuclear interaction in the 5-cm plate, but the class of events with $N = 0$ could include electrons stopped by multiplication in the lead plate. However, if many more positive than negative particles stop, the excess should be attributed to protons since there must be equal numbers of positive and negative electrons. At 3.4-km altitude in the momentum interval 1–4.8 Bev/c, 17 positive particles stopped in 5 cm of lead, whereas only 3 negative particles did likewise. This indicates that approximately $17 - 3 = 14$ particles were not electrons and hence should be designated as protons. On the other hand, at sea level 5 positive and 4 negative particles with $1.0 < p < 3.1$ Bev/c stopped in the 5-cm lead plate. There was no indication in this for the presence of protons.

Using the above classification, we have included the available information in Table I. Also included in parentheses are the corresponding data for the 1-cm lead plate. In some instances, the 1-cm plate could not supply the data. For instance, the measuring errors were so large that no scattering data were obtained. Also, it was impossible to identify events in which mesons were definitely produced because the criterion for this event was that the produced particles pass through an additional 1-cm plate without deflection or multiplication. This criterion could obviously not be used for the bottom plate.

The data listed in Table I under "Possible meson production" consist of shower events with low multiplicity (2–5), hard to distinguish from electron showers, because they did not satisfy the criterion for meson production listed above. However, these events did have two distinguishing features. First, about one-third of these events gave secondaries which appeared to diverge from a point rather deep in the 5-cm lead block, while ordinary electron showers of 4 or 5 particles appear to diverge from a point very near the surface. Second, all of the incident particles were positive. At sea level, the present experiment gave shower events with similar numbers of positive and negative initiating particles. Therefore, the observed events may well represent the production of mesons by protons.

Before calculating the total interaction cross section, we will compare the data obtained from the 1-cm plate with those from the 5-cm plate. The number 41 ± 7 of events in the 5-cm plate (4th to 6th row, last column, of

TABLE I. Data from 5-cm lead plate used for computing the scattering and total interaction cross sections for protons. Parentheses indicate same data for 1-cm lead plate.

	Momentum range			
	1–1.9 Bev/c	1.9–3.1 Bev/c	3.1–4.8 Bev/c	1–4.8 Bev/c
N_p	378 ± 50	122 ± 25	90 ± 15	590 ± 60
$(N_{\mu^+} + N_p)$	1043	694	442	2179
N_{μ^-}	596	479	317	1392
Stars $N = 0$	11 (0)	3 (0)	0 (0)	14 (0)
Stars $N = 1$	12 (1)	2 (0)	2 (0)	16 (1)
Stars $N \geqq 2$	5 (1)	4 (5)	2 (1)	11 (7)
Definite meson prod.	0	1	2	3
Possible meson prod.	4	4	0	8
Nuclear scattering	18 ± 11	10 ± 8		28 ± 14
Total No. of nuclear interactions				80 ± 16

Table I) can be compared directly with the corresponding number 8 ± 3 for the 1-cm plate if the latter number is increased by a factor of 4/3 to account for the difference in solid angle covered by the two plates. The resulting ratio of similar events becomes $(41\pm7)/(8\pm3)4/3=3.9\pm1.6$. This is somewhat smaller than the ratio of 5.0 for the thicknesses of the two plates, but it is not unreasonable for the small number of events observed. Therefore, this is additional evidence that all events occurring in the 5-cm plate were counted.

The mean free path for the total interaction of protons with $1.0<p<4.8$ Bev/c in lead will now be calculated on the basis of the data given in Table I. When 590 ± 60 protons are incident on 5 cm of lead, 80 ± 16 nuclear, interactions are produced. Calculating the mean free path for total interaction, one finds $(590\pm60)57/(80\pm16)=420\pm95$ g/cm^2. Since the geometrical cross section corresponds to about 160 g/cm^2 of lead, one finds that the above interaction length corresponds to $(0.38\pm0.09)\sigma_g$. This cross section is actually averaged over the momentum range from 1.0 to 4.8 Bev/c. Since a large part of the incident protons have momenta in the range 1.0 to 1.9 Bev/c, it is possible to calculate the cross section for this group alone. Table I gives all the necessary data. One calculates, therefore, a total interaction length of $(378\pm50)57/(50\pm13)=430\pm140$ g/cm^2. This corresponds to $(0.37\pm0.12)\sigma_g$.

VII, NUCLEAR INTERACTIONS OF PROTONS: DISCUSSION AND CONCLUSION

The present experiment has provided a cross section for the nuclear scattering of $(0.13\pm0.07)\sigma_g$ and for the total interaction of $(0.38\pm0.09)\sigma_g$ for protons in lead. The total cross section appears considerably smaller than one would expect on the basis of observed cross sections for neutrons and protons of lower energy. The experiments performed with 85- and 280-Mev neutrons indicate that lead exhibits nearly a geometrical cross section.[30] Presumably protons should interact with a lead nucleus in a similar manner. However, the present experiment deals with a more energetic beam of protons (0.43–3.5 Bev) which may exhibit a different interaction in lead nuclei. Recent experiments have given some information on the interaction of protons in photographic plates. Bernardini *et al.*[31] have performed an experiment in which the interaction of protons of 0.375 Bev was studied. They obtained a total interaction cross section of $(0.56\pm0.11)\sigma_g$. Camerini *et al.*[32] have investigated in photoplates nuclear interactions produced by very energetic cosmic-ray particles. Their results show that protons with energies <1.0 Bev suffer elastic interactions in silver and bromine and that other types of interaction become of comparable importance only for energies >2.0 Bev. Their results do not provide an absolute cross section for total interaction. In view of the results of Bernardini *et al.* and Camerini *et al.* obtained essentially for the interaction of protons with silver and bromine, one would expect that protons should interact with nearly geometrical cross section with a heavier nucleus like lead. Nevertheless, the results of the present experiment indicate a weaker interaction.

Experiments performed on the particles producing penetrating showers have shown that the more energetic particles (energy >10 Bev) interact strongly in matter. Boehmer and Bridge[33] have demonstrated that the neutral particles (presumably neutrons) producing events with the highest multiplicity have a mean free path in carbon of 85 ± 12 g/cm^2 and in lead of 143 ± 30 g/cm^2. Lead and carbon perhaps display a smaller cross section for neutrons of lower energy, but this is not certain because the efficiency of the detector of penetrating showers decreases in a complicated manner as the multiplicity and hence the energy of the incident particle decreases. Froehlich *et al.*[34] have shown that protons of about 10 Bev which produce penetrating showers have a mean free path in lead of about 160 to 190 g/cm^2.

The cross sections obtained in the present experiment indicate a weaker interaction of protons with lead nuclei in the energy range 0.43–3.5 Bev than is observed for protons of smaller and greater energy. The principal source of uncertainty for the result lies in the determination of the number of incident protons. This experiment has been used to determine the proton flux at 3.4-km altitude to an estimated accuracy of 10 percent. Similar measurements of Miller *et al.* gave a flux of protons which at an energy of 0.43 Bev is 25 percent smaller than that deduced from the present experiment. If one were to reduce our proton intensity by 25 percent, the scattering and total interaction cross sections become, respectively, $\sigma_s=(0.27\pm0.09)\sigma_g$, $\sigma_t=(0.60\pm0.08)\sigma_g$. If all the errors were to add in such a manner as to make the largest possible, although not likely, cross section, then $\sigma_t=0.68\sigma_g$. The total interaction cross section would be geometrical if the flux of protons were only 60 percent of that obtained from the present experiment, provided all the errors should add to give the largest possible cross section. Such a low value for the flux would not only be outside the limits of error of the present experiment by a factor of four but would also be considerably smaller than that determined by Miller. Therefore, one concludes that the cross section which protons (0.43–3.5 Bev) exhibit for interaction with lead is less than geometrical and is most probably $(0.38\pm0.09)\sigma_g$ with an upper limit that might be stretched to $0.68\sigma_g$.

[30] Fox, Leith, Wouters, and MacKensie, Phys. Rev. **80**, 23 (1950).
[31] Bernardini, Booth, and Lindenbaum, Phys. Rev. **85**, 826 (1952).
[32] Camerini, Davies, Franzinetti, Lock, Perkins, and Yekutieli, Phil. Mag. **42**, 1261 (1951).
[33] H. W. Boehmer and H. S. Bridge, Phys. Rev. **85**, 863 (1952).
[34] Froehlich, Harth, and Sitte, Phys. Rev. **87**, 504 (1952).

The ratio of the scattering cross section to the total interaction cross section is relatively unaffected by an uncertainty in the proton flux. The best value of this ratio r is $(0.13\pm0.07)/(0.38\pm0.09)=0.34\pm0.19$. If, on the other hand, the proton intensity should be 75 percent of that used in the present calculations, then $r=(0.27\pm0.09)/(0.60\pm0.08)=0.45\pm0.18$.

We have had the benefit of several discussions of mu-meson scattering with Professor B. Rossi, Professor W. Scott, and Mr. S. Olbert. Mr. Olbert kindly provided some of his results prior to publication. Professor Scott has also made available the results of the Snyder and Scott and the Molière scattering calculations in a form directly applicable to the present experiment.

PHYSICAL REVIEW VOLUME 88, NUMBER 6 DECEMBER 15, 1952

The Temperature Dependence of Electrical Resistance

W. V. HOUSTON
Rice Institute, Houston, Texas
(Received August 18, 1952)

The electrical resistance of a simple metal can be computed over a wide range of temperature by considering the thermal vibrations and the scattering from individual ions. Observations by MacDonald and Mendelssohn make possible a comparison with experiment from room temperature down to very low values. Moderate agreement for lithium and sodium can be obtained by a suitable choice of parameters, but the values necessary are not in close agreement with those suggested by other phenomena.

An approximate method for taking into account all three normal modes of vibration with a given propagation vector also gives moderate agreement with the observations.

THE current phase of the theory of electrical conductivity began in 1928 when Sommerfeld applied the Fermi-Dirac statistics to the Lorentz-Drude treatment of the conduction electrons in a metal.[1] It was then soon recognized that the electron scattering, to which electrical resistance is due, is similar in many respects to x-ray scattering. As long as the crystal ions are fixed in their lattice positions the electrons move without any obstructions, but the presence of irregularities due to strains, impurities, or thermal motions, gives rise to a random scattering and to resistance.

With this picture it is obvious why resistance decreases with decreasing temperature, but it was not at first clear why the zero-point motion of the ions does not produce, in all metals, a very large residual resistance. The explanation of this fact was given in 1929, when it was shown that the statistics of the electrons, combined with the conservation of energy in the scattering process, lead to a vanishing probability of scattering as the temperature approaches zero.[2]

The scattering of an electron wave occurs on a sound wave in the crystal. The scattering is subject to three restrictions:

1. There must be conservation of propagation vectors of the incident electron wave, the sound wave, and the scattered electron wave. The propagation vector of the scattered wave must be equal to the sum of the propagation vectors of the incident wave and the sound wave. This is analogous to conservation of momentum.

2. There must be conservation of energy in the scattering process. The sound wave can gain or lose $h\nu$ of energy and the electron must lose or gain the same amount. Since $h\nu$ for the sound wave is small compared with the electron energies, the electron will not have its energy changed very much. It can be scattered from a point near the surface of the Fermi distribution only to another point near the same surface. In particular, at very low temperatures, when the sound vibration in question has its zero-point energy and can lose no more, the electron cannot gain energy at all but can only lose it.

3. The statistical distribution must be taken into account because of the Pauli exclusion principle. At very low temperatures the electron cannot gain energy because the lattice vibration has no energy to lose. The electron can then only be scattered if it can lose energy to the lattice. But at such very low temperatures, the surface of the Fermi distribution is quite sharp. Practically all the states of energy lower than the one from which an electron is to be scattered are occupied. Hence, the electron is practically not scattered at all and the resistance reaches very low values.

The detailed analysis of these three restrictions, the conservation of propagation vector, the conservation of energy, and the Pauli exclusion principle, leads directly to a proportionality of the resistance to the fifth power of the temperature in the limit of very low temperatures.

Thus in the two temperature limits of high temperature and very low temperature, the behavior of electrical resistance of ordinary metals is rather well understood on the basis of general principles. For high enough temperatures the resistance is proportional to the temperature, and for low enough temperatures is proportional to the fifth power of the temperature. The intervening region shows the peculiarities characteristic of the individual metals, and it has long been recognized that no one-parameter curve can describe the resistances of all pure metals.

Until recently there have not been extensive measurements over a wide enough region to permit detailed

[1] A. Sommerfeld, Z. Physik **47**, 1 (1928).
[2] W. V. Houston, Phys. Rev. **34**, 279 (1929).

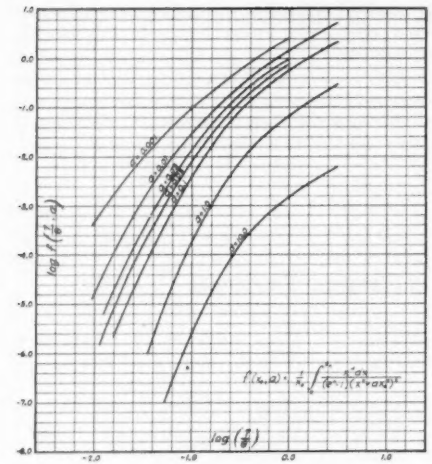

FIG. 1. Plot of $\log f(T/\theta, a)$ for several values of a.

comparison of theory and experiment. However, MacDonald and Mendelssohn[3] at Oxford have published measurements on the alkali metals which permit an extension of the resistance-temperature curve from the high temperature region clear down to the region in which the resistance is proportional to the fifth power of the temperature. It, therefore, becomes possible to make a beginning at interpreting these measurements.

The electron scattering in a metal is proportional to the number of sound waves per unit solid angle in the direction and with the wavelength suitable for a particular scattering process. It is also proportional to the mean square amplitude of the sound waves. But, in addition, the scattering will depend on the nature and extent of the individual ions. For a simple Coulomb field the scattering will follow the Rayleigh scattering law, but since the ion is not isolated, it is more appropriate to use a scattering law which corresponds to a finite ion. Wentzel gave in 1926 the scattering law for a shielded nucleus as[4]

$$S \approx \left(\sin^2\frac{\theta}{2}+\frac{1}{4\pi^2 b^2}\right)^{-2}.$$

If this law of scattering by individual ions is inserted into the theory and appropriate approximations are made, the resistance becomes proportional to the function

$$f(a, x_0)=\frac{1}{x_0}\int_0^{x_0}\frac{x^4 dx}{(e^x-1)(x^2+ax_0^2)^2},$$

where x_0 is taken as θ/T. The use of x_0 as θ/T is, of course, subject to all the well-known uncertainties. The parameter a is proportional to the square of the ratio of the wavelength of the shortest effective sound wave and the effective radius of the scattering ion. Large values of a correspond to small but isotropic scattering. Small values of a correspond to larger scattering but predominantly in forward directions.

When this law of resistance was published in 1929, there were no observations with which it could be compared, and only a general statement of its properties was given. An examination of the integral shows that for large values of a and of x_0 the resistance is inversely proportional to x_0^5 or directly proportional to T^5. For small values of a, however, when x_0 is not too large, the resistance will vary with a lower power of T, and only for extremely low values of T will the fifth-power dependence be reached.

Figure 1 gives the logarithm of f as a function of the logarithm of x_0 for several different values of a. The slopes of all of these curves approach 5 as x_0 becomes large, but for a given value of x_0 the different curves show different slopes. At $x_0=10$, for example, the slope varies from 1.9 for $a=0.001$ to 4.8 with $a=10.0$. Hence, one can understand in this way the principal result of MacDonald and Mendelssohn. It is interesting to note also that the better conductors will correspond to large values of a and will show the T^5 behavior at temperatures even above $\frac{1}{10}$ the Debye temperature.

It is to be expected that the theory would be most applicable to the alkali metals and so some of the observations of MacDonald and Mendelssohn have been plotted together with the theoretical curves. Figure 2 shows the result for sodium. Since both the Debye temperature and the parameter a can be adjusted, the observations do not determine both of them with much accuracy. However, if the Debye temperature is known from other observations, some adjustment of the fit is possible by means of the parameter a.

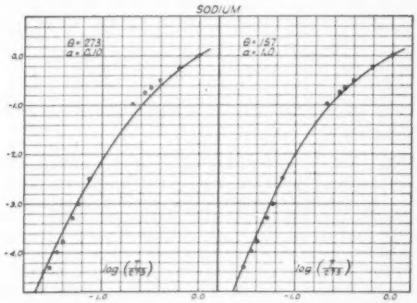

FIG. 2. Comparison of observed resistance in sodium with $f(T/\theta, a)$ for two pairs of values of θ and a.

[3] D. K. C. MacDonald and K. Mendelssohn, Proc. Roy. Soc. (London) A202, 103 (1950).
[4] G. Wentzel, Z. Physik 40, 590 (1926).

Blackman[5] has pointed out that in studying electrical resistance, one should use a Debye temperature based upon the velocity of the longitudinal waves only, since it is only the longitudinal waves that contribute to the electron scattering. If a is taken to be 0.10, a moderate fit can be attained as shown in Fig. 2, when θ is taken to be 273, which is near the temperature computed from the velocity of the longitudinal waves. If, however, the value of θ is taken as 157, more nearly corresponding to the characteristic temperature obtained from specific heat, a better fit is obtained with $a=1.0$.

For lithium a characteristic temperature of 544 represents the longitudinal waves (see Fig. 3). It is moderately satisfactory with $a=0.05$, although a still better fit is obtained with $\theta=238$ and $a=1.00$.

Thus, although it is possible to get a reasonable fit of the theoretical curve and the observed points, it is done only by the arbitrary selection of a characteristic temperature which is justified neither by the elastic constants nor by the specific heat data, and it becomes obvious that one must make a more careful analysis of the spectrum of the elastic vibrations and their effect in scattering electrons. The electron scattering due to very short elastic waves is more important than that due to the longer ones. This is because in the first place there are more of them, and in the second place each of them corresponds to scattering with a greater change in momentum. But on the other hand, the short elastic waves are less accurately described by the simple Debye theory.

Upon close examination of the normal vibrations of a crystal, it becomes evident that while the long wavelength vibrations rather closely follow the pattern of a continuum and can be strictly divided into longitudinal and transverse waves, the same is not true for the short waves near the limit of the spectrum.[6] In these waves, all three normal vibrations tend to have longitudinal components and will correspondingly contribute to the electron scattering. Hence, one might expect that while for low temperatures the resistance could be described entirely in terms of the predominantly longitudinal waves, for somewhat higher temperatures account must be taken of the other waves also.

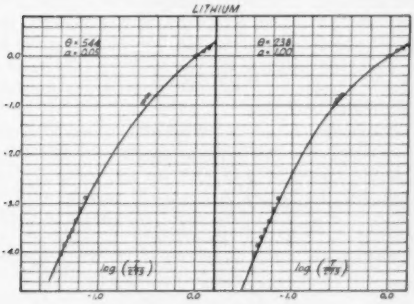

FIG. 3. Comparison of observed resistance in lithium with $f(T/\theta, a)$ for two pairs of values of θ and a.

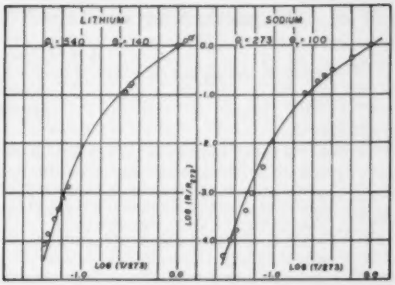

FIG. 4. Comparison of observed resistances in sodium and lithium with calculations based on both "longitudinal" and "transverse" vibrations.

If one makes a very crude approximation by saying that the transverse waves have longitudinal components whose effectiveness is roughly proportional to the square of the frequency and that at the maximum frequency all three normal vibrations participate equally, it is possible to derive simply an expression for the resistance which involves two different Debye temperatures. One may be called the longitudinal Debye temperature, and the other the transverse Debye temperature. Figure 4 shows the curves obtained from this idealization and with the assumption of isotropic scattering by each ion. By the use of appropriate temperatures for lithium and sodium, some approximation to the observed resistance is obtained. A variety of such approximate models can be set up, but a precise explanation of the observations must await a more detailed analysis of the elastic vibrations in particular cases.

[5] M. Blackman, Proc. Phys. Soc. (London) **A64**, 681 (1951).

[6] W. V. Houston, Rice Institute Pamphlet **32**, 123 (1945).

Magnetic Analysis of the $F^{19}(d, p)F^{20}$ and $F^{19}(d, \alpha)O^{17}$ Reactions*

H. A. Watson† and W. W. Buechner
Physics Department and Laboratory for Nuclear Science and Engineering, Massachusetts Institute of Technology, Cambridge, Massachusetts

(Received August 19, 1952)

The energy spectrum of protons from the $F^{19}(d, p)F^{20}$ reaction has been analyzed at 90 degrees to the incident deuteron beam, using an annular magnetic spectrograph with photographic detection. Nineteen proton groups have been observed and identified with this reaction. These correspond to the ground state of F^{20} and eighteen excited states in the range of excitation from 0 to 5.1 Mev. Deuteron bombarding energies ranging from 1.5 to 2.1 Mev were used.

Tracks of alpha-particles, arising from the $F^{19}(d, \alpha)O^{17}$ reaction, were also observed on the photographic plates. Alpha-particle groups corresponding to the ground state and ten excited levels of O^{17} in the range of excitation from 0 to 6.9 Mev were identified. Some of the groups corresponding to O^{17} levels of sufficient excitation to be unstable against neutron decay exhibited a broadening which may result from the natural width of the corresponding O^{17} levels.

I. INTRODUCTION

THE present investigation has been undertaken to measure the excited states of F^{20} using the $F^{19}(d, p)F^{20}$ reaction. The levels of this nucleus are of particular interest since they have been reported[1] to be spaced by integral multiples of 320 kev. Additional information, however, has been obtained about the excited states of O^{17} from observations on the energy spectrum of alpha-particles from the $F^{19}(d, \alpha)O^{17}$ reaction. The O^{17} nucleus and its mirror nucleus F^{17} are one of the few pairs of mirror nuclei whose energy levels are not difficult to observe. It is of particular interest, therefore, that their energy levels should be carefully measured in order that one might compare their energy-level diagrams.

Of the previous investigations of the F^{20} energy levels, the largest number of levels observed thus far are those recently reported by Burrows, Powell, and Rotblat,[2] who used 8.0-Mev cyclotron deuterons and measured the proton ranges in photographic emulsions. The ground-state Q-value was measured to be 4.39 Mev, and excitation energies of 0.63, 0.83, 1.00, 1.37, 2.55, 2.91, 3.49, 4.06, 4.31, and 4.73 Mev with errors of ± 0.05 Mev were reported for the ten excited F^{20} levels.

Other recent measurements have been made by Shull[3] and by Allen and Rall.[4] Shull made a magnetic analysis at 90 degrees of the proton spectrum using 10.3-Mev deuterons and identified proton groups corresponding to seven excited F^{20} states. A ground-state Q-value of 4.55 Mev was measured, and excitation energies of 0.69, 0.98, 2.20, 2.70, 3.12, 3.74, and 4.41 Mev were assigned to the seven excited states. Allen and Rall, using 3.76-Mev deuterons and range measurements, reported eight excited levels in approximately the same range having excitation energies of 0.64, 0.97, 1.31, 1.91, 2.52, 2.83, 3.45, and 4.01 Mev. The ground-state Q-value was measured to be 4.16 Mev. The results of these investigations are tabulated in Table II, together with those obtained in the present investigation.

Burrows, Powell, and Rotblat[2] have also investigated the energy levels of O^{17}. Measurements were made of the range in photographic emulsions of protons from the $O^{16}(d, p)O^{17}$ reaction and of alpha-particles from the $F^{19}(d, \alpha)O^{17}$ reaction. Eleven proton groups arising from the $O^{16}(d, p)O^{17}$ reaction and fourteen alpha-particle groups arising from the $F^{19}(d, \alpha)O^{17}$ reaction were identified. Excitation energies of 0.87, 3.06, 3.85, 4.58, 5.07, 5.31, 5.76, 6.24, 6.89, 7.51, 8.27, 8.59, and 9.06 Mev were calculated for thirteen O^{17} states by averaging the results of the two reactions. The ground-state Q-value for the $F^{19}(d, \alpha)O^{17}$ reaction was measured to be 10.04 ± 0.02 Mev.

Bockelman *et al.*[5] at Wisconsin observed seven resonances in the scattering of neutrons by O^{16}. Using a binding energy of 4.14 Mev for the neutron, these resonances correspond to excitation energies of 4.55, 5.08, 5.38, 5.70, 5.87, 5.94, and 6.37 Mev. The results obtained by Burrows, Powell, and Rotblat and by Bockelman are tabulated in Table III, together with those obtained in the present investigation.

Range measurements on the alpha-particle spectrum from the $F^{19}(d, \alpha)O^{17}$ reaction were also made by French, Meyer, and Treacy,[6] who observed four alpha-particle groups corresponding to excited O^{17} states and calculated their Q-values to be 6.79, 6.03, 5.26, and 2.81 Mev. The ground-state Q-value has previously been measured by this laboratory[7] to be 10.050 ± 0.010 Mev. In addition, French, Meyer, and Treacy also

* This work has been assisted by the joint program of the ONR and AEC.

† Now at the Bell Telephone Laboratories, Murray Hill, New Jersey.

[1] R. C. Allen and W. Rall, Phys. Rev. **78**, 337 (1950).

[2] Burrows, Powell, and Rotblat, Proc. Roy. Soc. (London) **A209**, 478 (1951).

[3] F. B. Shull, Phys. Rev. **83**, 875 (1951).

[4] R. C. Allen and W. Rall, Phys. Rev. **81**, 60 (1951).

[5] Bockelman, Miller, Adair, and Barschall, Phys. Rev. **84**, 69 (1951).

[6] French, Meyer, and Treacy, Proc. Phys. Soc. (London) **A63**, 666 (1950).

[7] Strait, Van Patter, Buechner, and Sperduto, Phys. Rev. **81**, 747 (1951).

observed an alpha-particle group that they identified with the $F^{19}(d,n)Ne^{20*}\rightarrow O^{16}+\alpha$-reaction. An excitation energy of 9.7 Mev was calculated for the Ne^{20} state, which gave rise to the group.

The present investigation with the magnetic spectrograph was undertaken to determine whether earlier investigations had been unable to resolve some of the levels in the regions surveyed and to obtain more accurately the excitation energies. The development of thin nickel-foil backings for targets made it possible to investigate the F^{20} levels up to excitations of about 4.8 Mev, using the magnetic spectrograph. The relatively high ground-state Q-value of the $F^{19}(d,\alpha)O^{17}$ reaction, on the other hand, permitted measurement of the O^{17} levels up to an excitation of 7.5 Mev. Thus, it was possible to check most of the regions covered in the previous investigations.

The measurements on the proton energy spectrum were carried out over a period of about a year starting in July, 1950. When this was completed, a number of additional exposures were taken to survey the alpha-particle spectrum from the (d,α) reaction at bombarding energies of 1.8 and 2.0 Mev. When these exposures were completed and before the data were analyzed, the spectrograph was dismantled and moved to another generator. As will be discussed in a later section, there are indications that appreciable surface contamination may have been present on the targets during these exposures for the alpha-particle groups. The results, however, are reported here since it may be some time before there is an opportunity to repeat this portion of the work.

II. APPARATUS AND EXPERIMENTAL PROCEDURE

The apparatus and experimental procedures used in the investigation are similar to those that have been described in earlier papers.[7-9]

The apparatus consisted essentially of the MIT 2.0-Mev air-insulated electrostatic generator, a deflecting magnet and slit system to define the energy of the deuteron beam, and an annular-magnet spectrograph with which the observations on the spectrum of charged particles leaving the reactions were made. Eastman NTA photographic plates were used to detect the charged particles deflected by the spectrograph. All observations were made at 90 degrees to the incident beam. The fluxmeter for the spectrograph was calibrated through measurements on the deflection of polonium alpha-particles. The energy of the incident beam was determined by measuring the energy of the deuterons scattered elastically by C^{12} and O^{16} nuclei in thin Formvar targets.

Several types of targets were used. In the investigation of proton groups having momenta between 210 and 350 kilogauss-centimeters at 1.8-Mev bombarding energy, thin layers of PbF_2 evaporated onto 10-mil platinum sheets were employed. In the range of $H\rho$ values below 272 kilogauss-centimeters, thin aluminum foils were placed in front of the photographic plates to absorb deuterons scattered elastically by the platinum nuclei in the target backing. These foils were of such a thickness that they would pass the protons at reduced velocity and absorb all the deuterons.

At still lower $H\rho$ values, below 210 kilogauss-centimeters, a thin-target technique was employed. The use of thin nickel foils as target backings has already been described by Bashkin and Goldhaber.[10] A somewhat modified method of using these foils has been found satisfactory for the present investigation.

Nickel foils of thicknesses 1000A and 750A, with attached copper backings, were obtained from the Chromium Corporation of America, Waterbury, Connecticut. In the present investigation, these were fixed to $\frac{3}{4}\times\frac{3}{4}$-inch wire frames with glyptal, the latter being in contact with the nickel rather than the copper. The frame was then mounted vertically in a jig and lowered into a chromic-acid solution which dissolved away the copper. While still wet, it was then successively immersed in several beakers of water to wash away the acid. By using extreme care in raising and lowering the foils in and out of the liquid, it was found that only about 10 percent of them were ruptured by the surface tension of the water, despite their extremely small thickness. Thin layers of BaF_2 were then evaporated onto the foils. Targets made in this manner seemed capable of withstanding almost indefinite bombardment (at least several thousand microcoulombs) at a beam intensity of 0.4 microampere.

In the investigation of the higher energy part of the alpha-particle spectrum, targets of BaF_2 and PbF_2 on platinum backings were used. The BaF_2 targets with thin nickel backings were again used in the study of the region in which elastically scattered deuterons would otherwise have covered the photographic plates.

In calculating the Q-values for the various groups, small corrections were applied, which took into account the following:

(1) A small measured departure of the median angle of observation from 90 degrees.

(2) The effect of the finite angle of acceptance of the spectrograph magnet ($\pm 0.2°$ about the median angle).

(3) The approximation in using the nonrelativistic Q-equation.

The first of these corrections arose from an earlier measurement which indicated that the incident deuteron beam was not quite perpendicular to the planes of the pole faces of the magnetic spectrograph and, hence, that the median angle of observation was not quite 90 degrees.

[8] Buechner, Strait, Stergiopoulos, and Sperduto, Phys. Rev. **74**, 1569 (1948).

[9] Buechner, Strait, Sperduto, and Malm, Phys. Rev. **76**, 1543 (1949).

[10] S. Bashkin and G. Goldhaber, Rev. Sci. Instr. **22**, 112 (1951).

III. RESULTS AND CONCLUSIONS

A. The $F^{19}(d, p)F^{20}$ Reaction

The spectrum of protons observed from the bombardment of fluorine targets with 1.8-Mev deuterons is shown in Figs. 1 and 2 as a function of their momentum in kilogauss-centimeters. In Fig. 1 the group of protons on the right, marked $F^{19}(O)$, results from individual events in which the ground state of F^{20} has been formed. Groups arising from eighteen excited states of the F^{20} nucleus are marked with the numbers 1 through 18. Other groups resulting from reactions with contaminant elements are marked according to the contaminant nuclei. The spectrum was surveyed using several targets so that it was necessary to normalize the yield of the various fluorine groups. This was done by taking exposures on the ground-state group for each target.

The energy of each group has been taken to be that corresponding to the point at one-third height on the high energy side of the peak. Selection of this point has been previously discussed.[8] Each of the fluorine groups was observed at two different bombarding energies. In the case of all except groups (6) and (15), a change in bombarding energy of 0.3 Mev or more was used. For groups (6) and (15), a change of 0.2 Mev was used. Bombarding energies of 1.5, 1.8, 2.0, and 2.1 Mev were used at various times during the investigation.

The two intense groups at $H\rho$ values of 287 and 150 kilogauss-centimeters have been observed in all previous surveys of this energy region and result from the $C^{12}(d, p)C^{13}$ reaction, leading to the formation of the ground state and first excited state, respectively, of C^{13}. Similarly, the two intense groups with $H\rho$ values of 263 and 228 result from the $O^{16}(d, p)O^{17}$ reaction, leading to the formation of the ground state and first excited state of O^{17}.

Identification of the weaker contaminant groups was made through calculation of their Q-values, assuming a given reaction, and comparison with the results previously measured for the same reaction. A list of the Q-values observed for the reactions leading to the weaker contaminant groups, together with those previously measured at this Laboratory for the same reactions, is given in Table I.[7,11–13]

Each contaminant group was also observed at a different bombarding energy to make certain that there was not a weak fluorine group superimposed on it. By changing the bombarding energy, groups resulting from reactions with contaminant elements shift in energy by different amounts than do the fluorine groups, because the residual nucleus in the case of a reaction with a contaminant element is of different mass than that of the F^{20} nucleus and carries away a different proportion of the change in bombarding energy. For an 0.3-Mev

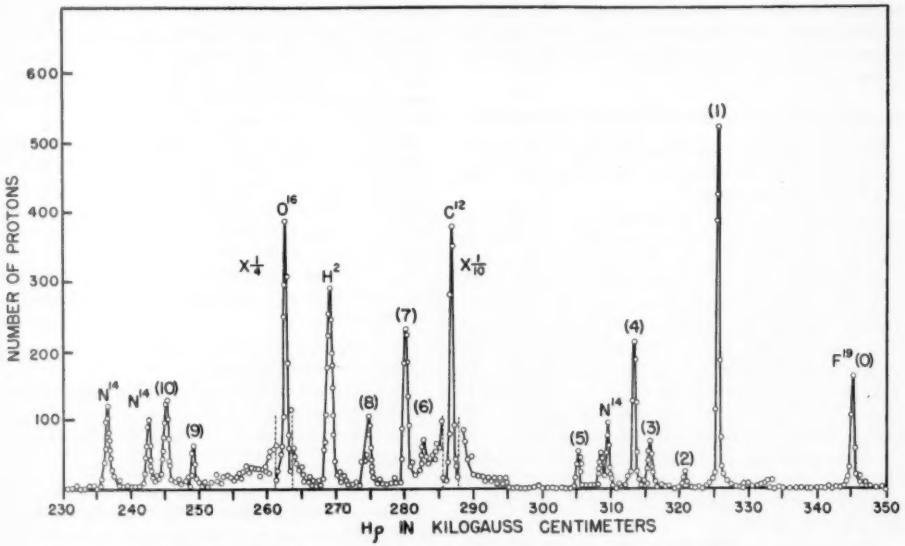

FIG. 1. Spectrum of protons from PbF_2 target bombarded with 1.8-Mev deuterons.

[11] R. Malm and W. W. Buechner, Phys. Rev. 80, 771 (1950).
[12] Laboratory for Nuclear Science and Engineering, Massachusetts Institute of Technology, Progress Report, May 31 (1951) (unpublished). The Q-value for this level, erroneously listed as -0.316 ± 0.006, should be -0.136 ± 0.006.
[13] Sperduto, Holland, Van Patter, and Buechner, Phys. Rev. 80, 769 (1950).

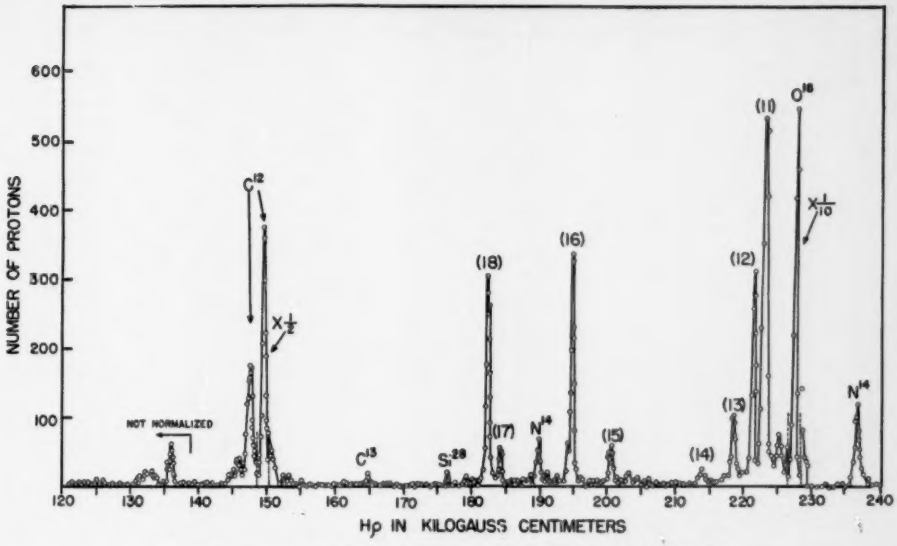

FIG. 2. Spectrum of protons from fluorine targets bombarded with 1.8-Mevdeuterons.

increase in deuteron energy, a Si^{28} group would increase in energy by 12.9 kev more than a F^{19} group, while a N^{14} group would increase 13.5 kev less than the F^{19} group. Since the widths of the fluorine and contaminant groups were usually between 9 and 15 kev, this shift in bombarding energy should have produced a definite structure to the observed group if it were comprised of a superposition of groups from two reactions. No such structure was observed, however.

The proton group at an $H\rho$ value of 226 kilogauss-centimeters in Fig. 2 was not observed when exposures were taken with targets having thin nickel backings. It is concluded therefore that this group definitely does not result from the $F^{19}(d,p)F^{20}$ reaction. It may be related in some manner to the oxygen group at an $H\rho$ of 228 kilogauss-centimeters, since no other contaminant groups are known to exist in this region; the reason for its appearance, however, does not seem easy to explain.

The proton groups with $H\rho$ values 133 and 136 kilogauss-centimeters were first observed on two exposures made with a PbF_2 target having a thin nickel backing. Later, the higher-energy group was again observed on an exposure taken with a BaF_2 target at the same bombarding energy. Several other attempts to observe these groups yielded no tracks at all on the photographic plates. Further efforts to determine the origin of the groups were not pursued, since extremely long exposures were needed, and the proton tracks in this energy region were sufficiently short so that counting was difficult and inaccurate. The group with the lower energy probably results from a reaction with a contaminant element which has accumulated on both sides of the target, since its width is considerably greater than would be expected for a fluorine group. The higher energy group, however, may quite possibly be another fluorine group. Its Q-value has been calculated on this assumption and is tabulated in Table II, along with the Q-values calculated for the other eighteen proton groups.

Also shown in Table II are the F^{20} excitation energies, together with those observed by Burrows *et al.*, by Shull, and by Allen and Rall. The excitation energies measured by these latter observers are listed on the same line as the closest excitation energy measured in the present investigation. In some cases, however, these observers may actually have been observing neighboring levels of greater intensity or were not able to resolve two or more closely spaced levels. The

TABLE I. Q-values of contaminant groups.

Contaminant	Kilogauss cm	Obs. Q-value (Mev)	Previously measured Q-value (Mev)	Reference
N^{14}	310	3.336	3.339±0.005	11
N^{14}	309	3.310	3.310±0.005	11
H^3	270	4.031	4.030±0.006	7
N^{14}	243	1.447	1.451±0.005	11
N^{14}	237	1.309	1.306±0.005	11
N^{14}	191	0.295	0.300±0.005	11
Si^{28}	177	−0.134	−0.136±0.006	12
C^{12}	165	−0.145	−0.148±0.005	13

TABLE II. Q-values and excited states in F^{20} from $F^{19}(d, p)F^{20}$ reaction.

Level	Q-value (Mev)	Excitation	Rel int.	Burrows *et al.*[a] excitation	Shull[b] excitation	Allen and Rall[c] excitation
(0)	4.373±0.007	0	1.0	0 (Q=4.39)	0 (Q=4.55)	0 (Q=4.16)
(1)	3.721±0.006	0.652±0.008	2.3	0.63±0.05	0.69	0.64±0.03
(2)	3.545±0.007	0.828±0.008	0.18	0.83±0.05		
(3)	3.385±0.007	0.988±0.008	0.44	1.00±0.05	0.98	0.97±0.05
(4)	3.314±0.006	1.059±0.008	1.2			
(5)	3.064±0.006	1.309±0.008	0.38	1.37±0.05		1.31±0.05
(6)	2.403±0.005	1.970±0.008	0.25			1.91±0.04
(7)	2.325±0.005	2.048±0.008	2.0			
(8)	2.178±0.005	2.195±0.008	0.85		2.20	
				2.55±0.05		2.52±0.04
(9)	1.503±0.005	2.870±0.008	0.53	2.91±0.05	2.70	2.83±0.04
(10)	1.407±0.005	2.966±0.008	1.2		3.12	
(11)	0.882±0.005	3.491±0.008	4.6	3.49±0.05		3.45±0.03
(12)	0.845±0.004	3.528±0.008	1.3			
(13)	0.787±0.004	3.586±0.008	0.37			
(14)	0.692±0.004	3.681±0.008	0.18		3.74	
(15)	0.412±0.004	3.961±0.009	0.61			
(16)	0.294±0.004	4.079±0.009	3.0	4.06±0.05		4.01±0.15
(17)	0.098±0.004	4.275±0.009	0.50			
(18)	0.063±0.004	4.310±0.009	3.2	4.31±0.05	4.41	
(19)	(−0.689±0.006)	(5.062±0.011)		4.73±0.05		

[a] See reference 2.
[b] See reference 3.
[c] See reference 4.

relative intensities of the proton groups observed at 1.8-Mev bombarding energy are also tabulated. These are probably correct only to within about 30 percent, since a number of targets were used and normalization of the intensities was difficult.

From Table II, it is evident that about six of the excited levels observed in the present investigation have not previously been reported. Some of these are fairly close to other levels, and it might be expected that the corresponding proton groups would not be detected with the lower resolution characteristic of methods used by other observers.

An energy-level diagram for the F^{20} nucleus is shown in Fig. 3. A scale indicating excitation energy in Mev is plotted on the left-hand side, while the measured excitations of the various levels are shown on the right.

Some of the separations between levels show an interesting regularity within the region of excitation investigated. As is shown to the right of the energy-level diagram in Fig. 3, separations having mean values of 0.661, 0.820, 0.989, 1.317, and 1.980 Mev are repeated a number of times. It is interesting to note that multiplying the energy 0.165 Mev by the integers 4, 5, 6, 8, and 12 yields the values 0.660, 0.825, 0.990, 1.320, and 1.980 Mev, respectively, which are in surprisingly good agreement with the observed spacings. It is unfortunate that it was not possible to investigate the levels in the region of higher excitations to see whether the regularity continued. One would hesitate to suggest, however, that the apparent repetition of the spacings between some of the levels and the evident agreement between the repeated spacings and integral multiples of 0.165 Mev is anything more than a coincidence of nature. The 165-kev spacing is approximately one-half the 320-kev spacing reported by Allen and Rall.[1]

B. The $F^{19}(d, \alpha)O^{17}$ Reaction

The spectrum of alpha-particles from thin layers of BaF_2 bombarded with 1.8-Mev deuterons is shown in Fig. 4 as a function of their momentum in kilogauss-centimeters. Here the group marked $F^{19}(O)$ at the right-hand side of the plot results from individual events in which the ground state of O^{17} has been formed. Ten more groups arising from the $F^{19}(d, \alpha)$ reaction are numbered from 1 through 10. Figure 5 shows the track distribution observed on an exposure taken for an additional survey of this spectrum, indicating more clearly that groups (8) and (9) are two separate groups.

A broad distribution of alpha-particles having an upper limit at an $H\rho$ of 351.7 kilogauss-centimeters can be seen in the plot. These particles probably result from the alpha-particle decay of excited Ne^{20} nuclei formed by the $F^{19}(d, n)Ne^{20}$ reaction. Assuming this to be the case, an excitation energy of 11.85 Mev has been calculated for the Ne^{20} state of greatest excitation, giving rise to the distribution. This calculation is based on a ground-state Q-value of 10.72 Mev[14] for the $F^{19}(d, n)$ reaction and a mass-difference equivalent to 4.78 Mev[14] between an O^{16} nucleus plus an alpha-particle and an unexcited Ne^{20} nucleus. It also assumes that the Ne^{20} state does not exhibit a natural width.

At an $H\rho$ of 373 in the plot shown in Fig. 4, a group of particles was observed that were found to be tritons from the $C^{13}(d, t)C^{12}$ reaction. At a given value of $H\rho$, tracks made by tritons are approximately the same

[14] Hornyak, Lauritsen, Morrison, and Fowler, Revs. Modern Phys. **22**, 291 (1950).

length as those made by alpha-particles. A group of tritons may be easily distinguished, however, using a change in bombarding energy.

As has been mentioned, the exposures for the $F^{19}(d,\alpha)O^{17}$ groups were made shortly before the spectrograph was disassembled. While the operation of the apparatus appeared normal during this period, subsequent analysis of the data gave Q-values for the alpha-particle groups from this reaction and from reactions of various contaminants which were consistently lower than those previously measured at this Laboratory.

The Q-values obtained are listed in Table III,[7,15] the values given for each of the contaminant reactions being an average of two results that agreed within 3 kev or less in each case.

While further measurements will be required to determine with certainty the reason for the discrepancy between the present values and those previously obtained, there are definite indications that the present low values were caused by layers of carbon contamination on the targets used. Two photographic plates that were exposed during the present survey were also read for proton tracks from the $C^{12}(d,p)C^{13}$ ground-state reaction. The ground-state Q-value for the $C^{12}(d,p)C^{13}$ reaction has been measured[7] to be 2.716 ± 0.005 Mev. The mean Q-value obtained from these two plates was 2.717 Mev. It seems probable, then, that the lower Q-values measured for the first, second, and fourth reactions listed above resulted from C^{12} contamination which accumulated on the target. The $C^{13}(d,t)C^{12}$ ground-state Q-value may have measured low because the observed triton groups used for the calculations were weak and poorly defined, making it difficult to estimate their energy.

Since the excitation energies as calculated from the observed Q-values are less affected by the presence of contamination than are the Q-values themselves, we have listed in Table IV only the excited states in O^{17} as determined from the present investigation. In calculating the probable error of these excitation energies, an estimate was made of the uncertainty caused by the target contamination. This amounted to 4 kev for the lower excited states and 8 kev for the six highest ones.

Also listed are the mean values obtained by Burrows *et al.*[2] from the $O^{16}(d,p)O^{17}$ and $F^{19}(d,\alpha)O^{17}$ reactions, together with the excitation energies obtained by Bockelman[8] from measurements on the scattering of neutrons by O^{16}. These latter excitation energies are obtained using a value of 4.14 Mev for the neutron binding energy in O^{17}. This binding energy is obtained from the sum of the $O^{16}(d,p)O^{17}$ ground-state Q-value measured at this Laboratory[7] and the binding energy of the deuteron measured by Mobley and Laubenstein.[16]

Because the binding energy of the last neutron of the O^{17} nucleus is only 4.14 Mev, neutron decay is at least energetically possible for most of the O^{17} levels that were observed in the present investigation. If neutron decay did take place from these levels, one might expect the alpha-particle groups involved to show widths greater than those usually observed with the particular experimental arrangement used. In the spectrum shown in Fig. 4, it is evident that group (7) is broader than others of approximately the same energy. Closer examination showed a small but finite broadening of

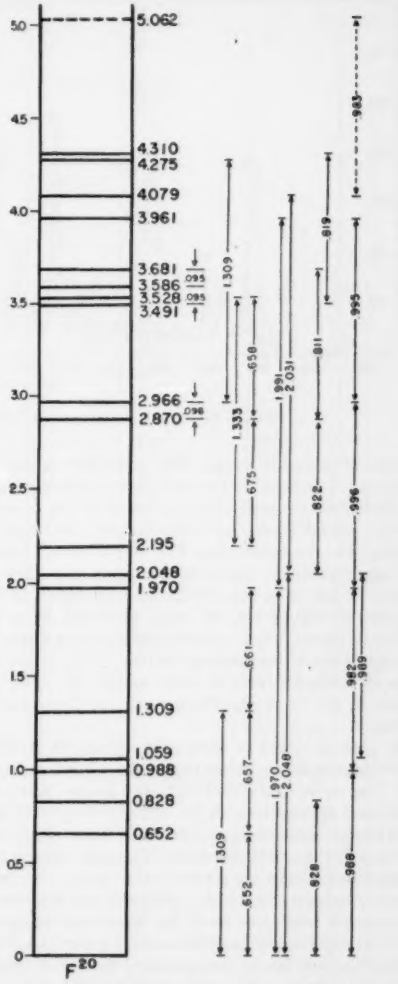

FIG. 3. Energy-level diagram for F^{20}. Excitation energies in Mev.

[15] R. Malm and W. W. Buechner, Phys. Rev. **81**, 519 (1951).
[16] R. C. Mobley and R. A. Laubenstein, Phys. Rev. **80**, 309 (1950).

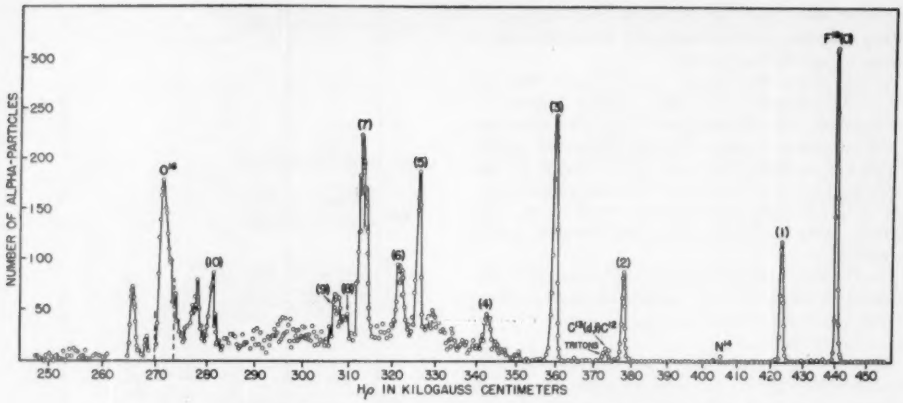

FIG. 4. Spectrum of alpha-particles from BaF_2 target bombarded with 1.8-Mev deuterons.

several of the other groups. The possibility cannot be ruled out, however, that group (7) and possibly some of the others are really superpositions of two or more closely spaced groups of approximately the same intensity. On the assumption that the observed groups are single groups of particles, the quantity V listed in Table IV has been calculated as an indication of the relative widths of the O^{17} levels observed. It is the width in kilovolts that must be added to the spread in energy of the alpha-particles leaving the target in the case of a narrow level in order to give the observed width of the track distributions on the photographic plates.

In general, there is reasonable agreement between the values listed in Table IV for the excited states of O^{17}. The value of 0.883 ± 0.011 Mev for the first level is in good agreement with the value 0.876 ± 0.009 Mev previously measured at this laboratory using the $O^{16}(d, p)O^{17}$ reaction. However, there are several discrepancies between the results of the three experiments listed. The level at 5.1 Mev, which was not observed in the present work, was found by Bockelman to have a width of 100 kev. If the alpha-particle group associated with this level has a corresponding spread in energy, it is probable it would be obscured by the background from the $F^{19}(d, n)Ne^{20*}\rightarrow O^{16}+\alpha$-reaction. Similarly, it is probable that alpha-particles corresponding to the broad level found by Bockelman at 6.37 Mev would also not have been observed. The level reported by Burrows *et al.*, at 6.24 Mev, which was not observed in either the present work or in that of Bockelman, may possibly correspond with this broad level.

The levels listed in Table IV as (11) and (12) are shown in parenthesis, since they were observed at only one bombarding energy. Although no contaminant nuclei are known to give rise to groups in the region of $H\rho$ of 278 and 267 kilogauss-centimeters where the groups corresponding to (11) and (12) were observed, there remains a question as to whether they arise from the $F^{19}(d, \alpha)O^{17}$ reaction. In a survey taken at a bombarding energy of 2.0 Mev, the groups were obscured by elastically scattered deuterons.

It is evident that the relative widths measured in

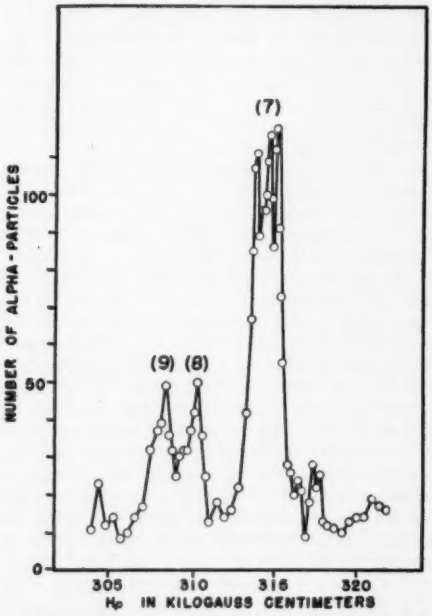

FIG. 5. Track distribution on single exposure showing groups (7), (8), and (9).

the present investigation show little agreement with those obtained for the same levels from the scattering measurements of Bockelman. Group (7), which was the widest observed in the present work, corresponds to an O^{17} level that showed relatively little width in the scattering measurements of Bockelman. It is possible that the $F^{19}(d,\alpha)O^{17}$ reaction is able to excite two or more closely spaced levels in this region that are not excited by neutron scattering. If these levels are sufficiently close, the alpha-particle groups arising from them would be superimposed and give the appearance of a single broad group. It is also interesting to note that level (5), which corresponds to a fairly intense group of alpha-particle tracks in Fig. 4, was not detected by Bockelman.

TABLE III. Comparison of Q-values with previous determinations.

Reaction	Calc Q Mev	Previously measured value at MIT	Reference
$F^{19}(d,\alpha)O^{17}$ ground state	10.028	10.050±0.010	7
$N^{14}(d,\alpha)C^{12}$ first excited state	9.116	9.137±0.006	15
$C^{13}(d,t)C^{12}$ ground state	1.300	1.310±0.006	7
$O^{16}(d,\alpha)N^{14}$ ground state	3.099	3.112±0.006	7

TABLE IV. Excited states in O^{17}. [Present results are from the $F^{19}(d,\alpha)O^{17}$ reaction; Burrows *et al.*, from $O^{16}(d,p)O^{17}$ and $F^{19}(d,\alpha)O^{17}$; Bockelman *et al.*, from neutron scattering from O^{16}.]

Level	Present results: Excitation	Rel int	Γ kev	Burrows *et al.*[a] excitation	Bockelman[b] Excit.	Width in kev
(0)	0 (Q=10.028)	1.0		0		
(1)	0.883±0.011	0.40		0.87±0.02		
(2)	3.069±0.010	0.36		3.06±0.03		
(3)	3.856±0.011	1.3		3.85±0.03		
(4)	4.567±0.014	0.23	22±8	4.58±0.02	4.55	40
				5.07±0.02	5.08	100
(5)	5.229±0.013	0.79	8±6	5.31±0.02		
(6)	5.397±0.014	0.46	15±8		5.38	35
(7)	5.723±0.014	0.87	28±7	5.76±0.02	5.70	≤7
(8)	5.875±0.015	0.16			5.87	≤10
(9)	5.947±0.015	0.31	$3<\Gamma\leq 12$		5.94	30
				6.24±0.02		
					6.37	120
(10)	6.869±0.014	0.39		6.89±0.03		
(11)	(6.986±0.015)	(0.33)	20±11			
(12)	(7.371±0.015)	(0.44)				
				7.51±0.03		
				8.27±0.04		
				8.59±0.04		
				9.06±0.04		

[a] See reference 2.
[b] See reference 5.

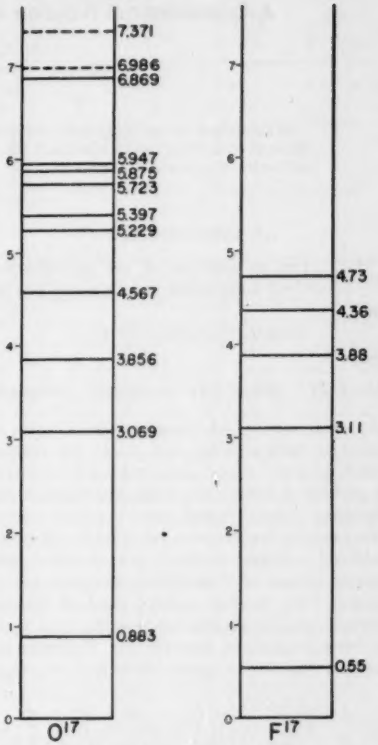

FIG. 6. Energy-level diagram for O^{17} and F^{17}. Excitation energies in Mev.

An energy-level diagram for the O^{17} nucleus, constructed from the results of the present investigation, is given in Fig. 6. On the right-hand side is shown the energy-level diagram for the mirror nucleus F^{17} constructed from the recent measurements of Laubenstein and Laubenstein.[17] Some correspondence seems to be present between the levels of the two nuclei.

It is a pleasure to acknowledge the assistance of the staff of the High Voltage Laboratory. Particular thanks are due Mr. Wilton Tripp, Miss Jane Pann, and Miss Helene Schwartz for reading the photographic plates.

[17] R. A. Laubenstein and M. S. Laubenstein, Phys. Rev. 84, 18 (1951).

A Combinatorial Solution of the Two-Dimensional Ising Model

M. KAC AND J. C. WARD
Institute for Advanced Study, Princeton, New Jersey
(Received June 2, 1952)

An elementary method which yields the partition function of a two-dimensional Ising model is described. The method is purely combinatorial and does not involve any of the algebraic apparatus used in this connection by Onsager and Kaufman.

I. INTRODUCTION

THE partition function of the two-dimensional square net Ising model can be easily put in the form[1]

$$(\cosh H)^h(\cosh H')^v\sum g(l,k)x^l y^k, \tag{1.1}$$

where

$$H=J/kT,\quad H'=J'/kT,\quad x=\tanh H,\quad g=\tanh H',$$

h the total number of horizontal links, v the total number of vertical links, and $g(l,k)$ the number of "closed polygons" with l horizontal and k vertical links. The problem is thus purely combinatorial and consists in counting closed polygons. Since the exact evaluation of the partition function was provided by Onsager[2] and Kaufman,[3] it seemed desirable to understand how the algebraic method of these authors performs the actual counting. This was the starting point of the present investigation. The authors felt that the exact formulas (for finite lattices) of Onsager and Kaufman should provide a clue to the proper method of counting and thus lead to an elementary combinatorial approach to the problem.

In the main body of the paper we shall explain in detail the method of counting which yields the partition function up to negligible terms due to boundary effects. Several combinatorial points will be dealt with a heuristic manner only. We do not go into the details of rigor because our main aim is not so much an alternative derivation of the Onsager-Kaufman formula but a demonstration that a combinatorial approach is indeed possible. Furthermore, the combinatorial approach provides a new insight into the problem and its difficulties. Although this new insight makes the three-dimensional Ising model look even more formidable than before, the authors hope that the method may find other useful application.

II. PRELIMINARIES

The exact formula for the partition function of an $n\times m$ lattice (wound on a torus) was found by Kaufman (see reference 3) to be of the form

$$Z=\frac{1}{2}\frac{(\sinh 2H)^{\frac{1}{2}mn}}{2^{\frac{1}{2}mn}}\left\{\prod_{r=1}^{n}\left(2\cosh\frac{m}{2}\gamma_{2r}\right)+\prod_{r=1}^{n}\left(2\sinh\frac{m}{2}\gamma_{2r}\right)+\prod_{r=1}^{n}\left(2\cosh\frac{m}{2}\gamma_{2r-1}\right)+\prod_{r=1}^{n}\left(2\sinh\frac{m}{2}\gamma_{2r-1}\right)\right\}, \tag{2.1}$$

where

$$\cosh\gamma_j=\cosh 2H^*\cosh 2H'-\sinh 2H^*\sinh 2H'\cos(\pi j/n),$$

or, equivalently,

$$\cosh\gamma_j=\frac{(1+x^2)(1+y^2)}{2x(1-y^2)}-\frac{(1-x^2)}{2x}\frac{2y}{1-y^2}\cos\frac{\pi j}{n}. \tag{2.2}$$

It is apparent that the complexity of formula (2.1) is due to taking boundary effects too seriously. For large lattices one expects the asymptotic formula

$$Z\sim\left(\frac{\sinh 2H}{2}\right)^{\frac{1}{2}mn}\prod_{r=1}^{n}\left(2\cosh\frac{m}{2}\gamma_{2r}\right),$$

which with the aid of the obvious relation,

$$\cosh l\theta=2^{l-1}\prod_{S=0}^{l-1}\left(\cosh\theta-\cos\frac{(2S+1)\pi}{2l}\right),$$

can be written as

$$Z\sim(\sinh 2H)^{\frac{1}{2}n}\prod_{r=1}^{n}\prod_{S=0}^{l-1}\left(\cosh\gamma_{2r}-\cos\frac{(2S+1)\pi}{2l}\right).$$

Here we set $m/2=l$ and assume that m is even. Making use of (2.2) one gets, after a few simple transformations,

$$Z\sim(\cosh H)^h(\cosh H')^v\prod_{r=1}^{n}\prod_{S=0}^{l-1}\left\{(1+x^2)(1+y^2)-2y(1-x^2)\cos\frac{2\pi r}{n}-2x(1-y^2)\cos\frac{(2S+1)\pi}{2l}\right\}.$$

For large lattices one can replace $(2S+1)$ by $2S$ and obtain finally

$$Z\sim(\cosh H)^h(\cosh H')^v\prod_{r=1}^{n}\prod_{S=1}^{\frac{1}{2}m}\left\{(1+x^2)(1+y^2)-2y(1-x^2)\cos\frac{2\pi r}{n}-2x(1-y^2)\frac{2\pi S}{m}\right\}. \tag{2.3}$$

[1] B. L. van der Waerden, Z. Physik **118**, 473 (1941).
[2] L. Onsager, Phys. Rev. **65**, 117 (1944).
[3] B. Kaufman, Phys. Rev. **76**, 1232 (1949).

(It may be pointed out that for a $n\times m$ lattice wound on a torus one has $h=v=mn$.) If one compares (2.3) with (1.1) one sees that, apart from boundary effects, one must have

$$\sum g(l,k)x^l y^k = \prod_{r=1}^{n}\prod_{S=1}^{m}\left\{(1+x^2)(1+y^2) - 2y(1-x^2)\cos\frac{2\pi r}{n} - 2x(1-y^2)\cos\frac{2\pi S}{m}\right\}. \quad (2.4)$$

III. THE PRINCIPLE OF THE METHOD

The way we propose to attack the problem is to construct a suitable determinant[4] with ones (1's) on the main diagonal and x's, y's, and 0's off the main diagonal. The construction would have to be such that to each nonvanishing term in the expansion of the determinant there would correspond a unique closed polygon and vice versa. If the signs of the terms in the expansion of the determinant could all be made positive, the value of the determinant would yield the generating function $\sum g(l,k)x^l y^k$. This approach meets immediately with several difficulties which we find instructive to discuss before writing down the actual determinant. A determinant with ones on the main diagonal,

$$\begin{vmatrix} 1 & A_{12} & A_{13} & \cdots & \cdots & A_{1p} \\ A_{21} & 1 & A_{23} & \cdots & \cdots & A_{2p} \\ A_{31} & A_{32} & 1 & A_{34} & \cdots & A_{3p} \\ \cdot & \cdot & \cdot & \cdot & \cdot & \cdot \\ \cdot & \cdot & \cdot & \cdot & \cdot & \cdot \\ A_{p1} & A_{p2} & \cdot & \cdot & \cdot & 1 \end{vmatrix},$$

can be expanded as follows:

$$\sum \pm (A_{i_1 i_2} A_{i_2 i_3}\cdots A_{i_{s(1)} i_1})(A_{j_1 j_2}\cdots A_{j_{s(1)} j_1})\cdots(A_{l_1 l_2}\cdots A_{l_{s(\nu)} l_1}). \quad (3.1)$$

The permutations of indices involved in these terms are products of cycles, and herein lies our hope of dentifying the terms of the expansion with closed polygons. In brief, we expect to identify closed polygons with cycles or, in case of closed polygons of several components, with products of cycles. We can now state the first difficulty which our approach encounters. If there is to be a one-to-one correspondence between terms in the expansion (3.1) and closed polygons, then terms like $A_{12}A_{23}A_{34}A_{41}$ and $A_{21}A_{14}A_{43}A_{32}$ should correspond to different closed polygons. On the other hand, the cycles involved in both of these terms, namely, (1234) and (2143), are inverses of each other and should be associated with the same polygon. It would thus seem that the determinant will, at best, count oriented polygons, whereas we are interested in the unoriented ones. This difficulty can be resolved by the following trick. Consider an $n\times 2m$ lattice (Fig. 1) and classify all closed polygons (unoriented) on this lattice into those which do and those which do not cut the middle line (dividing the $n\times 2m$ lattice into $2n\times m$ lattices). Disregarding the closed polygons which cut the middle line, we can associate with every other polygon an oriented polygon on the upper lattice by the following rule: The parts of the polygon in the upper lattice (if any) remain there and are oriented clockwise whereas the parts of the polygon in the lower lattice (if any) are replaced by their reflections through the middle line and are oriented counter-clockwise (Fig. 2). On the basis of this rule we can see that the generating function of unoriented closed polygons on the $n\times 2m$ lattice is equal (up to boundary effects due to neglecting figures which cut the middle line) to the generating function of oriented polygons on the $n\times m$ lattice.

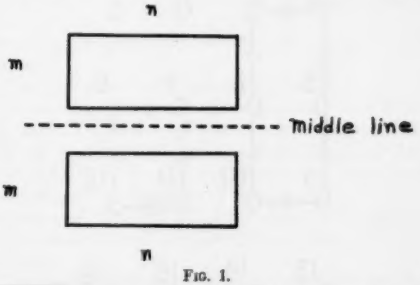

FIG. 1.

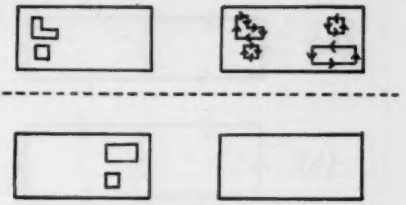

FIG. 2.

Since the partition function for an $n\times 2m$ lattice is (in the limit as n and m become simultaneously infinite) the square of the partition function for an $n\times m$ lattice, we should expect the product,

$$\prod_{r=1}^{n}\prod_{S=1}^{m}\left\{(1+x^2)(1+y^2) - 2y(1-x^2)\cos\frac{2\pi r}{n} - 2x(1-y^2)\cos\frac{2\pi S}{m}\right\}, \quad (3.2)$$

to be the generating function of oriented closed polygons on the $n\times m$ lattice. There is, however, one more difficulty. The oriented polygon [Fig. 3(a)] does not correspond to any unoriented polygon, whereas the

[4] We understand that Mr. Madox of Manchester University, England, has considered a similar idea. However, we are not aware of any publications on this subject.

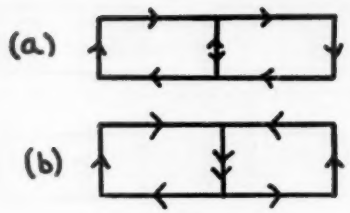

FIG. 3.

oriented polygon [Fig. 3(b)] does. This difficulty seems to spoil the one-to-one correspondence established above, but it can be resolved in the actual construction of the determinant. It will turn out that there will be no terms in the expansion of the determinant corresponding to figures like (b), whereas figures like (a) will be counted in a regular fashion. The fact that it is the "impossible" ones that one counted rather than the "possible" ones is of no consequence since, for counting purposes, the distinction is immaterial.

It should be noted finally that n and m enter symmetrically in (3.2), whereas in the Kaufman-Onsager formula they do not. This fact makes it apparent that the oriented closed polygons are the natural ones with which to deal. This in turn lends support to the naturalness of the determinant method because it is in this way that one is forced into considering oriented polygons.

IV. CONSTRUCTION OF THE DETERMINANT. FURTHER DIFFICULTIES AND THEIR RESOLUTION

We shall illustrate the construction of the determinant by considering a 4×4 lattice. The generalization to arbitrary size is easy and will be left to the reader. The oriented polygon shown in Fig. 4 is described as follows: (1,2)RD(2,6)DD(6,10)DL(10,9)LU(9,5)UU(5,1)UR(7,11)DR(11,12)RU(12,8)UL(8,7)LD. The numbers indicate which neighboring points are connected; the first of the letters R, L, D, U (Right, Left, Down, Up) indicates the direction in which the line joining the points is traversed, and the second letter the subsequent direction of motion. Symbols like (1,3) RD will not enter in describing closed polygons because 1 and 3 are not nearest neighbors. Neither will symbols like (1,2) RL and many others. Symbols like these will be called *improper*.

Let us now define a matrix $A_{(i,j)XY}$ $(i,j=1,2,3,4;$ $XY=\mathrm{R, L, U, D})$ as follows:

$$\begin{aligned}&A_{(i,j)XY}=0 \text{ if } (i,j)XY \text{ is improper;}\\ &A_{(i,j)XY}=x \text{ if } X=\mathrm{R} \text{ or } \mathrm{L} \text{ (and the symbol is proper);}\\ &A_{(i,j)XY}=y \text{ if } X=\mathrm{U} \text{ or } \mathrm{D} \text{ (and the symbol is proper).}\end{aligned} \tag{4.1}$$

On the main diagonal we put ones (1's). The rows and columns are labeled as follows:

R	L	R	L	D
1 2 3 4	1 2 3 4	13 14 15 16	13 14 15 16	1 5 9 13

U	D	U
1 5 9 13	4 8 12 16	4 8 12 16

With x's and y's placed according to (4.1) we see that to each oriented closed polygon there corresponds a term

$$\pm x^l y^k \tag{4.2}$$

in the expansion of the determinant, where l and k denote, respectively, the number of horizontal and vertical lines in the polygon. We must first modify the matrix elements in such a way as to get only positive signs in (4.2). We note that the sign of a cycle of length C is $(-1)^{C-1}$, and since we are dealing with cycles of even length the sign is always negative. If a polygon consists of r components, so that the corresponding permutation is a product of r cycles, the sign will be $(-1)^r$. The modification of matrix elements must be accomplished in such a way as to provide a minus sign for each one-component polygon. This is done by multiplying each x and y by

$$\alpha=e^{\frac{1}{2}i\pi}, \quad \alpha^{-1}=e^{-\frac{1}{2}i\pi}, \quad \text{or} \quad \alpha^0=1,$$

according as the turning which is described by letter indices is through $\frac{1}{2}\pi$ (counter-clockwise), $-\frac{1}{2}\pi$ (clockwise), or 0. Thus, terms with indices RR, LL, UU, DD will remain unaltered, those with indices RU, UL, LD, DR will be multiplied by α, and those with indices RD, DL, LU, UR by α^{-1}. If we now take a closed one-component polygon, the term in the expansion of the modified determinant will be

$$(-1)^{\Omega/2\pi}(-1)x^l y^k,$$

where Ω is the total angle through which one turns in

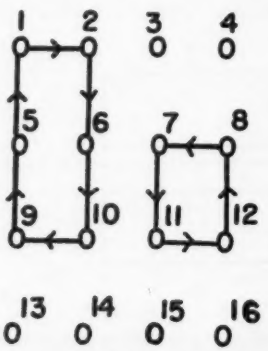

FIG. 4.

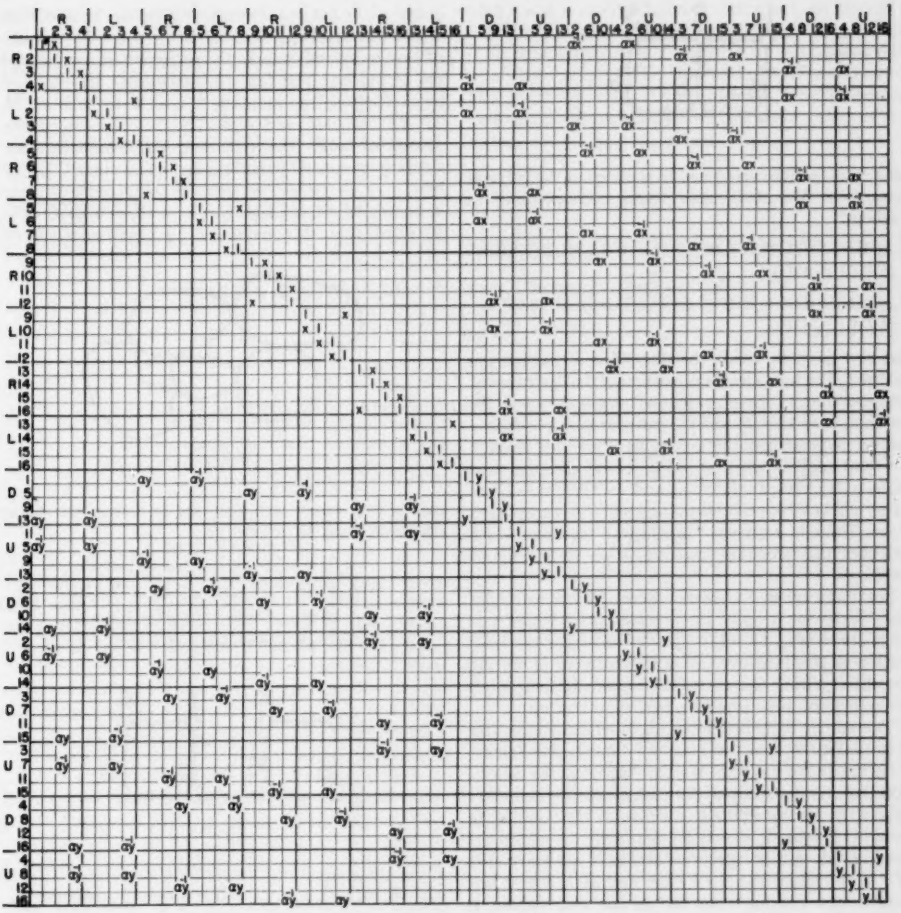

FIG. 5. The determinant for a 4×4 lattice.

describing the polygon. Since $\Omega=\pm 2\pi$, we get $+x^4y^4$ as desired.

The determinant is finally as given in Fig. 5.

Let us first see how the difficulty stated toward the end of Sec. 3 is resolved. Figure 6 is described symbolically as (1,2)RD(2,6)DL(6,5)LU(5,1)UR(2,3)LD(2,6)DR(6,7)RU(7,3)UL. This clearly does not correspond to any term in the expansion of our determinant because elements corresponding to (2,6)DL and (2,6)DR appear in the same row and only one element from each row is allowed.

There is finally one more difficulty, which fortunately resolves itself automatically. This difficulty is the following: There are terms in the expansion of our determinant which do not correspond to closed polygons. Some of these terms are trivial, like those which do not involve elements of the main diagonal or those like (1,2)RR(2,3)RR(3,4)RR(4,1)RR. The presence of these terms depends clearly on our decision to put the lattice on a torus, and hence they correspond to negligible boundary effects.

There are, however, also nontrivial terms. Such a nontrivial term can arise as shown in Fig. 6. Consider the closed polygon in Fig. 7, and note that it is a two-component figure and that hence it gives rise to 4 terms x^4y^4 corresponding to 4 distinct ways in which the two components can be traced out *separately*. But in the expansion of the determinant there will be 4

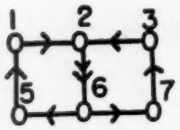

FIG. 6.

other terms which correspond to tracing out the polygon *unicursally*. We shall have terms corresponding to symbols:

(1,2)RD(2,6)DD(6,10)DR(10,11)RU(11,7)UL(7,6)LL (6,5)LU(5,1)UR,

(1,2)RD(2,6)DR(6,7)RD(7,11)DL(11,10)LU(10,6)UL (6,5)LU(5,1)UR,

and two more in which the directions of motion are reversed. The terms in the expansion of the determinant corresponding to these "unicursal" symbols cancel. To see this, note that in tracing out our polygon in the manner indicated by the first symbol we turn through the total angle 0, whereas in the second case the total angle is 2π. Since $(-1)^{0/2\pi}=1$ and $(-1)^{2\pi/2\pi}=-1$, the terms will be of opposite signs and will thus cancel each other. There is a general "topological" theorem which underlies this situation and which we state without proof:

Let there be $n(>1)$ plane closed curves such that each curve has a point in common with at least one other curve (Fig. 8). Then $\sum\epsilon^{\Omega/2\pi}=0$, where the summation is extended over all unicursal ways of tracing out the resulting figure and Ω denotes the total angle through which one turns in a particular tracing.

The reader is invited to check other situations, like that in Fig. 9, and see how the cancellation follows from the above theorem. We thus arrive at the conclusion that our determinant is equal, except for boundary effects, to the generating function of the number of closed polygons. It should be clear that the considerations of this section apply to lattices of arbitrary size. We have chosen the 4×4 case just as a convenient illustration. For an $n\times m$ lattice the determinant is $4mn\times4mn$.

V. THE EVALUATION OF THE DETERMINANT

An examination of the determinant reveals that it has a certain amount of cyclic structure, and consequently it is not too difficult to guess the eigenvectors of the corresponding matrix.[5] Let ϵ and δ be two 4th roots of unity and consider the vector whose components are as follows: The first 32 components are obtained by multiplying the numbers $1, \epsilon, \epsilon^2, \epsilon^3$ by $a, b, a\delta, b\delta, a\delta^2, b\delta^2, a\delta^3, b\delta^3$, and repeating them in consecutive groups of four. The remaining 32 components are similarly obtained by multiplying the numbers $1, \delta, \delta^2, \delta^3$ by $c, d, c\epsilon, d\epsilon, c\epsilon^2, d\epsilon^2, c\epsilon^3, d\epsilon^3$. The components are thus $a, a\epsilon, a\epsilon^2, a\epsilon^3, b\delta, b\delta\epsilon, b\delta\epsilon^2, b\delta\epsilon^3, \cdots, d\epsilon^3, d\epsilon^3\delta, d\epsilon^3\delta^2, d\epsilon^3\delta^3$. In order that this vector be an eigenvector of our

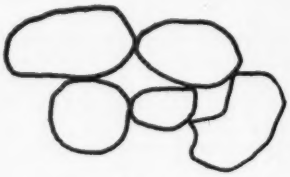

FIG. 8.

matrix it is easily seen that the following four linear equations must be satisfied:

$$\begin{aligned}(1+x\epsilon)a+0b+\alpha^{-1}x\epsilon c+dx\epsilon d&=\lambda a,\\ 0a+(1+x\epsilon^{-1})b+\alpha x\epsilon^{-1}c+\alpha^{-1}x\epsilon^{-1}d&=\lambda b,\\ dy\delta a+\alpha^{-1}y\delta b+(1+y\delta)c+0d&=\lambda c,\\ \alpha^{-1}y\delta^{-1}a+\alpha y\delta^{-1}b+0c+(1+y\delta^{-1})&=\lambda d.\end{aligned}\tag{5.1}$$

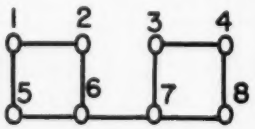

FIG. 9.

From these equations we get four eigenvalues $\lambda_1(\epsilon,\delta)$, $\lambda_2(\epsilon,\delta)$, $\lambda_3(\epsilon,\delta)$, $\lambda_4(\epsilon,\delta)$, and it is seen immediately that

$$\prod_{j=1}^{4}\lambda_j(\epsilon,\delta)=\begin{vmatrix}1+x\epsilon & 0 & \alpha^{-1}x\epsilon & \alpha x\epsilon\\ 0 & 1+x\epsilon^{-1} & \alpha x\epsilon^{-1} & \alpha^{-1}x\epsilon^{-1}\\ \alpha y\delta & \alpha^{-1}y\delta & 1+y\delta & 0\\ \alpha^{-1}y\delta^{-1} & \alpha y\delta^{-1} & 0 & 1+y\delta^{-1}\end{vmatrix}$$

$$=(1+x^2)(1+y^2)-y(1-x^2)(\epsilon+\epsilon^{-1})$$

$$-x(1-y^2)(\delta+\delta^{-1}).$$

The original determinant is the product of all eigen-

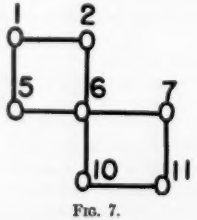

FIG. 7.

[5] After the determinant has been constructed and computed, several of our friends pointed out that a suitable reshuffling of rows and columns will reduce it to a form in which cyclicity is much more evident.

values and is thus equal to

$$\prod_{\epsilon,\delta}\prod_{j=1}^{4}\lambda_j(\epsilon,\delta)=\prod_{\epsilon,\delta}\{(1+x^2)(1+y^2)-y(1-x^2)(\epsilon+\epsilon^{-1})-x(1-y^2)(\delta+\delta^{-1})\},$$

which is precisely (2.4). Needless to say, in the $n\times n$ case ϵ and δ are nth roots of unity but the system of Eqs. (5.1) remains otherwise unchanged.

In conclusion, it is a pleasure to acknowledge the kind hospitality of The Institute for Advanced Study and to thank many of our friends for the healthy pessimism they showed during the early stages of this work.

PHYSICAL REVIEW VOLUME 88, NUMBER 6 DECEMBER 15, 1952

Magnetic Hyperfine Structure in Diatomic Molecules*·†

R. A. Frosch and H. M. Foley
Columbia University, New York, New York

(Received July 29, 1952)

A general theory of the magnetic hyperfine structure in diatomic molecules, including states other than $^1\Sigma$ states, is given. The magnetic hyperfine interaction is derived from the Dirac equation for the electron in the molecular potential field. First-order hyperfine structure formulas are given for the various vector coupling schemes characteristic of molecular states. The $^1\Sigma$ magnetic hyperfine structures are obtained from second order hyperfine interactions. Applications to the $N^{14}O^{16}$ and $O^{16}O^{17}$ microwave spectra are discussed.

1. INTRODUCTION

THE general theory of the nuclear hyperfine structure observed in atomic spectra has been worked and discussed extensively,[1] and even the detailed ...ures of the observed spectra are quite well understood. No such general treatment has apparently been given for diatomic molecules. In the case of diatomic molecules with no resultant electronic spin or orbital angular momentum ($^1\Sigma$), satisfactory phenomenological treatments of the magnetic interaction of the nuclear moment with the electronic currents, in the form of an $\mathbf{I}\cdot\mathbf{J}$ coupling with the molecular angular momentum vector, have been given.[2] Investigation has shown[3] that this effect arises for the most part from the effect in second order of the nondiagonal matrix elements of the nuclear magnetic interaction with the electronic currents. The interaction of the nuclear electric quadrupole moment with the electronic currents in these molecules has also been treated satisfactorily.[4] The development of microwave spectroscopy and molecular beam techniques have made it possible to examine the hyperfine spectra of paramagnetic gas molecules, i.e., molecules in states other than $^1\Sigma$. The present paper is devoted to the general treatment of the hyperfine spectra of diatomic molecules. For molecules with nonzero electronic angular momentum, it may be anticipated that the nuclear moment interaction with the electrons will be of the order of magnitude of atomic magnetic hyperfine couplings, and thus will be very much larger than typical nuclear electric quadrupole couplings. The strength and mode of the vector coupling of the nuclear spin to the various angular momentum vectors in the molecule will therefore be primarily determined by the magnetic interactions, and it will be sufficient in almost all cases to evaluate only the diagonal values of the electric quadrupole interaction, in a vector coupling representation determined by the magnetic interaction. The greater part of the present work will thus deal with the theory of the magnetic interaction of a single nuclear spin with the electronic currents in the various kinds of molecular states.

Typical features of the molecular magnetic hyperfine interactions may be compared with those of atoms. The interaction with electronic spins in the atomic case is treated quite differently in s states ($L=0$) and non-s states.[1] For non-s states, the spin coupling may be written as the interaction of two point magnetic dipoles in the form $3(\mathbf{I}\cdot\mathbf{R})(\mathbf{S}\cdot\mathbf{R})/R^5-(\mathbf{I}\cdot\mathbf{S})/R^3$, where $\mathbf{R}$ is the space vector from nucleus to electron. For s-states, this interaction vanishes (as does the orbital interaction), and the actual hyperfine coupling must be accounted for by a more refined treatment of the magnetic interaction. The most satisfactory method of treating the interaction of the nuclear magnetic moment with the electronic currents is via the Dirac equation for the

* Publication assisted by the Ernest Kempton Adams Fund for Physical Research of Columbia University.
† Assisted in part by the ONR.

[1] E. Fermi, Z. Physik **60**, 320 (1930); G. Breit and F. W. Doermann, Phys. Rev. **36**, 1732 (1930); H. B. G. Casimir, *On the Interaction Between Atomic Nuclei and Electrons* (Teyler's Tweede Genootschap, Haarlem, 1936); E. Fermi and E. Segrè, Z. Physik **82**, 729 (1933).

[2] Kellogg, Rabi, Ramsey, and Zacharias, Phys. Rev. **57**, 677 (1940); H. Zeiger and D. I. Bolef, Phys. Rev. **85**, 788 (1952); D. I. Bolef and H. J. Zeiger, Phys. Rev. **85**, 799 (1952).

[3] H. M. Foley, Phys. Rev. **72**, 504 (1947); G. C. Wick, Phys. Rev. **73**, 51 (1948).

[4] J. Bardeen and C. H. Townes, Phys. Rev. **73**, 97 (1948).

electron.[1] Advantage may be taken of the spherical symmetry of the potential field in which the electron moves to reduce the interaction for s-states to the form

$$W_{\text{hfs}}=(16/3)\pi g_I\mu_0\mu_N\psi_r^2(0)\mathbf{I}\cdot\mathbf{S}, \tag{1.1}$$

where $\psi_r^2(0)$ is the electron density at the origin (position of the nucleus).

In the case of the diatomic molecule the potential field possesses only axial symmetry and no classification of states according to a total angular momentum quantum number can be made. Thus, there can be no separation of the hyperfine interaction into characteristic s- and non-s forms. Nevertheless, effects similar to the atomic s-state interaction are found. In particular, a $^2\Sigma$ or $^3\Sigma$ molecular state with total rotational angular momentum zero shows a nonvanishing hyperfine structure.

For molecules, there is also the complicating feature of the introduction, in addition to the electronic l and s, of a third vector, the molecular rotational angular momentum. This brings about the well-known molecular coupling states (Hund's case a and case b),[5] and makes possible a number of different nuclear spin couplings. These possible couplings will be treated in detail in later sections.

2. THE MAGNETIC INTERACTION OF NUCLEAR MOMENT AND ELECTRONS

The general form of the interaction of the nuclear magnetic moment with a single electron has been given by Breit and Doermann.[1] Their Hamiltonian was derived by reducing the Dirac equation for the electron in the field of the nucleus from four component form to the approximately correct two component Pauli form. The hyperfine perturbation was obtained from the latter equation. Due to normalization difficulties, their result contains a non-Hermitian term which must be arbitrarily excluded.

We will derive the Pauli equation in a form suitable for our purposes by applying a series of unitary transformations to the Dirac Hamiltonian. This procedure, an extension of the method of Foldy and Wouthuysen,[6] avoids the normalization difficulty. A treatment of this problem using the Dirac equation with explicit consideration of normalization has recently been given by Karnaugh.[7]

We write the Dirac Hamiltonian in the conventional form

$$H_0=\beta mc^2-eV+c\boldsymbol{\alpha}\cdot(\mathbf{p}-(e/c)\mathbf{A}). \tag{2.1}$$

We apply to this Hamiltonian three successive unitary transformations of the form

$$H_i=e^{iS_i}H_{i-1}e^{-iS_i}, \tag{2.2}$$

where, if $\mathcal{E}=-\nabla V$,

$$S_1=-ic\beta\boldsymbol{\alpha}\cdot\{\mathbf{p}-(e/c)\mathbf{A}\}/2(mc^2-eV),$$

$$S_2=\frac{-ic\beta}{2(mc^2-eV)}\left[\frac{-eVc}{(mc^2-eV)}\boldsymbol{\alpha}\cdot\left(\mathbf{p}-\frac{e}{c}\mathbf{A}\right)-\frac{ie\beta c}{2(mc^2-eV)}\boldsymbol{\alpha}\cdot\boldsymbol{\mathcal{E}}\right],$$

$$S_3=\frac{-ic\beta}{2(mc^2-eV)}\left\{\frac{e^2V^2c^2}{mc^2-eV}\boldsymbol{\alpha}\cdot\left(\mathbf{p}-\frac{e}{c}\mathbf{A}\right)+\frac{ie^2V\beta c^2}{2(mc^2-eV)}\boldsymbol{\alpha}\cdot\boldsymbol{\mathcal{E}}+\frac{\text{const}\,c^3}{(mc^2-eV)^2}\boldsymbol{\alpha}\cdot\left(\mathbf{p}-\frac{e}{c}\mathbf{A}\right)\times[\sigma\cdot(p-e/cA)]^2\right\}\varphi=0. \tag{2.3}$$

We are left finally with

$$H_3=\beta mc^2-eV+\frac{\beta c^2}{2mc^2}\left[\boldsymbol{\sigma}\cdot\left(\mathbf{p}-\frac{e}{c}\mathbf{A}\right)\right]^2+\frac{iec^2}{8(mc^2-eV)^2}\left[\boldsymbol{\sigma}\cdot\left(\mathbf{p}-\frac{e}{c}\mathbf{A}\right),\boldsymbol{\sigma}\cdot\boldsymbol{\mathcal{E}}\right] \tag{2.4}$$

+terms of order $1/(mc^2)^3$ and higher. In the above, $[A, B]$ denotes $[AB-BA]$. This Hamiltonian yields the Pauli equation as

$$\left\{E+eV-\frac{1}{2m}\left[\boldsymbol{\sigma}\cdot\left(\mathbf{p}+\frac{e}{c}\mathbf{A}\right)\right]^2+\frac{c^2e\hbar}{8i(mc^2+eV)^2}\left[\boldsymbol{\sigma}\cdot\left(\mathbf{p}+\frac{e}{c}\mathbf{A}\right),\boldsymbol{\sigma}\cdot\boldsymbol{\mathcal{E}}\right]\right\}\varphi=0, \tag{2.5}$$

taking the electron charge to be $-e$. In the third term, the divergent denominator has been set equal to $2mc^2$. A term proportional to μ_N^2 has been neglected. The hyperfine part of (2.5) may be written in terms of the electronic orbital angular momentum L' as

$$\frac{e\hbar}{2mc}\frac{2\boldsymbol{\mu}\cdot\mathbf{L}'}{r_1^3}+\frac{2i\mu_0}{\hbar}\mathbf{S}\cdot[\mathbf{p}\times\mathbf{A}]+\frac{2e^2\hbar}{4m^2c^3}\mathbf{S}\cdot[\boldsymbol{\mathcal{E}}'\times\mathbf{A}], \tag{2.6}$$

in which $S=\sigma/2$, and we have set $E+mc^2+eV=2mc^2$ in the denominator of the first two terms. In the case of an atom, Eq. (2.6) becomes

$$\frac{2g_I\mu_0\mu_N}{r^3}\left\{\left[\mathbf{I}\cdot\mathbf{L}+\frac{3(\mathbf{I}\cdot\mathbf{r})(\mathbf{S}\cdot\mathbf{r})}{r^2}-\mathbf{I}\cdot\mathbf{S}\right]+\frac{2mc^2e^2\mathcal{E}_r}{[E+eV+mc^2]^2}\left[-\frac{(\mathbf{I}\cdot\mathbf{r})(\mathbf{S}\cdot\mathbf{r})}{r^2}+\mathbf{I}\cdot\mathbf{S}\right]\right\}. \tag{2.7}$$

The first term gives the hyperfine levels for non-s states and is zero for s-states. The second term may be

[1] G. Herzberg, *Molecular Spectra and Molecular Structure: I. Spectra of Diatomic Molecules* (D. Van Nostrand Company, Inc., New York, 1950), p. 218.

[6] L. L. Foldy and S. A. Wouthuysen, Phys. Rev. 78, 29 (1950).

[7] M. Karnaugh, dissertation, Yale University (1952) (unpublished).

written, after a partial integration, as (1.1). This term is proportional to the charge density at the nucleus, and is nonzero for s-states only.

Expression (2.6) will be the basis for our treatment of the hyperfine spectra of molecules. In the remainder of the paper we will write

$$2mc^2e^2\mathcal{S}_r/[E+eV+mc^2]^2=\delta(r), \qquad (2.8)$$

since the terms with this coefficient (except for neglected relativistic corrections, significant only for heavy nuclei) give appreciable contributions only from the region near the nucleus.

3. MOLECULAR QUANTIZATION

The rigorous theory of the quantum states of diatomic molecules, and in particular the approximate nature of the separation of rotation, vibration, and electronic motion have been discussed by Van Vleck and Kronig.[8] In a first-order theory of molecular hyperfine structure, it is necessary only to know the particular vector coupling representation of the electronic spin and the orbital and rotational angular momenta. The most important of these representations are Hund's case a, in which the spin is strongly coupled to the internuclear axis by the spin orbit interaction, and Hund's case b, in which the spin is decoupled by "gyroscopic" terms in the kinetic energy, and the spin vector is added to the total angular momentum of the molecule. Which of these vector coupling schemes most nearly describes any molecular state depends on the relative magnitudes of the spin orbit coupling and the gyroscopic term (proportional to $\hbar^2/2I$). In both of these cases, the component of electronic angular momentum parallel to the internuclear axis is a good quantum number Λ, and the separation of levels corresponding to different values of Λ is characteristically much greater than the level splittings due to rotation, spin orbit coupling, Λ doubling, or hyperfine structure. In this paper we shall be concerned for the most part with hyperfine and other interactions which are diagonal in Λ. Higher order effects due to matrix elements of the various interactions which are nondiagonal in Λ we consider in Sec. 7.

4. THE MAGNETIC HYPERFINE INTERACTION IN A MOLECULAR COORDINATE SYSTEM

The coordinate system for the molecule consists in the first place of a rectangular coordinate system XYZ fixed in the laboratory and with the center of mass of the molecule at the origin. The orientation of the internuclear axis in this frame is given by the polar and azimuthal angles θ and ψ with respect to the Z axis. The positions of the electrons are described in a rectangular coordinate system $x'y'z'$, fixed in the molecule, with z' along the internuclear axis and x' constrained to remain in the XY plane. In the usual treatment of the molecular problem,[8] an approximate separation of the Hamiltonian into electronic, vibrational, and rotational terms is made, and the wave function is the product of three corresponding factors:

$$\Psi=\psi_e(x', y', z')\psi_V(R)\psi_R(\theta, \psi). \qquad (4.1)$$

(The electron spin may be quantized in the laboratory or in the internal coordinate system according to Hund's case b or case a, respectively.)

We shall express the magnetic hyperfine interaction [expression (2.6)] in the internal coordinate system, replacing $x'y'z'$ by cylindrical coordinates $\rho'\varphi z'$ where $x'=\rho'\cos\varphi$ and $y'=\rho'\sin\varphi$. It is clear that the φ dependence of the electronic wave function is of the form

$$e^{\pm i\Lambda\varphi}/(2\pi)^{\frac{1}{2}}. \qquad (4.2)$$

(The effect of the degeneracy in $\pm\Lambda$ is described in Sec. 6.) To obtain the matrix elements of (2.6) diagonal in Λ we shall first average over φ.‡

In the first term of (2.6): $(2e/2mc)\boldsymbol{\mu}_N\cdot(\mathbf{r}_1\times\mathbf{p})/r_1^3$, $\mathbf{r}_1$ is the vector from the nucleus to the interacting electron. It is convenient to express this in terms of the orbital angular momentum about the center of mass. From Fig. 1, we note that $\mathbf{r}_1=\mathbf{r}-\tau\mathbf{k}'$, where τ is the distance from the center of mass to the nucleus with spin; and $\mathbf{k}'$ is a unit vector in the z' direction. This first term becomes

$$\frac{2g_I\mu_0\mu_N}{r_1^3}\mathbf{I}\cdot\mathbf{L}-\frac{e}{2mc}2\boldsymbol{\mu}\cdot[\tau\mathbf{k}'\times\mathbf{p}], \qquad (4.3)$$

where $\mathbf{L}\hbar=\mathbf{r}\times\mathbf{p}$ and $\mu_0=e\hbar/2mc$.

The second term of (4.3) has no matrix elements diagonal in Λ.

The second term of expression (2.6) may be expanded, and the only terms which do not vanish on averaging

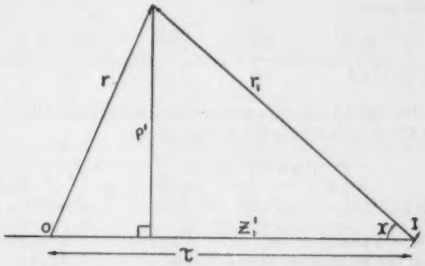

FIG. 1. Coordinates of the electron in the molecular frame of reference. The nucleus is located at I and the center of mass of the molecule at 0.

[8] R. de L. Kronig, *Band Spectra and Molecular Structure* (Cambridge University Press, Cambridge, 1930); J. H. Van Vleck, Phys. Rev. 33, 467 (1929).

‡ Throughout the paper the term "matrix elements" will frequently be used for operators which have been averaged over the electronic coordinates, but remain operators with respect to the spin and rotational coordinates.

over φ are

$$-\frac{\boldsymbol{\mu}\cdot\mathbf{S}}{r_1'^3}+\mu_{x'}S_{x'}\frac{3x'^2}{r_1'^5}+\mu_{y'}S_{y'}\frac{3y'^2}{r_1'^5}+\mu_{z'}S_{z'}\frac{3z_1'^2}{r_1'^5}. \quad (4.4)$$

The third term of expression (2.6) contains the factor $\mathbf{S}\cdot\boldsymbol{\mathcal{E}}'\times\mathbf{A}$, which may be written as

$$\mathbf{S}\cdot\left[\boldsymbol{\mathcal{E}}'\times\frac{\boldsymbol{\mu}\times\mathbf{r}_1}{r_1'^3}\right]=\frac{\boldsymbol{\mathcal{E}}'\cdot\mathbf{r}_1}{r_1'^3}\boldsymbol{\mu}\cdot\mathbf{S}+\boldsymbol{\mathcal{E}}'\cdot\boldsymbol{\mu}\frac{\mathbf{S}\cdot\mathbf{r}_1}{r_1'^3}. \quad (4.5)$$

The expansion of Eq. (4.5) in cylindrical coordinates and the integration over φ yields

$$[\boldsymbol{\mathcal{E}}'\times\mathbf{A}]\cdot\mathbf{S}=\frac{\mathcal{E}_{\rho'}'\rho'+\mathcal{E}_{z'}'z'}{r_1'^3}\boldsymbol{\mu}\cdot\mathbf{S}$$
$$-\frac{\mathcal{E}_{\rho'}'\rho'}{2r_1'^3}(\mu_{x'}S_{x'}+\mu_{y'}S_{y'})-\frac{\mathcal{E}_{z'}'z_1'}{r_1'^3}\mu_{z'}S_{z'}, \quad (4.6)$$

where $\mathcal{E}_{\rho'}$ and $\mathcal{E}_{z'}$ are the ρ' and z' components of the electric field produced by all charges except the interacting electron.

We now collect the terms of expressions (4.3), (4.4), and (4.6), and form the complete expression for the effective magnetic hyperfine operator for all matrix elements diagonal in Λ. We designate the angle between the molecular axis and the vector $\mathbf{r}_1'$ from the nucleus to the electron by $\chi=\tan^{-1}\rho'/z_1'$ (see Fig. 1), and write $\mathcal{E}'=e\mathcal{E}$. We obtain the operator in the form

$$aI_{z'}L_{z'}+b\mathbf{I}\cdot\mathbf{S}+cI_{z'}S_{z'}, \quad (4.7)$$

where

$$a=2g_I\mu_0\mu_N(1/r_1'^3)_{\text{av}},$$
$$b=2g_I\mu_0\mu_N\left[\frac{e^2 2mc^2}{[E+eV+mc^2]^2}\frac{\mathcal{E}_{\rho'}\rho'/2+\mathcal{E}_{z'}z_1}{r_1'^3}\right.$$
$$\left.-\frac{3\cos^2\chi-1}{2r_1'^3}\right]_{\text{av}}, \quad (4.8)$$
$$c=2g_I\mu_0\mu_N\left[\frac{e^2 2mc^2}{[E+eV+mc^2]^2}\frac{\mathcal{E}_{\rho'}\rho'/2-\mathcal{E}_{z'}z_1}{r_1'^3}\right.$$
$$\left.+\frac{3}{2}\frac{3\cos^2\chi-1}{r_1'^3}\right]_{\text{av}},$$

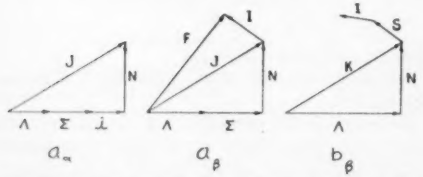

FIG. 2. The three molecular coupling states including nuclear spin. The various coupling possibilities for case b are discussed in Sec. 5 and appear in Fig. 3.

with the signs as indicated (μ_0 positive). This expression (4.7) may be employed to discuss all features of the hyperfine spectra in both Hund's case a and case b arising from matrix elements diagonal in Λ. The quantities in brackets $[\ ]_{\text{av}}$ are to be averaged over the electronic space coordinates for the particular states. The first term of b or c yields a nonvanishing contribution only in regions closer to the nucleus than the classical radius of the electron, $e^2/2mc^2$. In this region the nonvanishing component of the electron wave function is spherically symmetric (within our approximation). If we write $\mathcal{E}_{\rho'}\rho'=\mathcal{E}_r r_1\sin^2\chi$ and $\mathcal{E}_{z'}z_1'=\mathcal{E}_r r_1\cos^2\chi$, upon performing the average (assuming spherical symmetry) we obtain

$$b=2g_I\mu_0\mu_N\left[\frac{2}{3}\frac{\delta(r_1)}{r_1^2}-\frac{3\cos^2\chi-1}{2r_1^3}\right]_{\text{av}},$$
$$c=3g_I\mu_0\mu_N\left[\frac{3\cos^2\chi-1}{r_1^3}\right]_{\text{av}}. \quad (4.9)$$

The term in b with coefficient $\delta(r_1)$ arises because of the quasi-relativistic treatment leading to expression (2.6), and represents the departure of the actual hyperfine coupling from that expected from the interaction of two-point dipoles. If the electronic charge distribution were exactly spherical, the term $3\cos^2\chi-1$ would vanish and the term referred to above would give the whole hyperfine structure. In this case Eq. (4.7) reduces to the Fermi formula for s-states, Eq. (1.1). On the other hand, if this "s-term" interaction was absent we should have $3b+c=0$. Thus, the value of $3b+c$ from any observed spectrum is an indication of the presence of some spherical charge density bearing a free spin near the nucleus.

If more than one electron contributes to the total orbital or spin angular momentum, the hyperfine interaction operator has the form of expression (4.7), but the coefficient [Eq. (4.9)] contains a term from each interacting electron.

5. COUPLINGS AND MATRIX ELEMENTS

We consider now the vector coupling possibilities of a single nuclear spin to the various angular momenta of the molecule. In principle, representations can occur in which the nuclear spin is quantized either in the laboratory coordinate system or in the internal coordinate system of the molecule. Now a coupling of the nuclear moment to the internuclear axis will come about through the magnetic interaction with the electronic orbital angular momentum (and with the electron spin in Hund's case a). This interaction is the analog of the coupling of the electron spin to the molecular axis which leads to Hund's case a, but is about 1000 times smaller in magnitude since the magnetic moment of the nucleus is much smaller than that of the electron. The "gyroscopic" terms which act to decouple the spin from the axis are of the same order of magnitude for molecular

and electronic spins since they depend on the spins rather than the magnetic moments of the particles. We may distinguish the following important cases of vector coupling as (a) case a_α: Hund's case a with the nuclear spin space quantized with respect to the internuclear axis. (This includes the case where $S=0$); (b) case a_β: Hund's case a with the nuclear spin space quantized in the laboratory frame. (This includes the case where $S=0$); (c) case b_β: Hund's case b with the nuclear spin space quantized in the laboratory frame. The vector coupling possibilities are shown in Fig. 2. The several possible coupling schemes for case b are discussed later in this section.

Actually, because of the weak magnetic coupling of the nuclear spin to the molecular axis, case a_α is expected to be of extremely rare occurrence, and in the interests of brevity will not be considered here.[9]

Case a

The magnetic hyperfine operator (4.7) may be written as

$$aI_{z'}L_{z'}+b(I_{x'}S_{x'}+I_{y'}S_{y'})+(b+c)I_{z'}S_{z'}. \quad (5.1)$$

The second term has only nonzero matrix elements which are off-diagonal in Ω, and hence, in a molecule which is in a good case a state, the effects of this term will be very small and are neglected here. For a discussion of this term in cases intermediate between Hund's case a and case b and in $^1\Sigma$ states, see Sec. 7. Thus, the part of expression (5.1) diagonal in Λ becomes

$$[a\Lambda+(b+c)\Sigma]I_{z'}=d\mathbf{I}\cdot\mathbf{k}', \quad (5.2)$$

where $d=a\Lambda+(b+c)\Sigma$, and $\mathbf{k}'$ is the unit coordinate vector along the molecular axis. The magnetic hyperfine structure problem in case a_β is thus reduced to the calculation of the diagonal value of Eq. (5.2) in a representation in which the electronic wave function is that designated as Hund's case a, and the nuclear spin is quantized in the fixed laboratory system. To express this result, we require the matrix elements of the components of the unit coordinate vector $\mathbf{k}'$ in the fixed system. In Appendix I are given such matrix elements for the vectors of the internal molecular coordinate system. We write the matrix of (5.2) first in the "decoupled" representation in which JIm_Jm_I are good quantum numbers. Expansion of the scalar product and reference to Appendix I yield for the matrix elements diagonal in J

$$d\frac{\Omega}{J(J+1)}\mathbf{I}\cdot\mathbf{J}. \quad (5.3)$$

It should be pointed out that the coefficient of the I, J coupling varies with J. We may make use of the addition formulas of Condon and Shortley[10] to obtain the matrix elements in the weak field $IJFm_F$ representation:

$$(JIFm_F|\mathbf{I}\cdot\mathbf{k}'|JIFm_F)=\Omega\frac{F(F+1)-J(J+1)-I(I+1)}{2J(J+1)},$$

$$(IJFm_F|\mathbf{I}\cdot\mathbf{k}'|IJ-1Fm_F) \quad (5.4)$$
$$=\pm\frac{1}{2}\frac{(J^2-\Omega^2)^{\frac{1}{2}}}{J(4J^2-1)^{\frac{1}{2}}}[(F+J-I)(F+I-J+1)\times(F+I+J+1)(J+I-F)]^{\frac{1}{2}}.$$

The $J\rightarrow J+1$ matrix element follows from the Hermitian property of the matrix. It is expected that the effects of matrix elements nondiagonal in J will be small (inasmuch as the rotational energy is very much greater than the hyperfine structure) and may be taken into account as a second order perturbation.

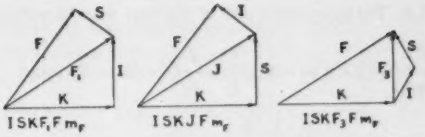

FIG. 3. The three simple coupling cases in case b_β. The "good" quantum numbers are indicated in each case.

Case b_β

Here both I and S are space quantized in the laboratory coordinate system. We may write expression (5.1) as

$$a\Lambda(\mathbf{I}\cdot\mathbf{k}')+b(\mathbf{I}\cdot\mathbf{S})+c(\mathbf{I}\cdot\mathbf{k}')(\mathbf{S}\cdot\mathbf{k}'). \quad (5.5)$$

In a completely "decoupled" representation (good quantum numbers are $ISKm_Im_Sm_K$) the matrix elements of $\mathbf{I}\cdot\mathbf{k}'$, $\mathbf{S}\cdot\mathbf{k}'$, $\mathbf{I}\cdot\mathbf{S}$ may be evaluated directly from Appendix I, and the last term calculated by matrix multiplication. The zero field problem is rather complicated, however, inasmuch as it involves the coupling of the three vectors I, K, S. The simplest possibilities are (see also Fig. 3)

$$K+I=F_1, \quad K+S=J, \quad I+S=F_3,$$
$$F_1+S=F, \quad J+I=F, \quad F_3+K=F.$$

We shall refer to these three representations as the F_1, J, and F_3 representations, respectively. The good quantum numbers are indicated in Fig. 3 for each case.

The part of the Hamiltonian of the system which must be discussed in the determination of the appropriate representation for this case includes the hyperfine couplings of expression (5.5) and the electron spin orbit interaction contained in the third term of Eq.

[9] R. A. Frosch, dissertation, Columbia University (1952) (unpublished).

[10] E. U. Condon and G. H. Shortley, *Theory of Atomic Spectra* (Cambridge University Press, Cambridge, 1951), pp. 69, 71.

(2.5). The appropriate part of this term may be written

$$\frac{e^2h}{4m^2c^2}\sigma\cdot[\mathcal{E}\times\mathbf{p}]=-2i\mu_0^2\Big\{\mathcal{E}_{x'}\frac{\partial}{\partial z'}(S_{x'}\sin\varphi-S_{y'}\cos\varphi)$$

$$+\mathcal{E}_{x'}\Big[-\frac{1}{\rho'}\frac{\partial}{\partial\varphi}(S_{x'}\cos\varphi+S_{y'}\sin\varphi)$$

$$+\frac{\partial}{\partial\rho'}(-S_{x'}\sin\varphi+S_{y'}\cos\varphi)\Big]+S_{x'}\frac{\mathcal{E}_{\rho'}}{\rho'}\frac{\partial}{\partial\varphi}\Big\}, \quad (5.6)$$

where $S=\sigma/2$. Only the last term of (5.6) yields matrix elements diagonal in Λ. In case b, S is quantized in the laboratory frame, and it is appropriate to write the part of (5.6) diagonal in Λ as

$$2\mu_0^2\Lambda\left(\frac{\mathcal{E}_{\rho'}}{\rho'}\right)_{kl}\mathbf{S}\cdot\mathbf{k}'=2\mu_0^2\left(\frac{\mathcal{E}_{\rho'}}{\rho'}\right)_{kl}\Lambda^2\frac{\mathbf{S}\cdot\mathbf{K}}{K(K+1)}, \quad (5.7)$$

for the term diagonal in K. Thus the electron spin orbit interaction represents a coupling of S to K. For states with $\Lambda\neq0$, expression (5.7) will in general be much larger than the hyperfine coupling term (5.5), and thus the J representation will be approximately correct. For Σ states, however, (5.7) vanishes, and the remaining effects of the spin orbit coupling are obtained from the second-order effects of the matrix elements of (5.6) between Σ and Π states. This coupling of S to K, known as ρ doubling for $^2\Sigma$ states,[8] may be shown to be of the form

$$\text{const }\mu_0B\frac{(\Sigma|L_\perp|\Pi)}{h\nu_{\Sigma\Pi}}[K(K+1)]^{\frac{1}{2}}S_\perp$$

$$+\text{const }\mu_0^2(S_\perp)^2, \quad (5.8)$$

where $S_\perp$ is the appropriate one of $S_{x'}\pm iS_{y'}$, and similarly for $L_\perp$. The first term of (5.8) becomes finally constant $\mathbf{S}\cdot\mathbf{K}$. The second term may be written as constant $(S^2-(\mathbf{S}\cdot\mathbf{k}')^2)$ and is a somewhat complicated coupling of S to K, as is seen from the discussion of expression (7.8) in Sec. 7. These couplings are of much smaller magnitude than (5.7) and are possibly of the same magnitude as the hyperfine interaction. A similar formula obtains for $^2\Sigma$ states.[11]

Although the hyperfine level pattern can in principle be obtained from any of the three representations F_1, J, F_2 by writing out the complete matrix of the hyperfine interaction (5.5) and the spin orbit coupling (5.6) in this representation and solving the secular determinant directly, it is usually much more convenient to choose a representation in which the diagonal values of (5.5) and (5.6) are large compared to off-diagonal elements. In this case the energy levels may be obtained by second order perturbation theory.

Hyperfine Matrix Elements in Case b_β

We give here the complete matrix elements (diagonal in Λ) of the operators $\mathbf{I}\cdot\mathbf{k}'$, $\mathbf{I}\cdot\mathbf{S}$, $\mathbf{S}\cdot\mathbf{k}'$, from which the hyperfine energy levels may be calculated by matrix multiplication according to (5.5), for the following cases:

(a) F_2 representation: $\mathbf{I}\cdot\mathbf{S}$, $\mathbf{I}\cdot\mathbf{k}'$, $\mathbf{S}\cdot\mathbf{k}'$, for all I, S, K,
(b) J representation: $\mathbf{I}\cdot\mathbf{S}$, $\mathbf{I}\cdot\mathbf{k}'$, for all I, S, K; and $\mathbf{S}\cdot\mathbf{k}'$, for $S=\frac{1}{2}$, 1 and all I, K,
(c) F_1 representation: $\mathbf{I}\cdot\mathbf{S}$, $\mathbf{S}\cdot\mathbf{k}'$, for all I, S, K; and $\mathbf{I}\cdot\mathbf{k}'$, for $I=\frac{1}{2}$, 1 and all S, K.

Diagonal values of $\mathbf{S}\cdot\mathbf{k}'$ in the J representation and of $\mathbf{I}\cdot\mathbf{k}'$ (for all S and I, respectively) may be written down directly from the vector model. We have made use of the results of Racah,[12] Condon and Shortley,[10] and Bardeen and Townes[4] in calculating these matrix elematrix elements. Details of the method are given in the dissertation of Frosch.[9] The actual formulas for the energy levels and spectral line frequencies in these representations are rather complicated, and it has not appeared worth while to work out the complete formulas, which may be obtained from the matrix elements below. One example is worked out in Sec. 10. The notation $(|A/B|)$ refers to the element of A or of B. When a double sign appears either the upper or the lower sign is to be taken throughout. Unlisted matrix elements are either zero or follow directly from the Hermitian properties of the matrices in the usual manner. We note, first of all, that in all representations

$$(K\vdots\mathbf{k}'\vdots K)=\Lambda/K(K+1),$$
$$(K\vdots\mathbf{k}'\vdots K-1)=(K^2-\Lambda^2)^{\frac{1}{2}}/K(4K^2-1)^{\frac{1}{2}}, \quad (5.9)$$
$$(IS\vdots\mathbf{I}/\mathbf{S}\vdots IS)=(KS\vdots\mathbf{I}/\mathbf{S}\vdots KS)=(KI\vdots\mathbf{I}/\mathbf{S}\vdots KI)=1.$$

Now

$$(KF_2F|\mathbf{I}\cdot\mathbf{S}|KF_2F)$$
$$=\tfrac{1}{2}[F_2(F_2+1)-I(I+1)-S(S+1)]. \quad (5.10)$$

We note

$$(SIF_2\vdots\mathbf{I}\vdots SIF_2)=\frac{F_2(F_2+1)-S(S+1)+I(I+1)}{2F_2(F_2+1)},$$
$$(SIF_2\vdots\mathbf{I}\vdots SIF_2-1)=\pm\frac{[(F_2-S+I)(F_2+S+I+1)(S+I-F_2+1)(F_2+S-I)]^{\frac{1}{2}}}{2F_2[(2F_2-1)(2F_2+1)]^{\frac{1}{2}}}. \quad (5.11)$$

[11] M. H. Hebb, Phys. Rev. **49**, 610 (1936).
[12] G. Racah, Phys. Rev. **61**, 186 (1942); **62**, 438 (1942); **63**, 237, 368 (Eq. 4) (1943).

The similar quantities for S are obtained by interchanging I and S and inverting the double sign. Then,

$$\begin{aligned}
&(F_3KF|\mathbf{I}\cdot\mathbf{k}'/\mathbf{S}\cdot\mathbf{k}'|F_3KF)=\tfrac{1}{2}(K|\mathbf{k}'|K)(F_3|\mathbf{I}/\mathbf{S}|F_3)\{F(F+1)-F_3(F_3+1)-K(K+1)\},\\
&(F_3KF|\mathbf{I}\cdot\mathbf{k}'/\mathbf{S}\cdot\mathbf{k}'|F_3K-1F)=\pm\tfrac{1}{2}(K|\mathbf{k}'|K-1)(F_3|\mathbf{I}/\mathbf{S}|F_3)\\
&\qquad\times[(F+K-F_3)(F+F_3-K+1)(F+F_3+K+1)(F_3+K-F)]^{\frac{1}{2}},\\
&(F_3KF|\mathbf{I}\cdot\mathbf{k}'/\mathbf{S}\cdot\mathbf{k}'|F_3-1KF)=\mp\tfrac{1}{2}(K|\mathbf{k}'|K)(F_3|\mathbf{I}/\mathbf{S}|F_3-1)\\
&\qquad\times[(F+F_3-K)(F+K-F_3+1)(F+F_3+K+1)(F_3+K-F)]^{\frac{1}{2}},\\
&(F_3KF|\mathbf{I}\cdot\mathbf{k}'/\mathbf{S}\cdot\mathbf{k}'|F_3-1K-1F)=-\tfrac{1}{2}(K|\mathbf{k}'|K-1)(F_3|\mathbf{I}/\mathbf{S}|F_3-1)\\
&\qquad\times[(F_3+K+F+1)(F_3+K+F)(F_3+K-F)(F_3+K-F-1)]^{\frac{1}{2}},\\
&(F_3KF|\mathbf{I}\cdot\mathbf{k}'/\mathbf{S}\cdot\mathbf{k}'|F_3+1K-1F)=\tfrac{1}{2}(K|\mathbf{k}'|K-1)(F_3|\mathbf{I}/\mathbf{S}|F_3+1)\\
&\qquad\times[(F+K-F_3-1)(F+K-F_3)(F+F_3-K+1)(F+F_3-K+2)]^{\frac{1}{2}},
\end{aligned}\tag{5.12}$$

In the J representation,

$$\begin{aligned}
&(JIF|\mathbf{I}\cdot\mathbf{S}|JIF)=\tfrac{1}{2}(I|\mathbf{I}|I)(J|\mathbf{S}|J)\{F(F+1)-J(J+1)-I(I+1)\},\\
&(JIF|\mathbf{I}\cdot\mathbf{S}|J-1IF)=\mp\tfrac{1}{2}(I|\mathbf{I}|I)(J|\mathbf{S}|J-1)[(F+J-I)(F+I-J+1)(F+J+I+1)(J+I-F)]^{\frac{1}{2}},
\end{aligned}\tag{5.13}$$

where

$$(KSJ|\mathbf{S}|KSJ)=(KS|\mathbf{S}|KS)\frac{J(J+1)-K(K+1)+S(S+1)}{2J(J+1)},$$

$$(KSJ|\mathbf{S}|KSJ-1)=\mp(KS|\mathbf{S}|KS)\cdot\frac{[(J-K+S)(J+K+S+1)(K+S-J+1)(J+K-S)]^{\frac{1}{2}}}{2J[(2J+1)(2J-1)]^{\frac{1}{2}}},\tag{5.14}$$

Now,

$$\begin{aligned}
&(JIF|\mathbf{I}\cdot\mathbf{k}'|JIF)=\tfrac{1}{2}(J|\mathbf{k}'|J)\{F(F+1)-J(J+1)-I(I+1)\},\\
&(JIF|\mathbf{I}\cdot\mathbf{k}'|J-1IF)=\pm\tfrac{1}{2}(J|\mathbf{k}'|J-1)[(F+J-I)(F+I-J+1)(F+I+J+1)(J+I-F)]^{\frac{1}{2}},
\end{aligned}\tag{5.15}$$

where

$$\begin{aligned}
&(KJ|\mathbf{k}'|KJ)=(K|\mathbf{k}'|K)\frac{J(J+1)-S(S+1)+K(K+1)}{2J(J+1)},\\
&(KJ|\mathbf{k}'|K-1J)=\pm(K|\mathbf{k}'|K-1)\frac{[(J-S+K)(J+S+K+1)(S+K-J)(J+S-K+1)]^{\frac{1}{2}}}{2J(J+1)},\\
&(KJ|\mathbf{k}'|KJ-1)=\mp(K|\mathbf{k}'|K)\frac{[(J-S+K)(J+S+K+1)(S+K-J+1)(J+S-K)]^{\frac{1}{2}}}{2J[(2J+1)(2J-1)]^{\frac{1}{2}}},\\
&(KJ|\mathbf{k}'|K-1J-1)=(K|\mathbf{k}'|K-1)\frac{[(J-S+K)(J+S+K+1)(J-S+K-1)(J+S+K)]^{\frac{1}{2}}}{2J[(2J+1)(2J-1)]^{\frac{1}{2}}},\\
&(KJ|\mathbf{k}'|K-1J+1)=-(K|\mathbf{k}'|K-1)\frac{[(S+K-J)(J+S-K+1)(S+K-J-1)(J+S-K+2)]^{\frac{1}{2}}}{2(J+1)[(2J+1)(2J+3)]^{\frac{1}{2}}}.
\end{aligned}\tag{5.16}$$

For $S=\frac{1}{2}$,

$$\begin{aligned}
&(KJ=K-\tfrac{1}{2}|\mathbf{S}\cdot\mathbf{k}'|K-1J=K-\tfrac{1}{2})\\
&\qquad=\pm(K^2-\Lambda^2)^{\frac{1}{2}}/2K,
\end{aligned}\tag{5.17}$$

and for $S=1$,

$$\begin{aligned}
&(KJ=K|\mathbf{S}\cdot\mathbf{k}'|K-1J=K)\\
&\qquad=\pm\frac{(K^2-\Lambda^2)^{\frac{1}{2}}}{K(2K+1)^{\frac{1}{2}}}(K+1)^{\frac{1}{2}},\\
&(KJ=K-1|\mathbf{S}\cdot\mathbf{k}'|K-1J=K-1)\\
&\qquad=\pm\frac{(K^2-\Lambda^2)^{\frac{1}{2}}}{K(2K-1)^{\frac{1}{2}}}(K-1)^{\frac{1}{2}}.
\end{aligned}\tag{5.18}$$

In general, for all S, the diagonal elements are

$$(KJ|\mathbf{S}\cdot\mathbf{k}'|KJ)=\frac{\Lambda\{J(J+1)-K(K+1)-S(S+1)\}}{2K(K+1)}.\tag{5.19}$$

In the F_1 representation the matrix elements are to be obtained from those in the J representation by interchanging I and S, and letting J become F_1.

In the case of triplet states, where two electron spins add to a resultant $S=1$, in addition to the matrix elements given above there are also some elements between the triplet states and singlet states of the same

values of Λ. These connect states with considerable energy difference, and are considered as higher order effects. The appropriate matrix elements of the hyperfine operators may be obtained using the methods outlined by Frosch,[9] in conjunction with the formulas of Condon and Shortley.[10]

The effect of the "s-state" part of the magnetic hyperfine interaction obtained specifically from the relativistic treatment, discussed in Sec. 4, becomes especially apparent in the case of the zero rotational state of a Σ electronic level ($K=0$, $\Lambda=0$). The appropriate representation is F_s, and the diagonal hyperfine energy level formula is

$$\tfrac{1}{6}(3b+c)\{F(F+1)-S(S+1)-I(I+1)\}. \quad (5.20)$$

In Sec. 4, it was shown that the nonvanishing of the coefficient of this expression is directly related to the presence of a distribution of electron spin moment near the nucleus similar to that of an atomic s-state.

Matrix elements in the partially decoupled representation in a weak magnetic field (quantum numbers $ISKF_1m_{F_1}m_S$, $ISKJm_Jm_I$, $ISKF_2m_{F_2}m_K$) may also be obtained from the above operators using the formulas of Condon and Shortley.[10]

6. THE EFFECT OF THE LAMBDA-DOUBLING

The treatment of hyperfine interactions in the previous section has been concerned only with matrix elements diagonal in Λ. Before discussing the effects due to interactions connecting electronic states of very different energies, it is appropriate to consider the effect of the near degeneracy of states of value $\pm\Omega$ ($\pm\Lambda$ in case b). This degeneracy is raised in some order of the perturbation theory by the action of a part of the kinetic energy of rotation which was neglected in the separation of rotation and electronic motion.[8] The matrix elements of this operator are given in Sec. 7, expression (7.9). The correct linear combinations of the degenerate wave functions are the symmetric and antisymmetric functions, e.g., $[f(\Lambda\Sigma)\pm f(-\Lambda-\Sigma)]/(2)^{\frac{1}{2}}$ in Hund's case a. For both case a and case b, we write these as $[f(+)\pm f(-)]/(2)^{\frac{1}{2}}$. The matrix elements of the hyperfine operator now may be written as

(a) Diagonal in Λ doubling state:

$$\begin{pmatrix}\text{symmetric}\\ \text{antisym.}\end{pmatrix}\Big|H_{\text{hfs}}\Big|\begin{matrix}\text{symmetric}\\ \text{antisym.}\end{matrix}\Big)=\tfrac{1}{2}\{(+|H|+)+(-|H|-)\pm 2(-|H|+)\}; \quad (6.1)$$

(b) Off-diagonal in Λ doubling state:

$$\begin{pmatrix}\text{symmetric}\\ \text{antisym.}\end{pmatrix}\Big|H_{\text{hfs}}\Big|\begin{matrix}\text{antisym.}\\ \text{symmetric}\end{matrix}\Big)=\tfrac{1}{2}\{(+|H|+)-(-|H|-)\}, \quad (6.2)$$

where the matrix elements $(+|H|+)$ etc., are obtained from the $f(+)$, $f(-)$ states, in which Λ is a good quantum number. The matrix elements $(+|H|+)$ and $(-|H|-)$ are thus diagonal in Λ and are among those already derived in Sec. 5. For case a_β, the hyperfine matrix elements diagonal in Λ and Ω are of the form

$$[a\Lambda+(b+c)\Sigma](\mathbf{I}\cdot\mathbf{k}'). \quad (6.3)$$

The matrix elements of this operator which are also diagonal in J are the same for the states $\pm\Omega$ whose degeneracy is removed in Λ doubling. The matrix elements nondiagonal in J are of opposite signs for $\pm\Omega$ so that $(+|H|+)=-(-|H|-)$ for $\Delta J=\pm 1$.

In addition to the magnetic hyperfine elements diagonal in Λ of Sec. 5, there are also matrix elements connecting states differing in Λ by $\Delta\Lambda=\pm 1,\pm 2$. Thus, there are interactions between the degenerate states for Π states only. Some of the matrix elements are diagonal and some off diagonal in J, and they yield the various quantities of Eq. (6.1). The hyperfine matrix elements nondiagonal in Λ and Ω are worked out in Sec. 7, and we employ here expression (7.3) written as

$$(+|H|-)=(+\Pi|t|-\Pi)(S_{x'}+iS_{y'})\mathbf{I}\cdot(\mathbf{x}'+i\mathbf{y}'). \quad (6.4)$$

We shall give here explicit formulas for the hyperfine splitting for a case a_β $^2\Pi_{\frac{1}{2}}$ molecular state, neglecting the hyperfine matrix elements nondiagonal in J. The matrix elements for $\Delta J=\pm 1$ may be worked out from Sec. 5 and the Appendix. Thus, we have for the symmetric and antisymmetric Λ doubling states

$$W_{S/A}=(+|H|+)\pm(+|H|-),$$

with

$$(+|H|+)=\left(a-\frac{b+c}{2}\right)\frac{\mathbf{I}\cdot\mathbf{J}}{2J(J+1)},$$

$$(+|H|-)=\frac{d(J+\tfrac{1}{2})}{2J(J+1)}\mathbf{I}\cdot\mathbf{J}, \quad (6.5)$$

where

$$d=(+\Pi|t|-\Pi)$$

$$=-\frac{g_I\mu_0\mu_N}{2}\left[\left(\frac{\delta(r_1)}{r_1^2}-\frac{3}{r_1^3}\right)\sin^2\chi\right]_{hy}.$$

Electronic wave functions which contribute to this $+\Pi\rightarrow-\Pi$ matrix element will vanish near the nucleus sufficiently rapidly so that the first term of the above expression for d will be negligible compared to the second.

For case b molecular states the same symmetry properties of the matrix elements obtain as in case a_β and the discussion given above applies for case b with the rotational angular momentum K replacing J. Expressions similar to Eq. (6.5) may be developed from the formulas of Sec. 7, with the important difference that in case b the electron spin is quantized in the laboratory rather than in the molecular frame.

7. SECOND-ORDER EFFECTS

In this section are considered effects which arise from those matrix elements of the magnetic hyperfine inter-

action [Eq. (2.6)] which are off diagonal in Λ, or off diagonal in Λ in Hund's case a. Levels which correspond to different values of the axial orbital angular momentum Λ, or in case a to differentel ectron spin components, are in general separated by energy intervals which are very large compared to the hyperfine interaction energy. The special features due to the $\pm\Omega$ degeneracy (Λ doubling) are treated in Sec. 6. These second-order effects in the general case give only small corrections to the first-order hyperfine structure, the theory of which is developed in Secs. 4 and 5. There are, however, several special cases in which these effects are of importance. In addition to the Λ doubling effects, there is the large class of molecular states with no first-order hyperfine structure, e.g., $^1\Sigma$ states, in which these second-order effects (and the nuclear electric quadrupole perturbation) constitute the whole of the hyperfine structure. The treatment of the hyperfine level structure in molecular cases intermediate between Hund's case a and case b also involves some of these off diagonal matrix elements.

The matrix elements of the first term of Eq. (2.6),

$$\frac{e}{mc}\frac{\mu\cdot L'}{r_1^3}, \tag{7.1}$$

may be written

$$2g_I\mu_0\mu_N\left(\Lambda\left|\frac{1}{r_1^3}[I_{x'}L_{x'}'+I_{y'}L_{y'}']\right|\Lambda\pm1\right). \tag{7.2}$$

The magnetic interaction of the nuclear spin moment with the electron spin moment [Eq. (2.6)] yields matrix elements off diagonal both with respect to Λ and with respect to Σ. The elements off diagonal in Λ arise from the terms in (2.6) of the form $(\mathbf{I}\cdot\mathbf{r})(\mathbf{S}\cdot\mathbf{r})$, which appear both in the ordinary spin-spin interaction and in the 'relativistic' term. The terms which contribute off diagonal matrix elements may be expanded in the molecular frame of reference as

$$\begin{aligned}2g_I\mu_0\mu_N&\left[\frac{3}{r_1^3}-\frac{\delta(r_1)}{r_1^3}\right]\\
&\times\left\{\frac{\sin^2\chi}{4}[e^{-2i\varphi}(I_{x'}+iI_{y'})(S_{x'}+iS_{y'})\right.\\
&+e^{2i\varphi}(I_{x'}-iI_{y'})(S_{x'}-iS_{y'})]\\
&+\sin\chi\cos\chi[e^{-i\varphi}[(I_{x'}+iI_{y'})S_{z'}\\
&+(S_{x'}+iS_{y'})I_{z'}]+e^{i\varphi}[(I_{x'}-iI_{y'})S_{z'}\\
&\left.+(S_{x'}-iS_{y'})I_{z'}]]\right\}.\end{aligned} \tag{7.3}$$

Clearly, the first term, with factors $e^{\pm2i\varphi}$, in this expression connects states of $\Delta\Lambda=\pm2$. These terms are discussed in connection with the Λ doubling of Π states in Sec. 6.

Terms in the hyperfine coupling which are off diagonal in Σ only are of interest in cases intermediate between Hund's case a and case b. Such matrix elements arise from the spin components perpendicular to the symmetry axis (in $\mathbf{I}\cdot\mathbf{S}$) in Eq. (4.7). In a Hund's case a representation, the operator may be written conveniently in the form

$$\begin{aligned}F(\rho,\chi)&\tfrac{1}{4}\{(I_{x'}-iI_{y'})(S_{x'}+iS_{y'})\\
&+(I_{x'}+iI_{y'})(S_{x'}-iS_{y'})\}\\
&=F(\rho\chi)\tfrac{1}{4}\{\mathbf{I}\cdot(\mathbf{x}'-i\mathbf{y}')(S_{x'}+iS_{y'})\\
&+\mathbf{I}\cdot(\mathbf{x}'+i\mathbf{y}')(S_{x'}-iS_{y'})\}.\end{aligned} \tag{7.4}$$

The $S_{x'}\pm iS_{y'}$ operator acts only on the internal electron spin wave function, and the matrix elements of $(\mathbf{x}'\pm i\mathbf{y}')/2$ are, with respect to the rotational wave function, the same as those of a unit vector $\mathbf{i}'$, and are given in Appendix I. Thus, the matrix elements of expression (7.4) connecting $\Sigma\rightarrow\Sigma+1$ and $\Omega\rightarrow\Omega+1$ have the form

$$A(\mathbf{I}\cdot\mathbf{i}')[(S+\Sigma)(S-\Sigma+1)]^{\frac{1}{2}}. \tag{7.5}$$

For a good case a state, the effect of these matrix elements between members of a multiplet may be taken into account as a second-order perturbation. For a real intermediate case these matrix elements would be subjected to the appropriate transformation from case a.

There is another interaction with matrix elements off diagonal in Λ which should be mentioned here. This is the interaction of the electric quadrupole moment of the nucleus with the electrons. This interaction has been discussed extensively by Casimir,[1] and its matrix elements diagonal in Λ have been given by many authors.[2,4] In our notation, this interaction may be written

$$\begin{aligned}\frac{eQ}{I(2I-1)}&\left\{\frac{3\cos^2\chi-1}{2r_1^3}\frac{3I_{z'}^2-I^2}{2}+\frac{3}{4}\frac{\sin\chi\cos\chi}{r_1^3}\right.\\
&\times[[I_{z'}(I_{x'}-iI_{y'})+(I_{x'}-I_{y'})I_{z'}]e^{i\varphi}\\
&+[I_{z'}(I_{x'}+iI_{y'})+(I_{x'}+iI_{y'})I_{z'}]e^{-i\varphi}]\\
&\left.+\frac{3}{8}\frac{\sin^2\chi}{r_1^3}[e^{2i\varphi}(I_{x'}-iI_{y'})^2+e^{-2i\varphi}(I_{x'}+iI_{y'})^2]\right\},\end{aligned} \tag{7.6}$$

where Q is the electric quadrupole moment of the nucleus as defined by Bardeen and Townes.[4] The terms in $e^{\pm2i\varphi}$ may affect the Λ doubling in case b.

Except for the case of Λ doubling described in Sec. 6, the matrix elements of (7.2) or (7.3) would by themselves yield negligible effects in a second-order calculation. There are, however, certain "molecular" matrix elements which are off diagonal in Λ and which, when taken in cross terms with (7.2) or (7.3) yield observable hyperfine structures, even in $^1\Sigma$ states.

We shall give here the effects in $^1\Sigma$ states which arise in second order from the interactions with the electron orbital currents, expression (7.2). The spin effects of

Eq. (7.3) are of the same general form. Semiclassical treatments (large values of J) have been given previously.[3] We write (7.2) in the form

$$\tfrac{1}{2}a[(L_{x'}+iL_{y'})(I_{x'}-iI_{y'})+(L_{x'}-iL_{y'})(I_{x'}+iI_{y'})]. \tag{7.7}$$

This term in second order yields§

$$\frac{a^2}{4}\sum_{\Pi}\frac{(\Sigma|L'_\perp|\Pi)^2}{\Delta E_{\Sigma\Pi}}[(\mathbf{I}\cdot\mathbf{k}')^2-I(I+1)], \tag{7.8}$$

in which the summation is extended over all Π states to which there is a nonvanishing $(\Sigma|L_\perp|\Pi)$ matrix element. The dependence on F of the expression in square brackets is given by $C(C+1)$ with $C=F(F+1)-I(I+1)-J(J+1)$. This is of exactly the same form as the hyperfine level perturbation developed by an electric quadrupole moment. The quantity $\sum_\Pi(\Sigma|L_\perp|\Pi)^2/\Delta E_{\Sigma\Pi}$ cannot, in general, be evaluated. For a very simple model with the total orbital angular momentum a good quantum number (Van Vleck's hypothesis of pure precession),[8] the value $L(L+1)/\Delta E_{\Sigma\Pi}$, is obtained for this quantity. The order of magnitude of this effect is $E_{hfs}^2/\Delta E_{\Sigma\Pi}$, which will be quite negligible in almost all cases.

The perturbation terms in the molecular Hamiltonian which arise from the nonseparability of electronic and rotational motion, and which lead to the "Λ doubling" observed in molecular spectra give nonvanishing matrix elements between Σ and Π states and these may form cross terms with the magnetic hyperfine operator (7.2). The Λ doubling operator is[8]

$$B(\Sigma|L_\perp|\Pi)[J(J+1)]^{\frac{1}{2}} =2B\left(\Sigma\left|L_{y'}+\frac{\tau p_{x'}}{\hbar}\right|\Pi\right)[J(J+1)]^{\frac{1}{2}}. \tag{7.9}$$

Another molecular operator with similar properties is the interaction of the electrons with an external magnetic field. For $^1\Sigma$ molecules there is no first-order interaction, but there exists the operator

$$\mu_0(L_{x'}\mathbf{x}'+L_{y'}\mathbf{y}')\cdot\mathbf{H}, \tag{7.10}$$

which has matrix elements of the form $\mu_0(\Sigma|L_\perp|\Pi)\mathbf{i}'\cdot\mathbf{H}$. The cross term of the first term of (7.9) with (7.2) is

$$\sum_\Pi 4aB\frac{(\Sigma|L'_\perp|\Pi)^2}{i\Delta E_{\Sigma\Pi}}[J(J+1)]^{\frac{1}{2}}(\mathbf{I}\cdot\mathbf{i}') =\sum_\Pi\frac{(\Sigma|L'_\perp|\Pi)^2}{\Delta E_{\Sigma\Pi}}2aB(\mathbf{I}\cdot\mathbf{J}). \tag{7.11}$$

This term accounts for most of the observed $\mathbf{I}\cdot\mathbf{J}$ interaction in $^1\Sigma$ states. There is a small contribution from the 'direct' $\mathbf{I}\cdot\mathbf{J}$ interaction of the nuclear motion discussed in Sec. 8. For the case of a positive nuclear moment the term above is positive.

The cross term of the second term of (7.9) with (7.1) gives a negligible hyperfine level shift. We will now examine the second-order cross term involving the matrix elements of the second term of (7.9) with those of $L_{y'}$ We have

$$\frac{e}{mc}\tau\mu_{y'} \times\sum_\Pi\frac{(\Sigma|p_{x'}|\Pi)(\Pi|L_{y'}/r_1^3|\Sigma)+(\Sigma|L_{y'}/r_1^3|\Pi)(\Pi|p_{x'}|\Sigma)}{\Delta E_{\Sigma\Pi}}. \tag{7.12}$$

The summation is extended to all excited Π states. Now, since

$$\frac{p_{kn}}{m}=\frac{i}{\hbar}[E_k-E_n]r_{kn}, \tag{7.13}$$

this expression becomes

$$\frac{e}{mc}\tau\mu_{y'}\frac{im}{\hbar}\left(\Sigma\frac{|L_{y'}x'-x'L_{y'}|}{r_1^3}\Sigma\right), \tag{7.14}$$

and since $[L_{y'}, x']=-iz_1'$ we have for the cross term

$$\frac{e}{c}\frac{2B}{\hbar}\mu_{y'}\tau[J(J+1)]^{\frac{1}{2}}\left(\frac{z_1'}{r_1^3}\right)_n=\frac{B}{\hbar c}\mathcal{S}_e(\boldsymbol{\mu}\cdot\mathbf{J})\tau, \tag{7.15}$$

noting that the matrix elements of $\boldsymbol{\mu}\cdot\mathbf{y}'$ are just $\mu_N(\mathbf{I}\cdot\mathbf{J})/2[J(J+1)]^{\frac{1}{2}}$. $\mathcal{S}_e$ is the magnitude of the electronic field produced by the electrons at the nucleus. The first term of Eq. (7.2) gives a contribution equal to (7.15), giving finally

$$2(B/\hbar c)\mathcal{S}_e(\boldsymbol{\mu}\cdot\mathbf{J})\tau. \tag{7.16}$$

This term is just canceled by an equal contribution from the rotational motion of the nuclei (see Sec. 8).

The cross term of (7.2) with (7.10) is

$$\sum_\Pi a\mu_0\frac{(\Sigma|L_\perp|\Pi)^2}{\Delta E_{\Sigma\Pi}}(I_{x'}-iI_{y'})(H_{x'}+iH_{y'}) =\sum_\Pi a\mu_0\frac{(\Sigma|aL_\perp|\Pi)^2}{\Delta E_{\Sigma\Pi}}[\mathbf{I}\cdot\mathbf{H}-(\mathbf{I}\cdot\mathbf{k}')(\mathbf{H}\cdot\mathbf{k}')]. \tag{7.17}$$

This expression represents the effect of the diamagnetic shielding of the nucleus by the electrons in the presence of an external magnetic field. This effect has been discussed extensively by Ramsey[13] and will not be considered further here.

For completeness we consider the cross term of (7.9)

§ In Eqs. (7.8), (7.11), and (7.17) the matrix elements have been written as if the radial integrals could be factored from the angular momentum operators.

[13] N. F. Ramsey, Phys. Rev. 78, 699 (1950).

and (7.10):

$$\sum_{\Pi} 2B\frac{(\Sigma|L_\perp|\Pi)^2}{i\Delta E_{\Sigma\Pi}}\mu_0[J(J+1)]^{\frac{1}{2}}(\mathbf{x}'-i\mathbf{y}')\cdot\mathbf{H}$$

$$=2\mu_0 B\sum_{\Pi}\frac{(\Sigma|L_\perp|\Pi)^2}{\Delta E_{\Sigma\Pi}}(\mathbf{J}\cdot\mathbf{H}), \quad (7.18)$$

which yields the electronic contribution to the molecular rotational magnetic moment:

$$2\mu_0 B\sum_{\Pi}\frac{(\Sigma|L_\perp|\Pi)^2}{\Delta E_{\Sigma\Pi}}\mathbf{J}. \quad (7.19)$$

8. NUCLEAR SPIN-ROTATION INTERACTION IN $^1\Sigma$ STATES

In addition to the second-order electronic $\mathbf{I}\cdot\mathbf{J}$ interaction of Sec. 7, there is also the interaction of the nuclear magnetic moment with the magnetic field produced by the rotation of the heavy particles themselves. This interaction term is

$$-Z_2\frac{e}{M_0c}\boldsymbol{\mu}_1\cdot\frac{[\boldsymbol{\rho}\times\mathbf{p}]}{\rho^3}, \quad (8.1)$$

where M_0 is the reduced mass, ρ the distance between the nuclei, and $\mathbf{p}=\mathbf{p}_2=-\mathbf{p}_1$. Account must be taken here of the relative motion of the two nuclei. Following the procedure of Sec. 7, we write (8.1) in the form

$$Z_2e\frac{\boldsymbol{\mu}_1\cdot[\tau\mathbf{k}'\times\mathbf{p}]}{c\rho^3M_0}+Z_2e\frac{\boldsymbol{\mu}_1\cdot[\boldsymbol{\rho}_2\times\mathbf{p}]}{M_0c\rho^3}$$

$$=\mathcal{E}_N\frac{\tau\boldsymbol{\mu}_1\cdot\mathbf{J}\hbar}{M_0\rho^2c}+\mathcal{E}_N\frac{\rho_2\hbar}{cM_0\rho^2}\boldsymbol{\mu}_1\cdot\mathbf{J}, \quad (8.2)$$

where $\mathcal{E}_N$ is the electric field produced at the position of nucleus 1 by nucleus 2. ρ_2 is the distance from the center of mass nucleus 2. The first term of (8.2) added to (7.16) gives just

$$\frac{\tau\hbar}{M_0\rho^2c}\times[\text{total electric field at 1}]. \quad (8.3)$$

The electric field at the equilibrium position of a nucleus is zero. The second term of (8.2) is to be added to (7.11) and contributes to the $\mathbf{I}\cdot\mathbf{J}$ interaction.

9. INTERACTION WITH AN EXTERNAL FIELD: SELECTION RULES AND INTENSITIES

The contribution of each electron to the electronic dipole moment is the vector $e\mathbf{r}'$ with components $e\mathbf{x}'$, $e\mathbf{y}'$, and $e\mathbf{z}'$ in the molecular coordinate system.

The magnetic dipole moment operator in case a_β is the sum of two parts:

(1) The electronic contribution, a vector in the molecular frame of reference with components:

$$(\mu_0L_{x'}+2\mu_0S_{x'})\mathbf{x}';$$
$$(\mu_0L_{y'}+2\mu_0S_{y'})\mathbf{y}';$$
and $$(\mu_0L_{z'}+2\mu_0S_{z'})\mathbf{z}.$$

(2) The nuclear moment vector $g_I\mu_N\mathbf{I}$ in the laboratory system.

In case b_β, the magnetic moment is the sum of:

(1) $\mu_0L_{x'}\mathbf{x}'$; $\mu_0L_{y'}\mathbf{y}'$; $\mu_0\Lambda\mathbf{z}'$ in the molecular coordinate system.

(2) The vector $2\mu_0\mathbf{S}+g_I\mu_N\mathbf{I}$ in the laboratory system.

Diagonal values of the magnetic moment operator yield the first order Zeeman effect. Nondiagonal values of the electric and magnetic dipole operators give the selection rules and the intensities in electric and magnetic dipole transitions, as well as higher order Zeeman and Stark effects. The diagonal matrix elements of the magnetic interaction in case a are

$$(\Lambda+2\Sigma)\mu_0\frac{\Omega}{J(J+1)}m_J H+g_I\mu_N m_I H \quad (9.1)$$

in strong fields, and

$$(\Lambda+2\Sigma)\mu_0\frac{\Omega}{J(J+1)}\frac{F(F+1)+J(J+1)-I(I+1)}{2F(F+1)}$$
$$+g_I\mu_N\frac{F(F+1)-J(J+1)+I(I+1)}{2F(F+1)} \quad (9.2)$$

in very weak fields. The presence of Λ doubling does not affect these diagonal values. In case b the diagonal magnetic interaction is

$$\mu_0\frac{\Lambda^2}{K(K+1)}\frac{J(J+1)-S(S+1)+K(K+1)}{2J(J+1)}m_J$$
$$+2\mu_0\frac{J(J+1)-K(K+1)+S(S+1)}{2J(J+1)}m_J$$
$$+g_I\mu_N m_I \quad (9.3)$$

in strong fields, and in weak fields for the J representation (Sec. 5) it is

$$\left\{\mu_0\frac{\Lambda^2}{K(K+1)}\frac{J(J+1)-S(S+1)+K(K+1)}{2J(J+1)}\right.$$
$$\left.+2\mu_0\frac{J(J+1)-K(K+1)+S(S+1)}{2J(J+1)}\right\}$$
$$\times\left\{\frac{F(F+1)-I(I+1)+J(J+1)}{2F(F+1)}\right\}m_F$$
$$+g_I\mu_N\frac{F(F+1)-J(J+1)+I(I+1)}{2F(F+1)}m_F. \quad (9.4)$$

The off diagonal matrix elements of the electric or magnetic dipole moment components may be worked out from the matrix elements of the direction cosines of the molecular coordinate system given in the Appendix, together with the formulas taking into account the vector coupling.[10] In the interest of brevity the results will not be given here.[9]

Some examples of the use of the off diagonal matrix elements have been given in Sec. 7. The selection rules for the diatomic molecule are well known[8] and need only be extended to include the usual rule, $\Delta F=0, \pm 1$.

10. APPLICATIONS

The oxygen and nitrogen oxide molecules appear to be the only examples so far observed of a first-order magnetic hyperfine spectrum.

$O^{16}O^{17}$

The coupling of the electron spin to the molecular rotation in a $^3\Sigma$ state has been shown[11] to arise in part from the second-order effect of the spin orbit interaction orbital angular momentum components perpendicular to the axis, and the Λ doubling interaction [expression (7.9)]. Matrix elements of these operators between $^3\Sigma$ and $^3\Pi$ states yield in second-order energy perturbations in the $^3\Sigma$ level of the form discussed in Sec. 6 Eq. (5.8). Kramers[14] has shown that, in addition to these second-order terms, there is the spin-spin interaction of the electrons, which contributes terms of the same form as the above. The final energy positions of the levels $J=K+1, K, K-1$ are then

$$\begin{aligned} W_{K+1}&=W_0-2\lambda\frac{K+1}{2K+3}+\mu(K+1),\\ W_K&=W_0,\\ W_{K-1}&=W_0-2\lambda\frac{K}{2K-1}-\mu K, \end{aligned} \tag{10.1}$$

for $\lambda \ll B$. A more exact formula has been given by Schlapp[15] for the case $B \cong \lambda$.

The first-order magnetic hyperfine structure for a $^3\Sigma$ state is given by the case b_β expression (5.5):

$$b\mathbf{I}\cdot\mathbf{S}+c(\mathbf{I}\cdot\mathbf{k}')(\mathbf{S}\cdot\mathbf{k}'). \tag{10.2}$$

This quantity must be expressed in the F_1, J, or F_2 representation. For O_2 we have $\lambda=1.984$ cm^{-1} and $\mu=-0.0084$ cm^{-1}.[8] Thus, it appears likely that the coupling of S to K will be greater than the hyperfine interaction, and the J representation is appropriate. The diagonal expressions for the hyperfine levels in this representation are

$$W_{FJK}=\frac{F(F+1)-J(J+1)-I(I+1)}{2J(J+1)} \times\begin{cases}(K+2)[b+c/(2K+3)] & \text{for } J=K+1\\ b+c & \text{for } J=K\\ (K-1)[-b+c/(2K-1)] & \text{for } J=K-1.\end{cases} \tag{10.3}$$

Higher order corrections, proportional to b^2, and c^2, etc., may be obtained from the matrix elements of (10.2) according to the methods given in Sec. 5. A comparison of (10.3) with the spectrum of $O^{16}O^{17}$ will be published separately by Dr. S. L. Miller.

$N^{14}O^{16}$

Beringer and Castle[16] have observed the microwave spectrum of NO gas in rather strong magnetic fields. Margenau and Henry, and Henry[17] have given theoretical analyses of the spectrum. Their results are derived from an incomplete Hamiltonian.

In the experiments of Beringer and Castle, the Λ doubling was not resolved. Its effects are not included in our analysis. (The writers have been informed by Professor Beringer[18] that in a considerably more accurate experiment, the Λ doubling and the related hyperfine structure effects in NO have been resolved. For this reason only, a summary of the analysis of the previous results will be given here.)

The ground state of NO is represented quite well by Hund's case *a*. In this representation the hyperfine Hamiltonian including all effects diagonal in Λ is

$$[a\Lambda+(b+c)\Sigma](\mathbf{I}\cdot\mathbf{k}')+b(I_{x'}S_{x'}+I_{y'}S_{y'}). \tag{10.4}$$

The second term gives matrix elements only between $^2\Pi_{\frac{1}{2}}$ and $^2\Pi_{\frac{3}{2}}$ states (see Sec. 7). This effect is expected to be small, and in fact it was possible to account for the observed spectrum without including it.

The energy levels in a strong magnetic field ($\sim$8500 gauss) were obtained in the following way: The Zeeman matrix, including elements of the Zeeman Hamiltonian connecting $J=3/2$ and $J=5/2$ was solved exactly. (The effect of the $J=7/2$ level on $J=3/2$ states was found to be negligible.) The resulting states were then corrected by a second-order calculation of the effects of the states of $^2\Pi_{\frac{1}{2}}$. This calculation employed the matrix elements of the magnetic field between $^2\Pi_{\frac{1}{2}}$ and $^2\Pi_{\frac{3}{2}}$ states, and the rotational distortion of the spin multiplets[8] (incipient case *b*). The final linear combination of eigenfunctions was employed to obtain the magnetic hyperfine structure from (10.4). An agreement with the observed spectrum to 0.05 percent was obtained employing $(a\Lambda+(b+c)\Sigma)=0.002607$ cm^{-1}.

[10] H. A. Kramers, Z. Physik **53**, 422 (1929).
[15] R. Schlapp, Phys. Rev. **51**, 342 (1937).
[16] R. Beringer and J. G. Castle, Jr., Phys. Rev. **78**, 581 (1950).
[17] H. Margenau and A. F. Henry, Phys. Rev. **78**, 587 (1950); A. F. Henry, Phys. Rev. **80**, 549 (1950).
[18] R. Beringer (private communication to the authors).

APPENDIX

We require matrix elements of operators of the form,

$$e^{\mp ik\varphi}\mathbf{I}\cdot(\mathbf{x}'\pm i\mathbf{y}'), \tag{A1}$$

where $k=0$, 1, 2. Since the wave functions are of the form,

$$\Theta_{J\Omega M}(\theta)e^{i\Lambda\varphi}e^{iM\psi}, \tag{A2}$$

the integrals giving matrix elements are of the form,

$$\int\Theta_{J\Omega M}{}^{*}e^{-i\Lambda\varphi}e^{-iM\psi}e^{\mp ik\varphi}\mathbf{I}\cdot(\mathbf{x}'\pm i\mathbf{y}')\Theta_{J'\Omega'M'}e^{i(\Lambda\pm k)\varphi}e^{iM'\psi}d\tau. \tag{A3}$$

If we perform the φ integral, we are left with the quantity,

$$\int\Theta_{J\Omega M}{}^{*}e^{-iM\psi}\mathbf{I}\cdot(\mathbf{x}'\pm i\mathbf{y}')\Theta_{J'\Omega'M'}e^{iM'\psi}\sin\theta d\theta d\psi, \tag{A4}$$

to evaluate. In this connection it is convenient to define a Cartesian coordinate system with unit vectors $\mathbf{i}'\mathbf{j}'\mathbf{k}'$, related to the fixed space frame through the usual Eulerian angles (see Fig. 4). In this Eulerian system, the $\mathbf{x}'$ axis is along the line of nodes, and the $\mathbf{y}'$ axis is related to it in the usual right-handed way. The electron is located on the $\mathbf{i}'$ axis. We may write

$$\begin{aligned}\mathbf{i}'&=\mathbf{x}'\cos\varphi+\mathbf{y}'\sin\varphi\\&=(\mathbf{x}'+i\mathbf{y}')(e^{-i\varphi}/2)+(\mathbf{x}'-i\mathbf{y}')(e^{i\varphi}/2),\end{aligned} \tag{A5}$$

and hence, we see that

$$(\Omega|\mathbf{i}'|\Omega\pm1)=\tfrac{1}{2}\int\Theta_{J\Omega M}{}^{*}\times e^{-iM\psi}(\mathbf{x}'\pm i\mathbf{y}')\Theta_{J'\Omega\pm1M'}e^{iM'\psi}\sin\theta d\theta d\psi. \tag{A6}$$

The unit vectors $\mathbf{i}'\mathbf{j}'\mathbf{k}'$ are $\mathbf{T}$ vectors in the notation of Condon and Shortley,[10] that is, they commute with the components of $\mathbf{J}$ in the laboratory system according to $[J_z, T_y]=i\hbar T_x$, etc. Then, their matrix elements are of the form,

$$\begin{aligned}(\alpha Jm|\mathbf{T}|\alpha'J+1m\pm1)&=\mp(\alpha J\vdots\mathbf{T}\vdots\alpha'J+1)\\&\quad\times\tfrac{1}{2}[(J\pm m+1)(J\pm m+2)]^{\frac{1}{2}}(\mathbf{i}\pm i\mathbf{j}),\\(\alpha Jm|\mathbf{T}|\alpha'J+1m)&=(\alpha J\vdots\mathbf{T}\vdots\alpha'J+1)\\&\quad\times[(J+1)^2-m^2]^{\frac{1}{2}}\mathbf{k},\\(\alpha Jm|\mathbf{T}|\alpha'Jm\pm1)&=(\alpha J\vdots\mathbf{T}\vdots\alpha'J)\\&\quad\times\tfrac{1}{2}[(J\mp m)(J\pm m+1)]^{\frac{1}{2}}(\mathbf{i}\pm i\mathbf{j}),\\(\alpha Jm|\mathbf{T}|\alpha'Jm)&=(\alpha J\vdots\mathbf{T}\vdots\alpha'J)m\mathbf{k},\\(\alpha Jm|\mathbf{T}|\alpha'J-1m\pm1)&=\pm(\alpha J\vdots\mathbf{T}\vdots\alpha'J-1)\\&\quad\times\tfrac{1}{2}[(J\mp m)(J\mp m-1)]^{\frac{1}{2}}(\mathbf{i}\pm i\mathbf{j}),\\(\alpha Jm|\mathbf{T}|\alpha'J-1m)&=(\alpha J\vdots\mathbf{T}\vdots\alpha'J-1)(J^2-m^2)^{\frac{1}{2}}\mathbf{k}.\end{aligned} \tag{A7}$$

in which $\mathbf{i}$, $\mathbf{j}$, $\mathbf{k}$ are the XYZ unit vectors in the laboratory system. From King, Hainer, and Cross[19] we obtain, with a change of phase to conform to the choice of

[19] Cross, Hainer, and King, J. Chem. Phys. 12, 210 (1944).

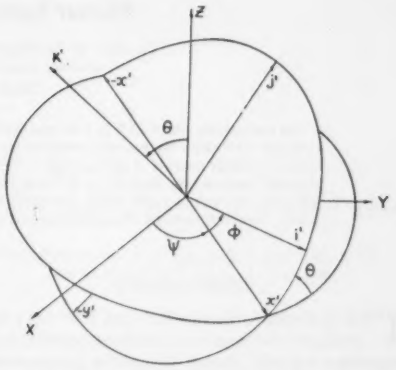

FIG. 4. The Eulerian coordinate system $\mathbf{i}'\mathbf{j}'\mathbf{k}'$ with θ and ψ as chosen by King, Hainer, and Cross. The plus and minus $\mathbf{x}'$ and minus $\mathbf{y}'$ axes are marked. For proper phase and angles as chosen by Condon and Shortley and Van Vleck one should let $\mathbf{j}\rightarrow\mathbf{i}$, $\mathbf{i}\rightarrow-\mathbf{j}$, and $\psi\rightarrow\psi+\pi$. ψ then is the angle between the $\mathbf{i}$ axis and the projection of $\mathbf{k}'$ on the $\mathbf{ij}$ plane.

angles of Van Vleck[8] and the phases of Condon and Shortley,[10]

$$\begin{aligned}(J\Omega\vdots\mathbf{k}'\vdots J+1\Omega)&=\frac{[(J+\Omega+1)(J-\Omega+1)]^{\frac{1}{2}}}{(J+1)[(2J+1)(2J+3)]^{\frac{1}{2}}},\\(J\Omega\vdots\mathbf{k}'\vdots J\Omega)&=\frac{\Omega}{J(J+1)},\\(J\Omega\vdots\mathbf{k}'\vdots J-1\Omega)&=\frac{(J^2-\Omega^2)^{\frac{1}{2}}}{J(4J^2-1)^{\frac{1}{2}}},\end{aligned} \tag{A8}$$

$$\begin{aligned}(J\Omega\vdots\mathbf{j}'/\mp i\mathbf{i}'\vdots J+1\Omega\pm1)&=\mp\frac{[(J\pm\Omega+1)(J\pm\Omega+2)]^{\frac{1}{2}}}{2(J+1)[(2J+1)(2J+3)]^{\frac{1}{2}}},\\(J\Omega\vdots\mathbf{j}'/\mp i\mathbf{i}'\vdots J\Omega\pm1)&=\frac{[(J\mp\Omega)(J\pm\Omega+1)]^{\frac{1}{2}}}{2J(J+1)},\\(J\Omega\vdots\mathbf{j}'/\mp i\mathbf{i}'\vdots J-1\Omega\pm1)&=\pm\frac{[(J\mp\Omega)(J\mp\Omega-1)]^{\frac{1}{2}}}{2J(4J^2-1)^{\frac{1}{2}}}.\end{aligned}$$

It should also be noted that, in the rotating frame,

$$(\Sigma|S_{y'}\pm iS_{x'}|\Sigma\pm1)=[S(S+1)-\Sigma(\Sigma\pm1)]^{\frac{1}{2}}, \tag{A9}$$

and, in the laboratory frame,

$$(m_S|S_X\mp iS_Y|m_S\pm1)=[S(S+1)-m_S(m_S\pm1)]^{\frac{1}{2}}, \tag{A10}$$

etc.

Nuclear Spectra of Rb^{82} and Rb^{84}†

CHARLES M. HUDDLESTON AND ALLAN C. G. MITCHELL
Indiana University, Bloomington, Indiana

(Received July 31, 1952)

The nuclear spectra of Rb^{82} (6.3 hr) and Rb^{84} (34 days) have been measured with a magnetic lens spectrometer. Rb^{82} emits two positron groups of energies 0.775 and 0.175 Mev. It also decays by orbital electron capture. A large number of gamma-rays accompanies the disintegration (Table I). Reasonable agreement with the gamma-rays emitted by Br^{82} has been obtained. Rb^{84} emits three groups of positrons having end-point energies of 1.629, 0.822, and 0.373 Mev. One gamma-ray whose energy is 0.890 Mev has been found. Level diagrams for these disintegrations are discussed.

1. INTRODUCTION

THE radioactive nuclei Rb^{82} and Rb^{84} have been studied by a number of authors. Bombardment of bromine by high energy α-particles produces Rb^{81} (4.7 hr), Rb^{82} (6.3 hr), Rb^{82} (107 days), and Rb^{84} (34 days). The mass assignment and periods of these activities were studied carefully by Reynolds, Karraker, and Templeton[1] and by Karraker and Templeton.[2] The mass assignments were made with the help of a mass-spectrograph and the half-lives were measured with a counter. They found that, for lower energy α-particles (<20 Mev), the α-$2n$ reaction was weak compared to the α-n, so that activities were characteristic of Rb^{82} and Rb^{84}. Both Rb^{82} and Rb^{84} are positron emitters, and there is some orbital electron capture. They state that the end point of the positron spectrum of Rb^{82} is 0.670 ± 0.05 Mev and that of Rb^{84} is 1.5 Mev, with a lower energy group about 0.37 Mev.

Beckham and Pool[3] bombarded krypton with α-particles and deuterons. The rubidium activity showed a half-life of 38 days. They found that both positrons and electrons were emitted, the positrons having an end-point energy of 1.3 Mev, as measured by aluminum absorption. This activity is ascribed to Rb^{84}.

TABLE I. Gamma-rays of Rb^{82}. Energies are in kev.

Present work			Confirmation	
Pb radiator	U radiator	Internal conv.	Siegbahn *et al.*	Hubert *et al.*
		188 *K*		
		248 *K* & *L*		
		322 *K* & *L*		
388 *K*	390 *K*	390 *K*		
423 *K*	423 *K*			
465 *K*	468 *K*	464 *K*		
545 *K*	550 *K*	558 *K*	550	547
610 *K*	610 *K* & *L*		610	615
690 *K*	690 *K*		692	682
768 *K*	770 *K* & *L*		769	752
	818 *K* & *L*		824	823
	1020 *K*	1018 *K*	1036	1026
		1314 *K*	1321	1306
	1464 *K* & *L*	1464 *K* & *L*		1453

It is clear that Rb^{82} decays to Kr^{82} and that Rb^{84} decays to Kr^{84} with some possibility of decay to Sr^{84}. The energy levels of both Kr^{82} and Kr^{84} have been at least partially investigated from a study of the decay of Br^{82} and Br^{84}.

Siegbahn, Hedgran, and Deutsch,[4] and Hubert and Laberrigue-Frolow,[5] have studied the radiations from Br^{82}. The former studied the gamma-rays by means of photoelectrons and internal conversion electrons, while the latter measured only the photoelectrons. In all, some eight gamma-rays were observed. Their energies are shown in Table I. Work on the beta-ray spectrum has not been published, but Siegbahn[6] has found at least three groups. The decay scheme appears to be quite complicated.

The beta-rays of Br^{84} have been investigated by Duffield and Langer[7] who found four groups of beta-rays having end-point energies of 4.679, 3.45, 2.53, 1.72 Mev. The gamma-rays were not measured.

In order to obtain additional information on the levels of Kr^{82} and Kr^{84} an investigation of the radiations from Rb^{82} and Rb^{84} has been undertaken.

2. PREPARATION OF SOURCES

The sources were prepared by bombarding ammonium bromide with alpha-particles in the Indiana University cyclotron. The material was covered with a 1-mil copper foil to reduce the energy of the alpha-particles, originally 23 Mev, below the threshold for the α,$2n$ reactions. The current to the target had to be kept low, around 5 microamperes, in order not to vaporize the NH_4Br.

After bombardment the source was dissolved and any extraneous copper removed by precipitation with H_2S. The material was then made $0.1N$ in HCl and run through an ion column, measuring the activity of aliquots as a function of time. The rubidium which came through the column was essentially carrier free.

Beta-ray sources were prepared by evaporating a drop of the concentrated material onto a thin zapon film. Gamma-ray sources were prepared by soaking up

† Supported by the joint program of the ONR and AEC.

[1] Reynolds, Karraker, and Templeton, Phys. Rev. **75**, 313 (1949).

[2] D. G. Karraker and D. H. Templeton, Phys. Rev. **80**, 646 (1950).

[3] C. Beckham and M. L. Pool, Phys. Rev. **80**, 125 (1950).

[4] Siegbahn, Hedgran, and Deutsch, Phys. Rev. **76**, 1263 (1949).

[5] P. Hubert and J. Laberrigue-Frolow, Compt. rend. **232**, 2420 (1951).

[6] K. Siegbahn (private communication).

[7] R. B. Duffield and L. M. Langer, Phys. Rev. **81**, 203 (1950).

a few drops of the concentrated material on cotton and placing this in a copper capsule.

3. MEASUREMENT OF THE SPECTRA

Measurements of the spectra were made in a magnetic lens spectrometer. Two different types of counters were used, one having a 4-mg/cm² mica window and one having a thin Zapon window capable of transmitting electrons down to 10 kev. Measurements of the beta-spectrum of both Rb^{82} and Rb^{84} were made. In measuring the spectrum of Rb^{82}, short bombardments of about 1 hour were made, the spectrum was measured, and the source was allowed to sit in the spectrometer until the 6.3-hour Rb^{82} had died away. The spectrum of the residual activity of Rb^{84} was then measured, and corrections were made to the Rb^{82} spectrum. In investigating Rb^{84}, 5-hour bombardments were used, and the Rb^{82} was allowed to die out before measuring the spectrum. The energies of the gamma-rays from Rb^{82} were determined by measuring the energies of the photoelectrons ejected from both lead and uranium radiators. The sources of Rb^{84} were not strong enough to permit measuring the gamma-rays in the magnetic lens.

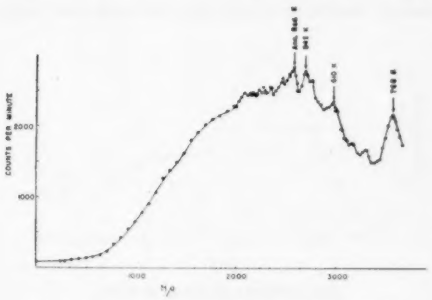

FIG. 1. Spectrum of photoelectrons ejected from Pb by gamma-rays of Rb^{82}. Energies are in kev.

4. RESULTS ON Rb^{82}

The distribution in energy of the photoelectrons ejected from lead and uranium radiators are shown in Figs. 1 and 2, respectively. It will be seen at once that a large number of gamma-rays are present, some of them of quite low intensity. The energies of these gamma-rays as determined from the measurements of the photoelectrons ejected from lead and uranium radiators as well as the values determined from internal conversion lines are given in Table I. Some of the very weak lines did not appear in more than one run and are left out of the table. Only those lines which appeared in at least two runs are given. Since the half-lives of Rb^{82} and Rb^{81} are not too different, it would be impossible to rule out Rb^{81} impurities on the basis of period measurements. It is felt, however, that the method of preparation excludes the possibility of any Rb^{81}. It is interesting to note that all of the lines found by Siegbahn, Hedgran and Deutsch, or Hubert and Laberrigue-Frolow in their measurements on Br^{82} have been found in Rb^{82} and all are internally converted. It was not possible to make relative intensity measurements on the lines. However, it is clear that the strongest line is that at 0.768 Mev.

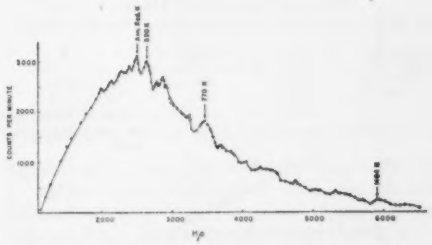

FIG. 2. Spectrum of photoelectrons ejected from U by gamma-rays of Rb^{82}. Energies are in kev.

The results of the measurements of the particle spectrum are shown in Fig. 3. These experiments were performed using a magnetic lens spectrometer without any device to separate particles of different sign. Both positrons and internal conversion electrons are recorded. It will be seen that many of the lines previously investigated in the gamma-ray experiments are internally converted. In addition, four other internal conversion lines, together with an Auger line, were found. The most intense internal conversion line is that whose gamma-ray energy is 0.188 Mev.

Figure 4 shows a Fermi plot of the positron spectrum. It will be seen that there are two groups whose end-point energies are 0.775 and 0.175 Mev. The energies, relative abundances, and values of $\log ft$ are given in Table II.

All of the gamma-ray lines, the two beta-ray groups, together with the three known beta-ray groups from Br^{82}—0.447, 0.323, and 0.181 Mev—can be fitted

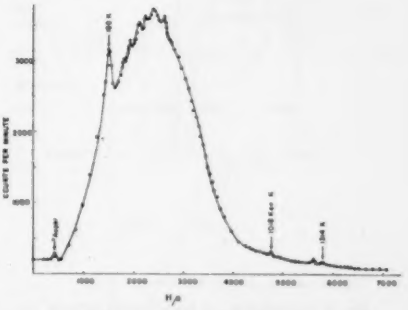

FIG. 3. Particle spectrum of Rb^{82}. Energies are in kev.

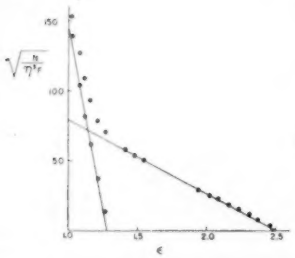

FIG. 4. Fermi plot of positrons from Rb^{82}.

reasonably well into a disintegration scheme. However, since the scheme is very complicated and the information on the intensity of the gamma-ray lines is meager, the scheme may not be unique. A possible tentative scheme, which omits only a line at 1.260 Mev, is shown in Fig. 5. The strongest line is the one at 0.768 Mev, and this would appear to be at the bottom of the

TABLE II. Positrons from Rb^{82}.

E(Mev)	Abundance (percent)	logft
0.775	76	4.93
0.175	24	4.88

scheme. No other line is of comparable intensity. The two positron groups feed the first excited level and the second excited level, respectively. The gamma-ray of 0.610 Mev corresponds to the difference in energy of these two states. The higher levels, fed by orbital electron capture, are less certain.

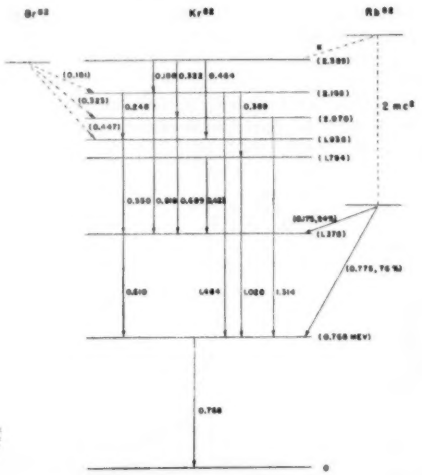

FIG. 5. Tentative energy level diagram of Kr^{82}. Energies are in Mev.

The values of logft for the two positron groups indicate that each is an allowed transition. The shell model would give several possibilities for the configurations of $_{37}Rb_{45}^{82}$ and $_{35}Br_{47}^{82}$. If one chooses the configuration $(f_{5/2}, p_{1/2})$ for Rb^{82}, this state will have even parity and a spin of 3. Thus the transition to the ground state of Kr^{82} (0, even) would be forbidden and the transitions to the first two excited states would be allowed if the spins and parities of the ground and first two excited states of Kr^{82} are 0, 2, 4 and even. For Br^{82}, on the other hand, the most likely configuration is $(p_{3/2}, g_{9/2})$ which would give a high spin and odd parity, explaining why no transitions to the lower excited states of Kr^{82} occur. The above configurations are in agreement with Nordheim's Rule.

5. EXPERIMENTS ON Rb^{84}

The beta-ray spectrum of Rb^{84} was measured both in a 180° spectrometer and in a magnetic lens spectrometer. The results in the two cases are essentially in agreement. The experiments using the 180° spectrometer assured, of course, that positrons were being

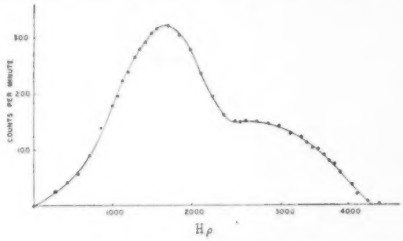

FIG. 6. Positron spectrum of Rb^{84}.

measured. The magnetic lens was used without a separating baffle.

The spectrum obtained using the lens spectrometer is shown in Fig. 6. A Fermi plot of the data is shown in Fig. 7. It will be seen at once that the high energy group of positrons has a forbidden shape. Applying the shape corrections for a transition of the type $\Delta j = \pm 2$ yes, a straight line Fermi plot was obtained. The spectrum could then be analyzed into three groups as shown in Table III. The lowest energy group is quite weak and may not be real. It is to be noted that the value of log$(W_0^2-1)ft$ for the highest energy group is in accord with the usual values obtained for transitions of the type $\Delta j = \pm 2$, yes.

Since the sources used were too weak to allow one to measure gamma-rays in a magnetic spectrograph, internal conversion electrons were sought in the 180° spectrometer and a gamma-ray was also found using a scintillation spectrometer. The electron spectrum as measured in the 180° spectrometer showed a weak internal conversion line corresponding to a gamma-ray of energy 0.890 Mev.

A careful search was made using a scintillation counter with a NaI(Tl) crystal. A gamma-ray, whose energy is 0.890 Mev, was found. No other gamma-rays, except a line at 0.510 Mev corresponding to annihilation radiation, were found.

In order to see whether or not the most energetic group of positrons goes to the ground state, the usual type of coincidence experiment was performed. A source was set up between two counters, one to measure gamma-rays and the other, an end-window counter, to measure positrons. With enough aluminum between both counters to stop all positrons, a gamma-gamma coincidence background was obtained. This, of course, included coincidences due to annihilation radiation. The positron-gamma coincidence rate was then measured as a function of the thickness of aluminum absorber. These measurements were corrected for chance,

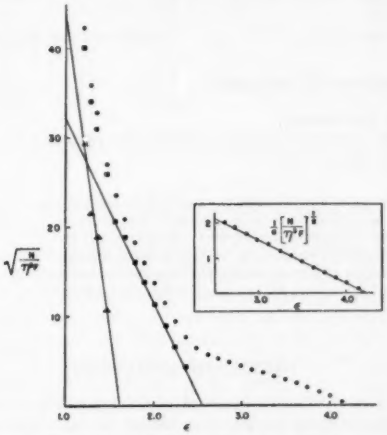

FIG. 7. Fermi plot for positrons from Rb^{84}.

cosmic-ray, and gamma-gamma coincidences. The results are shown in Fig. 8, in which the number of positron-gamma coincidences per recorded positron ($N_{\beta\gamma}/N_\beta \times 10^3$) is plotted against absorber thickness. There are no coincidences beyond 0.1 cm Al absorber (0.750 Mev), indicating that the highest energy group goes to the ground state. Coincidences are found for positrons of energies less than approximately 0.750 Mev, showing that the second group of positrons is followed by the emission of a gamma-ray.

Since Rb^{84} lies between two stable nuclides—Kr^{84} and Sr^{84}—it is possible that Rb^{84} also decays by electron emission. The experiments with the 180° spectrometer showed that there was a small background of electrons, which was only a few counts per minute above the background. If there is a group of electrons its intensity must be extremely small.

These experiments on Rb^{84} show that it disintegrates with the emission of three groups of positrons. The

TABLE III. Positron spectrum of Rb^{84}.

E_{Mev}	Abundance percent	logft	log$(W_0^2-1)ft$
1.629±0.005	39	9.24	10.44
0.822±0.05	58	8.15	—
0.373±0.05	3	8.87	—

highest energy group goes to the ground state and has a forbidden shape characteristic of a once forbidden spectrum with $\Delta j = \pm 2$. The second group goes to a state at 0.890 Mev above the ground state and is followed by the emission of a gamma-ray. The third group is extremely weak and no gamma-ray corresponding to transitions to the ground state has been found.

The results of this investigation are embodied in the decay scheme shown in Fig. 9, and it is of interest to discuss this scheme in the light of theoretical predictions. The shell model would predict the configuration

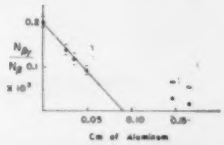

FIG. 8. Positron-gamma coincidences in Rb^{84}.

$(f_{5/2}, p_{1/2})$ or $(f_{5/2}, g_{9/2})$ for the ground state of $_{37}Rb_{47}^{84}$. Since the ground state of Kr^{84} has zero spin and even parity and since the positron transition from Rb^{84} to this state corresponds to $\Delta j = 2$ and a change of parity, it follows that the ground state of Rb^{84} has spin 2 and odd parity. This suggests the configuration $(f_{5/2}, g_{9/2})$ for the ground state of Rb^{84}. The second positron transition has an allowed shape and a value of logft = 8.2. This suggests that the transition is $\Delta j = 0$, yes, which would make the first excited state have spin 2

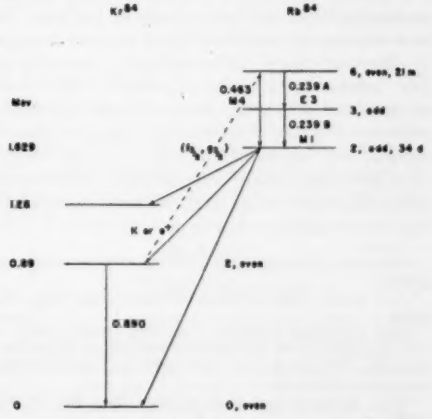

FIG. 9. Energy levels of Kr^{84}. Energies are in Mev.

and even parity. Flammersfeld[8] has shown that there is an excited state of Rb^{84} having a half-life of 23 min and emitting internal conversion electrons whose energy is approximately 0.320 Mev. Recent experiments in this laboratory[9] have delineated the excited states of Rb^{84} more exactly. The results of this investigation are shown for completeness in Fig. 9. The governing metastable state was found to have a half-life of 21 min.

It appeared difficult to reconcile the original decay scheme of Langer and Duffield[7] for Br^{84} with that proposed here for Rb^{84}. When the results of the present experiments became known, Dr. Langer and Dr. Duffield[10] measured the gamma-rays from Rb^{84} with the help of a scintillation spectrometer. Their results show a strong gamma-ray of energy 0.890 Mev and a weaker one of energy 1.89 Mev. It is now believed that the original decay scheme was incomplete and that the highest energy beta-ray group does not lead to the ground state, as originally supposed, but to an excited state from which the gamma-ray at 0.890 Mev is emitted.

The authors are indebted to Dr. M. B. Sampson and the cyclotron group for making the bombardments. They wish to thank Dr. R. G. Wilkinson for making the measurements on the 180° spectrometer and Mr. R. S. Caird for making the measurements with the scintillation spectrometer. They are indebted to Mr. Arthur Lessor for making the chemical separations.

[8] A. Flammersfeld, Z. Naturforsch. **5a**, 687 (1950).
[9] R. S. Caird and A. C. G. Mitchell (to be published).
[10] The authors are indebted to Dr. L. M. Langer for communicating to them the results of their experiments.

PHYSICAL REVIEW VOLUME 88, NUMBER 6 DECEMBER 15, 1952

Total Neutron Cross Section of Sodium*

P. H. STELSON† AND W. M. PRESTON‡
Laboratory for Nuclear Science and Engineering, Massachusetts Institute of Technology, Cambridge, Massachusetts
(Received July 2, 1952)

The total neutron cross section of sodium has been measured over the energy range 120 to 1000 kev using resolutions of 2.5 to 5 kev. A number of resonances, corresponding to excited states in the compound nucleus Na^{24} were investigated. In some cases it is possible to assign J and l values and to compute the effective level spacings $D_J{}^l$. Evidence is given to show that the $D_J{}^l$, which are a measure of the complexity of a state, differ by a factor of 8 for two states of the same type and at approximately the same excitation energy (7.5 Mev) in the Na^{24} nucleus. An anomalous S-wave resonance at 300 kev suggests that the potential scattering may be spin dependent.

INTRODUCTION

THE recent good resolution work on the $Na^{23}(d,p)Na^{24}$ reaction by Sperduto *et al.*[1] gives a detailed picture of the level structure of the Na^{24} nucleus up to an excitation energy of 4.6 Mev. The level structure at somewhat higher excitation energies (7.0 Mev and above) can be studied by measuring the total neutron cross section of sodium. Adair *et al.*[2] measured this cross section from 40 to 1000 kev using a resolution of 20 kev. Although they found a number of maxima, they concluded that their resolution was not adequate for any detailed interpretation. To learn more concerning these virtual levels we have measured the cross section using resolutions of 2.5 to 5 kev.

EXPERIMENTAL METHOD

The experimental procedure for measuring the total neutron cross section was similar to that previously described.[3] Monoenergetic neutrons were produced by allowing protons of well-defined energy from the Rockefeller electrostatic generator to strike thin targets of lithium. The original proton-recoil counter was replaced by a new counter with an o.d. of 1 inch, effective length of 4 inches and 2-mil center wire, filled to 5 atmospheres of hydrogen gas and operated with 3.5 kev on the center wire. This counter was approximately twice as efficient and had a better signal-to-noise ratio. The ambiguity caused by the presence of the second group of neutrons from the $Li(p,n)$ reaction at energies above 640 kev was removed, as before, by adjusting the bias to make the counter insensitive to the lower energy group.

A metallic sodium scatterer, one inch in diameter and 0.186×10^{24} nuclei/cm² thick, was encased in a thin-walled (5 mil), air-tight steel cylinder. The scatterer and counter were placed at mean distances of 13 and 30 cm, respectively, from the target in the forward

* This work was jointly supported by the ONR and the Bureau of Ships.
† Now at Oak Ridge National Laboratory, Oak Ridge, Tennessee.
‡ Now at Harvard University, Cambridge, Massachusetts.
[1] A. Sperduto and W. W. Buechner, Massachusetts Institute of Technology Progress Report LNSE (1952) (unpublished); Phys. Rev. (to be published).
[2] Adair, Barschall, Bockelman, and Sala, Phys. Rev. **75**, 1124 (1949).
[3] Hinchey, Stelson, and Preston, Phys. Rev. **86**, 483 (1952).

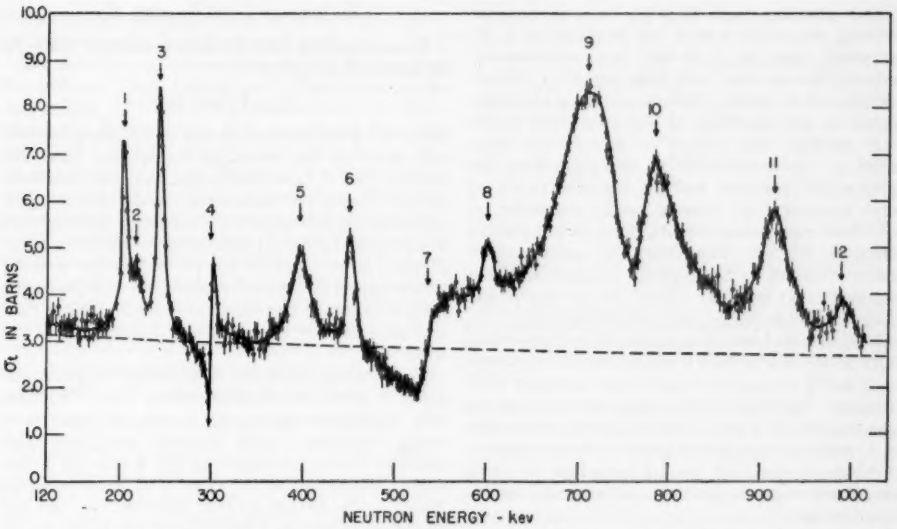

FIG. 1. Total neutron cross section of sodium. The dashed curve is the calculated potential scattering for an interactive radius of 5.1×10^{-13} cm.

direction. With this geometry, the scattering-in correction to the cross section is calculated to be approximately $7.0\times10^{-3}g\sigma$ barn, where σ is the cross section and g is the ratio of the differential scattering cross section in the forward direction to the average value. The value of g, although unknown, should not differ markedly from unity. The correction is therefore of the order of one percent. We have not applied the scattering-in correction since it is not precisely calculable and since it is less than the statistical error.

For total neutron cross section measurements, the energy resolution depends on the energy spread of the incident protons, the target thickness, and the angle subtended by the neutron detector. For our experimental arrangement, with resolutions of 2.5 to 5 kev, the principal contribution to energy spread is the target thickness. The target thickness was determined by measuring the sharp resonance at 585 kev in the total neutron cross section of sulfur.[4, 5]

The resulting curve of the total neutron cross section of sodium for the neutron energy range 120 to 1000 kev is shown in Fig. 1. In this energy range 12 resonances were observed. Not all of the experimental data are shown in Fig. 1; the resonances in the range 120 to 500 kev were measured several times. Data for each resonance have been listed in Table I. Column 2 gives the resonance energies in the laboratory system, corrected for target thickness. In the case of S-wave resonances, where the position of the maxima is shifted appreciably by interference with potential scattering, the resonance energy was determined by fitting a theoretical curve.

Columns 3, 4, and 5 give, respectively, Δ, the resolution with which the resonance was measured; Γ_M, the measured width; and Γ, the natural width calculated from the relation $\Gamma^2=\Gamma_m^2-\Delta^2$. This does not apply to resonance 4, a narrow S-wave resonance, which is discussed below.

In column 6 we list the experimentally determined values of the cross section for the resonances. In the case of resonances excited by S-wave neutrons, this is taken as the difference between the maximum and minimum values. For other resonances the value is taken as the height of the maximum value of σ_T above the estimated "background" level. Column 7 lists the values obtained after corrections have been applied to take account of the finite value of the resolution employed.

DISCUSSION

A. J Value Assignments

When the predominant interaction of neutrons with the nucleus is elastic scattering, a comparison of the measured value of the total resonance cross section with the predictions of theory permits the assignment of total angular momentum J. If the possibility exists

[4] Peterson, Barschall, and Bockelman, Phys. Rev. **79**, 593 (1950).

[5] If the measured width of the sulfur resonance is Γ_M, then $\Delta E_n=(\Gamma_m^2-\Gamma^2)^{\frac{1}{2}}$ where we take $\Gamma=1.5$ kev. From ΔE_n we calculate ΔE_p. From the knowledge of the variation of stopping power we obtain ΔE_p at other proton energies and then convert to ΔE_n, the resolution at corresponding neutron energies.

of other processes, such as (n,p), (n,α) or inelastic scattering, only a lower limit can be placed on J. In the present case, the (n,p) and (n,α) reactions are eliminated because they have large negative Q values. A decision as to whether inelastic scattering can occur depends on the knowledge of low-lying levels in the target nucleus. This region of sodium has been studied by the measurement of α-particles from the $Mg^{25}(d,\alpha)Na^{23}$ reaction[6] and by the observation of γ-rays resulting from inelastic proton scattering on Na^{23}.[7] Both experiments indicate a first excited state in sodium at 430 kev. This limits the assignment of definite J values to the first six resonances. These assignments are listed in column 9; the theoretical values of the cross section are given in column 8.

The agreement between experimental and theoretical values of the cross section is reasonable for resonances 1, 2, 4, and 6. Resonances 3 and 5 show unusually poor agreement. The experimental value for No. 3 is 1.5 barns high for $J=1$ and 1.3 barns low for $J=2$, while No. 5, which is a fairly broad symmetrical resonance, is 0.6 barn low for $J=1$ but 1.2 barns high for $J=0$. The differences are larger than our estimated experimental errors.

The computed values of the cross section for the case of purely elastic scattering are listed also for resonances 7 to 12. Since these resonances can give rise to inelastic scattering, the values serve only as lower limits for J. For example, resonance No. 11 has a measured cross section of 2.3 barns, indicating that J is at least 3. If No. 9 is a single resonance, the J value must be at least 5 which would require excitation by neutrons with 3 or more units of orbital angular momentum. It is probable that this peak is, instead, a superposition of at least two noninterfering states (i.e., states of different J or parity).

TABLE I. Summary of data relating to the neutron resonances in the total cross section of sodium. Energies are expressed in kev and cross sections in barns. Column 2 gives the resonance energies in the laboratory system. Columns 3, 4, and 5 give, respectively, Δ, the resolution with which the resonance was measured; Γ_M, the measured width; and Γ, the natural width. Column 6 lists the measured resonance cross sections; column 7, the cross section after applying corrections for resolution. Column 8 lists the theoretical values of the cross section for the corresponding J values listed in column 9. Column 11 lists the calculated values of $D_J{}^l$ for the corresponding values of l listed in column 10.

No.	$(E_R)_{lab}$	Δ	Γ_M	Γ	σ	σ^*	σ_{cal}	J	l	$D_J{}^l$
1	204	4.1	6.5	5	3.9	5.2	5.22	1	1	450
2	217	4.0	~14	~14	~1.3	~1.3	1.63	0	1	1150
3	243	3.8	8	7	5.0	5.9	4.38	1	1	480
							7.32	2		
4	297	3.6		4	3.4		3.57	1	0	67
		2.4		4	3.5					
5	396	~5	23	23	2.0	2.1	2.69	1	1	950
6	451	~5	10	9	2.2	2.5	2.37	1	1	320
									2	4000
7	542	~5		39	2.1		(2.0)	(1)	(0)	(520)
8	602	~5	~8	~6	1.1	1.4	(1.8)	(1)		
9	710	~5		72	~5.3		(5.5)	(5)		
10	784	~5		38	~2.6		(2.3)	(2)		
							(3.1)	(3)		
11	914	~5		36	~2.5		(2.7)	(3)		
12	988	~5		24	~1.0		(1.0)	(1)		

[6] Endt, Haffner, and Van Patter, Phys. Rev. **86**, 518 (1952).
[7] Stelson, Preston, and Goodman, Phys. Rev. **86**, 629 (1952).

B. Average Level Spacing, $D_J{}^l$

Theory suggests that the natural neutron width Γ_n be expressed as a product:

$$\Gamma_n = T_n{}^l D_J{}^l/2\pi,$$

where $T_n{}^l$ is the probability that the incoming neutron will penetrate the centrifugal barrier and enter the nucleus. The $T_n{}^l$ are readily calculable and, therefore, if the l value of the neutrons producing the excitation is known, one can compute the interesting quantity $D_J{}^l$. The reciprocal of $D_J{}^l$ is a measure of the inherent nuclear lifetime; large values of $D_J{}^l$ (~25 Mev for sodium) would suggest an interaction similar to a simple single-body interaction. The degree to which $D_J{}^l$ is less than this large value is a measure of the complexity of the state.

The potential scattering in the energy range investigated is small for neutrons having $l \geqslant 1$. Therefore, only resonances excited by S-wave neutrons show strong interference with potential scattering. This identifies the narrow resonance No. 4 as an $l=0$ resonance. The computed $D_J{}^l$ value is 67 kev. Resonance No. 7 is also excited by $l=0$ neutrons, but here the resonance energy is a little above the threshold for inelastic scattering. On the basis of purely elastic scattering, the two possible values for the resonance cross section are 1.92 and 3.18 barns for $J=1$ and 2, respectively. If the resonance were $J=2$, fairly strong inelastic scattering would be required to reduce the cross section to the experimental value of 2.1 barns. For this resonance, strong inelastic scattering is quite unlikely since the inelastic neutrons, having only 90 kev and an unknown l value, must compete with the outgoing elastic neutrons of 520 kev and $l=0$. On the other hand, the experimental value of 2.1 barns agrees reasonably well with the $J=1$ value for purely elastic scattering. If this interpretation is correct, i.e., that the resonance is mainly an elastic scattering resonance, we obtain a $D_J{}^l$ value of 520 kev. We have, then, evidence that in the Na^{24} nucleus at approximately the same excitation energy (7.5 Mev), two levels of the same type ($J=1$ and even parity) can differ in $D_J{}^l$ values by a factor of 8.

The resonances 1, 2, 3, 5, and 6 do not exhibit appreciable interference with the potential scattering, indicating that the excitation is by neutrons with l values larger than zero. For these resonances there is no straightforward method of determining the l value. Hence, the $D_J{}^l$ values are somewhat speculative. In addition, even if the l values were definitely known, the D_J cannot be as precisely determined as one proceeds to larger l values because the $T_n{}^l$ become increasingly sensitive to the value of the interaction radius R about which there is considerable uncertainty. For our calculations of the $T_n{}^l$ we have chosen $R=5.1\times10^{-13}$ cm. This is approximately midway between the values given by the expressions $1.5\times10^{-13}A^{\frac{1}{3}}$ and $1.5\times10^{-13}[A^{\frac{1}{3}}+1]$.

The calculated potential scattering for $R=5.1\times10^{-13}$ cm is shown in Fig. 1 by the dashed curve.

The possibility of resonance excitation by neutrons with sufficiently large l values can be eliminated because the resulting $D_J{}^l$ values are impossibly large, i.e., they exceed the Wigner limit. If it is assumed that the resonances 1, 2, 3, and 5 are excited by $l=2$ neutrons, the calculated $D_J{}^l$ (15 to 40 Mev) are approximately equal to the Wigner limit. Although not definitely excluded, such large D_J values seem unlikely, especially in view of the two $D_J{}^l$ values derived from the $l=0$ resonances, and we have therefore assigned $l=1$ to these resonances. However, one should be cautious with this argument as it may lead to an artificial uniformity in $D_J{}^l$. Resonance 6 yields $D_J{}^l$ values of 320 kev or 4 Mev for $l=1$ or 2, and either assignment seems acceptable. The l assignments and corresponding $D_J{}^l$ for the resonances are listed in columns 10 and 11 of Table I.

C. Spin Dependent Potential Scattering

Although the resonance cross section of the narrow S resonance, No. 4, given by the difference $\sigma_{max}-\sigma_{min}$, agrees well with the theoretical value for $J=1$, the absolute values of the maximum and minimum cross sections are not in good agreement with theory. From the statistical theory we have the result that the depth of the minimum is a fraction g of the total potential scattering,[8] where g is the statistical weight factor $(2J+1)/2(2I+1)$. Enlarged plots of data taken with 3.6- and 2.4-kev resolutions are shown in Fig. 2. The dashed curves in the figure are calculated from the theory (for infinitely good resolution) where we have taken the natural width as 4.0 kev and the total potential scattering σ_P as 3.0 barns. It is seen that, even with the finite experimental resolutions, the interference dip has considerably more depth than predicted by theory.

On first thought one might be tempted to match the experimental value of σ_{min} by reducing the value of the total potential scattering; a reduction to 2.4 barns is required. There are two arguments against this. First, as is seen in Fig. 1, the larger value, calculated for an interaction radius of 5.1×10^{-13} cm, seems to be reasonable throughout the energy range measured. In addition, it is in good agreement with other experimental data at lower energies. Second, while reducing the value of σ_P to 2.4 barns yields the correct σ_{min}, the actual depth of the interference dip is predicted to be only 0.9 barns, which is considerably less than is indicated by the experimental curve.

A similar anomalous situation in sodium has been observed at lower neutron energies. Hibdon *et al.*[9] found a neutron scattering resonance at 3 kev, which has a resonance cross section of 550 barns ($J=2$) and a width of 170 ev. However, there is no discernible

[8] This is true only if, as in the present case, l values larger than zero are negligible contributions to the total potential scattering.

[9] Hibdon, Muehlhause, Selove, and Woolf, Phys. Rev. **77**, 730 (1950).

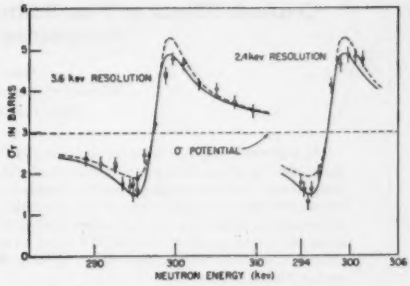

FIG. 2. Plots of data taken for the narrow S resonance, No. 4. The dashed and solid curves are calculated for the cases $\sigma_-/\sigma_+=1$ and $\sigma_-/\sigma_+=2$, respectively. The natural width and the total potential scattering are taken as 4.0 kev and 3.0 barns, respectively.

interference dip characteristic of $l=0$ excitation. Selove[10] has interpreted this as an indication that the S-wave potential scattering is strongly spin dependent. He finds $\sigma_-/\sigma_+=11$, where σ_+ and σ_- are the potential scattering cross sections for the $+$ and $-$ spin states. In this notation the total potential scattering σ_P equals $\frac{3}{4}\sigma_-+\frac{1}{4}\sigma_+$. This view also yields a consistent interpretation of the coherent scattering cross section of sodium measured by Shull and Wollan.[11,12]

Therefore, invoking spin dependent potential scattering to account for the unusually strong interaction of the S resonance at 300 kev, we have calculated the theoretical curve for the case $\sigma_-/\sigma_+=2.0$ (for infinitely good resolution) where, again, the natural width is taken as 4.0 kev and σ_P as 3.0 barns. These curves, giving a better fit, are shown in Fig. 2 by the solid line. However, even with the assumption of spin dependence, the actual shape of the experimental curve is not well represented by the calculated curve; the experimental points give a noticeably sharper interference dip.

The second S resonance, No. 7, gives a good fit with the assumption that the potential scattering is not dependent on the spin state. If these interpretations are correct, we have the result that the potential neutron scattering in sodium is strongly spin dependent at low energies, $\sigma_-/\sigma_+=11$ at 3 kev, reducing to a factor of 2.0 at 300 kev and becoming approximately 1 at 550 kev.

In conclusion we wish to express our appreciation to Mr. I. E. Slawson and Mr. D. C. Thompson for invaluable help with the Rockefeller generator.

[10] W. Selove, Phys. Rev. **80**, 290 (1950).

[11] C. G. Shull and E. O. Wollan, Phys. Rev. **81**, 527 (1951).

[12] The absence of a dip might also be explained by the assumption that even at this low neutron energy the excitation is due to P wave neutrons. In this connection it is interesting to calculate the $D_J{}^l$. Taking $R=5.1\times10^{-13}$ cm we find $D_J{}^l$ is 25 kev for S-wave and 6 Mev for P-wave neutrons. The 25-kev value is small, but it is not very different from the 67-kev value for resonance No. 4, while the 6-Mev value is large but certainly not impossibly large. The measurement of the angular distribution of the neutrons scattered by this resonance, if practicable, would probably decide the question of S-wave *vs* P-wave excitation.

Coulomb Effects in Pion Scattering by Protons under the Charge Independence Hypothesis*

LÉON VAN HOVE†
University of Rochester, Rochester, New York
(Received September 2, 1952)

The differential cross sections for scattering of charged π-mesons by protons, observed so far at energies and angles for which Coulomb effects are negligible, were found compatible with the assumption of charge independence for the nuclear interaction between pion and nucleon. For the future discussion of scattering experiments now being performed at lower energies, the Coulomb effects are calculated, retaining the charge independence hypothesis for the nuclear part of the interaction and describing it by the phase shifts used in the higher energy region. For 35-Mev pions, an estimate based on the known magnitude of the total π^+-p cross section shows the Coulomb effects to reach 50 percent for a scattering angle of the order of 50° in the center-of-mass system.

ALL the experimental data obtained so far on the scattering of π-mesons by protons were found compatible with the assumption of charge independence of the (nonelectromagnetic) pion-nucleon interaction, and could be analyzed in terms of six phase shifts corresponding to the states of total isotopic spins $T=\frac{1}{2}, \frac{3}{2}$ and angular momenta $s_{\frac{1}{2}}$, $p_{\frac{1}{2}}$, $p_{\frac{3}{2}}$.[1] These data refer to pion energies of the order of 100 Mev, for which the Coulomb forces between proton and charged pion have negligible effects at the observed scattering angles.

Since scattering experiments are now being performed at Rochester with pion energies of the order of 35 Mev, for which Coulomb effects are likely to be observable, these effects have been investigated, retaining the charge independence hypothesis for the nuclear part of the interaction and trying to describe it by the same six phase shifts mentioned above.

This description is possible under the reasonable assumption that the Coulomb energy may be neglected for any proton-pion separation r smaller than the range r_0 of the nuclear interaction (r_0 is of the order of the Compton wavelength of the pion). The wave function in the center-of-mass system, which is a Coulomb wave function for $r \geqq r_0$, has then to be continuously matched at $r=r_0$ to the wave function determined by the nuclear interaction for $r \leqq r_0$. At $r=r_0$, the latter wave function is completely expressible in terms of the phase shifts which would be produced by the nuclear interaction in the absence of Coulomb forces, i.e., the exact analogs of the phase shifts used in the analysis of the higher energy scattering experiments. We shall use six such phase shifts, corresponding to the isotopic spin and angular momentum states mentioned above, so that the matching of Coulomb and nuclear wave functions has to be performed for s- and p-waves only, whereas for higher l-values the nuclear interaction will be neglected and regular Coulomb wave functions can be used.

For each of the three types of scattering,

$$\pi^+ + p \to \pi^+ + p, \quad \pi^- + p \to \pi^- + p, \quad \pi^- + p \to \pi^0 + n,$$

the differential cross sections per steradian in the center-of-mass system, for scattering without and with nucleon spin flip, respectively, are found to have the form

$$\frac{d\sigma^{(nf)}}{d\Omega} = \frac{1}{4k^2}\left| -\frac{i\epsilon\alpha}{\sin^2(\theta/2)} \exp\left(-i\epsilon\alpha \log \sin^2\frac{\theta}{2}\right) + P + Q\cos\theta \right|^2, \quad (1)$$

$$\frac{d\sigma^{(f)}}{d\Omega} = \frac{1}{4k^2}|R|^2 \sin^2\theta. \quad (2)$$

θ is the scattering angle and hk the momentum in the center-of-mass system; $\alpha = mc^2/h^2k$, with ϵ the charge and m the reduced mass of pion and nucleon; ϵ is $+1$ for $\pi^+ + p \to \pi^+ + p$ scattering, -1 for $\pi^- + p \to \pi^- + p$ and 0 for $\pi^- + p \to \pi^0 + n$. P, Q, R are rather complicated expressions involving α and the six phase shifts which would be produced by the nuclear interaction in the absence of Coulomb forces. They are obtained as follows. Denote the latter phase shifts, for $T=\frac{1}{2}$, $\frac{3}{2}$, respectively, by η_1, η_3 for the $s_{\frac{1}{2}}$ wave, by η_{11}, η_{31} for the $p_{\frac{1}{2}}$-wave and by η_{13}, η_{33} for the $p_{\frac{3}{2}}$ wave. Consider the radial Schrödinger equation,

$$\frac{d^2u}{d\rho^2} + \left(1 - \frac{l(l+1)}{\rho^2} - \frac{2\epsilon\alpha}{\rho}\right)u = 0, \quad (\epsilon = \pm 1, 0; \rho = kr),$$

and denote by $u_\epsilon{}^l(\rho, \eta)$ its solution with asymptotic behavior ($\rho \gg 1$):[2]

$$u_\epsilon{}^l(\rho, \eta) \sim \sin\left(\rho - \frac{\pi}{2}l + \arg\Gamma(l+1+i\epsilon\alpha) + \eta - \epsilon\alpha \log 2\rho\right).$$

Starting from η_1 we define two phase shifts $\eta_1{}^+$, $\eta_1{}^-$

* This work was supported in part by the AEC.
† On leave from the Institute for Advanced Study, Princeton, New Jersey, during the summer of 1952.
[1] Anderson, Fermi, Long, and Nagle, Phys. Rev. **85**, 936 (1952); Anderson, Fermi, Nagle, and Yodh, Phys. Rev. **86**, 793 (1952); Fermi, Anderson, and Nagle (to be published) and private communication of E. Fermi to R. E. Marshak.
[2] N. F. Mott and H. S. W. Massey, *Theory of Atomic Collisions* (Oxford University Press, London, 1949), p. 53.

and two constants C_1^+, C_1^- by the equations

$$\left[\frac{d}{d\rho}\log u_{\pm 1}{}^0(\rho,\eta_1^{\pm})\right]_{\rho=kr_0}=\left[\frac{d}{d\rho}\log u_0{}^0(\rho,\eta_1)\right]_{\rho=kr_0};$$

$$C_1^{\pm}=\left[\frac{u_0{}^0(\rho,\eta_1)}{u_{\pm 1}{}^0(\rho,\eta_1^{\pm})}\right]_{\rho=kr_0}. \quad (3)$$

With η_3 we define similarly $\eta_3^{\pm}$ and $C_3^{\pm}$. Using $u_\epsilon{}^1(\rho,\eta)$ instead of $u_\epsilon{}^0(\rho,\eta)$, each p-phase shift $\eta_{\gamma\delta}$, $(\gamma,\delta=1,3)$ gives rise to $\eta_{\gamma\delta}^{\pm}$ and $C_{\gamma\delta}^{\pm}$. The quantities P, Q, R have then the following expressions:

For $\pi^+ + p \to \pi^+ + p$

$$P=\exp(2i\eta_3^+)-1,$$

$$Q=\frac{1+i\alpha}{1-i\alpha}[\exp(2i\eta_{31}^+)+2\exp(2i\eta_{33}^+)-3],$$

$$R=\exp(2i\eta_{33}^+)-\exp(2i\eta_{31}^+).$$

For $\pi^- + p \to \pi^- + p$

$$P=\zeta-1,\quad Q=\frac{1-i\alpha}{1+i\alpha}[\zeta_1+2\zeta_3-3],\quad R=\zeta_3-\zeta_1,$$

where

$$\zeta=\frac{2C_1^-\exp[i(\eta_1+\eta_1^-)]+C_3^-\exp[i(\eta_3+\eta_3^-)]}{2C_1^-\exp[i(\eta_1-\eta_1^-)]+C_3^-\exp[i(\eta_3-\eta_3^-)]}.$$

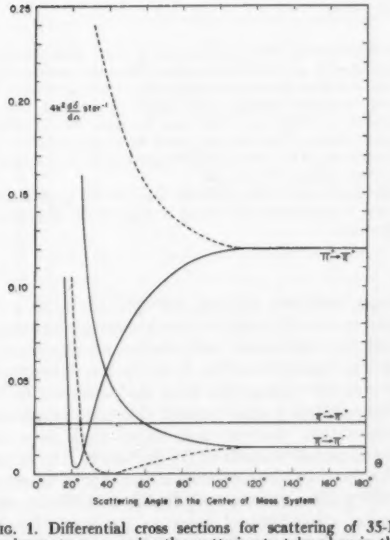

FIG. 1. Differential cross sections for scattering of 35-Mev pions by protons, assuming the scattering to take place in the $s_{\frac{1}{2}}$ state of isotopic spin $\frac{3}{2}$, with a phase shift of 10° (solid line) or −10° (dotted line).

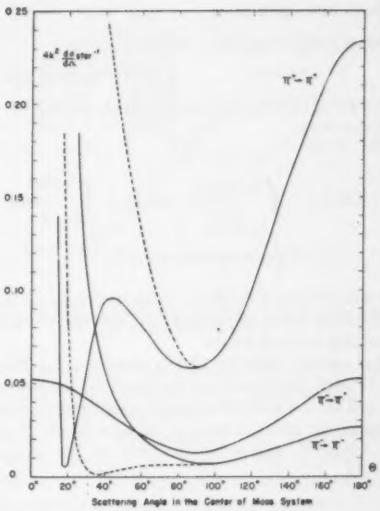

FIG. 2. Differential cross sections for scattering of 35-Mev pions by protons, assuming the scattering to take place in the $p_{\frac{1}{2}}$ state of isotopic spin $\frac{3}{2}$, with a phase shift of 7° (solid line) or −7° (dotted line).

ζ_1, ζ_3 are similar expressions with a second subscript 1,3, respectively, added in all C's and η's.

For $\pi^- + p \to \pi^0 + n$,

$$P=\chi,\quad Q=\left(\frac{1-i\alpha}{1+i\alpha}\right)^{\frac{1}{2}}[\chi_1+2\chi_3],\quad R=\chi_3-\chi_1,$$

with

$$\chi=\sqrt{2}\frac{\exp(2i\eta_3)-\exp(2i\eta_1)}{2C_1^-\exp[i(\eta_1-\eta_1^-)]+C_3^-\exp[i(\eta_3-\eta_3^-)]}.$$

χ_1 and χ_3 are again obtained by adding a second subscript, 1 and 3, respectively, in all C's and η's.

All foregoing formulas are nonrelativistic. If the proton were infinitely heavy compared to the pion, consideration of the Klein-Gordon equation shows that, apart from a negligible term containing the square of the Coulomb potential, the only relativistic corrections required would be to take for $\hbar k$ the relativistic momentum of the pion and to divide α by $(1-\beta^2)^{\frac{1}{2}}$, where βc is the relative velocity of proton and pion. In the absence of a conclusive treatment of relativistic two-body problems, it seems reasonable to apply similar corrections to our case: $\hbar k$ will be taken as the relativistic momentum of pion and nucleon in the center-of-mass system, and α will be divided by $(1-\beta^2)^{\frac{1}{2}}$, with βc the relative velocity of pion and proton.

Since in all practical cases one has $\alpha \ll 1$, a convenient way to treat Eq. (3) is by power expansion in α.[3] One

[3] The more conventional W. K. B. method is not well justified for the pion-proton separations and the energies here considered.

finds to first order in α,

$$\eta_1^{\pm}=\eta_1\pm\alpha[C+\log(2kr_0)-\mathrm{Ci}(2kr_0)\cos(2\eta_1)+\mathrm{si}(2kr_0)\sin(2\eta_1)], \quad (4)$$

$$C_1^{\pm}=1\mp\alpha[\mathrm{Ci}(2kr_0)\sin(2\eta_1)+\mathrm{si}(2kr_0)\cos(2\eta_1)] \quad (5)$$

with

$$\mathrm{Ci}(x)=-\int_x^{\infty}\frac{\cos x}{x}dx, \quad \mathrm{si}(x)=-\int_x^{\infty}\frac{\sin x}{x}dx,$$

$$C=\text{Euler's constant}=0.5772.$$

$\eta_3^{\pm}$ and $C_3^{\pm}$ have an identical expression in η_3. Similar expressions could be worked out for the η's and C's belonging to the p-waves.

For α of the order of 10^{-2} or smaller ($\alpha=1.25\times10^{-2}$ for 35 Mev pions) and not too small η_1, the α-terms in (4) and (5) are quite small and a good approximation is obtained by putting $\alpha=0$ in all expressions P, Q, R; the Coulomb effects reduce then to the α-term in Eq. (1).

To show the order of magnitude of the Coulomb effects for 35 Mev pions, the differential cross sections have been plotted for two choices of phase shifts: $\eta_3=\pm10°$, all other η's$=0$ (Fig. 1), and $\eta_{33}=\pm7°$, all other η's$=0$ (Fig. 2). These phase shifts correspond in each case to a total π^+ scattering cross section of the order of 18×10^{-27} cm^2, (in agreement with the data available so far).[4] The solid lines correspond to positive phase shifts, the dotted lines to negative ones. The difference between positive and negative phase shifts for $\pi^-\to\pi^0$ scattering at all angles and $\pi^-\to\pi^-$ or $\pi^+\to\pi^+$ scattering for $\theta>\pi/2$ is small and has been neglected. It is interesting to note that the effects are as large as 50 percent for θ below 50°, where θ is the scattering angle in the center-of-mass system.

A more detailed account of this work is available as a University of Rochester report (NYO-3223). The author wishes to thank Professor R. E. Marshak for suggesting this investigation and for many valuable discussions. He is indebted to Mr. R. Grover for computational help.

[4] Barnes, Clark, Perry, and Angell, Phys. Rev. **87**, 669 (1952).

PHYSICAL REVIEW VOLUME 88, NUMBER 6 DECEMBER 15, 1952

Disintegration Scheme of Fe^{59}†

FRANZ R. METZGER*
Physics Department, University of Illinois, Urbana, Illinois
(Received August 11, 1952)

The radiations accompanying the disintegration of Fe^{59} have been investigated using lens spectrometer and scintillation counter techniques. Three beta-ray spectra of end points 1560±8 kev (0.3 percent), 462±3 kev (53.9 percent), and 271±3 kev (45.8 percent) lead to the ground state, to 1098-kev and 1289-kev excited states of Co^{59}. The 1560-kev spectrum has a forbidden shape; the shapes of the other partial spectra are allowed. Gamma-rays of 191±2 kev (2.8 percent), 1098±6 kev (56.7 percent) and 1289±6 kev (43 percent) represent all the transitions possible between the three Co^{59}-states. The conversion coefficients characterize the 191-kev and the 1098-kev transitions as magnetic dipoles, the 1289-kev transition as electric quadrupole.

A disintegration scheme is presented in which spins and parities are assigned to all the levels involved. The single-particle orbitals corresponding to the assigned spins and parities agree with those of the spin-orbit coupling shell model. Accordingly, the first excited state (1098-kev) of Co^{59} is an $f_{5/2}$ state, and its 1098-kev energy difference from the $f_{7/2}$ gound state represents the spin-orbit splitting of the f-levels, which is responsible for the existence of a closed shell at N or $Z=28$.

The angular correlation of the 191 kev–1098 kev gamma-gamma cascade was measured and found to support the proposed spin assignment.

INTRODUCTION

THE radiations of 46-day Fe^{59} were studied by Deutsch and co-workers in 1942.[1] They analyzed the beta-ray spectrum into two components of approximately equal intensities with end points of 257 and 460 kev. They showed that the low energy beta-ray group is followed by a 1.30-Mev gamma-ray, the high energy group by a 1.10-Mev gamma-ray.

As the two high energy gamma-rays are not in coincidence with one another, Fe^{59} proved to be a very useful source with which to test gamma-gamma angular correlation equipment and similar arrangements for spurious coincidences due to scattering. When such a test was run without the usual lead absorbers in front of the counters, a small number of gamma-gamma coincidences was observed and traced back to a weak gamma-gamma cascade in the Fe^{59} decay, i.e., in Co^{59}.[2]

A subsequent investigation of the angular correlation in this gamma-gamma cascade did not allow an unambiguous assignment of spins to the levels involved. However, it was felt that most of the ambiguities could

† Supported in part by the joint program of the ONR and AEC.
* Now with the Bartol Research Foundation, Swarthmore, Pennsylvania.
[1] Deutsch, Downing, Elliott, Irvine, and Roberts, Phys. Rev. **62**, 3 (1942).
[2] F. R. Metzger, Phys. Rev. **85**, 727 (1952).

be eliminated by a study of the internal conversion of the gamma-rays and of the intensities of the beta-ray transitions. When, in the summer of 1951, high specific activity Fe^{59} became available through the radioisotopes program of the AEC, it was decided to reinvestigate the radiation emitted in the decay of Fe^{59}.

SOURCE MATERIAL

The first coincidence and scintillation spectrometer measurements[2] were carried out with low specific activity Fe^{59} (0.06 mC/g). All the experiments reported in this paper were performed with two shipments of high specific activity Fe^{59}, catalog item 26-PX of the Isotopes Division AEC. This Fe^{59} had been produced in a nuclear reactor by (n,γ)-reaction with enriched Fe^{58}.

Most of the final data were taken with a one millicurie shipment having a specific activity of 770 mC/g. This is to be compared with a specific activity of 1.3 mC/g available to Deutsch *et al.*[1]

COINCIDENCE EXPERIMENTS

Using NaI scintillation detectors in a coincidence arrangement of 10^{-7} seconds resolving time a small number of true gamma-gamma coincidences was observed in a Fe^{59} source. These coincidences were still present when two inches of lead separated the two counters; they therefore could not be attributed to Compton scattering from one counter to the other. The coincidence rate decreased with a half-life of 45 ± 3 days

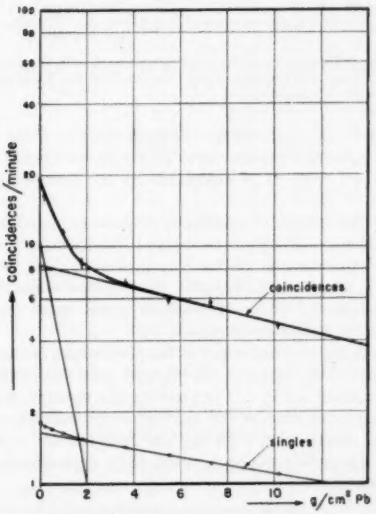

FIG. 1. Absorption of the γ-γ coincidences by lead absorbers in front of one counter. The absorption curve of the singles is included for comparison.

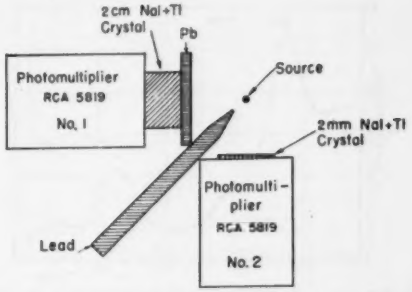

FIG. 2. Arrangement of the scintillation counters for the coincidence experiments.

which agrees with the half-life reported for Fe^{59},[3] indicating that a cascade in Co^{59} is the origin of these gamma-gamma coincidences.

Three g/cm² of lead in front of each counter reduced the single counting rates by about fifteen percent, but decreased the coincidence rate by a factor of thirty. This proves that one of coinciding components is a low energy gamma-ray.

The two coincident gamma-rays were clearly separated in a coincidence absorption experiment using lead absorbers in front of one of the two detectors. Figure 1 shows the coincidence absorption curve and its analysis into two components. The difference of the zero absorber values of the two components is due to a difference in the energy dependence of the detection efficiencies of the two scintillation detectors which differed somewhat in size and in the setting of the discriminators. From the absorption coefficient of the soft component one estimates a gamma-ray energy of about 200 kev. The absorption of the hard coincident gamma-ray follows closely the absorption of the bulk of the singles (Fig. 1). The slightly larger slope of the coincidence absorption curve is easily understood if one assumes that the 1.1-Mev gamma-ray is responsible for the coincidences, whereas a mixture of 1.1- and 1.3-Mev gamma-rays determines the absorption properties of the singles.

In order to determine the intensity of the 200-kev, 1.1-Mev cascade, coincidences were measured with the arrangement shown in Fig. 2. A NaI crystal, 2 cm thick and 3 cm in diameter with 5 g/cm² lead in front, detected the hard gamma-rays only. Another NaI crystal, No. 2, 2 mm thick and 3 cm in diameter, favored the soft gamma-ray.

The ratio of true coincidences to single counts in No. 1, N_{12}/N_1, is simply equal to $\alpha\cdot\omega_2\cdot\epsilon_2$, where α is the intensity of the cascade (per disintegration), $4\pi\omega_2$ is the solid angle in steradians subtended by the 2-mm crystal and ϵ_2 is the efficiency of the 2-mm crystal for

[3] See *Nuclear data*, National Bureau of Standards Circular No. 499 (1950), p. 52.

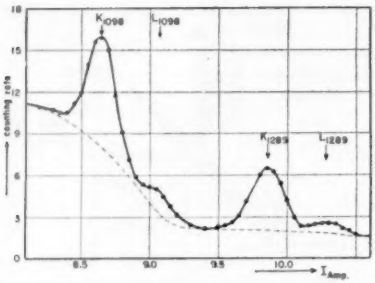

FIG. 3. Photoelectron spectrum of Fe^{59} using a gold converter. The dashed line represents the Compton background.

the detection of the 200-kev component. The measured values were $N_{12}=14.6$/min, $N_1=74{,}500$/min, $\omega_2=2.8\times10^{-5}$. For ϵ_2 we have used the value 0.25, which is close to the theoretical efficiency and in agreement with previous experience with this crystal. With these values one calculates $\alpha=(2.8\pm0.8)\times10^{-3}$. The error is tentative and mainly reflects the uncertainty in the efficiency value.

The above value of α is consistent with the analysis of a carefully measured singles absorption curve taking into account the energy dependence of the detection efficiency.

PHOTOELECTRON SPECTRUM

a. Energies of the Co^{59} Gamma-Rays

The spectrum of the electrons ejected by the Co^{59} gamma-rays from a 4.9 mg/cm² gold foil was measured in a lens spectrometer of 2.5 percent resolution and 0.5 percent transmission.

Superimposed on the Compton distribution, the photoelectron lines due to gamma-rays of 191 ± 2 kev, 1100 ± 6 kev, and 1287 ± 6 kev were identified. The spectrometer had been calibrated using the photoelectron lines of the 1172.9- and 1333.2-kev[4] Ni^{60} gamma-rays. If one accepts the 191-kev radiation as the transition between the 1287- and the 1100-kev levels, the best values for the energies of the Co^{59} gamma-rays are 191 ± 2, 1098 ± 6, and 1289 ± 6 kev.

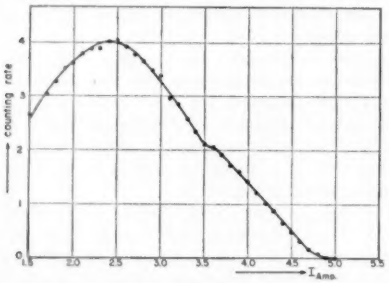

FIG. 4. β-ray spectrum of Fe^{59} in the energy region between 60 and 500 kev.

[4] Latest energy values according to a private communication from Professor Du Mond.

b. Intensity Ratio of the High Energy Gamma-Rays

The relative intensity of the 1.10- and 1.29-Mev gamma-rays is very important for the interpretation of the conversion data.

The intensity ratio can be inferred from the height of the photoelectron lines if the energy dependence of the gold converter efficiency is known. From previous experiments with gamma-rays above 550 kev the efficiency of our arrangement was known to be very nearly inversely proportional to the square of the gamma-ray energy. This was again checked using the two Ni^{60} gamma-rays, which have equal intensities for all practical purposes. With gold converter foils of thickness 25 mg/cm² and 4.9 mg/cm² a ratio of 1.29

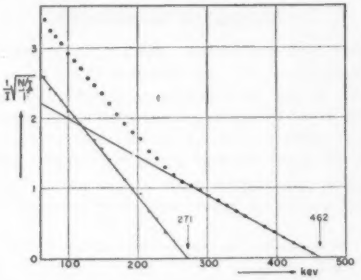

FIG. 5. Fermi plot of the β-ray spectrum of Fe^{59}. Circles represent the measured points, crosses the result of the subtraction of the 462-kev spectrum.

±0.05 was measured for the peak heights of the 1.17- and 1.33-Mev gamma-rays. This agrees with the ratio $(1.333/1.173)^2=1.29$ calculated by the inverse square law.

If the two Co^{59} gamma-rays were of equal intensities, one would expect a ratio $(1.289/1.098)^2=1.38$ for the photoelectron peaks. The measured peak heights are in a ratio of 1.78 ± 0.08. The 1.1-Mev transition is therefore $1.78/1.38=1.29\pm0.06$ times more intense than the 1.29-Mev transition.

A typical measurement of the photopeaks of the Co^{59} gamma-rays, using a 25-mg/cm² gold converter, is reproduced in Fig. 3. The presence of a strong Compton background renders the analysis more difficult. However, checks with a 4.9 mg/cm² gold foil and without any foil permit the background to be determined quite accurately.

THE BETA-RAY SPECTRUM

Beta-ray sources of one-quarter inch diameter were prepared by drying a drop of $FeCl_3$ solution on a Nylon-

Zapon film of approximately 20μg/cm^2. The beta-ray spectrum was then investigated in the lens spectrometer using a 195-μg/cm^2 window on the Geiger counter.

a. The Major Intensity Partial Beta-Ray Spectra

Figure 4 gives the beta-ray spectrum obtained with a source of about 3 μC strength. The break at 3.6 amp (277 kev) is rather pronounced and indicates the existence of two partial spectra. This is in agreement with Deutsch *et al.*,[1] but is contrary to the result of Mann and Hanson.[6] The Fermi plot, Fig. 5, shows the decomposition very clearly and yields for the end point energies 462±3 kev and 271±3 kev.

From a measurement of the areas under the two partial spectra it follows that 55 percent of the Fe^{59} disintegrations proceed via the 462-kev spectrum, whereas 45 percent take place through the 271-kev branch.

Preliminary experiments with sources of low specific activity had indicated the large influence of scattering, i.e., source thickness on the measured branching ratio. In order to estimate the magnitude of this effect, the beta-ray spectrum was measured with three sources of 3, 8 and 30 μC. The relative strengths of these sources had been determined to better than one percent by gamma-ray counting with a scintillation counter. Using the gamma-ray values for the relative strengths the measured counting rates were normalized to the same source strength and plotted in Fig. 6. The agreement of the three-spectra is very satisfactory in the upper part of the spectrum. The Fermi plot for the 462-kev spectrum, which is assumed to have an allowed shape below 271 kev, is therefore practically identical for all three sources. The contribution from the scattering is very substantial in the lower parts of the spectrum, especially for the 30 μC source. Consequently the Fermi plot of the 271-kev partial spectrum will strongly depend on the source thickness, as also will the intensity attributed to the 271-kev branch.

From the data of Fig. 6 it was estimated that the error in the area of the 271-kev spectrum due to scattering in the sources was between one and two percent for the 3 μC source. This correction has already been taken into account in the intensities stated earlier.

Using a half-life of 46 days and a 45 to 55 intensity ratio one calculates logft values of 5.9 for the 271-kev spectrum and of 6.7 for the 462-kev branch. The implications of these ft values will be discussed later.

b. Low Intensity, High Energy Beta-Ray Spectrum

With the 3 μC source the counting rates at energies higher than 480 kev did not vary by more than a few counts per minute. However, when a 100 μC source was used for the investigation of the conversion lines of the high energy gamma-rays, the counting rate above 480 kev was considerably larger than the background rate expected for a source of this strength. With a Co^{60} source of comparable strength and of comparable specific activity, the normal background counting rate was observed. The different behavior of the two sources is illustrated in Fig. 7. The counting rate at 12.5 amperes has been subtracted from all the measured points as normal background. The plateau-like regions to the left of the conversion peaks are due to Compton effect in the sources themselves. For the Co^{60} source the counting rate drops to zero in the region between the two conversion lines, whereas for the Fe^{59} source a residual counting rate of about 50 counts/minute is observed.

From the evidence summarized in Fig. 7 it is concluded that a high energy beta-ray spectrum is connected with the decay of Fe^{59}. Visual inspection suggests for the end point of this spectrum a current value of about 12 amperes, which corresponds to 1554 kev. This energy is very close to the total energy available for the $Fe^{59}-Co^{59}$ decay, namely, 462+1098=1560 kev. The high energy beta-ray spectrum is therefore considered to be the transition to the gound state of Co^{59}.

With the use of a 0.5 mC beta-source, the high energy

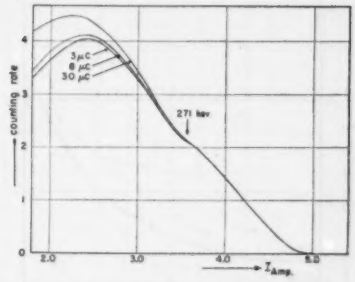

FIG. 6. The influence of source thickness on the shape of the β-ray spectrum of Fe^{59}. The three curves were normalized to the same source strength.

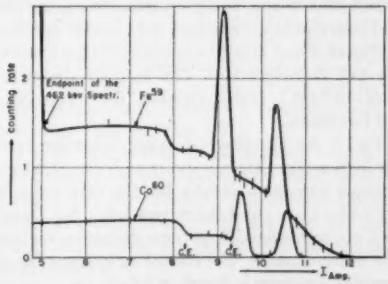

FIG. 7. High energy portion of the electron spectra of Fe^{59} and Co^{60}. Arrows indicate the maximum energies of the Compton electrons due to the Ni^{60} γ-rays.

[6] K. C. Mann and G. H. Hanson, Phys. Rev. **83**, 893 (1951).

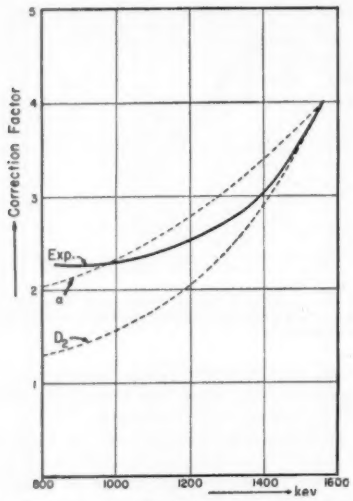

FIG. 8. Correction factors for Fe^{59} electrons. The full line represents the experimental correction factor for the 1560-kev spectrum. The dashed lines correspond to the unique correction factors for α-type ($\Delta I=2$, yes) and D_2 type ($\Delta I=3$, no) transitions. Ordinate scale is arbitrary.

spectrum was investigated in great detail. Unfortunately, only the regions from 1150 to 1210 kev and from 1340 kev to the end point are accessable and free from special corrections. In the upper third of the spectrum the conversion lines cover an appreciable portion of the beta-ray spectrum. Below 1100 kev (9.15 amp) the determination of the spectral shape is rendered uncertain by the presence of Compton electrons ejected out of the source material by the high energy gamma-rays. This effect was corrected for by using the shape of the distribution of Compton electrons suggested by the Co^{60} data of Fig. 7.

The Fermi plot obtained after applying all the necessary corrections indicated that the 1560-kev spectrum has a forbidden shape. Using a reasonable continuation of the Fermi plot to low energies, the 1560-kev spectrum was integrated and found to comprise 0.3 ± 0.1 percent of the Fe^{59} disintegrations. This intensity leads to a $\log ft$ of 10.9 ± 0.2, which classifies the transition as second forbidden.

In Fig. 8 the experimental shape correction factor for the high energy beta-ray spectrum is compared with the unique correction factors for the first forbidden α-type ($\Delta I=2$, yes) and the second forbidden D_2 type ($\Delta I=3$, no) transitions. Both these shapes are excluded by the measurements. The correct assignment for the high energy spectrum is therefore $\Delta I=2$, no.

The shell model assignment $f_{7/2}$ to the ground state of Co^{59} is in agreement with the measured spin and the new value for the magnetic dipole moment[6] of this nucleus. The character of the high energy beta-ray spectrum then determines the spin and parity of the Fe^{59} ground state as $\frac{3}{2}$, odd. A $p_{3/2}$ ground state for Fe^{59} with 33 neutrons is in accordance with the $p_{3/2}$ assignment for $_{33}As^{75}$ and for most of the nuclei with N or Z equal to 29, 31, 33, and 35.

It should be added that $h_{11/2}$ is another assignment for the ground state of Fe^{59} which is consistent with the existence of the high energy beta-ray spectrum. However, spins as high as 11/2 seem to occur only for much larger values of Z and N and even then only for excited states.

The results reported in this section are summarized in Table I.

CONVERSION ELECTRON SPECTRUM

a. Conversion of the 1.1- and 1.29-Mev Gamma-Rays

The theoretical K-conversion coefficients[7] for 1.1- and 1.29-Mev gamma-rays and different multipole orders are summarized in Table II.

$E2$ and $M1$, which do not involve a parity change, are with respect to their conversion, not only clearly separated from $E3$ or $M2$, but also from $E1$, which demands a parity change. Moderately accurate conversion data can therefore decide whether or not the high energy transitions in Co^{59} involve parity changes and they might also give some indication as to the electric or magnetic character of the transitions.

The same 0.5 mC source which had served in the investigation of the high energy beta-ray spectrum was used for the conversion measurements. The existence of the high energy spectrum and the presence of the "Compton step" due to the 1.29-Mev gamma-ray rendered the determination of the conversion line intensities more difficult. The best data obtained are presented in Fig. 9. From a comparison of peak heights as well as areas a value of 1.79 ± 0.06 was obtained for the relative number of 1.1- and 1.3-Mev conversion electrons.

In order to determine the conversion coefficients of the two transitions, the number of conversion electrons must be compared with the number of unconverted

TABLE I. Properties of the partial beta-ray spectra of Fe^{59}. "Allowed" f-values have been used throughout.

Endpoint energy (kev)	Intensity (percent of disint.)	$\log ft$	Shape
271 ± 3	44.9 ± 2	5.9	allowed
462 ± 3	54.8 ± 2	6.7	allowed
1560 ± 8	0.3 ± 0.1	10.9	forbidden $\neq\alpha$, $\neq D_2$

[6] W. G. Proctor and F. C. Yu, Phys. Rev. 77, 716 (1950).
[7] Rose, Goertzel, and Perry, Oak Ridge National Laboratory Report, ORNL 1023 (unpublished).

gamma-rays. In view of the very small conversion the number of unconverted gamma-rays is practically the same as the number of transitions. The combined intensities of the two gamma-transitions equals the combined intensities of the 271-kev and 462-kev beta-ray spectra. The 1.1-Mev transition is fed by the 462-kev beta-ray spectrum and by the 2.8 percent abundant 191-kev gamma-ray. The number of 1.29-Mev transitions is equal to the number of 271-kev beta-transitions reduced by the number of 191-kev gamma-rays. Using the beta-ray intensities of Table I, the 1.1-Mev transitions thus comprise $54.8+2.8=57.6$ percent of all Fe^{59} disintegrations, whereas the 1.29-Mev transitions comprise $44.9-2.8=42.1$ percent. The relative intensity of the two high energy transitions is therefore $57.6/42.1=1.37\pm0.09$. From the analysis of the photoelectron spectrum a ratio of 1.29 ± 0.06 was derived. The average is 1.32 ± 0.05. This corresponds to 56.7 percent 1.1-Mev transitions and 43 percent 1.29-Mev transitions. The conversion coefficient of the 1.1-Mev transitions is then obtained by dividing the number of 1.1-Mev conversion electrons by 56.7 percent of the total number of beta-rays. Likewise the conversion coefficient of the 1.29-Mev transition is obtained by dividing the corresponding number of conversion electrons by 43 percent of the total number of beta-rays.

The total area under the beta-ray spectrum of the 0.5 mC source could not be determined directly as the counting rates in the main spectrum were too high and in addition the source was rather thick. On the other hand, the beta-ray spectrum of the 3 μC source had been carefully investigated and the total area under the beta-ray spectrum had been determined. It was therefore only necessary to compare the strengths of the two sources by gamma-ray counting. This was done with the help of a third source of intermediate strength.

Combining all of this information the following total conversion coefficients were obtained:

$$\alpha_{\text{total}}(1.1\text{ Mev})=(18.3\pm0.7)\times10^{-5},$$
$$\alpha_{\text{total}}(1.29\text{ Mev})=(13.5\pm0.6)\times10^{-5}.$$

If a K/L ratio of 10 and an L/M ratio of 3 are assumed, the K-conversion coefficients become

$$\alpha_K(1.1\text{ Mev})=(16.1\pm0.6)\times10^{-5},$$
$$\alpha_K(1.29\text{ Mev})=(11.9\pm0.6)\times10^{-5}.$$

Comparing these values with the theoretical coefficients of Table II, one can immediately exclude $E1$, $M2$, $E3$, and $M3$ for both gamma-rays, leaving $M1$ and $E2$ as the only alternatives. Neither $M1$ nor $E2$ involve a change of parity. The $f_{7/2}$ ground state of Co^{59} and the 1.1-Mev and 1.29-Mev excited states have therefore all the same parity, namely, odd. Spin $\frac{1}{2}$ is excluded for either excited state of Co^{59}, because $E3$ and $M3$ are ruled out.

TABLE II. K-conversion coefficients of the high energy Co^{59} gamma-rays for different multipole orders (according to Rose *et al.*, reference 7).

	$E1$	$E2$	$E3$	$M1$	$M2$	$M3$
$10^5\times\alpha_K$(1.1 Mev)	6.7	16.2	33.0	14.9	31.0	60.0
$10^5\times\alpha_K$(1.29 Mev)	5.5	11.2	20.7	10.1	20.1	37.5

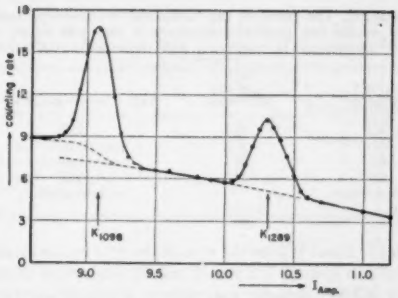

FIG. 9. Electron spectrum of Fe^{59} in the energy region between 1 Mev and 1.4 Mev. Dashed line represents background from 1560-kev β-ray spectrum and from Compton distribution of the 1.29-Mev γ-ray.

If the experimental K-conversion coefficients are accepted at face value, then both transitions are electric quadrupoles. However, when the difference between various assignments becomes so small, the absolute values might not be a very good guide. For example, the experimental values might change slightly owing to changes in some of the corrections and the theoretical values might change if screening is taken into account.[8] Most of these changes would presumably affect the absolute values much more than they would the ratio of the two coefficients. Moreover, the ratio is obtained more directly from experiment and is therefore more accurate. In order to decide between $M1$ and $E2$, it appears preferable therefore to consider the ratio of the conversion coefficients.

With the value 1.79 ± 0.06 for the relative number of conversion electrons and the value 1.32 ± 0.05 for the ratio of the gamma-ray intensities, the ratio of the total conversion coefficients becomes 1.36 ± 0.07. The K/L ratios for $M1$ and $E2$ transitions of very small Z^2/E are not known. It will be assumed that they are approximately equal and that the ratio 1.36 is also the ratio of the K-conversion coefficients of the 1.1 and 1.29-Mev gamma-rays. The ratios expected for the different possible assignments are compared with the experimental value in Table III.

The only theoretical ratio agreeing within the limits of error with the experimental value is the one assigning $M1$ to the 1.1-Mev transition and $E2$ to the 1.29-Mev transition. The $E2$–$E2$ and $M1$–$M1$ assignments are improbable, and the $E2$–$M1$ combination is definitely ruled out.

$M1$ for the 1.1-Mev transition leaves the possi-

[8] J. R. Reitz, Phys. Rev. **77**, 10 (1950).

TABLE III. The ratios of the theoretical K-conversion coefficients for the four possible assignments of multipole orders to the Co^{59} gamma-rays in comparison with the experimental value.

1.1-Mev gamma-ray	1.29-Mev gamma-ray	α_K(1.1 Mev)/α_K(1.29 Mev)
$M1$	$M1$	1.48
$M1$	$E2$	1.33
$E2$	$M1$	1.60
$E2$	$E2$	1.45
Experiment		1.36±0.07

bilities 7/2 and 5/2 for the spin of the first excited state of Co^{59}.[9] A spin of 7/2 would call for an α-type shape of the 462-kev beta-ray spectrum in contradiction with experiment. The first (1.1-Mev) excited state of Co^{59} has therefore spin 5/2, odd parity. If the single-particle model still holds at this excitation, spin and parity characterize the level as $f_{5/2}$.

$E2$ for the 1.29-Mev transition leads to a spin of $\frac{3}{2}$ and odd parity for the second excited state, $p_{3/2}$ being the appropriate single particle level.

It might be added that conversion measurements on Co^{60} yielded a value 1.34±0.09 for the ratio of the conversion coefficients of the Ni^{60} gamma-rays in very good agreement with the theoretical ratio 1.32 calculated for the accepted $E2$–$E2$ assignment.

b. Conversion of the 191-kev Gamma-Ray

The theoretical conversion coefficients of a 191-kev gamma-ray in Co are given in Table IV for different multipole orders. $E2$ and $M2$ are very well separated from $E1$ and $M1$ with regard to their conversion coefficients. If either $E2$ or $M2$ was the correct assignment, the counting rate in the conversion line should amount to five percent of the counting rate in the beta-ray spectrum on which the conversion line is superimposed. In the $E1$ or $M1$ case the contribution of the conversion line should be about 0.8 percent of the total counting rate. A quick survey did not reveal any conversion line, indicating that the contribution of the conversion line was smaller than two percent. After a careful investigation of the beta-ray spectrum, during which at least 10^6 counts were taken in every point, the conversion line of the 191-kev gamma-ray could be identified. The number of conversion electrons was found to be 0.02 percent of the total number of beta-rays. With a 2.8 percent abundance of the 191-kev transition one calculates a conversion coefficient of $(7\pm3)\times10^{-3}$, in very good agreement with the theoretical coefficients for either $E1$ or $M1$. As all Co^{59} levels have the same parity, $E1$ is excluded and the unique assignment to the 191-kev transition is $M1$. The same conclusion was reached on the basis of the conversion of the high energy gamma-rays. The measured value of the conversion coefficient restricts the maximum amount of $E2$ admixture to the 191-kev transition to 10 percent.

ANGULAR CORRELATION EXPERIMENTS

The existence of the 191-kev gamma-ray offers the possibility of measuring the angular correlation in the 191–1098-kev gamma-ray cascade of Co^{59}. However, one cannot expect to obtain a unique spin assignment from such an experiment with an odd-even nucleus where both transitions can be mixtures of magnetic and electric multipoles. By a suitable choice of the mixing ratios the coefficients of the angular correlation can be varied within wide limits,[10] and thus the same experimental data can be fitted with different spin assignments. Lifetime considerations will exclude some mixtures, but in general, they are not a very reliable guide in view of the large scatter observed in the magnitude of the nuclear matrix elements.[11]

If, on the other hand, the spins of the three cascade states are already known, the angular correlation can be used as a very sensitive means for determining the degree of mixture present in the transitions.

Using NaI crystals in a coincidence arrangement of 1.2×10^{-7} seconds resolving time the first correlation experiments were carried out with low specific activity Fe^{59} (0.06 mC/g). Due to the low coincidence rate obtainable with the weak (2.8 percent) cascade the data were rather inaccurate, and, although suggesting a small correlation, could not rule out the absence of any correlation. Thus, the preliminary correlation experiments could not exclude any assignment attributing spin $\frac{1}{2}$ to the intermediate level of the Co^{59} cascade. At this point it was decided that conversion measurements would answer the question of spin $\frac{1}{2}$ more directly and in addition would provide information concerning the parities of the Co^{59} states.

After most of the investigation described in the preceding sections had been completed and the assignment 3/2–5/2–7/2 had been established, the angular correlation of the 191–1098-kev cascade was measured again by Mr. Schiff of this laboratory using NaI crystals and an improved coincidence arrangement of 1.5×10^{-8} second resolving time. High specific activity Fe^{59} sources were used for these measurements. The correlation was studied between 90 degrees and 180 degrees in angular steps of 15 degrees. The measured points can be fitted with a $1+A_2\cos^2\theta$ distribution using a value of $A_2=0.080\pm0.016$, which definitely

TABLE IV. Theoretical K-conversion coefficients for a 191-kev gamma-ray in Co (according to Rose *et al.*, reference 7).

	$E1$	$E2$	$M1$	$M2$
$\alpha_K\times10^3$	6.2	41.5	7.1	43.5

[9] The ft-values of the main beta-ray spectra exclude spins larger than 7/2 for the excited states of Co^{59} if one discards spin $h_{11/2}$ for the ground state of Fe^{59} in favor of $p_{3/2}$.

[10] D. S. Ling and D. L. Falkoff, Phys. Rev. **76**, 1639 (1949).

[11] M. Goldhaber and A. W. Sunyar, Phys. Rev. **83**, 906 (1951).

excludes spin $\frac{1}{2}$ for the first excited state of Co^{59} in agreement with the conversion experiments.

The measured coefficient is compatible with the assignments 3/2–3/2–7/2 and 3/2–5/2–7/2 without the need of a mixture. The combination 5/2–5/2–7/2 would give rise to the observed correlation if about three percent $E2$ were admixed to the 1098-kev $M1$ transition. Such an admixture cannot be excluded, although from Weisskopf's lifetime formulas[12] one expects only about 0.1 percent $E2$. The cascade 5/2–3/2–7/2 cannot fit the experiment as long as the admixture of $E2$ to the 191-kev transition is kept below ten percent, the limit given by the conversion coefficient of the 191-kev line. Thus, of the four spin combinations compatible with the ft values of the beta-ray spectra and with the $E2$ or $M1$ character of the gamma-rays, the angular correlation eliminates one definitely, renders one unlikely, and leaves two as equally probable choices.

The experiment restricts the coefficient A_2 to values ranging from 0.064 to 0.096. Only an $A_2=0.077$ would give pure transitions for the 3/2–5/2–7/2 cascade. In order to match the other values, mixtures must be considered. As the admixture of $E2$ becomes more probable with increasing energy, it is assumed for reasons of simplicity, that only the 1098-kev transition is a mixture, the 191-kev gamma-ray being pure $M1$. Actually one expects from the lifetime relations[12] 0.002 percent $E2$ for the 191-kev gamma-ray and 0.1 percent $E2$ for the 1098-kev transition. Using the formulas given by Ling and Falkoff,[10] one finds that the admixture of $E2$ varies from 0.02 percent to zero percent and back to 0.06 percent as A_2 changes from 0.064 over 0.077 to 0.096. Thus the admixture of $E2$ to the 1098-kev transition is smaller than the 0.1 percent expected from Weisskopf's formulas. However, a factor of ten or even hundred in the transition probability is not considered serious, especially when it points in the direction of reduced $E2$ intensity.

CONCLUSIONS

Based on the experiments discussed in the preceding sections, the disintegration scheme shown in Fig. 10 is proposed. It agrees in the most intense radiation with that of Deutsch *et al.*[1] The intensities given in Fig. 10 are the adjusted values obtained by combining the beta-ray measurements with the gamma-ray data. The intensities of Table I, which are slightly different, were based on the beta-ray experiments alone.

If the excited levels of Co^{59} are single particle levels,

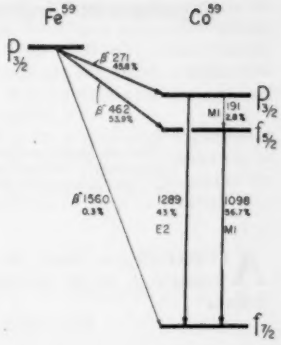

FIG. 10. Proposed disintegration scheme of Fe^{59}. Transition energies are given in kev.

the 1.098-Mev gamma-ray represents the splitting of the f-levels which, in the jj-coupling model of Mayer[13] and of Haxel, Jensen, and Suess,[14] gives rise to the shell at N or $Z=28$.

As all the levels involved in the decay of Fe^{59} have the same parity (odd), the beta-ray transitions can only be allowed or second forbidden. The logft value of 5.9 for the 271-kev spectrum is consistent with an allowed transition. The logft value of 6.7 of the 462-kev spectrum exceeds the range usually attributed to allowed transitions. However, the 462-kev spectrum involves a change of two units of orbital angular momentum; it therefore belongs to the l-forbidden group,[15] the extreme example of which is C^{14} with a logft value of 9.

According to our decay scheme the 191-kev $M1$ gamma-ray competes with the 1.29-Mev $E2$ transition. From Weisskopf's formulas[12] one would expect the 191-kev transition to be about twice as strong as the 1.29-Mev transition. Experimentally, however, the 1.29-Mev gamma-ray is fifteen times as intense as the 191-kev gamma-ray. The 191-kev $M1$ transition is probably thirty times weaker than expected because it involves a change of two units of orbital angular momentum. According to Sachs and Ross[16] such $\Delta l=2$ transitions, which would be forbidden for ordinary magnetic dipole effects, are allowed for certain forms of the interaction moment, but are expected to be somewhat weaker than the transitions involving no change in orbital angular momentum.

[12] V. Weisskopf, Phys. Rev. **83**, 1073 (1951).

[13] M. G. Mayer, Phys. Rev. **75**, 1946 (1949); **78**, 16 (1950).

[14] Haxel, Jensen, and Suess, Phys. Rev. **75**, 1766 (1949).

[15] Mayer, Moszkowski, and Nordheim, Revs. Modern Phys. **23**, 315 (1951); and L. W. Nordheim, Revs. Modern Phys. **23**, 322 (1951).

[16] R. G. Sachs and M. Ross, Phys. Rev. **84**, 379 (1951).

Experimental Verification of the Relationship between Diffusion Constant and Mobility of Electrons and Holes

TRANSISTOR TEACHERS SUMMER SCHOOL*
Bell Telephone Laboratories, Murray Hill, New Jersey
(Received August 4, 1952)

The relationship between diffusion constant and mobility, called the Einstein relationship, has been experimentally verified for electrons and holes in germanium. This has been accomplished by measuring the rate of increase in half concentration width of a pulse of minority carriers moving in an electric field.

ACCORDING to theory, the ratio of the diffusion constant D to the mobility μ of charged particles is

$$D/\mu = kT/q,$$

where T is the absolute temperature, k the Boltzmann constant, and q is the magnitude of the charge.[1]

This relation was verified by the following experiment. Sharp pulses of minority carriers were injected into single crystal rods of both P- and N-type germanium in which there was an electric field. As the pulse moved along the rod under the influence of the electric field, diffusion occurred, resulting in a continuous transition from a sharp to a broad pulse. The essential features of the pulse shape were determined at two different distances along the rod.

The pulse was injected at an emitter point and detected at a collector point, which was placed some distance away. The variation of current through the collector point was observed with an oscilloscope, using essentially the same arrangement employed by Haynes and Westphal in the determination of the mobility of holes and electrons in silicon.[2]

It can be shown that to a good approximation

$$\frac{D}{\mu} = \frac{V(\Delta t_1^2 - \Delta t_2^2)}{11.08 t_1 (t_1 - t_2)}$$

where Δt_1 = width of the pulse at half-maximum corresponding to the transit time t_1, Δt_2 = width of the pulse at half-maximum corresponding to the transit time t_2, and V = potential difference between emitter and collector positions for transit time t_1.

Using a constant electric field, the transit times and pulse widths were measured on the time base of the cathode-ray oscilloscope for two positions of the emitter point.

Since the determination of D/μ depends on a difference of squares of measured quantities, single observations do not have a high level of significance. Independent measurements were made by a large number of observers. The average value for D/μ obtained using injected electrons is within 1 percent of that obtained with holes. Since analysis shows that the data have a normal probability distribution, the method of least squares was used to evaluate the most probable value and its significance. The following results were

* A. B. Giordano, H. W. Schleuning, and Lucio M. Vallese, *Polytechnic Institute of Brooklyn, Brooklyn, New York;* H. E. Farnsworth and R. E. Schlier, *Brown University, Providence, Rhode Island;* W. J. Leivo and Norman Rostoker, *Carnegie Institute of Technology, Pittsburgh, Pennsylvania;* Forest Brammer, *Case Institute of Technology, Cleveland, Ohio;* G. E. McDuffie and R. L. Petritz, *Catholic University of America, Washington, D. C.;* Abraham Abramowitz, *City College, New York, New York;* D. G. Burkhard and F. C. Walz, *University of Colorado, Boulder, Colorado;* H. M. Foley, J. Millman, and L. H. O'Neill, *Columbia University, New York, New York;* P. Hartman, L. G. Parratt, and Clyde E. Ingalls, *Cornell University, Ithaca, New York;* Vernon Crawford and T. L. Weatherly, *Georgia Institute of Technology, Atlanta, Georgia;* Ralph D. Kodis and F. K. Willenbrock, *Harvard University, Cambridge, Massachusetts;* Edwin J. Scheibner, *Illinois Institute of Technology, Chicago, Illinois;* Peter Axel, *University of Illinois, Urbana, Illinois;* M. B. Gottlieb, *State University of Iowa, Iowa City, Iowa;* D. W. Gade, G. C. Danielson, and L. W. Von Tersch, *Iowa State College, Ames, Iowa;* W. H. Duerig, Donald E. Kerr, and C. Frank Miller, *The Johns Hopkins University, Baltimore, Maryland;* D. B. Wheeler, *Lehigh University, Bethlehem, Pennsylvania;* R. B. Adler, Eugene B. Hensley, Benjamin Lax, and Eugene P. Gross, *Massachusetts Institute of Technology, Cambridge, Massachusetts;* G. A. Woonton, *McGill University, Montreal, Canada;* L. A. Harris, *University of Minnesota, Minneapolis, Minnesota;* P. Greenstein and B. James Ley, *New York University, New York, New York;* R. J. Cashman and Donald A. Dobson, *Northwestern University, Evanston, Illinois;* E. M. Boone, *Ohio State University, Columbus, Ohio;* G. E. Knausenberger and Robert L. Riddle, *Pennsylvania State College, State College, Pennsylvania;* B. Roswell Russell and R. M. Showers, *University of Pennsylvania, Philadelphia, Pennsylvania;* G. Warfield, *Princeton University, Princeton, New Jersey;* Henry E. Breed and Kenneth E. Mortenson, *Rensselaer Polytechnic Institute, Troy, New York;* Harvey D. Polster, *University of Rochester, Rochester, New York;* Elmer C. Easton, D. A. Molony, and J. L. Potter, *Rutgers University, New Brunswick, New Jersey;* Melvin Lax and Henry Levinstein, *Syracuse University, Syracuse, New York;* Huntington W. Curtis, *United States Military Academy, West Point, New York;* Lawrence R. Quarles and Clifford M. Siegel, *University of Virginia, Charlottesville, Virginia;* D. A. Lind and R. C. Retherford, *University of Wisconsin, Madison, Wisconsin.*

[1] This equation is known as the Einstein relationship [see, for instance, N. F. Mott and R. W. Gurney, *Electronic Processes in Ionic Crystals* (Clarendon Press, Oxford, 1940), p. 63, or W. Shockley, *Electrons and Holes in Semiconductors* (D. Van Nostrand Company, Inc., New York, 1950), p. 300]. As pointed out by E. Spenke of Siemens-Schuckertwerke, however (private communication to W. Shockley), the essentials of this equation, published by A. Einstein [Ann. Physik **17**, 549 (1905)] had been published previously by J. S. Townsend [Trans. Roy. Soc. (London) **A193**, 129 (1900)] and by W. Nernst [Z. Physik. Chem. **9**, 613 (1884)]. Possibly it should be called the Nernst-Townsend-Einstein relationship since each derivation appears independent of the others.

[2] J. R. Haynes and W. C. Westphal, Phys. Rev. **85**, 680 (1952).

obtained:[3]

$$D/\mu = 0.0268 \pm 0.0013 \text{ ev},$$
$$T = 303 \pm 1°\text{K},$$
$$kT/q = 0.0262 \pm 0.0001 \text{ ev}.$$

[3] The probable error in the values of T and kT/q were not obtained using the method of least squares which would give a value much less than this. Generous allowance is made for systematic uncertainty in recording ambient temperature.

It would appear that these results verify the relation $D/\mu = kT/q$. Although there have been other experimental verifications of this relationship using colloidal particles and ions, this is the first direct experimental proof of the validity of this equation for electrons and holes of which we are aware.

The authors would like to express their appreciation to W. C. Westphal for assisting with apparatus, to J. R. Haynes for advice and encouragement, and to the Bell Telephone Laboratories for their hospitality.

PHYSICAL REVIEW VOLUME 88, NUMBER 6 DECEMBER 15, 1952

Gravitation and Electrodynamics

BEHRAM KURŞUNOĞLU*
Fitzwilliam House, University of Cambridge, Cambridge, England
(Received May 19, 1952)

In this paper Einstein's unified field theory is modified, and some of the physical implications of the new theory are examined. It entails: (1) a restriction of 4-current distribution, (2) an electromagnetic field consisting of short- and long-range parts, (3) a finite self-energy for the electron, (4) a classical description of pair production and annihilation as discussed by Feynman in his electrodynamics, (5) the Lorentz-force law for a charged particle moving in an external electromagnetic field, (6) the bending of light grazing the surface of the sun—the same as given by the general theory of relativity.

1. INTRODUCTION

THE arguments for the necessity of a unified field theory are well known, and therefore they will not be elaborated at length. The author believes that a correct and unified quantum theory of fields, without the need of the so-called renormalization of some physical constants, can be reached only through a complete classical field theory that does not exclude gravitational phenomena. It is true that one cannot feel very optimistic about the quantization of a nonlinear classical field theory. But one hopes that this difficulty may be overcome, partly, by starting the quantization procedure with a Lagrangian[1] formulation of the quantum field theory.

In this paper we propose a new version of Einstein's latest unified field theory.[1a] The reasons for this modification will be made clear in the following. The same formalism and notation of Einstein's theory are used. The total field is described by a Hermitian tensor $g_{\alpha\beta}$ given as

$$g_{\alpha\beta} = a_{\alpha\beta} + i\varphi_{\alpha\beta}, \tag{1.1}$$

where

$$a_{\alpha\beta} = \underset{\sim}{g}_{\alpha\beta} \quad \text{and} \quad \varphi_{\alpha\beta} = \underset{\sim}{g}_{\alpha\beta}, \quad i = (-1)^{\frac{1}{2}},$$

so that we have

$$(g_{\alpha\beta})^\dagger = (g_{\alpha\beta}). \tag{1.2}$$

The dagger (†) stands for Hermitian conjugate operation. We also have the general affine connection $\Gamma^\gamma_{\alpha\beta}$ given by

$$\Gamma^\gamma_{\alpha\beta} = \Gamma^\gamma_{\underset{\sim}{\alpha\beta}} + i\Gamma^\gamma_{\underset{\sim}{\alpha\beta}}. \tag{1.3}$$

The Hermitian property of $\Gamma^\gamma_{\alpha\beta}$ in the covariant indices α and β is obvious.

Now, if we define $a^{\alpha\beta}$ as the normalized minors of $\mathrm{Det}a_{\alpha\beta} = a$, then, we have

$$a_{\alpha\mu}a^{\gamma\mu} = \delta_\alpha{}^\gamma.$$

The determinant of $g_{\alpha\beta}$, because of (1.2), is real and can be expressed as

$$g = a(1 - \Omega - \Lambda^2), \tag{1.4}$$

where

$$\Omega = \tfrac{1}{2}\varphi_{\mu\nu}\varphi^{\mu\nu} \quad \text{(is an invariant)},$$
$$\Lambda = \tfrac{1}{4}f^{\mu\nu}\varphi_{\mu\nu} \quad \text{(is a pseudoscalar)},$$

and

$$f^{\alpha\beta} = \frac{1}{2(-a)^{\frac{1}{2}}}\epsilon^{\alpha\beta\mu\nu}\varphi_{\mu\nu}, \tag{1.5}$$

where $\epsilon^{\alpha\beta\mu\nu}$ is zero whenever any two indices are equal and is ± 1 for even and odd permutations. All indices are raised by $a^{\alpha\beta}$.

We also have the contravariant tensor $g^{\alpha\beta}$ given by

$$g_{\alpha\mu}g^{\beta\mu} = \delta_\alpha{}^\beta.$$

* Now at Laboratory of Nuclear Studies, Cornell University, Ithaca, New York.

[1] J. Schwinger, Phys. Rev. 82, 914 (1951).

[1a] A. Einstein, *The Meaning of Relativity* (Methuen, London, 1951).

It can easily be shown that $\mathfrak{g}^{\alpha\beta}[=(-g)^{\frac{1}{2}}g^{\alpha\beta}]$ can be expressed in terms of $g_{\alpha\beta}$ as

$$\underset{\sim}{\mathfrak{g}}^{\alpha\beta}=(-g)^{\frac{1}{2}}a^{\alpha\beta}+\underset{\sim}{\mathfrak{g}}^{\alpha\mu}\varphi_{\mu}^{\ \beta}, \tag{1.6}$$

$$\underset{\sim}{\mathfrak{g}}^{\alpha\beta}=(-a)^{\frac{1}{2}}(\varphi^{\alpha\beta}+\Delta f^{\alpha\beta})/(1-\Omega-\Delta^2)^{\frac{1}{2}}. \tag{1.7}$$

In (1.6) we used the expression

$$\delta_{\beta}^{\ \alpha}\Lambda=f^{\alpha\mu}\varphi_{\beta\mu}.$$

The components of the affine connection $\Gamma^{\gamma}_{\alpha\beta}$ are defined by solving the equations

$$\underset{+-}{g_{\alpha\beta;\gamma}}=g_{\alpha\beta,\gamma}-g_{\alpha\beta}\Gamma^{\mu}_{\alpha\gamma}-g_{\alpha\mu}\Gamma^{\mu}_{\gamma\beta}=0. \tag{1.8}$$

By splitting up symmetric and antisymmetric parts (or by taking real and imaginary parts) of (1.8) it is easy to show that

$$\Gamma^{\gamma}_{\underset{\sim}{\alpha\beta}}=\left\{\begin{matrix}\gamma\\ \alpha\beta\end{matrix}\right\}_a+a^{\gamma\mu}(\varphi_{\beta\mu}\Gamma^{\nu}_{\underset{\sim}{\alpha\nu}}+\varphi_{\nu\alpha}\Gamma^{\nu}_{\underset{\sim}{\mu\beta}}), \tag{1.9}$$

where $\left\{\begin{matrix}\gamma\\ \alpha\beta\end{matrix}\right\}_a$ are the Christoffel symbols formed from $a_{\alpha\beta}$.

Equations (1.8), when solved with respect to $\Gamma^{\gamma}_{\underset{\sim}{\alpha\beta}}$, give[2]

$$\Gamma^{\gamma}_{\underset{\sim}{\alpha\beta}}=-\tfrac{1}{2}I^{\gamma}_{\underset{\sim}{\alpha\beta}}+a^{\gamma\mu}\varphi_{\alpha\beta o\mu}, \tag{1.10}$$

where the sign (o) stands for covariant differentiation with respect to $\Gamma^{\gamma}_{\underset{\sim}{\alpha\beta}}$, so that (1.10) is only an implicit solution of (1.8), and $I^{\gamma}_{\underset{\sim}{\alpha\beta}}=a^{\gamma\mu}I_{\alpha\beta\mu}$ is defined by

$$I_{\alpha\beta\gamma}=\varphi_{\alpha\beta,\gamma}+\varphi_{\beta\gamma,\alpha}+\varphi_{\gamma\alpha,\beta}. \tag{1.11}$$

Equation (1.11) represents the 4-current density, the dual of which is

$$\mathfrak{I}^{\alpha}=(1/3!)\epsilon^{\mu\nu\rho\alpha}I_{\mu\nu\rho}. \tag{1.12}$$

We add the four field conditions,

$$\Gamma_{\alpha}=\Gamma^{\gamma}_{\underset{\sim}{\alpha\gamma}}=0, \tag{1.13}$$

to Eqs. (1.8).

Equations (1.13) imply, because of (1.8), the four equations

$$\underset{\sim}{\mathfrak{g}}^{\alpha\beta}_{\ \ ,\beta}=0. \tag{1.14}$$

2. THE EQUATIONS OF THE TOTAL FIELD

The existence of Bianchi identities have been of great use in the mathematical formulation of the ideas of general relativity. The right-hand sides of $G_{\alpha\beta}-\frac{1}{2}a_{\alpha\beta}G=-8\pi\bar{\gamma}T_{\alpha\beta}$ are the phenomenological descriptions of the sources of the gravitational field, but the fact that covariant divergence of the left-hand side vanishes identically has induced one to stick-in $T_{\alpha\beta}$ in an *ad hoc* manner. In unified field theory we can start, formally, in the same way and derive the sources of the field direct from the elements of the theory itself.

We first note that if we multiply both sides of (1.11) by $\underset{\sim}{\mathfrak{g}}^{\alpha\beta}$ and use Eqs. (1.14), the identities

$$\underset{\sim}{\mathfrak{g}}^{\alpha\mu}_{\ \ |\mu}=-\tfrac{1}{2}\underset{\sim}{\mathfrak{g}}^{\mu\nu}I^{\alpha}_{\mu\nu} \tag{2.1}$$

follow immediately. The stroke (|) in (2.1) stands for covariant differentiation with respect to $\left\{\begin{matrix}\gamma\\ \alpha\beta\end{matrix}\right\}_a$.

If (1.8) and (1.13) are granted, it can be shown that the Hermitian tensor $R_{\alpha\beta}$ satisfies Bianchi-Einstein identities for the nonsymmetric field derived by Einstein[3] as

$$\mathfrak{g}^{\alpha\beta}[\underset{+-}{R_{\alpha\beta;\gamma}}-\underset{++}{R_{\alpha\gamma;\beta}}-\underset{-+}{R_{\gamma\beta;\alpha}}]=0. \tag{2.2}$$

These identities hold for all fields satisfying (1.8) and (1.13). It is now easy to verify the identity, with proviso (1.8) and (1.13),

$$\mathfrak{g}^{\alpha\beta}[\underset{+-}{g_{\alpha\beta;\gamma}}-\underset{++}{g_{\alpha\gamma;\beta}}-\underset{-+}{g_{\gamma\beta;\alpha}}]=0, \tag{2.3}$$

which is equivalent to (2.1).

After performing the semi-colon covariant differentiations and using

$$\underset{\sim}{\mathfrak{g}}^{\alpha\beta}_{\ \ ,\beta}=-\underset{\sim}{\mathfrak{g}}^{\mu\nu}\Gamma^{\alpha}_{\mu\nu}$$

(which follows from $\underset{+-}{\mathfrak{g}^{\alpha\beta}_{\ \ ;\gamma}}=0$), the identity (2.2) can be written in a suggestive form as

$$(\underset{\sim}{\mathfrak{g}}^{\alpha\mu}\underset{-+}{R_{\beta\mu}}-\tfrac{1}{2}\delta^{\alpha}_{\beta}\underset{\sim}{\mathfrak{g}}^{\mu\nu}\underset{-+}{R_{\mu\nu}})_{||\alpha}=-\tfrac{1}{2}\underset{\sim}{\mathfrak{g}}^{\mu\nu}(\underset{-+}{R_{\mu\nu,\beta}}+\underset{-+}{R_{\nu\beta,\mu}}+\underset{-+}{R_{\beta\mu,\nu}}), \tag{2.4}$$

and (2.3) or (2.1) are equivalent to

$$(\underset{\sim}{\mathfrak{g}}^{\alpha\mu}a_{\beta\mu}-\tfrac{1}{2}\delta^{\alpha}_{\beta}\underset{\sim}{\mathfrak{g}}^{\mu\nu}a_{\mu\nu})_{||\alpha}=-\tfrac{1}{2}\underset{\sim}{\mathfrak{g}}^{\mu\nu}(\varphi_{\mu\nu,\beta}+\varphi_{\nu\beta,\mu}+\varphi_{\beta\mu,\nu}), \tag{2.5}$$

where $(||)$ stands for covariant differentiation with respect to Christoffel symbols formed from $b_{\alpha\beta}$ which is defined by

$$b^{\alpha\beta}=\underset{\sim}{\mathfrak{g}}^{\alpha\beta}/(-\mathrm{Det}\underset{\sim}{\mathfrak{g}}^{\alpha\beta})^{\frac{1}{2}}.$$

Hence,

$$\underset{\sim}{\mathfrak{g}}^{\alpha\beta}=(-b)^{\frac{1}{2}}b^{\alpha\beta},\quad b=\mathrm{Det}b_{\alpha\beta}=\mathrm{Det}\underset{\sim}{\mathfrak{g}}^{\alpha\beta}, \tag{2.6}$$

and

$$b_{\alpha\mu}b^{\gamma\mu}=\delta_{\alpha}^{\gamma}. \tag{2.7}$$

The form of (2.4) does not change with respect to the transformation

$$\underset{\sim}{R_{\alpha\beta}}\rightarrow\underset{\sim}{R_{\alpha\beta}}+(\partial_{\alpha}B_{\beta}-\partial_{\beta}B_{\alpha}).$$

[2] B. Kurşunoğlu, Phys. Rev. **82**, 289 (1951).

[3] A. Einstein, Can. J. Math. **2**, 120 (1950).

This fact will be made use of in the Hamiltonian principle of the theory.

When $\varphi_{\alpha\beta}=0$, (2.4) reduces to

$$(\mathfrak{g}^{\alpha\mu}G_{\beta\mu}-\tfrac{1}{2}\delta^{\alpha}_{\beta}\mathfrak{g}^{\mu\nu}G_{\mu\nu})_{|\alpha}=0,$$

where $\mathfrak{g}^{\alpha\beta}=(-g)^{\frac{1}{2}}g^{\alpha\beta}$; hence the symmetric tensor $b_{\alpha\beta}$ may be taken as the generalized "metric" of the spacetime. From the conservation laws of general relativity one might jump to the conclusion that the right-hand sides of (2.4) ought to vanish so that they would constitute a set of four field equations, but this is *non-sequitur*. Instead, we shall follow the analogy with the electromagnetic theory. In (2.4) the right-hand side being a covariant divergence of a symmetric tensor density [left-hand side of (2.4)] has the appearance of a generalized electromagnetic force density, that this is so will be shown more explicitly later on.

The identity (2.4) can be satisfied by taking $R_{\alpha\beta}=0$ (Einstein's theory), or we may reconcile the two identities by putting $R_{\alpha\beta}=\lambda\varphi_{\alpha\beta}$ (Schrödinger's theory).[4] In both cases the field equations are over-determined (since we also have Eqs. (1.14) the total number of the field equations are 20; for consistency 8 identities are required, but there are only 4+1 identities), and also the forms of the identities are destroyed. It is very important to preserve the form of the identities, i.e., the reconciliation of (2.4) and (2.5) can be carried through by preserving the forms of "matter tensor" and "force-density," so that only in this way a consistent number of field equations can be secured. The expression in the bracket on the left-hand side of (2.4) can be regarded as a tensor describing the energy and momentum of the total field. We can think the same for (2.5) so that the required unification of the physical fields will be achieved, if we introduce a "fundamental constant" p of the dimension of (length)$^{-1}$ by writing

$$\mathfrak{g}^{\alpha\mu}R_{\beta\mu}-\tfrac{1}{2}\delta^{\alpha}_{\beta}\mathfrak{g}^{\mu\nu}R_{\mu\nu}+f\delta^{\alpha}_{\beta}(-b)^{\frac{1}{2}} = -p^2(\mathfrak{g}^{\alpha\mu}a_{\beta\mu}-\tfrac{1}{2}\delta^{\alpha}_{\beta}\mathfrak{g}^{\mu\nu}a_{\mu\nu}), \quad \text{(I)}$$

and

$$R_{\alpha\beta,\gamma}+R_{\beta\gamma,\alpha}+R_{\gamma\alpha,\beta}=-p^2(\varphi_{\alpha\beta,\gamma}+\varphi_{\beta\gamma,\alpha}+\varphi_{\gamma\alpha,\beta}), \quad \text{(II)}$$

where, in I, the third term on the left-hand side is a consequence of the covariant differentiation with respect to $\left\{\begin{matrix}\gamma\\ \alpha\beta\end{matrix}\right\}_b$, and f is a constant.

The minus sign before p^2 is very important and will explain itself when we consider the solutions of the field equations.

By contracting (I) with respect to β and α and arranging the terms, we obtain I as

$$R_{\alpha\beta}=-p^2a_{\alpha\beta}+fb_{\alpha\beta}.$$

The constant f can be defined by imposing the condition that our field equations must reduce, in the absence of $\varphi_{\alpha\beta}$, to the free field equations of general relativity. Thus, we finally obtain

$$R_{\alpha\beta}=-p^2(a_{\alpha\beta}-b_{\alpha\beta}), \quad (2.8)$$

$$R_{\alpha\beta,\gamma}+R_{\beta\gamma,\alpha}+R_{\gamma\alpha,\beta}=-p^2I_{\alpha\beta\gamma}, \quad (2.9)$$

$$\mathfrak{g}^{\alpha\beta}{}_{,\beta}=0. \quad (2.10)$$

In this way we have obtained 18 field equations for 16 field variables plus two trivial identities that follow by differentiation of (2.9) and (2.10). Hence, we have a consistent number of field equations. Note that p^2 is not a cosmological constant. The same field equations can also be obtained from an action principle,

$$\delta\int\mathfrak{L}d^4x=\delta\int[\mathfrak{g}^{\alpha\beta}R_{\alpha\beta}-2p^2\{(-b)^{\frac{1}{2}}-(-g)^{\frac{1}{2}}\}]d^4x=0. \quad (2.11)$$

The term in curly brackets can also be written as

$$\{[-\mathrm{Det}\mathfrak{g}^{\alpha\beta}]^{\frac{1}{2}}-[-\mathrm{Det}\mathfrak{g}^{\alpha\beta}]^{\frac{1}{2}}\} =(\sqrt{-b})[1-(1-M-L^2)^{\frac{1}{2}}],$$

where

$$M=\tfrac{1}{2}\chi_{\mu\nu}\chi^{\mu\nu}, \quad L=\tfrac{1}{4}\chi^{*\mu\nu}\chi_{\mu\nu},$$

$$\chi_{\mu\nu}=\frac{b_{\alpha\mu}b_{\beta\gamma}}{\sqrt{-b}}\mathfrak{g}^{\alpha\beta}, \quad \chi^{*\mu\nu}=\frac{1}{\sqrt{-b}}\epsilon^{\mu\nu\alpha\beta}\chi_{\alpha\beta}.$$

In order to impose the conditions (1.14), we add the term $\mathfrak{g}^{\alpha\beta}B_{\alpha\beta}$ and regard B_α as auxiliary field variable which can be eliminated from the field equations. Lagrangians of Einstein and Schrödinger theories are

$$\mathfrak{L}_E=\mathfrak{g}^{\alpha\beta}R_{\alpha\beta}$$

and

$$\mathfrak{L}_S=\mathrm{Det}(-R_{\alpha\beta})^{\frac{1}{2}} \text{ (or } \mathfrak{g}^{\alpha\beta}R_{\alpha\beta}-2\lambda(-g)^{\frac{1}{2}}).$$

The variation of $I=\int\mathfrak{L}d^4x$ consists of adding the independent effects of changing the field components at each point by $\delta_0\mathfrak{g}^{\alpha\beta}$, $\delta_0\Gamma^{\gamma}_{\alpha\beta}$, δ_0B_α and of altering the region of integration by a displacement δx^μ of the points on the boundary surfaces. The first kind of variations lead to the field equations and the second one to the Bianchi-Einstein identities for the nonsymmetric field. The variation of the first term in (2.11) is given in Einstein's theory, and that of the second term can easily be obtained.

3. CONSERVATION LAWS

Now, let us introduce the pseudo quantity

$$\mathfrak{B}=\mathfrak{g}^{\alpha\beta}\mathfrak{B}_{\alpha\beta}, \quad (3.1)$$

where

$$\mathfrak{B}_{\alpha\beta}=\Gamma^{\gamma}_{\alpha\beta}\Gamma^{\nu}_{\gamma\nu}-\Gamma^{\gamma}_{\alpha\nu}\Gamma^{\nu}_{\gamma\beta}, \quad (3.2)$$

[4] E. Schrödinger, Proc. Roy. Irish Acad. LI. **A213** (1948).

which is the nonlinear part of

$$R_{\alpha\beta}=\Gamma^{\gamma}_{\alpha\beta,\gamma}-\Gamma^{\gamma}_{\alpha\gamma,\beta}+\Gamma^{\gamma}_{\alpha\beta}\Gamma^{\mu}_{\gamma\mu}-\Gamma^{\gamma}_{\alpha\mu}\Gamma^{\mu}_{\gamma\beta}=R_{\alpha\beta}+iR_{\alpha\beta}, \quad (3.3)$$

where

$$\Gamma^{\gamma}_{\alpha\gamma}=\partial \log(-g)^{\frac{1}{2}}/\partial x^{\alpha}.$$

The variation of (3.1), using $\mathfrak{g}^{(\alpha\beta)}_{+\ ;\gamma}=0$, gives

$$\delta\mathfrak{B}=-\mathfrak{B}_{\alpha\beta}\delta\mathfrak{g}^{\alpha\beta}+\mathfrak{B}^{\gamma}_{\alpha\beta}\delta\mathfrak{g}^{\alpha\beta}{}_{,\gamma}, \quad (3.4)$$

where

$$\mathfrak{B}^{\gamma}_{\alpha\beta}=\Gamma^{\gamma}_{\alpha\beta}-\delta^{\gamma}_{\beta}\Gamma^{\mu}_{\alpha\mu}. \quad (3.5)$$

The Hamiltonian derivatives of $\mathfrak{B}$ with respect to $\mathfrak{g}^{\alpha\beta}$ results in

$$\frac{\partial\mathfrak{B}}{\partial\mathfrak{g}^{\alpha\beta}}-\frac{\partial}{\partial x^{\gamma}}\frac{\partial\mathfrak{B}}{\partial\mathfrak{g}^{\alpha\beta}{}_{,\gamma}}=-R_{\alpha\beta}. \quad (3.6)$$

Multiplying (3.6) by $\mathfrak{g}^{\alpha\beta}{}_{,\mu}$, we get

$$-\mathfrak{g}^{\alpha\beta}{}_{,\gamma}R_{\alpha\beta}=\frac{\partial}{\partial x^{\mu}}(\delta^{\mu}_{\gamma}\mathfrak{B}-\mathfrak{g}^{\alpha\beta}{}_{,\gamma}\mathfrak{B}^{\mu}_{\alpha\beta}), \quad (3.7)$$

or we can write

$$-\frac{1}{2}\mathfrak{g}^{\alpha\beta}{}_{,\gamma}R_{\alpha\beta}=-\frac{1}{2}\mathfrak{g}^{\alpha\beta}{}_{,\gamma}R_{\alpha\beta}+\frac{1}{2}\frac{\partial}{\partial x_{\mu}}(\delta^{\mu}_{\gamma}\mathfrak{B}-\mathfrak{g}^{\alpha\beta}{}_{,\gamma}\mathfrak{B}^{\mu}_{\alpha\beta}). \quad (3.8)$$

We can cancel the left-hand side of (3.8) by writing the identities (2.2) as,

$$\tfrac{1}{2}\mathfrak{g}^{\alpha\beta}{}_{,\gamma}R_{\alpha\beta}=-\tfrac{1}{2}\mathfrak{g}^{\alpha\beta}(R_{\alpha\beta,\gamma}+R_{\beta\gamma,\alpha}+R_{\gamma\alpha,\beta})$$
$$-(\mathfrak{g}^{\alpha\beta}R_{\alpha\gamma}-\tfrac{1}{2}\delta^{\beta}_{\gamma}\mathfrak{g}^{\mu\nu}R_{\mu\nu})_{,\beta}. \quad (3.9)$$

On adding up (3.8) and (3.9) and using the field equations (1.14), i.e., we are again using the 4-hermiticity conditions $\Gamma_{\alpha}=0$, it follows that

$$\mathfrak{T}^{\beta}_{\gamma,\beta}=0, \quad (3.10)$$

where

$$4\pi p^{2}\mathfrak{T}^{\beta}_{\gamma}=(\mathfrak{g}^{\alpha\beta}R_{\alpha\gamma}-\tfrac{1}{2}\delta^{\beta}_{\gamma}\mathfrak{g}^{\mu\nu}R_{\mu\nu})$$
$$-(\mathfrak{g}^{\alpha\beta}R_{\alpha\gamma}-\tfrac{1}{2}\delta^{\beta}_{\gamma}\mathfrak{g}^{\mu\nu}R_{\mu\nu})+\tfrac{1}{2}(\mathfrak{g}^{\mu\nu}{}_{,\gamma}\mathfrak{B}^{\beta}_{\mu\nu}-\delta^{\beta}_{\gamma}\mathfrak{B}) \quad (3.11)$$

is the pseudo stress-energy-momentum tensor of the total field.

If we set $\varphi_{\alpha\beta}=0$, (3.11) reduces to

$$\mathfrak{a}^{\alpha\beta}G_{\alpha\gamma}-\tfrac{1}{2}\delta^{\beta}_{\gamma}\mathfrak{a}^{\mu\nu}G_{\mu\nu}+\tfrac{1}{2}(\mathfrak{a}^{\mu\nu}{}_{,\gamma}\mathfrak{L}^{\beta}_{\mu\nu}-\delta^{\beta}_{\gamma}\mathfrak{L}), \quad (3.12)$$

where $\mathfrak{L}^{\beta}_{\mu\nu}$ and $\mathfrak{L}$ are the corresponding expressions of $\mathfrak{B}^{\beta}_{\mu\nu}$ and $\mathfrak{B}$ in general relativity. The expression (3.12) is the total energy momentum tensor of general relativity, and it is conserved. In the absence of matter, when the field equations $G_{\alpha\beta}=0$ are used, (3.12) consist merely of the last term representing gravitational field energy density.

A similar situation appears to be the case in Einstein's theory. When the field equations $R_{\alpha\beta}=0$ are used in (3.11) the energy momentum tensor of Einstein's field consists again of the last pseudo term of (3.11), and there is nothing to take the place of the matter in the ordinary sense, and Einstein's field equations are not complete.

There is one important point to be noticed: Because of the existence of the electromagnetic field the last term of (3.11) differs considerably from its counterpart $\mathfrak{L}$ in general relativity; e.g., it cannot be made to vanish at a point in any special coordinate system. Despite this the pseudo term cannot represent the total field energy density.[5]

The above arguments, as far as a nonsymmetric generalization of general relativity is concerned, make it clear beyond any shadow of doubt that the expression (3.11) is the genuine energy momentum tensor of the total field, and its form is most suggestive and provides another argument in favor of the fact that the field equations are neither $R_{\alpha\beta}=0$ nor $R_{\alpha\beta}=\lambda g_{\alpha\beta}$ both of which cause the vanishing of the field energy density.

If in (3.11) we use the field equations (2.8), we get

$$4\pi p^{2}\mathfrak{T}^{\beta}_{\gamma}=-p^{2}[\delta^{\beta}_{\gamma}((-b)^{\frac{1}{2}}-(-g)^{\frac{1}{2}}-\tfrac{1}{2}\mathfrak{g}^{\mu\nu}\varphi_{\mu\nu})+\mathfrak{g}^{\beta\mu}\varphi_{\gamma\mu}]$$
$$-(\mathfrak{g}^{\alpha\beta}R_{\alpha\gamma}-\tfrac{1}{2}\delta^{\beta}_{\gamma}\mathfrak{g}^{\mu\nu}R_{\mu\nu})+\tfrac{1}{2}(\mathfrak{g}^{\mu\nu}{}_{,\gamma}\mathfrak{B}^{\beta}_{\mu\nu}-\delta^{\beta}_{\gamma}\mathfrak{B}). \quad (3.13)$$

The expression in square brackets in (3.13), when the cubes and higher orders of φ's are neglected, reduces to

$$-(-a)^{\frac{1}{2}}(\tfrac{1}{4}\delta^{\beta}_{\gamma}\varphi_{\mu\nu}\varphi^{\mu\nu}-\varphi^{\beta\mu}\varphi_{\gamma\mu}).$$

The reason for not having a minus sign before $\mathfrak{T}^{\alpha}_{\beta}$ in (3.11) is due to the fact that the tensor $R_{\alpha\beta}$ defined by (3.3) has an opposite sign to that of conventional form of $R_{\alpha\beta}$.

We may also define an energy-momentum 4-vector by writing

$$\mathfrak{P}_{\alpha}=\int_{\sigma}\mathfrak{T}^{\beta}_{\alpha}d\sigma_{\beta}, \quad (3.14)$$

where $\mathfrak{P}_{\alpha}$ is a pseudo vector, and $d\sigma_{\beta}$ is a four-dimensional surface element.

Finally it can be shown that, because of $\Gamma_{\alpha}=0$, the field equations are gauge-invariant.

4. LINEAR APPROXIMATIONS TO THE FIELD EQUATIONS

The two spherically symmetric static solutions of Einstein-Schrödinger theories were obtained by Papapetrou.[6] It would be of great interest if one could obtain

[5] B. Kurşunoğlu, Proc. Phys. Soc. (London) **A65**, 81 (1952).
[6] A. Papapetrou, Proc. Roy. Irish Acad. **A52**, 69 (1948).

the same for the present theory. But this is found to be more difficult in this case. In order to see more explicitly the form of the right-hand sides of the field equations (2.8) we first introduce a constant q (with the dimensions of an electric field strength) and write the physical tensor $g_{\alpha\beta}$ as

$$g_{\alpha\beta}=a_{\alpha\beta}+iq^{-1}\varphi_{\alpha\beta}. \tag{4.1}$$

The numerical value of q will be calculated in later sections. For the static spherically symmetric case the right-hand sides of (2.8) have the forms

$$-p^2(a_{11}-b_{11})=-p^2a_{11}\left(1-\frac{1}{(1-E^2/q^2)^{\frac{1}{2}}}\right),$$

$$-p^2(a_{22}-b_{22})=-p^2a_{22}(1-(1-E^2/q^2)^{\frac{1}{2}}),$$

$$-p^2(a_{33}-b_{33})=-p^2a_{33}(1-(1-E^2/q^2)^{\frac{1}{2}})\sin^2\theta,$$

$$-p^2(a_{44}-b_{44})=-p^2a_{44}\left(1-\frac{1}{(1-E^2/q^2)^{\frac{1}{2}}}\right).$$

The comparison of these with the kinetic energy $-m_0c^2[1-(1-v^2/c^2)^{-\frac{1}{2}}]$ is most suggestive;[7] while the latter puts a limit to the velocity of light, the former puts a limit to the electric field strength E. Thus for the consistency of the above expressions we have to impose the condition

$$|E|<q \tag{4.2}$$

upon the electric field E.

Now the symmetric and the antisymmetric parts of $R_{\alpha\beta}$ are

$$R_{\underline{\alpha\beta}}=(\Gamma^{\gamma}_{\underline{\alpha\beta},\gamma}-\Gamma^{\gamma}_{\underline{\alpha\gamma},\beta}+\Gamma^{\gamma}_{\underline{\alpha\beta}}\Gamma^{\rho}_{\gamma\rho}-\Gamma^{\gamma}_{\underline{\alpha\rho}}\Gamma^{\rho}_{\gamma\beta})+\Gamma^{\gamma}_{\underline{\alpha\gamma}}\Gamma^{\rho}_{\gamma\beta}, \tag{4.3}$$

$$R_{\underline{\alpha\beta}}=\Gamma^{\gamma}_{\underline{\alpha\beta},\gamma}+\Gamma^{\gamma}_{\underline{\alpha\beta}}\Gamma^{\gamma}_{\gamma\mu}-\Gamma^{\mu}_{\underline{\alpha\mu}}\Gamma^{\gamma}_{\gamma\beta}-\Gamma^{\mu}_{\underline{\alpha\beta}}\Gamma^{\gamma}_{\alpha\gamma}=\Gamma^{\gamma}_{\underline{\alpha\beta},\gamma}. \tag{4.4}$$

We split up the field variables in the form

$$g_{\alpha\beta}=-\delta_{\alpha\beta}+h_{\alpha\beta}+i\varphi_{\alpha\beta}, \tag{4.5}$$

where $h_{\alpha\beta}$ and $\varphi_{\alpha\beta}$ represent weak gravitational and electromagnetic fields, respectively, where we use the convention $x_4=icl$.

Let us assume that we can neglect

(1) the squares of $h_{\alpha\beta}$;

(2) the cubes and higher orders of $\varphi_{\alpha\beta}$;

(3) gravitational and electromagnetic interaction terms.

Then, using (1.9) and (1.10), one can write

$$\Gamma^{\gamma}_{\underline{\alpha\beta}}=\tfrac{1}{2}I_{\alpha\beta\gamma}-\partial_\gamma\varphi_{\alpha\beta}, \tag{4.6}$$

$$\Gamma^{\gamma}_{\underline{\alpha\beta}}=\tfrac{1}{2}(\partial_\gamma h_{\alpha\beta}-\partial_\beta h_{\alpha\gamma}-\partial_\alpha h_{\beta\gamma})$$
$$+\tfrac{1}{2}(\varphi_{\beta\rho}I_{\alpha\gamma\rho}+\varphi_{\alpha\rho}I_{\beta\gamma\rho})+\varphi_{\beta\rho}\partial_\rho\varphi_{\alpha\gamma}+\varphi_{\alpha\rho}\partial_\rho\varphi_{\gamma\beta}. \tag{4.7}$$

[7] M. Born and L. Infeld, Proc. Roy. Soc. (London) CXLIV, A425 (1934).

The remaining field variables are

$$g=-h+(1-\Omega), \tag{4.8}$$

$$b=1-h=a, \tag{4.9}$$

$$b_{\alpha\beta}=-\delta_{\alpha\beta}+h_{\alpha\beta}-T'_{\alpha\beta}, \tag{4.10}$$

where

$$T_{\alpha\beta}=\tfrac{1}{4}\delta_{\alpha\beta}\varphi_{\mu\nu}\varphi_{\mu\nu}-\varphi_{\alpha\mu}\varphi_{\beta\mu}. \tag{4.11}$$

From (1.11) and (1.12) we can write

$$I_{\alpha\beta\gamma}=\epsilon_{\alpha\beta\gamma\mu}J_\mu, \tag{4.12}$$

$$\partial_\beta f_{\alpha\beta}=J_\alpha, \tag{4.13}$$

where

$$f_{\alpha\beta}=-\tfrac{1}{2}\epsilon_{\alpha\beta\mu\nu}\varphi_{\mu\nu}=\partial_\alpha A_\beta-\partial_\beta A_\alpha, \tag{4.14}$$

and A_α are the potentials of the electromagnetic field. Using (4.14), $T'_{\alpha\beta}$ becomes

$$T'_{\alpha\beta}=\tfrac{1}{4}\delta_{\alpha\beta}\varphi_{\mu\nu}\varphi_{\mu\nu}-\varphi_{\alpha\mu}\varphi_{\beta\mu}=-(\tfrac{1}{4}\delta_{\alpha\beta}f_{\mu\nu}f_{\mu\nu}-f_{\alpha\mu}f_{\beta\mu})=-T_{\alpha\beta}.$$

With these results the field equations (2.8) reduce to

$$\tfrac{1}{2}\Box h_{\alpha\beta}+\tfrac{1}{2}(\delta_{\alpha\beta}J_\mu J_\mu-J_\alpha J_\beta)+\partial_\alpha\varphi_{\beta\rho}\partial_\rho\varphi_{\alpha\rho}$$
$$+\partial_\alpha\partial_\beta(\tfrac{1}{4}f_{\mu\nu}f_{\mu\nu})+\tfrac{1}{2}(f_{\alpha\mu}J_{\beta\mu}+f_{\beta\mu}J_{\alpha\mu}$$
$$-\delta_{\alpha\beta}f_{\mu\nu}J_{\mu\nu})=p^2T_{\alpha\beta}, \tag{4.15}$$

where

$$J_{\alpha\beta}=\partial_\alpha J_\beta-\partial_\beta J_\alpha, \text{ and } \Box=\partial_\mu\partial_\mu, \text{ and } \partial_\alpha=\partial/\partial x^\alpha, \tag{4.16}$$

and the coordinate conditions

$$\partial_\mu h_{\alpha\mu}=\tfrac{1}{2}\partial_\alpha h, \quad (h=h_{\mu\mu}) \tag{4.17}$$

are used. Because of the Bianchi-Einstein identities for the nonsymmetric field the conditions (4.17) are consistent with the field equations.

In the absence of charges we have

$$\tfrac{1}{2}\Box h_{\alpha\beta}+\partial_\mu\varphi_{\beta\rho}\partial_\rho\varphi_{\alpha\mu}+\partial_\alpha\partial_\beta(\tfrac{1}{4}f_{\mu\nu}f_{\mu\nu})=p^2T_{\alpha\beta}. \tag{4.18}$$

A general solution of the wave equation (4.18) for the gravitational potentials $h_{\alpha\beta}$ can be obtained by expressing $\varphi_{\alpha\beta}$ as a superposition of plain waves by means of Fourier integral representation of $\varphi_{\alpha\beta}$. It follows, by differentiation, from (1.11) that $\varphi_{\alpha\beta}$ satisfy

$$\Box\varphi_{\alpha\beta}=0, \tag{4.19}$$

which is solved by

$$\tfrac{1}{2}\varphi_{\alpha\beta}(x)=\int[\varphi_{\alpha\beta}(k)+\overset{*}{\varphi}_{\alpha\beta}(k)]$$
$$\times\exp(ik_\mu x_\mu)\delta(k_\mu{}^2)d^4k, \tag{4.20}$$

where the coefficients $\varphi_{\alpha\beta}$ are undefined, and $\delta(k_\mu{}^2)$ is Dirac's δ-function. The vector k_μ is the wave-number four vector. For the functions $h_{\alpha\beta}$ we write

$$\tfrac{1}{2}h_{\alpha\beta}(x)=\int[h_{\alpha\beta}(k)+\overset{*}{h}_{\alpha\beta}(k)]\exp(ik_\mu x_\mu)d^4k. \tag{4.21}$$

When these are substituted in (4.18), one obtains the gravitational potentials as functions of Maxwell's radi-

ation field. To these solutions one adds the solutions for free gravitational fields.

We identify $\varphi_{\alpha\beta}$ and its dual $f_{\alpha\beta}$ in accordance with the Maxwell's equations (1.11) and (1.14) as

$$\begin{aligned}(\varphi_{23},\ \varphi_{31},\ \varphi_{12};\ \varphi_{41},\ \varphi_{42},\ \varphi_{43})&\\ =(iE_1,\ iE_2,\ iE_3;\ H_1,\ H_2,\ H_3),&\\ (f_{23},\ f_{31},\ f_{12};\ f_{41},\ f_{42},\ f_{43})=(H_1,\ H_2,\ H_3;\ iE_1,\ iE_2,\ iE_3).&\end{aligned}\tag{4.22}$$

By using (4.1) and comparing (4.15) with $G_{\alpha\beta}=-2\bar{\gamma}T_{\alpha\beta}$ of general relativity, we get

$$p^2q^{-2}=2\bar{\gamma}/c^4,\tag{4.23}$$

where $\bar{\gamma}$ = gravitational constant.

5. THE STRUCTURE OF THE ELECTRON

The most interesting feature of the unified field theory is its restriction of the charge-current distribution. This is the essential deviation from Maxwell-Lorentz electrodynamics and is expressed by the field equations (2.9). With the above approximation it works out as

$$(\Box-\kappa^2)J_\alpha=0,\tag{5.1}$$

where

$$\kappa^2=2p^2.\tag{5.2}$$

For an electron at rest the charge density, as follows from (5.1), is

$$\rho=-iJ_4=(e\kappa^2/4\pi)e^{-\kappa r}/r,$$

so that

$$\int\rho dV=4\pi\int_0^\infty\rho r^2dr=e.\tag{5.3}$$

For sufficiently large κ the function ρ behaves as a delta-function multiplied by $4\pi/\kappa^2$ regardless of the order of limits ($r\to0$, $\kappa\to\infty$) or otherwise ($\kappa\to\infty$, $r\to0$). It is easy to see that when the origin $r=0$ is included the function ρ is a solution of

$$(\nabla^2-\kappa^2)\rho=-e\kappa^2\delta(\mathbf{r}),\tag{5.4}$$

where

$$\delta(\mathbf{r})=\delta(x)\delta(y)\delta(z).$$

When rationalized units are used Eqs. (4.13) can be written as

$$\Box A_\alpha=-4\pi J_\alpha\quad\text{and}\quad\partial_\mu A_\mu=0,$$

so that in a static spherically symmetric case the potential $\varphi=-iA_4$ is given by

$$\varphi=(e/r)(1-e^{-\kappa r}),\tag{5.5}$$

where we use the fact that, in case $J_\alpha=0$, the electrodynamics is the same as classical theory.

Our charge distribution has the range of nuclear forces (κ will follow in the next section). It may be objected that the charge of an electron is an indivisible unit; therefore a shape factor κ is out of place, but this is no more an unreasable description of the electron than is the point electron model.[8]

The second term $-(e/r)e^{-\kappa r}$ of φ may be interpreted as causing a force holding the electron to itself.

A further approximation to the field equations (2.9) can be obtained by retaining gravitational and interaction terms in the equations. On multiplying both sides of (2.9) by $\epsilon^{\alpha\beta\gamma\rho}$ we obtain

$$-\kappa^2J_\rho=\epsilon^{\alpha\beta\gamma\rho}\underset{\sim}{\Gamma}^{\sigma}_{\alpha\beta|\sigma,\gamma}.\tag{5.6}$$

Hence, using the expressions for the Γ's, after some lengthy calculations we get

$$\begin{aligned}(\Box-\kappa^2)J_\alpha=&-\kappa^2\gamma J_\alpha-\tfrac{1}{2}(\partial_\mu\gamma)J_{\alpha\mu}+(\partial_\gamma J_\mu)\partial_\mu\gamma_{\alpha\gamma}\\ &-(2\partial_\gamma J_\mu)\partial_\alpha\gamma_{\mu\gamma}+(2\partial_\gamma f_{\mu\nu})\partial_\rho\partial_\alpha\gamma_{\gamma\mu}+(\tfrac{1}{2}\partial_\rho\partial_\mu\gamma)\partial_\rho f_{\alpha\mu}\\ &-(\tfrac{1}{2}\partial_\alpha\gamma)\partial_\alpha J_\mu-(\partial_\beta\partial_\gamma J_\alpha)\gamma_{\beta\gamma}+4(\partial_\beta\partial_\gamma f_{\alpha\mu})\partial_\beta\gamma_{\mu\gamma}\\ &\times(\partial_\rho f_{\gamma\alpha})\partial_\rho\partial_\gamma\gamma-(\partial_\alpha\partial_\gamma\gamma)J_\gamma+(2\partial_\mu J_\alpha)\partial_\mu\gamma,\end{aligned}\tag{5.7}$$

where

$$\gamma_{\alpha\beta}=h_{\alpha\beta}-\tfrac{1}{2}\delta_{\alpha\beta}h,\quad\gamma=-h,\quad\partial_\beta\gamma_{\alpha\beta}=0.$$

The effect of the terms on the right-hand side of (5.7) may be of significance only for heavy particles or for an assembly of particles. The right-hand side of (5.7) is a 4-vector and it is of course conserved. In general, we are going to assume that the effect of those terms are equivalent to a delta-singularity and replace (5.7) by

$$(\Box-\kappa^2)\mathbf{J}_\alpha=-\kappa^2\mathbf{j}_\alpha,\tag{5.8}$$

where

$$\begin{aligned}j_\alpha(x)&=\int_{-\infty}^{s}e\delta(x-\xi)V_\alpha(\xi)ds,\\ \delta(x)&=\delta(x_1)\delta(x_2)\delta(x_3)\delta(x_4),\end{aligned}\tag{5.9}$$

and ξ_α represent the center of the electron and V_α is a four-vector of the second order.

The 4-vector $\mathbf{j}_\alpha$ acts as the source of the 4-current J_α. This may also be regarded as a boundary condition imposed on the current density. We infer from (5.8) that the charge distribution of the electron has a range κ^{-1}.

The electrostatic field due to an electron at rest is

$$E=-d\varphi/dr=(e/r^2)[1-e^{-\kappa r}-\kappa re^{-\kappa r}],\tag{5.10}$$

from which the field at $r=0$ comes out as

$$E(0)=e\kappa^2/2,\tag{5.11}$$

and the potential has its maximum at $r=0$ as

$$\varphi(0)=e\kappa.\tag{5.12}$$

At $r=0$, φ and E have a finite discontinuity.

[8] A point electron may be regarded as an infinitely compressed form of the actual (extended) electron, and for this process of localization into a point an infinite amount of energy has to be used. This may also be seen quite easily by expanding the delta-function in terms of the eigenfunctions of a suitable energy operator $\mathbf{I}$, of course, leads to the so-called infinite self-energy of the electron in classical and quantum field theories.

Unified field theory describes the charge density of an elementary particle as a short range field. It is not possible to measure the effects of an electron "radius" κ^{-1} by having two electrons collide with an energy of the order mc^2. Quantum theoretically the wavelength corresponding to this energy is $\hbar/mc$, which is much larger than κ^{-1}. Thus it is impossible to locate the electron at that energy better than within $\hbar/mc$. During a collision their average distance will never be within a distance comparable with κ^{-1}.

A solution of (5.8) can be obtained by means of Fourier integral representation as

$$J_\alpha^{\rm ret}(x)=\kappa^2\int\bar{\Delta}^{\rm ret}(x-x')j_\alpha(x')d^4x', \qquad (5.13)$$

where

$$\bar{\Delta}^{\rm ret}(x)=\bar{\Delta}(x)-\tfrac{1}{2}\Delta(x)$$

are Lorentz invariant scalar functions,[9] and they vanish outside the light cone and are singular on the light cone so that the solutions (5.13) are causally correct. The 4-current $J_\alpha^{\rm ret}$ given by (5.13) is conserved.

It can easily be seen, by writing (5.13) in terms of Fourier components, that

$$\int_{-\infty}^{\infty}J_4(x)dt=\frac{e\kappa^2}{4\pi}\frac{e^{-\kappa r}}{r}.$$

The equations,

$$\Box A_\alpha=-4\pi J_\alpha, \quad (\Box-\kappa^2)J_\alpha=-\kappa^2 j_\alpha, \qquad (5.14)$$

in quantum electrodynamics, imply a two-particle picture (photon+meson). Their combined form, i.e., a fourth-order equation in A_α, have been discussed extensively,[10] and it is found that a fourth-order partial differential equation is not, because of occurrence of negative probabilities, consistent with the physical reality. In the present case this objection does not arise, since Eqs. (5.14) can be replaced by

$$\Box A_\alpha=-4\pi\kappa^2\int\bar{\Delta}^{\rm ret}(x-x')j_\alpha(x')d^4x', \qquad (5.15)$$

which means that electromagnetic field can be split up as a "short-range" and "long-range" parts. Thus one can regard a neutral vector meson field as part of the electromagnetic field. Equations (5.15) are solved by

$$A_\alpha^{\rm ret}(x)=4\pi\kappa^2\int D^{\rm ret}(x-x')\bar{\Delta}^{\rm ret}(x'-x'')\times j_\alpha(x'')d^4x'd^4x'', \qquad (5.16)$$

where $D^{\rm ret}(x)$ is obtained by putting $\kappa=0$ in the expression of $\bar{\Delta}^{\rm ret}(x)$. In actual case there was no need for the definition of the current density J_α given by (1.11). Equations (2.9) approximate to

$$(\Box-\kappa^2)\partial_\beta f_{\alpha\beta}=-\kappa^2 j_\alpha, \qquad (5.17)$$

so that the second set of Maxwell's equations are to be obtained by solving (5.17). In this sense, we can say that the sources of the electromagnetic field are contained in our field equations.

In the present theory, if one attempted to construct an S-matrix of quantum electrodynamics in interaction representation, then the interaction Hamiltonian would be $\mathfrak{H}=-(1/c)J_\mu^{\rm ret}A_\mu$ instead of $(1/c)j_\mu A_\mu$. The former contains the invariant function $\bar{\Delta}^{\rm ret}(x-x')$. Strictly speaking the S-matrix,

$$P\exp\left[-\frac{i}{hc}\int_{-\infty}^{\infty}\mathfrak{H}(x)d^4x\right],$$

when expanded will have, with each term, associated various powers of $\bar{\Delta}^{\rm ret}(x)$ so that one expects the results for any physical process to be convergent. It, of course, is not possible to say without going into details, that this proposition will be free of objections.

6. THE NATURE OF THE ELECTROMAGNETIC MASS

The energy-momentum tensor (3.13), when the approximation procedure of Sec. 4 is used, can easily be put into the form

$$4\pi p^2\mathfrak{T}_{\alpha\beta}=-p^2T_{\alpha\beta}+\tfrac{1}{2}f_{\beta\mu}J_{\alpha\mu}+\tfrac{1}{4}\delta_{\alpha\beta}J_\mu J_\mu -\tfrac{1}{8}\delta_{\alpha\beta}\Box(f_{\mu\nu}f_{\mu\nu})+\tfrac{1}{2}J_\mu\partial_\beta f_{\alpha\mu} +\tfrac{1}{2}\partial_\alpha f_{\mu\nu}\partial_\beta f_{\mu\nu}-\tfrac{1}{4}\delta_{\alpha\beta}J_{\mu\nu}f_{\mu\nu}. \qquad (6.1)$$

The tensor $\mathfrak{T}_{\alpha\beta}$ is nonsymmetric; it can be symmetrized by using a standard method[11] so as to secure the conservation of the angular momenta, but for the following purpose its symmetrization is only of an academic interest and, therefore, no attempt will be made for it.

For the static spherically symmetric case, in spherically polar coordinates diagonal components of $\mathfrak{T}_{\alpha\beta}$ are given by

$$4\pi p^2\mathfrak{T}_{11}=\tfrac{1}{2}p^2E^2-4\pi^2\rho^2+\tfrac{1}{4}\nabla^2E^2 -2\pi E\frac{d\rho}{dr}+\frac{1}{4}\frac{1}{r}\frac{dE^2}{dr}+\frac{1}{2}\sin^2\theta\cos^2\varphi \times\left[\frac{1}{2r}\frac{dE^2}{dr}-\left(\frac{dE}{dr}\right)^2+4\pi E\frac{d\rho}{dr}-\kappa^2E^2\right],$$

$$4\pi p^2\mathfrak{T}_{22}=\tfrac{1}{2}p^2E^2-4\pi^2\rho^2+\tfrac{1}{4}\nabla^2E^2 -2\pi E\frac{d\rho}{dr}+\frac{1}{4}\frac{1}{r}\frac{dE^2}{dr}+\tfrac{1}{2}\sin^2\theta\sin^2\varphi \times\left[\frac{1}{2r}\frac{dE^2}{dr}-\left(\frac{dE}{dr}\right)^2+4\pi E\frac{d\rho}{dr}-\kappa^2E^2\right], \qquad (6.2)$$

[9] J. Schwinger, Phys. Rev. **75**, 677 (1949).
[10] A. Pais and G. E. Uhlenbeck, Phys. Rev. **79**, 145 (1950).
[11] G. Wentzel, *Quantum Theory of Fields* (Interscience Publications, New York, 1949).

$$4\pi\rho^2\mathfrak{T}_{22}=\tfrac{1}{2}\rho^2E^2-4\pi^2\rho^2+\tfrac{1}{4}\nabla^2E^2$$
$$-2\pi E\frac{d\rho}{dr}+\frac{1}{4}\frac{1}{r}\frac{dE^2}{dr}+\tfrac{1}{2}\cos^2\theta$$
$$\times\left[\frac{1}{2r}\frac{dE^2}{dr}-\left(\frac{dE}{dr}\right)^2+4\pi E\frac{d\rho}{dr}-\kappa^2E^2\right],$$

$$4\pi\rho^2\mathfrak{T}_{44}=-\tfrac{1}{2}\rho^2E^2-4\pi^2\rho^2+\tfrac{1}{4}\nabla^2E^2, \tag{6.3}$$

where the electrostatic field E is given by

$$-if_{4s}=E_s=(x_s/r)\,|E|, \quad (s=1,2,3) \tag{6.4}$$

and $|E^2|=E_1^2+E_2^2+E_3^2$ is a function of r only.

By integrating $\mathfrak{T}_{44}$ through the whole of space we can calculate the constant κ in terms of the mass and charge of the electron. The following integrals will be used throughout the following discussions:

$$\int E^2dV=4\pi\int_0^\infty\frac{d\varphi}{dr}\frac{d\varphi}{dr}r^2dr=2\pi e^2\kappa,$$

$$\int\rho^2dV=4\pi\int^\infty r^2\left(\frac{e\kappa^2}{4\pi}\frac{\bar{e}^{\kappa r}}{r}\right)^2dr=\frac{1}{8\pi}e^2\kappa^3, \tag{6.5}$$

$$\int\nabla^2E^2dV=4\pi\left[r^2\frac{dE^2}{dr}\right]_0^\infty=0, \quad \int E\frac{d\rho}{dr}dV=-\tfrac{1}{2}e^2\kappa^3.$$

Now

$$-\mathfrak{T}_{44}=\text{energy density}=\sigma c^2,$$

where $\sigma=$ mass density, so that

$$-4\pi\rho^2\int\mathfrak{T}_{44}dV=\tfrac{1}{2}\rho^2\int E^2dV+4\pi^2\int\rho^2dV.$$

Hence,

$$m_0c^2=\tfrac{1}{2}\kappa e^2,$$

and

$$\kappa=2m_0c^2/e^2. \tag{6.6}$$

Note that each term in the above contributes half of the rest mass of the electron. The appearance of the factor 2 in (6.6) is a most important feature of the entire theory. This we shall explain a little later. The constant p follows as

$$p=(1/\sqrt{2})\kappa=\sqrt{2}m_0c^2/e^2.$$

The constant q, using (4.23), is

$$q=m_0c^4/e^2\sqrt{\gamma}=1.2\times10^{37}\text{ esu.}^{11a} \tag{6.7}$$

Thus the inequality (4.2) finds its most convincing explanation. It follows also from (5.11) that

$$E^2(0)/q^2=4\cdot\gamma m_0^2/e^2$$
$$=4\cdot\text{gravitational force/electrostatic force.}$$

[11a] From (6.7), (5.11), and (4.2) it follows that the rest mass of any elementary charged particle satisfies the inequality:

$$m_0<\tfrac{1}{2}|e|/\sqrt{\gamma}\approx10^{-6}\text{ g.}$$

For the radial and transverse stress components we have

$$\int\mathfrak{T}_{11}dV=\int\mathfrak{T}_{22}dV=\int\mathfrak{T}_{33}dV=0, \tag{6.8}$$

which is the so-called Laue theorem. Thus, our electron is a stable structure.

The integrals of the rest of $\mathfrak{T}_{\alpha\beta}$ give

$$\int\mathfrak{T}_{mn}dV=0, \quad \int\mathfrak{T}_{4m}dV=\int\mathfrak{T}_{m4}dV=0, \ m\neq n.$$

Now, a few words on the electromagnetic mass are necessary. The potential $\varphi(r)$ reaches its maximum at $r=0$, and it is $\varphi(0)=e\kappa=2m_0c^2/e$. Since the entire mass is contributed by an electromagnetic field with a "short-range" and a "long-range" parts, then, from a classical point of view in bringing a positron and electron charge together all external fields are canceled out, and an energy of $2m_0c^2$ is released which is the rest mass of these particles in virtue of their fields. This may also mean that the rest mass of the two particles is equivalent to the work done in separating them against their mutual attraction after they "are created."[12] Similar arguments may be applied for the origin of the neutral matter.

7. EQUATIONS OF MOTION

It has been shown[13] that in the presence of an electromagnetic field the equations $G_{\alpha\beta}=-2\bar{\gamma}T_{\alpha\beta}$ gave a correct law of motion for a charged particle. It has also been shown[14] that Einstein's theory gives no interaction between a charged particle and electromagnetic field: a result that could be deduced immediately from our discussion on the energy-momentum tensor of the field.

In the present theory a particle is to be represented as a concentration of the field energy density into a very small space-time region where, contrary to the assumption of a singularity, the laws of field are known and the magnitude of the field strength can be expressed in terms of finite but large numbers. Thus the application of the methods of general relativity to the present case is not suitable, and it has to be modified. The surface integral conditions[15] of general relativity are empty in this case.

It is quite easy to show from the assumption that mass is entirely of an electromagnetic origin and from the field equations that the equations of motion of an electron in an external field have the correct form.

Now let

$$f_{\alpha\beta}=\overset{(s)}{f}_{\alpha\beta}+\overset{(e)}{f}_{\alpha\beta}, \tag{7.1}$$

[12] R. P. Feynman, Phys. Rev. **74**, 939 (1948).
[13] L. Infeld and P. R. Wallace, Phys. Rev. **57**, 797 (1940).
[14] L. Infeld, Acta Polonica **X**, 284 (1951).
[15] A. Einstein and L. Infeld, Can. J. Math. **1** (1949).

where

$\overset{(e)}{f}_{\alpha\beta}$ = proper field of the electron,

$\overset{(e)}{f}_{\alpha\beta}$ = external field.

We assume that the acceleration of the particle is not too large, so that we can make use of a Lorentz transformation.

When the field equations (1.8) are granted, then, as in general relativity, the field equations can also be obtained from an action principle[4]

$$\delta\int \mathfrak{H}d^4x=0,$$

where

$$-8\pi p^2\mathfrak{H}=\mathfrak{B}+2p^2(-b)^{\frac{1}{2}}-(-g)^{\frac{1}{2}}. \tag{7.2}$$

In this case the field variables $\mathfrak{g}^{\alpha\beta}=\mathfrak{g}^{\alpha\beta}{}_{,\gamma}$ and $\mathfrak{g}^{\alpha\beta}$ are to be varied independently. The complete antisymmetric tensor density $\mathfrak{g}^{\alpha\beta\gamma}=\epsilon^{\alpha\beta\gamma\delta}A_\delta$ is the dual of A_α. With the approximation of Sec. 4 we have

$$\mathfrak{B}=\tfrac{1}{2}J_\mu J_\mu-(\varphi_{\mu\nu}\varphi_{\gamma\mu})_{,\gamma\nu},$$

the last term of which can be dropped from the action principle, and we get

$$-4\pi p^2\int \mathfrak{H}d^4x=\delta\int(\tfrac{1}{4}p^2f_{\mu\nu}f_{\mu\nu}+\tfrac{1}{4}J_\mu J_\mu)d^4x. \tag{7.3}$$

Now, using (7.1) we obtain

$$-4\pi\int \mathfrak{H}d^4x=\delta\int[\tfrac{1}{4}\overset{(e)}{f}_{\mu\nu}\overset{(e)}{f}_{\mu\nu}+\tfrac{1}{4}p^{-2}J_\mu J_\mu]d^4x$$
$$+\tfrac{1}{2}\delta\int \overset{(e)}{f}_{\mu\nu}\overset{(e)}{f}_{\mu\nu}d^4x+\tfrac{1}{4}\delta\int \overset{(e)}{f}_{\mu\nu}\overset{(e)}{f}_{\mu\nu}d^4x. \tag{7.4}$$

We define the quantity $\mathfrak{L}$ by

$$4\pi\mathfrak{L}=\int \overset{(e)}{\mathfrak{H}}d^3x+\int \tfrac{1}{2}\overset{(e)}{f}_{\mu\nu}\overset{(e)}{f}_{\mu\nu}d^3x. \tag{7.5}$$

Hence,

$$4\pi\delta\int \mathfrak{H}d^4x=4\pi\delta\int \mathfrak{L}dt,$$

where

$$\overset{(e)}{\mathfrak{H}}=\tfrac{1}{4}\overset{(e)}{f}_{\mu\nu}\overset{(e)}{f}_{\mu\nu}+\tfrac{1}{4}p^{-2}J_\mu J_\mu.$$

The last term in (7.4), because of $\partial_\nu f^{(e)}{}_{\mu\nu}=0$, drops out, also in the rest frame of the electron we have (writing $4\pi J_\alpha$ for J_α)

$$-4\pi\int \overset{(e)}{\mathfrak{H}}d^3x=\tfrac{1}{2}\int E^2dV+4\pi^2p^{-2}\int \rho^2dV=4\pi m_0c^2,$$

so that we can write

$$-\int \overset{(e)}{\mathfrak{H}}d^3x=m_0c^2(1-v^2/c^2)^{\frac{1}{2}},$$

where v = velocity of the center of the electron.

From these results it follows that (7.4) is

$$\delta\int m_0c^2\left(1-\frac{v^2}{c^2}\right)^{\frac{1}{2}}dt+\tfrac{1}{2}\delta\int \overset{(e)}{f}_{\mu\nu}\overset{(e)}{f}_{\mu\nu}d^4x=0. \tag{7.6}$$

Now, we have

$$\overset{(e)}{f}_{\mu\nu}=\partial_\mu\overset{(e)}{A}_\nu-\partial_\nu\overset{(e)}{A}_\mu,\quad \partial_\nu\overset{(e)}{f}_{\mu\nu}=4\pi J_\mu.$$

Using these equations in (7.6) and integrating by parts and dropping the divergence terms we get

$$\mathfrak{L}=m_0c^2(1-v^2/c^2)^{\frac{1}{2}}-\int \overset{(e)}{A}_\mu J_\mu d^3x. \tag{7.7}$$

Thus we have obtained the action function of Maxwell-Lorentz theory. An electron behaves as a mechanical system with the rest mass m_0 acted on by the external field $\overset{(e)}{f}_{\alpha\beta}$.

If we assume that the electron is moving in a constant external field $\overset{(e)}{A}_\mu$, then we obtain

$$\int \mathfrak{L}dt=\int m_0c^2(1-v^2/c^2)^{\frac{1}{2}}dt-e\int A_\mu V_\mu dtd^3x.$$

Thus in a slowly varying field the generally covariant force law can be stated as

$$\frac{dV^\alpha}{d\tau}+\left\{\begin{matrix}\alpha\\ \beta\gamma\end{matrix}\right\}_b V^\beta V^\gamma=\frac{e}{m_0c^2}\Psi^{\alpha\mu}V_\mu, \tag{7.8}$$

where $V_\mu=dx_\mu/d\tau$,

$$\Psi_{\alpha\beta}=-\tfrac{1}{2}\epsilon_{\alpha\beta\mu\nu}\mathfrak{Q}^{\mu\nu}=(f_{\alpha\beta}-\Lambda\varphi_{\alpha\beta})/(1-\Omega-\Lambda^2)^{\frac{1}{2}}, \tag{7.9}$$

and

$$d\tau^2=b_{\alpha\beta}dx^\alpha dx^\beta. \tag{7.10}$$

We must mention the fact that these results could also be deduced, without making the above approximations, merely from the fact that the expression (7.2) is already contained in $\mathfrak{T}_4{}^4$ and contributes the total rest mass m_0 of the electron. In (7.8) $\Psi_{\alpha\beta}$ refers to the actual field, i.e., the external field plus the field produced by the particles themselves.

8. DEFLECTION OF LIGHT

For a static spherically symmetric field, Eqs. (4.15), in spherical polar coordinates, give

$$\nabla^2\tfrac{1}{2}h_{44}=\tfrac{1}{2}p^2q^{-2}E^2, \tag{8.1}$$

$$\nabla^2\tfrac{1}{2}h_{11}=-\tfrac{1}{2}p^2q^{-2}E^2+4\pi q^{-2}E\frac{d\rho}{dr}+8\pi^2\rho^2q^{-2}$$
$$-\frac{1}{2}q^{-2}\frac{1}{r}\frac{dE^2}{dr}+q^{-2}\sin^2\theta\cos^2\varphi$$
$$\times\left[\left(\frac{dE}{dr}\right)^2-\frac{1}{2}\frac{1}{r}\frac{dE^2}{dr}+p^2E^2\right],$$

$$\nabla^2\tfrac{1}{2}h_{22}=-\tfrac{1}{2}p^2q^{-2}E^2+4\pi q^{-2}E\frac{d\rho}{dr}+8\pi^2\rho^2q^{-2}$$
$$-\frac{1}{2}q^{-2}\frac{1}{r}\frac{dE^2}{dr}+q^{-2}\sin^2\theta\sin^2\varphi$$
$$\times\left[\left(\frac{dE}{dr}\right)^2-\frac{1}{2}\frac{1}{r}\frac{dE^2}{dr}+p^2E^2\right], \quad (8.2)$$

$$\nabla^2\tfrac{1}{2}h_{33}=-\tfrac{1}{2}p^2q^{-2}E^2+4\pi q^{-2}E\frac{d\rho}{dr}+8\pi^2\rho^2q^{-2}$$
$$-\frac{1}{2}q^{-2}\frac{1}{r}\frac{dE^2}{dr}+q^{-2}\cos^2\theta$$
$$\times\left[\left(\frac{dE}{dr}\right)^2-\frac{1}{2}\frac{1}{r}\frac{dE^2}{dr}+p^2E^2\right].$$

All other components vanish because of spherical symmetry.

Now if we consider the gravitational field of an electron at rest the above expressions, when integrated through the whole of space, give

$$\int-\nabla^2h_{11}dV=\int-\nabla^2h_{22}dV=\int-\nabla^2h_{33}dV$$
$$=\int\nabla^2h_{44}dV=2\pi e^2\kappa p^2q^{-2}=\frac{8\pi\bar{\gamma}}{c^2}m_0. \quad (8.3)$$

The contributions of the terms on the right-hand side of the equations (8.2) to the mass of the electron, except the first term, vanish.[16]

From (8.3) it follows that for a macroscopic distribution of mass density Eqs. (8.1)–(8.2) can be written as

$$\nabla^2h_{44}=\kappa_0\sigma, \quad (8.4)$$
$$\nabla^2h_{11}=-\kappa_0\sigma+\kappa_0\sigma_1+\kappa_0\sigma_2\sin^2\theta\cos^2\varphi, \quad (8.5)$$
$$\nabla^2h_{22}=-\kappa_0\sigma+k_0\sigma_1+\kappa_0\sigma_2\sin^2\theta\sin^2\varphi, \quad (8.6)$$
$$\nabla^2h_{33}=-\kappa_0\sigma+\kappa_0\sigma_1+\kappa_0\sigma_2\cos^2\theta, \quad (8.7)$$

where

$$\sigma=(1/4\pi c^2)\textstyle\sum_n E_n^2=\text{density of mass per unit volume}, \quad (8.8)$$

and

$$\kappa_0=8\pi\bar{\gamma}/c^2.$$

The densities σ_1 and σ_2 represent the rest of the terms on the right-hand sides of the equations (8.2). Note that because of (8.3), we have

$$\int(\sigma_1+\sigma_2\sin^2\theta\cos^2\varphi)dV=\int(\sigma_1+\sigma_2\sin^2\theta\sin^2\varphi)dV$$
$$=\int(\sigma_1+\sigma_2\cos^2\theta)dV=0. \quad (8.9)$$

In (8.8) E_n can be replaced by its maximum value $\frac{1}{2}e_n\kappa^2$ where κ can take two values κ_e and κ_p for electron and proton, respectively, so that

$$E_n=2e_n(m_{0n}c^2/e_n^2)^2,$$

and

$$E_n^2=4m_{0n}c^2(m_{0n}c^2/e_n^2)^2.$$[17]

If we put

$$V_0=\pi(e^2/m_0c^2)^3=\text{"volume of the particle,"}$$

then, we get

$$\sigma=\textstyle\sum_n(m_{0n}/V_n).$$

With the arguments given at the end of Sec. 6 we are now in a position to regard the system (8.4)–(8.7) as representing the equations of a gravitational field produced by the density σ of matter. The solutions of (8.4)–(8.7) can be written down at once, as

$$h_{44}=-\frac{\kappa_0}{4\pi}\int\frac{\sigma(r')dV'}{|r-r'|}, \quad (8.10)$$

$$h_{11}=h_{22}=h_{33}=\frac{\kappa_0}{4\pi}\int\frac{\sigma(r')dV'}{|r-r'|}$$
$$-\frac{\kappa_0}{4\pi}\int\frac{\sigma_1(r')}{|r-r'|}dV'-\frac{\kappa_0}{4\pi}\frac{1}{3}\int\frac{\sigma_2(r')dV'}{|r-r'|}. \quad (8.11)$$

Hence, because of the second and third terms on the right-hand side of (8.11), the potentials h_{11}, h_{22}, h_{33} are different from that of general relativity. But since our main interest is, as will be seen in the following, in the partial derivatives of h_{11}, h_{22}, h_{33}, h_{44} with respect to the coordinate x and integration of the results between the limits $(-\infty, \infty)$, the contribution of the second and third terms on the right-hand side of (8.11) will, because of (8.9), vanish, *viz.*,

$$\int_{-\infty}^{\infty}\frac{\partial h_{11}}{\partial x}dz=\frac{\kappa_0}{4\pi}\int\int_{-\infty}^{\infty}\sigma(r')dV'\frac{\partial}{\partial x}\left(\frac{1}{|r-r'|}\right)dz$$
$$-\frac{\kappa_0}{4\pi}\int[\sigma_1(r')+\tfrac{1}{3}\sigma_2(r')]dV'$$
$$\times\int_{-\infty}^{\infty}\frac{\partial}{\partial x}\left(\frac{1}{|r-r'|}\right)dz=-\frac{\kappa_0}{2\pi}MR^{-1},$$

where

$$M=\int\sigma(r')dV'=\text{total mass}.$$

[16] It is clear that the value of κ given by (6.6) enables us to regard m_0, calculated as an electromagnetic mass, also as the gravitational mass of a particle. The same constant m_0 in Sec. 7 behaves as a mechanical mass. Thus electromagnetic mass = inertial mass = gravitational mass, which is the statement of the "principle of equivalence." The constant κ could also be calculated from (8.3).

[17] This gives a density of matter of the order 10^{13} g cm^{-3}, which is similar to the liquid drop model of the nucleus.

Now, if we neglect the term $q^{-2}T_{\alpha\beta}dx^\alpha dx^\beta$ in the expression of the metric of the space-time, we can write

$$d\tau^2=-\left(1+\frac{\kappa_0}{4\pi}\int\frac{\sigma(r')}{|r-r'|}dV'\right)(dx^2+dy^2+dz^2)$$
$$+c^2\left(1-\frac{\kappa_0}{4\pi}\int\frac{\sigma(r')dV'}{|r-r'|}\right)dt^2. \quad (8.12)$$

This result is the same as the one obtained by Einstein in general relativity. The required deflection of light passing near a strong gravitational field follows from

$$d\tau^2=0.$$

Hence, if L is the velocity of light, we have approximately

$$L=c\left(1-\frac{\kappa_0}{4\pi}\int\frac{\sigma(r')}{|r-r'|}dV'\right), \quad (8.13)$$

so that the deflection of light is

$$\alpha=\int_{-\infty}^{\infty}\frac{1}{L}\frac{\partial L}{\partial x}dz=\frac{\kappa_0 M}{2\pi R}=1.75', \quad (8.14)$$

in complete agreement with the result of general relativity.[18]

The author is not aware of any other unified field theory comprising the results obtained in the foregoing. We think that these implications of the theory are important enough to warrant our confidence in its validity as a correct physical theory.

The author is grateful to Professor P. A. M. Dirac and to Dr. C. A. Hurst for many useful discussions and finally to the Turkish Government for the award of a scholarship.

[18] It can easily be seen that for $\kappa=0$ the above theory reduces to Einstein's version of the unified field theory.

PHYSICAL REVIEW VOLUME 88, NUMBER 6 DECEMBER 15, 1952

Mobility in High Electric Fields

E. M. Conwell*
Bell Telephone Laboratories, Murray Hill, New Jersey
(Received July 17, 1952)

An extension of conductivity theory to high fields, subject to the usual simplifying assumptions, is carried out for the cases in which the change of energy of an electron in a collision can be neglected. This yields a relationship between mobility and relaxation time which is valid over a wide range of fields.

THE formal theory of conduction can be extended simply to cover the case of high fields when the scattering processes which give rise to the resistance are to a good approximation elastic. This condition is satisfied in monatomic solids for the range of temperature and field strength in which collisions are mainly with acoustical modes of lattice vibrations and impurities. Experiments indicate that in germanium at room temperature, for example, this is the case up to about 4000 volts per cm.[1] This condition is also satisfied for electrons in a gas when the collisions are nonionizing ones with atoms or ions.

The distribution function for the electrons in an electric field will be denoted by $f(\mathbf{k}, \mathbf{E})$, where $\mathbf{k}$ is the wave vector and $\mathbf{E}$ is the electric field intensity. If we neglect crystal anisotropy, since the scattering is elastic the distribution function in the presence of the field will be nearly isotropic in k space. It can be shown that it is a good approximation to take

$$f(\mathbf{k}, \mathbf{E})=f_0(k, E)-f_1(k, E)\cos\theta, \quad (1)$$

where θ is the angle between $\mathbf{k}$ and the field direction, chosen as the z axis, and f_1 is much smaller than f_0. In low fields, of course, f_0 will be the zero field equilibrium distribution. In the steady state, the rate of change of f due to the field must be balanced by the rate of change due to collisions, or

$$(eE/\hbar)(\partial f/\partial k_z)+(\partial f/\partial t)_c=0. \quad (2)$$

It has been shown that probabilities of scattering by lattice vibrations or imperfections are independent of electric field intensity up to fields of the order of 6×10^5 volts per cm.[2] In the approximation that the scattering is elastic, transitions will take place to states on the constant energy surface. Let the probability of transition per unit time from a state near $\mathbf{k}$ to one of a group of states in area dS' of the constant energy surface be denoted by $P(\mathbf{k}, \mathbf{k}')dS'$. Then

$$(\partial f/\partial t)_c=-\int_{S'}[f(\mathbf{k}, \mathbf{E})P(\mathbf{k}, \mathbf{k}')$$
$$-f(\mathbf{k}', \mathbf{E})P(\mathbf{k}', \mathbf{k})]dS'. \quad (3)$$

To carry this further it is necessary to assume that $P(\mathbf{k}, \mathbf{k}')=P(\mathbf{k}', \mathbf{k})$ and depends only on the angle between $\mathbf{k}$ and $\mathbf{k}'$. Since collisions can only redistribute electrons around the constant energy surface, f_0 does not contribute to this term. The rate of change of f_1 may be found by considering an element of phase

* On leave from Brooklyn College, Brooklyn, New York.
[1] W. Shockley, Bell System Tech. J. **30**, 990 (1951).
[2] J. Bardeen and W. Shockley, Phys. Rev. **80**, 69 (1950).

space along the **k** vector parallel to **E**. Using (1), we obtain

$$(\partial f_1/\partial t)_c = +\int_{S'} f_1(k, E)(1-\cos\theta)P(\theta)dS', \quad (4)$$

$$(\partial f_1/\partial t)_c = +[f_1(k, E)]/[\tau(k)], \quad (5)$$

where τ is the zero field relaxation time. Equation (2) then takes the form

$$(eE/h)(df/dk)+(f_1/\tau)=0, \quad (6)$$

for high as well as low fields.[3]

Since the isotropic part of the distribution will not contribute to the current, the current density is given by

$$j=\int\int\int \frac{\hbar k}{m}\cos\theta(-f_1\cos\theta)\frac{2}{(2\pi)^3}k^2\sin\theta d\theta d\phi dk, \quad (7)$$

where the integration is over all k space. Using (6) to eliminate f_1, we obtain

$$j=\frac{2}{(2\pi)^3}\frac{e^2}{m}E\int\int\int\tau\frac{df}{dk}k^3\cos^2\theta\sin\theta d\theta d\phi dk. \quad (8)$$

We now make the assumption that the energy surfaces are spherical. The integration can then be carried out, giving

$$j=\frac{1}{3\pi^2}\frac{e^2}{m}E\left[(k^3\tau f)\Big|_0^\infty-\int_0^\infty f\frac{d}{dk}(k^3\tau)dk\right]. \quad (9)$$

For the mechanisms of scattering under consideration, $k^3\tau$ vanishes at the lower limit, and the first term makes no contribution to j. The expression can then be written

$$j=-\frac{e^2}{3m}E\int_0^\infty\frac{1}{k^2}\frac{d}{dk}(k^3\tau)f(k)\frac{1}{\pi^2}k^2dk$$

$$=\frac{e^2}{3m}En\left\langle\frac{1}{k^2}\frac{d}{dk}(k^3\tau)\right\rangle, \quad (10)$$

where n is the number of electrons per unit volume, and the quantity in brackets is to be averaged over all electrons. In terms of the mobility, this result is

$$\mu=\frac{e}{3m}\left\langle\frac{1}{k^2}\frac{d}{dk}(k^3\tau)\right\rangle. \quad (11)$$

In this form the result is valid for low fields and high within the limits that the scattering is nearly elastic. It yields a field-dependent mobility at high fields because the electron distribution is field-dependent.

It is easily checked that this gives correct results in all familiar low field cases. For example, in the case of lattice or impurity scattering in nondegenerate semiconductors at low fields it gives the same mobility as $(e/m)\langle v^2\tau\rangle/\langle v^2\rangle$, which is valid for a Maxwell-Boltzmann distribution.[4] At high fields it gives the correct drift velocity for electrons in a gas, for which the high field distribution is known.[5] It has been pointed out by Wannier that this expression for the mobility is derivable in the high field case from the equation system (17) of his paper.[6]

[3] Essentially this equation is derived for electrons in a gas in high fields in S. Chapman and T. G. Cowling, *Mathematical Theory of Non-Uniform Gases* (Cambridge University Press, Cambridge, 1939), p. 346.

[4] W. Shockley, *Electrons and Holes in Semiconductors* (D. Van Nostrand Company, Inc., New York, 1950), p. 276.

[5] See reference 3, p. 351.

[6] G. Wannier, Phys. Rev. **83**, 281 (1951).

PHYSICAL REVIEW VOLUME 88, NUMBER 6 DECEMBER 15, 1952

The Comparison between the Longitudinal Correlation and the Time Correlation in a Turbulent Flow*

F. N. Frenkiel
Applied Physics Laboratory, The Johns Hopkins University, Silver Spring, Maryland

(Received June 20, 1952)

Some preliminary applications of high speed computing to the analysis of experimental data on turbulence are reported. A time correlation curve is determined from a recording of velocity fluctuations measured with a single hot-wire anemometer. The shape of the time correlation curve differs from the shape of the longitudinal correlation curve measured in the same fluid flow. One must, therefore, be cautious in reaching conclusions from experiments based on the assumption that time and space spectra of turbulence are identical. A more extensive study of the relation between time and space characteristics of turbulence is in process.

WHEN the relation between a spectrum of turbulence and a correlation coefficient was first found by Taylor,[1] an assumption was made that the turbulence pattern moves in the fluid stream without changing. This assumption was necessary, since Taylor's spectrum described a statistical characteristic of velocity fluctuations at a fixed point of the fluid flow while his correlation coefficient referred to simultaneous velocity fluctuations along the mean velocity direction. Taylor's

* This work was supported by the U. S. Navy Bureau of Ordnance.

[1] G. I. Taylor, Proc. Roy. Soc. (London) **A164**, 476 (1938).

assumption is, of course, meant as an approximation and in many cases its use is fully justified. In a field of decaying turbulence the time-spectrum[1] cannot be identical with the one-dimensional longitudinal spectrum[2]; if it were, there would not be any decay whatsoever. One must, therefore, be rather cautious in reaching conclusions concerning the decay of turbulence when these conclusions are based on the assumption that the time-spectrum and the longitudinal spectrum are identical. The relation between certain time and space characteristics has been discussed elsewhere.[2,3] It is difficult to establish a rigorous theoretical relation between these characteristics without other assumptions. A direct experimental comparison between them may, therefore, be valuable. The present note describes some preliminary data obtained during the preparation of an extensive investigation in this field.

Oscillographic recordings of the fluctuations of the turbulent velocity made with a hot-wire anemometer were used for this investigation. The measurements (made available by Dr. G. B. Schubauer of the National Bureau of Standards) were obtained in a wind-tunnel at a point 10 feet downstream of a 3½-inch mesh grid at a wind speed of 20 feet per second. The velocity was determined as a function of the time by reading, on the oscillographic recording, the velocity at 1779 instants, $t_1, t_2, \cdots$ spaced at intervals equal to approximately 1/3100 second.

Various statistical characteristics of turbulence, including frequency distributions and second- and third-order correlation curves, were then determined using punch-card computing machines.[4] The second-order time correlation coefficient for the turbulent velocities u_i' and u_{i+h}' at two instants t_i and t_{i+h} separated by an

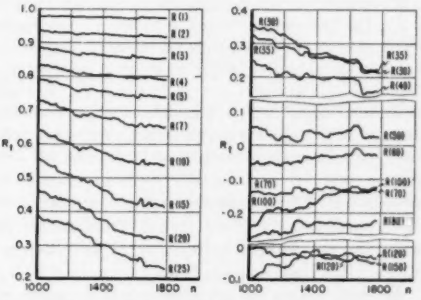

FIG. 1. Time-correlation coefficient $R_t(h)$ as a function of the length of the oscillographic recording. The interval of time h and the length of the recording n are expressed in multiples of 1/3100 second.

[2] F. N. Frenkiel, Compt. rend. **222**, 367 (1946).
[3] F. N. Frenkiel, Proc. 7th Int. Congr. Appl. Mech. **2**, 112 (1948).
[4] Frenkiel, Edelson, and Rawling, Nav. Ord. Lab. Memo 10815 (1950) (unpublished).

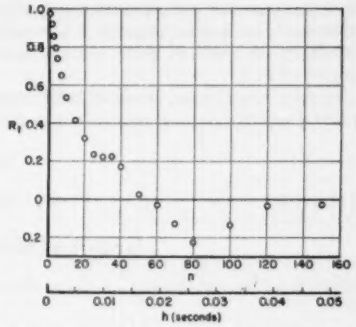

FIG. 2. Time-correlation curve calculated using the total length of the oscillographic recording ($n=1779$ corresponding to about 0.57 second).

interval of time h was calculated with the formula

$$R_t(h)=\sum_{i=1}^{i=n-h} u_i'u_{i+h}'\Big[\sum_{i=1}^{i=n-h}(u_{i+h}')^2\Big]^{-1},$$

with $n=1, 2, \cdots, 1779$ and h the interval of time measured in multiples of 1/3100 second. Figure 1 represents the time-correlation coefficient for several values of the interval of time h as a function of the number of points used for its computation. The curves show a general trend indicating the limits toward which the correlation coefficient values appear to tend. Figure 2, representing the correlation coefficient R_t as a function of h, is given only as an illustration of the general shape of the time-correlation curve. One notices immediately the large negative values of the correlation coefficient for h in the region of 0.02 to 0.04 second. None of the available measurements of longitudinal correlation coefficients made under the same experimental conditions present such large negative values.[5] While the length of the oscillographic recording was too small to give very accurate numerical values for the correlation coefficients, one can conclude from Fig. 1 that the negative values of $R_t(h)$ are of the order of magnitude of those represented on Fig. 2. From these preliminary investigations, it appears that the time-correlation curve has a sensibly different shape than the longitudinal correlation curve.

If the time correlation curve $R_t(h)$ is compared with the longitudinal correlation curve $R_x(hU)$ (U is the mean velocity and $hU=x$ is the distance between the two points for which the correlation between the u-velocity components is measured), one may expect that the difference between R_t and R_x will decrease as h decreases. However, even if this difference is negligible for small h, it does not necessarily follow that the

[5] Dryden, Schubauer, Mock, and Skramstad, National Advisory Committee for Aeronautics, Rept. 581 (1937).

difference between time and space velocity gradients is negligible, and there may be, therefore, a non-negligible difference between time and space microscales of turbulence.

An extensive investigation is needed before complete experimental results can be given concerning the relation between time and space characteristics of turbulence. This work is now in process in cooperation with the National Bureau of Standards.[6]

[6] New experimental measurements, now in process, are being made in cooperation with Dr. J. Laufer (National Bureau of Standards) and Mr. I. Katz (Applied Physics Laboratory).

PHYSICAL REVIEW VOLUME 88, NUMBER 6 DECEMBER 15, 1952

Statistical Mechanics of Irreversibility*

HERBERT B. CALLEN AND MURRAY L. BARASCH, *Department of Physics, University of Pennsylvania, Philadelphia, Pennsylvania*

AND

JULIUS L. JACKSON, *Applied Physics Laboratory, Johns Hopkins University, Silver Spring, Maryland*

(Received July 25, 1952)

The fluctuation-dissipation theorem relating spontaneous equilibrium fluctuations to the conductance in a dissipative thermodynamic system is extended to the case of several variables, using a quantum statistical analysis. The conductance matrix is shown to be subject to certain symmetry relations, providing a generalization of the Onsager reciprocity theorem. The susceptance matrix is also shown to be subject to similar symmetries. The symmetries apply to all frequency components, and hence to arbitrary transient processes.

1. INTRODUCTION

THE theory of irreversible processes consists essentially of two types of theorems. The first of these theorems is the reciprocity relations of Onsager, treating of the symmetry of the mutual interference among several simultaneously occurring irreversible processes.[1,2] The second is the fluctuation-dissipation theorem, relating the spontaneous fluctuations in an equilibrium system and the parameter (the conductance) which characterizes the dissipative aspects of an irreversible process.[3-5] The purpose of this and the following paper is to extend the fluctuation-dissipation theorem to several variables and to exhibit its relation to a generalization of the Onsager reciprocity theorem.

Both the Onsager theorem and the fluctuation-dissipation theorem have been investigated by quantum statistical and thermodynamic methods. In the present paper we shall be concerned exclusively with the quantum statistical analysis.

We shall show that the fluctuation-dissipation theorem may be interpreted as a matrix equation when extended to several variables. The mean square fluctuation of a single variable $\langle Q^2 \rangle$ is replaced by a matrix, the elements of which are the spontaneous mutual correlation moments of two fluctuating variables $\langle Q_j Q_k \rangle$. The admittance (and hence the conductance) is replaced by an admittance matrix, the element Y_{jk} describing the response of the variable Q_j to the force V_k. Furthermore, we shall show that both the conductance and susceptance matrices are subject to a symmetry relation. The symmetries so established apply to all frequency components and consequently are applicable to arbitrary types of transient processes. An indication will be given of the application of this reciprocity theorem to steady-state processes.

2. THE ADMITTANCE MATRIX

In this section we shall define the admittance matrix and develop a useful quantum statistical expression for it.

We consider a system whose Hamiltonian in isolation is H_0. Let the system be acted on by a perturbation which induces the irreversible processes of interest. For a single variable this perturbation may be written in the form[3] $V(t)Q(\cdots q_r \cdots p_r \cdots)$, in which $V(t)$ is a time-dependent scalar which measures the instantaneous strength of the applied perturbation, and which therefore plays the role of a driving force, and in which $Q(\cdots q_r \cdots p_r \cdots)$ is a function of the coordinates and momenta of the particles composing the system. For the general case in which several simultaneous perturbations act, we shall write the total perturbation as $\sum_k V_k(t) Q_k(\cdots q_r \cdots p_r \cdots)$.

We shall assume the perturbations to be sufficiently small so that first-order perturbation theory is valid. As we shall see, this assumption linearizes the system in the following sense. Under the influence of the perturbations, the expectation value of Q_j becomes a function of time, and if $\dot{Q}_j(\omega)$ denotes the Fourier component of the time derivative of this expectation value, then $\dot{Q}_j(\omega)$ is a linear function of the Fourier

* This work was supported by the ONR, and the Bureau of Ordnance of the U. S. Navy.

[1] L. Onsager, Phys. Rev. **37**, 405 (1931); **38**, 2265 (1931).
[2] H. B. G. Casimir, Revs. Modern Phys. **17**, 343 (1945).
[3] H. B. Callen and T. A. Welton, Phys. Rev. **83**, 34 (1951).
[4] J. L. Jackson, Phys. Rev. **87**, 471 (1952).
[5] H. B. Callen and R. F. Greene, Phys. Rev. **86**, 702 (1952).

components $V_k(\omega)$ of the several driving forces. That is,

$$\dot{Q}_j(\omega) = -\sum_k Y_{jk}(\omega) V_k(\omega). \tag{2.1}$$

The minus sign[6] is here included in order to indicate explicitly the tendency of $\dot{Q}_j$ to be of such a sign as to decrease the perturbing energy V_jQ_j.[4] The matrix $\{Y_{jk}\}$ may be called the admittance matrix. The elements of this matrix are, in general, complex, indicating by the usual convention the phase relations between the response and the several driving forces. That is,

$$Y_{jk}(\omega) = g_{jk}(\omega) - ib_{jk}(\omega). \tag{2.2}$$

The real and imaginary parts of the admittance matrix are respectively the conductance and susceptance matrices, $\{g_{jk}\}$ and $\{b_{jk}\}$.

The method we use in order to obtain explicit expressions for the elements of the admittance matrix is simply to compute the time dependent expectation value of $\dot{Q}_j$ in the perturbed states of the system.[4] The initial state of the system is represented by an ensemble in which the occupation numbers of the unperturbed energy states are in accordance with the equilibrium distribution associated with a temperature T.

In the presence of sinusoidal perturbations $V_k(t) = V_k^0 \sin\omega t$, the Hamiltonian for the system is

$$H = H_0(\cdots q_r \cdots, \cdots p_r \cdots) + \sum_k V_k^0 \sin\omega t Q_k(\cdots q_r \cdots, \cdots p_r \cdots), \tag{2.3}$$

where

$$H_0\Psi_n = E_n\Psi_n. \tag{2.4}$$

Writing the perturbed wave functions as

$$\Phi_n = \sum_m b_{nm}(t)\Psi_m \exp(-iE_mt/\hbar), \tag{2.5}$$

we find, to first order, that for $n \neq m$

$$2ib_{nm}(t) = -\sum_k V_k^0 \langle\Psi_m|Q_k|\Psi_n\rangle \times\left\{\frac{\exp[-it(E_n-E_m+\hbar\omega)/\hbar]-1}{E_n-E_m+\hbar\omega} - \frac{\exp[-it(E_n-E_m-\hbar\omega)/\hbar]-1}{E_n-E_m-\hbar\omega}\right\}, \tag{2.6}$$

and for $n = m$

$$b_{nn}(t) = 1 + (1/i\hbar)\sum_k V_k^0\langle\Psi_n|Q_k|\Psi_n\rangle(1-\cos\omega t)/\omega. \tag{2.7}$$

The expectation value $\langle\Phi_n|\dot{Q}_j|\Phi_n\rangle$ of $\dot{Q}_j$ in the nth perturbed eigenstate may now be computed.

The operator associated with $\dot{Q}_j$ is given by the commutator $[H, Q_j]/\hbar$ from which, keeping only first-order terms, we have

$$\langle\Phi_n|\dot{Q}_j|\Phi_n\rangle = \frac{1}{2\hbar}\sum_k\sum_{m\neq n} V_k^0\langle E_n|Q_j|E_m\rangle \times\langle E_m|Q_k|E_n\rangle(E_m-E_n) \times\left\{\frac{e^{-i\omega t}-e^{-it(E_m-E_n)/\hbar}}{E_n-E_m+\hbar\omega} - \frac{e^{i\omega t}-e^{-it(E_m-E_n)/\hbar}}{E_n-E_m-\hbar\omega}\right\} + \text{complex conjugate.} \tag{2.8}$$

[6] The negative sign was unfortunately omitted in Eqs. (2.12) and (2.14) of reference 3.

Now to obtain the response for a macroscopic system we average (2.8) over the ensemble. The summations over both n and m may be replaced by integrations over energy.[3] Introducing the density of levels $\rho(E)$ and the distribution function

$$f(E_n) = (\text{const.})\exp(-E_n/kT), \tag{2.9}$$

we find

$$\langle\dot{Q}_j\rangle = \frac{1}{2\hbar}\int_0^\infty\int_0^\infty dE_m dE_n \rho(E_m)\rho(E_n)f(E_n)(E_m-E_n) \times\sum_k V_k^0\langle E_m|Q_j|E_n\rangle\langle E_n|Q_k|E_m\rangle \times\left\{\frac{e^{i\omega t}-e^{it(E_m-E_n)/\hbar}}{E_n-E_m+\hbar\omega}\right\} - \frac{1}{2\hbar}\int_0^\infty\int_0^\infty dE_m dE_n \rho(E_m)\rho(E_n)f(E_n)(E_m-E_n) \times\sum_k V_k^0\langle E_m|Q_j|E_n\rangle\langle E_n|Q_k|E_m\rangle \times\left\{\frac{e^{-i\omega t}-e^{it(E_m-E_n)/\hbar}}{E_n-E_m-\hbar\omega}\right\} + \text{complex conjugate.} \tag{2.10}$$

For large t the first integral becomes

$$\frac{i\pi\omega}{2}\exp(i\omega t)\int_0^\infty dE_m\rho(E_m)\rho(E_m-\hbar\omega)f(E_m-\hbar\omega) \times\sum_k V_k^0\langle E_m|Q_j|E_m-\hbar\omega\rangle\langle E_m-\hbar\omega|Q_k|E_m\rangle + \frac{\exp(i\omega t)}{2\hbar}\int_0^\infty\int_0^\infty dE_m dE_n\rho(E_m)\rho(E_n) \times f(E_n)(E_m-E_n)\sum_k\frac{\langle E_m|Q_j|E_n\rangle\langle E_n|Q_k|E_m\rangle}{E_n-E_m+\hbar\omega},$$

and the other integrals may be evaluated similarly. As in reference 3, these integrals may be further reduced, yielding

$$\langle\dot{Q}_j\rangle = -\sin\omega t\sum_k g_{jk}V_k^0 + \cos\omega t\sum_k b_{jk}V_k^0, \tag{2.11}$$

with

$$g_{jk} = \tfrac{1}{2}\pi\omega(1-\exp[-\hbar\omega/kT]) \times\int_0^\infty dE_m\rho(E_m)\rho(E_m+\hbar\omega)f(E_m) \times\{\langle E_m+\hbar\omega|Q_k|E_m\rangle\langle E_m|Q_j|E_m+\hbar\omega\rangle + \text{c.c.}\} + 2\omega\int_0^\infty\int_0^\infty dE_m dE_n\frac{\rho(E_m)\rho(E_n)f(E_n)(E_n-E_m)}{(E_n-E_m)^2-(\hbar\omega)^2} \times\text{Im}\{\langle E_m|Q_k|E_n\rangle\langle E_n|Q_j|E_m\rangle\}, \tag{2.12}$$

and

$$b_{jk}=\pi\omega(1-\exp[-\hbar\omega/kT])$$
$$\times\int_0^\infty dE_m\rho(E_m)\rho(E_m+\hbar\omega)f(E_m)$$
$$\times\mathrm{Im}\{\langle E_m+\hbar\omega|Q_k|E_m\rangle\langle E_m|Q_j|E_m+\hbar\omega\rangle\}$$
$$+\omega\int_0^\infty\int_0^\infty dE_m dE_n\frac{\rho(E_m)\rho(E_n)f(E_n)(E_m-E_n)}{(E_n-E_m)^2-(\hbar\omega)^2}$$
$$\times\{\langle E_m|Q_k|E_n\rangle\langle E_n|Q_j|E_m\rangle+\text{c.c.}\}. \quad (2.13)$$

3. THE SPONTANEOUS FLUCTUATIONS IN EQUILIBRIUM

Having in the previous section investigated the response of a system to a driving force, we now turn our attention to the spontaneous fluctuations in equilibrium. In particular, we shall compute the correlation moment $\langle Q_jQ_k\rangle$ of two arbitrary functions of the coordinates and momenta of the particles of the system.

We shall find it convenient to first compute $\langle\dot{Q}_j\dot{Q}_k\rangle$, from which the moment $\langle Q_jQ_k\rangle$ may easily be obtained. We proceed in this calculation by formulating the expectation value of $\dot{Q}_j\dot{Q}_k$ in a pure state of the system and then averaging over all pure states in accordance with the equilibrium distribution function. Since the quantum-mechanical operators $\dot{Q}_j$ and $\dot{Q}_k$ do not necessarily commute, the appropriate operator for which we seek the expectation value becomes $\frac{1}{2}(\dot{Q}_j\dot{Q}_k+\dot{Q}_k\dot{Q}_j)$. The expectation value of $\dot{Q}_j\dot{Q}_k$ in the unperturbed state Ψ_n is then

$$\tfrac{1}{2}\langle E_n|\dot{Q}_j\dot{Q}_k+\dot{Q}_k\dot{Q}_j|E_n\rangle=1/2\hbar^2[\textstyle\sum_m(E_n-E_m)^2$$
$$\times\langle E_n|Q_k|E_m\rangle\langle E_m|Q_j|E_n\rangle+\text{c.c.}]. \quad (3.1)$$

The summation over m may be replaced by an integration over E_m. With the substitution

$$\hbar\omega=|E_n-E_m|, \quad (3.2)$$

we then obtain

$$\tfrac{1}{2}\langle E_n|\dot{Q}_j\dot{Q}_k+\dot{Q}_k\dot{Q}_j|E_n\rangle=\frac{1}{2\hbar^2}\int_0^\infty(\hbar\omega)^2$$
$$\times\langle E_n+\hbar\omega|Q_k|E_n\rangle\langle E_n|Q_j|E_n+\hbar\omega\rangle\rho(E_n+\hbar\omega)\hbar d\omega$$
$$+\frac{1}{2\hbar^2}\int_0^\infty(\hbar\omega)^2\langle E_n-\hbar\omega|Q_k|E_n\rangle$$
$$\times\langle E_n|Q_j|E_n-\hbar\omega\rangle\rho(E_n-\hbar\omega)\hbar d\omega+\text{c.c.} \quad (3.3)$$

We compute the macroscopic correlation moment by summing over unperturbed states Ψ_n, weighting them by $f(E_n)$ as previously. This summation may also be replaced by an integration over E_n. Using the transformation

$$E\rightarrow E'+\hbar\omega \quad (3.4)$$

as before, we have the result

$$\langle\dot{Q}_j\dot{Q}_k\rangle=\frac{1}{2}\int_0^\infty d\omega\hbar\omega^2(1+\exp[-\hbar\omega/kT])$$
$$\times\int_0^\infty dE_m\rho(E_m)\rho(E_m+\hbar\omega)f(E_m)$$
$$\times[\langle E_m+\hbar\omega|Q_k|E_m\rangle\langle E_m|Q_j|E_m+\hbar\omega\rangle+\text{c.c.}]. \quad (3.5)$$

Since the Fourier component of Q_j is simply the Fourier component of $\dot{Q}_j$ divided by $i\omega$, it follows that

$$\langle Q_jQ_k\rangle=\frac{1}{2}\int_0^\infty d\omega\hbar(1+\exp[-\hbar\omega/kT])$$
$$\times\int_0^\infty dE_m\rho(E_m)\rho(E_m+\hbar\omega)f(E_m)$$
$$\times[\langle E_m+\hbar\omega|Q_k|E_m\rangle\langle E_m|Q_j|E_m+\hbar\omega\rangle+\text{c.c.}]. \quad (3.6)$$

These two equations constitute our desired expressions for the correlation moments of the spontaneously fluctuating variables in an equilibrium system.

4. THE FLUCTUATION-DISSIPATION THEOREM

A theorem has previously been proved[3] which is equivalent to a relation between the diagonal elements of the fluctuation-correlation matrix and of the conductance matrix. In this section we obtain an extension of this theorem to the off-diagonal elements of the respective matrices.

Comparison of Eqs. (3.6) and (2.12) yields directly the theorem

$$\langle Q_jQ_k\rangle=\frac{2}{\pi}\int_0^\infty d\omega E(\omega,T)\left[\frac{g_{jk}(\omega)+g_{kj}(\omega)}{2\omega^2}\right]. \quad (4.1)$$

Here

$$E(\omega,T)\equiv\tfrac{1}{2}\hbar\omega+\hbar\omega[\exp(\hbar\omega/kT)-1]^{-1}, \quad (4.2)$$

which is formally the mean energy at temperature T of a harmonic oscillator of natural frequency ω. It may be noted that at high T ($kT\gg\hbar\omega$), $E(\omega,T)$ assumes the classical limiting value of kT.

It is sometimes useful to introduce fictitious fluctuating forces defined in such a way that they would induce the observed values of the fluctuating responses. It is clearly possible to use relations of the form $V=Z\dot{Q}$ to transform (4.1) into an expression for the correlation moments of these fictitious forces. Because of the artificiality of such forces and because the expressions for the off-diagonal elements become rather complicated in such a formulation, we prefer to restrict ourselves to the theorem as stated in Eq. (4.1). The diagonal form of Eq. (4.1), written in terms of the fluctuating forces, has been applied elsewhere to the problems of Brownian motion, the fluctuating electric field in the vacuum, and pressure fluctuations in gases.[3]

5. SYMMETRY PROPERTIES OF THE ADMITTANCE MATRIX

In this section we shall consider certain symmetry properties of the admittance matrix.

We have

$$Y_{jk}(\omega, A)=g_{jk}(\omega, A)-ib_{jk}(\omega, A), \tag{5.1}$$

where we have explicitly indicated that the admittance matrix may depend upon an applied magnetic field, described by the vector potential A. We consider the behavior of the admittance matrix under the simultaneous transformations $j\leftrightarrow k$ and $A\rightarrow -A$; that is, we shall investigate the relationship of $Y_{jk}(\omega, A)$ and $Y_{kj}(\omega, -A)$. It may be noted that the dependence of $Y_{jk}(\omega, A)$ on the indices j and k and on the field A is only through constructs of the form $\langle E_m|Q_j|E_n\rangle \times\langle E_n|Q_k|E_m\rangle$. The transformation $j\leftrightarrow k$ is equivalent to the replacement of each of these matrix elements by its complex conjugate. Thus, we are led to study the behavior of the unperturbed wave functions and the operators Q_k (these being the quantities entering into the matrix elements) under a particular operator T. This operator is so defined that applied to a given wave function which depends parametrically on A, it takes the complex conjugate of that function and also replaces A by $-A$:

$$T\Psi(\cdots q\cdots, \cdots A\cdots) = \Psi^*(\cdots q\cdots, \cdots -A\cdots). \tag{5.2}$$

The unperturbed wave functions may be chosen as real in the absence of a magnetic field. In the presence of a field, the momenta in the unperturbed Hamiltonian are replaced by (P_r-e_r/cA_r) and thence by $-ih[\nabla_r-(e_r/hc)iA_r]$. Therefore, the convention which made the wave functions real in the absence of a field will cause them to involve both i and A only through the product iA. The unperturbed wave functions are therefore invariant under the T operation.

Similarly the classical function Q_j is a real function of the coordinates and of the quantities (P_r-e_r/cA_r). The operator Q_j is consequently a function of the coordinates and of the quantities $-ih[\nabla_r-(e_r/hc)iA_r]$. Since the T operator leaves the square bracket invariant, it merely replaces (P_r-e_r/cA_r) by $-(P_r-e_r/cA_r)$. That is, the symmetry of the operator Q_j under T is equivalent to the symmetry of the classical function Q_j under the reversal of all particle velocities.

In the above discussion we have, for convenience, implied a scalar wave function and thereby ignored spin. If spin is included the operator T must also be considered as causing the reversal of all spins. The T operator is essentially the Wigner time-reversal operator.[7] The symmetry of the operator Q_j under T is then equivalent to the symmetry of the semiclassical function Q_j under the simultaneous reversal of all particle velocities *and spins*.

[7] A simple discussion of the time-reversal operator is given by M. J. Klein, Am. J. Phys. **20**, 65 (1952).

Returning now to Eq. (5.1), we recall that $Y_{jk}(\omega, A)$ depends on j and k only through constructs of the form $\langle E_m|Q_j|E_n\rangle\langle E_n|Q_k|E_m\rangle$. The simultaneous transformation $j\leftrightarrow k$ and $A\rightarrow -A$ corresponds to the application of the T operation within these matrix elements. The T operation leaves the unperturbed wave functions invariant, and yields a symmetry, in its action on the Q_j, which derives from the dependence of the Q_j on the particle velocities and spins. If both Q_j and Q_k are even under the reversal of particle velocities and spins, then $Y_{jk}(\omega, A)$ is invariant under the transformation considered. If both Q_j and Q_k are odd under the reversal of particle velocities and spins, then $Y_{jk}(\omega, A)$ is again invariant, whereas if Q_j is even and Q_k odd (or vice versa), $Y_{jk}(\omega, A)$ changes sign under this transformation.

Thus, we have derived our basic symmetry relations. If Q_j and Q_k are both odd or both even under reversal of the particle velocities and spins,

$$Y_{jk}(\omega, A)=Y_{kj}(\omega, -A). \tag{5.3}$$

If Q_j is even and Q_k odd (or vice versa) under reversal of the particle velocities and spins,

$$Y_{jk}(\omega, A)=-Y_{kj}(\omega, -A). \tag{5.4}$$

It may now be noted that the general case, in which the Q_j and Q_k are neither even nor odd in the particle velocities and spins, may be easily subsumed under the above analysis by a simple artifice. It is always possible to write any given function Q_j as the sum of two functions, one even, $\equiv Q_j^{(e)}$ and one odd, $\equiv Q_j^{(o)}$, in the particle velocities and spins. The case in which there is a single driving force associated with the single function Q_j may, therefore, be considered to be a special case of the situation in which there are two independent driving forces for $Q_j^{(e)}$ and $Q_j^{(o)}$, these two driving forces being taken equal:

$$V_jQ_j=V_j^{(e)}Q_j^{(e)}+V_j^{(o)}Q_j^{(o)}, \tag{5.5}$$

with

$$V_j^{(e)}=V_j^{(o)}=V_j. \tag{5.6}$$

This device reduces any situation to one in which all functions Q_j or Q_k are either even or odd under reversal of the particle velocities and spins.

The symmetry theorem expressed in Eqs. (5.3) and (5.4) is a generalization of the reciprocity theorem of Onsager. Whereas the Onsager theorem applies only to relaxation processes, the above theorem applies to all frequency components and hence to arbitrary transient processes. Both the real and the imaginary components of the admittance are subject to the symmetry relations.

6. THE APPLICATION TO STEADY-STATE PROCESSES

The application of the symmetry theorem to steady-state processes requires an extension of the analysis and the introduction of a particular type of approxi-

mation. This situation exists also in the application of the Onsager theorem to steady-state processes.[8,9] An appropriate extension of the analysis will appear in a subsequent paper, but it seems desirable to indicate briefly here the general aspects of the relationship of the symmetry theorem to steady-state processes.

It is immediately apparent that our formalism is not appropriate for a direct application to steady-state processes. The admittance as given in Eqs. (2.12) and (2.13) vanishes for zero frequency, whereas in a steady-state process a time-independent force leads to a nonzero time-independent response. A specific example brings out very clearly the essential difference in the situations described by our formalism and those appropriate to the study of steady-state phenomena. Consider, in particular, the application of an electric field to a conductor. As indicated in reference 3, this situation may be described by taking the driving force V as the applied potential difference and Q as $\sum_i e_i x_i/L$, wherein e_i is the charge on the ith particle, x_i its distance from one end of the conductor, and L the total length of the conductor. The system which is properly described by this Hamiltonian is an electrical resistor placed between two condenser plates which impress the voltage V across it, the resistor, however, *not* being in electrical contact with the external circuit. As indicated above, the time independent applied driving force V eventually leads to a vanishing current $\dot{Q}$. On the other hand, a steady-state process results if the electrical isolation between the conductor and the potential source is destroyed. Whereas the distribution of electrons along the length of the conductor is radically different from the equilibrium distribution in the situation discussed (the electrons accumulating toward one end of the conductor), the effect of making an actual physical contact between the conductor and the rest of the circuit is to provide an external reservoir of electrons which attempts to maintain the equilibrium distribution.

The above example suggests one approximate method of applying our analysis to steady-state processes: this method has been previously employed in a discussion of the Onsager relations by one of us.[9] A steady-state process may be considered as involving the action of two distinct external agencies on the dissipative system. One of these applies a perturbation to the system; the second is an agency which attempts to restore the equilibrium statistical distribution function. The analysis of such a steady-state process may then be conveniently carried out by an artifice which successfully avoids the requirement of explicit consideration of the restoring agency. We assume that the response $\dot{Q}$ observed in the steady-state is equal to the instantaneous response $\dot{Q}(\tau)$ which would be exhibited at some particular time τ in a system which is not acted on by a restoring agency but to which is applied, at time $t=0$, the driving force V. We see that for such a system the distribution function is of precisely the equilibrium form immediately after the application of the perturbation. If the restoring agency is a very effective one, so that in its competition with the applied perturbation it is able to maintain very nearly the equilibrium distribution function in the steady-state process, the parameter τ which appears in our analysis will be very small; conversely, weak restoring agencies and/or strong perturbations are represented in our formalism by large values of τ. By this device the action of the restoring agency is represented approximately by a single parameter τ, and the analysis of steady-state processes is reduced to the calculation of the response, at a particular time, of an appropriately defined transient process; this latter type of process being completely within the scope of the formalism previously developed.

We consider, then, a system to which are applied the driving forces

$$V_j(t)=\begin{cases} V_j^0, & t>0, \\ 0, & t<0, \end{cases} \tag{6.1}$$

and we seek the response at time τ. It follows immediately from Eq. (2.1) and from the transform $1/i\omega$ of the unit step function that

$$\dot{Q}_j(\tau)=\sum_k L_{jk}V_k^0, \tag{6.2}$$

where

$$L_{jk}=\frac{1}{2\pi}\int_{-\infty}^{\infty} d\omega \exp(i\omega\tau)\frac{Y_{jk}(\omega)}{i\omega}. \tag{6.3}$$

$\dot{Q}_j(\tau)$ is to be interpreted as the *time-independent* response in the steady-state process. It is evident from Eq. (6.3) that the L_{jk} satisfy symmetry relations identical in form to those satisfied by the Y_{jk}, these symmetries being the basis of the modern theory of steady-state irreversible processes.[8,10]

[8] See H. B. Callen, Phys. Rev. **73**, 1349 (1948).
[9] H. B. Callen, thesis, Massachusetts Institute of Technology, 1947, unpublished.
[10] S. R. DeGroot, *Thermodynamics of Irreversible Processes* (North-Holland Publishing Company, Amsterdam, Netherlands, 1951).

On a Theorem of Irreversible Thermodynamics. II*

RICHARD F. GREENE, *Department of Physics, University of Illinois, Urbana, Illinois*

AND

HERBERT B. CALLEN, *Department of Physics, University of Pennsylvania, Philadelphia, Pennsylvania*

(Received July 25, 1952)

The fluctuation-dissipation theorem, which relates the equilibrium fluctuations to the admittance of a thermodynamic linear dissipative system, is generalized for more than a single extensive parameter. The real part of the admittance is shown to be symmetric, supplying thereby an extension of the reciprocity theorem of Onsager. The analysis is macroscopic and thermodynamic in nature, and is carried out for adiabatic constraints as well as for microcanonical constraints.

1. INTRODUCTION

THIS paper is a sequel to an earlier paper of the same title,[1] to be referred to as "I," and is the thermodynamic counterpart of the preceding statistical paper.[2]

In "I" we established the relations

$$\langle \xi^2 \rangle = -\frac{2}{\pi} k \int d\omega \sigma_S(\omega) \omega^{-2}, \tag{1.1}$$

and

$$\langle \xi^2 \rangle = -\frac{2}{\pi} kT \int d\omega \sigma_V(\omega) \omega^{-2}, \tag{1.2}$$

where $\langle \xi^2 \rangle$ is the mean square fluctuation of an extensive parameter in the frequency interval determined by the range of integration, and where $\sigma_S(\omega)$ and $\sigma_V(\omega)$ are conductances which characterize the irreversible response of the system to an applied force. The first of the above equations applies to systems in which all extensive parameters other than the one of interest are held constant, whereas the second equation applies to systems similarly constrained except that the constraint on the energy is replaced by the condition of adiabatic insulation. In this paper we shall generalize these results to the case in which several extensive parameters are permitted to fluctuate spontaneously, and in which the several associated forces act on the system to induce an irreversible composite process. The analysis parallels the quantum statistical analysis of the preceding paper and augments it by the consideration of adiabatic constraints. The symmetry of the real part of the admittance matrix is established by thermodynamic reasoning, but that of the imaginary part does not follow from our thermodynamic analysis.

2. THE METHOD

As in "I" the proof of the fluctuation-dissipation theorem (here established for multiple extensive variables) is based on the Wiener-Khinchin formula,

$$G_{ij}(\omega) = \frac{1}{(2\pi)^{\frac{1}{2}}} \int_{-\infty}^{\infty} d\tau \langle \xi_i(t) \xi_j(t+\tau) \rangle e^{-i\omega\tau}, \tag{2.1}$$

which reduces the problem of determining the spectral density matrix $G_{ij}(\omega)$ to that of determining the autocorrelation matrix $\langle \xi_i(t) \xi_j(t+\tau) \rangle$. This latter quantity may be written as

$$\langle \xi_i(t) \xi_j(t+\tau) \rangle = \int d\xi_0' \cdots \int d\xi_r' \xi_i' W_1(\xi_0' \cdots \xi_r') \times \langle \tau, \xi_0' \cdots \xi_r' | \xi_j \rangle, \tag{2.2}$$

where $W_1(\xi_0' \cdots \xi_r') d\xi_0' \cdots d\xi_r'$ is the probability of finding $\xi_0 \cdots \xi_r$ in the range $d\xi_0' \cdots d\xi_r'$, and $\langle \tau, \xi_0' \cdots \xi_k' | \xi_j \rangle$ is the expectation value of ξ_j at a time τ after the variables $\xi_0 \cdots \xi_r$ had the value $\xi_0' \cdots \xi_r'$. Thus random variable theory provides us with the spectral density of the equilibrium fluctuations if we know the two quantities $W_1(\xi_0 \cdots \xi_r)$ and $\langle \tau, \xi_0' \cdots \xi_r' | \xi_j \rangle$. Now $W_1(\xi_0 \cdots \xi_r)$ is the familiar distribution function of statistical thermodynamics, so that the calculation of $\langle \tau, \xi_0' \cdots \xi_r' | \xi_j \rangle$ is the crux of the derivation. But the mean decay curve $\langle \tau, \xi_0' \cdots \xi_r' | \xi_j \rangle$ of a spontaneous extensive parameter fluctuation is identical to the observed curve of macroscopic drift into equilibrium. The latter curve, finally, may be expressed in terms of the admittance matrix describing such irreversible processes. Thus the conditional mean $\langle \tau, \xi_0' \cdots \xi_r' | \xi_j \rangle$ can be written in terms of the admittance matrix so that Eqs. (2.1) and (2.2) yield the desired relation between $G_{ij}(\omega)$ and $Y_{ij}(\omega)$.

During derivation of the connection between $\langle \tau, \xi_0' \cdots \xi_r' | \xi_j \rangle$ and Y_{ij}, recourse is made to the principle of microscopic reversibility, whereby $\langle \tau, \xi_0' \cdots \xi_r' | \xi_j \rangle$ appears as an even function of τ. By this means we then derive the symmetry of the real part of the matrix Y_{ij}, obtaining a set of generalized reciprocity relations.

The derivation outlined is carried out for systems under two distinct types of constraints. In the first type, all of the extensive parameters are either rigidly fixed (microcanonical) or free to vary (these "canonical" variables being those of which the fluctuations are studied). In the second type of constraint, the micro-

* This work was supported in part by the ONR under contract with the University of Pennsylvania.

[1] H. B. Callen and R. F. Greene, Phys. Rev. **86**, 702 (1952).

[2] Callen, Barasch, and Jackson, preceding paper, Phys. Rev. **88**, 1382 (1952).

canonical constraint on the energy is relaxed and replaced by the condition of adiabatic insulation. For this latter type of system it is necessary to augment the derivation by the construction of a theory of fluctuations of several extensive parameters under adiabatic constraint; this theory is given in Appendix A.

3. THE ADMITTANCE OF THERMODYNAMIC SYSTEMS

In this section we recall briefly the thermodynamic definition of the admittance function which characterizes the response of the system to an applied force and the analytic properties of this admittance function. We state these definitions and analytic properties appropriately to a system with several driven parameters.

We frame our thermodynamic analysis in the "entropy language," in which the entropy S is taken as the dependent function of the equilibrium values of the energy X_0 and the various other extensive parameters:

$$S=S(X_0, X_1, \cdots, X_r). \tag{3.1}$$

The intensive parameters in the entropy language are

$$F_k\equiv\partial S/\partial X_k, \quad k=0, 1, \cdots, r. \tag{3.2}$$

Here F_0 is the inverse temperature, and the other F_k are simply $-1/T$ times the corresponding intensive parameters, in the more conventional energy language.

The instantaneous deviation of an extensive parameter x_j from its equilibrium value X_j is denoted by ξ_j:

$$\xi_j\equiv x_j-X_j. \tag{3.3}$$

The intensive forces which enter into the succeeding analysis are the intensive parameters of the driving reservoir with which the system is presumed to be in interaction. This reservoir is assumed to have characteristic relaxation times small compared to the reciprocal of any of the frequencies of interest, so that it is always in quasi-static equilibrium.

Let $\beta_i(\omega)$ be the Fourier amplitude of the ith driving force

$$f_i(t)=F_i+\frac{1}{(2\pi)^{\frac{1}{2}}}\int_{-\infty}^{\infty}d\omega\beta_i(\omega)e^{i\omega t}, \tag{3.4}$$

and let $\alpha_j(\omega)$ be the Fourier amplitude of the jth extensive parameter

$$x_j(t)=X_j+\frac{1}{(2\pi)^{\frac{1}{2}}}\int_{-\infty}^{\infty}d\omega\alpha_j(\omega)e^{i\omega t}. \tag{3.5}$$

For sufficiently small amplitudes α_j and β_i will be linearly related, thus defining the admittance matrix $Y_{ji}(\omega)$:

$$i\omega\alpha_j(\omega)=\sum_{i=0}^{r}Y_{ji}(\omega)\beta_i(\omega). \tag{3.6}$$

The condition that a constant applied force leads to constant values of the extensive parameters gives, as in "I,"

$$Y_{ji}(\omega)=i\omega\partial X_j/\partial F_i+O(\omega^2), \tag{3.7}$$

where the partial derivative is to be taken with all the other intensive parameters held constant.

The causal relationship between the applied forces and the induced response has its analytic statement in the further requirement that the matrix elements $Y_{ji}(\omega)$ have no poles in the lower half of the ω-plane.

4. THE CONDITIONAL EXPECTATION VALUE

Having formulated a thermodynamic definition of the admittance function, we proceed with the plan outlined in Sec. II: We must calculate $\langle\tau, \xi_0'\cdots\xi_r'|\xi_j\rangle$, the expectation value of ξ_j at a time τ after the set $\xi_0\cdots\xi_r$ had exactly the value $\xi_0'\cdots\xi_r'$.

For a reason explained in "I" we may equate $\langle\tau, \xi_0'\cdots\xi_r'|\xi_j\rangle$ to the decay function which describes the macroscopic behavior of ξ_j after the microcanonical constraint $\xi_0\cdots\xi_r=\xi_0'\cdots\xi_r'$ is lifted. This decay function is simple to get. Rather than impose a constraint which is to be lifted at $t=0$, we may instead impose an appropriately chosen set of "forces" which is, again, to be lifted at $t=0$. This set of forces, of course, is chosen so as to induce the same initial macroscopic state as would the constraints it replaces. That is, we consider that until $t=0$ the system is in equilibrium with a set of applied forces $F_i+\delta F_i$ of such magnitude as to produce values $X_i+\xi_i'$ of the set of x_i. At time $t=0$ the applied forces are suddenly changed to F_0, F_1, $\cdots$, F_r, and the macroscopically observed value of ξ_j at time $t=\tau$ is $\langle\tau, \xi_0'\cdots\xi_r'|\xi_j\rangle$. The problem is now in a form suitable for analysis in terms of the admittance function. The applied forces are

$$\delta f_i=\begin{cases}\sum_{k=0}^{r}\dfrac{\partial F_i}{\partial X_k}\xi_k', & t<0,\\ 0, & t\geqslant 0,\end{cases} \tag{4.1}$$

or

$$\delta f_i=\frac{1}{(2\pi)^{\frac{1}{2}}}\sum_{k=0}^{r}\frac{\partial F_i}{\partial X_k}\xi_k'\int_{-\infty}^{\infty}d\omega \times\left[\left(\frac{\pi}{2}\right)^{\frac{1}{2}}\delta(\omega)+\frac{i}{\omega(2\pi)^{\frac{1}{2}}}\right]e^{i\omega\tau}. \tag{4.2}$$

For this improper integral we take the Cauchy principle value. The response to this applied force is, according to Eq. (3.6),

$$\xi_j(t)=\frac{1}{(2\pi)^{\frac{1}{2}}}\sum_{i,k=0}^{r}\frac{\partial F_i}{\partial X_k}\xi_k'\int_{-\infty}^{\infty}d\omega Y_{ij}(\omega)/i\omega \times\left[\left(\frac{\pi}{2}\right)^{\frac{1}{2}}\delta(\omega)+\frac{i}{\omega(2\pi)^{\frac{1}{2}}}\right]e^{i\omega\tau}. \tag{4.3}$$

Equation (3.7) now gives

$$\xi_j(\tau)=\tfrac{1}{2}\xi_j'+\frac{1}{2\pi}\sum_{i,k}\xi_k'\frac{\partial F_i}{\partial X_k}\int_{-\infty}^{\infty}d\omega Y_{ij}(\omega)\omega^{-2}e^{i\omega\tau}. \quad (4.4)$$

This formula is correct for $\tau>0$, but to find $\xi_j(\tau)$ for negative τ we must invoke the principle of microscopic reversibility. We here assume that the extensive parameters are even functions of the particle momenta and that there are no magnetic or Coriolis fields; the more general cases follow through precisely as in the previous paper[2] in this journal. Then the principle of microscopic reversibility insures that $\xi_j(\tau)$ is an even function of τ, whence

$$\langle\tau,\xi_0'\cdots\xi_r'|\xi_j\rangle=\frac{1}{2\pi}\sum_{i,k}\xi_k'\frac{\partial F_i}{\partial X_k}\int_{-\infty}^{\infty}d\omega\omega^{-2}\times[Y_{ij}(\omega)+Y_{ij}^*(\omega)]e^{i\omega\tau}. \quad (4.5)$$

5. THE SPECTRAL DENSITY OF THE SPONTANEOUS FLUCTUATIONS

Having now computed the quantity $\langle\tau,\xi_0'\cdots\xi_r'|\xi_j\rangle$, we may find the correlation moment $\langle\xi_i(t)\xi_j(t+\tau)\rangle$ by Eq. (2.2), and thence the spectral density $G_{ij}(\omega)$ by Eq. (2.1). Thus

$$\langle\xi_i(t)\xi_j(t+\tau)\rangle=\frac{1}{2\pi}\sum_{l,k}\frac{\partial F_l}{\partial X_k}\langle\xi_i\xi_k\rangle\int_{-\infty}^{\infty}d\omega\omega^{-2}\times[Y_{lj}(\omega)+Y_{lj}^*(\omega)]e^{i\omega\tau}, \quad (5.1)$$

and

$$G_{ij}(\omega)=\frac{1}{(2\pi)^{\frac{1}{2}}}\sum_{l,k}\frac{\partial F_l}{\partial X_k}\langle\xi_i\xi_k\rangle\omega^{-2}[Y_{lj}(\omega)+Y_{lj}^*(\omega)]. \quad (5.2)$$

The fluctuation moment $\langle\xi_i\xi_k\rangle$ is well known from conventional thermodynamic fluctuation theory for systems with canonical and microcanonical constraints. In fact, we have

$$\sum_k\frac{\partial F_l}{\partial X_k}\langle\xi_i\xi_k\rangle=-k\delta_{il}. \quad (5.3)$$

Restricting ourselves temporarily to systems with canonical and microcanonical constraints (the adiabatic constraint will be considered in the next section), we thus find

$$G_{ij}(\omega)=-\left(\frac{2}{\pi}\right)^{\frac{1}{2}}k\omega^{-2}\sigma_{Sij}(\omega), \quad (5.4)$$

where the conductance matrix σ_{Sij} is the real part of the admittance matrix

$$\sigma_{Sij}=\tfrac{1}{2}[Y_{ij}(\omega)+Y_{ij}^*(\omega)]. \quad (5.5)$$

By the definition of the spectral density, we now have our generalization of the fluctuation-dissipation theorem

$$\langle\xi_i\xi_j\rangle=-\frac{2}{\pi}k\int_{-\infty}^{\infty}d\omega\omega^{-2}\sigma_{Sij}(\omega). \quad (5.6)$$

6. SPECTRAL DENSITY UNDER ADIABATIC CONSTRAINT

In the previous section we have found the form of the fluctuation-dissipation theorem appropriate to a system with several extensive parameters canonically constrained and with all other extensive parameters microcanonically constrained. We now wish to consider the case in which the constraint on the energy is replaced by the condition that the system is adiabatically insulated; that is, no heat flow is possible through the boundary of the system. For such a system it is most convenient to employ the energy language, based on the fundamental relation

$$X_0=X_0(S,X_1,\cdots,X_r), \quad (6.1)$$

with the intensive parameters defined by

$$P_k\equiv\partial X_0/\partial X_k)_{S,X_1,\cdots,X_r}. \quad (6.2)$$

Under the adiabatic constraint the first-order entropy change is zero during a fluctuation, and the energy change is simply

$$\delta x_0=\sum_1^r P_k\delta x_k. \quad (6.3)$$

The forces are now taken as the energy language intensive parameters of the driving reservoir,

$$p_i(t)=P_i+\frac{1}{(2\pi)^{\frac{1}{2}}}\int_{-\infty}^{\infty}d\omega\beta_i(\omega)e^{i\omega t}, \quad (6.4)$$

and the admittance function now has the dimensions of $\omega x/p$ rather than of $\omega x/f$. As a function of ω we again have the condition

$$Y_{ji}(\omega)=i\omega\partial X_j/\partial P_i)_S+O(\omega^2), \quad (6.5)$$

and the partial derivative is now to be taken with all other intensive parameters (except P_i and T) and with the entropy constant.

We then find, in analogy with (5.2), that the spectral density matrix is

$$G_{ij}(\omega)=\frac{1}{(2\pi)^{\frac{1}{2}}}\sum_{k,l}\frac{\partial P_i}{\partial X_k}\langle\xi_k\xi_l\rangle\omega^{-2}[Y_{lj}(\omega)+Y_{lj}^*(\omega)], \quad (6.6)$$

or

$$G_{ij}(\omega)=\left(\frac{2}{\pi}\right)^{\frac{1}{2}}\sum_{k,l}\frac{\partial P_i}{\partial X_k}\langle\xi_k\xi_l\rangle\omega^{-2}\sigma_{Ulj}, \quad (6.7)$$

where

$$\sigma_{Ulj}=\tfrac{1}{2}[Y_{lj}(\omega)+Y_{lj}^*(\omega)]. \quad (6.8)$$

The subscript U is now written explicitly to indicate that σ_U is the real part of the energy language admittance.

In Appendix A we calculate the fluctuation moment $\langle \xi_k \xi_l \rangle$ under adiabatic constraints as

$$\langle \xi_k \xi_l \rangle = kT \partial X_k / \partial P_l)_S. \tag{6.9}$$

This gives the fluctuation-dissipation theorem for adiabatic constraints:

$$\langle \xi_k \xi_l \rangle = \frac{2}{\pi} kT \int_0^\infty d\omega \omega^{-2} \sigma_{Ukl}(\omega). \tag{6.10}$$

7. RECIPROCITY RELATIONS

We now show that the conductance matrix is symmetric under our assumptions of vanishing magnetic field and parameters even in the particle momenta. This symmetry is a generalization of the reciprocity theorem of Onsager.

For simplicity we consider canonical and microcanonical constraints, although the theorem follows identically for the adiabatic constraint. We have

$$G_{ij}(\omega) = -(2/\pi)^{\frac{1}{2}} k \omega^{-2} \sigma_{Sij}(\omega), \tag{7.1}$$

and

$$G_{ij}(\omega) = \frac{1}{(2\pi)^{\frac{1}{2}}} \int_{-\infty}^{\infty} d\omega \langle \xi_i(t) \xi_j(t+\tau) \rangle e^{-i\omega\tau}. \tag{7.2}$$

Now, according to the principle of microscopic reversibility we have[3]

$$\langle \xi_i(t) \xi_j(t+\tau) \rangle = \langle \xi_i(t) \xi_j(t-\tau) \rangle, \tag{7.3}$$

and as we are dealing with a stationary random process we can substitute $t+\tau$ for t in the right-hand member, yielding

$$\langle \xi_i(t) \xi_j(t+\tau) \rangle = \langle \xi_j(t) \xi_i(t+\tau) \rangle. \tag{7.4}$$

With Eqs. (7.1) and (7.2) this immediately yields the reciprocity theorem

$$\sigma_{Sij}(\omega) = \sigma_{Sji}(\omega). \tag{7.5}$$

Similarly, for adiabatic constraints,

$$\sigma_{Uij}(\omega) = \sigma_{Uji}(\omega). \tag{7.6}$$

APPENDIX A. FLUCTUATIONS UNDER AN ADIABATIC CONSTRAINT

Let us consider the thermodynamic fluctuations of a system canonical with respect to several extensive parameters $x_1, x_2, \cdots, x_r$ and under an adiabatic constraint.

The probability of a fluctuation to instantaneous values $x_0, x_1, \cdots, x_r$ is[4]

$$W(x_0, \cdots, x_r) = \Omega_0 \times \exp\left\{ \left[s - S + \sum_{k=1}^{r} P_k \delta x_k - \frac{1}{T} \delta x_0 \right] \Big/ k \right\}, \tag{A.1}$$

where

$$\delta x_k = x_k - X_k = \xi_k, \tag{A.2}$$

and

$$s = S(x_0, x_1, \cdots, x_r). \tag{A.3}$$

Now under an adiabatic constraint,

$$\delta x_0 = \sum_{k=1}^{r} P_k \delta x_k. \tag{A.4}$$

If we delete from our ensemble those states inconsistent with (A.4) the probability (A.1) becomes

$$W_S = \Omega_0 \exp\{[s-S]/k\}. \tag{A.5}$$

But now

$$s - S = \frac{\partial s}{\partial x_0} \delta x_0 + \sum_{k=1}^{r} \frac{\partial s}{\partial x_k} \delta x_k + \tfrac{1}{2} \left[\sum_{k,l=1}^{r} \frac{\partial^2 s}{\partial x_k \partial x_l} \delta x_k \delta x_l + 2 \sum_{k=1}^{r} \frac{\partial^2 s}{\partial x_0 \partial x_k} \delta x_k \delta x_0 + \frac{\partial^2 s}{\partial x_0^2} (\delta x_0)^2 \right] + \cdots, \tag{A.6}$$

which becomes, using (A.4),

$$s - S = \tfrac{1}{2} \sum_{k,l=1}^{r} \delta x_k \delta x_l \left[\frac{\partial^2 s}{\partial x_k \partial x_l} + 2 P_l \frac{\partial^2 s}{\partial x_0 \partial x_k} + P_k P_l \frac{\partial^2 s}{\partial x_0^2} \right], \tag{A.7}$$

dropping the higher order terms. (These various derivatives are, of course, to be evaluated at the "point" $x_k = X_k$.) Now in general, for any quantity

$$\delta(\ ) = \frac{\partial}{\partial x_0}(\ ) \delta x_0 + \sum_{k=1}^{r} \frac{\partial}{\partial x_k}(\ ) \delta x_k;$$

so under the constraint (A.4), which we denote by a subscript s,

$$\frac{\partial}{\partial x_l}(\ )_S = P_l \frac{\partial}{\partial x_0}(\ ) + \frac{\partial}{\partial x_l}(\ ). \tag{A.8}$$

We may apply (A.8) to a re-expressed form of (A.7):

$$\begin{aligned} s - S &= \tfrac{1}{2} \sum_{k,l} \delta x_k \delta x_l \left[\frac{\partial}{\partial x_l} \left(-\frac{P_k}{T} \right) + 2 P_l \frac{\partial}{\partial x_0} \left(-\frac{P_k}{T} \right) + P_k P_l \frac{\partial}{\partial x_0} \left(\frac{1}{T} \right) \right] \\ &= \tfrac{1}{2} \sum_{k,l} \delta x_k \delta x_l \left[\frac{\partial}{\partial x_l} \left(-\frac{P_k}{T} \right)_S + P_l \frac{\partial}{\partial x_0} \left(-\frac{P_k}{T} \right) + P_k P_l \frac{\partial}{\partial x_0} \left(\frac{1}{T} \right) \right]. \end{aligned} \tag{A.9}$$

Now if we put

$$P_l \frac{\partial}{\partial x_0} \left(-\frac{P_k}{T} \right) = P_l \frac{\partial^2 s}{\partial x_0 \partial x_k} = P_l \frac{\partial}{\partial x_k} \left(\frac{1}{T} \right), \tag{A.10}$$

[3] L. Onsager, Phys. Rev. **37**, 405 (1931); **38**, 2265 (1931).
[4] See M. J. Klein and L. Tisza, Phys. Rev. **76**, 1861 (1949).

then (A.9) becomes

$$s-S=\tfrac{1}{2}\sum_{k,l}\delta x_k\delta x_l\left[\frac{\partial}{\partial x_l}\left(-\frac{P_k}{T}\right)_S+P_l\frac{\partial}{\partial x_k}\left(\frac{1}{T}\right)+P_kP_l\frac{\partial}{\partial x_0}\left(\frac{1}{T}\right)\right]. \quad (A.11)$$

Now, using (A.8) again, we find

$$s-S=\tfrac{1}{2}\sum_{k,l=1}^{r}\delta x_k\delta x_l\left[-\frac{1}{T}\frac{\partial P_k}{\partial x_l}\right)_S-P_k\frac{\partial}{\partial x_l}\left(\frac{1}{T}\right)_S+P_l\frac{\partial}{\partial x_k}\left(\frac{1}{T}\right)_S\Bigg]. \quad (A.12)$$

Now the summation of the last two terms in the summand gives zero, so

$$s-S=\frac{-1}{2T}\sum_{k,l=1}^{r}\frac{\partial P_k}{\partial X_l}\Big)_S\delta x_k\delta x_l. \quad (A.13)$$

We note that

$$\partial P_k/\partial X_l)_S=\partial P_l/\partial X_k)_S\equiv\alpha_{lk}. \quad (A.14)$$

Thus

$$W_S=\Omega_0\exp\left[-\frac{1}{2kT}\sum_{k,l=1}^{r}\frac{\partial P_k}{\partial X_l}\Big)_S\delta x_k\delta x_l\right]. \quad (A.15)$$

In this expression we must consider that explicit dependence upon x_0 has been removed by means of Eq. (A.4). Let us put

$$\pi_l=\frac{1}{kT}\sum_{k=1}^{r}\alpha_{lk}\delta x_k. \quad (A.16)$$

Then

$$\langle\pi_i\delta x_j\rangle=\frac{\int dx_0\cdots\int dx_r\,\pi_i\delta x_j\exp\left[\dfrac{-1}{2kT}\displaystyle\sum_{k,l=1}^{r}\alpha_{lk}\delta x_k\delta x_l\right]}{\int dx_0\cdots\int dx_r\exp\left[\dfrac{-1}{2kT}\displaystyle\sum_{k,l=1}^{r}\alpha_{lk}\delta x_k\delta x_l\right]}$$

$$=\delta_{ij},\text{ the Kronecker delta.} \quad (A.17)$$

Then (except at critical points) we may insert (A.15)

$$\delta x_k=2kT\textstyle\sum_l\alpha_{kl}^{-1}\pi_l,$$

whence

$$\langle\delta x_i\delta x_k\rangle=2kT\textstyle\sum_l\alpha_{kl}^{-1}\langle\delta x_i\pi_l\rangle$$

$$=2kT\alpha_{ki}^{-1} \quad (A.18)$$

$$=2kT\partial X_i/\partial P_k)_S, \quad (A.19)$$

since $\partial X_i/\partial P_k)_S$ and $\partial P_k/\partial X_i)_S$ are inverse matrices.

Propagation in Electron-Ion Streams

R. Q. Twiss
Services Electronics Research Laboratory, Baldock, Herts, England
(Received March 17, 1952. Revised manuscript received July 30, 1952)

A mathematical theory is given for the propagation of electromagnetic waves in electron-ion streams composed of N discrete beams. The solution, which is fully relativistic, is obtained in vector form by an extension of Hansen's theory and takes explicit account of the initial and boundary conditions. When certain restructions are placed upon the transverse boundary conditions the general solution satisfying arbitrary initial conditions can be expanded in terms of a complete orthogonal set of elementary vector solutions. For this case the necessary and sufficient conditions are found for amplification and instability both in the terminated and the unterminated stream. The correct physical interpretation of the conventional "Ansatz" solutions is found together with the conditions under which they are valid. One is then able to distinguish amplified growing waves from reverse waves attenuated in the reverse direction. Finally the analysis is extended to the continuous velocity distribution. It is shown that the present treatment differs significantly from Landau's theory for the thermal plasma and the consequences of this are discussed.

1. INTRODUCTION

THE development of electronic tubes such as the traveling and space-charge wave amplifiers and the discovery that sunspots and solar flares can produce excess noise radiation has led several writers[1–5] to extend the magneto-ionic theory of Appleton to the more general case where the medium contains moving electron-ion streams. However there is considerable disagreement over the physical interpretation of these theories, particularly as to the conditions under which a medium can amplify a given initial disturbance or radiate nonthermal energy into free space. Furthermore some of this work is open to criticism on purely mathematical grounds, especially in those treatments which assume a continuous velocity distribution in the stream.

It is probable that much of the trouble has arisen because the mathematical analysis upon which these theories are usually based contains no explicit reference to the initial and boundary conditions, a procedure the dangers of which have been recently emphasized by Pierce.[6]

It has not proved possible to carry through, in closed form, a complete solution for the propagation in an electron-ion stream which satisfies arbitrary initial and boundary conditions, but this can be done when certain restrictions are placed upon the latter. The resulting solution covers cases of considerable practical importance, which enable one to form an unambiguous picture of the physical nature of the propagation in a moving ionized medium. In particular it enables one to discriminate between waves that are excited directly and those that are excited only by reflections, to find necessary and sufficient conditions under which amplification or instability can take place, and to compare the energy carried by the radiation field to that carried by the moving space charge.

The first part of this paper is largely mathematical and the nature of the solution is discussed only in general terms. The theory is applied to specific cases to establish the physical conditions which can lead to amplification and instability in nature.

2. SIMPLIFYING ASSUMPTIONS AND INITIAL CONDITIONS

The theory of propagation in moving ionized media has been developed along three main lines to apply respectively to gas discharges, to the ionosphere, and to electron wave tubes, and the simplifying approximations employed have naturally depended on which of these cases is to be studied. In the present paper the analysis has been restricted as little as possible consistent with the over-all aim of getting a complete solution under at least some physically realizable boundary conditions. However when a choice has to be made it has been taken with the last two applications in mind rather than with the case of the gas discharge. In fact the starting point of this paper is the fundamental article by Hahn[7] on electron beams and, as far as possible, the symbolism has been chosen to coincide with his. On this standpoint the limiting assumptions are as follows.

(1) *Linearity.* We consider the small signal case, where the square and cross product terms of the time dependent field and space-charge quantities may be neglected, when the Maxwell-Lorentz equations become linear.

(2) *Rectilinear flow.* We assume that the stream is composed of a system of N superimposed beams of charged particles, both electrons and ions, moving in rectilinear unaccelerated paths. Ideally such a flow can be established as discussed by Hahn.[7] In the text we restrict ourselves to the case where all these paths are parallel and where the external force system consists simply of an axial magnetic field. The extension to the cases where the beams are not all parallel and where the external magnetic field has a transverse component can only be achieved with a considerable increase in complexity and in a Cartesian system of coordinates.

[1] V. A. Bailey, Australian J. Sci. Research **A.1**, 351 (1948); Phys. Rev. **83**, 439 (1951).
[2] E. P. Gross, Phys. Rev. **82**, 232 (1951).
[3] D. Bohm and E. P. Gross, Phys. Rev. **75**, 1851, 1864 (1949).
[4] A. V. Haeff, Proc. Inst. Radio Engrs. **37**, 1 (1949).
[5] J. Feinstein and H. K. Sen, Phys. Rev. **83**, 405 (1951).
[6] J. R. Pierce, Bell System Tech. J. **XXX**, no. 3, 626 (1951).
[7] W. C. Hahn, Gen. Elec. Rev. **42**, 258 (1939).

The general case, where the charged particles follow nonrectilinear paths under arbitrary external fields, appears as yet quite intractable in a relativistic theory.

(3) *Uniform flow.* We assume that the beams are uniform in cross section so that the dc velocity and space charge density in the stream are independent of position. The analysis will therefore not be applicable to a slipping stream, but the limitation appears essential if the initial conditions are to appear explicitly in a solution in closed form.

(4) *Collisions.* Owing to the discrete nature of the space charge and the presence of ions and neutral molecules both electron-electron and electron-ion scattering will take place. In this paper we follow the usual procedure and treat the stream as if it were a charged jelly. That is we take e/m equal to its experimental value while letting e and m tend to zero. The effects of scattering are then allowed for by introducing a force term $\nu_s m_s \mathbf{v}_s$ into the into the Lorentz force equation where ν_s is the collision frequency of a particle mass m_s and velocity $\mathbf{v}_s$.

This procedure is taken over from the propagation theory of the ionosphere; its extention to the general electron-ion stream is of dubious validity. Thus in a thermal plasma the velocity distribution of the charged particles will presumably be everywhere Maxwellian, but when nonthermal beams are present scattering will change the velocity distribution along the beam; since this is a nonlinear effect it cannot be allowed for by our theory which will only apply when the scattering frequency ν_s is small. Another objection to this procedure is that it cannot allow for the production of radiation by free-free transitions the cross sections of which are proportional to e^2 so that the total incoherent radiation is proportional to Ne^2 or eI which tends to zero on this approximation. This fact must be borne in mind when considering the escape of radiation from an electron-ion stream. However despite these drawbacks we should get a qualitatively accurate approximation for the effects of scattering on coherent phenomena such as amplification or instability.

(5) *Initial conditions.* We assume that the stream is excited by an arbitrary initial spatial distribution of disturbance concentrated between the planes $z=0$, $z=d$, and by a time dependent disturbance at the plane $z=0$ which is not necessarily a surface of discontinuity in the medium.

The principal symbols used in this paper are as follows:

$\mathbf{a}=(0, 0, 1)$; a unit vector parallel to the z axis.
$\mathbf{B}_0=(0, 0, B_0)$; the dc magnetic flux density.
c; the velocity of light in vacuum.
$-e_s$; the electric charge on particles of the sth beam.
$\mathbf{E}(x^1, x^2, z, t)$, $\mathbf{H}(x^1, x^2, z, t)$; the electric and magnetic field vectors.
$E_l(z, t)$, $H_l(z, t) l=1-3$; coefficients in the vector expansions of $\mathbf{E}(x^1, x^2, z, t)$, $\mathbf{H}(x^1, x^2, z, t)$, respectively.
k; the L_z-transform mate of z.
$K_s=1/(1-u_{0s}^2/c^2)$.
m_{0s}, m_s; the rest and relativistic transverse mass of particles of the sth beam, respectively.
$\mathbf{L}$, $\mathbf{M}$, $\mathbf{N}$; fundamental vectors $\nabla\phi(x^1, x^2)$, $\nabla\phi(x^1, x^2)\times\mathbf{a}$, $\phi(x^1, x^2)\mathbf{a}$, respectively.
N; the number of individual beams of charged particles.
p; the mode parameter; $\nabla^2\phi(x^1, x^2)+p^2\phi(x^1, x^2)=0$.
$r_s(z, l)$; a factor of the space charge density. $\rho_s(x^1, x^2, z, t) = r_s(z, l)\phi(x^1, x^2)$.
$\mathbf{u}_{0s}=(0, 0, u_{0s})$, $\mathbf{v}_s$; the dc and ac velocities of particles of the sth beam, respectively.
(x^1, x^2, z); generalized cylindrical co-ordinates.
ϵ_0; the dielectric coefficient of free space $=1/(\mu_0 c^2)$.
μ_0; the magnetic permeability of free space $=4\pi\cdot 10^{-7}$.
ν_s; collision frequency of particles of sth beam.
ρ_{0s}, $\rho_s(x^1, x^2, z, t)$; dc and ac space charge density of particles of sth beam respectively.
$\phi(x^1, x^2)$; the scalar quantity from which the vector solution is derived.
ω; the L_t-transform mate of t.
$\omega_{H,s}=e_s B_0/m_s$; the cyclotron angular frequency of particles of sth beam.
$\omega_{0s}=(-e_s\rho_{0s}/\epsilon_0 m_s)^{\frac{1}{2}}$; the plasma angular frequency of particles of sth beam.
Ω_0; angular frequency of external signal.
$L_t\{f(z, t)\}=f^t(z, \omega)=f^t$; the Laplace transform of $f(z, t)$ with respect to t.
$L_t\{f(0, t)\}=f^t(0, \omega)=f^t(0)$.
$L_z\{f^t(z, \omega)\}=f^{z,t}(k, \omega)=f^{z,t}$; the Laplace transform of $f^t(z, \omega)$ with respect to z.
$L_z\{f(z, 0)\}=f^z(k, 0)=f^z(0)$.

3. AN ELEMENTARY SOLUTION

We shall now obtain an elementary solution for the Maxwell-Lorentz equations in an electron-ion stream of uniform cross section composed of N discrete superimposed beams moving, with dc velocities, u_{01}, $u_{02}\cdots u_{0N}$ and dc charge densities ρ_{01}, $\rho_{02}\cdots\rho_{0N}$, respectively, under the action of an external axial magnetic field of flux density $\mathbf{B}=(0, 0, B_0)$. The conditions under which the general solution can be represented as a linear sum over a set of orthogonal elementary solutions are discussed below.

The electromagnetic fields satisfy the Maxwell equations which in MKS units may be written

$$\left.\begin{aligned} &\nabla\times\mathbf{E}=-\partial\mathbf{B}/\partial t, \quad \nabla\times\mathbf{H}=\sum_{s=1}^{N}\rho_s\mathbf{v}_s+\partial\mathbf{D}/\partial t,\\ &\nabla\cdot\mathbf{D}=\sum_{s=1}^{N}\rho_s, \qquad \nabla\cdot\mathbf{B}=0, \end{aligned}\right\} \tag{3.1}$$

where the summations are taken over the N electron velocity classes. Since the electron flow is in vacuum we have the further relations:

$$\mathbf{B}=\mu_0\mathbf{H}, \quad \mathbf{D}=\epsilon_0\mathbf{E}, \tag{3.2}$$

where $\mu_0=4\pi\times10^{-7}$ and $\mu_0\epsilon_0=1/c^2$.

Since the charge associated with any one beam is conserved we have the N conservation equations

$$\partial\rho_s/\partial t+\nabla\cdot(\rho_s\mathbf{v}_s)=0, \quad (s=1\cdots N). \tag{3.3}$$

Finally each charged particle moves under the Lorentz force equation which for particles of charge $-e_s$ may be written

$$(\partial/\partial t+\nu_s+\mathbf{v}_s\cdot\nabla)m_s\mathbf{v}_s=-e_s(\mathbf{E}+\mathbf{v}_s\times\mathbf{B}) \quad (s=1\cdots N), \tag{3.4}$$

where $m_s=m_{0s}(1-v_s^2/c^2)^{-1}$ is the transverse relativistic mass, and ν_s is the collision frequency appropriate for

particles of the sth beam. In what follows we shall feel free to omit the subscript s whenever this may be done without ambiguity.

In the small signal theory we express the field and charge variables as the sum of a time independent and a time dependent quantity, and neglect second-order time dependent terms. In the present case

$$\mathbf{v}_{0s}=(0,0,u_{0s}),\quad \mathbf{E}_0=(0,0,0),\quad \mathbf{B}_0=(0,0,B_0),$$

where the z-axis is taken parallel to the direction of flow.

Hence, to the first order, we may write

$$\rho_s\mathbf{v}_s=\rho_{0s}u_{0s}\mathbf{a}+\rho_{1s}u_{0s}\mathbf{a}+\rho_{0s}\mathbf{v}_{1s}, \tag{3.5}$$

$$m_s\mathbf{v}_s=m_{0s}(\mathbf{v}_{0s}+\mathbf{v}_{1s})(1-u_{0s}^2/c^2)^{\frac{1}{2}} -m_{0s}(1-u_{0s}^2/c^2)^{-\frac{1}{2}}(u_{0s}^2/c^2)(\mathbf{v}_{1s}\cdot\mathbf{a})\mathbf{a}, \tag{3.6}$$

where $\mathbf{a}=(0,0,1)$ is a unit vector parallel to the direction of flow. Zero-order quantities are denoted by a zero subscript and first-order quantities by a subscript 1 which will in future be omitted.

The time dependent part of Eqs. (3.1), (3.3), and (3.4) may therefore be written

$$\left.\begin{aligned}\nabla\times\mathbf{E}&=-\mu_0\partial\mathbf{H}/\partial t,\\ \nabla\times\mathbf{H}&=\textstyle\sum(\rho_s u_{0s}\mathbf{a}+\rho_{0s}v_s)+\epsilon_0\partial E/\partial t\\ \nabla\cdot\mathbf{E}&=\textstyle\sum\rho_s/\epsilon_0,\quad \nabla\cdot\mathbf{H}=0\end{aligned}\right\} \tag{3.7}$$

$$\partial\rho_s/\partial t+\nabla\rho_s\cdot u_{0s}\mathbf{a}+\rho_{0s}\nabla\mathbf{v}_s=0\quad (s=1\cdots N) \tag{3.8}$$

$$(\partial/\partial t+\nu_s+u_{0s}\mathbf{a}\cdot\nabla)[m_s\mathbf{v}_s+m_s(u_{0s}^2/c^2)\times(1-u_{0s}^2/c^2)^{-1}(\mathbf{v}_s\cdot\mathbf{a})\mathbf{a}] =-e_s[\mathbf{E}+\mathbf{v}_s\times B_0\mathbf{a}+\mu_0u_{0s}\mathbf{a}\times\mathbf{H}]\quad (s=1\cdots N). \tag{3.9}$$

These are the equations to be solved subject to the initial conditions stated above. The conventional procedure used by Bailey[1] and other writers,[2-5] is to look for plane wave solutions where all quantities have a time-spatial dependence of the form $\exp i(\mathbf{k}\cdot x+\omega t)$, and thus obtain a characteristic equation relating $\mathbf{k}$ and ω. Despite its simplicity this method has many drawbacks. In particular it breaks down when the electron velocity distribution is continuous and has to be modified in electron tube theory where the cross section of the stream is normally circular-cylindrical rather than rectangular. The principal objection however arises from the difficulty of interpreting the characteristic equation without knowing the actual boundary and initial conditions of which this "Ansatz" procedure takes no explicit account.

A possible line of attack is to make use of the stream function introduced by Bunemann[6] into the theory of the magnetron. In principle, with this method, one does not have to restrict oneself to the linear approximation, but the differential equations determining the stream function are normally too complex to be solved except for the small signal theory. This removes much of the attraction of this method. Furthermore the scalar stream function, defined by

$$\nabla\psi_s=(m_sv_s-e_s\mathbf{A}), \tag{3.10}$$

only exists when

$$\nabla\times(m_s\mathbf{v}_s-e_s\mathbf{A})=0, \tag{3.11}$$

where $\mathbf{A}$ is the vector potential. Equation (3.11) is not a consequence of the Maxwell-Lorentz equations but an additional restriction imposed upon them which is not satisfied when, as in the present case, the charged particles have a dc component of velocity in the direction of the external magnetic field. The vector stream function of Gabor,[9] which may be used under the more general conditions when

$$\mathbf{v}_s\times[\nabla\times(m_s\mathbf{v}_s-e_s\mathbf{A})]=0, \tag{3.12}$$

suffers from similar limitations.

None of these alternatives will be employed here; instead we shall employ a method similar to that developed by Hansen[10] in the theory of antenna radiation in which a set of independent vector solutions are derived from a scalar quantity.

In a source free medium the field vectors all satisfy the dissipative wave equation

$$\nabla(\nabla\cdot\mathbf{C})-\nabla\times\nabla\times\mathbf{C}+h^2\mathbf{C}=0, \tag{3.13}$$

where $h^2=\epsilon\mu\omega^2-i\sigma\mu\omega$, and where all quantities are assumed to vary with time as $\exp(-i\omega t)$.

If ψ is a solution of the scalar wave equation,

$$\nabla^2\psi+h^2\psi=0, \tag{3.14}$$

and if $\mathbf{a}$ is a constant unit vector, then three independent vector solutions of Eq. (3.13) are

$$\left.\begin{aligned}\mathbf{L}'&=\nabla\psi(x^1x^2,z),\quad \mathbf{M}'=\nabla\psi(x^1,x^2,z)\times\mathbf{a},\\ \mathbf{N}'&=1/h\nabla\times\mathbf{M}',\end{aligned}\right\} \tag{3.15}$$

where (x^1, x^2, z) are generalized cylindrical coordinates.

Hansen showed that a complete general solution can be constructed of elementary solutions of the type of Eq. (3.15) when $\psi(x^1, x^2, z)$ is any function satisfying Eq. (3.14) and the boundary conditions.

In charge free space such a solution can also be carried through in spherical coordinates, though not in more complex coordinate systems, but this is not possible when moving charge is present.

For our present purposes it is more convenient to select as independent vectors the time independent orthogonal triad

$$\mathbf{L}=\nabla\phi(x^1,x^2),\ \mathbf{M}=\nabla\phi(x^1,x^2)\times\mathbf{a},\ N=\phi(x^1,x^2)\mathbf{a}, \tag{3.16}$$

where $\mathbf{a}$ is the unit constant vector $(0, 0, 1)$ and $\phi(x^1, x^2)$ is a scalar function.

By analogy with the charge free case, we are led to

[6] O. Bunemann, C.V.D. Report, Mag. 37 (1944) (unpublished); also L. R. Walker in *Microwave Magnetrons*, MIT Radiation Laboratory series No. 6 (McGraw-Hill Book Company, Inc., New York, 1948).

[9] D. Gabor, Proc. Inst. Radio Engrs. 33, 792 (1945).

[10] W. W. Hansen, Phys. Rev. 47, 139 (1935).

look for a solution of the field variables of the form

$$\mathbf{E}=E_1(z,t)\mathbf{L}+E_2(z,t)\mathbf{M}+E_3(z,t)\mathbf{N}, \quad (3.17)$$

and

$$\mathbf{H}=H_1(z,t)\mathbf{L}+H_2(z,t)\mathbf{M}+H_3(z,t)\mathbf{N}. \quad (3.18)$$

Similarly for the velocity variables we shall look for a solution

$$\mathbf{v}_s=v_{1s}(z,t)\mathbf{L}+v_{2s}(z,t)\mathbf{M}+v_{3s}(z,t)\mathbf{N} \quad (s=1\cdots N), \quad (3.19)$$

and shall show that Eqs. (3.17)–(3.19) are consistent with the Maxwell-Lorentz equations (3.7)–(3.9) provided that $\phi(x^1, x^2)$ satisfies a two-dimensional wave equation of the form

$$\nabla^2\phi(x^1,x^2)+p^2\phi(x^1,x^2)=0. \quad (3.20)$$

$E_1(z,t)$, etc., should not be confused with (E_{x^1}, E_{x^2}, E_z), the components of $\mathbf{E}(x^1, x^2, z, t)$, which are given by

$$\left.\begin{aligned} E_{x^1}(x^1,x^2,z,t)&=E_1(z,t)[\partial\phi/\partial x^1]/h_1 \\ &\quad +E_2(z,t)[\partial\phi/\partial x^2]/h_2, \\ E_{x^2}(x^1,x^2,z,t)&=E_1(z,t)[\partial\phi/\partial x^2]/h_2 \\ &\quad -E_2(z,t)[\partial\phi/\partial x^1]/h_1, \\ E_z(x^1,x^2,z,t)&=E_3(z,t)\phi. \end{aligned}\right\} \quad (3.21)$$

The fundamental vectors **L**, **M**, **N** form a mutually orthogonal triad so that a linear vector equation involving those three vectors alone will be everywhere satisfied if and only if the coefficient of these vectors on each side of the equation be everywhere equal.

Now if we inspect Eqs. (3.7) to (3.9) which are to be solved we see that the vector operations are of two kinds; namely taking the vector product of a field or charge variable with either ∇ or **a**. If the latter operator be applied to a vector of the form

$$\mathbf{F}=f_1(z,t)\mathbf{L}+f_2(z,t)\mathbf{M}+f_3(z,t)\mathbf{N}, \quad (3.22)$$

we get

$$\mathbf{F}\times\mathbf{a}=-f_2\mathbf{L}+f_1\mathbf{M}, \quad (3.23)$$

which leaves the general form of **F** invariant, However,

$$\nabla\times\mathbf{F}=\partial f_2/\partial z\mathbf{L}+(f_3-\partial f_1/\partial z)\mathbf{M}-f_2\nabla^2\phi\mathbf{a}. \quad (3.24)$$

If we apply this last result to the Maxwell equation,

$$\nabla\times\mathbf{E}=-\mu_0\partial\mathbf{H}/\partial t,$$

we see that Eqs. (3.18) and (3.19) are only self-consistent for all (x^1, x^2) if ϕ and $\nabla^2\phi$ are linearly related, that is if ϕ satisfies the two-dimensional wave equation (3.20), where p^2 is a scalar quantity independent of (x^1, x^2, z, t).

Accordingly we get that

$$\nabla\times\mathbf{F}=\partial f_2/\partial z\mathbf{L}+(f_3-\partial f_1/\partial z)\mathbf{M}+p^2f_2\mathbf{N}. \quad (3.25)$$

The scalar operations in Eqs. (3.7) to (3.9) on the other hand either involve taking the scalar product of a field or space charge vector with ∇ or with **a**, or operating on a vector with $\partial/\partial t$ or $\mathbf{a}\cdot\nabla\equiv\partial/\partial z$. The last two operations clearly leave the form of **F** invariant, while the scalar product of **a** or ∇ with **F** is a scalar linearly proportional to $\phi(x^1, x^2)$. Thus

$$\mathbf{a}\cdot\mathbf{F}=f_3\phi, \quad (3.26)$$

while

$$\nabla\cdot\mathbf{F}=[-p^2f_1+\partial f_3/\partial z]\phi. \quad (3.27)$$

From this it follows that the vector equations of Eqs. (3.7) to (3.9) reduce to equations of the general form

$$\alpha(z,t)\mathbf{L}+\beta(z,t)\mathbf{M}+\gamma(z,t)\mathbf{N}=0, \quad (3.28)$$

while the scalar equations are all of the form

$$a(z,t)\phi=0, \quad (3.29)$$

when **E**, **H**, and $\mathbf{v}_s$ are all of the form of Eq. (3.22) and ϕ satisfies Eq. (3.20).

If these equations are everywhere to be consistent we must have

$$\alpha(z,t)=\beta(z,t)=\gamma(z,t)=a(z,t)=0, \quad (3.30)$$

except in the trivial case when $\phi(x^1, x^2)\equiv 0$.

On substituting for **E**, **H**, $\mathbf{v}_s$ from Eqs. (3.17)–(3.19) in the continuity equations (3.8), we get

$$(\partial/\partial t+u_{0s}\partial/\partial z)\rho_s=-\rho_{0s}[-p^2v_{1s}+\partial v_{2s}/\partial z]\phi \quad (s=1\cdots N), \quad (3.31)$$

using Eq. (3.27), so that we may write

$$\rho_s(x^1,x^2,z,t)=r_s(z,t)\phi(x^1,x^2) \quad (s=1\cdots N), \quad (3.32)$$

where

$$(\partial/\partial t+u_{0s}\partial/\partial z)r_s=-\rho_{0s}[-p^2v_{1s}+\partial v_{2s}/\partial z] \quad (s=1\cdots N). \quad (3.33)$$

From the scalar Maxwell equations of (3.7) we get

$$-p^2E_1+\partial E_3/\partial z=\sum r_s/\epsilon_0, \quad (3.34)$$

$$-p^2H_1+\partial H_3/\partial z=0. \quad (3.35)$$

From the vector Maxwell equations of (3.7) we get

$$\left.\begin{aligned} \partial H_2/\partial z&=\sum\rho_{0s}v_{1s}+\epsilon_0\partial E_1/\partial t, \\ H_3-\partial H_1/\partial z&=\sum\rho_{0s}v_{2s}+\epsilon_0\partial E_2/\partial t, \\ p^2H_2&=\sum(u_{0s}r_s+\rho_{0s}v_{3s})+\epsilon_0\partial E_3/\partial t, \end{aligned}\right\} \quad (3.36)$$

and

$$\left.\begin{aligned} \mu_0\partial H_1/\partial t&=-\partial E_2/\partial z; \\ \mu_0\partial H_2/\partial t&=(E_2-\partial E_1/\partial z); \\ \mu_0\partial H_3/\partial t&=-p^2E_2. \end{aligned}\right\} \quad (3.37)$$

Finally, from the Lorentz force, Eq. (3.9), we get

$$\left.\begin{aligned} (\partial/\partial t+\nu_s+u_{0s}\partial/\partial z)m_sv_{1s}& \\ \quad=-e_s[E_1+u_{0s}\mu_0H_2]+m_s\omega_{Hs}v_{2s}, & \\ (\partial/\partial t+\nu_s+u_{0s}\partial/\partial z)m_sv_{2s}& \\ \quad=-e_s[E_2-u_{0s}\mu_0H_1]-m_s\omega_{Hs}v_{1s}, & \\ (\partial/\partial t+\nu_s+u_{0s}\partial/\partial z)m_sK_sv_{3s}=-e_sE_3, & \end{aligned}\right\} \quad (3.38)$$

where

$$\omega_{Hs}=e_sB_0/m_s \quad (3.39)$$

is the cyclotron angular frequency associated with particles of the sth beam, and where $K_s=(1-u_{0s}^2/c^2)^{-1}$.

These equations are just sufficient to determine the set of unknown quantities in terms of the initial conditions. It follows that a particular solution of Eqs. (3.7) to (3.9) can be found in the form of Eqs. (3.17) to (3.19).

To this stage the solution is valid even when the dc quantities are arbitrary functions of z. We now assume that these quantities are all independent of position, and take the Laplace transforms of Eqs. (3.33) to (3.38) first with respect to t and then with respect to z, where

$$\left.\begin{aligned} L_t\{f(z,t)\}&=f^t(z,\omega)\\ &=\int_0^\infty f(z,t)\exp(-i\omega t)dt,\\ L_t^{-1}\{f^t(z,\omega)\}&=f(z,t)\\ &=\frac{1}{2\pi}\int_{-\infty-i\gamma_1}^{\infty-i\gamma_1}\exp(i\omega t)f^t(z,\omega)d\omega, \end{aligned}\right\}\quad(3.40)$$

and

$$\left.\begin{aligned} L_z\{f^t(z,\omega)\}&=f^{z,t}(k,\omega)\\ &=\int_0^\infty f^t(z,\omega)\exp(-ikz)dz,\\ L_z^{-1}\{f^{z,t}(k,\omega)\}&=f^t(z,\omega)\\ &=\frac{1}{2\pi}\int_{-\infty-i\gamma_2}^{\infty-i\gamma_2}f^{z,t}(k,\omega)\exp(ikz)dk. \end{aligned}\right\}\quad(3.41)$$

γ_1, γ_2 are positive real numbers such that all the singularities of $f^t(z,\omega)$ lie above the line $\mathrm{Im}(\omega)+\gamma_1=0$ and all the singularities of $f^{z,t}(k,\omega)$ lie above the line $\mathrm{Im}(k)+\gamma_2=0$ in the complex ω and k-planes, respectively.[11]

There is no agreed nomenclature for double Laplace or Fourier transforms of the Maxwell equations. The present choice has the virtue of being self-explanatory and seems as good a compromise as any. We shall normally write $f^{z,t}(k,\omega)$ as $f^{z,t}$ while $f^t(0,\omega)$, which defines conditions over the initial surface $z=0$, will be written $f^t(0)$. Similarly $f^z(k,0)$ will be written $f^z(0)$ whenever this may be done without ambiguity.

Applying these transformations to Eq. (3.33) we get, for $r_s^{z,t}$, the equation

$$\begin{aligned} i(\omega+u_{0s}k)r_s^{z,t}&=r_s^z(0)+u_{0s}r_s^t(0)\\ &\quad-\rho_{0s}[-p^2v_{1s}^{z,t}+ikv_{3s}^{z,t}-v_{2s}^t(0)]. \end{aligned}\quad(3.42)$$

From Eq. (3.37) we get for $\mathbf{H}^{z,t}$ the equations

$$\left.\begin{aligned} i\omega\mu_0H_1^{z,t}&=-ikE_2^{z,t}+\mu_0H_1^z(0)+E_2^t(0),\\ i\omega\mu_0H_2^{z,t}&=-[E_3^{z,t}-ikE_1^{z,t}+E_1^t(0)]\\ &\quad+\mu_0H_2^z(0),\\ i\omega\mu_0H_3^{z,t}&=-p^2E_2^{z,t}+\mu_0H_2^z(0). \end{aligned}\right\}\quad(3.43)$$

From the transform of Eq. (3.35), $H_3^z(0)$ is given in terms of $H_1^z(0)$ by the equation

$$ikH_3^z(0)=p^2H_1^z(0)+H_3(0,0),\quad(3.44)$$

while, from Eq. (3.34), $E_3^z(0)$ is given in terms of $E_1^z(0)$ and $r_s^z(0)$ by the equation

$$-p^2E_1^z(0)+ikE_3^z(0)-E_3(0,0)=\sum r_s^z(0)/\epsilon_0.\quad(3.45)$$

Taking transforms of Eq. (3.38) and eliminating the magnetic field components by Eq. (3.43) we get three equations for $v_{1s}^{z,t}$ which may be solved in terms of $E_1^{z,t}$ and the initial conditions. Finally, taking transforms of Eq. (3.36) and eliminating $r_s^{z,t}$, $H_1^{z,t}$, and $v_{1s}^{z,t}$, we get three linear nonhomogeneous equations for $E_1^{z,t}$ which, in matrix notation, may be written

$$\mathfrak{E}(k,\omega)\mathfrak{A}(k,\omega)=\mathfrak{C}^*(k,\omega)+\mathfrak{C}^\dagger(k,\omega),\quad(3.46)$$

where $\mathfrak{E}(k,\omega)$ is the row matrix $(E_1^{z,t}, E_2^{z,t}, E_3^{z,t})$.

$\mathfrak{A}(k,\omega)$ is the 3×3 matrix with element $a_{lm}(k,\omega)$ defined by

$$\mathfrak{A}(k,\omega)=$$

$$\begin{pmatrix} \left[k^2-\frac{\omega^2}{c^2}+\frac{1}{c^2}\sum\frac{\omega_0^2\omega_b\omega_{bs}}{\omega_{bs}^2-\omega_H^2}\right], & -\frac{1}{c^2}\sum\frac{i\omega_0^2\omega_b\omega_H}{\omega_{bs}^2-\omega_H^2}, & \left[ik+\frac{i}{c^2}\sum\frac{u_0\omega_0^2\omega_b}{\omega_{bs}^2-\omega_H^2}\right],\\ \frac{1}{c^2}\sum\frac{i\omega_0^2\omega_b\omega_H}{\omega_{bs}^2-\omega_H^2}, & \left[k^2+p^2-\frac{\omega^2}{c^2}+\frac{1}{c^2}\sum\frac{\omega_0^2\omega_b\omega_{bs}}{\omega_{bs}^2-\omega_H^2}\right], & -\frac{1}{c^2}\sum\frac{u_0\omega_H\omega_0^2}{\omega_{bs}^2-\omega_H^2},\\ p^2\left[ik+\frac{i}{c^2}\sum\frac{u_0\omega_0^2\omega_{bs}}{\omega_{bs}^2-\omega_H^2}\right], & \frac{p^2}{c^2}\sum\frac{u_0\omega_H\omega_0^2}{\omega_{bs}^2-\omega_H^2}, & \frac{\omega^2}{c^2}\left[1-\sum\frac{\omega_0^2}{K\omega_b\omega_{bs}}\right]-p^2\left[1+\frac{1}{c^2}\sum\frac{u_0^2\omega_{bs}\omega_0^2}{\omega_b(\omega_{bs}^2-\omega_H^2)}\right] \end{pmatrix},\quad(3.47)$$

where

$$\omega_b=\omega+u_{0s}k\quad\text{and}\quad\omega_{bs}=\omega+u_{0s}k-iv_s,\quad(3.48)$$

and $\omega_{0s}^2=(-e_s\rho_{0s}/\epsilon_0m_s)^{\frac{1}{2}}$ is the plasma angular frequency associated with the sth beam.

It may be noted that ω_0^2, ω_b, ω_{bs}, K, and u_0 all depend on s and therefore must be included under the summation sign.

$\mathfrak{C}^*(k,\omega)$ is the column matrix with elements $C_l^*(k,\omega)$

[11] It will be noted that these transforms are rotated through an angle $\pi/2$ in the complex k and ω-planes from the conventional definitions for the Laplace transforms, so that a direct comparison may be made between the present analysis and the "Ansatz" procedure.

proportional to the values of the field and space charge variables at $z=0$, defined by

$$\left.\begin{aligned} C_1^*(k,\omega) &= -ik_1E_1{}^t(0)-i\omega\mu_0H_2{}^t(0)-\sum\left\{\frac{u_0\omega_0{}^2}{c^2}\Delta_1[E^t(0)]-i\omega\mu_0\rho_0u_0\Delta_1[v_s{}^t(0)]\right\},\\ C_2^*(k,\omega) &= -ikE_2{}^t(0)+i\omega\mu_0H_1{}^t(0)-\sum\left\{\frac{u_0\omega_0{}^2}{c^2}\Delta_2[E^t(0)]-i\omega\mu_0\rho_0u_0\Delta_2[v_s{}^t(0)]\right\},\\ C_3^*(k,\omega) &= p^2E_1{}^t(0)+\sum\left\{\frac{u_0\omega\mu_0}{\omega_b}\left[u_0r_s{}^t(0)+\rho_0v_{3s}{}^t(0)\left(1+\frac{\omega}{\omega_{bs}}\right)\right]-\frac{p^2u_0{}^2}{\omega_b}\left(\frac{i\omega_0{}^2}{c^2}\Delta_1[E^t(0)]+\omega\mu_0\rho_0\Delta_1[v_s{}^t(0)]\right)\right\}, \end{aligned}\right\} \quad (3.49)$$

and $\mathfrak{C}^t(k,\omega)$ is the column matrix with elements $C_l{}^t(k,\omega)$, proportional to the values of the field and space charge variables at $t=0$, defined by

$$\left.\begin{aligned} C_1{}^t(k,\omega) &= \frac{i\omega}{c^2}E_1{}^s(0)+ik\mu_0H_2{}^s(0)+\mu_0\sum\left\{\frac{u_0\omega_0{}^2}{c^2}\Delta_2[H^s(0)]+i\omega\rho_0\Delta_1[v_s{}^s(0)]\right\},\\ C_2{}^t(k,\omega) &= \frac{i\omega}{c^2}E_2{}^s(0)-\frac{i\mu_0(p^2+k^2)}{k}H_1{}^s(0)-\mu_0\sum\left\{\frac{u_0\omega_0{}^2}{c^2}\Delta_1[H^s(0)]-i\omega\rho_0\Delta_2[v_s{}^s(0)]-\frac{iH_3(0,0)}{k}\right\},\\ C_3{}^t(k,\omega) &= -\frac{\omega p^2}{c^2k}E_1{}^s(0)-\mu_0\sum\left\{\frac{\omega^2}{\omega_b}\left[\frac{r_s{}^s(0)}{k}-\frac{\rho_{0s}v_{3s}{}^s(0)}{\omega_{bs}}\right]-\frac{\omega}{c^2k}E_3(0,0)-p^2\mu_0H_2{}^s(0)\right.\\ &\qquad \left.+p^2u_0\left(\frac{\omega_0{}^2}{c^2}\Delta_2[H^s(0)]-\frac{i\omega\rho_0}{\omega_b}\Delta_2[v_s{}^s(0)]\right)\right\}, \end{aligned}\right\} \quad (3.50)$$

where

$$\left.\begin{aligned} \Delta_1[F] &= (i\omega_{bs}F_1+\omega_HF_2)/(\omega_{bs}{}^2-\omega_H{}^2),\\ \Delta_2[F] &= (-\omega_HF_1+i\omega_{bs}F_2)/(\omega_{bs}{}^2-\omega_H{}^2), \end{aligned}\right\} \quad (3.51)$$

and F is any one of $E_l{}^s(0)$, $H_l{}^t(0)$, etc.

By Cramer's rule the solution of Eq. (3.46) may be written

$$E_l{}^{s,t}(k,\omega)=\sum_{m=1}^{3}[C_m^*(k,\omega)+C_m{}^t(k,\omega)]A_{ml}(k,\omega)/\det\mathfrak{A}(k,\omega), \quad (3.52)$$

where $A_{ml}(k,\omega)$ is the co-factor of $a_{ml}(k,\omega)$ in the matrix $\mathfrak{A}(k,\omega)$ defined by Eq. (3.47).

We have thus obtained an elementary solution of the Maxwell-Lorentz equations of the form of Eqs. (3.17) to (3.19), where

$$E_l(z,t)=\left(\frac{1}{2\pi}\right)^2\int_{-\infty-i\gamma_1}^{\infty-i\gamma_1}\exp(i\omega t)d\omega\int_{-\infty-i\gamma_2}^{\infty-i\gamma_2}\exp(ikz)dk \times\sum_{m=1}^{3}[C_m^*(k,\omega)+C_m{}^t(k,\omega)]\frac{A_{ml}(k,\omega)}{\det\mathfrak{A}(k,\omega)}, \quad (3.53)$$

together with similar expressions for $H_l(z,t)$, $v_{ls}(z,t)$ and $r_s(z,t)$, which is valid inside the electron-ion stream provided that $\phi(x^1,x^2)$ satisfies the two-dimensional wave equation (3.20).

It still remains to find the transverse boundary conditions satisfied by the elementary solution. For the stream of infinite cross section the transverse boundary conditions require only that the solution be well behaved at infinity. We show below that this is so if we restrict our choice of p, in Eq. (3.17), to the real numbers $-\infty<p<\infty$, when the general solution satisfying arbitrary initial conditions can be expressed in terms of a continuous orthogonal set of elementary solutions.

For the stream of finite cross section the transverse boundary conditions are only satisfied by a single elementary solution under the limited conditions discussed in Sec. 4.

4. THE GENERAL SOLUTION FOR THE STREAM OF INFINITE CROSS SECTION

The elementary solution of Eq. (3.53) does not satisfy arbitrary initial conditions. On the contrary it was assumed that the initial conditions depended upon the transverse coordinates in a manner determined uniquely by the particular choice of the scalar $\phi(x^1,x^2)$ from which the solution was derived. Specifically we assumed that the initial spatial distribution of velocity modulation on the sth beam at time $t=0$ could be written in the form

$$\mathbf{v}_s(x^1,x^2,z,0)=v_{1s}(z,0)\nabla\phi-v_{2s}(z,0)\mathbf{a}\times\nabla\phi+v_{3s}(z,0)\phi\mathbf{a}, \quad (4.1)$$

where ϕ satisfies Eq. (3.20) and $\mathbf{a}=(0,0,1)$ is a unit axial vector, together with similar assumptions as to the initial values of the transverse components of the electromagnetic field and the velocity and density modulations at the surface $z=0$.

It follows that the general solution can only be expressed by an integral representation over the set of elementary solutions if an arbitrary vector field can be expressed as an integral over a set of terms of the general form of Eq. (4.1).

The proof that this is possible involves the classical theory of orthogonal integral representation which is amply covered in the literature. The only new feature of the present case arises because of the vector nature of the expansion. To illustrate this let us consider the solution in the special case of a Cartesian coordinate system.

In Cartesian coordinates (x, y, z, t) a typical solution of Eq. (3.20) is

$$\phi(x, y)=\exp[i(mx+ny)], \tag{4.2}$$

where $m^2+n^2=p^2$, when the general solution can be given by an integral representation over the set of $\phi(x, y)$ obtained by letting m, n take all real values in the range $-\infty<m<\infty$, $-\infty<n<\infty$ as long as an arbitrary vector field can be expressed in the form

$$\mathbf{F}(x, y, z, t)=\left(\frac{1}{2\pi}\right)^2\int_{-\infty}^{\infty}dm\int_{-\infty}^{\infty}dn\{f_1(m, n, z, t)\nabla - f_2(m, n, z, t)\mathbf{a}\times\nabla+f_3(m, n, z, t)\mathbf{a}\} \times\exp[i(mx+ny)]. \tag{4.3}$$

To prove that this is possible we first obtain a Fourier integral expansion of the three scalars $\mathbf{F}\cdot\mathbf{a}$, $(\nabla-\mathbf{a}\partial/\partial z)\cdot\mathbf{F}$ and $\mathbf{a}\cdot[\nabla\times\mathbf{F}]$, and then apply the Fourier integral theorem to show that

$$f_3(m, n, z, t)=\int_{-\infty}^{\infty}dx\int_{-\infty}^{\infty}dy(\mathbf{a}\cdot\mathbf{F}) \times\exp[-i(mx+ny)], \tag{4.4}$$

$$f_1(m, n, z, t)=\frac{-1}{(m^2+n^2)}\int_{-\infty}^{\infty}dx\int_{-\infty}^{\infty}dy(\nabla-\mathbf{a}\partial/\partial z)\cdot\mathbf{F} \times\exp[-i(mx+ny)], \tag{4.5}$$

$$f_2(m, n, z, t)=\frac{1}{(m^2+n^2)}\int_{-\infty}^{\infty}dx\int_{-\infty}^{\infty}\mathbf{a}\cdot[\nabla\times\mathbf{F}] \times\exp[-i(mx+ny)], \tag{4.6}$$

provided that $\mathbf{F}$ and its first derivatives belong to $L^2(-\infty, \infty)$.

Let us suppose that an expansion of the form of Eq. (4.1) has been carried through for all the given initial vector fields $\mathbf{v}_s(x^1, x^2, 0, t)$, $E(x^1, x^2, z, 0)$, etc. In each expansion we then select the component appropriate to a particular choice of m, n and obtain the elementary solution of Eq. (4.1) in the form

$$E_l(m, n, z, t)=\left(\frac{1}{2\pi}\right)^2\int_{-i\gamma_1-\infty}^{-i\gamma_1+\infty}d\omega\int_{-i\gamma_2-\infty}^{-i\gamma_2+\infty}dk \times E_l^{s,t}(m, n, k, \omega)\exp[i(kz+\omega t)]. \tag{4.7}$$

By the superposition principle the general solution may then be expressed by the fourfold integral

$$\mathbf{E}(x^1, x^2, z, t)=\left(\frac{1}{2\pi}\right)^4\int_{-\infty}^{\infty}dm\int_{-\infty}^{\infty}dn\int_{-i\gamma_1-\infty}^{-i\gamma_1+\infty}dk \times\int_{-i\gamma_2-\infty}^{-i\gamma_2+\infty}dk\exp[i(kz+\omega t)]\{E_1^{s,t}(m, n, k, \omega)\nabla - E_2^{s,t}(m, n, k, \omega)\mathbf{a}\times\nabla+E_3^{s,t}(m, n, k, \omega)\mathbf{a}\} \times\exp[i(mx+ny)]. \tag{4.8}$$

That the set of elementary solution is orthogonal follows immediately from the Fourier integral theory. A similar analysis can be carried through in any other orthogonal cylindrical coordinate system.

5. THE STREAM OF FINITE CROSS SECTION

For the stream of finite cross section the transverse boundary conditions are satisfied by a single elementary solution only in the very restricted case when

(i) The boundaries of the stream coincide with one or other of the orthogonal cylindrical coordinate surfaces.

(ii) The tangential components of the electric vector are identically zero at the boundary of the stream.

(iii) The electromagnetic fields decompose into independent TE and TM modes for which $E_1(z, t)\equiv 0$ $\equiv E_3(z, t)$ and $E_2(z, t)\equiv 0$, respectively. As in the single-beam theory of Hahn,[7] this is only possible when $\omega_H=0$, or $\omega_H=\infty$ or $\omega_0^2=0$.

It is implicit in Hahn's analysis[7] that these conditions are necessary even for the simple case of the single beam stream excited in the symmetrical mode. To show that they are sufficient for the general case let us assume that the boundary of the stream coincides with the coordinate surfaces

$$x^1=a_1, a_2; \quad x^2=b_1, b_2, \tag{5.1}$$

and that $\phi(x^1, x^2)$ is separable in (x^1, x^2) so that we may write

$$\phi(x^1, x^2)=X(x^1)Y(x^2). \tag{5.2}$$

When condition (ii) is satisfied the transverse boundary condition may be written

$$\mathbf{E}\times\mathbf{n}=0 \tag{5.3}$$

where $\mathbf{n}$ is a unit vector normal to the boundary surfaces of Eq. (5.1). From Eq. (3.21) we have on

substituting in Eq. (5.3), that

$$\left.\begin{aligned} &E_3(z,t)X(a)Y(x^2)=0 \quad a=a_1,a_2, \quad b_1<x^2<b_2,\\ &E_3(z,t)X(x^1)Y(b)=0 \quad a_1<x^1<a_2, \quad b=b_1,b_2, \end{aligned}\right\} \tag{5.4}$$

together with

$$E_1(z,t)Y(b)(\partial X/\partial x^1)/h_1 - E_2(z,t)(X(x^1)/h_2)[\partial Y/\partial x^2]_{x^1=b}=0, \tag{5.5}$$
$$b=b_1,b_2 \quad \text{and} \quad a_1<x^1<a_2,$$

$$E_1(z,t)(X(a)/h_2)(\partial Y/\partial x^2) + E_2(z,t)(Y(x^2)/h_1)[\partial X/\partial x^1]_{x^1=a}=0, \tag{5.6}$$
$$a=a_1,a_2 \quad \text{and} \quad b_1<x^2<b_2.$$

If these conditions are to be satisfied for all $0<z<d$ and all $t>0$ we must in general have either

$$\left.\begin{aligned} &\text{(i)}\ X(a)=Y(b)=0; \quad a=a_1,a_2; \quad b=b_1,b_2\\ &\text{and}\\ &\qquad E_3(z,t)\equiv 0, \end{aligned}\right\} \tag{5.6}$$

or

$$\left.\begin{aligned} &\text{(ii)}\ [\partial X/\partial x^1]_{x^1=a}=[\partial Y/\partial x^2]_{x^2=b}=0;\\ &\qquad\qquad a=a_1,a_2; \quad b=b_1,b_2\\ &\text{and}\\ &\qquad E_1(z,t)\equiv 0\equiv E_2(z,t), \end{aligned}\right\} \tag{5.7}$$

which is possible if and only if condition (iii) is satisfied.

In this case the boundary conditions define two independent sets of orthogonal eigenfunctions in terms of which the general *TE* and the general *TM* solution can be expanded, respectively.

In the special case where the boundary surfaces reduce to a pair of coordinate surfaces $x^1=a_1, a_2$, and when $\phi(x^1, x^2)$ is independent of x^2 a certain simplification results when conditions (i) and (iii) are met as then general transverse boundary conditions can be satisfied independently by either the *TE* or the *TM* modes.

Even in this case, however, the transverse boundary conditions cannot in general be satisfied by a single elementary solution. The only exceptions occur when the moving stream is replaced by a stationary plasma or when $\omega_{H_s}=\infty$ and only the *TE* waves are excited. The solution is then effectively the same as that for a dielectric filled wave guide which has been extensively analyzed in the literature.[12]

When the limiting conditions (i)–(iii) are not satisfied the general solution cannot be represented as an orthogonal sum over a set of the elementary solutions, and the initial conditions cannot be included explicitly in the solution as developed here. Essentially this is because we have taken too simple a form for the elementary solutions. However elementary solutions of a form complex enough to satisfy arbitrary transverse boundary conditions have not yet been found. It may be that complete orthogonal sets of such solutions do not exist and it is certainly open to question as to whether they can be derived from a single scalar quantity.

At present our only resource is to fall back upon an "Ansatz" and develop the method given by Hahn[7] in a form appropriate to the vector solution of this paper. In this procedure one represents the general solution as the sum over an infinite set of partial waves the propagation constants of which are determined by the angular frequency ω. The amplitudes of these waves can then be found in terms of the initial and terminal boundary conditions by matching across the terminal surfaces of discontinuity at $z=0$ and $z=d$. Unfortunately the transverse distribution functions associated with the allowable propagation modes in the stream form a nonorthogonal and indeed overcomplete set. One therefore has to introduce an auxiliary set of orthogonal functions which do form a complete set in the region over which the matching has to be carried out. Both the initial conditions and the solution in the stream have then to be expanded in terms of this auxiliary set, thus giving an infinite sequence of infinite equations to determine the amplitudes of the various partial waves, the exact solutions of which involve the ratio of two infinite determinants.

This procedure is straightforward and can, in principle, be used to yield an approximation of arbitrarily high order as we have shown elsewhere,[13] but even in the simplest cases the algebra is very heavy and the solution too complicated to throw light on the physical nature of the propagation. Accordingly it will not be considered further here. For the rest of this paper we shall confine attention to the elementary solution of Eq. (3.53) and assume that the transverse boundary conditions can be satisfied for suitable real values of p.

6. THE SOLUTION UNDER PARTICULAR INITIAL CONDITIONS

In earlier treatments of the unbounded plasma it has been customary to assume an initial distribution of disturbance which depends upon z as $\exp(ik_0z)$, where k_0 is an arbitrary real number.

As pointed out by Landau[14] this choice involves no loss of generality in a small signal theory since any initial disturbance that is physically realizable can be expanded as a Fourier integral of the form

$$F(z,0)=\frac{1}{2\pi}\int_{-\infty}^{\infty} f(k_0)\exp(ik_0z)dk_0. \tag{6.1}$$

Alternatively we can assume that the initial disturbance is concentrated at a single point in the medium when formally it may be expressed by the Dirac δ-function. This procedure is also quite general since an arbitrary initial disturbance may be expressed by

[12] J. A. Stratton, *Electromagnetic Theory* (McGraw-Hill Book Company, Inc., New York, 1941).

[13] R. Q. Twiss, Services Electronics Research Lab. Tech. J. 1 (1951).

[14] L. Landau, J. Phys. (U.S.S.R.) **10**, 25 (1946).

the integral

$$F(z, 0) = \int_{-\infty}^{\infty} f(z_0)\delta(z-z_0)dz_0. \quad (6.2)$$

Both these choices have advantages which can be combined by assuming that

$$E_l(z, 0) = E_l(k_0)\exp(ik_0z) + E_l(z_0)\delta(z-z_0), \quad (6.3)$$

together with similar expressions for the other field and space charge variables. In this case the Laplace-Fourier transform of $E_l(z, 0)$ with respect to z is given by

$$E_l^s(k, 0) = E_l^s(0) = E_l(k_0)/i(k-k_0) + E_l(z_0)\exp(-ikz_0). \quad (6.4)$$

Substituting from Eq. (6.4) in Eq. (3.52), we have that

$$E_l^{s,t}(k, \omega) = \sum_{m=1}^{2}[C_m^*(k, \omega) + C_m^{z_0}(k, \omega)\exp(-ikz_0) + C_m^{k_0}(k, \omega)/i(k-k_0)]A_{ml}(k, \omega)/\det\mathfrak{A}(k, \omega) \quad (6.5)$$

where $C_m^{z_0}(k, \omega)$, $C_m^{k_0}(k, \omega)$ are given by Eq. (3.50) with $E_l^s(0)$ replaced by $E_l(z_0)$ and $E_l(k_0)$, respectively, and where $C_m^*(k, \omega)$ depends only upon the time-dependent fields at $z=0$.

Now $E_l^{s,t}(k, \omega)$ as given by Eq. (6.5) is a meromorphic function of k which is $O(k^{-1})$ as $k \to \infty$ along the line $\mathrm{Im}(k)+\gamma_2=0$, while it can be shown by direct expansion of Eq. (3.47) that all the poles of $E_l^{s,t}(k, \omega)$ except that at $k-k_0=0$ occur at the zeros of the equation

$$\prod_{s=1}^{N}[(\omega_{b,s}^2 - \omega_{H,s}^2)(\omega_{b,s}\omega_{H,s})]\det\mathfrak{A}(k, \omega) = 0. \quad (6.6)$$

A rational equation for k of the $(4N+4)$th order.[18]

If we had used an "Ansatz," and assumed that all ac quantities were proportional to $\exp[i(kz+\omega t)]$ one would have obtained Eq. (6.6) as the characteristic equation relating k, ω though further discussion would now be needed to determine whether the zeros of the first two factors ever gave nontrivial roots or whether all the solutions could be derived from the zeros of the characteristic determinant,

$$\det\mathfrak{A}(k, \omega) = 0. \quad (6.7)$$

This point is clearly particularly relevant for the continuous velocity distribution when $N \to \infty$, and we show below that Eq. (6.7) does not yield all the solutions in this case.

If $k_n(\omega)$ be any root of Eq. (6.6), then $E_l^t(z, \omega)$, defined by

$$E_l^t(z, \omega) = \frac{1}{2\pi}\int_{-\infty-i\gamma_2}^{\infty-i\gamma_2} \exp(ikz)E_l^{s,t}(k, \omega)dk, \quad (6.8)$$

may be expressed as a sum of partial waves by the equation

$$E_l^t(z, \omega) = \sum_{m=1}^{2}[C_m^{k_0}(k_0, \omega)A_{ml}(k_0, \omega)/\det\mathfrak{A}(k_0, \omega)] \times \exp(ik_0z) + i\sum_{m=1}^{2}\sum_{n=1}^{4N+4}\alpha_{ml}(k_n\omega)[C_m^*(k_n, \omega) + C_m^{z_0}(k_n, \omega)\exp(-ik_nz_0)U(z-z_0) + C_m^{k_0}(k_n, \omega)/i(k_n-k_0)]\exp(ik_nz), \quad (6.9)$$

where $U(z)$ is the Heaviside unit step function, and where $\alpha_{ml}(k_n, \omega)$ is the residue of $A_{ml}(k, \omega)/\det\mathfrak{A}(k, \omega)$ at the pole $k=k_n$.

This result is derived on the assumption that all the roots of the characteristic equation are distinct, which will be the case except at a finite number of points in the complex ω plane. As ω tends to the value at which $k_r(\omega)=k_s(\omega)$, say, the terms proportional to $\exp(ik_rz)$ and $\exp(ik_sz)$ tend to infinity. However their sum remains finite and tends uniformly to a limit proportional to

$$\exp(ik_rz)\lim_{k_s\to k_r}\frac{\sin(k_r-k_s)z}{k_r-k_s} \sim z\exp(ik_rz). \quad (6.10)$$

Therefore $E_l^t(z, \omega)$ may be expressed by Eq. (6.9) even when some of the $k_n(\omega)$ are equal as long as the infinite terms are grouped so that their sum is finite. This will always be possible unless $E_l^t(z, \omega)$ has a singularity at a multiple root in the ω-plane. In this case however the point lies by definition above the line $\mathrm{Im}(\omega)+\gamma_2=0$ along which $E_l^t(z, \omega)$ is to be integrated.

Instead of discussing the solution in the general case we shall consider separately the three special cases where the medium is excited (i) by an external signal incident on $z=0$ at $t=0$, (ii) by an initial disturbance concentrated at the point $z=z_0$, (iii) by an initial sinusoidal distribution of disturbance. Between them these cover most of the cases of physical interest. The physical situations to which they apply have been discussed by Feinstein and Sen.[5]

The Externally Excited Medium

In this case where we take $C_m^{z_0} \equiv C_m^{k_0} \equiv 0$, the solution of Eq. (6.9) is not expressed entirely in terms of known quantities since $C_m^*(k_n, \omega)$ depends upon $E_s^t(0)$, $H_s^t(0)$ $(s=1, 2)$, which are determined by the boundary conditions at $z=0$, $z=d$, on the transverse components of the electromagnetic field. These conditions yield four independent linear nonhomogeneous equations relating $E_s^t(0)$, $H_s^t(0)$ to the external fields and the initial density and velocity modulations on the stream which are just sufficient to determine the former quantities uniquely.

In the general case, the elimination of these unknown quantities is very cumbersome, and not essentially

[18] Using Eqs. (3.44) and (3.45) it can be shown that there is no pole at $k=0$.

different from that given in an earlier paper,[16] referred to hereafter as I, for the special case of pure transverse propagation. The principal conclusions will therefore be stated without the mathematical proofs which are straightforward extensions of those in I.

To begin with, let us assume that all the beams composing the stream are moving in the positive direction, and let us consider the contribution to the solution at (z, t) from a partial wave with propagation constant $k_r(\omega)$. As shown in I, this depends upon the asymptotic nature of $k_r(\omega)$ as $\omega \to \infty - i\gamma_2$.

From Eq. (3.47) it can be shown that two of the roots of Eq. (6.6) $\sim +\omega/c$ as $\omega \to \infty$ and therefore are to be associated with the reverse field waves. As in I it can be shown that these waves can only be excited by reflection, and do not contribute to the solution at z until a time $t > (2d-z)/c$.

Two other roots such that $k \sim -\omega/c$ as $\omega \to \infty$ correspond to the forward field waves. The remaining space charge waves have propagation constants for which

$$k \sim (-\omega/u_r)(1+\epsilon_r) \quad r = 1 \cdots N,$$

where ϵ_r is a small quantity $\to 0$ as $\omega \to \infty$ which can take one of four different values for given r.

It can be shown as in I, that a space charge or forward field wave will not contribute to the disturbance at a point z until a time

$$t > z \operatorname*{Lim}_{\omega \to \infty - i\gamma_1} (-k_r/\omega).$$

Furthermore the expressions for $E_s^t(0)$, $H_s^t(0)$ involving the terminal boundary conditions can be expanded as a sum of partial waves which can be interpreted as arising from successive reflections at the terminal boundaries. If $E_s^t(0)$, $H_s^t(0)$ have any poles in the complex ω-plane below the real axis, instability will result due to the presence of reflected waves.

When the stream consists in part of reverse beams of charged particles, the solution for the terminated stream becomes prohibitively complicated. The density and velocity modulations on the reverse beams at $z=0$ can no longer be given *a priori* but depend on the manner in which these beams enter the interaction space. However when the terminal surface at $z=d$ is infinitely remote, things become much simpler since, as is proved below, the space charge waves associated with the reverse beams can only be excited by reflection. Accordingly, the density and velocity modulations on these reverse beams at $z=0$ can be determined immediately from the requirement that the amplitudes of the reverse space charge waves, for which

$$\operatorname*{Lim}_{\omega \to \infty - i\gamma_1} (k_r/\omega) > 0, \tag{6.11}$$

be identically zero.

Even when $d \to \infty$, it is not possible to evaluate explicitly the transient solution,

$$E_1(z, t) = \frac{1}{2\pi} \int_{-\infty - i\gamma_1}^{\infty - i\gamma_1} \exp(i\omega t) E_1^t(z, \omega) d\omega, \tag{6.12}$$

except in the very simplest cases. The difficulties arise largely because the $k_n(\omega)$, and therefore $E_1^t(z, \omega)$, are multivalued functions of ω which cannot in general be found explicitly, since this would involve the algebraic solution of an equation of the $(4N+4)$th degree.

It may be however that the only contribution to $E_1(z, t)$ which does not decay with time is that proportional to $\exp(i\Omega_0 t)$, where Ω_0 is the angular frequency of the external signal. In this case we have the steady-state solution

$$E_1(z, t) = i \sum_{n=M}^{4N+4} \alpha_{n1}(k_n, \Omega_0) C_n^*(k_n \Omega_0) \exp[i(k_n z + \Omega_0 t)],$$

where M is chosen to exclude all the partial waves for which the inequality of Eq. (6.11) is satisfied. However, the condition that the transient part of the solution decays with time must be established by a separate investigation. This steady-state solution is the same as that obtained by an "Ansatz" in which the characteristic equation is solved for k with $\omega = \Omega_0$.

One important result of this discussion is to settle the ambiguity between amplified growing waves and growing waves attenuated in the negative direction, since the latter satisfy the inequality (6.11).

It is usually a simple matter to identify the reverse field waves, except perhaps in the neighborhood of the cyclotron frequency, but more care is needed to discriminate between the forward and reverse space charge waves.

The Medium Excited at a Single Internal Point

In this case $C_n^{in}(k, \omega) \equiv 0$, but $C_n^*(k_n, \omega)$ must be found in terms of $E_1(z_0)$, etc., from the terminal boundary conditions at $z=0$ and $z=d$.

In a frame of reference in which all the beams in the stream are moving in the positive direction one can extend the analysis of I to show that the reverse field waves do not exist in the region $z > z_0$ until a time $t > (d-z)/c$, while in the region $z < z_0$ they provide the only terms that contribute to the disturbance as long as $t < z/c$. As in the case of the externally excited medium, the space charge waves can be grouped in sets of four such that the front edge of their contribution to the disturbance propagates at the velocity u_r of the associated beam. If we now transform to a new frame of reference in which some of the beams are moving in the reverse direction, it follows that none of the space charge waves associated with these beams contribute to the disturbance in the region $z > z_0$ in the new frame. More generally we conclude that no partial wave can be excited directly in the region $z > z_0$ by an internal disturbance originally localized in the region $z < z_0$ or

[16] R. Q. Twiss, Phys. Rev. **84**, 448 (1951).

by an external disturbance incident at $z=z_0$, if the associated propagation constant obeys the inequality (6.11).

For the infinite unterminated medium it can be shown that $E_l{}^t(z,\omega)$ is given by choosing $C_m{}^*(k_n,\omega)$ so that

$$C_m{}^*(k_n,\omega)+C_m{}^{s0}(k_n,\omega)\exp(ik_nz_0)=0 \quad (6.13)$$

for all $k_n(\omega)$ for which the inequality (6.11) holds good, and

$$C_m{}^*(k_n,\omega)=0$$

for all other $k_n(\omega)$. These $4N+4$ equations are just sufficient to determine the $4N+4$ unknowns in $C_m{}^*(k_0,\omega)$.

The Medium Excited Sinusoidally

In this case it can be shown, along the lines employed in I, that the only term of $E_l{}^t(z,\omega)$ that contributes to $E_l(z,t)$ for $t<z/c$ and $t<(d-z)/c$ is that proportional to $\exp(ik_0z)$, so that

$$E_l{}^t(z,\omega)=\sum_{m=1}^{8}[C_m{}^{k_0}(k_0,\omega)A_{ml}(k_0,\omega)/\det\mathfrak{A}(k_0,\omega)]\times\exp(ik_0z) \quad (6.14)$$

for $t<z/c$ and $t<(d-z)/c$. For the infinite unterminated medium where $z=d-z=\infty$, it follows from Eq. (6.9) that

$$C_m{}^*(k_n,\omega)+C_m{}^{k_0}(k_n,\omega)/i(k_n-k_0)=0 \quad (n=1\cdots 4N+4).$$

Since $E_l{}^t(z,\omega)$ is a rational function of ω, $O(\omega^{-1})$ as $\omega\to\infty$, we have immediately that

$$E_l(z,t)=i\sum_{n=1}^{4N+4}\beta_{nl}\exp[i(k_0z+\omega_nt)], \quad (6.15)$$

where ω_n is any root of the characteristic equation (6.6) with $k=k_0$, and where β_{nl} is the residue of

$$\sum_{m=1}^{8}C_m{}^{k_0}(k_0,\omega)A_{ml}(k_0,\omega)/\det\mathfrak{A}(k_0,\omega)$$

at the pole $\omega=\omega_n$. The solution of Eq. (6.15) is the same as that given by an "Ansatz" in which one solves the characteristic equation for ω with $k=k_0$.

If some of these characteristic roots lie in the lower half of the complex ω plane for certain ranges of k_0, then an initial spatial disturbance with Fourier components in these ranges will build up exponentially with time since in general the β_{nl} are all nonzero.

However one cannot decide without further discussion whether the stream is amplifying or unstable since the two phenomena are indistinguishable if the initial distribution of disturbance is sinusoidal. To differentiate one must consider the stream excited by a disturbance concentrated initially at $z=z_0$. If the disturbance remains finite within a finite distance of $z=z_0$ for all t then the stream is stable in this particular frame of reference and vice versa. In practice the distinction is only important in a frame of reference in which all the charge is moving in one direction, when only the reverse field waves exist in the region $z<z_0$ of an infinite unterminated medium. Hence in this case one would only expect instability to arise if one of the ω_n that lie below the real ω axis for some real k_0 can be identified as a field wave, that is if

$$\lim_{k_0\to\infty-i\gamma_2}[\omega_n(k_0)/k_0]=\pm 1/c.$$

This is rarely if ever the case. In general it is amplification rather than instability that can arise in an unterminated stream.

This discussion serves to underline the similarities between the two alternative "Ansatz" solutions. It is misleading to assert that one solution gives conditions for instability, the other conditions for amplification. As has been pointed out by Feinstein and Sen,[5] the physical differences between the two lies only in the different initial conditions, and either solution can be used to find whether amplification is possible in an unterminated stream. If the infinite stream is neither unstable nor amplifying, this can be shown more easily by solving the characteristic equation for ω for arbitrary real k_0, than by examining the steady-state solution, since, in the latter case, one must also prove that any growing waves are also reverse waves. On the other hand the former procedure can only be applied to the terminated stream when the solution can be represented by standing waves as in the charge free resonator with perfectly conducting walls. If such a resonator is filled with moving charge one has to use the steady state analysis to find the resonant frequencies, which are given, in this case, by the values of ω for which $H_x{}^t(0)$ is a maximum. Admittedly, to the first approximation, the only effect of the moving charge on the field waves is to alter the effective dielectric constant of the medium, and to this order the resonant frequencies may still be found from the roots of the characteristic equation for ω. However this procedure goes badly astray when the energy carried by the space charge waves becomes comparable with that carried by the field waves, as happens in the neighborhood of the cyclotron frequency or when the charge velocity approaches that of light.

7. THE CONTINUOUS VELOCITY DISTRIBUTION

Until now we have assumed that the electron-ion stream consists of a finite number of separate beams. When the number of these beams becomes very large, as in the case of a thermal plasma, the discrete analysis becomes excessively complicated and one is led to approximate the discontinuous velocity distribution of physical reality by an idealized continuous distribution.[17]

The solution of Eqs. (3.47) to (3.52) can formally be

[17] It must be remembered that one is here concerned with the actual velocity distribution at a given time rather than with the ensemble average distribution.

applied both to the discrete and the continuous case if we replace the summations over the N electron-ion beams by Riemann-Stieltjes integrals. To justify this step one has to show that the operations of evaluating the integral of Eq. (6.8) and proceeding to the limit $N\to\infty$ are commutable. The proof is a straightforward exercise in ϵ-analysis and will not be given here since its validity does not appear to be in dispute. When the stream is composed of two or more kinds of particles, electrons and ions say, one distinguishes between the separate velocity distribution and replaces terms such as

$$\sum_{s=1}^{N}\frac{\omega_{0s}^2\omega_{bs,s}\omega_{H,s}}{\omega_{bs,s}^2-\omega_{H,s}^2}$$

by a sum of Riemann-Stieltjes integrals of the form

$$\sum_{l=1}^{L}\int_{u_{1l}}^{u_{2l}}du\frac{\omega_{0l}^2(u)\omega_{Hl}(u)\omega_{bs,l}(u)}{\omega_{bs,l}^2(u)-\omega_{Hl}^2(u)},$$

where L is the number of different particles and

$$\omega_{Hl}(u)=(eB_0/m_{0l})(1-u^2/c^2)^{\frac{1}{2}},\quad \omega_{bs,l}(u)=\omega+uk-i\nu_l(u).$$

For the sake of simplicity however we shall assume in this section that there is only one class of charged particles, though the more general case does lead to new results when the axial magnetic field is nonzero.

In the continuous case the "Ansatz" solution breaks down in that it does not yield the complete solution. This was pointed out by Landau in his criticism of Vlasov's theory[18] of the thermal plasma but the former's treatment is also open to objection, since it is only rigorously valid for the physically impossible case where the velocity distribution of the charged particles is analytic up to infinite velocities. It is possible to modify Landau's theory to cover the case where the electron velocities are always finite, but the solution then becomes much more complex, while it is only valid when both the dc and the ac velocity distributions are analytic functions of velocity.

Accordingly we shall develop an alternative theory valid for any form of velocity distribution. In order to compare this procedure with that followed by Landau we shall consider the special case

$$p^2=\omega_H=\nu=0, \tag{7.1}$$

in which the stream is excited by an initial sinusoidal distribution of density modulation of the form

$$\rho_u(z,0)=g(u)\exp(ik_0z). \tag{7.2}$$

The general case is discussed briefly below.

If in Eqs. (3.47) to (3.52) we make the further substitution

$$\omega_0^2(u)K(u)=\omega_0^2f_0(u),$$

we get

$$E_3(z,t)=\frac{1}{2\pi}\int_{-\infty-i\gamma_1}^{\infty-i\gamma_1}\exp(i\omega t)E_3'(z,\omega)d\omega, \tag{7.3}$$

where

$$E_3'(z,\omega)=\frac{\dfrac{-1}{\epsilon_0}\displaystyle\int_{u_1}^{u_2}g(u)du/k_0(\omega+uk_0)}{1-\omega_0^2\displaystyle\int_{u_1}^{u_2}f_0(u)du/(\omega+uk_0)^2}, \tag{7.4}$$

and where u_1u_2 are the limits of the continuous velocity distribution.

If $f_0(u)$ has a first derivative throughout the range $u_1<u<u_2$ the denominator in Eq. (7.4) may be written in the equivalent form,

$$1-\omega_0^2\int_{u_1}^{u_2}du[df_0(u)/du]/k_0(\omega+uk_0),$$

as long as $f_0(u_1)=0=f_0(u_2)$, when our solution is identical with that of Landau allowing for the change of symbolism

The difference arises at the next stage in the inversion from the ω-plane onto the real t axis and centers on the treatment of the integrals

$$I_1=\int_{u_1}^{u_2}g(u)du/(\omega+uk_0), \tag{7.5}$$

$$I_2=\int_{u_1}^{u_2}f_0(u)du/(\omega+uk_0)^2, \tag{7.6}$$

which are undefined when $\omega+uk_0=0$.

As defined by the Laplace integral,

$$E_3'(z,\omega)=\int_0^\infty E_3(z,t)\exp(-i\omega t)dt$$

only converges on and below the line $\mathrm{Im}(\omega)+\gamma_1=0$, and in this region I_1, I_2 and $E_3'(z,\omega)$ are single valued analytic functions of ω.

However to find $E_3(z,t)$ explicitly it is desirable to use Eq. (7.4) to define $E_3'(z,\omega)$ by analytic continuation in the upper half of the complex ω plane. One way of doing this is to insert a cut along the real ω axis between the points

$$\omega=-u_1k_0,\quad \omega=-u_2k_0.$$

This removes the singularities of I_1 and I_2 which are now single valued analytic functions of ω all over the accessible regions of the ω plane, and $E_3'(z,\omega)$ is now a single valued function of ω everywhere analytic except at the isolated poles at the zeros of

$$1-\omega_0^2\int_{u_1}^{u_2}f_0(u)du/(\omega+uk_0)^2=0. \tag{7.7}$$

[18] A. Vlasov, J. Exptl. Theoret. Phys. (U.S.S.R.) 8, 291 (1938); J. Phys. (U.S.S.R.) 9, 25 (1945).

We now form a closed contour from the line

$$\mathrm{Im}(\omega)+\gamma_1=0,$$

and the infinite upper half-circle together with contours around the isolated poles of $E^t(z,\omega)$ and around the cut, within which $E_3{}^t(z,\omega)$ is everywhere analytic and $O(\omega^{-1})$ as $\omega\to\infty$.

By Cauchy's theorem the integral of Eq. (7.6) for $t>0$ is equal to $2\pi i$ times the sum of the residues of the isolated poles of $E_3{}^t(z,\omega)$ together with the contribution from the contour around the cut taken in a counter clockwise direction. By Jordan's lemma the contribution from the infinite half-circle is zero.

The contribution from around the cut is in general nonzero, as is shown in Appendix II for the special case where $g(u)$ and $f_0(u)$ are analytic functions of u, and can be split into three separate terms. The first term arises when one of the zeros of Eq. (7.7) lies on the cut. As we show in Appendix II this is never the case when $f_0(u)$ is analytic in the neighborhood of the real axis in the complex u plane, but such zeros do occur when $f_0(u)$ is discontinuous, as witness the simple case

$$f_0(u)=f_1 \quad u_1<u<\bar{u},$$
$$f_0(u)=f_2 \quad \bar{u}<u<u_2.$$

The second term in the integral around the cut arises because I_1, of Eq. (7.5) has, in general, a discontinuity equal to $2\pi i g(-\Omega_0/k_0)$ as we cross the cut from the upper to the lower half of the complex ω plane at the point $\omega=\Omega_0$. As a typical example consider the case

$$g(u)=f_0(u)=1 \quad u_1<u<u_2,$$

where the integral around the cut is equal to

$$\frac{i}{\epsilon_0 k_0}\int_{u_1}^{u_2} du \frac{1}{1-\omega_0^2(u_2-u_1)/(\omega+u_2k_0)(\omega+u_1k_0)}.$$

This term is nonzero even when $\omega_0^2=0$ and corresponds to the so-called "gas modes" discussed by Bohm and Gross.[3] Finally a third term arises due to the fact that the I_2, of Eq. (7.6), has a discontinuity as one crosses the cut equal to

$$2\pi i[df_0(-\Omega_0/k_0)/du]/k_0,$$

when $f_0(u)$ has a derivative for all $u_1<u<u_2$. The presence of such terms is ignored in the usual "Ansatz" solutions which often omit the "gas modes" as well.

Admittedly I_2 becomes continuous across the cut if we represent $f_0(u)$ as the limit of a series of square pulse functions

$$f_0(u)=f(n) \quad u_n<u<u_{n+1}, \quad n=1\cdots M,$$

where

$$u_{n+1}-u_n=\Delta u=(u_2-u_1)/M,$$

which can be done as long as $f_0(u)$ is integrable in the sense of Riemann.

However this simplification only arises in the special case of Eq. (7.1). In general the characteristic determinant is discontinuous across the cut whatever the form of $f_0(u)$, except when $f_0(u)$ can be represented as the sum of a series of δ functions. This last case is trivial since the stream now reduces to a system of discrete beams when the cut is redundant.

The procedure, that we have just outlined, is the normal one in transform theory valid whatever the nature of $f_0(u)$ and $g(u)$ as long as these functions are integrable in some sense. In particular there is no need for $f_0(u)$ and $g(u)$ to be analytic functions of u; they can be represented by a sum of δ functions or of square pulse functions or by a power series, whichever is the more convenient.

However this is certainly not possible in the treatment given by Landau as we show in Appendix III.

When ω_H, ν and p^2 are all nonzero we see by inspection of Eqs. (3.47) to (3.50) that cuts must be made in the ω plane along the lines

$$\omega=\omega_H-uk_0+i\nu(u); \quad \omega=-uk_0+i\nu(u); \quad \omega=-uk_0,$$

which all lie on or above the real ω-axis.

A similar procedure must be followed for the medium excited by an external signal or by an initially localized disturbance before inverting from the complex k plane onto the real ω-axis. In this case also the contributions from the cuts are, in general, nonzero and can be of importance particularly in the noise theory of the terminated stream.

8. DISCUSSION

The vector solution of this paper can be applied in principle to a stream of charged particles with different charge/mass ratios and arbitrary velocity distributions under arbitrary initial and boundary conditions. Unlike the theories that employ a stream function one is not restricted to the case of zero axial magnetic field and since the analysis is fully relativistic there is no need to treat the transverse and longitudinal fields separately.

However the general theory is very complex and in this paper we have discussed only the special case where the solution satisfying arbitrary initial conditions can be expanded as a sum over a complete orthogonal set of independent elementary solutions. Such an expansion can always be carried out for the stream of infinite cross section, but for the finite stream it is only possible under the limited transverse boundary conditions of Sec. 5. Each elementary solution can then be expressed explicitly in terms of the initial conditions by means of a double Laplace transform.

The use of a Laplace transform was introduced by Landau[14] in his theory of the longitudinal oscillations in a thermal plasma. However his treatment is only valid when the ac and dc velocity distribution functions are analytic, and, in its original form, can only be applied to the unphysical case where the electron velocity distribution extends to infinity. The solution of this paper is free from these restrictions and contains

terms, which are inevitably omitted in an "Ansatz" solution where one assumes *ab initio* that all ac quantities are proportional to $\exp[i(\mathbf{k}\cdot\mathbf{z}+\omega t)]$. This "Ansatz" procedure, which is used by the majority of writers, only gives the necessary conditions that a solution should satisfy the Maxwell-Lorentz equations. It is therefore much less informative than the more rigorous Laplace transform analysis which gives the complete solution under given initial conditions, and from which one can find both the physical interpretation of the "Ansatz" solutions and the initial conditions to which they correspond.

In one "Ansatz" procedure one solves the characteristic equation for ω in terms of fixed $k=k_0$, where k_0 is a real propagation constant, and obtains $4N+4$ possible modes of oscillation, where N is the number of discrete velocity beams. We have shown that this solution only applies in general to the infinite unterminated stream excited by an initial distribution of disturbance proportional to $\exp(ik_0z)$. For the stream terminated at $z=0$ the solution is only valid for $t<z/c$ except in the very special circumstances discussed in Sec. 6. If any of the roots of the characteristic equation lie in the lower half of the complex ω-plane for certain real k_0, then an associated initial disturbance will build up exponentially with time. However one cannot tell from this whether the stream is amplifying or unstable, a distinction that is important when the stream is excited by a disturbance confined initially to a small region of the stream. We concluded on heuristic rather than rigorous grounds that the stream would only be unstable in a frame of reference in which all the charge is moving in one direction if one of the growing roots was associated with a field wave; that is if $\mathrm{Lim}(\omega_n/k_0)=\pm 1/c$ as $k_0\to\infty-i\gamma_2$, where $\omega_n(k_0)$ lies below the real ω axis for some real k_0 and where γ_2 is chosen so as to avoid any multiple roots of the characteristic determinant. The distinction between instability and amplification is usually unimportant in a frame of reference moving with the stream as both processes will normally occur together.

The alternative "Ansatz" solution is found by solving the characteristic equation for k in terms of fixed $\omega=\Omega_0$, when one obtains $4N+4$ possible values for the propagation constant. This solution applies to a stream excited at a material boundary by an external signal of frequency Ω_0, and is only valid when the transient part of the solution for the singly terminated stream decays with time. The conditions when this last restriction is satisfied can be found from the first "Ansatz" solution when all the charge is moving in one direction. However when reverse beams are present together with amplified growing waves the stream is often unstable so that no steady-state solution exists.

In order to interpret this solution one must be able to distinguish between waves that are directly excited at the incident surface $z=0$, and those that can only be excited by reflection from some subsequent surface or region of discontinuity. When all the charge is moving in the positive direction we showed in an earlier paper[16] that the asymptotic value of the propagation constant of the reflected waves is given by $\mathrm{Lim}[k_n(\Omega_0)/\Omega_0]=+1/c$ as $\Omega_0\to\infty-i\gamma_1$. When reverse beams are present we have shown that the associated space charge waves can only be excited by reflection so that we now have the general result that $\mathrm{Lim}[k_n(\Omega_0)/\Omega_0]>0$ as $\Omega_0\to\infty-i\gamma_1$ for all reflected waves and vice versa.

Although the two "Ansatz" solutions correspond to quite different initial conditions, there are many similarities between them. In particular either procedure can be used to find whether the unterminated stream can amplify. This is contrary to some earlier interpretations where one "Ansatz" is used to find whether the stream is unstable the other to find whether it can amplify. To some extent the confusion is merely a matter of terminology, but it can easily lead to false conclusions. Thus some writers have argued that amplified growing waves can exist in a stream even if all the roots of the characteristic equation lie on or above the real axis in the ω-plane. However in this case any growing waves with propagation constants in the lower half of the complex k plane are always reverse waves attenuated in the reverse direction.

The vector solution of Eqs. (3.17) to (3.19) is valid even when the dc quantities such as u_{0z}, ρ_z, etc., are functions of z. In this case one can integrate Eqs. (3.33), (3.37), and (3.38) to find $\mathbf{r}_s{}^t(z,\omega)$, $H_l{}^t(z,\omega)$, and $v_{ls}{}^t(z,\omega)$ explicitly in terms of $E_l{}^t(z,\omega)$. On substituting in Eq. (3.37) one gets a system of integro-differential equations for $E_l{}^t(z,\omega)$, but these can no longer be reduced to algebraic equations by a Laplace transform with respect to z and small progress has been made toward their solution.

The theory can also be extended to the case where the dc magnetic field and the dc velocities have transverse as well as axial components as discussed in Appendix I. However this can only be carried through in Cartesian coordinates and the algebra in the general case is very cumbersome. The best hope is then to look for some approximate solution in which, for example, one considers only the transverse or only the longitudinal part of the solution. The errors involved in this and similar simplifications are discussed.

Acknowledgment is made to the Admiralty for permission to submit this paper for publication.

APPENDIX I

In the text the dc components of the external magnetic flux density and of space charge velocity were assumed to be of the form $\mathbf{B}_0=(0,0,B_0)$ and $\mathbf{u}_0=(0,0,u_0)$, respectively. We shall now show how the analysis may be extended when these vectors possess transverse components so that $\mathbf{B}_0=\mathbf{B}_{r0}+B_0\mathbf{a}$, $\mathbf{u}_0=\mathbf{u}_{r0}+u_0\mathbf{a}$ where $\mathbf{B}_{r0}\cdot\mathbf{a}=\mathbf{u}_{r0}\cdot\mathbf{a}=0$ and $\mathbf{B}_{r0}$, $\mathbf{u}_{r0}$ are constant vectors independent of position. In order to maintain the steady-state flow it is necessary to introduce

additional dc **E**-fields but as these do not affect the small signal ac equations they will be left unspecified.

Assuming, for the moment that $\mathbf{u}_{r0}=0$, the only effect of the transverse components of the dc magnetic field is to add additional terms to the Lorentz force equation which, in its linear approximation, may now be written

$$(\partial/\partial t+v_s+u_{0s}\partial/\partial z)(m_s\mathbf{v}_s+m_sK_s(u_{0s}^2/c^2)(\mathbf{v}_s\cdot\mathbf{a})\mathbf{a}) = -e_s[\mathbf{E}+\mathbf{v}_s\times B_0\mathbf{a}+\mu_0u_{0s}\mathbf{a}\times\mathbf{H}+\mathbf{v}_s\times\mathbf{B}_{r0}], \quad (I.1)$$

differing from Eq. (3.9) in the term $\mathbf{v}_s\times\mathbf{B}_{r0}$.

The elementary solution derived above for the case $\mathbf{B}_{r0}=0$ relied on the fact that all the vector Maxwell-Lorentz equations could be expressed as linear combinations of the three fundamental vectors **L**, **M**, **N** defined in (3.16). These vectors determine an auxiliary coordinate system in which we may express $\mathbf{B}_{r0}$ by the vector equation

$$\mathbf{B}_{r0}=B_{01}\mathbf{L}+B_{02}\mathbf{M}, \quad (I.2)$$

where B_{01}, B_{02} are scalar coefficients that depend upon (x^1, x^2) in such a manner that $\mathbf{B}_{r0}$ is a constant vector.

Substituting for $\mathbf{B}_{r0}$ in Eq. (I.1) and assuming that $\mathbf{v}_s$ is given by (3.19) the term $\mathbf{v}_s\times\mathbf{B}_{r0}$ may be written

$$\mathbf{v}_s\times\mathbf{B}_{r0}=-B_{02}v_{2s}\phi\mathbf{L}-B_{01}v_{2s}\phi\mathbf{M} +(B_{01}v_{2s}-B_{02}v_{1s})[\nabla\phi]^2/\phi\mathbf{N}. \quad (I.3)$$

In the general case where ϕ is any solution of the two-dimensional wave equation (3.20) consistency requires that

$$B_{0l}\phi(x^1, x^2) \quad \text{and} \quad B_{0l}[\nabla\phi(x^1, x^2)]^2/\phi(x^1, x^2) \quad l=(1, 2)$$

must both be independent of (x^1, x^2). This is only possible in Cartesian coordinates and then only when the solution of Eq. (3.20) is expressed as a traveling wave

$$\phi(x^1, x^2)=\exp[i(lx+my)],$$

where $l^2+m^2=p^2$.

In this case $B_{0l}\sim\phi^*(x^1, x^2)$, the complex conjugate of $\phi(x^1, x^2)$ when $\mathbf{B}_{r0}$ as defined by Eq. (I.2) is indeed independent of position, so that a consistent solution can be obtained.

A similar discussion shows that the same restriction must be imposed on the coordinate system when the dc velocity has transverse components. In the latter case especially the algebra becomes extremely cumbersome and its importance does not seem sufficiently great to warrant even a summary of the solution.

APPENDIX II

When $g(u)$ the ac velocity distribution function of Sec. 7 is analytic we can immediately find the discontinuity in I_1, defined by Eq. (7.5), as we cross the real ω axis.

Since $g(u)$ is analytic we may expand $g(u)\equiv g(u+\omega/k_0-\omega/k_0)$ as a Taylor series in (ω/k_0+u) to give

$$g(u)=g(-\omega/k_0)+\sum_{n=1}^{\infty}g^n(-\omega/k_0)(u+\omega/k_0)^n/n!.$$

If we substitute in Eq. (7.5) and integrate we get

$$I_1=g(-\omega/k_0)\log\left(\frac{u_2+\omega/k_0}{u_1+\omega/k_0}\right) +\sum_{n=1}^{\infty}\frac{g^n(-\omega/k_0)}{nn!k_0}\left[\left(u_2+\frac{\omega}{k_0}\right)^n-\left(u_1+\frac{\omega}{k_0}\right)^n\right].$$

As we cross the real ω axis at the point $\omega=-\tilde{u}k_0\equiv\Omega_0$, $u_1<\tilde{u}<u_2$, the logarithmic term in I_1 changes from

$$i\pi g(+\tilde{u})\equiv i\pi g(-\Omega_0/k_0)$$

just above the real ω-axis to

$$-i\pi g(-\tilde{u})\equiv -i\pi g(-\Omega_0/k_0)$$

just below the real ω-axis.

Similarly if $f_0(u)$ is analytic we may write

$$f_0(u)=f_0(-\omega/k_0)+\sum_{n=1}^{\infty}f_0^n(-\omega/k_0)(u+\omega/k_0)^n/n!,$$

when substituting in Eq. (7.6), and integrating term by term we get

$$I_2=\frac{f_0(-\omega/k_0)}{k_0^2}\cdot\frac{u_2-u_1}{(u_2+\omega/k_0)(u_1+\omega/k_0)} +\frac{f_0'(-\omega/k_0)}{k_0^2}\cdot\log\left(\frac{u_2+\omega/k_0}{u_1+\omega/k_0}\right) +\sum_{n=1}^{\infty}\frac{f^n(-\omega/k_0)}{(n-1)n!k_0^2}[(u_2+\omega/k_0)^{n-1}-(u_1+\omega/k_0)^{n-1}],$$

which has a discontinuity of

$$2\pi i[f_0'(-\Omega_0/k_0)]/k_0^2$$

across the real ω-axis, when $\omega=-\tilde{u}k_0\equiv\Omega_0$ and $u_1<\tilde{u}<u_2$.

It follows from this that the characteristic equation of Eq. (7.7) has no zeros on or immediately above the cut between the points $-u_2k_0<\omega<-u_1k_0$ if $f_0(u)$ is analytic, except possibly at the zeros of $f_0'(-\Omega_0/k_0)$. However these zeros form a set of measure zero if $f_0(u)$ is an integral function of u as do the zeros of Eq. (7.7) so that this possibility can effectively be ignored.

APPENDIX III

In the solution given in Sec. 7 for the stream with a continuous velocity distribution it was only necessary that $f_0(u)$ and $g(u)$, the dc and ac velocity distribution functions should be integrable.

However in the alternative solution given by Landau[14] it is necessary that $f_0(u)$ and $g(u)$ be integral functions

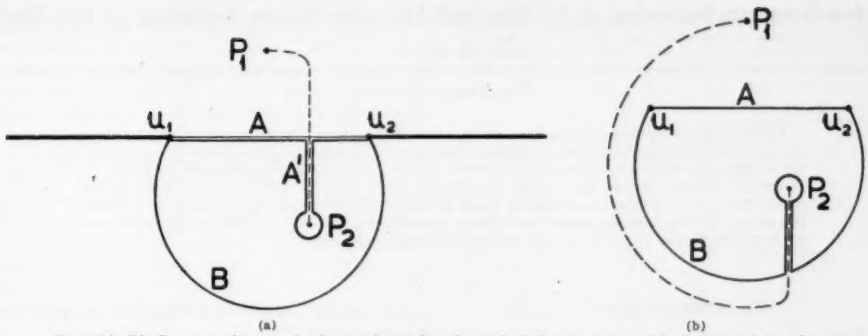

FIG. 1(a), (b). Contours of integration in complex u plane for analytical continuation of I_1, I_2 in complex ω plane.

of u, while this writer's procedure has to be further modified when one allows for the fact that no material particle can have a velocity greater than c.

Instead of inserting a cut in the complex ω-plane, Landau obtains the analytic continuation of $E_z{}^t(z, \omega)$ by deforming the contours of integration of I_1 and I_2, defined by Eqs. (7.5) and (7.6), respectively, in the complex u *plane*. For values of ω lying in the lower half of the complex ω plane the point $u=-\omega/k_0$ lies in the upper half of the complex u plane if k_0 is positive and the contour of integration may be taken along the real u axis, contour A in Fig. 1(a). Provided that $f_0(u)$ and $g(u)$ are integral functions of u this contour may be deformed into contour B without affecting the value of I_1 and I_2. Let us now suppose that the point $u=-\omega/k_0$ is allowed to move into the lower half of the complex u *plane* to the point P_2, crossing the real axis between $u_1<u<u_2$. The contour B may now be deformed into the contour A' giving a different value for I_1I_2 than that obtained by integrating along the contour A. By this means one can obtain an analytic continuation of I_1I_2 and $E_z{}^t(z, \omega)$ into the upper half of the complex ω plane. However this procedure does not lead to a single valued expression for I_1I_2 since the point P_2 could have been approached by a path that crosses the real u axis outside the range $u_1<u<u_2$, as shown in Fig. 1(b), when the contour B can be deformed back into the contour A. Admittedly this difficulty does not arise in the case considered by Landau when $(u_1, u_2)\equiv(-\infty, \infty)$, but when u_1u_2 are finite we must insert cuts into the real u axis in the ranges $-\infty>u>u_1$, $u_2<u<\infty$ to ensure that I_1, I_2 are single valued. In this case I_1, I_2 are undefined at values of $\omega=-\tilde{u}k_0$ where $\tilde{u}$ lies on these cuts and we must introduce a corresponding system of cuts into the complex ω-plane in the ranges $-\infty<\omega<-u_2k_0$, $-u_1k_0<\omega<\infty$.

Thus Landau's procedure leads to no increase in simplicity over the alternative we have followed in the text, while it is only valid when $f_0(u)$, $g(u)$ are integral functions of u. Furthermore some of his conclusions as to the nature of the solution for the thermal plasma have to be modified appreciably when one takes account of the fact that $|u_1|$, $|u_2|$ are both less than c, since it is not now possible to deform the contour of integration of Eq. (7.3) into the upper half of the complex ω plane outside the range $-u_2k_0<\omega<-u_1k_0$. The physical consequences of this are discussed.

Proton-Deuteron Scattering at 5.1 Mev and Deuteron-Proton Scattering at 10.2 Mev*

K. B. MATHER
Commonwealth Scientific and Industrial Research Organization, Physics Department, University of Melbourne, Melbourne, Australia
(Received July 21, 1952)

A photographic scattering chamber has been used to study the elastic scattering of 5.1-Mev protons by deuterium and 10.2-Mev deuterons by hydrogen, these being the same process in the center-of-mass system. Differential cross sections were obtained from 16.4° to 172.9°. These are in good agreement with other experimental data at about the same energy. Comparison is made with the theoretical angular distribution due to Buckingham, Hubbard, and Massey, based on a symmetrical exchange force. Agreement is close at this energy, favoring exchange rather than ordinary force theories. However, at higher energies (~10-Mev $p-d$) the BHM calculations do not represent the interaction satisfactorily.

I. INTRODUCTION

THE proton-deuteron interaction has now been studied at various energies from 250 kev to ~10 Mev, including three studies at approximately 5 Mev.[1] The present report contributes further data at 5.1 Mev over a somewhat wider range of angles. The data were acquired by scattering both 5.1-Mev protons from deuterium and 10.2-Mev deuterons from hydrogen, the combination of the techniques having obvious advantages in revealing special errors to which either one is liable.

II. METHOD

The apparatus employed consisted of the photographic scattering chamber described in an earlier publication[2] on proton-proton scattering, and its manner of use was essentially unchanged in the present work. However, in $p-d$ scattering, scattered and recoil particles are different and distinguishable and were counted separately, leading to the differential scattering cross section in the laboratory system by the following formula:[3]

$$\sigma(\Theta)=n_a Rh \sin\Theta/N_{cc}N_t 2b \sin\Phi.$$

Conversion to center-of-mass cross section $\sigma(\theta)$ at center-of-mass angle θ is achieved by formulas:

$$\sigma(\theta)=\sigma(\Theta_1)\cdot(\sin\Theta_1/\sin\theta)^2\cdot\cos(\theta-\Theta_1)$$

if *scattered* tracks at angle Θ_1 are counted, and

$$\sigma(\theta)=\sigma(\Theta_2)/4\cos\Theta_2$$

if *recoil* tracks at angle Θ_2 are counted, the angle relationship being:

$$\theta=(\pi-2\Theta_2).$$

In $p-d$ scattering the proton may be scattered at all laboratory angles from 0 to 180° the deuteron recoiling at angle from 0 to 90°. In $d-p$ scattering the deuteron has a maximum angle of scatter of 30°, the proton recoiling at angles from 0 to 90°. Owing to the fact that there are two kinds of collision (hard and soft) which can scatter the deuteron at any angle less than 30°, three distinct track lengths appear in the photographic emulsion at all angles below 30°—a short deuteron track, a long deuteron track, and a recoil proton track.

Approximate ranges in Nuclear Research Emulsions (Ilford C2) are listed in column 4 of Tables I and II, for $p-d$ and $d-p$ cases, respectively. It will be observed that it is always possible and generally easy to distinguish, by their ranges, the several particles which appear at any angle. The fact that one plate can, for $d-p$ scattering below 30°, yield three scattering cross sections endows the method with special merit. These three values serve as related "triplets" since they derive from the same slit unit and precisely the same geometry is used in computing them. They should therefore be very reliable in relative value. Similarly, in $p-d$ scattering below 90° there are related "doublets."

III. EXPERIMENTAL DETAILS

The source of protons and deuterons was the Washington University 45-inch cyclotron. The beam energy was redetermined during every run by measuring ranges in a photographic plate placed at the 45° position at a small angle, $\Phi=3°$. The range-energy data of Rotblat[4] were used, leading to average energy values at the scattering volume of 5.1±0.1 Mev for the protons and 10.2±0.2 Mev for the deuterons, in the laboratory system.

The energy of each individual run could be stated rather more precisely than this but as the beam energy appeared to vary slightly from run to run, average

* The experimental portion of this work was conducted at Washington University, St. Louis, Missouri, assisted by the ONR and AEC.

[1] R. F. Taschek, Phys. Rev. **61**, 13 (1942), 250 and 275 kev; Tuve, Heydenberg, and Hafstad, Phys. Rev. **50**, 806 (1936), 830 kev; Sherr, Blair, Kratz, Bailey, and Taschek, Phys. Rev. **72**, 662 (1947), 1.51, 2.08, 2.53, 3.00, and 3.49 Mev; Heitler, May, and Powell, Proc. Roy. Soc. (London) **A190**, 180 (1947), 4.2 Mev; Rodgers, Leiter, and Kruger, Phys. Rev. **78**, 656 (1950), 4.97 Mev; Karr, Bondelid, and Mather, Phys. Rev. **81**, 37 (1950), 5.0 Mev; L. Rosen and J. C. Allred, Phys. Rev. **82**, 777 (1951), 5.2 Mev; Armstrong, Allred, Bondelid, and Rosen, Phys. Rev. **83**, 218 (1951), 9.7 Mev.

[2] K. B. Mather, Phys. Rev. **82**, 133 (1951).

[3] This formula appeared incorrectly in reference 2. The symbols are defined there.

[4] J. Rotblat, Nature **167**, 550 (1951).

values have been quoted together with uncertainties which cover the extreme limits encountered.

The deuterium and hydrogen used as scattering gases were 99.5 and 99.8 percent pure, respectively. Experiments were usually conducted at a gas pressure of approximately 1.4 cm Hg which was low enough to prevent any serious multiple scattering effects.

The $p-d$ data were much "cleaner" than the $d-p$ due particularly to the heavy neutron flux which is always associated with a cyclotron accelerating deuterons. During preliminary runs it was found that the background on the plates due to knock-on protons was heavy and would have complicated the scanning unnecessarily. This was reduced to a few percent by surrounding the scattering chamber with a concrete fort 16 inches thick on the side facing the cyclotron and reinforced about the collimator with timber blocks.

Runs were made at several different exposures so as to give optimum track density over each range of angles to facilitate scanning. The method of scanning was the same as described in reference 2. In certain cases, however, e.g., $d-p$ runs 5 and 6, for $\Theta<30°$, only short deuteron tracks were counted as these could be counted quickly. Counting long deuterons and protons was more tedious, requiring ideal exposure conditions, and was only considered worthwhile for run 7.

IV. RESULTS AND DISCUSSION

The final values of seven runs are listed in Table I ($p-d$) and Table II ($d-p$) ranging from $\theta=16.4°$ to 172.9°, and all data are shown in Fig. 1 as $\sigma(\theta)$ *versus* θ. The total number of tracks counted was 105,500. The number contributing to each value is given in parentheses after the value and determines the standard deviation of the value imposed by the counting. Other errors are the same as listed in Sec. VIII of reference 2. The probable error in relative values, excluding the statistical error, is ~0.4 percent.

Corrections had to be applied to the $p-d$ data as follows: (1) Scattering volume. This is not exactly the same as implied in the formula for $\sigma(\Theta)$ in Sec. II. A correction had to be applied only at $\Theta=165°$ and amounted to 0.7 percent. (2) Air leakage, degassing of plates and equipment, and impure gas. This amounted to ~5 percent at $\Theta=11°$ and declined rapidly at larger angles. (3) Slit width. This applied only where the cross section was changing rapidly, *viz.*, at small laboratory angles where it amounted in several cases to a few percent.

Similar corrections pertained to the $d-p$ runs. On the whole, the $p-d$ scanning was more straightforward. Fewer cases of ambiguous track lengths occurred and hence runs 1 and 2 should carry rather more weight.

In run 6 the tracks were so congested that only short deuteron tracks could be counted confidently and even there it was felt that some tracks might be overlooked. This may account for the tendency towards lower values in this run. The $d-p$ data show considerable scatter at $\theta=30°$ to 40°. This is due to the difficulty of counting accurately the short proton tracks, especially at 30°. These tracks are only 7μ in mean range and, allowing for straggling, some of the tracks are too short to be established with certainty. In run 4 the value at 30° is a lower limit. About 10 percent more "probables" were recorded and it seems likely that others escaped notice altogether.

Beyond about 160° the same trouble operates. Some short deuterons, expecially at $\theta=168.6°$ and 172.9° may be missed. The $p-d$ data which have better statistics in this region would be expected to suffer from

Table I. Differential cross sections derived from two $p-d$ scattering runs at 5.1 Mev. The figures in parenthesis are numbers of tracks contributing to the values. In the third column, p indicates scattered proton and d recoil deuteron.

Θ	θ	Kind of track	Range in μ	$\sigma(\theta)\times10^{25}$ cm² steradian⁻¹ Run 1	Run 2
11	16.4	p	168	x3.90 (1200)	
	158.0	d	89	2.29 (1212)	
15	22.4	p	162		
	150.0	d	84		
16	23.9	p	162	2.48 (1158)	
	148.0	d	83	1.72 (1355)	
21	31.1	p	155	2.27 (966)	
	138.0	d	77	1.17 (845)	
25	37.2	p	148	2.00 (1733)	
	130.0	d	71	0.846 (1245)	
30	44.5	p	138	1.86 (735)	
	120.0	d	61	0.602 (401)	
35	51.7	p	129	1.63 (1242)	
	110.0	d	52	0.533 (680)	
40	58.7	p	118	1.47 (1294)	1.49 (1207)
	100.0	d	42	0.646 (911)	0.631 (841)
45	65.7	p	106		
	90.0	d	33		0.84 (188)
50	73.5	p	92	1.21 (968)	
	80.0	d	26	1.00 (1205)	
55	79.2	p	82	1.02 (721)	1.12 (861)
	70.0	d	19	1.25 (1294)	1.24 (1382)
60	85.6	p	71		0.862 (1200)
	60.0	d	13		1.37 (2570)
65	91.9	p	62	0.743 (611)	0.734 (919)
	50.0	d	8	1.71 (1736)	1.60 (2457)
70	98.0	p	54		0.651 (1112)
	40.0	d	5		
75	103.9	p	48	0.550 (511)	0.616 (1006)
	30.0	d	~3		
85	114.9	p	35		0.577 (1037)
	10.0	d	—		
95	124.5	p	26	0.618 (367)	0.712 (990)
105	133.8	p	19		1.01 (1121)
115	141.9	p	15	1.24 (534)	1.36 (1141)
125	149.1	p	12		1.77 (1305)
135	155.7	p	10		2.22 (1028)
145	161.6	p	8		/2.60 (1240)
155	167.2	p	7		/2.84 (1217)
165	172.4	p	~7		/2.96 (2488)

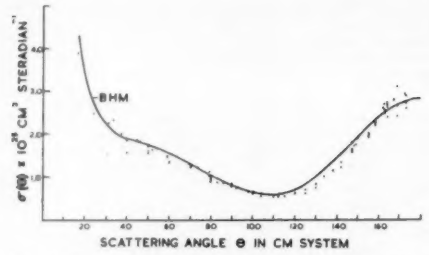

FIG. 1. Differential $p-d$ and $d-p$ cross sections in center-of-mass coordinates. All values listed in Tables I and II are plotted. The full curve (BHM) is theoretical, based on calculations for the same energy by Buckingham, Hubbard, and Massey.

the same cause but seem to be rather higher in value. Probably the curve begins to flatten off at or near 160° as predicted by the Buckingham, Hubbard, and Massey theory, but this region is difficult to study and the present data are not conclusive beyond about 160°.

Moreover, where this error exists, multiple scattering losses will also be at their worse and due to the complicated "compensating" mechanism (see Sec. VIII of reference 2) it is very difficult to estimate the consequences. Lower limit values are prefixed in the tables by *l*. Other values which are suspected for any reason (poor scanning conditions, heavy background, etc.) are prefixed by *x*.

In the present work absolute values were determined by two methods: (a) By measuring the charge collected on a standard condenser as described in the earlier publications. (b) By assuming a value for the absolute cross section of $p-p$ scattering (which is established to a higher degree of precision than any other scattering process) and determining $p-d$ and $d-p$ cross sections relative to $p-p$. The reason for introducing (b) is that as a result of a recheck by the Bureau of Standards some doubts have arisen concerning the true values of the condensers at the time this work was carried out.

Cross sections were therefore determined relative to the $p-p$ results of reference 2, which appear to be consistent with other results at or near this energy; i.e., assuming absolute $p-p$ cross sections to be in accordance with pure S-wave scattering of phase shift $\delta_0=54.5°$. The derived absolute $p-d$ and $d-p$ cross sections agreed with those measured directly (method (a)) to ~2 percent. The cross sections in Tables I and II are the mean of both methods and are believed to have an accuracy in absolute value of ±2 percent (probable error) taking account of all sources of systematic error which have been recognized but not including the effect of statistical error on the individual values.

TABLE II. Differential cross sections derived from five $d-p$ scattering runs at 10.2 Mev. In the third column *ld* indicates long deuteron track, *sd* short deuteron track and *p* recoil proton track. Prefix *l* indicates lower limit value and *x* doubtful value.

				$\sigma(\theta)\times10^{25}$ cm² steradian^{-1}							
		Kind of	Range	Run 3		Run 4		Run 5		Run 6		Run 7	
	θ	track	in μ										
7	21.1	*ld*	325										
	166.0	*p*	440										
	172.9	*sd*	13					*l*2.73	(532)	*l*2.6	(118)	*l*2.9	(314)
11	33.4	*ld*	300									2.32	(430)
	158.0	*p*	425									2.31	(187)
	168.6	*sd*	15					*l*2.68	(1120)	*l*2.42	(996)	*l*3.11	(81)
15	46.1	*ld*	264									1.82	(1129)
	150.0	*p*	403									1.91	(504)
	163.9	*sd*	16	2.63	(889)			2.69	(1536)	2.40	(1859)	2.74	(262)
16	49.4	*ld*	260										
	148.0	*p*	396										
	162.5	*sd*	16	2.57	(946)			2.49	(1320)			2.70	(724)
21	66.8	*ld*	238									1.30	(1132)
	138.0	*p*	359									1.14	(390)
	155.2	*sd*	20					1.92	(1404)	1.99	(488)	2.04	(375)
25	82.7	*ld*	196			0.954	(1236)					0.875	(1709)
	130.0	*p*	324			0.839	(384)					0.752	(544)
	147.3	*sd*	25			1.80	(722)	*x*1.58	(994)	1.66	(1280)	1.60	(973)
30	120.0	*p*	276			0.639	(316)						
35	110.0	*p*	230	0.536	(1903)	0.563	(1070)	0.545	(2400)			0.610	(1049)
40	100.0	*p*	184	0.637	(2180)	0.613	(739)	0.622	(2267)			0.666	(1075)
45	90.0	*p*	141	0.780	(291)								
50	80.0	*p*	104	0.957	(2365)	0.945	(1047)	0.879	(2488)				
55	70.0	*p*	70					1.21	(2906)				
60	60.0	*p*	47					1.34	(1828)				
65	50.0	*p*	28	1.55	(2270)			*x*1.56	(2392)				
70	40.0	*p*	15	1.85	(1918)			1.58	(1905)				
75	30.0	*p*	7			*l*1.52	(220)						

In Fig. 1 all the experimental points of the present work have been plotted. The point at $\theta=16.4°$ is uncertain but seems to be consistent with purely Rutherford-Darwin scattering indicating that the scattering is essentially Coulombian below this angle. The minimum cross section at this energy occurs at approximately 112° in the center-of-mass system.

The full curve (BHM) represents the calculated angular distribution of 5-Mev protons due to Buckingham *et al.*[5] based on a symmetrical exchange force as in the earlier work of Buckingham and Massey, but including allowance for *D*-wave scattering. The new calculations are markedly superior in representing the observations at large angles (see comparison with earlier theory made by Karr *et al.*, reference 1) and appear to represent the experimental facts of $p-d$ scattering fairly satisfactorily from about 2 to 5 Mev. In absolute value at 5 Mev the theoretical curve would fit the data better if ~9 percent lower.

However, the recent $p-d$ scattering at 9.7 Mev carried out at Los Alamos by Armstrong *et al.* (see reference 1) can be compared roughly with the BHM calculations at 11.5 Mev and here the agreement is poor. The experimental curve rises much more steeply at large angles and also shows no tendency to flatten off between about 30° and 60° as predicted by BHM. These discrepancies seem to be paralleled also by high energy $n-d$ scattering.

Part of the scanning involved in this project was carried out at Birmingham University, England, assisted by an Imperial Chemical Industries Fellowship.

[5] Buckingham, Hubbard, and Massey, Proc. Roy. Soc. (London) **A211**, 183 (1952).

PHYSICAL REVIEW VOLUME 88, NUMBER 6 DECEMBER 15, 1952

The Relativistic Configuration Space Formulation of the Multi-Electron Problem*

MARIAN GÜNTHER
Institute of Theoretical Physics, University of Warsaw, Warsaw, Poland
(Received July 16, 1952)

A relativistic configuration space (many-time) presentation of quantum electrodynamics is developed, which, being equivalent to the Tomonaga-Schwinger formalism, may be expected to have the advantage of its direct applicability to bound-state problems of multi-electron systems. The main purpose of this paper is therefore to get an evidently relativistically invariant description of the interactions between individual electrons, in such a way, however, as to avoid those divergence difficulties which may be accounted for by the use of electron plane waves for building up the actual state of the system. The order of the presentation is as follows: a general relativistically invariant proof of equivalence of the Tomonaga-Schwinger formalism and the many-time formalism of Dirac, Fock, and Podolski given in Sec. I will provide a necessary starting point for further generalization in the form of Eq. (53). This equation, when eventually solve in Sec. II, gives rise to a formal extension of the multi-electron wave function concept into regions for which the latter remained hitherto undefined. In Sec. III a method of elimination of virtual processes is outlined and invariant expressions for the multi-electron interactions are derived. All explicit derivations in this paper are carried out to terms of the order of e^2. An example, a relativistic two-electron wave equation, is given. This equation accounts for the Coulomb and Breit interactions.

I. MANY-TIME AND TOMONAGA-SCHWINGER THEORIES

A FORMALISM based on the relativistic configuration space concept was introduced for the first time by Dirac, Fock, and Podolski[1] (referred to in the following as D.F.P.). This formalism is usually called the many-time theory, because an introduction of separate sets of spatial coordinates for individual electrons necessitates an introduction of a separate time variable for each electron. Our first task will be to show the equivalence of the Schwinger-Tomonaga theory[2] (referred to later on as T-Sch.) and the D.F.P. theory, if Fermi-Dirac statistics is assumed in the latter. The method employed is thoroughly invariant in form. We start with the basic equations of the D.F.P. theory:

$$[\gamma_k{}^\mu((\partial/\partial x_k{}^\mu)-(ie/\hbar c)A_\mu(x_k))+(mc/\hbar)]\times\varphi(x_1\cdots x_k\cdots x_\nu)=0;\quad k=1,2,3\cdots\nu;\quad(1)$$

$$\Box A_\mu=0;\quad(2)$$

$$[A_\mu(x),A_\nu(x')]_-=i\hbar c\delta_{\mu\nu}D(x-x');\quad(3)$$

$$[\partial A_\mu(x)/\partial x^\mu-e\sum_{k=1}^{\nu}D(x-x_k)]\varphi(x_1\cdots x_\nu)=0;\quad(4)$$

where A_μ stand for the components of the potential four-vector of the radiation field, and $\varphi(x_1\cdots x_\nu)$ is the wave function of the system containing ν-electrons. Each x, when without upper index, stands for all the

* This part of the work submitted to the Faculty of Mathematics, Physics, and Chemistry of the University of Warsaw for obtaining the "Venia Legendi" (May, 1951).

[1] Dirac, Fock, and Podolski, Physik. Z. Sowjetunion **2**, 468 (1932).

[2] S. Tomonaga, Prog. Theor. Phys. **1**, 27 (1946); J. Schwinger, Phys. Rev. **74**, 1439 (1948).

four-space and time variables of the kth electron. It is to be understood, of course, that the wave function $\varphi(x_1 \cdots x_\nu)$ depends not only on the electron coordinates, but also on the radiation field variables, e.g., on the population numbers of different plane-wave components of the radiation field, and is therefore subject to A_μ operators. $D(x)$ denotes further the well-known singular function introduced by Pauli for the radiation field, with a δ-singularity on the light cone. The wave function of the D.F.P. formalism can only be uniquely defined if all interelectron distances are space-like. This is due to the fact that the system (1) ceases to be compatible as soon as we try to enter with one electron into the time-like part of the light cone of another,[3] and the A_μ operators do not commute on the light cone. We proceed now as follows: First, we introduce an infinite set of functions, $u_n(x)$, uniquely defined for all points of space-time, all of them satisfying the field-free Dirac equation

$$[\gamma^\mu(\partial/\partial x^\mu)+(mc/\hbar)]u_n(x)=0, \tag{5}$$

and a condition of orthogonality and normalization of the form

$$i\int_\sigma \bar{u}_n(x)\gamma^\mu u_m(x)d\sigma_\mu=\delta_{nm}. \tag{6}$$

We shall further assume that the $u_n(x)$-set is "complete" on every space-like surface σ, i.e., every function defined for all points of such a surface may be expressed as an expansion in terms of the set. The $d\sigma_\mu$ in (6) stand for the four components of the surface element of σ and are

$$d\sigma_\mu \equiv (dxdydz/i,\ dydzd(ct),\ \cdots,\ \cdots);$$

further, we have

$$\bar{u}_n = u_n{}^*\gamma^4. \tag{7}$$

The conditions (6) hold for every surface σ as a consequence of

$$(\partial/\partial x^\mu)[\bar{u}_n(x)\gamma^\mu u_m(x)]=0, \tag{8}$$

the last equality being a consequence of (5) and its conjugate.

We consider now a certain σ-surface, containing the points $x_1 \cdots x_\nu$. Then we can write

$$\varphi(x_1 \cdots x_\nu)=\sum_{n_1 n_2 \cdots n_\nu} a[\sigma](n_1 \cdots n_\nu) \times u_{n_1}(x_1)\times \cdots \times u_{n_\nu}(x_\nu). \tag{9}$$

It is of importance to note that the $a[\sigma](n_1 \cdots n_\nu)$ coefficients defined by (9) acquire functional dependence on σ while passing from one of those surfaces to another, for $\varphi(x_1 \cdots x_\nu)$ does not in general obey the field-free Dirac equation. We will try now to build up the state vector $\Psi[\sigma]$ of T-Sch. in terms of these coefficients. The dependence on the radiation field variables is also contained in the $a[\sigma](n_1 \cdots n_\nu)$ coefficients, as it should be if $\Psi[\sigma]$ is to have a proper definition. In order to find out what this proper definition will be and what (functional) differential equations the state vector will satisfy, we must first try to get the functional differential equations for the coefficients. Our first step will be to write down the Dirac equation for a single electron in terms of functionals and functional derivatives. We start with a development of an (arbitrary at first) spinor function $\psi(x)$ in terms of the set of functions defined by (5) and (6):

$$\psi(x)=\sum_n a[\sigma](n)u_n(x), \tag{10}$$

for all points x of σ. The coefficients $a[\sigma](n)$ do not change therefore as long as we move the point x along the σ-surface. Thus, on multiplying (10) from the left by $\bar{u}_n(x)\gamma^\mu$ and integrating along σ we get

$$a[\sigma](n)=i\int_\sigma \bar{u}_n(x)\gamma^\mu\psi(x)d\sigma_\mu, \tag{11}$$

and this gives us a straightforward way to determine the coefficients of (10). We now differentiate (11) with respect to σ at the point x. We use here the definition of T-Sch. of a functional derivative. A functional derivative of a functional F is given by the expression

$$\delta F[\sigma]/\delta\sigma(x)=\lim_{V(\sigma,\sigma')\to 0}\{F[\sigma]-F[\sigma']\}/V(\sigma,\sigma'), \tag{12}$$

where σ and σ' differ only in the immediate neighborhood of the point x, V being the four-dimensional volume contained between σ and σ'. This is the volume in the x, y, z, ct continuum and is a real number. Thus we get

$$\begin{aligned}\delta a[\sigma](n)/\delta\sigma(x) &= i\lim_{V(\sigma,\sigma')\to 0}\frac{\left\{\int_\sigma \bar{u}_n(x')\gamma^\mu\psi(x')d\sigma_\mu' - \int_{\sigma'}\bar{u}(x')\gamma^\mu\psi(x')d\sigma_\mu'\right\}}{V(\sigma,\sigma')} \\ &= i\lim_{V(\sigma,\sigma')\to 0}\frac{\left\{\int_{V(\sigma,\sigma')}(\partial/\partial x^\mu')[\bar{u}_n(x')\gamma^\mu\psi(x')]d^4x'\right\}}{V(\sigma,\sigma')} \\ &= i(\partial/\partial x^\mu)[\bar{u}_n(x)\gamma^\mu\psi(x)].\end{aligned} \tag{13}$$

Owing to (5) and its conjugate we have

$$\delta a[\sigma](n)/\delta\sigma(x)=i\bar{u}_n(x)[\gamma^\mu(\partial/\partial x^\mu)+(mc/\hbar)]\psi(x). \tag{14}$$

If we assume now that $\psi(x)$ satisfies the Dirac equation for an electron in an electromagnetic field described by the potential four-vector $A_\mu(x)$:

$$[\gamma^\mu((\partial/\partial x^\mu)-(ie/\hbar c)A_\mu(x))+(mc/\hbar)]\psi(x)=0, \tag{15}$$

we finally get

$$\delta a[\sigma](n)/\delta\sigma(x)=-(e/\hbar c)\bar{u}_n(x)\gamma^\mu A_\mu(x)\psi(x). \tag{16}$$

Using once more the expansion (10) on the right-hand

[3] F. Bloch, Physik. Z. Sowjetunion **5**, 301 (1934).

side of (16), this becomes

$$\delta a[\sigma](n)/\delta\sigma(x) = -(e/\hbar c)\sum_m (n|A(x)|m)a[\sigma](m), \quad (17)$$

where

$$(n|A(x)|m) = \bar{u}_n(x)\gamma^\mu A_\mu(x)u_m(x). \quad (18)$$

Equation (17) plays an essential part in our considerations and can easily be generalized for the case of many electrons if only all their mutual distances should remain space-like. The expansion of the wave function of the D.F.P. theory was already been given by (9). By an easy generalization of (11) we have

$$a[\sigma](n_1\cdots n_\nu) = (i)^\nu \int_\sigma \cdots \int_\sigma \bar{u}_{n_1}(x_1)\gamma_1^{\mu_1}\times\cdots$$
$$\times \bar{u}_{n_\nu}(x_\nu)\gamma_\nu^{\mu_\nu}\varphi(x_1\cdots x_\nu)d\sigma_1^{\mu_1}\cdots d\sigma_\nu^{\mu_\nu}, \quad (19)$$

whereas instead of (13) we get

$$\delta a[\sigma](n_1\cdots n_\nu)/\delta\sigma(x)$$
$$= (i)^\nu \sum_k \sum_{n_1\cdots n_\nu} \int_\sigma \cdots \int_\sigma \int_\sigma \cdots \int_\sigma \bar{u}_{n_1}(x_1)\gamma_1^{\mu_1}\times\cdots$$
$$\times u_{n_{k-1}}(x_{k-1})\gamma_{k-1}^{\mu_{k-1}}\times\bar{u}_{n_k}(x)[\gamma_k^{\mu_k}(\partial/\partial x_k^\mu)+$$
$$+(mc/\hbar)]\times\bar{u}_{n_{k+1}}(x_{k+1})\gamma_{k+1}^{\mu_{k+1}}\times\cdots$$
$$\times\bar{u}_{n_\nu}(x_\nu)\gamma_\nu^{\mu_\nu}\varphi(x_1\cdots x_{n-1}x\cdot x_{k+1}\cdots x_\nu)$$
$$\times d\sigma_1^{\mu_1}\cdots d\sigma_{k-1}^{\mu_{k-1}}d\sigma_{k+1}^{\mu_{k+1}}\cdots d\sigma_\nu^{\mu_\nu}. \quad (20)$$

Finally, if $\varphi(x_1\cdots x_\nu)$ obeys Eqs. (1) of the D.F.P. formalism, we get instead of (17)

$$\frac{\delta a[\sigma](n_1\cdots n_\nu)}{\delta\sigma(x)} = -\left(\frac{e}{\hbar c}\right)\sum_{k=1}^{\nu}\sum_{m_k}(n_k|A(x)|m_k)$$
$$\times a[\sigma](n_1\cdots n_{k-1}m_k n_{k+1}\cdots n_\nu), \quad (21)$$

where $(n|A(x)|m)$ is still given by (18).

If Fermi-Dirac statistics for the electrons is taken into account, Eq. (21) assumes the well-known form of the T-Sch. equation of motion for the state vector $\Psi[\sigma]$. To show this, we observe first that in the case of Fermi-Dirac statistics the functionals $a[\sigma](n_1\cdots n_\nu)$ must satisfy the condition

$$a[\sigma](n_1\cdots n_\nu) = \pm a[\sigma](p(n_1\cdots n_\nu)), \quad (22)$$

where p denotes any permutation of the numbers $n_1\cdots n_\nu$ and we must use the + or − sign according to whether this permutation is even or odd. We introduce now the well-known Jordan-Wigner[4] electron creation and annihilation operators[4]

$$a_n = \begin{pmatrix}1 & 0\\ 0 & -1\end{pmatrix}\times\cdots\times\begin{pmatrix}0 & 1\\ 0 & 0\end{pmatrix}\times\begin{pmatrix}1 & 0\\ 0 & 1\end{pmatrix}\times\cdots,$$
$$\uparrow$$
$$n\text{th place} \quad (23)$$
$$\downarrow$$
$$a_n^* = \begin{pmatrix}1 & 0\\ 0 & -1\end{pmatrix}\times\cdots\times\begin{pmatrix}0 & 0\\ 1 & 0\end{pmatrix}\times\begin{pmatrix}1 & 0\\ 0 & 1\end{pmatrix}\times\cdots.$$

The symbol $\times$ denotes here Kronecker products of the matrices, whereas every first row (column) and every second row (column) of any of the matrices corresponds to there being one or no electrons, respectively, in the nth state. The operators satisfy the following commutation relations:

$$[a_n, a_m]_+ = [a_n^*, a_m^*]_+ = 0, \quad [a_n^*, a_m]_+ = \delta_{nm}. \quad (24)$$

The components $\langle\Psi[\sigma]|N_1, N_2\cdots\rangle$ of the state vector $\Psi[\sigma]$ can now be defined by[5]

$$a[\sigma](n_1\cdots n_\nu) = \langle 0\cdots 0|\, a_{n_1}\cdots a_{n_\nu}\Psi[\sigma]\rangle, \quad (25)$$

where the "bra" $\langle 0\cdots 0|$ or a one-column matrix of the form:

$$\begin{pmatrix}1\\0\end{pmatrix}\times\begin{pmatrix}1\\0\end{pmatrix}\times\cdots \quad (26)$$

corresponds to the state where there are no electrons (not even in negative energy states), whereas the "ket" $|N_1, N_2\cdots\rangle$ corresponds to a state where there are N_1, $N_2\cdots$ electrons in the states u_1, u_2, $\cdots$, respectively. Following a well-known procedure (second quantization), e.g., that given by Dirac,[5] we get instead of (21)

$$\delta\Psi[\sigma]/\delta\sigma(x) = -(e/\hbar c)\sum_n\sum_m a_n^*(n|A(x)|m)a_m\Psi[\sigma], \quad (27)$$

and this is exactly the most important equation of the T-Sch.-theory. It assumes its usual form if we introduce the operators

$$\psi(x) = \sum_n a_n u_n(x), \quad \bar{\psi}(x) = \sum_n a_n^*\bar{u}_n(x), \quad (28)$$

and the current four-vector operator

$$j_\mu(x) = (iec)\bar{\psi}(x)\gamma^\mu\psi(x). \quad (29)$$

It is then

$$(i\hbar c)(\delta\Psi[\sigma]/\delta\sigma(x)) = -(1/c)j_\mu(x)A_\mu(x)\Psi[\sigma]. \quad (30)$$

It is a simple consequence of (5), that

$$[\gamma^\mu(\partial/\partial x^\mu)+(mc/\hbar)]\psi(x) = 0. \quad (31)$$

From (24) it then follows that

$$[\psi(x), \psi(x')]_+ = [\bar{\psi}(x), \bar{\psi}(x')]_+ = 0,$$
$$[\psi(x), \bar{\psi}(x')]_+ = \sum_n u_n(x)\times\bar{u}_n(x') = (1/i)S(x-x'). \quad (32)$$

It can be easily shown that the S-function defined by (32) is the same as the S-function of the T-Sch.-formalism. The $u_n(x)\times\bar{u}_n(x')$ products which appear in (32) are the Kronecker products of the spinors $u_n(x)$

[4] P. Jordan and E. Wigner, Z. Physik 47, 631 (1928).

[5] P. A. M. Dirac, *The Principles of Quantum Mechanics* (Clarendon Press, Oxford, 1947), pp. 291–297.

and $\bar{u}_n(x')$, their components being all the products of all the components of $u_n(x)$ by all components of $\bar{u}_n(x')$. They are therefore of the shape of the Dirac γ operators, and, as it should be, of the type of the S-function of T-Sch. The S-function of the T-Sch. formalism can be uniquely defined by the condition, that for any function $\chi(x)$ satisfying the field-free Dirac equation:

$$[\gamma^\mu(\partial/\partial x^\mu)+(mc/\hbar)]\chi(x)=0, \tag{33}$$

but arbitrary otherwise, for any space-like surface σ and for every point x' not necessarily lying on this surface, one should have

$$\chi(x')=\int_\sigma S(x-x')\gamma^\mu\chi(x)d\sigma_\mu. \tag{34}$$

This condition is indeed satisfied by the S-function defined by (32). Because of (33) $\chi(x)$ can be developed in a series of the type of (10), with all the coefficients being constant functionals, i.e., having the same values for any space-like σ. The nth term of this series is, therefore, apart from a constant factor, simply the $u_n(x)$-function, for which, owing to (6), we have

$$u_n(x')=i\sum_m u_m(x')\times\int_\sigma \bar{u}_m(x)\gamma^\mu u_n(x)d\sigma_\mu, \tag{35}$$

and this leads to

$$\chi(x')=i\int_\sigma \sum_n u_n(x')\times\bar{u}_n(x)\gamma^\mu\chi(x)d\sigma_\mu. \tag{36}$$

The expression $i\sum_n u_n(x')\times u_n(x)$ represents therefore the S-function of T-Sch.

To complete the derivation of T-Sch. from D.F.P. we now turn to the Lorentz condition, expressed within the framework of the latter by Eq. (4). On multiplying (4) from the left by the Kronecker products of the form

$$\bar{u}_{n_1}(x_1)\gamma_1{}^{\mu_1}\times\cdots\times\bar{u}_{n_\nu}(x_\nu)\gamma_\nu{}^{\mu_\nu},$$

and integrating ν times over the σ-surface, we finally get

$$\left[(\partial A_\mu(x)/\partial x^\mu)-\int_\sigma D(x-x')(1/c)j_\mu(x')d\sigma'^\mu\right]\Psi[\sigma]=0, \tag{37}$$

and this is again the form which the Lorentz condition assumes in the T-Sch. theory. Our derivation of the T-Sch. theory is thus completed. The equations of the T-Sch. theory are Eq. (30) together with the definition of the current four-vector (29), and further, (2), (3), (31), (32), and (37).

We will now go over to the second part of our proof of equivalence of the two theories. Namely, we shall derive the D.F.P. theory from T-Sch.-formalism. We have proved so far that every antisymmetric function $\varphi(x_1\cdots x_\nu)$ obeying the equations of D.F.P. can be expanded in a series (9), and that the coefficients of this expansion can be interpreted as the components of a state vector $\Psi(\sigma)$. What we are going to prove now will enable us to show that, inversely, the components of every solution of the equations of T-Sch., $\langle\Psi[\sigma]|N_1\cdots\rangle$, are coefficients of an expansion of the type (9) of a function which obeys the equations of D.F.P. The method developed here will be of immediate importance for our further generaliations of the many-time formalism. This is because the question it chiefly concerns is: "What are the conditions, which must be satisfied by a given infinite set of functionals of the space-like surface σ, in order that they may be interpreted as the expansion coefficients, of the type of the right-hand side of (9), of a function depending only on one or more distinct points situated on this surface?"

It is immediately clear that an arbitrary set of functionals cannot in general be interpreted as a set of coefficients of the aforesaid expansion, for the left-hand side of (9) will in general change if we change σ even at points different from those which appear as arguments of the u_n-functions on the right-hand side of (9).

We show first that the components of $\Psi[\sigma]$ can rightly be interpreted as the expansion coefficients of a "pure" function of distinct points. To avoid all unnecessary complications we confine ourselves at first to the case of two electrons. The generalization for any number of them will then be obvious. We start with the definition of a functional:

$$\Phi[\sigma](x_1,x_2)=(1/2)!\sum_m\sum_{n<m}[u_m(x_1)\times u_n(x_2) -u_n(x_1)\times u_m(x_2)]\times\langle\psi[\sigma]|0\cdots 1_n\cdots 1_m\cdots\rangle, \tag{38}$$

and investigate the conditions for its being a "pure" function of x_1, x_2, provided x_1 and x_2 lie on the surface σ. We differentiate (38) with respect to σ at the point x, which is in general different from x_1 and x_2, and get

$$\delta\Phi[\sigma](x_1,x_2)/\delta(x) =(1/2)!\sum_m\sum_{n<m}[u_m(x_1)\times u_n(x_2)-u_n(x_1)\times u_m(x_2)] \times(\delta/\delta\sigma(x))\langle\Psi[\sigma]|0\cdots 1_n\cdots 1_m\cdots\rangle. \tag{39}$$

Because $\Psi[\sigma]$ satisfies (29), and taking into account (30), (29), (28), (22), we get

$$\begin{aligned}
&(i\hbar c)(\delta/\delta\sigma(x))\langle\Psi[\sigma]|0\cdots 1_n\cdots 1_m\rangle\\
&=-(ie)\langle\bar{\psi}(x)\gamma^\mu A_\mu(x)\psi(x)\Psi[\sigma]|0\cdots 1_n\cdots 1_m\cdots\rangle\\
&=-(ie)\langle\bar{u}_n(x)\gamma^\mu A_\mu\psi(x)\Psi[\sigma]|0\cdots 1_m\cdots\rangle\\
&\quad+(ie)\langle\bar{u}_m(x)\gamma^\mu A_\mu(x)\psi(x)\Psi[\sigma]|0\cdots 1_n\cdots\rangle\\
&=-(ie)\sum_{s<m}\bar{u}_n(x)\gamma^\mu A_\mu(x)u_s(x)\langle\Psi[\sigma]|0\cdots 1_s\cdots 1_m\cdots\rangle\\
&\quad+(ie)\sum_{s>m}\bar{u}_n(x)\gamma^\mu A_\mu(x)u_s(x)\langle\Psi[\sigma]|0\cdots 1_m\cdots 1_s\cdots\rangle\\
&\quad+(ie)\sum_{s<n}\bar{u}_m(x)\gamma^\mu A_\mu(x)u_s(x)\langle\Psi[\sigma]|0\cdots 1_s\cdots 1_n\cdots\rangle\\
&\quad-(ie)\sum_{s>n}\bar{u}_m(x)\gamma^\mu A_\mu(x)u_s(x)\\
&\qquad\qquad\times\langle\Psi[\sigma]|0\cdots 1_n\cdots 1_s\cdots\rangle,
\end{aligned} \tag{40}$$

which amounts to

$$(i\hbar c)(\delta\Phi[\sigma](x_1, x_2)/\delta\sigma(x)) = -(ie)\sum_s u_s(x_1)\times\bar{u}_s(x)\gamma_1^\mu A_\mu(x)\Phi[\sigma](x, x_2) - (ie)\sum_s u_s(x_2)\times\bar{u}_s(x)\gamma_2^\mu A_\mu(x)\Phi[\sigma](x_1, x), \quad (41)$$

or, taking into account (32),

$$(i\hbar c)(\delta\Phi[\sigma](x_1, x_2)/\delta\sigma(x)) = -eS_1(x_1-x)\gamma_1^\mu A_\mu(x)\Phi[\sigma](x, x_2) + -eS_2(x_2-x)\gamma_2^\mu A_\mu(x)\Phi[\sigma](x_1, x). \quad (42)$$

The answer to our question concerning $\Phi[\sigma](x_1, x_2)$ is given by the last equation. Indeed, $\Phi[\sigma](x_1, x_2)$ can be interpreted as a "pure" function of x_1 and x_2 only if they lie on σ and if the latter is (as always assumed) space-like. This follows immediately from the well-known properties of the S-functions of T-Sch., which vanish for all space-like arguments except zero. This means that

$$\delta\Phi[\sigma](x_1, x_2)/\delta\sigma(x) = 0 \quad (43)$$

if all x_1, x_2, and x lie on σ and if x does not coincide with x_1 or x_2. Therefore we can simply put

$$\Phi[\sigma](x_1, x_2) \underset{df}{\equiv} \varphi(x_1, x_2) \quad (44)$$

if only x_1 and x_2 lie on σ, and try to set up a differential equation satisfied by $\varphi(x_1, x_2)$. This is easily achieved if we differentiate $\varphi(x_1, x_2)$ with respect to σ at a certain point x. The functional differntiation of a "pure" function involved here is explained in the following way. A "pure" function $\vartheta(x)$ is interpreted as a special case of a functional whose value does not change when any deformation of σ outside x is being performed. Before carrying out the functional differentiation we shall write $\vartheta(x')$ in the form

$$\vartheta(x') = \int_\sigma S(x'-x)\gamma^\mu\vartheta(x)d\sigma_\mu, \quad (45)$$

where a well-known property of the S-function has been used, namely, that apart from the coefficient γ^4 it is the Dirac δ-function for the space-like arguments. It is assumed therefore that σ contains x'. Owing to the fact that S satisfies a field free Dirac equation we can also write

$$\vartheta(x') = \int_{\sigma_0} S(x'-x)\gamma^\mu\vartheta(x)d\sigma_\mu + \int^{\sigma} S(x'-x)[\gamma^\mu(\partial/\partial x^\mu)+(mc/\hbar)]\vartheta(x)d^4x, \quad (46)$$

where σ_0 is another space-like surface prior to σ. This is just the form most suitable for functional differentiation. On performing it we get

$$\delta\vartheta(x')/\delta\sigma(x) = S(x'-x)[\gamma^\mu(\partial/\partial x^\mu)+(mc/\hbar)]\vartheta(x). \quad (47)$$

The same can be done for the two-electron function $\varphi(x_1, x_2)$. We get thus

$$\delta\varphi(x_1, x_2)/\delta\sigma(x) = S_1(x_1-x)[\gamma_1^\mu(\partial/\partial x^\mu)+(mc/\hbar)]\varphi(x, x_2) + S_2(x_2-x)[\gamma_2^\mu(\partial/\partial x^\mu)+(mc/\hbar)]\varphi(x_1, x). \quad (48)$$

Comparison of (42) and (48) yields then, owing to (44),

$$[\gamma_1^\mu((\partial/\partial x_1^\mu)-(ie/\hbar c)A_\mu(x_1))+(mc/\hbar)]\varphi(x_1, x_2) = 0,$$

and

$$[\gamma_2^\mu((\partial/\partial x_2^\mu)-(ie/\hbar c)A_\mu(x_2))+(mc/\hbar)]\varphi(x_1, x_2) = 0, \quad (49)$$

and these are again the most important equations of D.F.P.

The results obtained can be easily generalized for any number of electrons. Let us define a functional:

$$\Phi[\sigma](x_1\cdots x_\nu) = (\nu!)^{-\frac{1}{2}} \sum_{n_\nu>\cdots>n_2>n_1} \times\begin{vmatrix} u_{n_1}(x_1)\cdots u_{n_1}(x_\nu) \\ \cdots\cdots\cdots \\ u_{n_\nu}(x_1)\cdots u_{n_\nu}(x_\nu)\end{vmatrix} \langle\Psi[\sigma]|\cdots 1_{n_1}\cdots 1_{n_2}\cdots 1_{n_\nu}\cdots\rangle, \quad (50)$$

where ν is the number of electrons. On differentiating it with respect to σ at an extra point x of this surface, and taking into account (29), we get instead of (42):

$$(i\hbar c)\frac{\delta\Phi[\sigma](x_1\cdots x_\nu)}{\delta\sigma(x)} = -e\sum_{i=1}^{\nu} S_i(x_i-x)\gamma_i^\mu A_\mu(x) \times\Phi[\sigma](x_1\cdots x_{i-1}, x, x_{i+1}\cdots x_\nu). \quad (51)$$

The conclusion drawn from it is the same as that drawn from (42) and yields a definition of a multi-electron wave function,

$$\Phi[\sigma](x_1\cdots x_\nu) \underset{df}{\equiv} \varphi(x_1\cdots x_\nu), \quad (52)$$

for all points $x_1\cdots x_\nu$ lying on σ. For this function we get then, in analogy to (48),

$$\frac{\delta\varphi(x_1\cdots x_\nu)}{\delta\sigma(x)} = \sum_{i=1}^{\nu} S_i(x_i-x)[\gamma_i^\mu(\partial/\partial x^\mu)+(mc/\hbar)] \times\varphi(x_1\cdots x_{i-1}, x, x_{i+1}\cdots x_\nu). \quad (53)$$

Comparing the left-hand sides of (51) and (53) and taking into account (52), we then get system (1) of the basic equations of D.F.P. It is a trivial matter to show that the Lorentz condition (36) assumes its original form

$$\left[\frac{\partial A_\mu(x)}{\partial x^\mu} - e\sum_{i=1}^{\nu} D(x-x_i)\right]\varphi(x_1\cdots x_\nu) = 0, \quad (4)$$

$\varphi(x_1\cdots x_\nu)$ being now defined by (50) and (52).

The equivalence of D.F.P.+Fermi-Dirac statistics and T-Sch. is therefore complete.

II. A GENERALIZATION OF THE MANY-TIME FORMALISM

Our main purpose now is to extend the definition of $\varphi(x_1 \cdots x_\nu)$ so as to cover all points (each one determined jointly by all $x_1, x_2 \cdots x_\nu$) of our 4ν-dimensional configuration space. It is quite obvious that such a function, if properly defined, cannot satisfy (1) for all points corresponding to any two or more electrons separated by time-like distances, this being the consequence of incompatibility of (1) for such configurations. On the other hand, a generalized $\varphi(x_1 \cdots x_\nu)$ function must simply be equal to that hitherto used [as defined, e.g., by (50) and (52)] for all space-like electron configurations and therefore must obey Eqs. (1) for the latter type of configurations. This, besides the formal argument, is to be demanded, because we want $\varphi(x_1 \cdots x_\nu)$ to retain its physical meaning as a wave function for all space-like electron configurations. The purpose of the extension in view will be clear as soon as we are able to write down equations (of an integral or integro-differential form) which are compatable for all configurations whatsoever. It will then be possible to solve such equations, approximately at least, by means of ordinary methods, which cannot be done when dealing with (1). We start with Eq. (53) which we write now in the form

$$(i\hbar c)\delta\Phi[\sigma](x_1 \cdots x_\nu)/\delta\sigma(x) = \mathcal{H}(x; x_1 \cdots x_\nu)\Phi[\sigma](x_1 \cdots x_\nu), \quad (54)$$

where

$$\mathcal{H}(x; x_1 \cdots x_\nu) = -e\sum_{i=1}^{\nu} S_i(x_i - x)\gamma_i^\mu A_\mu(x) Q(x_i \rightarrow x), \quad (55)$$

and where $Q(x_i \rightarrow x)$ stand for the "argument exchange operators," defined by

$$f(x_1 \cdots x_{i-1}, x, x_{i+1} \cdots x_\nu) = Q(x_i \rightarrow x) f(x_1 \cdots x_{i-1}, x_i, x_{i+1}, \cdots x_\nu). \quad (56)$$

Equation (54) can be formally solved by means of the Dyson method of chronological products.[6] It is well known that a solution of the equation of motion of T-Sch. (29) can, for instance, be given in the form

$$\Psi[\sigma] = \left\{ \sum_{n=0}^{\infty} (1/n!)[1/i\hbar c]^n \int_{-\infty}^{\sigma} d^4x^{(n)} \cdots \times \int_{-\infty}^{\sigma} d^4x^{(1)} P[H(x^{(n)}), \cdots H(x^{(1)})] \right\} \Psi[-\infty], \quad (57)$$

where

$$H(x) = -(1/c) j_\mu(x) A_\mu(x). \quad (58)$$

The chronological product $P[H(x^{(n)}, \cdots H(x^{(1)})]$ of operators $H(x^{(n)}) \cdots H(x^{(1)})$ denotes the product of those operators arranged in the order, reading from right to left, in which the points $x^{(1)}, \cdots x^{(n)}$ "occur in time." If some of the points $x^{(1)}, \cdots x^{(n)}$ lie space-like with respect to each other, the phrase in the quotation marks has a definite meaning in a given Lorentz frame only, unless the operators defined commute for space-like distances. This is actually the case for operators defined by (58), so that a chronological product $P[H(x^{(n)}), \cdots H(x^{(1)})]$ is an invariant concept. By the same argument we can write now a solution of (54):

$$\Phi[\sigma](x_1 \cdots x_\nu) = \left\{ \sum_{n=0}^{\infty} (1/n!)[1/i\hbar c]^n \int_{-\infty}^{\sigma} d^4x^{(n)} \cdots \times \int_{-\infty}^{\sigma} d^4x^{(1)} P[\mathcal{H}(x^{(n)}; x_1, \cdots x_\nu), \cdots \times \mathcal{H}(x^{(1)}; x_1, \cdots x_\nu)] \right\} \chi(x_1 \cdots x_\nu), \quad (59)$$

where the chronological products are again invariants and are taken with respect to the integration variables $x^{(1)}, \cdots x^{(n)}$ only. It is important to note that in solving (54) we treated $x_1, \cdots x_\nu$ as constant parameters. The function $\chi(x_1 \cdots x_\nu)$ in (59) is an analog of $\Psi[-\infty]$ in (57) and we have

$$\Phi[-\infty](x_1 \cdots x_\nu) = \chi(x_1, \cdots x_\nu). \quad (60)$$

Consequently, $\chi(x_1, \cdots x_\nu)$ satisfies a field-free Dirac equation as a function of all its arguments:

$$[\gamma_k^\mu(\partial/\partial x_k^\mu) + (mc/\hbar)]\chi(x_1, \cdots x_\nu) = 0 \qquad k = 1; 2; \cdots \nu. \quad (61)$$

This is because, owing to (38) or (50), and $\sigma = -\infty$ being fixed, $\Phi[\sigma](x_1 \cdots x_\nu)$ is a linear combination of functions satisfying the field-free Dirac equation with respect to every x_k. It is important to note that, because of the $Q(x_i \rightarrow x)$ operators, the integration in (59) is also performed with respect to the arguments on which $\chi(x_1 \cdots x_\nu)$ does depend, as is illustrated by

$$\int_{-\infty}^{\sigma} \mathcal{H}(x; x_1, \cdots x_\nu) d^4x \chi(x_1 \cdots x_\nu) = -e\sum_i \int_{-\infty}^{\sigma} S_i(x_i - x)\gamma_i^\mu A_\mu(x) \times \chi(x_1, \cdots x_{i-1}, x, x_{i+1}, \cdots x_\nu) d^4x. \quad (62)$$

If all $x_1, \cdots x_\nu$ lie space-like with respect to each other, then according to (52) we get

$$\varphi(x_1 \cdots x_\nu) = \left\{ \sum_{n=0}^{\infty} (1/n!)[1/i\hbar c]^n \int_{-\infty}^{\sigma} d^4x^{(n)} \cdots \times \int_{-\infty}^{\sigma} d^4x^{(1)} P[\mathcal{H}(x^{(n)}; x_1, \cdots x_\nu), \cdots \times \mathcal{H}(x^{(1)}; x_1, \cdots x_\nu)] \right\} \chi(x_1 \cdots x_\nu), \quad (63)$$

[6] F. J. Dyson, Phys. Rev. **77**, 219 (1950).

where σ is now any space-like surface which passes through all points $x_1, \cdots x_\nu$. Equation (63) can be rewritten in a form where the irrevelant σ-dependence is made to disappear. This is done with the help of a "retarded" S-function,

$$S^{\mathrm{Ret}}(x-x') = \eta(x, x')S(x-x'), \tag{64}$$

where

$$\eta(x, x') = \begin{cases} 0 & \text{for } x' \text{ later than } x, \\ 1 & \text{for } x' \text{ sooner than } x. \end{cases} \tag{65}$$

The retarded S-function is a relativistically invariant concept, notwithstanding the fact that $\eta(x. x')$ is not an invariant, since an S-function vanishes for all space-like arguments. On introducing an invariant function $\mathfrak{H}^{\mathrm{Ret}}(x; x^1, \cdots x_\nu)$ connected with S^{Ret} by means of the relation,

$$\mathfrak{H}^{\mathrm{Ret}}(x; x_1, \cdots x_\nu) = -e\sum_{i=1}^{\nu} S_i^{\mathrm{Ret}}(x_i - x)\gamma_i^\mu A_\mu(x) \times Q(x_i \to x), \tag{66}$$

we can easily verify that,

$$\int_{-\infty}^{\sigma} d^4x^{(n)} \cdots \int_{-\infty}^{\sigma} d^4x^{(1)} P[\mathfrak{H}(x^{(n)}; x_1 \cdots x_\nu), \cdots \times \mathfrak{H}(x^{(1)}; x_1, \cdots x_\nu)]\chi(x_1, \cdots x_\nu)$$

$$= \int_{-\infty}^{+\infty} d^4x^{(n)} \cdots \int_{-\infty}^{+\infty} d^4x^{(1)} P[\mathfrak{H}^{\mathrm{Ret}}(x^{(n)}; x_1, \cdots x_\nu), \cdots \times \mathfrak{H}^{\mathrm{Ret}}(x^{(1)}; x_1, \cdots x_\nu)]\chi(x_1, \cdots x_\nu). \tag{67}$$

Equation (63) then finally reads,

$$\varphi(x_1, \cdots x_\nu) = \left\{ \sum_{n=0}^{\infty} (1/n!)[1/i\hbar c]^n \int_{-\infty}^{+\infty} d^4x^{(n)} \cdots \times \int_{-\infty}^{+\infty} d^4x^{(1)} P[\mathfrak{H}^{\mathrm{Ret}}(x^{(n)}; x_1, \cdots x_\nu), \cdots \times \mathfrak{H}^{\mathrm{Ret}}(x^{(1)}; x_1, \cdots x_\nu)] \right\} \chi(x_1, \cdots x_\nu). \tag{68}$$

The last equation has been derived on the assumption that all $x_1, \cdots x_\nu$ are space-like, but it is, on the other hand, the most natural definition of $\varphi(x_1 \cdots x_\nu)$ for all points of the 4ν-dimensional configuration space. This definition being adopted, it can be directly verified by a straightforward calculation that $\varphi(x_1 \cdots x_\nu)$ satisfies Eqs. (1) of D.F.P. for all space-like electron configurations. In order to get the most general equation for $\varphi(x_1 \cdots x_\nu)$ it is convenient to "invert" the relation (68) and to express $\chi(x_1, \cdots x_\nu)$ by means of $\varphi(x_1, \cdots x_\nu)$, rather than to work with a somewhat formal expansion for $\varphi(x_1, \cdots x_\nu)$. This is physically the most advisable thing to be done, especially in the case of bound states, for the "step by step computation" of $\varphi(x_1, \cdots x_\nu)$ by means of (68) corresponds to the building up of the actual (bound!) state of the system as a result of an infinite series of "elementary mutual scatterings" of the electrons (and corresponds to the well-known Feynman-Dyson computations of the S-matrix). The "inverted" relation (68) reads

$$\chi(x_1, \cdots x_\nu) = \left\{ \sum_{n=0}^{\infty} (1/n!)[-1/i\hbar c]^n \int_{-\infty}^{+\infty} d^4x^{(n)} \cdots \times \int_{-\infty}^{+\infty} d^4x^{(1)} P^I[\mathfrak{H}^{\mathrm{Ret}}(x^{(n)}; x_1, \cdots x_\nu), \cdots \times \mathfrak{H}^{\mathrm{Ret}}(x^{(1)}; x_1, \cdots x_\nu)] \right\} \varphi(x_1, \cdots x_\nu), \tag{69}$$

where $P^I[\cdots]$ stands for the antichronological product of the operators $\mathfrak{H}^{\mathrm{Ret}}(x^{(\lambda)}; x_1 \cdots x_\nu)$, denoting that now, reading from right to left, they should occupy places in the order inverse to that in which the points $x^{(1)}, \cdots x^{(n)}$ occur in time. The transformations (68) and (69) are inverse with respect to each other, because, quite generally, an inversion to a transformation of the type

$$\Gamma = \left\{ \sum_{n=0}^{\infty} (1/n!)[1/i\hbar c]^n \int_{-\infty}^{+\infty} d^4x^{(n)} \cdots \times \int_{-\infty}^{+\infty} d^4x^{(1)} P[H(x^{(n)}), \cdots H(x^{(1)})] \right\} \Omega, \tag{70}$$

is

$$\Omega = \left\{ \sum_{n=0}^{\infty} (1/n!)[-1/i\hbar c]^n \int_{-\infty}^{+\infty} d^4x^{(n)} \cdots \times \int_{-\infty}^{+\infty} d^4x^{(1)} P^I[H(x^{(n)}), \cdots H(x^{(1)})] \right\} \Gamma. \tag{71}$$

Equation (69) is now the basic equation of our formalism. It is a gain of the form of an expansion in powers of the coupling constant, so that seemingly not much has been gained over the standard "S-matrix" methods. One should bear in mind, however, that a nonrelativistic treatment of the multi-electron problem using only Coulomb potentials yields already a very good approximation for problems where the bound states are concerned. This corresponds in our case to terms up to the order of e^2 being taken into account. The usefulness of the e-power expansion, as far as the terms in Eq. (69) are concerned, seems also to be supported by the fact that, for ν-electrons, only the first ν-terms of (69) survive, all the rest being identifically zero. This can easily be seen owing to the form of $\mathfrak{H}^{\mathrm{Ret}}(x; x_1, \cdots x_\nu)$ given by (66) and because the operators $A_\mu(x)$ commute outside of each other's light-cone. This latter property of the expansion (69) cannot unforunately be of much help in any of the actual calculations, because after the virtual processes of the radiation field are eliminated, all the infinite number of expansion terms reappear. Our multi-electron problem can be also formulated by means of a system of ν integro-differential equations instead of the one integral Eq. (69). Those we get on multiplying

(69) from the left by the operators $[\gamma_k{}^\mu(\partial/\partial x_k{}^\mu)+(mc/\hbar)]$, where $k=1, 2, \cdots \nu$, and taking into account (61):

$$[\gamma_k{}^\mu(\partial/\partial x_k{}^\mu)+(mc/\hbar)]\Big\{\sum_{n=0}^{\infty}(1/n!)[-1/i\hbar c]^n\int_{-\infty}^{+\infty}d^4x^{(n)}\cdots$$

$$\times\int_{-\infty}^{+\infty}d^4x^{(1)}P^I[\mathfrak{C}^{\mathrm{Ret}}(x^{(n)};x_1,\cdots x_\nu),\cdots\mathfrak{C}^{\mathrm{Ret}}(x^{(1)};x_1,\cdots x_\nu)]\Big\}\varphi(x_1,\cdots x_\nu)=0. \quad (72)$$

$$k=1, 2, \cdots \nu.$$

The last equations do not explicitly depend on the initial condition expressed by $\chi(x_1,\cdots x_\nu)$ and present a direct generalization of the D.F.P. Eqs. (1).

III. VIRTUAL PROCESSES ELIMINATION METHOD AND THE TWO-ELECTRON PROBLEM

We shall now turn to the explicit working out of (69) in an approximation where only the terms of order of e^2 are considered. Owing to (60) and (66) we can write

$$\chi(x_1,\cdots x_\nu)=\varphi(x_1,\cdots x_\nu)+(e/i\hbar c)\int_{-\infty}^{+\infty}\sum_i S_i{}^{\mathrm{Ret}}(x_i-x)\boldsymbol{A}_i(x)\varphi(x_1,\cdots x_{i-1},x,x_{i+1},\cdots x_\nu)d^4x$$

$$-(e^2/2\hbar^2c^2)\Big[\sum_i\sum_{j\neq i}\int_{-\infty}^{+\infty}d^4x^{II}\int_{-\infty}^{+\infty}d^4x^I S_i{}^{\mathrm{Ret}}(x_i-x^{II})S_j{}^{\mathrm{Ret}}(x_j-x^I)P^I(\boldsymbol{A}_i(x^{II}),\boldsymbol{A}_j(x^I))$$

$$\times\varphi(x_1,\cdots x_{i-1},x^{II},x_{i+1},\cdots x_{j+1},x^I,x_{j+1},\cdots x_\nu)-\sum_i\int_{-\infty}^{+\infty}d^4x^{II}\int_{-\infty}^{+\infty}d^4x^I$$

$$\times P^{II}(S_i{}^{\mathrm{Ret}}(x_i-x^{II})\boldsymbol{A}_i(x^{II}),S_i{}^{\mathrm{Ret}}(x^{II}x^I)\boldsymbol{A}_i(x^I))\varphi(x_1,\cdots x_{i-1},x^I,x_{i+1}\cdots)\Big]+\cdots, \quad (73)$$

where

$$\boldsymbol{A}_i(x)=\gamma_i{}^\mu A_\mu(x), \quad (74)$$

and

$$P^{II}(S_i{}^{\mathrm{Ret}}(x_i-x^{II})\boldsymbol{A}_i(x^{II}),S_i{}^{\mathrm{Ret}}(x^{II}-x^I)\boldsymbol{A}_i(x^I))\varphi(x_1,\cdots x_{i-1},x^I,x_{i+1},\cdots x_\nu)$$

$$=\begin{cases}S_i{}^{\mathrm{Ret}}(x_i-x^{II})\boldsymbol{A}_i(x^{II})S_i{}^{\mathrm{Ret}}(x^{II}-x^I)\boldsymbol{A}_i(x^I)\varphi(x_1,\cdots x_{i-1},x^I,x_{i+1},\cdots x_\nu) & \text{for } x^I \text{ later than } x^{II}\\ S_i{}^{\mathrm{Ret}}(x_i-x^I)\boldsymbol{A}_i(x^I)S_i{}^{\mathrm{Ret}}(x^I-x^{II})\boldsymbol{A}_i(x^{II})\varphi(x_1,\cdots x_{i-1},x^{II},x_{i+1},\cdots x_\nu) & \text{for } x^I \text{ sooner than } x^{II}\end{cases}=0 \quad (75)$$

because $S^{\mathrm{Ret}}(x-x')$ vanishes for all x' later than x. On multiplying (73) from the left by the operator $[\gamma_i{}^\mu(\partial/\partial x_k{}^\mu)+(mc/\hbar)]$ and using a well-known formula

$$[\gamma^\mu(\partial/\partial x^\mu)+(mc/\hbar)]\int_{-\infty}^{+\infty}d^4x'S^{\mathrm{Ret}}(x-x')f(x')=f(x), \quad (76)$$

which is often expressed in the form

$$[\gamma^\mu(\partial/\partial x^\mu)+(mc/\hbar)]S^{\mathrm{Ret}}(x-x')=\delta^{(4)}(x-x'), \quad (77)$$

and from which it follows further that

$$[\gamma_i{}^\mu(\partial/\partial x_i{}^\mu)+(mc/\hbar)]\int_{-\infty}^{+\infty}S_i{}^{\mathrm{Ret}}(x_i-x)\boldsymbol{A}_i(x)\varphi(x_1,\cdots x_{i-1},x,x_{i+1},\cdots x_\nu)d^4x=\boldsymbol{A}_i(x_i)\varphi(x_1,\cdots x_\nu), \quad (78)$$

and

$$[\gamma_i{}^\mu(\partial/\partial x_i{}^\mu)+(mc/\hbar)]\int_{-\infty}^{+\infty}d^4x^{II}\int_{-\infty}^{+\infty}d^4x^I S_i{}^{\mathrm{Ret}}(x_i-x^{II})S_j{}^{\mathrm{Ret}}(x_j-x^I)P^I(\boldsymbol{A}_i(x^{II}),\boldsymbol{A}_j(x^I))$$

$$\times\varphi(x_1,\cdots x_{i-1},x^{II},x_{i+1},\cdots x_{j-1},x^I,x_{j+1},\cdots x_\nu)$$

$$=\int_{-\infty}^{+\infty}d^4xS_j{}^{\mathrm{Ret}}(x_j-x)P^I(\boldsymbol{A}_i(x_i),\boldsymbol{A}_j(x))\varphi(x_1,\cdots x_{j-1},x,x_{j+1},\cdots x_\nu), \quad (79)$$

we finally get

$$0=[\gamma_k^\mu(\partial/\partial x_k^\mu)+(mc/\hbar)]\varphi(x_1,\cdots x_\nu)-(ie/\hbar c)\boldsymbol{A}_k(x_k)\varphi(x_1,\cdots x_\nu)+$$
$$-(ie/\hbar c)\sum_{i\neq k}\int_{-\infty}^{+\infty}S_i^{\mathrm{Ret}}(x_i-x)\boldsymbol{A}_i(x)[\gamma_k^\mu(\partial/\partial x_k^\mu)+(mc/\hbar)]\varphi(x_1,\cdots x_{i-1},x,x_{i+1},\cdots x_\nu)d^4x+$$
$$-(e^2/\hbar^2c^2)\sum_{i\neq k}\int_{-\infty}^{+\infty}S_i^{\mathrm{Ret}}(x_i-x)P^I(\boldsymbol{A}_k(x_k),\boldsymbol{A}_i(x))\varphi(x_1,\cdots x_{i-1},x,x_{i+1},\cdots x_\nu)d^4x+$$
$$-(e^2/\hbar^2c^2)\sum_{i\neq k}\sum_{\substack{j\neq k\\ j\neq i}}\int_{-\infty}^{+\infty}d^4x^{II}\int_{-\infty}^{+\infty}d^4x^I S_i^{\mathrm{Ret}}(x_i-x^{II})S_j(x_j-x^I)P^I(\boldsymbol{A}_i(x^{II}),\boldsymbol{A}_j(x^I))$$
$$\times[\gamma_k^\mu(\partial/\partial x_k^\mu)+(mc/\hbar)]\varphi(x_1,\cdots x_{i-1},x^{II},x_{i+1},\cdots x_{j-1},x^I,x_{j+1},\cdots x_\nu)+\cdots. \quad (80)$$

By means of an easy "iteration" we can free the right-hand side of (80) from the $[\gamma_k^\mu(\partial/\partial x_k^\mu)+(mc/\hbar)]$ operators, getting in the same approximation.

$$0=[\gamma_k^\mu((\partial/\partial x_k^\mu)+(ie/\hbar c)\boldsymbol{A}_\mu(x_\mu))+(mc/\hbar)]\varphi(x_1\cdots x_\nu)$$
$$+(e^2/\hbar^2c^2)\sum_{i\neq k}\int_{-\infty}^{+\infty}S_i^{\mathrm{Ret}}(x_i-x)[\boldsymbol{A}_i(x)\boldsymbol{A}_k(x_k)-P^I(\boldsymbol{A}_k(x_k),\boldsymbol{A}_i(x))]\varphi(x_1,\cdots x_{i-1},x,x_{i+1},\cdots x_\nu)d^4x. \quad (81)$$

The expression $[\boldsymbol{A}_i(x)\boldsymbol{A}_k(x_k)-P^I(\boldsymbol{A}_k(x_k),\boldsymbol{A}_i(x))]$ vanishes for all x sooner than x_k or lying space-like with respect to x_k, for then, either the order of the operators in $P^I(\boldsymbol{A}_k(x_k),\boldsymbol{A}_i(x))$ is the same as in $\boldsymbol{A}_i(x)\boldsymbol{A}_k(x_k)$, or else (for space-like distances) they commute. This expression may therefore be only different from zero for x lying inside of the past-part of a light-cone with the apex at x_k. Thanks to (3) and (74) we have then

$$[\boldsymbol{A}_i(x)\boldsymbol{A}_k(x_k)-P^I(\boldsymbol{A}_k(x_k),\boldsymbol{A}_i(x))]=(i\hbar c)D^{\mathrm{Ret}}(x-x_k)(\gamma_i^\mu\gamma_k^\mu), \quad (82)$$

where

$$D^{\mathrm{Ret}}(x-x')=\eta(x',x)D(x-x'), \quad (83)$$

and where $\eta(x',x)$ is given by (65). Instead of (81) we then get

$$0=[\gamma_k^\mu((\partial/\partial x_k^\mu)-(ie/\hbar c)A_\mu(x_k))+(mc/\hbar)]$$
$$\times\varphi(x_1,\cdots x_{i-1},x_i,x_{i+1}\cdots x_\nu)$$
$$+(ie^2/\hbar c)\sum_{i\neq k}\int_{-\infty}^{+\infty}S_i^{\mathrm{Ret}}(x_i-x)(\gamma_i^\mu\gamma_k^\mu)D^{\mathrm{Ret}}(x-x_k)$$
$$\times\varphi(x_1,\cdots x_{i-1},x,x_{i+1},\cdots x_\nu)d^4x+\cdots. \quad (84)$$

For space-like electron configurations the additional e^2-term vanishes and we are left with the D.F.P. equations. This illustrates the general feature of our formalism in the approximation considered. We want now to derive equations appropriate for bound state problems. This is understood to correspond to the elimination of virtual processes of the radiation field. As far as the e^2-terms are concerned it will correspond to an elimination of the first-order processes only, and this is easily achieved by elimination of the linear terms in A.

To do this we can write, owing to (69),

$$\varphi(x_1,\cdots x_\nu)=\chi(x_1\cdots x_\nu)$$
$$+(ie^2/\hbar c)\sum_i\int_{-\infty}^{+\infty}S_i^{\mathrm{Ret}}(x_i-x)\boldsymbol{A}_i(x)$$
$$\times\varphi(x_1,\cdots x_{i-1},x,x_{i+1}\cdots x_\nu)d^4x+\cdots. \quad (85)$$

On substituting the right-hand side of (85) into the term of (84) containing A we then get

$$0=[\gamma_k^\mu(\partial/\partial x_k^\mu)+(mc/\hbar)]\varphi(x_1\cdots x_\nu)$$
$$+(e^2/\hbar^2c^2)\sum_{i\neq k}\int_{-\infty}^{+\infty}S_i^{\mathrm{Ret}}(x_i-x)P(\boldsymbol{A}_k(x_k),\boldsymbol{A}_i(x))$$
$$\times\varphi(x_1,\cdots x_{i-1},x,x_{i+1},\cdots x_\nu)d^4x$$
$$+(e^2/\hbar^2c^2)\int_{-\infty}^{+\infty}\boldsymbol{A}_k(x_k)S_k^{\mathrm{Ret}}(x_k-x)\boldsymbol{A}_k(x)$$
$$\times\varphi(x_1,\cdots x_{k-1},x,x_{k+1},\cdots x_\nu)d^4x$$
$$-(ie^2/\hbar c)\boldsymbol{A}_k(x_k)\chi(x_1,\cdots x_\nu)+\cdots. \quad (86)$$

The only linear term in A which here reappears again does not contain $\varphi(x_1,\cdots x_\nu)$ but is only connected with the state of the system in the remote past, and will not enter our final equation for bound states. A bound state belongs to a wider class of states which we should call stable, the definition of the latter being that no real light quantum (at least in the approximation considered) should be present in those states throughout the whole history of the system. It follows that all those components of the wave function $\varphi(x_1,\cdots x_\nu)$ should vanish which correspond to the presence of any number of

photons (except zero). This is the case for all space-like configurations of the electrons. If we denote by $\varphi^{(0)}(x_1, \cdots x_\nu)$ and $\chi^{(0)}(x_1, \cdots x_\nu)$ the components of $\varphi(x_1, \cdots x_\nu)$ and $\chi(x_1, \cdots x_\nu)$, respectively, corresponding to the absence of photons, and by $\varphi^{(f)}(x_1, \cdots x_\nu)$ and $\chi^{(f)}(x_1, \cdots x_\nu)$ all other components of those functions, the sufficient condition for a stable state reads

$$\varphi^{(f)}(x_1, \cdots x_\nu) = \chi^{(f)}(x_1, \cdots x_\nu) = 0. \tag{87}$$

We have then also

$$\{A_k(x_k)\chi(x_1, \cdots x_\nu)\}^{(0)} = 0, \tag{88}$$

where $\{A_k(x_k)\chi(x_1, \cdots x_\nu)\}^{(0)}$ denotes the components of $A_k(x_k)\chi(x_1, \cdots x_\nu)$ corresponding to there being no photons. It is easily seen that the condition,

$$\chi^{(f)}(x_1, \cdots x_\nu) = 0,$$

is automatically satisfied if only there were no photons in the remote past (or on any given space-like surface σ, prior to the configuration determined by $x_1, \cdots x_\nu$), this being the direct consequence of (61) where there is no interaction with the radiation field. Because of (87) and (88), Eq. (86) can now be rewritten in the form

$$\begin{aligned} 0 = &[\gamma_k{}^\mu(\partial/\partial x_k{}^\mu) + (mc/\hbar)]\varphi^{(0)}(x_1 \cdots x_\nu) \\ &+ (ie^2/\hbar c)\sum_{i+k}\int S_+^{\mathrm{Ret}}(x_i - x)(\gamma_i{}^\mu\gamma_k{}^\mu)D_F(x_k - x) \\ &\times \varphi^{(0)}(x_1, \cdots x_{i-1}, x, x_{i+1}, \cdots x_\nu)d^4x \\ &+ (ie^2/\hbar c)\int_{-\infty}^{+\infty} \gamma_k{}^\mu S^{\mathrm{Ret}}(x_k - x)\gamma_k{}^\mu D_F(x_k - x) \\ &\times \varphi^{(0)}(x_1, \cdots x_{k-1}, x_k, x_{k+1}, \cdots x_\nu)d^4x + \cdots, \end{aligned} \tag{89}$$

where $D_F(x)$ denotes the well-known "causal D-function" introduced by Feynman, which can be defined by

$$\langle 0 | P(A_\mu(x), A_\nu(x')) | 0 \rangle = i\hbar c\delta_{\mu\nu}D_F(x - x'), \tag{90}$$

and where $\langle 0 | \cdots | 0 \rangle$ denotes that the vacuum expectation value should be taken. Equation (89) is (in the approximation considered) the necessary condition for $\varphi^{(0)}(x_1, \cdots x_\nu)$ to describe a stable state. Since $\varphi^{(0)}(x_1, \cdots x_\nu)$ only appears in (89), it is desirable to express the sufficient condition (87) also by means of this function only. This reads then

$$\int \cdots \int |\varphi^{(0)}(\mathbf{x}_1, t; \mathbf{x}_2, t; \cdots \mathbf{x}_\nu, t)|^2 d^3x_1 \cdots d^3x_\nu = 1, \tag{91}$$

and must hold for every t, or when expressed in the invariant notation

$$(i)^\nu \int_\sigma \cdots \int_\sigma \bar{\varphi}^{(0)}(x_1, \cdots x_\nu)\gamma_1{}^{\mu_1} \cdots \gamma_\nu{}^{\mu_\nu} \times \varphi^{(0)}(x_1, \cdots x_\nu)d\sigma_{\mu_1} \cdots d\sigma_{\mu_\nu} = 1, \tag{92}$$

and must hold for every space-like σ. Condition (91) is indeed sufficient for the electromagnetic vacuum to be preserved permanently, for it necessitates (87). This can easily be seen with the help of the wave function normalization condition:

$$\int \cdots \int |\varphi^{(0)}(\mathbf{x}_1, t; \mathbf{x}_2, t; \cdots \mathbf{x}_\nu, t)|^2 d^3x_1 \cdots d^3x_\nu + \sum_{\text{all } f} \int \cdots \int |\varphi^{(f)}(\mathbf{x}_1, t; \mathbf{x}_2, t; \cdots \mathbf{x}_\nu, t)|^2 \times d^3x_1 \cdots d^3x_\nu = 1, \tag{93}$$

where, in the most general case, the summation is extended on all components of the wave function $\varphi(x_1, \cdots x_\nu)$ except $\varphi^{(0)}(x_1, \cdots x_\nu)$. Equations (89) and (92) can now be considered as the relativistic wave equations for bound state problems of multi-electron systems. It must only be remebered that (92) holds unchanged in any approximation regarding virtual processes elimination, whereas (89) has to be corrected if exchange of two or more light quanta is to be taken into account. Elimination of the higher order processes of the radiation field proceeds on the same lines as for the first-order processes. The procedure is determined by the following recursive rule: After the elimination of the radiation processes involving n light quanta is accomplished, one should again use (85) in all terms of order n whose (electromagnetic) vacuum expectation value does not vanish. On taking the vacuum expectation value again, one then obtains all the stable state contributions due to virtual processes involving $(n+1)$ photons. For reasons to be explained below, however, this elimination method is not to be trusted, or else is not practically applicable for radiation processes of order higher than the first, if the formalism is not slightly changed so as to be "adapted" to the "hole-theory" and vacuum polarization problems. Equations (89) are nevertheless unaffected and yield as an typical example the relativistic two-electron problem expressed by the equations

$$\begin{aligned} &[\gamma_1{}^\mu(\partial/\partial x_1{}^\mu) + (mc/\hbar)]\varphi^{(0)}(x_1, x_2) \\ &\quad + (ie^2/\hbar c)\int_{-\infty}^{+\infty} S_2^{\mathrm{Ret}}(x_2 - x)(\gamma_1{}^\mu\gamma_2{}^\mu) \\ &\quad \times D_F(x_1 - x)\varphi^{(0)}(x_1, x)d^4x = 0, \\ &[\gamma_2{}^\mu(\partial/\partial x_2{}^\mu) + (mc/\hbar)]\varphi^{(0)}(x_1, x_2) \\ &\quad + (ie^2/\hbar c)\int_{-\infty}^{+\infty} S_1^{\mathrm{Ret}}(x_1 - x)(\gamma_1{}^\mu\gamma_2{}^\mu) \\ &\quad \times D_F(x_2 - x)\varphi^{(0)}(x, x_2)d^4x = 0, \end{aligned} \tag{94}$$

and the wave function normalization condition

$$(i)^2 \int_\sigma \int_\sigma \bar{\varphi}^{(0)}(x_1, x_2)\gamma_1{}^{\mu_1}\gamma_2{}^{\mu_2}\varphi^{(0)}(x_1, x_2)d\sigma_{\mu_1}d\sigma_{\mu_2} = 1. \tag{95}$$

The infinite terms

$$(ie^2/\hbar c)\int_{-\infty}^{+\infty}\gamma_k^{\mu}S^{\mathrm{Ret}}(x_k-x)\gamma_k^{\mu}D_F(x_k-x)\times\varphi^{(0)}(x_1,\cdots x_{k+1},x,x_{k+1},\cdots x_r)d^4x, \quad (96)$$

which clearly correspond to the electromagnetic self-energy of the electron, have been omitted in (94), and this does not spoil the integrability of those equations. On applying the $[\gamma_k^{\mu}(\partial/\partial x_k^{\mu})+(mc/\hbar)]$ or $[\gamma_i^{\mu}(\partial/\partial x_i^{\mu})+(mc/\hbar)]$ operators to the first or second of Eqs. (94) respectively, one can obtain a single second-order differential equation which, as far as the e^2-approximation is concerned, can with equal rights with (94) be considered as a basic equation for two-electron problem. This equation reads[7]

$$[\gamma_1^{\mu}(\partial/\partial x_1^{\mu})+(mc/\hbar)]\times[\gamma_2^{\mu}(\partial/\partial x_2^{\mu})+(mc/\hbar)]\varphi^{(0)}(x_1,x_2)+(ie^2/\hbar c)(\gamma_1^{\mu}\gamma_2^{\mu})D_F(x_1-x_2)\varphi^{(0)}(x_1,x_2)=0. \quad (97)$$

It is finally clear that for problems where in addition to the mutual interactions the electrons are subjected to the influence of an external field (that of a proton for instance), the derivatives

$$(\partial/\partial x_i^{\mu}) \quad (98)$$

are to be replaced by

$$(\partial/\partial x_i^{\mu})+(ie/\hbar c)A_{\mu}^{\mathrm{ext}}(x_i). \quad (99)$$

IV. FINAL REMARKS

As already mentioned, the formalism developed so far, and especially the virtual processes elimination method, is not suitable to handle problems of vacuum phenomena of the electron field. This is because of the infinite number of electrons occupying states of negative energy. The presence of those electrons cannot be neglected because of many-body forces which come into play (as forces acting between three electrons at least) if two or more light quanta are exchanged, giving rise to the vacuum polarization phenomena, and above all because no actual stable states can then exist. On the other hand, if they are taken into account, we are left with equations for a wave function $\varphi(x_1,\cdots x_r)$ which depends on an infinite number of x-arguments, and this makes them useless for any practical application. This essential difficulty of the formalism can be overcome if we treat the "sea" of negative energy electrons as an additional quantized field indistinguishable to some extent from the radiation field, and only treat the additional electrons or positrons by means of a configuration space, the forces between the latter being transmitted both by the radiation field and by the "sea." The fact that the additional electrons or positrons together with the "sea" form one physical entity can then be expressed by means of certain conditions imposed on their wave function. The details will be given in a subsequent paper concerned with the adaptation of the present formalism to Dirac's "hole-theory." Equations (94) or (97) account for Coulomb and Breit[8] interactions between two electrons, because they correspond to all relativistic effects connected with the exchange of a single light quantum. For the same reason all the retardation corrections to the Breit terms are also taken into account. Those terms, if treated with the aid of "one-time theory," appear to be strongly singular, whereas in (94) there is no place for singularities stronger than $1/r$ as indicated by the form of the integration kernel. This is easily explained by the fact that, if one tries to approximate the retardation by "static" potentials, one is forced to use essentially an expansion of the form

$$\delta(t\pm r/c)=\delta(t)\pm(r/c)\delta'(t)+(1/2)(r/c)^2\delta''(t)+\cdots,$$

which clearly leads to the aforementioned fictitious singularities.

I am indebted to the Polish Prime Minister's Committee for the Promotion of Science and Art for granting the scholarship enabling me to complete this work. I wish also to express my thanks to Professor F. J. Dyson, L. Infeld, H. A. Kramers, R. E. Peierls, and A. Rubinowicz for their interest and encouragement and interesting discussions.

[7] This equation has been recently published for the two-nucleon system by H. A. Bethe and E. E. Salpeter, Phys. Rev. **82**, 309 (1951).

[8] G. Breit, Phys. Rev. **34**, 553 (1929).

Letters to the Editor

PUBLICATION of brief reports of important discoveries in physics may be secured by addressing them to this department. The closing date for this department is five weeks prior to the date of issue. No proof will be sent to the authors. The Board of Editors does not hold itself responsible for the opinions expressed by the correspondents. Communications should not exceed 600 words in length and should be submitted in duplicate.

The Spontaneous Magnetization of a Two-Dimensional Rectangular Ising Model

C. H. CHANG
University of Washington, Seattle, Washington
(Received September 17, 1952)

THE present letter gives the spontaneous magnetization of a two-dimensional rectangular Ising Model. This is obtained by the method used in a paper by Yang[1] which treats the same problem except for a square lattice. The only difference in setting up the problem for a rectangular lattice is that instead of having the same H for both the vertical and the horizontal interactions, we have H_1 and H_2 (which are Kaufman's H and H'^*) for the vertical and the horizontal interactions, respectively; i.e.,

$$V_1=\exp\{H_1^*\sum_1^n C_r\},\quad V_2=\exp\{H_2\sum_1^n s_r s_{r+1}\}.$$

This leads to the condition $(x_1+1)(x_2+1)<2$ for temperatures below the critical temperature, where $x_1=\exp(-2H_1)$ and $x_2=\exp(-2H_2)$. The spontaneous magnetization I is expressed as an off-diagonal matrix element as before and the limiting process used there for reducing the calculation of I to an eigenvalue problem remains the same. In other words, all the results in Sec. I and II[2] of Yang's paper are unchanged.

In Sec. III, where an infinite crystal is considered, all the analysis remains the same except that H and H^* are replaced by H_2 and H_1^* in Eq. (60), and Eqs. (62) for A and B are replaced by

$$A=\coth H_2\coth H_1^*=(1+x_2)/x_1(1-x_2),$$
$$B=\tanh H_2\coth H_1^*=(1-x_2)/x_1(1+x_2).$$

In consequence, the modulus k in the elliptic integral is given by, instead of Eq. (78),

$$k=2k_{-1}^{\frac{1}{2}}/(1+k_{-1})=[2x_1/(1-x_1^2)][2x_2/(1-x_2^2)]=1/\sinh 2H_1\sinh 2H_2.$$

In Sec. IV the elliptic transformation (81) is replaced by

$$z=-(\mathrm{cn}u-i[1+k_1]^{\frac{1}{2}}\,\mathrm{sn}u)(\mathrm{dn}u-i[k_1+k_1k_2]^{\frac{1}{2}}\,\mathrm{sn}u)/(1+k_1\,\mathrm{sn}^2u),$$

with

$$\frac{1}{z}\frac{dz}{du}=-i\frac{1-k^2}{(1+k_1)^{\frac{1}{2}}}\frac{1}{\mathrm{dn}u-[k_1(1+k_2)/(1+k_1)]^{\frac{1}{2}}\,\mathrm{cn}u},$$

where $k_1=\sinh^{-2}2H_1$ and $k_2=\sinh^{-2}2H_2$. The essential properties of the variable z as a function of u remain the same as in the square lattice. There are still two singularities per unit cell $(4K\times 4iK')$, although their positions are changed.

In terms of the variable u, one reduces the integral equation (69) again into the integral equation (84). The change in the positions of the singularities of z does not affect one important property of the kernel $J(u', u)$ relevant in our calculation, namely, that $J(u', u)$ has only one simple pole inside a unit cell $(4K\times 4iK')$. This can be shown by examining the zeros of the factors **I** and **III** in $J(u', u)$. The remainder of Sec. V is unchanged except for Eq. (95) which is now

$$\prod_2^\infty\frac{l_n}{4}=\frac{4}{\pi^2}[K(k)]^2(1-k^2)^{\frac{1}{2}}=\frac{4}{\pi^2}K^2\left[1-\left(\frac{2x_1}{1-x_1^2}\frac{2x_2}{1-x_2^2}\right)^2\right]^{\frac{1}{2}}.$$

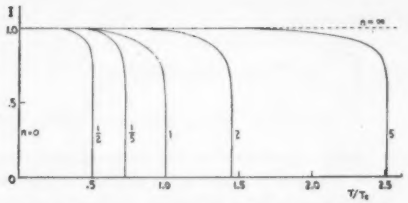

FIG. 1. The spontaneous magnetization of a two-dimensional rectangular Ising model.

The spontaneous magnetization I of a rectangular lattice is therefore

$$I=k'^4=(1-k^2)^{1/8}=\left[1-\left(\frac{2x_1}{1-x_1^2}\frac{2x_2}{1-x_2^2}\right)^2\right]^{1/8},$$

which is the same result as obtained by Kaugman and Onsager[4] for the long range order of the rectangular lattice using a different method. It reduces to the expression (96) for a square lattice.

Near the critical temperature the spontaneous magnetization varies proportionally to $(T_c-T)^{1/8}$. It is perhaps noteworthy that the exponent $\frac{1}{8}$ does not change with varying ratios of the vertical and horizontal interactions. One is tempted to conclude that the exponent is dependent only on the dimensionality of the lattice and not on the number of nearest neighbors.

In Fig. 1, I is plotted against T/T_c for various n's, where n is the ratio J_2/J_1 and T_c is the critical temperature for a square lattice with $J=J_1$.

The writer wishes to express his deep gratitude to Dr. C. N. Yang for suggesting this problem and for his guidance throughout this work.

[1] C. N. Yang, Phys. Rev. **85**, 808 (1952).
[2] B. Kaufman, Phys. Rev. **76**, 1232 (1949).
[3] All the section and equation numbers refer to Yang's paper.
[4] L. Onsager, Nuovo cimento **VI**, Suppl. p. 261 (1949).

The Nuclides Ba^{127}, Ba^{128}, and Cs^{128}

M. LINDNER AND R. N. OSBORNE
California Research and Development Company, Livermore, California
(Received October 6, 1952)

IN the course of study of radioactive nuclides in the region of barium which decay through the electron capture process, a previously unreported isotope of barium was encountered. In addition, further studies were made on the decay characteristics of the isobaric chain

$$Ba^{128}\ 2.4\ \text{days}\longrightarrow Cs^{128}\ 3.1\ \text{min}\longrightarrow Xe^{128},$$

with which 3.0-Mev positrons are reported to be associated.[1,2]

A barium fraction was removed from a cesium nitrate target which had been bombarded with 190-Mev deuterons. The short-lived Cs^{128} daughter was separated from the parent barium by the addition of chilled absolute alcohol to a previously fumed and chilled perchloric acid solution of the barium to which cesium carrier had been added. The resultant precipitate of cesium perchlorate was collected in a sintered glass filter and washed with alcohol. The time interval from separation to counting could be made less than a minute. In three independent determinations, half-life values of 3.80, 3.75, and 3.80 minutes were obtained. No other activity was detectable when decay was followed through five half-lives. The cesium daughter accounted for at least 90 percent of the activity present in the barium fraction, as determined on an end-window argon-alcohol-filled counter. This figure does not include the loss of cesium sustained during its chemical separation. Thus, essentially all the activity in the 2.4-day decay is due to Cs^{128}. In addition, the curve for growth of the 3.8-minute

cesium into a rapidly purified sample of barium followed that to be expected for the growth of a positron emitter into a parent which contained too small a quantity of particulate radiation to be detected with the end-window counter employed in the experiment. From these two facts it appears that Ba^{139} must decay principally by electron capture, since the equilibrium mixture of isobars contained the positrons reported by Fink and Templeton.[1] K-x-radiation was also found to be associated with the 3.8-minute cesium daughter as determined on a single-channel scintillation pulse analyzer. If these x-rays be due to electron capture rather than conversion of gamma-radiation, it would appear that 25 percent of the Cs^{138} decayed through electron capture. A barium sample was investigated for gamma-radiation on the pulse analyzer, but interference because of Compton recoils from the annihilation radiation rendered results inconclusive.

A barium isotope of 12-minute half-life was found whose radiations were not directly characterized. However, positron emission is probable since electromagnetic radiation seemed to comprise no more than five percent of the total activity detectable on an end-window counter. By four rapid chemical separations made at ten-minute intervals a cesium activity was obtained from the barium whose half-life and radiation characteristics agree with those reported for Cs^{137}.[2] Furthermore, the yield of this nuclide diminished roughly by a factor of two in each of the four successive separations. The 12-minute barium activity is thus Ba^{137}.

[1] R. W. Fink and D. H. Templeton, J. Am. Chem. Soc. **72**, 2818 (1950).
[2] R. W. Fink and E. O. Wiig, J. Am. Chem. Soc. **73**, 2365 (1951).
[3] Fink, Reynolds, and Templeton, Phys. Rev. **77**, 614 (1950).

The Cottrell-Bilby Theory of Yielding of Iron

TAKEO YOKOBORI
Institute of Science and Technology, University of Tokyo, Komaba-machi, Meguro-ku, Tokyo, Japan
(Received September 29, 1952)

ALTHOUGH the mechanism of yielding of iron by Cottrell and Bilby[1] (C-B theory) is the best one that has been proposed, there seem to be ambiguities concerning the method of deriving the equation of temperature and strain rate dependence. It may be much more reasonable to derive it from the following equation:

$$dm/dt = m^3, \tag{1}$$

in which m denotes the transition probability. Equation (1) was previously developed by the author,[2] considering the yield phenomenon as a Markoff process. In the C-B theory, m refers to the probability that a dislocation is released from the carbon atmosphere by an external stress, and it is given by

$$m = B\exp[-U(\sigma/\sigma_0)/kT]. \tag{2}$$

Hence, substituting the value of m from Eq. (2) into Eq. (1), we find

$$\log(v/BkT) + \log(-\partial U/\partial\sigma) = -U/kT, \tag{3}$$

in which $v = d\sigma/dt$ = stress velocity. The change of T involved in $\log(1/T)$ may be neglected compared with that involved in U/kT. Only when the term $\log(-\partial U/\partial\sigma)$ is negligible, does Eq. (3) become

$$BkT = v\exp(U/kT), \tag{4}$$

which is the same formula as in the C-B theory.[1]

Corresponding to each four series of U–σ/σ_0 curves in the C-B paper,[1] the curves of $U/\alpha(2AW\rho)^{\frac{1}{2}}$ *versus* σ/σ_0 were drawn as solid lines (as shown in Fig. 1), which approximate the curves in the C-B paper. In Fig. 1 the α's are suitably chosen constants, which are different for each four series, respectively; and $\alpha(2AW\rho)^{\frac{1}{2}}$ has such a unit that the ordinates become dimensionless. It is found that these curves are approximately equivalent to the curve of $-\log(\sigma/\sigma_0)$, as shown by the dashed line in Fig. 1. That is,

$$U \doteqdot -(1/n)\log(\sigma/\sigma_0), \tag{5}$$

where $1/n = \alpha(2AW\rho)^{\frac{1}{2}}$. Substituting $U = -(1/n)\log(\sigma/\sigma_0)$ in Eq. (3) gives

$$\log(v/nBkT\sigma_0) = (1/nkT+1)\log(\sigma/\sigma_0). \tag{6}$$

Since $1/nkT$ was found to be much larger than unity in the cases corresponding to these four series of U–σ/σ_0 curves, Eq. (6) becomes

$$nkT\log(v/nBkT\sigma_0) = \log(\sigma/\sigma_0). \tag{7}$$

Thus, the logarithm of yield stress should be proportional to the absolute temperature. The experimental results[3] are in good agreement with Eq. (7), as shown in Fig. 2.

It is interesting that from Eq. (7) the dependence of yield stress on strain rate $\dot{\epsilon}$ is given by the power law:

$$\sigma \propto \dot{\epsilon}^{nkT}. \tag{8}$$

If one uses the parameters corresponding to the No. 2 curve in the C-B paper,[1] then the exponent at room temperature is

$$nkT = 0.022,$$

which is in good agreement with the value 0.020 obtained in Deutler's experiments[4] upon mild steel.

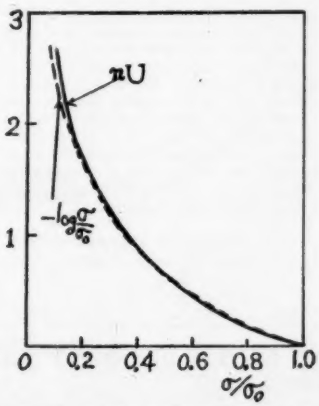

FIG. 1. The activation energy as a function of σ/σ_0 (from data of Cottrell and Bilby).

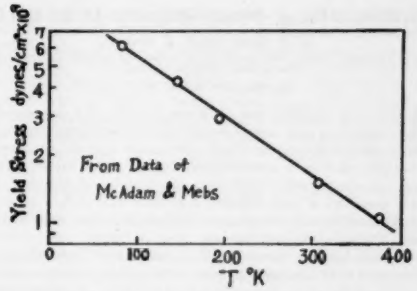

FIG. 2. The dependence of yield stress on temperature (from data of McAdam and Mebs).

[1] A. H. Cottrell and B. A. Bilby, Proc. Phys. Soc. (London) **62A**, 49 (1949).
[2] T. Yokobori, J. Phys. Soc. Japan **7**, 44 (1952).
[3] D. J. McAdam, Jr. and R. W. Mebs, Proc. Am. Soc. Testing Materials **43**, 661 (1943).
[4] C. Zener and J. H. Hollomon, J. Appl. Phys. **15**, 22 (1944).

Lifetimes of the μ^--Meson Stopped in Li, Be, and C

W. E. BELL[a] AND E. P. HINCKS
Physics Division, Atomic Energy of Canada Limited, Chalk River Laboratories, Chalk River, Ontario, Canada

(Received October 30, 1952)

THE time distributions of delays between the stopping of cosmic-ray μ-mesons in several light elements and the emission of decay electrons have been determined with the apparatus previously used[1] for a measurement of the μ^+-meson lifetime. The measurements reported here were obtained by substituting, in turn, absorbers of pure lithium, beryllium, and carbon to stop μ-mesons of the sea-level mixture, in place of the iron used previously. Details of the absorbers are given in Table I.

For each element about 30,000 meson decays, with delays in the range 1 to 11 μsec, were counted. After making the appropriate corrections[1] the decay curve for each of the three absorbers, when plotted, appears to be a single exponential. The contribution to each curve from μ^+-decays was estimated by computing the relative number of μ^+-mesons stopped in the absorber, brass counter walls, and iron supports, (assuming a sea-level positive excess of 20 percent for momenta of 500–1000 Mev/c) and attributing to the μ^+-meson a mean life, $\tau^+ = 2.22 \pm 0.02$ μsec.[1] Figure 1 shows the measured composite ($\mu^+ + \mu^-$) decay curve for carbon, together with the μ^--decay curve obtained by subtracting the μ^+-component.

In Table I are given values, for each absorber, of the fraction f^- of the total initial electron emission rate estimated as being due to μ^--mesons, the apparent mean life τ' from the composite curve, the mean life τ^- for the μ^--meson, and the inferred nuclear capture rate A for the μ^--meson.

TABLE I. Details of the absorbers and results.[a]

Absorber	Physical form	Mass (kg)	f^-	τ' (μsec)	τ^- (μsec)	A (10^4 sec^{-1})
Lithium	Metal cast in thin-walled steel box	6.5	0.27	2.20 ± 0.02	2.15 ± 0.09	<3.5
Beryllium	Metal bricks	12.4	0.42	2.15 ± 0.02	2.05 ± 0.06	3.7 ± 1.5
Carbon	Graphite block	25.4	0.42	2.12 ± 0.02	1.98 ± 0.06[b]	5.5 ± 1.5

[a] Preliminary results with a sodium fluoride absorber give $\tau^-_{NaF} = 1.4 \pm 0.2$ μsec, in agreement with Ticho's value 1.28 ± 0.12 μsec (see reference 3).
[b] H. A. Morewitz and M. H. Shamos [Phys. Rev. **87**, 241 (1952)] have recently reported a measurement of τ^- for carbon which is slightly lower than that given here.

The difference $(\tau^+ - \tau^-_{Li}) = +0.07 \pm 0.09$ μsec indicates that the μ^+ and μ^- *decay* lifetimes are equal within the experimental error. The effect of nuclear capture by the Li nucleus is expected to be small, the correction to be added to τ^-_{Li} to get τ^-_{decay} being $A_{Li}(\tau^-_{Li})^2$ if $A_{Li} \ll 1/\tau^-_{decay}$. By using the relation $A \propto Z^4$ proposed by Wheeler[2] to extrapolate from results[3,4] obtained at higher atomic number (Z), where capture predominates over decay, we estimate that $A_{Li} \sim 0.3 \times 10^4$ sec^{-1}, and, therefore, $A_{Li}(\tau^-_{Li})^2 \sim 0.01$ μsec. On this basis the difference $(\tau^+ - \tau^-_{decay})$ is equal to $+0.06 \pm 0.09$ μsec; it could only differ significantly from zero (becoming negative) should the above estimate of A_{Li} be too low by a factor $\gg 10$.

The nuclear capture rates A were calculated from the relation

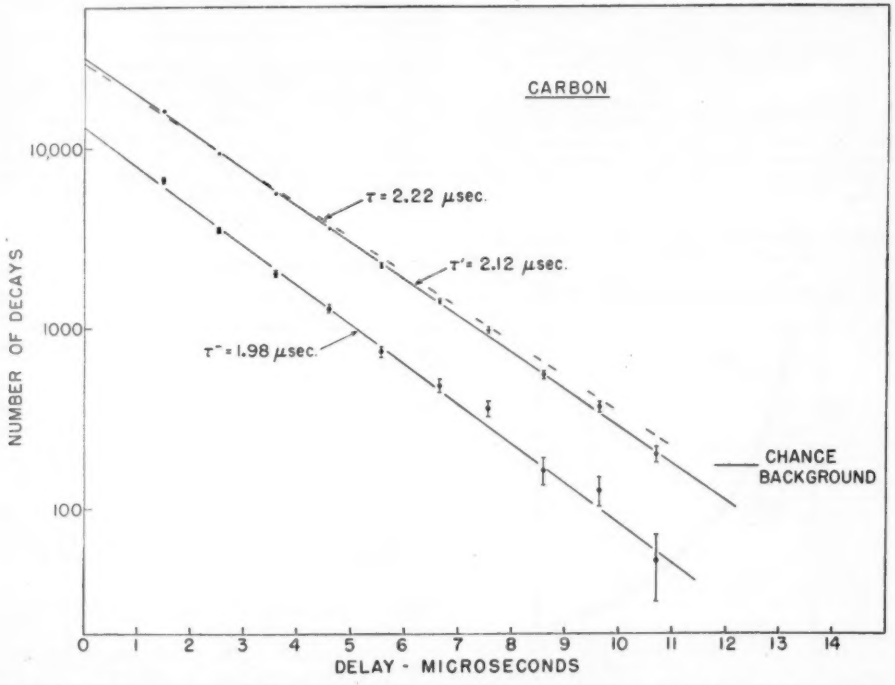

FIG. 1. Differential decay curves obtained with a carbon absorber. The upper curve is for the ($\mu^+ + \mu^-$) mixture, and the lower one is the corrected curve for μ^--mesons only. The errors shown are standard deviations, and the best straight lines were determined by least squares fit. The dashed curve with $\tau = 2.22$ μsec is shown for comparison.

$\Lambda=1/\tau^{-}-1/\tau^{-}_{\text{decay}}$, assuming that τ^{-}_{decay} is, in fact, equal to 2.22 ± 0.02 μsec. They do not depart significantly from the values obtained by extrapolating with a Z^4 dependence the results of previous measurements[2,4] for $Z>7$. Our experimental value of Λ for carbon may be compared with the values calculated by Preston and Duret[5] assuming a charge-exchange reaction with a coupling constant equal to that determined from the neutron β-decay. The comparison indicates that the coupling constants for μ-capture and β-decay are equal to within about 30 percent, strengthening the argument for a universal interaction between pairs of fermions.

* Now with Newmont Exploration Ltd., Jerome, Arizona.
[1] W. E. Bell and E. P. Hincks, Phys. Rev. **84**, 1243 (1951).
[2] J. A. Wheeler, Revs. Modern Phys. **21**, 133 (1949).
[3] H. K. Ticho, Phys. Rev. **74**, 1337 (1948).
[4] An account of existing data, with references, may be found in B. Rossi, *High Energy Particles* (Prentice-Hall, Inc., New York, 1952), Sec. 4.9.
[5] M. A. Preston and M. F. Duret, following Letter [Phys. Rev. **88**, 1425 (1952)].

The Coupling Constant of the Nucleon-μ-Meson Interaction

M. A. PRESTON AND M. F. DURET*
Physics Department, University of Toronto, Toronto, Ontario, Canada
(Received October 31, 1952)

ON the hypothesis of a "universal" interaction for particles of spin $\frac{1}{2}\hbar$, μ-capture ($P+\mu^{-}\rightarrow N+\nu$) and β-decay will be described by interaction Hamiltonians containing the same five coupling constants g_K, $K=S, V, T, A, P$. We write $g_S^2+g_V^2=(1-x)g^2$, $g_T^2+g_A^2=xg^2$, $G^2=(1+2x)g^2$. Recent β-decay evidence[1] suggests $\frac{1}{3}\lesssim x\lesssim\frac{1}{2}$. The decay of the neutron gives $G_\beta=(3.12\pm0.4)\times10^{-49}$ erg cm³. From μ-capture data, Tiomno and Wheeler[2] have estimated $G_\mu\sim10^{-49}$ erg cm³.

More recently, Kennedy has used a shell model to study the experimental results with heavy elements[3] and finds $G_\mu\sim3\times10^{-49}$ erg cm³. We have attempted to obtain a more reliable value of G_μ based on the μ-capture rate in C^{12}, since this has been measured and considerable information about the momentum distribution in this nucleus is now available.

We have expressed Λ, the transition probability for μ-meson capture, in terms of the nucleon momentum distribution. With a "gas" model approximation, we have

$$\Lambda=Mh^{-4}G_\mu^2\Psi^2\int_0^{y_0}dq\ q\int_0^{\infty}\rho W(\mathbf{p}_P)[1-W(\mathbf{p}_N)]dy.$$

Here $\mathbf{p}_P$, $\mathbf{p}_N$, and $\mathbf{q}$ are proton, neutron and neutrino momenta, $cq_0=\mu c^2-\Delta$, $y=|\mathbf{p}_P\times\mathbf{q}/q|$, and $\mu c^2=cq+\Delta+(p_N^2-p_P^2)/2M$, where Δ = mass of B^{12} atom − mass of C^{12} atom + meson binding energy + mc^2. The momentum distribution is $\rho W(\mathbf{p})$, where ρ is a density of order (nuclear dimensions/$\hbar$)³ determined explicitly by the normalization of the momentum distribution and $W(\mathbf{p})$ is the probability that a nucleon with momentum $\mathbf{p}$ is in one of the states which is occupied in the initial nucleus. The average over the nucleus of the K-shell meson probability density is Ψ^2.

High energy (n, d),[4] (p, p),[5] and (p, π)[6] experiments on C^{12} agree with a momentum distribution represented by (a) a Gaussian of average energy 14–19 Mev or (b) the Chew-Goldberger $(\alpha^2+p^2)^{-2}$ distribution cutoff at 72 Mev. Taking $G_\mu=3.12\times10^{-49}$ erg cm³, we find for Λ the values in the second column of Table I.

TABLE I. Calculated transition probabilities and the values of G_μ.

Model	$\Lambda(10^4\ \text{sec}^{-1})$ with $G_\mu=3.12\times10^{-49}$	$G_\mu(10^{-49}$ erg cm³)
Gaussian: $\bar{E}=18$ Mev	8.65	2.5 ± 0.3
Chew-Goldberger-Temmer	8.86	2.5 ± 0.3
Shell: $x=0.8$	4.67	3.4 ± 0.4
Shell: $x=0.5$	4.48	3.5 ± 0.4
Shell: $x=0.8$	2.11*	5.0 ± 0.7*
Shell: $x=0.5$	1.92*	5.3 ± 0.8*

We have also made calculations using the shell model. Here we would expect the results to be reliable for transitions to low-lying bound states only. We use spherical potential wells to represent the nuclei. Their depths are found from the known separation energies of the $1p$ protons of C^{12} and $1p$ neutrons of B^{12}. On this model there are then no higher bound single particle states in B^{12}, and the matrix elements required are those from the various $s_{\frac{1}{2}}$ and $p_{\frac{1}{2}}$ states of C^{12} to the $p_{\frac{3}{2}}$ states of B^{12}. Using the above value for G_μ, we obtain for the transition probability to the bound states:

$$(1+2x)^{-1}[3.62(1-x)+4.76(3x)]\times10^4\ \text{sec}^{-1}.$$

Some of these states, which are bound on the shell model, have excitations of ~11 Mev. Since the shell model is not reliable in these cases, we have also shown the transition probabilities excluding these states. (These values are labelled with an asterisk in Table I.)

Comparing the calculated values in the second column of Table I with the value $\Lambda=5.5\pm1.5\times10^4$ sec^{-1} determined by Bell and Hincks,[7] we find the values of G_μ given in column three. We may safely conclude that G_μ lies in the range (2.5 to 5.0) $\times10^{-49}$ erg cm³, and for reasons discussed in a fuller account (to be submitted to the Canadian Journal of Physics), we feel that the most likely value of G_μ is about 3.2×10^{-49} erg cm³.

* Holder of a National Research Council of Canada Studentship.
[1] O. Kofoed-Hansen and A. Winther, Phys. Rev. **86**, 428 (1952); R. Nataf and R. Bouchez, Phys. Rev. **87**, 155 (1952); J. M. Blatt, unpublished.
[2] J. Tiomno and J. A. Wheeler, Revs. Modern Phys. **21**, 153 (1949).
[3] Keuffel, Harrison, Godfrey, and Reynolds, Phys. Rev. **87**, 942 (1952); J. M. Kennedy, Phys. Rev. **87**, 953 (1952).
[4] G. F. Chew and M. L. Goldberger, Phys. Rev. **77**, 470 (1950).
[5] G. M. Temmer, Phys. Rev. **83**, 1067 (1951); Cladis, Hess, and Moyer, Phys. Rev. **87**, 425 (1952); P. A. Wolff, Phys. Rev. **87**, 434 (1952).
[6] E. M. Henley and R. H. Huddlestone, Phys. Rev. **82**, 754 (1951).
[7] W. E. Bell and E. P. Hincks, preceding Letter [Phys. Rev. **88**, 1424 (1952)].

The *g* Factor of Ferrites

TOSHIHIKO OKAMURA, YOSHIARU TORIZUKA, AND YUZO KOJIMA
Research Institute for Scientific Measurements, Tohoku University, Sendai, Japan
(Received October 16, 1952)

THE microwave resonance in Ni ferrite and Mn ferrite was observed in polycrystalline specimens at several frequencies from 9450 Mc/sec to 47,000 Mc/sec, and it was found that the frequency dependence of the apparent g factors could be explained in relation to the anisotropic internal field in the material.

Many spherical specimens whose diameter varied from about 3 mm to 0.3 mm were polished from a sintered block, and after studying the size effect[1] on the g factor at each frequency, the resonance fields H_s were determined by extrapolating to zero diameter. These are shown in Table I. The g factor at each frequency, designated g^* in the table, was calculated by Kittel's formula,[2]

$$\nu=(\gamma^*/2\pi)H_s, \qquad (1)$$

where $\gamma^*=g^*e/2mc$. This g factor was found to depend on the frequency, approaching the value of $g^*=2$ at shorter wavelengths.

As Landé's factor is a materially constant factor, it should have the same value at any frequency. We, therefore, substituted

TABLE I. g^* calculated by Kittles' formula $\nu=(\gamma^*/2\pi)H_s$.

Material	Frequency (Mc/sec)	Resonance field H_s (oersteds)	g^*
$NiOFe_2O_3$	9450	2780	2.43
	18,400	5930	2.22
	23,500	7660	2.19
	47,000	15,870	2.12
$MnOFe_2O_3$	9450	3120	2.16
	18,400	6320	2.08
	23,500	8190	2.05
	47,000	16,620	2.02

TABLE II. g values calculated by $\nu=(\gamma/2\pi)(H_s+H_i)$.

Material	Frequency (Mc/sec)	g
$NiOFe_2O_3$	9450	2.05
	18,400	2.04
	23,500	2.06
	47,000	2.05
$MnOFe_2O_3$	9450	1.99
	18,400	1.99
	23,500	1.98
	47,000	1.99

in Kittel's formula as follows:

$$\nu=(\gamma/2\pi)(H_s+H_i), \tag{2}$$

where $\gamma=ge/2mc$, and H_i denote the internal field in the material, which must be independent of frequency.

By use of the resonance data in Table I, the most probable values of H_i were calculated by the method of least squares to be 507 oersteds for Ni ferrite and 278 oersteds for Mn ferrite. Substituting these values in Eq. (2), we obtained for both ferrites the g values shown in the last column of Table II. These g values are independent of the frequency within the limits of experimental error. It should be noted that the g factor of Mn ferrite calculated from Eq. (2) agrees with the theoretical value of 2, showing good evidence for quenching of the orbital contribution of the Mn^{++} ion.

H_i may be the internal field[1-3] caused by the magnetocrystalline anisotropic energy, and seems to be equal to the internal field discussed by Rado et al.;[4] they reported that the internal field in Ferramic A would contribute to the resonance by domain rotation in the material.

This work will be reported in detail in the near future.

[1] Yager, Meritt, and Guillaud, Phys. Rev. **81**, 477 (1951); T. Okamura and Y. Kojima, Phys. Rev. **86**, 1040 (1952). Our data which were reported in Phys. Rev. **80**, 910 (1950) cannot be used in connection with the present discussion, because they were obtained without taking into consideration the size effect.
[2] C. Kittel, Phys. Rev. **73**, 155 (1948).
[3] L. Landau and E. Lifshitz, Physik. Z. Sowjetunion **8**, 158 (1935).
[4] Rado, Wright, and Emerson, Phys. Rev. **80**, 273 (1950).
[5] J. B. Birks, Proc. Phys. Soc. (London) **B63**, 65 (1950).

Ferroelectricity in Oxides of Fluorite Structure

W. R. COOK, JR. AND HANS JAFFE
The Brush Development Company, Cleveland, Ohio
(Received October 31, 1952)

A HIGH dielectric constant with a strong negative temperature coefficient recently has been reported for the new cadmium niobate composition $Cd_2Nb_2O_7$ by Bousky[1] and by Wainer and Wentworth.[2] These authors do not describe the crystal structure of this compound, but their discussion implies it to be a perovskite.

We have made powder x-ray diffraction patterns of this compound, prepared at 1150°C and found, not a perovskite structure, but a face-centered cubic structure of lattice constant 5.185 ±0.003A. The pattern is very sharp and shows no evidence of splitting in the back reflection lines, nor any indication of a superlattice. The relative intensities of the diffraction lines are very similar to those of cerium dioxide, which has the calcium fluoride structure.

This pattern can be accounted for by an arrangement of one molecule of $Cd_2Nb_2O_7$, with oxygens occupying statistically seven out of the eight anionic positions, and niobium and cadmium distributed statistically over the cationic positions of the fluorite structure. Periodic alternation of cadmium and niobium, or oxygen and vacant positions, are not compatible with the face-centered cubic structure. The O—O distance, 2.59A, is unusually small, probably because of the absence of $\frac{1}{8}$ of the oxygen atoms. The density calculated from the lattice constant is 6.24. Direct measurement on a ceramic body gave 5.89.

The high dielectric constant reported by Bousky[1] and by Wainer and Wentworth[2] was confirmed. A disk of the material fired to 1300°C shows a relative dielectric constant of 450 at room temperature. This rises to a peak of 2850 at −103°C, the Curie point. Hysteresis loops taken at −196°C show it to be ferroelectric below its Curie point.

We have also studied the analogous compound $Pb_2Nb_2O_7$, not previously described in the literature. We find a dielectric constant of 110 and a dielectric loss factor of 0.004 at 100 kc/sec, measured at room temperature. The dielectric constant rises with falling temperature from a value of 80 at 400°C to 245 at −196°C, the limit of measurement, with indications of a Curie point at somewhat lower temperatures.

The x-ray diffraction pattern of $Pb_2Nb_2O_7$ shows a distorted fluorite structure of rhombohedral symmetry. The lattice parameters are $a_0=5.285\pm0.003$A and $\alpha=89°15'$. Again there is no indication of any superstructure.

These results are significant in that they show ferroelectricity in a simple structure type where it was previously not suspected.

We thank E. J. Brajer for preparation of the samples and G. N. Cotton for the dielectric measurements which established the Curie point of $Cd_2Nb_2O_7$.

[1] S. Bousky, U. S. Patent No. 2,584,324, February 5, 1952.
[2] E. Wainer and C. Wentworth, J. Am. Ceram. Soc. **35**, 207 (1952).

The Ratio of Positive to Negative π-Meson Production from Deuterium

J. CAROTHERS AND C. G. ANDRÉ
Radiation Laboratory, Department of Physics, University of California, Berkeley, California
(Received October 28, 1952)

THE ratio of positive to negative π-meson production from deuterium at 0° to the 340-Mev proton beam of the Berkeley cyclotron has been measured by a method which permits a direct comparison of the positive and negative production. The mesons were separated from the proton background by using a double magnet arrangement as shown in Fig. 1. Double coincidences were made between photomultiplier signals 1 and 2, and 3 and 4 in diode bridge type coincidence circuits which had resolving times of about 5×10^{-9} second. The outputs of the two bridges were combined in a slow mixer (about 10^{-8} second resolving time), and the resulting triple coincidences were taken as being due to particles that had traveled the trajectory laid out. Several checks were made to assure that this was so. Turning off either magnet reduced the triples counting rate to about one percent of the rate with the fields on. This was the same as the accidental rate measured by inserting a time delay equal to one rf cycle ($\sim6\times10^{-8}$ sec) in the signal lines from photomultipliers 1 and 3. The number of negative particles counted when the target was filled with hydrogen was the same as that from the empty target. Range curves

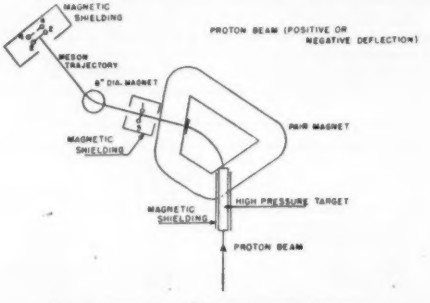

FIG. 1. Arrangement of the experimental apparatus.

TABLE I. π^+ to π^- ratio as a function of the laboratory meson energy.

E_π, Mev	π^+/π^- ratio
42	5.8±2.5
51	7.4±1.7
60	21.6±8.9
70	22.1±3.5
79	20.8±7.1
88	36.5±6.2
98	34 ±14
108	—
126	—

indicated a less than 5 percent contamination of particles with ranges greater than the expected meson ranges.

The target used was a high pressure gas target 24 in. long, which contained deuterium at 1400 psi at liquid nitrogen temperature. This placed 3.3 grams per square centimeter of deuterium in the beam, and since the end windows of the target contained only 1.7 grams per square centimeter of stainless steel, the production from the deuterium was greater than that from the target windows. Magnetic shielding was placed around the target to prevent the fringe fields of the first magnet from effecting the paths of the mesons produced in the far end of the target.

The ratios observed were obtained by measuring the meson production from the container plus gas at a series of energies, reversing the fields in both magnets, and measuring the mesons produced at the same energies. The gas was then removed from the container and similar measurements were made for the production from the end windows of the target. The values of the field strengths corresponding to various meson energies were obtained by using a current carrying wire to give the trajectories of the mesons of various energies. The fields were adjusted so the trajectory for each energy was the same. Use of the wire showed that reversing the magnetic fields delivered particles of the same energy but of opposite sign to the same position on the rear counters.

Checks of the counter efficiency were made using a Co^{60} source, and reversal of the magnetic fields was found to effect the counting rate in counters 1 and 3 by less than one percent. Counters 2 and 4 could not be tested in this manner, but the measured magnetic field at these counters was less than that at the position of counters 1 and 3.

The values of the π^+ to π^- ratio obtained for deuterium are given in Table I. Errors shown are standard deviations. Values are not shown for 108 and 126 Mev because no negative mesons were found at these energies. The ratios shown are those obtained by simply reversing the magnetic fields at a particular meson energy. The production curves are being corrected at the present time for the energy resolution of the apparatus, and any changes in the results will be published in a forthcoming article which will also include the results obtained for He, Be, C, and Pb.

The results that were obtained agree with the previous work on deuterium[1] in that they show a value higher than expected. Previous theoretical work[2] indicated that a ratio of about 8 might be expected. Some theoretical implication of these results are discussed in the following letter.

[1] Passman, Block, and Havens, Phys. Rev. **85**, 370 (1952).
[2] H. P. Noyes, Phys. Rev. **81**, 924 (1951).

The π^+ to π^- Ratio from Proton Bombardment of Deuterium*

MALVIN A. RUDERMAN†
Physics Department, Radiation Laboratory, University of California, Berkeley, California
(Received October 28, 1952)

NOYES[1] has calculated the expected ratio of negative to positive π-mesons in the forward direction when deuterium is bombarded by 345-Mev protons. Most of the mesons in collisions with free target nucleons have 60-Mev to 70-Mev energy in the laboratory system. To obtain π-mesons in this energy range from $p-d$ collisions, the production must come mostly when the internal momentum of the deuteron is small. For these cases, when the proton and neutron are far apart, the uncertainties in the deuteron wave function are minimized and Noyes' assumptions are most likely to be valid. He finds a π^+ to π^- ratio of 8.2±0.8 at 60 Mev if the $p+p\to\pi^+$ cross section differs from $p+n\to\pi^-$ only in a factor of two for the two protons and in the different interactions between the final nucleons. The final proton and neutron after π^+ production are taken to be in a ^3S state. Any admixture of singlet lessens the ratio. The matrix elements are assumed to be energy independent. If they vary like the square root of the meson center of mass kinetic energy, the ratio is a few percent smaller.

The experimental[2] value of the forward π^+ to π^- ratio at 60 Mev is about three times larger than predicted, implying that the $p+n\to\pi^-$ matrix element is suppressed relative to $p+p\to\pi^+$. This also seems to be true at 90°.[3]

If isotopic spin is conserved in meson production and the π^- meson is emitted predominantly into a p-state, the initial $p-n$ system is ^3S or ^1D and therefore has isotopic spin zero. Then in the final state of a π^- meson and two protons, the π^- and either proton must be in a state of isotopic spin one-half. To the extent that the interaction is strong only when leading to π^--proton states of isotopic spin $\frac{3}{2}$, the π^- production will be forbidden.[4] It is interesting to note that while isotopic spin does not contribute a selection rule for $p+p\to\pi^+$, the angular distribution indicates that the final state is one in which the π^+ and either nucleon have angular momentum $\frac{3}{2}$.[5]

* This work was performed under the auspices of the AEC.
† Now at Columbia University, New York, New York.
[1] H. P. Noyes, Phys. Rev. **81**, 924 (1951).
[2] J. Carothers and C. G. André, preceding Letter [Phys. Rev. **88**, 1426 (1952)].
[3] Passman, Block and Havens, Phys. Rev. **85**, 370 (1952).
[4] This would not necessarily imply that, at these energies, the scattering of π-mesons in hydrogen should be strong only in isotopic spin 3/2 states, since the scattering could involve matrix elements which cannot contribute to single meson production, viz., a meson pair coupling [J. V. Lepore, Phys. Rev. **88**, 750 (1952); G. Wentzel, Phys. Rev. **86**, 802 (1952)].
[5] K. Brueckner and K. M. Watson, Phys. Rev. **86**, 923 (1952).

Optical and Infrared Reflectivity of Metals at Low Temperatures

T. HOLSTEIN
Westinghouse Research Laboratories, East Pittsburgh, Pennsylvania
(Received November 3, 1952)

THE theory of the anomalous skin effect in metals was developed by Reuter and Sondheimer[1] to cover the case, often encountered at low temperatures, in which the electron mean free path is comparable to, or larger than the skin depth, as computed from the conventional theory.[2] Under such conditions explicit account must be taken of the motion of electrons in a spatially inhomogeneous electric field, with the result that the standard relation,[3]

$$\mathbf{j}(\mathbf{r})=\sigma(\omega)\mathbf{E}(\mathbf{r})=(ne^2\tau/m)(1+i\omega\tau)^{-1}\mathbf{E}(\mathbf{r}), \tag{1}$$

between the current density and electric field must be replaced by a more general expression of the form:

$$\mathbf{j}(\mathbf{r})=\int G(\mathbf{r},\mathbf{r}')\mathbf{E}(\mathbf{r}')dV'. \tag{2}$$

With regard to the "relaxation" region $\omega\gg 1/\tau$ with which we are primarily concerned here, Reuter and Sondheimer make the plausible statement that, when the skin depth

$$\delta\gg v/\omega, \tag{3}$$

i.e., when the skin depth is large compared to the distance traversed by an electron in a period of electromagnetic oscillation, the conventional theory based upon (1) should apply. Nevertheless, their results (reference 1, Fig. 4) on metallic absorptivity in the optical and near infrared regions, in which (3) is valid, are generally in disagreement with the prediction of this theory. In the

present note, we explain the disagreement in terms of a mechanism of electromagnetic loss which operates even when the relaxation time τ is infinite.

In our treatment, we assume that the validity of Eq. (3) permits us to consider the electromagnetic field to be essentially that associated with a stationary but otherwise free electron gas—the model provided by Eq. (1) with $\tau=\infty$. For the case of normal incidence of a plane electromagnetic wave upon a plane-parallel metallic surface, one readily obtains

$$E=E_s e^{-x/\delta_f}\cos(\omega t+\alpha), \tag{4}$$

where

$$\delta_f=(4\pi ne^2/mc^2)^{-\frac{1}{2}} \tag{5}$$

and

$$E_s=(2i\omega\delta_f/c)E_i. \tag{6}$$

(E_i is the amplitude of the incident field, α an arbitrary phase angle, and x the coordinate perpendicular to the surface.)

In the approximation of a stationary free-electron gas there is no loss of electromagnetic energy. However, when account is taken of the motion of the electrons to and from the metallic surface, one obtains a finite transfer of energy from the electromagnetic field to the electrons. The computation of this transfer will now be sketched briefly.

For the case in which an electron is specularly reflected, its terminal velocity $\mathbf{v}_t$ which it possesses upon leaving the boundary region in which the field is effectively contained is given by

$$\mathbf{v}_t=\mathbf{v}_i+(e/m)\int_{-\infty}^{+\infty}\boldsymbol{\varepsilon}(t)dt,$$

where $\boldsymbol{\varepsilon}(t)$, the field seen by the electron, is obtained from Eq. (4) by substituting[4] $x=v_i|t|\cos\theta$. The energy ΔE_{sp} transferred to the electron is then readily seen to be

$$\Delta E_{sp}=\left\langle\left[(e/m)\int_{-\infty}^{+\infty}\boldsymbol{\varepsilon}(t)dt\right]^2\right\rangle_{Av}, \tag{7}$$

the average[5] being taken with respect to the arbitrary phase angle α.

In the case of diffuse reflection at the metallic surface, the electron velocity is "randomized" at $t=0$; as a result, the energy gain ΔE_d turns out to be

$$\Delta E_d=\left\langle(e/m)^2\left[\left(\int_{-\infty}^{0}\boldsymbol{\varepsilon}(t)dt\right)^2+\left(\int_{0}^{\infty}\boldsymbol{\varepsilon}(t)dt\right)^2\right]\right\rangle_{Av}. \tag{8}$$

One obtains the rate of energy transfer per unit surface by multiplying (7) or (8) by the differential current,[6]

$$dI=nv(\sin\theta\cos\theta d\theta/2)(3v_0^2dv/v_0^3), \tag{9}$$

and integrating over all angles of incidence and all velocities from zero to v_0. Upon dividing the result by the incident flux per unit surface $cE_i^2/8\pi$, one obtains the absorptivity, which may be written in the general form

$$A=p\frac{2\pi ne^2}{m\omega^2}\frac{v_0^2}{c^2}+(1-p)\frac{3}{4}\frac{v_0}{c}, \tag{10}$$

where p is the fraction of electrons incident on the metallic surface which are specularly reflected, the remainder being diffusely reflected.

In the case of specular reflection ($p=1$), Eq. (10) gives

$$A_{sp}=(2\pi ne^2/m\omega^2)(v_0^2/c^2),$$

which agrees substantially with the graphical result of Reuter and Sondheimer in the optical and near infrared regions (reference 1, Fig. 4). However, the diffuse absorptivity $A_d=\frac{3}{4}v_0/c$, in contrast to the other cases treated by Reuter and Sondheimer, ($\omega\gtrsim 1/\tau$), may exceed A_{sp} by orders of magnitude. Namely, from Eqs. (5) and (3), we have

$$\frac{A_d}{A_{sp}}=\frac{3}{2}\frac{m\omega^2}{4\pi ne^2}\frac{c^2}{v_0^2}=\frac{3}{2}\left(\frac{\omega\delta_f}{v_0}\right)^2\gg 1.$$

We may finally report an observation of Pippard[7] that in the case of copper, if we assume one free electron per atom, we have $v_0\sim 1.5\times 10^8$ cm/sec, which gives $A_d\sim 0.4$ percent, in order of magnitude agreement with the experimental result, 0.62 percent, obtained by Ramanathan.[8]

A more complete report of this work will be presented at a later date.

[1] G. E. H. Reuter and E. H. Sondheimer, Proc. Roy. Soc. (London) **A195**, 336 (1948).
[2] See, e.g., A. H. Wilson, *The Theory of Metals* (Cambridge University Press, Cambridge, 1936), Chap. V, Sec. 4.1.
[3] In Eq. (3), ω is the circular frequency of the incident field and τ the relaxation time for attainment of thermal equilibrium between electrons and lattice.
[4] Here $\mathbf{v}_i$ is the initial random velocity and θ the angle of incidence (and reflection). We may without loss of generality take the origin of time to be the instant the electron strikes the surface.
[5] In this averaging operation, the cross term in the square of the right-hand side of (7) vanishes.
[6] We assume isotropically directed velocities with magnitudes varying from 0 to $v_0=(\hbar/m)(3\pi/8\pi)^{\frac{1}{3}}$ according to the Fermi distribution at absolute zero.
[7] A. B. Pippard, private communication.
[8] K. G. Ramanathan, Proc. Phys. Soc. (London) **A65**, 532 (1952).

Dependence of Gamma-Radiation Lifetimes on Nucleon Configurations

R. D. Hill
Physics Department, University of Illinois, Urbana, Illinois
(Received November 3, 1952)

It has been pointed out[1] that the gamma-radiation lifetimes of $M4$ transitions deviate by less than 30 percent from the mean lifetime τ_γ, given by a simple empirical formula of the Weisskopf type.[2] For other multipole radiations there is no such good agreement with empirical formulas. In particular, it has been observed[1] for $E3$ transitions that the squares of the matrix element, $|M|^2$, defined as $\tau_\gamma(\text{theoretical})/\tau_\gamma(\text{experimental})$, vary by as much as $10^{\pm 2}$ from a median value.

In connection with an investigation of a 14-hour isomeric decay of Os^{191}, an extremely slow $E3$ transition has recently been observed.[3] Since one of the states involved in this transition was identified as having a complex nucleon configuration, it seemed of interest to investigate whether there existed other evidence of a

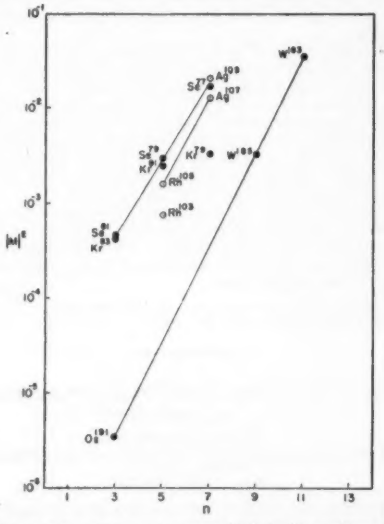

FIG. 1. Variation of the matrix element, $|M|^2$, for $E3$ transitions of the $7/2+\rightleftarrows 2g_{\frac{9}{2}}$ type, with complexity n of the $7/2+$nucleon configuration. Full circle points refer to even Z-odd N isomeric transitions. Open circle points refer to odd Z-even N isomeric transitions.

dependence of gamma-transition lifetime on nucleon configuration. The data presented in Fig. 1 show that there is, in fact, some evidence to this effect.

In Fig. 1, the values of the matrix elements $|M|^2$ for all the evaluable $E3$ transitions of the $7/2+\rightleftarrows p_{\frac{1}{2}}$ type are plotted against a number n, representing the complexity of the nucleon configuration. For odd-proton nuclei (open circle points), n is the number of protons coupling to form the $7/2+$state, and for odd-neutron nuclei (full circle points) n is the number of neutron holes in the configuration forming the $7/2+$state. Reasonable estimates of n can be arrived at in the case of $g_{9/2}$ proton and neutron configurations by consideration of the energy systematics of the $7/2+$levels.[4] For the cases of Os^{191}, W^{183}, and W^{185}, however, the n-values for the $i_{13/2}$ holes can be regarded as no more than judicious shell-theory guesses. It is apparent from the plot that $|M|^2$ increases steeply with n and at approximately the same rate for odd protons of the $g_{9/2}$ shell, and for odd neutrons of both the $g_{9/2}$ and $i_{13/2}$ sub-shells. To indicate the odd-proton variation, the Rh^{103} and Ag^{107} points have been joined by a line because these isomers have equal neutron numbers. There appears to be some evidence from the plot that there is a systematic effect of adding pairs of neutrons and protons. The departure of Kr^{79} from the general trend may be due to experimental inaccuracy.

Since the factors involved in the estimates[2] of transition probabilities are the same for both odd-proton and odd-neutron transitions and since the single nucleon $p_{\frac{1}{2}}$ states are common to all transitions, the differences of $|M|^2$ should be attributed to the differences of nucleon electric moment of the $7/2+$states. It is not surprising that the electric moment of the odd-proton $7/2$ states should increase with increasing numbers of protons in the outer-shell configurations. It is also reasonable to expect that an increasing number of neutrons in the outer shell configurations should tend to crowd protons into the core, thus affecting the electric moment in an inverse manner to the odd-proton states. This is equivalent to saying that for odd-neutron states the electric moment should increase with the number of neutron holes in the configuration.

If the argument for the variation of $|M|^2$ with configuration complexity be accepted for the $E3$ transitions, it may be conversely argued that the constancy of $|M|^2$ for the $M4$ transitions also indicates relatively pure configurations. Analysis of the $M4$ cases makes this indeed appear so, for there are only two cases (Ag^{110} and In^{110}) which have $|M|^2$ values departing significantly from the mean, and these configurations are, in fact, the only ones which are not describable in terms of a single nucleon. It may well be, therefore, that large departures of $|M|^2$ values from the mean value for a particular multipole transition are associated either with departures of one or both of the states from single nucleon configurations or alternatively with actual mixing of multipole radiations as, for example, in the case of $M1$ and $E2$ transitions.

[1] M. Goldhaber and A. W. Sunyar, Phys. Rev. **83**, 906 (1951).
[2] J. M. Blatt and V. F. Weisskopf, *Theoretical Nuclear Physics* (John Wiley and Sons, Inc., New York, 1952).
[3] J. B. Swan and R. D. Hill, Phys. Rev. **88**, 831 (1952); R. D. Hill and J. W. Mihelich (to be published).
[4] M. Goldhaber and R. D. Hill, Revs. Modern Phys. **24**, 179 (1952).

The Inherent Half-Width of K-Conversion Lines

HILDING SLÄTIS AND GUNNAR LINDSTRÖM
Nobel Institute of Physics, Stockholm, Sweden
(Received October 21, 1952)

IN 1951, one of us[1] found that the well-known F line (which is a K-conversion line) in the beta-spectrum of ThB was broader than the I line (L_{I} line). The half-widths in momentum were 0.14 and 0.10 percent, respectively. The observation was made in the semicircular beta-spectrometer constructed by Lindström and confirmed with the double focusing spectrometer.

Later, one of us measured the broadening effect in his permanent magnet beta-ray spectrometer of high resolving power[2]

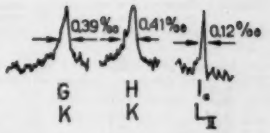

FIG. 1. Broadening effect of the K lines in the beta-spectrum of ThB. The relative half-widths are given in parts per thousand.

(half-width of the I_s line, which is an L_{II} line, only 1.2 parts in 10,000). The difference in half-width between the K and L lines was now found to be 3 parts in 10,000. In addition, the G and H lines, which also are K lines, were found to be 3 parts in 10,000 broader than the I_s line (Fig. 1). This broadening effect in momentum corresponds to about 80 ev in energy, and seems to be the same for all observed K-conversion lines in the β-spectrum of ThB.

Professor Kai Siegbahn has suggested the following explanation of the observed inherent line width of conversion lines: The fact that all the K-conversion lines investigated so far in the ThB spectrum have the same width indicates that the line broadening is essentially independent of the particular nuclear configuration of the states between which the transition takes place. The refilling of the empty place in the K shell, which occurs within a time which is very short compared to the life-time of the nuclear state, is accompanied mainly by the emission of $K\alpha$-radiation. The width of this radiation must, therefore, be expected to show up also in the width of the emitted K-electron line. An inspection of existing data[3] on $K\alpha$-line widths gives quantitative support to this view. For $Z=20$ to 40 the $K\alpha$-line widths increase from 1.7 to 6.8 ev. At $Z=74$ (W) the $K\alpha$-line width is already 42.5 ev, and a reasonable extrapolation to $Z=83$ yields here a line width of 70 ± 5 ev, in remarkably good agreement with the widths of the K-conversion lines reported above. The widths of the L-conversion lines should be expected to be about 10 ev, which is just too small to be observed at present.

The authors are indebted to Professor K. Siegbahn and Professor L. Hulthén for valuable discussions.

[1] G. Lindström, Arkiv Fysik **4**, No. 1 (1952).
[2] H. Slätis, Arkiv Fysik (to be published).
[3] A. H. Compton and S. K. Allison, *X-Rays in Theory and Experiment* (D. Van Nostrand and Company, New York, 1935).

Activation Energy for Fission*

GLENN T. SEABORG
Radiation Laboratory and Department of Chemistry, University of California, Berkeley, California
(Received November 3, 1952)

THE rate of spontaneous fission for even-even nuclides has a simple exponential dependence [1-3] on Z^2/A, and a plot of the logarithm of the "half-life" for this process *vs* Z^2/A (Fig. 1 of references 1 and 3) yields the relationship

$$T=10^{-21}\times10^{178-2.75Z^2/A}\ \text{sec}. \tag{1}$$

It is the purpose of this note to point out how this information can be related to the activation energy for fission and, hence, be correlated with the known information on slow neutron and photofission of heavy nuclides.

The barrier penetration probability for spontaneous fission has been shown to have the general form $10^{-k\Delta E}$, where ΔE is the energy deficit at the saddle point.[4,5] In particular Frankel and Metropolis[5] have derived for the liquid drop model the relationship

$$T=10^{-21}\times10^{7.85\Delta E}\ \text{sec}, \tag{2}$$

where ΔE is in Mev. On the assumption that their treatment for the rate process is essentially correct so that the general form of (2) is valid, even though the calculation of ΔE is not, as evidenced from the failure to account for experimental spontaneous fission

TABLE I. Correlation of slow neutron fissionability with potential barrier to fission and corresponding neutron binding energy.

Nuclide	ΔE (Mev)	NBE[a] (Mev)	$NBE-\Delta E$ (Mev)	SNF[b]
Ra^{226}	6.7	4.9	−1.8	−
Ra^{228}	6.8	4.6	−2.2	−
Ac^{227}	6.5	5.1	−1.4	−
Th^{227}	6.2	7.0	0.8	+
Th^{228}	6.3	5.4	−0.9	−
Th^{229}	6.3	6.7	0.4	+
Th^{230}	6.4	4.6	−1.8	−
Th^{232}	6.5	4.8	−1.7	−
Th^{234}	6.6	4.7	−1.9	−
Pa^{230}	6.1	6.9	0.8	+
Pa^{231}	6.1	5.4	−0.7	−
Pa^{232}	6.2	6.7	0.5	+
Pa^{233}	6.3	5.1	−1.2	−
U^{232}	5.9	5.9	0.0	+
U^{233}	6.0	6.7	0.7	+
U^{234}	6.0	5.4	−0.6	−
U^{235}	6.1	6.5	0.4	+
U^{236}	6.2	4.8	−1.4	−
Np^{236}	5.7	7.1	1.4	+
Np^{237}	5.9	5.2	−0.7	−
Np^{238}	6.0	6.4	0.4	+
Np^{239}	6.0	5.0	−1.0	−
Pu^{238}	5.7	5.7	0.0	+
Pu^{239}	5.8	6.5	0.7	+
Pu^{241}	5.9	6.2	0.3	+
Am^{241}	5.5	5.3	−0.2	−
Am^{242m}	5.6	6.5	0.9	+
Am^{242}	5.6	6.5	0.9	+
Am^{243}	5.7	5.2	−0.5	?
Cm^{242}	5.4	5.9	0.5	?

[a] Neutron binding energy for nuclide with mass number $A+1$, from reference 6.
[b] Slow neutron fissionability: + denotes σ_f greater than about 1 barn; − denotes σ_f less than about 1 barn.

rates,[1] we can relate (1) and (2) and obtain

$$T=10^{-21}\times 10^{7.85(22.7-0.477Z^2/A)} \text{ sec}, \quad (3)$$

where

$$\Delta E=(22.7-0.477Z^2/A) \text{ Mev}. \quad (4)$$

However, (2) actually applies only to U^{238} ($Z^2/A=35.56$) of different degrees of excitation, and extension to different values of Z^2/A leads to a somewhat more complicated expression. When this is related to (1), we find that ΔE can be approximately represented over a limited range of Z^2/A by

$$\Delta E=(19.0-0.36Z^2/A) \text{ Mev}. \quad (5)$$

When ΔE is calculated using (5) and compared with the binding energy (NBE) of the added neutron[6] for each of the nuclides whose slow neutron fission cross sections[7] or upper limits are known, remarkable agreement is observed as shown in the last two columns of Table I. Something approaching a quantitative correlation is attained if the individual values of $NBE-\Delta E$ are compared with the corresponding values of σ_f/σ_τ (σ_f = fission, $\sigma_\tau=n,\gamma$ cross section for slow neutrons) for each nuclide; since the probability for gamma-emission might be approximately the same for all these nuclides, the ratio σ_f/σ_τ may give a good measure of the relative probability for fission[8] and, hence, can be used to better advantage for comparative purposes than σ_f alone. Such a plot is shown in Fig. 1 where the available points, perhaps fortuitously, are rather well represented by a straight line with some exceptions discussed below.

Perhaps all of the presently available data on three types of fission (spontaneous, slow neutron, photo) are consistent with the view that an odd nucleon has the effect of slowing the fission process (possibly due to larger radii than corresponding even-even nuclides, giving smaller values of Z^2/r^3 which Z^2/A is meant to represent). In the spontaneous fission case, nuclides with odd nucleons have rates up to some 10^3 times slower than corresponding even-even nuclides (Fig. 1 in reference 1). In the case of photofission,[9] odd nucleon nuclides like U^{232}, U^{235}, and Pu^{239} have thresholds 0.4–0.5 Mev nearer the top of the barrier than U^{233} and Th^{232} corresponding to rates some 10^2–10^3 times slower than those of U^{235} or Th^{230}, indicating that the slowing effect of an odd nucleon is operative even at excitation to near the top of the barrier. However, the probability for gamma re-emission may be less for the even-even nuclides, because of a larger level spacing, which means that fission is relatively favored and would occur at lower excitation relative to the barrier height; thus, the odd nucleon may slow the photofission process. (1) in a manner analogous to the effect in spontaneous fission or (2) relative to gamma-emission owing to its effect on level spacing and, therefore, on the probability for competitive gamma-emission. If we apply these considerations to slow neutron fission, we must think in terms of the intermediate fissioning nucleus which is formed upon capture of the neutron. Thus, it would be interesting to see if even-odd nuclides (even protons, odd neutrons), where the intermediate fissioning nuclei are of the even-even type, undergo slow neutron induced fission with greater probability than other nuclear types at comparable excitation energy. Unfortunately, there are no presently known cases of the ratio σ_f/σ_τ for nuclides with $NBE-\Delta E<0$ but only for nuclides which are apparently excited above the barrier in the slow neutron fission process; those that form intermediates with an odd nucleon (see especially Cm^{243}) seem to be slower in undergoing this process; again either of the two mechanisms for the slowing effect of an odd nucleon may be operative. The variation in the positions of the points for the even-odd nuclides in the region above the barrier ($NBE-\Delta E>0$) may perhaps be explained by a small nonuniform variation in the probability for gamma-emission.

The empirical relationship (1) depends, of course, upon how the line is drawn through the points representing the measured spontaneous fission rates of the even-even nuclides. In order to examine this point further, other possibilities were examined; for example, a line drawn somewhat higher with a steeper slope gives more weight to the point[2] for U^{234} and passes somewhat above such points as those for Cm^{244}, U^{238}, and Th^{232} as it might do if these latter nuclides have slightly shrunken radii because of proximity to closed subshells. Such considerations lead to somewhat different constants in relation (5) but do not change per-

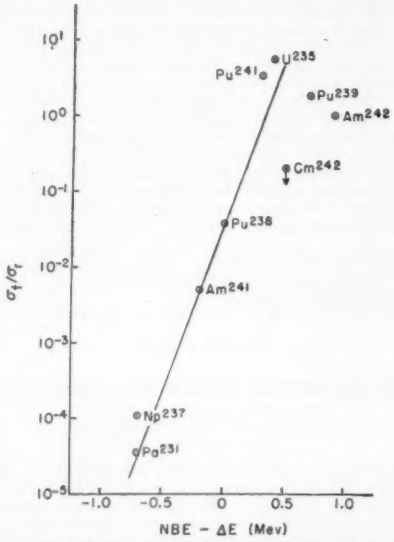

FIG. 1. Plot of comparative slow neutron fissionability. σ_f/σ_τ denotes ratio of slow neutron fission to n,γ-cross section (♀ signifies upper limit). $NBE-\Delta E$ denotes difference between neutron binding energy and potential barrier.

ceptibly the results in the correlations presented in Table I and Fig. 1.

It is a pleasure to acknowledge helpful discussions with J. O. Rasmussen, Jr., J. M. Hollander, D. R. Inglis, and G. Friedlander, and the help of M. J. Hollander with a number of the calculations.

* This work was performed under the auspices of the AEC.
[1] G. T. Seaborg, Phys. Rev. **85**, 157 (1952); U. S. Atomic Energy Commission Declassified Document AECD-3261 (July, 1951).
[2] W. J. Whitehouse and W. Galbraith, Nature **169**, 494 (1952).
[3] Ghiorso, Higgins, Larsh, Seaborg, and Thompson, Phys. Rev. **87**, 163 (1952).
[4] J. Frenkel, J. Phys. (U.S.S.R.) **10**, 533 (1946).
[5] S. Frankel and N. Metropolis, Phys. Rev. **72**, 914 (1947).
[6] Seaborg, Glass, and Thompson, unpublished work (1952).
[7] Data taken from forthcoming National Nuclear Energy Series, Plutonium Project Record, Vol. 14A, *The Actinide Elements* edited by G. T. Seaborg and J. J. Katz (McGraw-Hill Book Company, Inc., New York).
[8] J. R. Huizenga and R. B. Duffield, Phys. Rev. **88**, 959 (1952).
[9] Koch, McElhinney, and Gasteiger, Phys. Rev. **77**, 329 (1950).

The Vapor Pressure of He^3-He^4 Mixtures*

RAYMOND A. NELSON† AND WILLIAM BAND
Department of Physics, State College of Washington, Pullman, Washington
(Received October 27, 1952)

THE saturated vapor pressure of helium isotopes and mixtures of the helium isotopes can be discussed on the basis of the clustering avalanche theory of condensation applied to quantum degenerate gases.[1] The saturated vapor pressure is expressed in this theory in terms of the surface energy of small clusters. We calculated the surface energy per atom in clusters in pure He^4 and in pure He^3 to fit the theory to observed vapor pressures of the pure isotopes.[2,3] We then tentatively adopted an interpolation formula in an attempt to predict the vapor pressure of mixtures of the two isotopes. This formula was linear in the concentration; in other words, it assumed the same average concentration of He^3 in the surface of the clusters as in the vapor.

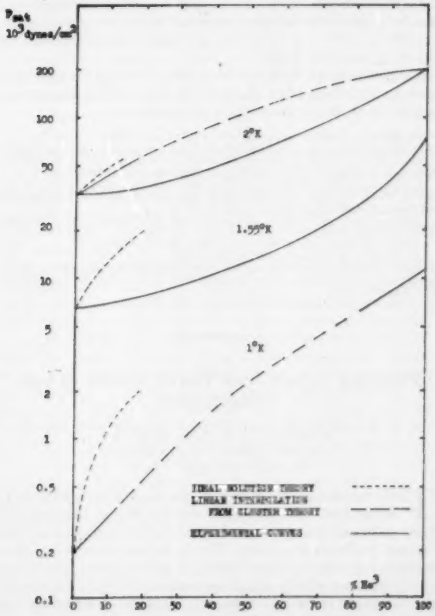

FIG. 1. Saturated vapor pressure as a function of He^3 concentration.

The results of these calculations were given in detail in a technical report to the Office of Naval Research dated June 16th, 1952. Since then the experimental data of Sommers[4] have become available. Figure 1 shows the theoretical curves we found at 2°K and 1°K compared with the ideal solution theory curves and smoothed curves for 2° and 1.55°K taken from Sommers' data. Clearly, although the theoretical curves lie appreciably lower than those of an ideal solution, the experimental curves are very considerably lower still.

This can be accounted for in theory if we use another interpolation formula that is nonlinear in the concentration, and is such as to decrease the average concentration of He^3 in the surface of clusters compared with that in the vapor. A long and tedious computation, however, is needed to find the best formula, and we plan to complete this before publishing a full report.

Sommers analyzed the relation between his saturated vapor pressures and the relative concentrations in the liquid phase, and noted that it was quite doubtful whether there was any significant effect resulting from the lambda-transition in the liquid. Our point of view coincides with this in that the liquid phase does not enter our analysis as such: saturation is an effect of clustering in the vapor. However, we do find that an anomalous decrease of He^3 in the surfaces of clusters is required to explain the data at 2°K. Whether this anomaly is connected with the similar anomaly that exists in the liquid phase below the lambda-point is an open question. It can perhaps be decided after we find whether or not the same anomaly in the clusters is required to explain the vapor pressure curves above as below the lambda-transition.

* Supported in part by the ONR.
† Now at Bell Telephone Laboratories, Murray Hill, New Jersey.
[1] W. Band, Phys. Rev. **79**, 871 (1950).
[2] W. H. Keesom, *Helium* (Elsevier, New York, 1942).
[3] Abraham, Osborne, and Weinstock, Phys. Rev. **80**, 366 (1950).
[4] H. S. Sommers, Jr., Phys. Rev. **88**, 113 (1952).

Multiple Coulomb Scattering of High Energy Pions in Photographic Emulsions*

MEERA BACKUS, J. J. LORD, AND MARCEL SCHEIN
Department of Physics, University of Chicago, Chicago, Illinois
(Received October 9, 1952)

THE small angle scattering in photographic plates of negative pions from the Chicago cyclotron[1] has been measured by the saggitta method. The measurements were undertaken in order to provide information on the multiple scattering of high energy pions over very long cell lengths which is of great importance in numerous cosmic-ray studies.

This investigation was made by methods similar to those initiated by Goldschmidt-Clermont *et al.*[2] and Fowler[3] which were worked out in considerable detail by others.[4,5] Negative pions of 226±7 Mev energy were allowed to pass through two Ilford G5 plates 200 microns in thickness with surfaces nearly parallel to the pion beam. The microscope and techniques were identical to those described by Berger *et al.*[4] The lateral displacement of the tracks y_j were measured at equal distances l (cell length) along a straight line defined by the rectilinear motion of the precision microscope stage.[4] The set of second differences of these lateral displacements $\Delta^2 y_j = y_{j+2} - 2y_{j+1} + y_j$ obtained from the tracks provides a measure of the multiple scattering of the pions. The 89 tracks which were measured were selected along a line 2 cm from the edge of the plate. Then only tracks nearly parallel to the surface were selected and measurements made until they were 5 microns from the surface. The energy of the pion beam before entering the plates was 227±7 Mev from previous calibrations.[1] When corrections were made for energy loss in the plates and wrapping material, the average energy of the pions used in this experiment was 218±11 Mev. The average measured length of the tracks in this investigation was 8000 microns and only 10 percent were shorter than 5600 microns. No measured length of track shorter than 3500 microns was found by the above selection

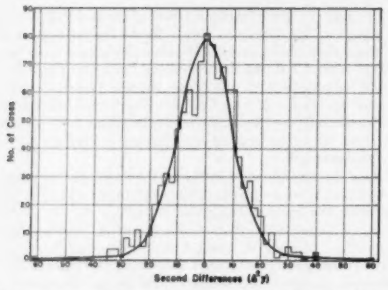

FIG. 1. Frequency distribution of 2nd differences for 218±11 Mev negative pions, using a 250-micron cell length. One unit of the abscissa equals 0.0693 micron. Second differences greater than 4 times the mean absolute value are shaded. The solid curve is the theoretical curve calculated from theory.

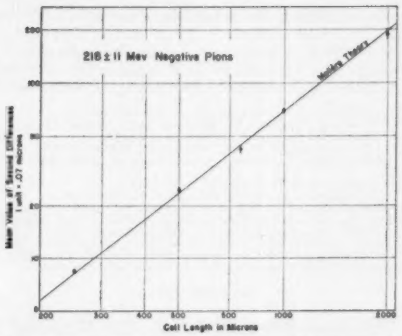

FIG. 2. Variation with cell length of the average absolute value of the second difference computed with quantities 4 times the calculated mean excluded. The solid curve is from theory (Molière). One unit of the ordinate is equal to 0.0693 micron.

scheme. This serves to indicate that the finite thickness of the emulsion (200 microns) had little tendency to bias the data in favor of tracks with small scattering. The influence of emulsion distortion was tested by a statistical analysis of the distribution of the algebraic signs of the observed successive second coordinate differences (run test) and found to be negligible within statistical fluctuations.

The measurements were made in a temperature controlled room with a special precision stage[4] described previously. Evaluation of the noise level was first determined from cosmic-ray tracks of extreme energy[5] (>15 Bev) for which the average value of the second differences is only the result of "noise" and in this case $\langle|\Delta^2 y|\rangle_{Av}=0.06$ micron. Since each measurement of the coordinate y_i is a length averaged over about a 10-micron section of the track, it is to be expected that the noise level would be dependent upon the degree of scattering of the track. This was determined by making 10 successive measurements of relatively strongly scattered tracks (pions and protons of energies from 200 to 400 Mev) at 30 positions. A statistical analysis then showed that the noise level for the tracks measured in this experiment was $\langle|\Delta^2 y|\rangle_{Av}=0.21$ micron.

The relation of the measure of multiple scattering to cell length, energy, and type of the scattered particle is given by:

$$\langle|\alpha|\rangle_{Av}=\langle|\Delta^2 y|\rangle_{Av}57.3/t=\frac{K_1 z Z(t/100)^{\frac{1}{2}}}{pv},$$

where $\langle|\alpha|\rangle_{Av}$ is the mean angle in degrees between successive chords through the points dividing the track into cells of length t in microns. Z, p, and v are the charge, momentum, and velocity of the scattered particle with pv expressed in Mev. The scattering factor K_1[6] is only slightly dependent upon Z, v, and t; and in accordance with convention $\langle|\Delta^2 y|\rangle_{Av}$ and $\langle|\alpha|\rangle_{Av}$ refer here to averages based only on those values less than 4 times the experimental mean. A histogram of the frequency distribution of $\Delta^2 y$ is given in Fig. 1 for cell lengths of 250 microns. The curve drawn through the histogram and normalized to equal area is calculated for convenience from the theory of Molière,[6] although the agreement with experiments would be quite as satisfactory for other theories.[7] In Table I a summary is given of the average second differences and scattering factors for the pions as well as for previous measurements with protons[4] and carbon nuclei.[8] In the last column of Table I comparison is made with the Molière[6] theory, which is in general agreement with the other theories.[7] Figure 2 gives the variation of the average second difference with cell length, and it is to be noticed that this variation with cell length is slightly less than that predicted from theory. This slight difference from theory was also present in the previous scattering data for protons.[4] By using cell lengths of 2000 microns and longer, it might be of interest to further investigate this dependency of scattering upon cell length.

TABLE I. Summary of multiple scattering data.

Particle	Energy Mev	Cell length, microns	$\langle\|\Delta^2 y\|\rangle$ micron	Scatt. factor K_1[a] (4 ×mean excluded) Expt.	Theory
Pions (neg.)	218±11	250	0.58±0.014	25.5±0.7	24.5
		500	1.69±0.28	26.3±0.7	25.5
		750	2.85±0.14	24.4±1.0	26.0
		1000	4.75±0.104	26.0±0.9	26.4
		2000	12.89±0.693	24.9±1.5	27.3
Protons	337±1	500		24.5±0.7	25.8
	218±2	500		25.4±1.0	26.2
Carbon nuclei	10 to 1000	250		24.8±1.4	26.4
		500		26.2±2.2	27.2

We wish to thank Professor H. L. Anderson and the cyclotron group for extending to us the facilities of the Chicago cyclotron, and Dr. M. J. Berger for valuable discussions.

* Assisted by the joint program of the ONR and AEC.

[1] Anderson, Fermi, Long, Martin, and Nagle, Phys. Rev. **85**, 934 (1952).
[2] Goldschmidt-Clermont, King, Muirhead, and Ritson, Proc. Phys. Soc. (London) **61**, 183 (1948); P. H. Fowler, Phil. Mag. **41**, 169 (1950).
[3] L. Voyvodic and E. Pickup, Phys. Rev. **81**, 471, 890 (1951); D. R. Corson, Phys. Rev. **83**, 217 (1951); Gottstein, Menon, Mulvey, O'Ceallaigh, and Rochat, Phil. Mag. **42**, 708 (1951).
[4] Berger, Lord, and Schein, Phys. Rev. **83**, 850 (1951); M. J. Berger, Phys. Rev. **88**, 59 (1952).
[5] Lord, Fainberg, and Schein, Phys. Rev. **80**, 970 (1950).
[6] G. Molière, Z. Naturforsch. **3a**, 78 (1951).
[7] E. J. Williams, Proc. Roy. Soc. (London) **A169**, 531 (1939); H. S. Snyder and W. T. Scott, Phys. Rev. **76**, 220, (1949); W. T. Scott, Phys. Rev. **85**, 245 (1952).
[8] Chou, Fry, and Lord, Phys. Rev. **87**, 671 (1952).

Polarized γ-Rays from Nuclei Aligned at Low Temperatures

G. R. BISHOP,* J. M. DANIELS,* G. GOLDSCHMIDT,† H. HALBAN, N. KURTI, AND F. N. H. ROBINSON†
Clarendon Laboratory, Oxford, England
(Received November 3, 1952)

THE γ-radiations from aligned nuclei, besides exhibiting an anisotropic polar diagram which depends on the multipole order of the transition, should also be polarized in a manner which depends on the parity change. The technique for aligning cobalt nuclei has already been established.[1,2] We have used this method to produce an assembly of aligned nuclei and have observed that the radiations are in fact polarized. We have investigated both Co^{60} and Co^{58}; our result for Co^{60} is in agreement with the well-

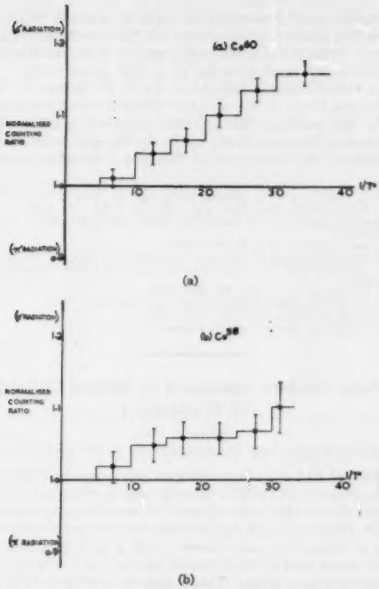

FIG. 1. (a) Polarization of γ-rays from Co^{60}; (b) Polarization of γ-rays from Co^{58}.

established fact[3,4] that the transitions are both $E2$; for Co^{58} we find the transition to be $E2$ also.

The source in each case was a stack of single crystals of the composition (1 percent Co, 12 percent Cu, 87 percent Zn) $Rb_2(SO_4)_2 \cdot 6H_2O$ mounted in a demagnetization cryostat with the b axis and the K_1 axis both horizontal. (K_1 is the direction of maximum susceptibility for the Co^{++} ions in this salt.) There are two axes of alignment in these crystals each making an angle of 53° to the b axis. For complete alignment, the radiation emitted along the b axis should be elliptically polarized (see Condon and Shortley[5]) with the major axis of the ellipse described by the electric vector vertical or horizontal, corresponding to $E2$ or $M2$ transitions, respectively.

The radiations emitted along the b axis were observed using a polarimeter, which relies on the fact that the differential cross section for Compton scattering is dependent on the polarization of the initial γ-ray. Radiation is collimated on to a liquid scintillator (4 percent terphenyl in toluene) where it is scattered. Radiation scattered through 90° in the horizontal and vertical directions is detected by two NaI crystals, which are screened from the direct radiations of the source by the collimator. The coincidence counting rates between each NaI crystal and the liquid scintillator give the number of γ-rays scattered by the scintillator in each direction. For unpolarized γ-rays these counting rates are the same, except for small geometrical differences. Polarized γ-rays are preferentially scattered in a direction perpendicular to the electric vector, and thus the ratio of the coincidence counting rates is in general different from unity. For partially polarized γ-radiation, the coincidence counting rate ratio has a value intermediate between unity and the value for plane polarized radiation. A detailed calculation by Steenberg[6] and Tolhoek and Cox[7] shows that the counting ratio increases from unity to its limiting value as the nuclear alignment becomes more and more complete. The limiting value for complete alignment is greatest for radiation emitted along the b axis (along which we observed).

The salt containing radioactive cobalt was cooled by adiabatic demagnetization to a temperature of approximately 0.01°K, and as the salt warmed up to 1°K the coincidence rates were observed for 15-second intervals. Simultaneously the temperature of the salt was obtained by measuring its magnetic susceptibility. The ratio of coincidence rates normalized to the ratio at 1°K is plotted in Fig. 1 as a function of $1/T^*$ (T^* is the temperature found according to Curie's Law from the susceptibility). Each point is an average obtained from several demagnetizations and the errors indicated are the standard deviations. Frequent tests demonstrated that the counters were stable and that the counting rates observed follow the usual Gaussian curve.

In Co^{60} two $E2$ γ-rays are emitted in a 4–2–0 cascade; the electric vectors of the two γ-rays are therefore parallel at all corresponding positions on each polar diagram. Our results [Fig. 1(a)] are consistent with this scheme. In consequence of imperfect screening, some of the coincidences observed are the result of the cascade γ-rays. The coincidence rate resulting from this cause is temperature dependent and would give a ratio mistakable for an $M2$ transition. However, calculation and experimental data show that the coincidence ratio is not changed by more than 2 percent.

The decay of Co^{58} by K capture (85.5 percent) and β^+ (14.5 percent) branching leads to the 805-kev excited level of Fe^{58}. The observed coincidence ratio [Fig. 1(b)] is of the same nature as that found for Co^{60} indicating that the transition to the ground state of Fe^{58} is electric. Previous measurement of the polar diagram[8] of the emitted radiation establishes the transition as quadrupole. There are some coincidences resulting from the annihilation radiation produced by the positrons, which can bring the coincidence ratio closer to unity but cannot alter the nature of the result. An $E2$ transition from the first excited state of the even-even nucleus Fe^{58} is expected from shell model considerations.[9]

We wish to thank Professor F. E. Simon for his continued interest and encouragement and Dr. P. F. D. Shaw of this Laboratory for his help in the preparation of the crystals.

* Imperial Chemical Industries Research Fellow.
† Nuffield Research Fellow.

[1] Daniels, Grace, and Robinson, Nature **168**, 780 (1951).
[2] Gorter, Poppema, Steenland, and Beun, Physica **17**, 1050 (1951).
[3] F. Metzger and M. Deutsch, Phys. Rev. **78**, 551 (1950).
[4] E. L. Brady and M. Deutsch, Phys. Rev. **78**, 558 (1950).
[5] E. U. Condon and G. Shortley, *Theory of Atomic Spectra* (Cambridge University Press, Cambridge, 1935).
[6] N. R. Steenberg, (to be published).
[7] H. A. Tolhoek and J. A. M. Cox, Physica **18**, 357 (1952).
[8] Daniels, Grace, Halban, Kurti, and Robinson, Phil. Mag. (to be published).
[9] M. Goldhaber and A. Sunyar, Phys. Rev. **83**, 906 (1951).

Angular Dependence of Inelastic Scattering of Protons on Be^9†

K. E. DAVIS
Reed College, Portland, Oregon
(Received October 28, 1952)

THE fact that the 2.4-Mev level in Be^9 was apparently quite sharp and clearly separated from any neighbors[1-7] made it an appropriate subject for studying the angular dependence of inelastic scattering of protons. A modified form of a camera originally developed by Wilkins[8] (Fig. 1) was used to obtain intensities for scattering angles between 20° and 160° at ten-degree intervals. Eastman NTB plates (1 in.×3 in.) were used and were inclined at about 4° to the scattered protons. Al stopping foils of appropriate thickness were interposed between the target and the various detector plates so as to reduce the track length and resultant background of elastically scattered protons, while at the same time making the tracks of inelastically scattered protons shorter and more easily recognized. The University of Rochester 26-inch cyclotron was used as the source of the 7.1-Mev incident protons, with an appropriate slit system in the fringing field of the cyclo-

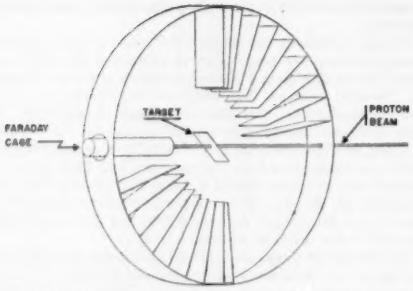

FIG. 1. Scattering camera with 7.1-Mev protons incident from right.

tron. The magnetic flux density in the camera proper was nowhere found to be greater than 40 gauss and at the target was determined to be less than 30 gauss. In view of these measurements, curvature of the proton paths in the camera was extremely small, and all trajectories were taken as straight lines without serious distortion of scattering angles. A control run in the absence of a rarget foil showed the background owing to slit edge scattering and similar sources to be negligible. The early apparent narrowness of the 2.4-Mev level has been confirmed in refined measurements by later observers[5] and is of particular interest since the level is a virtual one, being more than 780 kev above the dissociation energy.

The experimental results are given in Fig. 2. It can be seen that the scattering is essentially isotropic over the range 60° to 160° but then rises to more than three times this value by the time it reaches 20°. It is clear that the counts at the smaller angles cannot be attributed to elastically scattered protons since the distinction in length was easily and clearly made. Longmire[9] has calculated the expected angular distribution on the basis of the simplified model of a neutron and Be[8] previously used by Caldirola. His results gave either (a) isotropic scattering (for $n-p$ force completely exchange) or (b) average predominance of forward and backward compared to 90° scattering as 3 to 1 ($n-p$ force of ordinary, nonexchange, type). If the sharp increase in scattering observed in the forward direction is interpreted as *inelastic Coulomb* scattering, one secures general agreement with (a) i.e., a pure exchange force between n and p since the theoretical calculations did not include the Coulomb force on the proton.[10] It would seem that the rise is too fast for nuclear scattering. If

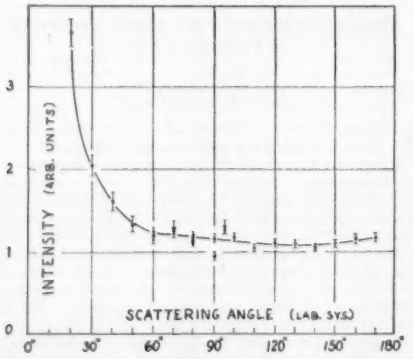

FIG. 2. Angular distribution of inelastically scattered protons from Be[9] (2.4-Mev level).

information could be secured at angles as small as 10°, a continued steep rise would tend to bear out this hypothesis. Longmire properly points out that the model used is a highly simplified one and conclusions based on it cannot be made in fine detail.

The author is deeply indebted to Dr. S. W. Barnes, Dr. G. B. Collins, and Dr. R. E. Marshak for their help and advice in undertaking this problem. He gratefully acknowledges the skilled assistance of Margaret Harris and Molly Hungate in scanning the plates and J. R. Graham and W. Harris in making the exposures.

† Work supported by the Research Corp. and the University of Rochester.

[1] K. E. Davis and E. M. Hafner, Phys. Rev. **73**, 1473 (1948).
[2] E. H. Rhoderick, Proc. Roy. Soc. (London) **A201**, 348 (1950).
[3] Buechner, Huang, Van Patter, Sperduto, and Strait, Phys. Rev. **81**, 233 (1951).
[4] R. Britten, Phys. Rev. **82**, 295 (1951).
[5] Browne, Williamson, Craig, and Donahue, Phys. Rev. **83**, 179 (1951).
[6] G. A. Dissanaike and J. O. Newton, Proc. Phys. Soc. (London) **A65**, 675 (1952).
[7] J. A. Harvey, Phys. Rev. **88**, 162 (1952).
[8] T. R. Wilkins and G. Kuerti, Phys. Rev. **55**, 1134 (1939).
[9] C. Longmire, Phys. Rev. **74**, 1773 (1948).
[10] C. Longmire, private communication.

Color Centers Generated in Sodium Chloride by Electrolysis

HENRY F. IVEY
Shiatron Electronics and Television Corporation, New York, New York

HACSKAYLO and Groetzinger[1] have recently reported the existence in sodium chloride crystals subjected to electrolysis of two ultraviolet absorption bands lying at 2260A and 2850A. These writers do not speculate on the origin of these bands. It is of interest to note, however, that a band identified as V_2 has been observed in NaCl colored by x-rays at 2226A by Casler, Pringsheim, and Yuster.[2] This V-band is attributed to trapping of "holes." Furthermore, Uchida, Ueta, and Nakai[3] have reported a band, designated K, at 2900–2950A in NaCl colored by electrolysis. It appears likely that these are the two bands observed by Hacskaylo and Groetzinger.

[1] M. Hacskaylo and G. Groetzinger, Phys. Rev. **87**, 789 (1952).
[2] Casler, Pringsheim, and Yuster, J. Chem. Phys. **18**, 1564 (1950).
[3] Uchida, Ueta, and Nakai, J. Phys. Soc. Japan **6**, 57 (1949); **6**, 107 (1951).

Errata

Similarity Properties of the Two-Fluid Model of Superconductivity, E. MAXWELL [Phys. Rev. **87**, 1126 (1952)]. Through an oversight a minus sign was omitted in Eq. (2). The first part of Eq. (2) should read: $F_s = -\frac{1}{2}\gamma T^2 x^{\alpha}$.

Optical Focusing in Constant Radius Accelerators, DAVID C. DEPACKH [Phys. Rev. **86**, 433 (1952)]. It has come to the attention of the writer that Wideröe[1] published the idea for sequential focusing by magnetic lenses in 1947. It would appear that all work subsequent to that time on sequential focusing in constant radius accelerators, including the writer's, must admit this prior claim, and the writer regrets his not having encountered reference 1 before his own publication.

[1] R. Wideröe, Schweiz. Arch. angew. Wiss. u. Tech. **8**, 10 (1947).

Interaction between Electron and One-Dimensional Electromagnetic Field, NATHAN ROSEN [Phys. Rev. **87**, 940 (1952)]. Equation (14) is incorrect in the general case and corresponds to the assumption that the electromagnetic field is moving in the positive direction of the Z axis. For consistency with this assumption further changes in the calculations are necessary, including the deletion of Eq. (22a). The final result remains essentially unchanged, but is subject to the restriction of this assumption.

Faraday Rotation of Guided Waves, H. SUHL AND L. R. WALKER [Phys. Rev. **86**, 122 (1952)]. In the expression for α_s in case (1) (ferrite case), the suffix zero should be shifted from the second β^2 to the first. Thus α_s should read as follows:

$$\alpha_s = (\chi_s/\zeta_s)[\beta_0^2 - \beta^2 + 2\zeta_s R_p H_0 - 4R_p^2 H_0^2].$$

Dielectric Constant and Permeability of Various Ferrites in the Microwave Region, TOSHIHIKO OKAMURA, TADAO FUJIMURA, AND MUNEYUKI DATE [Phys. Rev. **85**, 1041 (1952)]. The values of μ_1 in Table I were incorrectly calculated. They are as follows:

μ_1 (incorrect)	μ_1 (correct)
1.20	0.80
2.84	−0.84
1.94	0.06
1.38	0.62
1.57	0.43
1.90	0.10
1.74	0.26
1.47	0.53
2.31	−0.31

The values of $\tan\delta_\mu$ in the last column of Table I should be deleted.

The Theory of Spin Waves in Ferromagnetic Media, CONYERS HERRING AND CHARLES KITTEL [Phys. Rev. **81**, 869 (1951)]. The last β in Eq. (25) should be 2β. This error was perpetuated in the preparation of Fig. 1: the quantities $(BH)^{\frac{1}{2}}\beta$ and $H\beta$ on the left of the figure should be $2(BH)^{\frac{1}{2}}\beta$ and $2H\beta$, respectively, and the middle curve should run parallel to the lower parabola. Also, the $\xi\zeta$ on the left of Eq. (25) should be $\xi\zeta$. In two places the equations, though written for a general system of units, are valid only in special units: The statement following Eq. (12) should be changed to say that $h^{\frac{1}{2}}P_{\pm}$ is canonically conjugate to $h^{\frac{1}{2}}Q_{\pm}$. Equation (34) and the equation preceding it should each have the Bohr magneton β inserted in the denominator of the last fraction written; similarly β^2 should be inserted in the last denominators of (35) and (36).

The Solidification Curve of Helium II, B. M. CWILONG [Phys. Rev. **88**, 135 (1952)]. During further work on the solid-liquid interface of helium II an experiment was performed with an intention to compare the blocked capillary results with the results with the bellows.[1] For the U-tube a copper capillary 0.5-mm i.d. was employed, 40 cm of the U were immersed in the helium bath. A carbon resistance thermometer and its copper container formed the bottom of the U. Two 6-inch Bourdon gauges served for pressure measurement. No absolute pressure measurements were attempted. To the thermometer, a piezometer as described in (1) was attached. The thermometer was calibrated against the vapor pressure of the helium bath, with the U-tube evacuated.

No significant temperature difference could be detected when helium was introduced into the U-tube, at various pressures, up to solidification of helium. Also no significant difference in pressure could be observed between the blocking of the capillary and jamming of the magnetic needles in the piezometer. The melting curve obtained has the same gradient as that of Swenson.[2]

In view of these facts the author considers his contention as to the heat leakage through "helium II wire" to be invalid. It seems that previous results were the result of some spring effect of the bellows, probably an excessive friction owing to buckling of the bellows and solidification of helium within the bellows. The coincidence of this with the author's contention made him fairly confident of the results. He regrets the erroneous conclusions. He also thanks Dr. Swenson and Professor Simon for their interest and helpful correspondence.

However, in consequence of this error, in the meantime, a visual technique in the magnetic region of cooling was developed in this laboratory. The cavitation effect[3] was observed and is under investigation. Also a volume decrease in liquid helium, when cooled from 0.8 to 0.4°K was observed—a most interesting fact, which is also under investigation now.

[1] B. M. Cwilong, Phys. Rev. **88**, 135 (1952).
[2] C. A. Swenson, Phys. Rev. **86**, 870 (1952).
[3] Cwilong, Lees, and Manchester, Phys. Rev. **88**, 138 (1952).

High Energy Electron-Electron Scattering, WALTER H. BARKAS, ROBERT W. DEUTSCH, F. C. GILBERT AND CHARLES E. VIOLET [Phys. Rev. **86**, 59 (1952)]. In the above article it was noted that in two cases tracks of 185-Mev particles rather mysteriously stopped abruptly in the emulsion. In our opinion the events were real, and we could not disregard them. The behavior was considered anomalous because there was good reason to believe that the electrons being studied were negative. The direction of the analyzing magnetic field had been carefully established by the direction of the force on a current carrying conductor.

Since it is obviously important to understand the process in question, we have followed up the original study with a further investigation of this behavior. These additional observations now satisfy us that we were mistaken regarding the sign of the particles studied.

With the original plates a number of other plates were exposed simultaneously to electrons of various energies of the same and the opposite signs. On scanning[1] some of these plates we have obtained the following results:

1. Particles of ~36 Mev and of the same sign as those which were found to disappear were studied. Six disappearances were found when 185 cm of track was scanned.
2. Particles of ~36 Mev and of the opposite sign were then studied. In scanning 171 cm of track no disappearances were found.
3. Particles of ~185 Mev of the opposite sign were also studied. In scanning 53 cm of track no disappearances were observed.

Apparently particles of the same sign as those in the original experiment disappear, but particles of the opposite sign do not. This is the anticipated behavior if the original particles were positive electrons which annihilate in flight. That they actually are positive must be concluded from another experiment[2] carried out by one of us in collaboration with Dr. S. A. Colgate who suggested the investigation. This experiment utilized the same equipment as before, but the particle disappearances were detected by counters. The signs of the particles were established with certainty, and positive particles were found to be lost from the beam in traversing matter much more frequently than negative particles in accordance with the theory of Dirac. All the observations were consistent if we assume that between the time the direction of the magnetic field was established and the time the original plates were exposed the position of the reversing switch in the magnet circuit was (unexplainably) altered. The scattering experiment should be then interpreted as a study of the scattering of positive electrons by negative electrons. No observable difference between positron-electron and electron-electron scattering in the region investigated is to be expected.

It is believed that this is the first time that the annihilation in flight of high energy positrons has been directly observed, although the effect is well known from studies of the annihilation photons. We have looked for electron pairs from photons produced when the tracks terminate, but have found none. However, we estimate that the probability of a pair being found in the volume of emulsion which could be searched beyond the termini of the tracks is only 0.1.

In the above article on page 61, line 36 a typographical error should also be corrected. For "relative humidity was maintained at 10 percent" read "relative humidity was maintained at 100 percent."

[1] We are greatly indebted to Mr. P. C. Giles who did much of the additional microscope work necessary for this erratum.
[2] F. C. Gilbert and Stirling A. Colgate, Phys. Rev. **88**, 164 (1952).

Author Index to Volume 88

References with (A) are to abstracts of papers presented at meetings of the American Physical Society, and those with (T) designate title only. References with (L) are to Letters to the Editor.

Aamodt, R. Lee, Vincent Peterson, and Robert Phillips. $C^{12}(p,pn)C^{11}$ cross section from threshold to 340 Mev—739

Abrahams, Elihu and C. Kittel. Spin-lattice relaxation in ferromagnets—1200(L)

Adair, R. K. (see Miller, D. W.)—83

Adel, Arthur. Atmospheric window, 16 to 24 microns, and the second fundamental of N_2O—128

Ajzenberg, Fay. Deuteron bombardment of Be^9 and classification of levels of B^{10}—298

Alburger, David E. β-decay of F^{20}—1257

—— Decay of Rh^{104}—339

Allen, A. J. (see Arthur, J. S.)—1291

—— (see Hausman, H. J.)—1296

Allen, N. L. and E. Pickup. Collisions of heavy primary nuclei in emulsions—172(A)

Allred, J. C., A. H. Armstrong, R. O. Bondelid, and Louis Rosen. Elastic scattering of 9.7-Mev protons by D and by H—433

——, **A. H. Armstrong, A. M. Hudson, R. M. Potter, E. S. Robinson, Louis Rosen, and E. J. Stovall, Jr.** Elastic scattering of 10-Mev deuterons by H^3 and He^3—425

—— (see Rosen, Louis)—431

Amacher, H. C. (see Metzger, F. R.)—147(L)

Anderson, A. B. C. Dependence of Pfeifenton (pipe tone) frequency on pipe length, orifice diameter, and gas discharge pressure—161(A)

Anderson, James L. (see Bergmann, Peter G.)—1216(A)

Anderson, Paul A. Direct comparison of Kelvin and electron beam methods of contact potential measurements—655

Anderson, P. W. Concept of spin-lattice relaxation in ferromagnetic materials—1214(L)

André, C. G. (see Carothers, J.)—1426(L)

Andrews, C. L. Two new Peltier demonstrations—1216(T)

Annis, M. and N. F. Harmon. τ-meson decay in flight—1202(L)

Anslow, Gladys A., Irene S. White, and Rika Sarfaty. Confirmation of polymer and dimer absorptions in uv spectra of alcohols—154(A)

Anthony, Romuald. Observation of non-Rayleigh scattering in very near infrared spectrum of day sky—157(A)

Antonoff, George. Experimental demonstration of kinks—177(A)

—— Kinks in gases—160(A)

Apker, L. and E. Taft. Field emission from photoconductors—1037

—— **and E. A. Taft.** Photoconduction in anodic Ta_2O_5—58

Armstrong, A. H. (see Allred, J. C.)—425; 433

Arnold, W. R., J. A. Phillips, G. A. Sawyer, E. J. Stovall, Jr., and J. L. Tuck. $d-d$ cross sections 14–110 kev—159(A)

—— (see Phillips, J. A.)—159(A)

—— (see Stovall, E. J., Jr.)—159(A)

—— (see Tuck, J. L.)—159(A)

Arthur, J. S., A. J. Allen, R. S. Bender, H. J. Hausman, and C. J. McDole. Energy levels in light nuclei—1291

—— (see Hausman, H. J.)—1296

Asaro, Frank and I. Perlman. α-particles of Ra—129

—— **and I. Perlman.** α-spectra of Pu^{239} and Pu^{240}—828

Atkinson, William R. (see Fowler, Richard G.)—137(L)

Austern, N. Limit on repulsive core from 100-Mev deuteron photoeffect—1207(L)

Avery, E. C. (see Smaller, B.)—414(L)

Axtell, James C., Emmett H. Wiley, and S. W. Bass. Rf mass spectrometer—164(A)

Backman, Marvin E. New data on electrical phenomena associated with freezing of dilute aqueous solutions—165(A)

Backus, Meera and J. J. Lord. Multiple scattering of fast pions in photographic emulsions—169(A)

——, **J. J. Lord, and Marcel Schein.** Multiple Coulomb scattering of high energy pions in photographic emulsions—1431(L)

Baker, Paul, Jr., and Arthur Waltner. Angular distribution of neutrons from $d-d$ reaction—1213(L)

Ballard, Stanley S. (see Combes, Lewis S.)—153(A)

—— (see McCarthy, Kathryn A.)—153(A)

Band, William (see Nelson, Raymond A.)—1431(L)

Baranger, M., F. J. Dyson, and E. E. Salpeter. Fourth order vacuum polarization—680(L)

Barasch, Murray L. (see Combes, Herbert B.)—1382

Barfield, W. D. and A. A. Broyles. Coulomb functions for heavy nuclear particles—892

Barkas, Walter H., Robert W. Deutsch, F. C. Gilbert, and Charles E. Violet. High energy electron-electron scattering, erratum—1435(L)

Barnett, S. J. and Louis A. Giamboni. New gyromagnetic effect in permalloy and iron—28

Barschall, H. H. (see Coon, J. H.)—162(A); 562

Bartlett, James H. Iterative procedures and He wave equation—525

Bartnoff, S. (see Mingins, C. R.)—154(A)

Bass, S. W. (see Axtell, James C.)—164(A)

Battat, M. E. and F. L. Ribe. Cross sections for $Li^6(n,p)He^6$, $Li^7(n,d)He^6$, and $Be^9(n,\alpha)He^6$ for 14-Mev neutrons—159(A)

Baum, R. M. and C. S. Hung. Activation energy of heat treatment introduced lattice defects in Ge—134(L)

Bauserman, George W. Instantaneous measurement of transient flame temperatures—174(A)

Beattie, J. W. (see Ovadia, J.)—165(A)

Bell, E. E., R. L. Hansler, and R. A. Oetjen. Infrared rotational spectrum of H_2S—174(A)

Bell, W. E. and E. P. Hincks. Lifetimes of μ-meson stopped in light elements—apparatus—168(A); Lifetimes of μ-meson stopped in Li, Be, and C—1424(L)

—— (see Hincks, E. P.)—168(A)

Bender, R. S. (see Arthur, J. S.)—1291

—— (see Hausman, H. J.)—1296

Bennett, Willard H. Measurements of ionization efficiencies—165(A)

—— (see Harned, Boyd W.)—165(A)

Berger, Martin J. Multiple scattering of fast protons in photographic emulsions—59

Bergmann, Peter G., Ralph Schiller, and James L. Anderson. Lagrangian formulation of quantum theories—1216(A)

—— (see Thomson, Alice)—1216(A)

—— (see Thomson, Robert)—1216(A)

Beringer, R. (see Rawson, E. B.)—677(L)

Berlincourt, Ted G. de Haas-van Alphen effect in enriched Sn isotopes—242

Bernardini, G., E. T. Booth, and S. J. Lindenbaum. Interaction of high-energy nucleons with nuclei. II—1017

Berry, Chester R. Electron diffraction from small crystals—596

Bethe, H. A. Fundamental particles of physics—1215(T)

Biedenharn, L. C., Keith Boyer, and R. A. Charpie. Angular correlations of radiations from deuteron stripping reactions—517

Biondi, Manfred A. Diffusion, de-excitation, and ionization cross sections for metastable atoms. I—660

Bishop, G. R., J. M. Daniels, G. Goldschmidt, H. Halban, N. Kurti, and F. N. H. Robinson. Polarized γ-rays from nuclei aligned at low temperatures—1432(L)
Blair, John S. and Benjamin Segall. Impulse approximation and field theoretical calculations. I.—621
Blatt, J. M. (see Kalos, M. H.)—173(A)
Blau, M. and E. O. Salant. T-tracks in nuclear emulsions—954(L)
Blewett, J. P. Radial focusing in linear accelerator—1197
Block, M. M., S. Passman, and W. W. Havens, Jr. Production of charged π-mesons in H, D, C, Cu, and Pb by 381-Mev protons—1239
—— (see Passman, S.)—1247
Bloom, M. (see Perlman, M. M.)—1290
Bloom, Stewart D. Internal pair conversion in Mg^{24}—312
Bockelman, C. K. (see Miller, D. W.)—83
Bondelid, R. O. (see Allred, J. C.)—433
Bonner, W., J. P. Conner, and A. B. Lillie. Cross section and angular distribution of $He^3(d,p)He^4$ nuclear reaction—473
——, **A. B. Lillie, and H. L. Taylor.** Response of organic crystals to neutrons—162(A)
—— (see Conner, J. P.)—158(A); 468
Booth, E. T. (see Bernardini, G.)—1017
Bostick, Winston H. and Morton A. Levine. Direct observation of presence of magnetohydrodynamic waves in ionized He gas—153(A)
—— (see Levine, Morton A.)—153(A)
Boyd, G. E. and R. A. Charpie. Mass assignment and γ-radiation of 7-hr Mo isomer—681(L)
Boyer, Keith (see Biedenharn, L. C.)—517
Bozorth, R. M. Recent advances in theory of magnetization—171(T)
—— **and J. G. Walker.** Magnetostriction of single crystals of Co and Ni ferrites—1209(L)
Bramson, H. J., A. M. Seifert, and W. W. Havens, Jr. Energy spectrum of positrons from decay of μ-meson—304
Brand, Frank A. (see Jacobs, Harold)—492
Bransden, B. H. and A. Dalgarno. Variational method for radiationless transitions—148(L)
Bray, Ralph (see Navon, D.)—165(A)
Breit, G. and R. M. Thaler. Relativistic corrections to magnetic moments of nuclear particles—1214(L)
Brennan, J. G. and R. G. Sachs. Nuclear photoprocesses at high energy—824
Bridge, H. S. and R. H. Rediker. Ionization chamber measurements of absorption of N-component of cosmic rays in Pb—206
Britten, Roy. Scattering of 31.5-Mev protons from several elements—283
Brittin, Wesley E. and James H. Marable. Euclidean tensors—160(A)
Brockhouse, B. N. and D. G. Hurst. Energy distribution of slow neutrons scattered from solids—542
Brolley, J. E., Jr., J. L. Fowler, and L. K. Schlacks. $(n,2n)$ reactions in Cl^{37}, Cu^{63}, and Mo^{92}—618
Bromley, D. A. Ground state parity of N^{14}—565
—— (see Fulbright, H. W.)—700
Brook, Marx (see Kaplan, Joseph)—157(A)
Brown, B. M. and D. H. Tomboulian. Nuclear moments of Ta^{181}—1158
Brown, F. B., Jr., and A. V. Masket. Statistical study of distribution of stars in nuclear emulsions—1204(L)
Brown, R. J. S., George D. Freier, H. D. Holmgren, W. R. Stratton, and J. L. Yarnell. Differential cross-section measurements for the scattering of protons by deuterons—253
Broyles, A. A. (see Barfield, W. D.)—892
Broxon, James W. New barometric and temperature coefficients for small cosmic-ray bursts—173(A)
Brundy, Richard J. (see Eldridge, John A.)—163(A)
Bruner, J. A. (see Fulbright, H. W.)—700
Buechner, W. W. (see Enge, H. A.)—963
—— (see Sperduto, A.)—574
—— (see Watson, H. A.)—1324
Burgus, W. H. Radiations of Ce^{143}—1129
Bustamante, Enrique. Elementary particles at rest—1179
Butler, S. T. Stripping and the nuclear shell model—685(L)
—— **and E. E. Salpeter.** Stripping and pick-up differential cross sections—133(L)
Button, Kenneth J. Nuclear cross section for 37-Mev positive pions in Pb—956(L)

Caird, R. S. (see Smith, Alan B.)—150(L)
Caldwell, David O. Evaluation of range straggling for heavy particles—131
Calfee, Robert F., David M. Gates, and Byron E. Cohn. Atmospheric water vapor determination by infrared solar spectroscopy—157(A)
—— (see Gates, David M.)—157(A)
Callen, Herbert B., Murray L. Barasch, and Julius L. Jackson. Statistical mechanics of irreversibility—1382
—— (see Greene, Richard F.)—1387
Camac, M. Pair production by electrons—745
——, **A. D. McGuire, J. B. Platt, and H. J. Schulte.** X-rays from mesic atoms—134(L)
Cannitz, H. G. (see Noyes, H. P.)—1206(L)
Carothers, J. and C. G. André. Ratio of π^+ to π^- meson production from D—1426(L)
Carr, H. Y. and E. M. Purcell. Interaction between nuclear spins in HD gas—415(L)
Castner, Stanley V. and D. H. Templeton. Neutron deficient Sr isotopes—1126
Chambers, G. R. Review of tropospheric propagation data at distances far beyond the horizon—167(T)
Chang, C. H. Spontaneous magnetization of two-dimensional rectangular Ising model—1422(L)
Charpie, R. A. (see Biedenharn, L. C.)—517
—— (see Boyd, G. E.)—681(L)
Chartres, B. A. (see Green, H. S.)—1277
Chaudhury, M. L. Geiger-Nuttal relation and α-ray spectra—137(L)
Cheng, L. S., J. L. Dick, and J. D. Kurbatov. β-spectra of Co^{56}, Co^{57}, and Co^{61}—887
—— (see Elliott, M. W.)—263
—— (see Haskins, J. R.)—876
Cheston, W. B. (see Gallaher, L. J.)—684(L)
Chisholm, D. A., J. C. F. MacDonald, M. F. Crawford, and H. L. Welsh. Induced infrared absorption in H_2 and H_2-foreign gas mixtures at pressures up to 1500 atmos—957(L)
Chou, C. N. Internal absorption of fluorescent light in large plastic scintillators—167(A)
Choudhury, D. C. Production of E-layer in oxygen dissociation region in upper atmosphere—405
Choyke, W. J. and C. E. Nielsen. Low pressure He diffusion cloud chamber—167(A)
—— (see Nielsen, C. E.)—165(A)
Church, E. L. and J. J. Kraushaar. Geometrical correction in angular correlation measurements—419(L)
Cocconi, G. and A. Silverman. Production of π^0 mesons in H and D by high energy γ-rays—1230
Cohen, E. Richard. Rydberg constant and atomic mass of electron—353
Cohen, V. W. (see Kikuchi, C.)—142(L)
Cohn, Byron E. (see Calfee, Robert F.)—157(A)
—— (see Gates, David M.)—157(A)
Colgate, Stirling A. Use of annihilation of positrons in flight to give peaked γ-ray spectrum—164(A)
—— (see Gilbert, F. C.)—164(A)
Colli, Laura and Ugo Facchini. Discharge mechanism in A counters—987

Collins, C. B., R. M. Farquhar, and R. D. Russell. Variations in relative abundances of isotopes of common Pb—1275
Combes, Lewis S., Stanley S. Ballard, and David L. Honkonen. Inelastic deformation (cold flow) of certain crystalline materials under flexural stress—153(A)
Compton, Walter D. (see Fowler, Richard G.)—137(L)
Condit, R. I. Local atmospheric ion concentrations as basis for personnel and plant protection—158(A)
—— (see Graves, J. D.)—157(A)
Conklin, G. L. (see Mandeville, C. E.)—554
Conner, J. P., T. W. Bonner, and J. R. Smith. $H^3(d,n)He^4$ cross section—158(A); 468
—— (see Bonner, T. W.)—473
Conwell, E. M. Mobility in high electric fields—1379
Cook, C. Sharp (see Porter, Fred T.)—170(A)
Cook, W. R., Jr. and Hans Jaffe. Ferroelectricity in oxides of fluorite structure—1426(L)
Coon, J. H., E. R. Graves, and H. H. Barschall. Total cross sections for 14-Mev neutrons—162(A); 562; Leonard S. Goodman—686(L)
Cooper, H. G. (see Marx, J. W.)—106
Coppola, Patrick P. (see Hughes, Ray C.)—364
Corben, H. C. Current density in quantum electrodynamics—677(L)
Cork, J. M., J. M. LeBlanc, W. H. Nester, and F. B. Stumpf. Energy levels associated with radioactive decay of Gd^{153} and Tb^{161}—685(L)
Cotton, E. S. (see Curtis, H. O.)—173(A)
Courant, Ernest D., M. Stanley Livingston, and Hartland S. Snyder. Strong-focusing synchrotron—new high energy accelerator—1190
Craig, D. S., D. J. Donahue, and K. W. Jones. Electrostatic analysis of nuclear reaction energies. II—808
Cranna, N. G. (see Petch, H. E.)—1201(L)
Crawford, M. F. (see Chisholm, D. A.)—957(L)
Creedon, John E. (see Udelson, Burton J.)—145(L)
Cunningham, B. B. (see Fleming, E. H., Jr.)—642
Curtis, A. J. (see McGeer, P. L.)—174(A)
Curtis, H. O. and E. S. Cotton. Effects of atmosphere on penetrating cosmic radiation—173(A)
Cwilong, B. M. Solidification curve of He II—135(L); erratum—1435(L)
——, **J. F. Lees, and F. D. Manchester.** Cavitation effect in He II—138(L)

Dalgarno, A. (see Bransden, B. H.)—148(L)
Danforth, W. E. (see Weinreich, O. A.)—953(L)
Daniels, J. M. (see Bishop, G. R.)—1432(L)
Darden, S. E. (see Miller, D. W.)—83
Date, Muneyuki (see Okamura, Tosihiko)—1435(L)
Daunt, J. G. and T. S. Smith. Superconductivity of Re—309
—— (see Horowitz, M.)—1182
—— (see Smith, T. S.)—1172
Davies, T. H. (see Wexler, Sol)—1203(L)
Davila-Aponte, J. (see del Rosario, L.)—998
Davis, K. E. Angular dependence of inelastic scattering of protons on Be^9—1433(L)
——, **J. B. Marion, J. F. Delord, and K. M. King.** Close pair effect in cosmic-ray stars—368
Davis, L. R. (see Perlow, G. J.)—321
Davis, R. W. (see Phillips, D. D.)—600
de Carvalho, Hervasio and Herman Yagoda. Range of α-particles in H_2O—273
Delord, J. F. (see Davis, K. E.)—368
del Rosario, L. and J. Davila-Aponte. Range distribution of sea level mesons at low geomagnetic latitudes—998
dePackh, David C. Optical focusing in constant radius accelerators, erratum—1434(L)
der Mateosian, E. and A. Smith. Scintillation spectrometer study of Tl^{204} decay—1186
Detwiler, D. P. and Henry A. Fairbank. Thermal resistivity of superconductors—1049
Deutsch, Robert W. (see Barkas, Walter H.)—1435(L)
Dick, J. L. (see Cheng, L. S.)—887
Dodder, D. C. and J. L. Gammel. Elastic scattering of protons and neutrons by He—520
Doerner, Edward C. (see McCarthy, Kathryn A.)—153(A)
Donahue, D. J. (see Craig, D. S.)—808
Donaven, T. W., D. N. Kundu, John K. Long, and M. L. Pool. Cyclotron bombardments with 21-Mev He^3—158(A)
Drell, S. D. and E. M. Henley. Pseudoscalar mesons with applications to meson-nucleon scattering and photoproduction—1053
Driggers, F. E. Burst production in material of low atomic number by cosmic rays at sea level—173(A)
Dropesky, Bruce and Edwin E. Wiig. Three new neutron deficient Xe isotopes—683(L)
Duerig, William H. and Jordan J. Markham. Color centers in alkali halides at 5°K—1043
Duffield, Robert B. (see Huizenga, John R.)—959(L)
Duller, M. N., W. D. Walker, and J. D. Sorrels. Interactions of secondary particles from penetrating showers—172(A)
—— (see Walker, W. D.)—173(A)
DuMond, Jesse W. M. (see Muller, David E.)—775
Durbin, R. P., H. H. Loar, and W. W. Havens, Jr. Lifetimes of π^+- and π^--mesons—179
—— (see Loar, H.)—168(A)
Duret, M. F. (see Preston, M. A.)—1425(L)
Duval, J. E. (see Haskins, J. R.)—876
Dyson, F. J. (see Baranger, M.)—680(L)

Ebel, M. E. and W. F. Fry. Atomic electron ejection in large-angle scatterings—1306
Edwards, D. A. (see Tongiorgi, V. Cocconi)—145(L)
Eldridge, John A. and Richard J. Brundy. Roughness of nuclear energy surface—163(A)
Elliott, M. W., L. S. Cheng, J. R. Haskins, and J. D. Kurbatov. Nuclear spectroscopy of Ba^{131}—263
Elsasser, W. M. Theory of infrared radiation in atmosphere—158(T)
—— (see Evans, D. C.)—160(A)
Emerson, W. H. (see Rado, G. T.)—909
Enge, H. A., W. W. Buechner, and A. Sperduto. Magnetic analysis of $Al^{27}(d,p)Al^{28}$—963
Engelkemeir, D. W. (see Freedman, Melvin S.)—1155
—— (see Wagner, F., Jr.)—171(A)
Erginsoy, Cavid. Energy states of overlapping impurity carriers in semiconductors—893
Evans, D. C. and W. M. Elsasser. Utah digital computer—160(A)
Evans, G. E. and P. M. Stier. Space distribution of ionization—165(A)
—— (see Stier, P. M.)—164(A)
Evans, John E. Two-plate method of measuring anisotropic fast neutron spectra—163(A)

Facchini, Ugo (see Colli, Laura)—987
Fagg, L. W. and S. S. Hanna. Polarization of O^{16} γ-rays—1205(L)
Fairbank, Henry A. (see Detwiler, D. P.)—1049
Fan, H. Y. (see Navon, D.)—165(A)
—— (see Taylor, W. E.)—867
Farquhar, R. M. (see Collins, C. B.)—1275
Feinstein, J. Recent developments in theory of electromagnetic wave propagation through spherically stratified media—167(T)
Feldman, David. Meson-nucleon scattering and classical strong-coupling theory—890
—— (see Goldfarb, L. J. B.)—1099

Feshbach, Herman. Coulomb scattering of relativistic electrons and positrons by nuclei—295
—— **and S. I. Rubinow.** Variational principle for scattering—484
—— (see Lax, Melvin)—509
—— (see Pease, Robert L.)—945
Feuer, Paula. Electronic states in crystals under large overall perturbations—92
Finkelstein, R. J. *V*-particle and the composite pion—555
Fisher, L. H. (see Kachickas, G. A.)—878
Fleming, E. H., Jr., A. Ghiorso, and B. B. Cunningham. Specific α-activities and half-lives of U^{234}, U^{235}, and U^{236}—642
Fletcher, Harvey. Perception of speech by deafened listeners and relation to design of hearing aids—175(T)
Foldy, Leslie L. (see Kroll, Norman M.)—1177
Foley, H. M. (see Frosch, R. A.)—1337
Foner, Simon. Hall effect in Ni ferrite—955(L)
Forbes, Stuart G. Activation cross sections for 14-Mev neutrons—1309
Fowler, J. L., W. H. Jones, and J. H. Paehler. Fission asymmetry as function of excitation energy of compound nucleus—71
—— (see Brolley, J. E., Jr.)—618
Fowler, Richard G., William R. Atkinson, Walter D. Compton, and Robert J. Lee. Shock waves in low pressure spark discharges—137(L)
Fox, A. G. (see Weiss, M. T.)—146(L)
Frank, R. M. (see Yudowitch, K. L.)—759
Franken, Peter and Seymour Koenig. Determination of $g_J(^2S_{\frac{1}{2}})$ of K in terms of proton gyromagnetic ratio—199
Fraser, J. S. Angular distribution of prompt neutrons emitted in fission—536
Freedman, Melvin S., F. Wagner, Jr., and D. W. Engelkemeir. β-spectra of Pu^{239}, Pu^{240}, and Pu^{241}—1155
—— (see Wagner, F., Jr.)—171(A)
Freely, John (see Jacobs, Harold)—492
Freeman, J. J. Relation between conductance and noise power spectrum of certain electronic streams—164(A)
Freier, George D. (see Brown, R. J. S.)—253
—— (see Stratton, T. F.)—261
—— (see Stratton, W. R.)—257
French, A. P. (see Seed, J.)—1007
Frenkiel, F. N. Comparison between longitudinal and time correlations in turbulent flow—1380
Fried, Burton David. Electron-neutron interaction as deduced from pseudoscalar meson theory—1142
Friedland, Stephen S. and Henry S. Katzenstein. Deterioration of self-quenching counters—168(A)
Froehlich, Fritz E. and Kurt Sitte. Interaction mean free path of π-mesons in Pb—169(A)
Froman, Darol. Nuclear transparency and nucleon cross section for penetrating-shower producing cosmic radiation—172(A)
Frosch, R. A. and H. M. Foley. Magnetic hfs in diatomic molecules—1337
Frost, A. D., C. R. Mingins, and R. W. Perry. Equivalent electrical network of quartz plate used as filter—154(A)
Frost, R. H. (see Nielsen, C. E.)—165(A)
Fry, W. F. (see Ebel, M. E.)—1306
Fujimura, Tadao (see Okamura, Toshiko)—1435(L)
Fulbright, H. W., J. A. Bruner, D. A. Bromley, and L. M. Goldman. Angular distributions of protons and tritons from deuteron-induced reactions on Be^9—700
Fultz, S. C., R. J. Nash, R. L. Woodward, and M. L. Pool. Radiations of Rh^{69} and Ga^{67}—170(A)

Gallagher, C. J. Plastic deformation of Ge and Si—721
Gallaher, L. J. and W. B. Cheston. Angular correlation in $(d,p\gamma)$ reactions—684(L)
Gammel, J. L. (see Dodder, D. C.)—520
Gates, David M., Robert F. Calfee, and Byron E. Cohn. Spectral solar energy in near infrared—157(A)
—— (see Calfee, Robert F.)—157(A)
Ghiorso, A. (see Fleming, E. H., Jr.)—642
Giamboni, Louis A. (see Barnett, S. J.)—28
Gilbert, F. C. and Stirling A. Colgate. Annihilation of positrons in flight at 100 and 200 Mev—164(A)
—— (see Barkas, Walter H.)—1435(L)
Gilbert, W. S. and J. W. Rosengren. Deuteron photodisintegration at high energies—901
Gilmore, Earl H. Spectral distribution of energy in fluorescence of Na fluorescein—174(A)
Glenn, Howard B. Reaction $Li^6(\gamma,d)He^4$ at 2.76 Mev—418(L)
Glick, H. L. (see Halteman, E. K.)—1205(L)
Gluckstern, R. L. (see McIntosh, J. S.)—752
Goad, Walter. Cosmic radiation at great depths—169(A)
Goldberg, Colman. Acceptors produced in Ge by quenching from high temperatures—920
Goldberg, E. Low-lying levels of Al^{28} observed from $Mg^{24}(d,\alpha)Al^{28}$—159(A)
—— (see Kaufmann, S. G.)—673
Goldberg, M. D. (see Hughes, D. J.)—163(A)
Goldfarb, L. J. B. and D. Feldman. High energy $p-p$ scattering and associated polarization effects—1099
Goldman, L. M. (see Fulbright, H. W.)—700
Goldschmidt, G. (see Bishop, G. R.)—1432(L)
Goldwasser, E. L., F. E. Mills, and A. O. Hanson. Ionization loss and straggling of fast electrons—1137
Good, R. H., Jr. (see Miller, Stanley C., Jr.)—160(A)
Goodman, Leonard S. Total cross sections for 14-Mev neutrons—686(L)
Goodwin, Aurel, Jr., and Mario Iona. Temperature effect on counting rate of B neutron counters—168(A)
Gora, E. Lower limits for interaction times in photon scattering processes—1212(L)
Gorter, C. J. Heat pulses in He II below 1°K—681(L)
Grantham, G. E. Use of the Zidicon tube with television to illustrate small-scale effects—1216(T)
Graves, A. C. Physics and atomic-bomb tests—167(T)
Graves, E. R. (see Coon, J. H.)—162(A); 562
—— (see Phillips, D. D.)—600
Graves, G. A., L. M. Langer, and R. D. Moffat. K/L internal conversion ratio in $M4$ transitions—169(A); 344
Graves, J. D., W. R. Ketler, and R. I. Condit. Atmospheric ion monitor—157(A)
Green, H. S. and H. Messel. Spread of soft component of cosmic radiation—331
——, **H. Messel, and B. A. Chartres.** Angular distribution functions for high energy cosmic-ray particles—1277
Greene, Richard F. and Herbert B. Callen. Theorem of irreversible thermodynamics. II—1387
Greenwood, Allan. Pulse-free discharges in negative point-to-plane corona—91
Griswold, T. W., A. F. Kip, and C. Kittel. Microwave spin resonance absorption by conduction electrons in metallic Na—951(L)
Gross, E. P. Effective mass of electrons in polar crystals—153(A)
Guernsey, Gordon L., G. Mott, and B. K. Nelson. Differential $n-p$ scattering cross section for 220-Mev neutrons—15
—— (see Mott, George R.)—9
—— (see Nelson, B. K.)—1
Günther, Marian. Relativistic configuration space formulation of multi-electron problem—1411
Gurney, Ronald W. Lattice vibrations in graphite—465
—— Scattering of slow neutrons in polycrystalline media—466
Guttman, Lester (see Stout, J. W.)—703; 713

Hahn, E. L. and D. E. Maxwell. Spin echo measurements of nuclear spin coupling in molecules—1070

Halban, H. (see Bishop, G. R.)—1432(L)
Hall, D. B. Los Alamos fast reactor and its experimental use—176(T)
Hall, R. N. $p-n$ junctions produced by growth rate variation—139(L)
—— Recent developments in $p-n$ junction transistors—1215(T)
Halliday, David (see Wheatley, John)—424(L)
Halpern, J., A. K. Mann, and R. Nathans. (γ,pn) reaction in P—958(L)
——, **R. Nathans, and A. K. Mann.** Photon absorption cross sections in Bi and Ta—679(L)
Halpern, Otto. Magnetic quenching of three-quantum annihilation of positronium—164(A)
—— Multiple scattering of neutrons. III. Scattering by spin-dependent forces and polarization phenomena—232
—— Neutron optics—1003
Halsted, Richard E. Atomic masses from Pd through Xe—666
Halteman, E. K., G. F. Mechlin, and H. L. Glick. Isothermal ordering of Cu_3Au at 200°C—1205(L)
Hamermesh, Bernard and Virginia Hummel. Neutron capture γ-ray spectra from elements $Z=17$–30 and $Z=45$–57—916
Hanna, S. S. (see Fagg, L. W.)—1205(L)
Hansler, R. L. (see Bell, E. E.)—174(A)
Hanson, A. O. (see Goldwasser, E. L.)—1137
Harmon, N. F. (see Annis, M.)—1202(L)
Harned, Boyd W. and Willard H. Bennett. Efficiencies of multiple ionization of Hg—165(A)
Harrick, N. J. and N. F. Ramsey. Rotational magnetic moment, magnetic susceptibilities, and electron distribution in H_2—228
Harth, Erich M. Photoproduction of isomeric pair of Br^{80}—170(A)
Harvey, J. A. Inelastic scattering of 7.7-Mev protons—162(A)
—— (see Hughes, D. J.)—163(A)
Haskin, D. M. (see Lord, J. J.)—172(A)
Haskins, J. R., J. E. Duval, L. S. Cheng, and J. D. Kurbatov. Radioactivity of Sc^{43}—876
—— **and J. D. Kurbatov.** Disintegration of I^{131}—884
—— (see Elliott, M. W.)—263
Hausman, H. J., A. J. Allen, J. S. Arthur, R. S. Bender, and C. J. McDole. Energy levels in Mg, V, Cr, and Mn—1296
—— (see Arthur, J. S.)—1291
Havens, W. W., Jr. (see Block, M. M.)—1239
—— (see Bramson, H. J.)—304
—— (see Durbin, R. P.)—179
—— (see Loar, H.)—168(A)
—— (see Passman, S.)—1247
—— (see Smith, R. R.)—163(A)
Henderson, J. W. (see Marx, J. W.)—106
Henderson, W. J. (see Ovadia, J.)—165(A)
Henley, E. M. (see Drell, S. D.)—1053
Henry, Warren E. Anomalous paramagnetism of $CuSO_4\cdot 5H_2O$—166(A)
—— Spin paramagnetism of Cr^{+++}, Fe^{+++}, and Gd^{+++} at liquid He temperatures and in strong magnetic fields—559
Henshaw, C. L. Demonstrations of (a) random molecular motion, and (b) motor and generator—1216(T)
Herman, Frank. Electronic structure of diamond crystal—1210(L)
Herring, Conyers and Charles Kittel. Theory of spin waves in ferromagnetic media, erratum—1435(L)
Hershberger, W. D. and H. N. Leifer. Paramagnetic resonance in phosphors—714
Hibdon, C. T. and C. O. Muehlhause. Internal conversion of neutron capture γ-rays—943
Hiby, J. W. and M. Pahl. Influence of binary collisions on molecular gas flow—414(L)
Hill, R. D. Dependence of γ-radiation lifetimes on nucleon configurations—1428(L)
—— (see Swan, J. B.)—171(A); 831
Hincks, E. P. and W. E. Bell. Lifetimes of μ^--meson stopped in light elements—results—168(A)
—— (see Bell, W. E.)—168(A); 1424(L)
Hintz, Norton M. and Norman F. Ramsey. Excitation functions to 100 Mev—19
Hoerlin, Herman and Frank Kaszuba. Wavelength independent photographic dosimeter employing terphenyl intensifying screens—174(A)
Hofstadter, Robert (see Hudson, Alvin)—589
Holmes, John R. (see Parker, Lee W.)—174(A)
Holmgren, H. D. (see Brown, R. J. S.)—253
Holstein, T. Optical and infrared reflectivity of metals at low temperatures—1427(L)
Honkonen, David L. (see Combes, Lewis S.)—153(A)
Hopkins, N. J. Isomeric levels in Pb^{201} and Pb^{203}—680(L)
Horowitz, M., A. A. Silvidi, S. F. Malaker, and J. G. Daunt. Specific heat of Pb in temperature range 1°K to 75°K—1182
Houston, J. M. Slope of logarithmic plots of Fowler-Nordheim equation—349
Houston, W. V. Temperature dependence of electrical resistance—1321
Howard, L. A. (see Mingins, C. R.)—154(A)
Howell, Barton J. Table model computer for Fourier synthesis—160(A)
Hoyt, Harry C. Precision measurement of annihilation radiation and decay schemes of Ta^{182} and Ir^{192}—176(T)
—— (see Muller, David E.)—775
Huang, Su-Shu. Variational method for problems of neutron diffusion and of radiative transfer—50
Huddleston, Charles M. and Allan C. G. Mitchell. Nuclear spectra of Rb^{83} and Rb^{84}—1350
Hudson, Alvin and Robert Hofstadter. Energy loss of cosmic-ray μ-mesons in NaI crystals—589
Hudson, A. M. (see Allred, J. C.)—425
Hudson, Ralph P. Properties of Cr^{+++} ion in paramagnetic alums at low temperatures—570
Hughes, D. J., J. A. Harvey, and M. D. Goldberg. Mirror measurement of neutron-electron interaction—163(A)
Hughes, Ray C. and Patrick P. Coppola. Conductivity of oxide emitters—364
Huizenga, John R. and Robert B. Duffield. Fission to capture cross section ratio—959(L)
Hummel, Virginia (see Hamermesh, Bernard)—916
Hung, C. S. (see Baum, R. M.)—134(L)
Hurst, D. G. (see Brockhouse, B. N.)—542
Hutchinson, D. R. and M. L. Wiedenbeck. Reinvestigation of radioactivity of Sb^{124}—699
Hutchison, D. A. (see Smaller, B.)—414(L)

Iona, Mario (see Goodwin, Aurel, Jr.)—168(A)
Israel, Harvey I. Soft radiation from Pu^{239}—682(L)
Ivey, Henry F. Color centers generated in NaCl by electrolysis—1434(L)

Jackson, Julius L. (see Callen, Herbert B.)—1382
Jacobs, Harold, John Freely, and Frank A. Brand. Mechanism of field dependent secondary emission—492
Jaffe, George. Diffusion of neutrons—603
Jaffe, Hans (see Cook, W. R., Jr.)—1426(L)
Jakobson, Mark J. (see White, R. Stephen)—836
James, N. R., S. Legvold, and F. H. Spedding. Resistivity of La, Ce, Pr, and Nd at low temperatures—1092
James, Ralph A. (see Tewes, Howard A.)—860
Janzen, H. Absorption of high energy x-rays in various materials—653
Jentschke, W. K. (see Remley, M. E.)—162(A)

Jesse, William P. and John Sadauskis. α-particle ionization in mixtures of noble gases—417(L)
Johnson, Walter H., Jr. Mass of K^{40}—1213(L)
Jones, G. A. and D. H. Wilkinson. $Li^7(\alpha,\gamma)B^{11}$ and states of B^{11}—423(L)
Jones, K. W. (see Craig, D. S.)—808
Jones, L. M. Gravitational separation in upper atmosphere —176(T)
Jones, W. H. (see Fowler, J. L.)—71
Jost, Res and Walter Kohn. Equivalent potentials—382

Kac, M. and J. C. Ward. Combinatorial solution of the 2-dimensional Ising model—1332
Kachickas, G. A. and L. H. Fisher. Formative time lags of uniform field breakdown in N_2—878
Kalos, M. H. and J. M. Blatt. Lateral structure of electronic showers in air—173(A)
Kaplan, Joseph and Marx Brook. Recombination processes in O_2—157(A)
Kaplon, M. F. and D. M. Ritson. Emulsion cloud chamber observations on interactions of high energy primary cosmic radiation—386
Kaszuba, Frank (see Hoerlin, Herman)—174(A)
Katzenstein, Henry S. (see Friedland, Stephen S.)—168(A)
Kauffman, J. W. and J. S. Koehler. Quenching in of lattice vacancies in pure Au—149(L)
Kaufmann, S. G., E. Goldberg, L. J. Koester, and F. P. Mooring. Energy levels in Si^{28} excited by α-particles on Mg^{24}—673
Keck, James and Raphael Littauer. Production of photo-mesons in D—139(L)
Keepin, G. R. (see Stratton, W. R.)—257
Keesom, P. H. and N. Pearlman. Anomaly in low temperature atomic heat of Ag—140(L)
—— (see Pearlman, N.)—397
Keffer, Frederic. Spin-spin relaxation in ferromagnetic resonance—686(L)
Kennedy, William B. Wind and temperature measurements above lower isothermal region of atmosphere by acoustic propagation studies (July 1950–May 1951)—158(A)
Ketler, W. R. (see Graves, J. D.)—157(A)
Kikuchi, C., M. H. Sirvetz, and V. W. Cohen. Nuclear spin of V^{50} by paramagnetic resonance—142(L)
Kim, Y. B. (see Salvini, G.)—40
King, J. I. Radiative transfer and equilibrium associated with far infrared bands in atomsphere—157(A)
King, J. S. and W. C. Parkinson. Further test of shell model —141(L)
King, K. M. (see Davis, K. E.)—368
Kip, A. F. (see Griswold, T. W.)—951(L)
Kissinger, C. W. (see Perlow, G J.)—321
Kittel, Charles (see Abrahams, Elihu)—1200(L)
—— (see Griswold, T. W.)—951(L)
—— (see Herring, Conyers)—1435(L)
Klein, David J. (see Muller, David E.)—775
Kloepper, Robert M., E. S. Lennox, and M. L. Wiedenbeck. Angular and direction-polarization correlation for Co^{60}, Cs^{134}, and Sb^{124}—695
Koehler, J. S. (see Kauffman, J. W.)—149(L)
Koehler, W. F. Multiple-beam interferometric study of topaz cleavage faces and polished glass surfaces—175(A)
Koenig, Seymour H., A. G. Prodell, and P. Kusch. Anomalous magnetic moment of the electron—191
—— (see Franken, Peter)—199
Koester, L. J. (see Kaufmann, S. G.)—673
Kohn, Walter (see Jost, Res)—382
Kojima, Yuzo (see Okamura, Tosihiko)—1425(L)
Konopinski, E. J. (see Mahmoud, H. M.)—1266
Kramish, Arnold. Spontaneous fission *vs* α-decay—1201(L)
Kraushaar, J. J. (see Church, E. L.)—419(L)
Kretschmar, George G. and Henry W. Wedaa. Study of impinging liquid jets in liquid stream—161(A)
Kroll, Norman M. and Leslie L. Foldy. Effect of charge symmetry on nuclear reactions—1177
Kruger, P. G. (see Remley, M. E.)—162(A)
Kundu, D. N. (see Donaven, T. W.)—158(A)
—— (see Long, John K.)—171(A)
Kurath, D. States of light nuclei from *jj*-coupling model—804
Kurbatov, J. D. (see Cheng, L. S.)—887
—— (see Elliott, M. W.)—263
—— (see Haskins, J. R.)—876; 884
Kurşunoğlu, Behram. Gravitation and electrodynamics—1369
Kurti, N. (see Bishop, G. R.)—1432(L)
Kusch, P. (see Koenig, S. H.)—191
—— (see Prodell, A. G.)—184

Langer, L. M. and R. J. D. Moffat. β-spectrum of T and mass of neutrino—169(A); 689
—— (see Graves, G. A.)—169(A); 344
Laquer, Henry L. and Adam F. Schuch. Low temperature thermal expansion of U—166(A)
Larson, G. A. (see McDonough, R. R.)—154(A)
Laughlin, J. S. (see Ovadia, J.)—165(A)
Lauritsen, T. (see Thomas, R. G.)—969
Lax, Melvin and Herman Feshbach. Photoproduction of mesons in D—509
LeBlanc, J. M. (see Cork, J. M.)—685(L)
Lee, Robert J. (see Fowler, Richard G.)—137(L)
Lee, Tsung-Dao and David Pines. Motion of slow electrons in polar cyrstals—960(L)
Lees, J. F. (see Cwilong, B. M.)—138(L)
Legvold, S. (see James, N. R.)—1092
Leifer, H. N. (see Hershberger, W. D.)—714
Lennox, E. S. (see Kloepper, Robert M.)—695
Lepore, Joseph V. Symmetrical pseudoscalar meson theory of nuclear forces—750
Levine, Morton A. Measurements of lateral distribution of extensive air showers—154(A)
—— **and Winston H. Bostick.** Probe technique for measuring ion densities in afterglow of pulsed discharge—153(A)
—— (see Bostick, Winston H.)—153(A)
Levy, Maurice M. Meson theory of nuclear forces and low energy properties of $n-p$ system—725
—— Non-adiabatic treatment of relativistic two-body problem—72
Lewis, H. W. and G. H. Wannier. Spherical model of a ferromagnet—682(L)
Li, C. W. Nuclear mass determinations from disintegration energies; O to S—1038
Libby, W. F. (see Sugihara, T. T.)—587
Lillie, A. B. (see Bonner, T. W.)—162(A); 473
Lindenbaum, S. J. (see Bernardini, G.)—1017
Lindner, M. and R. N. Osborne. Nuclides Ba^{137}, Ba^{133}, and Cs^{132}—1422(L)
Lindström, Gunnar (see Slätis, Hilding)—1429(L)
Littauer, Raphael (see Keck, James)—139(L)
Livingston, M. Stanley (see Courant, Ernest D.)—1190
Lloyd, Stuart P. Explicit $\gamma-\gamma$ angular correlations. II. Polarization correlations—906
Loar, H. H. (see Durbin, R. P.)—179
Logan, John K. and Jules A. Marcus. Hall effect in Zn crystals at low temperatures—1234
Long, John K., M. L. Pool, and D. N. Kundu. Radioactivity of Pm^{143}, Pm^{145}, Pm^{146}, Pm^{149}, and Sm^{146}—171(A)
—— (see Donaven, T. W.)—158(A)
Lord, J. J., D. M. Haskin, and Marcel Schein. Narrow angle pairs from nuclear disintegrations—172(A)
—— (see Backus, Meera)—169(A); 1431(L)
Lovberg, R. H. (see Yarnell, J. L.)—158(A)

Low, Francis. Natural line shape—53
Lucy, F. A. (see Willig, F. J.)—161(A)

Ma, S. T. Bound states and interaction representation—1211(L)
MacDonald, A. D. High frequency breakdown in Ne—420(L)
MacDonald, D. K. C. Minimum of electrical resistance at low temperatures—148(L)
—— **and W. B. Pearson.** Residual resistance in dilute Cu alloys—149(L)
MacDonald, J. C. F. (see Chisholm, D. A.)—957(L)
MacLeod, D. W. (see McDonough, R. R.)—154(A)
Madansky, Leon (see Robinson, Berol L.)—1065
Magnusson, L. B. (see Wagner, F., Jr.)—171(A)
Mahmoud, H. M. and E. J. Konopinski. Evidence of once-forbidden spectra for law of β-decay—1266
Malaker, S. F. (see Horowitz, M.)—1182
Manchester, F. D. (see Cwilong, B. M.)—138(L)
Mandeville, C. E., E. Shapiro, R. I. Mendenhall, E. R. Zucker, and G. L. Conklin. γ-rays from Sn^{125}—554
Mann, A. K. (see Halpern, J.)—679(L); 958(L)
Manning, L. A. Study of upper atmospheric winds by echo methods—176(T)
Marable, James H. (see Brittin, Wesley E.)—160(A)
Marcus, Jules A. (see Logan, John K.)—1234
Marcus, Paul M. Free energies and phase transition of cylindrical superconductor—373
Margolis, B. Neutron capture cross section—327
Marion, J. B. (see Davis, K. E.)—368
Markham, Jordan J. Speculation on formation of *F*-centers during irradiation—500
—— (see Duerig, William H.)—1043
Marquez, Luis. Spallation of Cu with high energy neutrons—225
Marshak, R. E. *S*-wave in pion-nucleon scattering—1208(L)
—— (see Messiah, A. M. L.)—678(L)
—— (see Van Hove, L.)—1208(L)
Marshall, J. F. Theory of secondary emission—416(L)
Marshall, J., L. Marshall, V. A. Nedzel, and S. D. Warshaw. π^0-production cross section for 430-Mev protons on H and Be—632
Marshall, L. (see Marshall, J.)—632
Marx, J. W., H. G. Cooper, and J. W. Henderson. Radiation damage and recovery in Cu, Ag, Au, Ni, and Ta—106
Masket, A. V. (see Brown, F. B., Jr.)—1204(L)
Mason, W. P. Properties of tetragonal antiferroelectric crystal—480
—— **and B. T. Matthias.** Piezoelectric, dielectric, and elastic properties of $ND_4D_2PO_4$ (heavy water ADP)—477
Mather, K. B. $p-d$ scattering at 5.1 Mev and $d-p$ scattering at 10.2 Mev—1408
Matthias, B. T. (see Mason, W. P.)—477
Maxwell, D. E. (see Hahn, E. L.)—1070
Maxwell, E. Similarity properties of the two-fluid model of superconductivity, erratum—1434(L)
McCarthy, Kathryn A., Stanley S. Ballard, and Edward C. Doerner. Thermal conductivity of sapphire and rutile as function of temperature—153(A)
McCasker, C. B. A., H. Messel, D. D. Millar, and N. A. Porter. Experimental investigation of nucleon cascade in water—1216(A)
McDole, C. J. (see Arthur, J. S.)—1291
—— (see Hausman, H. J.)—1296
McDonough, R. R., D. W. MacLeod, and G. A. Larson. Stepped-surface piezoelectric filters—154(A)
McGeer, P. L., A. J. Curtis, G. B. Rathmann, and C. P. Smyth. Microwave absorption and dielectric relaxation in long-chain esters—174(A)
McGuire, A. D. (see Camac, M.)—134(L)
McIntosh, J. S., R. L. Gluckstern, and S. Sack. $p-T$ interaction—752
McMichael, B. D. and S. Mrozowski. Frequency response of PbS cells—1216(A)
McNish, A. G. Lunar tides in ionosphere—176(T)
McReynolds, A. W. Neutron monochromator crystals—Fe_3O_4 and Ge—958(L)
Meadows, J. W. High energy nuclear reactions and Goldberger model—143(L)
Mechlin, G. F. (see Halteman, E. K.)—1205(L)
Mei, J. Y. and E. Pickup. Close pairs of tracks in showers in emulsions—172(A)
Mendenhall, R. I. (see Mandeville, C. E.)—554
Merz, Walter J. Domain properties in $BaTiO_3$—421(L)
Messel, H. and R. B. Potts. Plural theories for shower component in high energy nuclear disintegrations—488
—— (see Green, H. S.)—331; 1277
—— (see McCasker, C. B. A.)—1216(A)
Messiah, A. M. L. Very long lifetime of C^{14} β-decay—151(L)
—— **and R. E. Marshak.** X-rays from π-mesic atom—678(L)
Metzger, Franz R. Disintegration scheme of Fe^{55}—1360
—— **and H. C. Amacher.** Internal conversion of Sr^{88} γ-rays—147(L)
Mihelich, J. W. Probability of internal conversion of *K*-series radiation of Au arising from interaction of *L* sub-shells—415(L)
Mileikowsky, Curt and Ward Whaling. Reaction energies of $Ne^{21}(d,\alpha)F^{19}$ and $Ne^{21}(d,p)Ne^{22}$ from magnetic analysis—1254
Millar, D. D. (see McCasker, C. B. A.)—1216(A)
Miller, D. W., R. K. Adair, C. K. Bockelman, and S. E. Darden. Total cross sections of heavy nuclei for fast neutrons—83
Miller, Maurice M. Excited levels in Ti^{48}—516
Miller, Stanley C., Jr., and R. H. Good, Jr. WKB method—160(A)
Mills, F. E. (see Goldwasser, E. L.)—1137
Mills, Robert G. Low pressure cloud chamber investigation of range-energy relations—168(A)
Mingins, C. R., S. Bartnoff, and L. A. Howard. High frequency electromechanical filters—154(A)
—— (see Frost, A. D.)—154(A)
Mitchell, Allan C. G. (see Huddleston, Charles M.)—1350
—— (see Smith, Alan B.)—150(L)
Mobley, R. C. Proposed method for producing short intense monenergetic ion pulses—360
Moffat, R. D. (see Graves, G. A.)—169(A); 344
—— (see Langer, L. M.)—169(A); 689
Mooring, F. P. (see Kaufmann, S. G.)—673
Morrison, H. L. and G. J. Plain. Minimum temperature gradient required for formation of tracks in cloud-ion chamber—167(A)
—— (see Rogers, F. T., Jr.)—161(A)
—— (see Plain, G. J.)—170(A); 177(A)
Moshinsky, Marcos. Diffraction in time—625
Mott, George R., Gordon L. Guernsey, and Bruce K. Nelson. Total cross sections of C and H for high energy neutrons—9
—— (see Guernsey, G.)—15
—— (see Nelson, B. K.)—1
Mousuf, A. K. K^{40} radioactive decay: its branching ratio and its use in geological age determinations—150(L)
Mrozowski, S. (see McMichael, B. D.)—1216(A)
Muehlhause, C. O. (see Hibdon, C. T.)—943
Muller, David E., Harry C. Hoyt, David J. Klein, and Jesse W. M. DuMond. Precision measurements of nuclear γ-ray wavelengths of Ir^{192}, Ta^{182}, RaTh, Rn, W^{187}, Cs^{137}, Au^{198}, and annihilation radiation—775

Nakabayasi, K. and I. Sato. Nuclear forces in pseudoscalar meson theory—144(L)
Nash, R. J. (see Fultz, S. C.)—170(A)
Nathans, R. (see Halpern, J.)—679(L); 958(L)
Naugle, J. E. High energy nuclear interaction—172(A)
Navon, D., Ralph Bray, and H. Y. Fan. Lifetime of injected carriers in Ge—165(A)
Nedzel, V. A. (see Marshall, J.)—632
Nelson, Bruce K., G. Guernsey, and G. Mott. Neutron energy distributions from Be, C, and Pb bombarded by 245-Mev protons—1
—— (see Guernsey, G.)—15
—— (see Mott, George R.)—9
Nelson, Raymond A. and William Band. Vapor pressure of He^3-He^4 mixtures—1431(L)
Nereson, Norris. Fission neutron spectrum of Pu^{239}—823
Nester, W. H. (see Cork, J. M.)—685(L)
Neugebauer, Hans J. Clausius-Mosotti equation for anisotropic crystals—1210(L)
Newell, H., Jr. Atmospheric temperatures and pressures at high altitudes—176(T)
Newhall, H. S. Demonstrations of 2 simple electrical experiments: (a) power transmission line and (b) damped oscillations in RLC circuit—1216(T)
Nielsen, C. E., R. H. Frost, and W. J. Choyke. Average energy loss per ion pair of slow electrons in He—165(A)
—— (see Choyke, W. J.)—167(A)
Nowick, A. S. Anelastic measurements of atomic mobility in substitutional solid solutions—925
Noyes, H. P. and H. G. Camnitz. Interference between Coulomb and nuclear scattering in $p-p$ collisions at 240 Mev—1206(L)

Odell, N. H. (see Taylor, W. E.)—867
Odencrantz, F. K. α-particle bombardment of PbS semiconductors—166(A)
Oetjen, R. A. (see Bell, E. E.)—174(A)
Okamura, Tosihiko, Tadao Fujimura, and Muneyuki Date. Dielectric constant and permeability of various ferrites in microwave region erratum—1435(L)
——, **Yosiharu Torizuka, and Yuzo Kojima.** g-factor of ferrites—1425(L)
Olds, R. H. and G. B. Shook. Mathematical studies of thermal processes relating to reaction rates in solid fuels—166(A)
—— (see Shook, G. B.)—166(A)
Osborne, M. F. M. Number theory and magnetic properties of electron gas—438
Osborne, R. N. (see Lindner, M.)—1422(L)
Ovadia, J., J. S. Laughlin, J. W. Beattie, and W. J. Henderson. Total specific ionization in air, A, and H from 17.5-Mev electrons—165(A)

Packard, Martin E. and Harry E. Weaver. Nuclear relaxation time of H_2 gas—163(A)
Paehler, J. H. (see Fowler, J. L.)—71
Pahl, M. (see Hiby, J. W.)—414(L)
Pais, A. (see Van Hove, L.)—1211(L)
Palmatier, E. D. Electronic component at low altitudes produced by π-meson decay—761
Parker, E. N. Application of generalization of Heisenberg's model of turbulence to critical Reynold's numbers—161(A)
Parker, Lee W. and John R. Holmes. Survey of isotope shift in O I—174(A)
Parkinson, W. C. (see King, J. S.)—141(L)
Passman, S., M. M. Block, and W. W. Havens, Jr. Excitation function for charged π-meson production in H and C by 345-Mev protons—1247
—— (see Block, M. M.)—1239
Pearlman, N. and P. H. Keesom. Atomic heat of Si below 100°K—397
—— (see Keesom, P. H.)—140(L)
Pearson, W. B. (see MacDonald, D. K. C.)—149(L)
Pease, Robert L. and Herman Feshbach. Theory of H^3—945
Peaslee, D. C. Photon-induced reactions—812
Pellam, John R. and Bernard Weinstock. Rayleigh disk measurements in He^3-He^4 mixtures—162(A)
Perlman, I. (see Asaro, Frank)—129; 828
Perlman, M. M. and M. Bloom. Nuclear resonance modulation correction—1290
Perlow, G. J., L. R. Davis, C. W. Kissinger, and J. D. Shipman, Jr. Rocket determination of ionization spectrum of charged cosmic rays at $\lambda = 41°$N—321
Perry, R. W. (see Frost, A. D.)—154(A)
Petch, H. E., G. M. Volkoff, and N. G. Cranna. Second order effects in nuclear electric quadrupole interaction of Al^{27} in spodumene—1201(L)
Peterson, Vincent (see Aamodt, R. Lee)—739
Phillips, D. D., R. W. Davis, and E. R. Graves. Inelastic collision cross sections for 14-Mev neutrons—600
Phillips, J. A., W. R. Arnold, G. A. Sawyer, E. J. Stovall, Jr., and J. L. Tuck. Absolute low energy cross section experiment—159(A)
—— (see Arnold, W. R.)—159(A)
—— (see Stovall, E. J., Jr.)—159(A)
—— (see Tuck, J. L.)—159(A)
Phillips, M. Perturbations of atomic g values—202
Phillips, Robert (see Aamodt, R. Lee)—739
Pickup, E. (see Allen, N. L.)—172(A)
—— (see Mei, J. Y.)—172(A)
Pieper, George F. Nuclear energy levels in 28-neutron shell region—1299
Pines, David (see Lee, Tsung-Dao)—960(L)
Plain, G. J. and H. L. Morrison. Use of radioactive vapor in continuously operating diffusion cloud chamber—177(A)
——, **H. L. Morrison, and F. T. Rogers, Jr.** Low energy portion of S^{35} β-spectrum—170(A)
—— (see Morrison, H. L.)—167(A)
Platt, J. B. (see Camac, M.)—134(L)
Pomerance, H. Thermal neutron capture cross sections—412
Pool, M. L. (see Donaven, T. W.)—158(A)
—— (see Fultz, S. C.)—170(A)
—— (see Long, John K.)—171(A)
Porter, Fred T. and C. Sharp Cook. Disintegration of Ce^{144} and Pr^{144}—170(A)
Porter, N. A. (see McCasker, C. B. A.)—1216(A)
Potter, R. M. (see Allred, J. C.)—425
Potts, R. B. Spontaneous magnetization of a triangular Ising lattice—352
—— (see Messel, H.)—488
Pratt, George W., Jr. Wave functions and energy levels for Cu^+ as found by Slater approximation to Hartree-Fock equations—1217
Preston, M. A. and M. F. Duret. Coupling constant of nucleon-μ-meson interaction—1425(L)
Preston, W. M. (see Stelson, P. H.)—1354
Preston-Thomas, H. Superconducting transition in Ta—325
Price, E. W. (see Wedaa, H. W.)—174(A)
Prodell, A. G. and P. Kusch. Hfs of H and D—184
—— (see Koenig, S. H.)—191
Pruett, Charles H. (see Roggenkamp, Paul L.)—1262
Pryor, M. J. Luminous lens-graph—1216(T)
Purcell, E. M. (see Carr, H. Y.)—415(L)

Rado, G. T., R. W. Wright, W. H. Emerson, and A. Terris. Ferromagnetism at very high frequencies. IV. Temperature dependence of magnetic spectrum of a ferrite—909
Ramsey, N. F. (see Harrick, N. J.)—228
—— (see Hintz, Norton M.)—19
Rankin, D. (see Stratton, W. R.)—257
Rathmann, G. B. (see McGeer, P. L.)—174(A)

Rawson, E. B. and R. Beringer. Atomic oxygen g-factors—677(L)
Ravenhall, D. G. (see Wolfenstein, L.)—279
Rediker, R. H. (see Bridge, H. S.)—206
Redlich, Martin. Discontinuities in binding energies of neutrons and protons in light nuclei—38
Regener, V. H. Experiments on penetrating cosmic-ray showers—167(T)
Reid, C. Scintillators and energy transfer processes—422(L)
Remley, M. E., W. K. Jentschke, and P. G. Kruger. $n-p$ scattering using organic crystal scintillation detectors—162(A)
Reynolds, F. W. and G. R. Stilwell. Mean free paths of electrons in evaporated metal films—418(L)
Reynolds, S. E. Thunderstorm-precipitation growth and electrical-charge generation—167(T)
Ribe, F. L. (see Battat, M. E.)—159(A)
Richardson, John M. Electron removal in Kr afterglows—895
Ridgway, S. L. (see Tomlinson, E. P.)—170(A)
Rinehart, John S. Scabbing of metals under explosive attack: Multiple scabbing—162(A)
Ritson, D. M. (see Kaplon, M. F.)—386
Robinson, Berol L. and Leon Madansky. Polarization correlations of γ-rays of Cs^{134} and of annihilation radiation—1065
Robinson, E. S. (see Allred, J. C.)—425
Robinson, F. N. H. (see Bishop, G. R.)—1432(L)
Rocket Panel. Pressures, densities, and temperatures in upper atmosphere—1027
Roe, Glenn M. Convergence of intermolecular force series—659
Rogers, F. T., Jr., and H. L. Morrison. Analog computation in theory for critical stability of fluid—161(A)
—— (see Plain, G. J.)—170(A)
Roggenkamp, Paul L., Charles H. Pruett, and Roger G. Wilkinson. Disintegration scheme of V^{48}—1262
Rosen, Louis. Measurements of neutron-spectra using nuclear emulsion techniques—176(T)
—— **and J. C. Allred.** $d-d$ elastic scattering at 10.5 Mev—431
—— (see Allred, J. C.)—425; 433
Rosen, Nathan. Interaction between electron and one-dimensional electromagnetic field, erratum—1434(L)
Rosenblum, E. S., E. F. Shrader, and R. M. Warner, Jr. Absorption of 5.3-Mev, 10.3-Mev, and 17.6-Mev γ-rays—612
Rosengren, J. W. (see Gilbert, W. S.)—901
Rosenzweig, Norbert. Configuration interaction between odd terms in Fe group—580
Ross, Marc. Evidence for non-additivity of nucleon moments in heavy nuclei—935
Rostoker, Norman. Interpretation of electron-inertia experiment for metals with positive Hall coefficients—952(L)
Rubinow, S. I. (see Feshbach, Herman)—484
Ruderman, Malvin A. π^+ to π^- ratio from proton bombardment of D—1427(L)
Russell, R. D. (see Collins, C. B.)—1275

Sachs, R. G. (see Brennan, J. G.)—824
Sack, S. (see McIntosh, J. S.)—752
Sadauskis, John (see Jesse, William P.)—417(L)
Salant, E. O. (see Blau, M.)—954(L)
Salpeter, E. E. Nuclear reactions in stars. I. $p-p$ chain—547
—— (see Baranger, M.)—680(L)
—— (see Butler, S. T.)—133(L)
Salvini, G. and Y. B. Kim. Production cross section and frequency of neutral mesons in cosmic rays—40
Sarfaty, Rika (see Anslow, Gladys A.)—154(A)
Sato, I. (see Nakabayasi, K.)—144(L)
Sawyer, G. A. (see Arnold, W. R.)—159(A)
—— (see Phillips, J. A.)—159(A)
—— (see Stovall, E. J., Jr.)—159(A)
—— (see Tuck, J. L.)—159(A)
Schein, Marcel (see Backus, Meera)—1431(L)
—— (see Lord, J. J.)—172(A)
Schlacks, L. K. (see Brolley, J. E., Jr.)—618
Schremp, E. J. Phase space of nonlocalizable elementary particle—161(A)
Schuch, Adam F. (see Laquer, Henry L.)—166(A)
Schulte, H. J. (see Camac, M.)—134(L)
Schulz, Alvin G. (see White, R. Stephen)—836
Seaborg, Glenn T. Activation energy for fission—1429(L)
Seed, J. and A. P. French. Angular correlations in $F^{18}(p,\alpha\gamma)O^{15}$—1007
Seeger, R. J. Shock-wave phenomena—175(T)
Segall, Benjamin (see Blair, John S.)—621
Seifert, A. M. (see Bramson, H. J.)—304
Seitz, Frederick. Plasticity of Si and Ge—722
Seliger, H. H. Backscattering of positrons and electrons—408
Sen, Hari K. Solar "enhanced radiation" and plasma oscillations—816
Shapiro, E. (see Mandeville, C. E.)—554
Shapiro, Maurice M. and Bertram Stiller. Ionization loss at relativistic velocities in nuclear emulsions—169(A)
Shipman, J. D., Jr. (see Perlow, G. J.)—321
Shockley, W. Interpretation of e/m values for electrons in crystals—953(L)
Shook, G. B. and R. H. Olds. Measurement of reaction rates for solids—166(A)
—— (see Olds, R. H.)—166(A)
Shrader, E. F. (see Rosenblum, E. S.)—612
Shreffler, R. G. (see Willig, F. J.)—161(A)
Shutt, R. P. (see Whittemore, W. L.)—1312
Silverman, A. and M. Stearns. Production of π^0 mesons by γ-rays on H—1225
—— (see Cocconi, G.)—1230
Silvidi, A. A. (see Horowitz, M.)—1182
Sirvetz, M. H. (see Kikuchi, C.)—142(L)
Sitte, Kurt. Collision cross sections in cosmic-ray interactions—172(A)
—— (see Froehlich, Fritz E.)—169(A)
Slätis, Hilding and Gunnar Lindström. Inherent half-width of K-conversion lines—1429(L)
Smaller, B., E. L. Yasaitis, E. C. Avery, and D. A. Hutchison. Spin-spin interaction in HD nuclear resonance—414(L)
Smith, A. (see der Mateosian, E.)—1186
Smith, Alan B., R. S. Caird, and Allan C. G. Mitchell. Experiments on Ge^{75} and Ge^{75m}—150(L)
Smith, J. R. (see Conner, J. P.)—158(A); 468
Smith, R. R., T. I. Taylor, and W. W. Havens, Jr. Paramagnetic neutron scattering cross section of various transition group ions at long neutron wavelengths—163(A)
Smith, T. S. and J. G. Daunt. Properties of superconductors below 1°K. III. Zr, Hf, Cd, and Ti—1172
—— (see Daunt, J. G.)—309
Smyth, C. P. (see McGeer, P. L.)—174(A)
Snyder, Hartland S. (see Courant, Ernest D.)—1190
Sommers, H. S., Jr. Vapor pressures of He^3–He^4 mixtures below λ-point—113
Sorrels, J. D. (see Duller, M. N.)—172(A)
—— (see Walker, W. D.)—173(A)
Spedding, F. H. (see James, N. R.)—1092
Spencer, L. V. Penetration and diffusion of x-rays: Calculation of spatial distributions by semi-asymptotic methods—793
Sperduto, A. and W. W. Buechner. Magnetic analysis of proton groups from $Na^{23}(d,p)Na^{24}$—574
—— (see Enge, H. A.)—963
Squire, William. Electronegativity and work function—1216(A)
Staras, H. Effect of scattering by turbulent atmosphere on received field deep in shadow region—167(T)

Stasch, B. H. Pupil-built apparatus for teaching Pascal's principle—1216(T)
Stearns, M. (see Silverman, A.)—1225
Steele, M. C. Application of theory of numbers to magnetic properties of free electron gas—451
Steffen, Rolf M. and W. Zobel. Angular correlation of γ-rays emitted from excited states of Cd^{114}—170(A)
Stelson, P. H. and W. M. Preston. Total neutron cross section of Na—1354
Stephens, W. E. and M. E. Toms. Photoprotons from heavy elements—160(A)
Sternheimer, R. M. Density effect for ionization loss in various materials—851
Stier, P. M. and G. E. Evans. Range-energy relation for heavy ions—164(A)
—— (see Evans, G. E.)—165(A)
Stiller, Bertram (see Shapiro, Maurice M.)—169(A)
Stilwell, G. R. (see Reynolds, F. W.)—418(L)
Stout, J. W. and Lester Guttman. Electrical resistivity of In-Tl solid solutions—713
—— **and Lester Guttman.** Superconductivity of In-Tl solid solutions—703
Stovall, E. J., Jr., W. R. Arnold, J. A. Phillips, G. A. Sawyer, and J. L. Tuck. TD cross sections 15–125 kev—159(A)
—— (see Allred, J. C.)—425
—— (see Arnold, W. R.)—159(A)
—— (see Phillips, J. A.)—159(A)
—— (see Tuck, J. L.)—159(A)
Stratton, T. F. and George D. Freier. Angular distribution of α-particles from $d-T$ reactions—261
—— (see Stratton, W. R.)—257
—— (see Yarnell, J. L.)—158(A)
Stratton, W. R., G. D. Freier, G. R. Keepin, D. Rankin, and T. F. Stratton. Elastic scattering of deuterons by tritons —257
—— (see Brown, R. J. S.)—253
—— (see Yarnell, J. L.)—158(A)
Stumpf, F. B. (see Cork, J. M.)—685(L)
Sugihara, T. T. and W. F. Libby. Negative pion activation of Br—587
Suhl, H. and L. R. Walker. Faraday rotation of guided waves, erratum—1435(L)
Swan, J. B. and R. D. Hill. Radioactivity of Os—171(A)
—— **and R. D. Hill.** Radioisotopes of Os—831
Swartz, J. C. and J. W. Trischka. Rf spectra of Li^6F^{19} by molecular beam method—1085

Taft, E. A. (see Apker, L.)—58; 1037
Taylor, H. L. (see Bonner, T. W.)—162(A)
Taylor, T. I. (see Smith, R. R.)—163(A)
Taylor, W. E., N. H. Odell, and H. Y. Fan. Grain boundary barriers in Ge—867
Templeton, D. H. (see Castner, Stanley V.)—1126
Terris, A. (see Rado, G. T.)—909
Tessman, Jack R. Parallel susceptibility of an antiferromagnet at low temperatures—1132
Tetenbaum, S. J. 6-mm spectra of OCS and N_2O—772
Tewes, Howard A. and Ralph A. James. Proton induced reactions of Th—fission yield curves—860
Thaler, R. M. (see Breit, G.)—1214(L)
Thie, Joseph A. Photomesons from the deuteron—420(L)
Thomas, L. H. Use of large-scale computing in physics—1215(T)
Thomas, R. G. Analysis of the energy levels of mirror nuclei, C^{13} and N^{13}—1109
—— **and T. Lauritsen.** Magnetic lens spectrometer measurements of radiations from light nuclear reactions—969
Thomson, Alice and Peter G. Bergmann. Generalized statistical mechanics and Onsager relations—1216(A)
Thomson, D. M. Evidence for new level in Be^7—954(L)
Thomson, Robert and Peter G. Bergmann. Spin and angular momentum in general theory of relativity—1216(A)
Ticho, Harold K. Absorption mean free path of large hard showers in air—236
Tomboulian, D. H. (see Brown, B. M.)—1158
Tomlinson, E. P. and S. L. Ridgway. β-spectrum of As^{76}—170(A)
Toms, M. E. (see Stephens, W. E.)—160(A)
Tongiorgi, V. Cocconi and D. A. Edwards. Neutrons produced in absorption of negative π-mesons at rest—145(L)
Torizuka, Tosiharu (see Okamura, Tosihiko)—1425(L)
Transistor Teachers Summer School. Experimental verification of relationship between diffusion constant and mobility of electrons and holes—1368
Trischka, J. W. (see Swartz, J. C.)—1085
Tuck, J. L., W. R. Arnold, J. A. Phillips, G. A. Sawyer, and E. J. Stovall, Jr. He^3D cross sections 35–100 kev—159(A)
—— (see Arnold, W. R.)—159(A)
—— (see Phillips, J. A.)—159(A)
—— (see Stovall, E. J., Jr.)—159(A)
Twiss, R. Q. Propagation in electron-ion streams—1392

Udelson, Burton J. and John E. Creedon. Comparison of electron density in different regions of dc glow discharge—145(L)
Urey, Harold C. Abundances of elements—248

Van Allen, J. A. Distribution of atmospheric O_3 between 25- and 65-km altitude—176(T)
Van Hove, Leon. Coulomb effects in pion scattering by protons under charge independence hypothesis—1358
——, **R. Marshak, and A. Pais.** Charge independence and multiple pion production—1211(L)
Varney, Robert N. Drift velocities of ions in Kr and Xe—362
Vidale, Marcello L. Intensity of soft and hard component of cosmic radiation as function of altitude at geomagnetic latitudes of 28°N, 41°N, and 55°N—266
Violet, Charles E. (see Barkas, Walter H.)—1435(L)
Volkoff, G. M. (see Petch, H. E.)—1201(L)
Voyvodic, L. Mass determinations of fast cosmic-ray particles in emulsions—171(A)

Wada, W. W. Scattering of charge symmetric pseudoscalar mesons by nucleons—1032
Wagner, F., Jr., M. S. Freedman, D. W. Engelkemeir, and L. B. Magnusson. Radiations of Bi^{212}, Pb^{209}, and Tl^{202}—171(A)
—— (see Freedman, Melvin S.)—1155
Walker, J. G. (see Bozorth, R. M.)—1209(L)
Walker, L. R. (see Suhl, H.)—1435(L)
Walker, W. D. μ-meson-electron scattering—168(A)
——, **N. M. Duller, and J. D. Sorrels.** Angular distribution of penetrating secondary particles from showers in C and Pb—173(A)
—— (see Duller, M. N.)—172(A)
Walske, M. C. Stopping power of K-electrons—1283
Waltner, Arthur (see Baker, Paul, Jr.)—1213(L)
Wannier, G. H. (see Lewis, H. W.)—682(L)
Ward, J. C. (see Kac, M.)—1333
Warner, R. M., Jr. (see Rosenblum, E. S.)—612
Warshaw, S. D. (see Marshall, J.)—632
Watkins, D. A. Noise in electron beams at microwave frequencies—171(T)
Watson, H. A. and W. W. Buechner. Magnetic analysis of the $F^{19}(d,p)F^{20}$ and $F^{19}(d,\alpha)O^{17}$ reactions—1324
Watson, Kenneth M. Effect of final state interactions on reaction cross sections—1163
Weaver, Harry E. (see Packard, Martin E.)—163(A)
Wedaa, Henry W. and E. W. Price. Contrast and color in interference fringes—174(A)

—— (see Kretschmar, George G.)—161(A)
Weinreich, O. A. and W. E. Danforth. Optical properties of crystalline thoria—953(L)
Weinstock, Bernard (see Pellam, John R.)—162(A)
Weiss, M. T. and A. G. Fox. Magnetic double refraction at microwave frequencies—146(L)
Welsh, H. L. (see Chisholm, D. A.)—957(L)
Wenzel, W. A. and Ward Whaling. Cross section and angular distribution of D(d,p)T—1149
Westermark, Torbjorn. Production of P^{33} with thermal neutrons—573
Wexler, Sol and T. H. Davies. Average electric charge of daughter atoms from β-decay and isomeric transition—1203(L)
Whaling, Ward (see Mileikowsky, Curt)—1254
—— (see Wenzel, W. A.)—1149
Wheatley, John and David Halliday. Quenching of ortho-positronium decay by magnetic field—424(L)
White, Irene S. (see Anslow, Gladys A.)—154(A)
White, R. Stephen, Mark J. Jakobson, and Alvin G. Schulz. Production of charged photomesons from D and H. I—836
Whittemore, W. L. and R. P. Shutt. Coulomb and nuclear interactions of cosmic-ray mesons and protons in Pb—1312
Wick, G. C., A. S. Wightman, and E. P. Wigner. Intrinsic parity of elementary particles—101
Wiedenbeck, M. L. (see Hutchinson, D. R.)—699
—— (see Kloepper, Robert M.)—695
Wightman, A. S. (see Wick, G. C.)—101
Wigner, E. P. (see Wick, G. C.)—101
Wiig, Edwin O. (see Dropesky, Bruce)—683(L)
Wiley, Emmett H. (see Axtell, James C.)—164(A)
Wilkinson, D. H. (see Jones, G. A.)—423(L)
Wilkinson, Roger G. (see Roggenkamp, Paul L.)—1262
Willig, F. J., F. A. Lucy, and R. G. Shreffler. Fast jets from collapsing cylinders—161(A)
Wilson, Robert R. Radii of mirror nuclei—350
Witmer, Enos E. New conception of nuclei and elementary particles—163(A)
Wolfenstein, L. and D. G. Ravenhall. Consequences of invariance under charge conjugation—279
Woodward, R. L. (see Fultz, S. C.)—170(A)
Wright, R. W. (see Rado, G. T.)—909

Yagoda, Herman (see de Carvalho, Hervasio)—273
Yarnell, J. L., R. H. Lovberg, T. F. Stratton, and W. R. Stratton. Angular distribution of protons from $He^3(d,p)He^4$—158(A)
—— (see Brown, R. J. S.)—253
Yasaitis, E. L. (see Smaller, B.)—414(L)
Yennie, Donald R. Quantum corrections to classical nonlinear meson theory—527
Yokobori, Takeo. Cottrell-Bilby theory of yielding of Fe—1423(L)
Yudowitch, K. L. and R. M. Frank. Small angle x-ray scattering from compact identical particles—759

Zobel, W. (see Steffen, Rolf M.)—170(A)
Zucker, E. R. (see Mandeville, C. E.)—554

Analytic Subject Index to Volume 88

References with (A) are to abstracts of papers presented at meetings of the American Physical Society. References with (L) are to Letters to the Editor.

Absorption of radiation (see **Radiation**)
Acoustics
Dependence of Pfeifenton (pipe tone) frequency on pipe length, orifice diameter, and gas discharge pressure, A. B. C. Anderson—161(A)
Afterglow (see **Discharge of electricity in gases**)
Alloys (see **Crystalline state**)
Annihilation (see **Pair production and annihilation**)
Antiferroelectric phenomena (see **Ferroelectric and antiferroelectric phenomena**)
Antiferromagnetism (see **Magnetic properties**)
Arcs (see **Discharge of electricity in gases**)
Astrophysics
Nuclear reactions in stars. I. $p-p$ chain, E. E. Salpeter—547
Solar "enhanced radiation" and plasma oscillations, Hari K. Sen—816
Variational method for problems of neutron diffusion and of radiative transfer, Su-Shu Huang—50
Atmosphere (see also **Meteorology**)
Atmospheric ion monitor, J. D. Graves, W. R. Ketler, and R. I. Condit—157(A)
Atmospheric water vapor determination by infrared solar spectroscopy, Robert F. Calfee, David M. Gates, and Byron E. Cohn—157(A)
Local atmospheric ion concentrations as basis for personnel and plant protection, R. I. Condit—158(A)
Pressures, densities, and temperatures in upper atmosphere, Rocket Panel—1027
Production of *E*-layer in oxygen dissociation region in upper atmosphere, D. C. Choudhury—405
Radiative transfer and equilibrium associated with far infrared bands in atmosphere, J. I. King—157(A)
Wind and temperature measurements above lower isothermal region of atmosphere by acoustic propagation studies, William B. Kennedy—158(A)
Atomic and molecular beams
Rf spectra of Li^6F^{19} by molecular beam method, J. C. Swartz and J. W. Trischka—1085
Atomic mass (see **Isotopes and atomic mass; Mass spectroscopy**)
Atomic structure (see **Spectra, atomic**)

Boson theory (see **Field theory**)
Bremsstrahlung (see **Radiation**)

Chemical reactions
Mathematical studies of thermal processes relating to reaction rates in solid fuels, R. H. Olds and G. B. Shook—166(A)
Measurement of reaction rates for solids, G. B. Shook and R. H. Olds—166(A)
Cold emission (see **Field currents**)
Compton effect (see **Scattering of radiation**)
Conductivity, electrical (see **Electrical conductivity**)
Conductivity, thermal (see **Thermal conductivity**)
Constants, physical standards
Rydberg constant and atomic mass of the electron, E. Richard Cohen—353
Contact potentials
Direct comparison of Kelvin and electron beam methods of contact potential measurements, Paul A. Anderson—655
Cosmic radiation
Absorption mean free path of large hard showers in air, Harold K. Ticho—236
Absorption of *N*-component in Pb, H. S. Bridge and R. H. Rediker—206
Angular distribution functions for high energy cosmic-ray particles, H. S. Green, H. Messel, and B. A. Chartres—1277
Angular distribution of penetrating secondary particles from showers in C and Pb, W. D. Walker, N. M. Duller, and J. D. Sorrels—173(A)
Burst production in material of low atomic number at sea level, F. E. Driggers—173(A)
Close pair effect in cosmic-ray stars, K. E. Davis, J. B. Marion, J. F. Delord, and K. M. King—368
Close pairs of tracks in showers in emulsions, J. Y. Mei and E. Pickup—172(A)
Collision cross sections in cosmic-ray interactions, Kurt Sitte—172(A)
Collisions of heavy primary nuclei in emulsions, N. L. Allen and E. Pickup—172(A)
Cosmic radiation at great depths, Walter Goad—169(A)
Coulomb and nuclear interactions of cosmic-ray mesons and protons in Pb, W. L. Whittemore and R. P. Shutt—1312
Effects of atmosphere on penetrating cosmic radiation, H. O. Curtis and E. S. Cotton—173(A)
Electronic component at low altitudes produced by π-meson decay, E. D. Palmatier—761
Emulsion cloud-chamber observations on interactions of high energy primaries, M. F. Kaplon and D. M. Ritson—386
Energy loss of μ-mesons in NaI crystals, Alvin Hudson and Robert Hofstadter—589
Experimental investigation of nuclear cascade in water, C. B. A. McCasker, H. Messel, D. D. Millar, and N. A. Porter—1216(A)
Frequency of neutral mesons, G. Salvini and Y. B. Kim—40
High energy nuclear interaction, J. E. Naugle—172(A)
Intensity of soft and hard component as function of altitude at geomagnetic latitudes of 28°N, 41°N, and 55°N, Marcello L. Vidale—266
Interactions of secondary particles from penetrating showers, M. N. Duller, W. D. Walker, and J. D. Sorrels—172(A)
Lateral distribution of extensive air showers, Morton A. Levine—154(A)
Lateral structure of electronic showers in air, M. H. Kalos and J. M. Blatt—173(A)
Lifetimes of μ^- meson stopped in light elements—apparatus, W. E. Bell and E. P. Hincks—168(A); 1424(L); results, E. P. Hincks and W. E. Bell—168(A)
Mass determinations of fast cosmic-ray particles in emulsions, L. Voyvodic—171(A)
Narrow angle pairs from nuclear disintegrations, J. J. Lord, D. M. Haskin, and Marcel Schein—172(A)
New barometric and temperature coefficients for small bursts, James W. Broxon—173(A)
Nuclear transparency and nucleon cross section for penetrating-shower producing cosmic radiation, Darol Froman—172(A)
Plural theories for shower component in high energy nuclear disintegrations, H. Messel and R. B. Potts—488
Range distribution of sea level mesons at low geomagnetic latitudes, L. del Rosario and J. Davila-Aponte—998
Rocket determination of ionization spectrum of charged cosmic rays at $\lambda = 41°N$, G. J. Perlow, L. R. Davis, C. W. Kissinger, and J. D. Shipman, Jr.—321
Spread of soft component, H. S. Green and H. Messel—331
Statistical study of distribution of stars in nuclear emulsions, F. B. Brown, Jr., and A. V. Masket—1204(L)

Cosmic radiation (continued)
T-tracks in nuclear emulsions, M. Blau and E. O. Salant—954(L)
Cross section, measurements, theory (see also **Scattering of electrons**)
Absolute low energy cross section experiment with deuterons, J. A. Phillips, W. R. Arnold, G. A. Sawyer, E. J. Stovall, Jr., and J. L. Tuck—159(A)
Of C and H for high energy neutrons, George R. Mott, Gordon L. Guernsey, and Bruce K. Nelson—9
Differential cross-section measurements for scattering of protons by deuterons, R. J. S. Brown, George D. Freier, H. D. Holmgren, W. R. Stratton, and J. L. Yarnell—253
Differential $n-p$ scattering for 220-Mev neutrons, Gordon L. Guernsey, G. Mott, and B. K. Nelson—15
Effect of final state interactions on reaction cross sections, Kenneth M. Watson—1163
Inelastic collision cross sections for 14-Mev neutrons, D. D. Phillips, R. W. Davis, and E. R. Graves—600
Neutron capture cross sections, B. Margolis—327
Stripping and pick-up differential cross sections, S. T. Butler and E. E. Salpeter—133(L)
Thermal neutron capture cross sections, H. Pomerance—412
Total cross sections for 14-Mev neutrons, J. H. Coon, E. R. Graves, and H. H. Barschall—162(A); 562; Leonard S. Goodman—686(L)
Total cross sections of heavy nuclei for fast neutrons, D. W. Miller, R. K. Adair, C. K. Bockelman, and S. E. Darden—83
Total neutron cross section of Na, P. H. Stelson and W. M. Preston—1354
Crystal counters (see **Methods and instruments**)
Crystalline state
Acceptors produced in Ge by quenching from high temperatures, Colman Goldberg—920
Anelastic measurements of atomic mobility in substitutional solid solutions, A. S. Nowick—925
Clausius-Mosotti equation for anisotropic crystals, Hans J. Neugebauer—1210(L)
Color centers generated in NaCl by electrolysis, Henry F. Ivey—1434(L)
Color centers in alkali halides at 5°K, William H. Duerig and Jordan J. Markham—1043
Dielectric constant and permeability of ferrites in microwave region, erratum, Tosihiko Okamura, Tadao Fujimura, and Muneyuki Date—1435(L)
Effective mass of electrons in polar crystals, E. P. Gross—153(A)
Electron diffraction from small crystals, Chester R. Berry—596
Electronic states in crystals under large overall perturbations, Paula Feuer—92
Electronic structure of diamond crystal, Frank Herman—1210(L)
Energy distribution of slow neutrons scattered from solids, B. N. Brockhouse and D. G. Hurst—542
Formation of *F*-centers during irradiation, Jordan J. Markham—500
Grain boundary barriers in Ge, W. E. Taylor, N. H. Odell, and H. Y. Fan—867
Inelastic deformation (cold flow) of certain crystalline materials under flexural stress, Lewis S. Combes, Stanley S. Ballard, and David L. Honkonen—153(A)
Isothermal ordering of Cu_3Au at 200°C, E. K. Halteman, G. F. Mechlin, and H. L. Glick—1205(L)
Lattice vibrations in graphite, Ronald W. Gurney—465
Motion of slow electrons in polar crystals, Tsung-Dao Lee and David Pines—960(L)
Multiple-beam interferometric study of topaz cleavage faces and polished glass surfaces, W. F. Koehler—175(A)
Optical and infrared reflectivity of metals at low temperatures, T. Holstein—1427(L)
Optical properties of crystalline thoria, O. A. Weinreich and W. E. Danforth—953(L)
Parallel susceptibility of antiferromagnet at low temperatures, Jack R. Tessman—1132
Plastic deformation of Ge and Si, C. J. Gallagher—721
Plasticity of Si and Ge, Frederick Seitz—722
Quenching in of lattice vacancies in pure Au, J. W. Kauffman and J. S. Koehler—149(L)
Radiation damage and recovery in Cu, Ag, Au, Ni, and Ta, J. W. Marx, H. G. Cooper, and J. W. Henderson—106
Residual resistance in dilute Cu alloys, D. K. C. MacDonald and W. B. Pearson—149(L)
Spontaneous magnetization of triangular Ising lattice, R. B. Potts—352

Diamagnetism (see **Magnetic properties**)
Dielectrics and dielectric properties
Clausius-Mosotti equation for anisotropic crystals, Hans J. Neugebauer—1210(L)
Dielectric constant and permeability of ferrites in microwave region, erratum, Tosihiko Okamura, Tadao Fujimura, and Muneyuki Date—1435(L)
Microwave absorption and dielectric relaxation in long-chain esters, P. M. McGeer, A. J. Curtis, G. B. Rathmann, and C. P. Smyth—174(A)
Of $ND_4D_2PO_4$, W. P. Mason and B. T. Matthias—477
Diffraction of electrons (see **Electron diffraction**)
Diffraction of neutrons (see **Neutron diffraction**)
Diffraction of radiation (see **Radiation**)
Diffusion (see also **Thermal diffusion**)
Of metastable atoms, Manfred A. Biondi—660
Of neutrons, George Jaffe—603
Penetration and diffusion of x-rays: Calculation of spatial distributions by semi-asymptotic methods, L. V. Spencer—793
Relationship between diffusion constant and mobility of electrons and holes, Transistor Teachers Summer School—1368
Variational method for problems of neutron diffusion and of radiative transfer, Su-Shu Huang—50
Discharge of electricity in gases
Direct observation of presence of magnetohydrodynamic waves in ionized He gas, Winston H. Bostick and Morton A. Levine—153(A)
Discharge mechanism in A counters, Laura Colli and Ugo Facchini—987
Electron density in different regions of dc glow discharge, Burton J. Udelson and John E. Creedon—145(L)
Electron removal in Kr afterglows, John M. Richardson—895
Formative time lags of uniform field breakdown in N_2, G. A. Kachickas and L. H. Fischer—878
High frequency breakdown in Ne, A. D. MacDonald—420(L)
Probe technique for measuring ion densities in afterglow of pulsed discharge, Morton A. Levine and Winston H. Bostick—153(A)
Pulse-free discharges in negative point-to-plane corona, Allan Greenwood—91
Recombination processes in O_2, Joseph Kaplan and Marx Brook—157(A)
Shock waves in low pressure spark discharges, Richard G. Fowler, William R. Atkinson, Walter D. Compton, and Robert J. Lee—137(L)
Disintegration and excitation of nucleus (see also **Nuclear spectra; Photodisintegration; Radioactivity**)

Absolute low energy cross-section experiment, J. A. Phillips, W. R. Arnold, G. A. Sawyer, E. J. Stovall, Jr., and J. L. Tuck—159(A)
Activation cross sections for 14-Mev neutrons, Stuart G. Forbes—1309
Al^{26} low-lying levels from $Mg^{24}(d,n)Al^{25}$, E. Goldberg—159(A)
$Al^{27}(d,p)Al^{28}$ magnetic analysis, H. A. Enge, W. W. Buechner, and A. Sperduto—963
Angular correlation in $(d,p\gamma)$ reactions, L. J. Gallaher and W. B. Cheston—684(L)
Angular correlations in $F^{19}(p,\alpha\gamma)O^{16}$, J. Seed and A. P. French—1007
Angular distribution of α-particles from $d-T$ reactions, T. F. Stratton and George D. Freier—261
Angular distribution of neutrons from $d-d$ reaction, Paul Baker, Jr., and Arthur Waltner—1213(L)
Angular distributions of protons and tritons from deuteron-induced reactions on Be^9, H. W. Fulbright, J. A. Bruner, D. A. Bromley, and L. M. Goldman—700
Angular distributions of protons from $He^3(d,p)He^4$, J. L. Yarnell, R. H. Lovberg, T. F. Stratton, and W. R. Stratton—158(A)
$C^{13}(p,pn)C^{12}$ cross section from threshold to 340 Mev, R. Lee Aamodt, Vincent Peterson, and Robert Phillips—739
Cyclotron bombardments with 21-Mev He^3, T. W. Donaven, D. N. Kundu, John K. Long, and M. L. Pool—158(A)
Deuteron bombardment of Be^9 and levels of B^{10}, Fay Ajzenberg—298
$d-d$ cross sections 14–110 kev, W. R. Arnold, J. A. Phillips, G. A. Sawyer, E. J. Stovall, Jr., and J. L. Tuck—159(A)
$D(d,p)T$, cross section and angular distribution, W. A. Wenzel and Ward Whaling—1149
d-He^3 cross sections 35–100 kev, J. L. Tuck, W. R. Arnold, J. A. Phillips, G. A. Sawyer, and E. J. Stovall, Jr.—159(A)
$d-T$ cross sections 15–125 kev, E. J. Stovall, Jr., W. R. Arnold, J. A. Phillips, G. A. Sawyer, and J. L. Tuck—159(A)
Effect of charge symmetry on nuclear reactions, Norman M. Kroll and Leslie L. Foldy—1177
Electrostatic analysis of nuclear reaction energies, D. S. Craig, D. J. Donahue, and K. W. Jones—808
Energy levels in light nuclei, J. S. Arthur, A. J. Allen, R. S. Bender, H. J. Hausman, and C. J. McDole—1291
Energy levels in Mg, V, Cr, and Mn, H. J. Hausman, A. J. Allen, J. S. Arthur, R. S. Bender, and C. J. McDole—1296
Energy levels in Si^{29} excited by α-particles on Mg^{26}, S. G. Kaufmann, E. Goldberg, L. J. Koester, and F. P. Mooring—673
Evidence for new level in Be^7, D. M. Thomson—954(L)
Excitation functions to 100 Mev, Norton M. Hintz and Norman F. Ramsey—19
$F^{19}(d,p)F^{20}$ and $F^{19}(d,\alpha)O^{17}$, magnetic analysis, H. A. Watson and W. W. Buechner—1324
Further test of the shell model, J. S. King and W. C. Parkinson—141(L)
$He^3(d,p)He^4$, cross section and angular distribution, T. W. Bonner, J. P. Conner, and A. B. Lillie—473
High energy nuclear interaction, J. E. Naugle—172(A)
High energy nuclear reactions and Goldberger model, J. W. Meadows—143(L)
$H^3(d,n)He^4$ cross section, J. P. Conner, T. W. Bonner, and and J. R. Smith—158(A); 468
Interaction of high energy nucleons with nuclei, G. Bernardini, E. T. Booth, and S. J. Lindenbaum—1017
$Li^6(n,p)He^6$, $Li^7(n,d)He^6$, and $Be^9(n,\alpha)He^6$ cross sections for 14-Mev neutrons, M. E. Battat and F. L. Ribe—159(A)
$Li^7(\alpha,\gamma)B^{11}$ and states of B^{11}, G. A. Jones and D. H. Wilkinson—423(L)
Magnetic lens spectrometer measurements of radiations from light nuclear reactions, R. G. Thomas and T. Lauritsen—969
Narrow angle pairs from nuclear disintegrations, J. J. Lord, D. M. Haskin, and Marcel Schein—172(A)
$Ne^{21}(d,\alpha)F^{19}$ and $Ne^{21}(d,p)Ne^{22}$ reaction energies from magnetic analysis, Curt Mileikowsky and Ward Whaling—1254
Neutron energy distributions from Be, C, and Pb bombarded by 245-Mev protons, Bruce K. Nelson, G. Guernsey, and G. Mott—1
$(n,2n)$ reactions in C^{12}, Cu^{63}, and Mo^{92}, J. E. Brolley, Jr., J. L. Fowler, and L. K. Schlacks—618
N^{14} ground state parity, D. A. Bromley—565
Nuclear energy levels in region of 28-neutron shell, George F. Pieper—1299
Nuclear reactions in stars. I. $p-p$ chain, E. E. Salpeter—547
Polarization of O^{16} γ-rays, L. W. Fagg and S. S. Hanna—1205(L)
Production of P^{32} with thermal neutrons, Torbjorn Westermark—573
Scattering of 31.5-Mev protons from several elements, Roy Britten—283
$Na^{23}(d,p)Na^{24}$, magnetic analysis of proton groups, A. Sperduto and W. W. Buechner—574
Spallation of Cu with high energy neutrons, Luis Marquez—225
Stripping and pick-up differential cross sections, S. T. Butler and E. E. Salpeter—133(L)

Dissociation
Production of E-layer in oxygen dissociation region in upper atmosphere, D. C. Choudhury—405

Dynamics
Euclidean tensors, Wesley E. Brittin and James H. Marable—160(A)

Elasticity
Cottrell-Bilby theory of yielding of Fe, Takeo Yokobori—1423(L)
Of $ND_4D_2PO_4$, W. P. Mason and B. T. Matthias—477

Electrical conductivity and resistance (see also **Semiconductors; Superconductivity**)
Of In-Tl solid solutions, J. W. Stout and Lester Guttman—713
Interpretation of electron-inertia experiment for metals with positive Hall coefficients, Norman Rostoker—952(L)
Of La, Ce, Pr, and Nd at low temperatures, N. R. James, S. Legvold, and F. H. Spedding—1092
Mean free paths of electrons in evaporated metal films, F. W. Reynolds and G. R. Stilwell—418(L)
Minimum at low temperatures, D. K. C. MacDonald—148(L)
Mobility in high electric fields, E. M. Conwell—1379
Of oxide emitters, Ray C. Hughes and Patrick P. Coppola—364
Radiation damage and recovery in Cu, Ag, Au, Ni, and Ta, J. W. Marx, H. G. Cooper, and J. W. Henderson—106
Residual resistance in dilute Cu alloys, D. K. C. MacDonald and W. B. Pearson—149(L)
Temperature dependence, W. V. Houston—1321

Electrodynamics (see **Electromagnetic theory and electrodynamics**)

Electrolysis
Color centers generated in NaCl by electrolysis, Henry F. Ivey—1434(L)
Electromagnetic theory and electrodynamics (see also **Quantum electrodynamics**)
Gravitation and electrodynamics, Behram Kurşunoğlu—1369
Electron diffraction
From small crystals, Chester R. Berry—596
Electronic tubes
Relation between conductance and noise power spectrum of certain electronic streams, J. J. Freeman—164(A)
Electrons (see also **E/m**; **Electromagnetic theory and electrodynamics**; **Positrons**)
Anomalous magnetic moment, S. H. Koenig, A. G. Prodell, and P. Kusch—191
Mirror measurement of neutron-electron interaction, D. J. Hughes, J. A. Harvey, and N. D. Goldberg—163(A)
Electrons in metals
Interpretation of electron-inertia experiment for metals with positive Hall coefficients, Norman Rostoker—952(L)
Interpretation of e/m values for electrons in crystals, W. Shockley—953(L)
Mean free paths of electrons in evaporated metal films, F. W. Reynolds and G. R. Stilwell—418(L)
Electrons, scattering of
Backscattering of positrons and electrons, H. H. Seliger—408
High energy electron-electron scattering, erratum, Walter H. Barkas, Robert W. Deutsch, F. C. Gilbert, and Charles E. Violet—1435(L)
Electrons, secondary
Mechanism of field dependent secondary emission, Harold Jacobs, John Freely, and Frank A. Brand—492
Theory of secondary emission, J. F. Marshall—416(L)
Elements (see **Isotopes**)
Energy loss of particles (see **Range and energy loss of particles**)
Energy states of atoms (see **Spectra, atomic**)
Energy states of molecules (see **Molecular structure and constants**; **Spectra, molecular**)
Energy states of nucleus (see **Disintegration and excitation of nucleus**; **Nuclear spectra**; **Nuclear structure**)
Errata
Dielectric constant and permeability of various ferrites in microwave region, Toshiko Okamura, Tadao Fujimura, and Muneyuki Date—1435(L)
Faraday rotation of guided waves, H. Suhl and L. R. Walker—1435(L)
High energy electron-electron scattering, Walter H. Barkas, Robert W. Deutsch, F. C. Gilbert, and Charles E. Violet—1435(L)
Interaction between electron and one-dimensional electromagnetic field, Nathan Rosen—1434(L)
Optical focusing in constant radius accelerators, David C. dePackh—1434(L)
Similarity properties of two-fluid model of superconductivity, E. Maxwell—1435(L)
Solidification curve of He II, B. M. Cwilong—1435(L)
Theory of spin waves in ferromagnetic media, Conyers Herring and Charles Kittel—1435(L)
Excitation of nuclei (see **Disintegration and excitation of nucleus**; **Nuclear spectra**; **Nuclear structure**)
Explosion phenomena (see also **Shock waves**)
Fast jets from collapsing cylinders, F. J. Willig, F. A. Lucy, and R. G. Shreffler—161(A)
Scabbing of metals under explosive attack: Multiple scabbing, John S. Rinehart—162(A)
Faraday effect (see **Magneto-optical effects**)
Ferroelectric and antiferroelectric phenomena
Domain properties in $BaTiO_3$, Walter J. Merz—421(L)
Ferroelectricity in oxides of ferrite structure, W. R. Cook, Jr., and Hans Jaffe—1426(L)
Properties of $ND_4D_2PO_4$, W. P. Mason and T. B. Matthias—477
Properties of tetragonal antiferroelectric crystal, W. P. Mason—480
Ferromagnetism (see **Magnetic properties**)
Field currents
Field emission from photoconductors, L. Apker and E. Taft—1037
Slope of logarithmic plots of Fowler-Nordheim equation, J. M. Houston—349
Field theory (see also **Quantum electrodynamics**)
Electron-neutron interaction as deduced from pseudoscalar meson theory, Burton David Fried—1142
Impulse approximation and field theoretical calculations, John S. Blair and Benjamin Segall—621
Invariance under charge conjugation, L. Wolfenstein and D. G. Ravenhall—279
Lagrangian formulation of quantum theories, Peter G. Bergmann, Ralph Schiller, and James L. Anderson—1216(A)
Meson-nucleon scattering and classical strong-coupling theory, David Feldman—890
Meson theory of nuclear forces and low energy properties of $n-p$ system, Maurice M. Lévy—725
Non-adiabatic treatment of relativistic two-body problem, Maurice M. Lévy—72
Nuclear forces in pseudoscalar meson theory, K. Nakabayasi and I. Sato—144(L)
Pseudoscalar mesons with applications to meson-nucleon scattering and photoproduction, S. D. Drell and E. M. Henley—1053
Quantum corrections to classical nonlinear meson theory, Donald R. Yennie—527
Scattering of charge symmetric pseudoscalar mesons by nucleons, W. W. Wada—1032
Symmetrical pseudoscalar meson theory of nuclear forces, Joseph V. Lepore—750
V-particle and the composite pion, R. J. Finkelstein—555
Films, properties of
Mean free paths of electrons in evaporated metal films, F. W. Reynolds and G. R. Stilwell—418(L)
Fission of nucleus (see also **Disintegration and excitation of nucleus**)
Activation energy for fission, Glenn T. Seaborg—1429(L)
Angular distribution of prompt neutrons emitted in fission, J. S. Fraser—536
Fission asymmetry as function of excitation energy of compound nucleus, J. L. Fowler, W. H. Jones, and J. H. Paehler—71
Fission neutron spectrum of Pu^{239}, Norris Nereson—823
Fission to capture cross section ratio, John R. Huizenga and Robert B. Duffield—959(L)
Proton induced reactions of Th-fission yield curves, Howard A. Tewes and Ralph A. James—860
Spontaneous fission *vs* α-decay, Arnold Kramish—1201(L)
Fluctuation phenomena
Relation between conductance and noise power spectrum of certain electronic streams, J. J. Freeman—164(A)
Fluid dynamics (see also **Aerodynamics**; **Hydrodynamics**)
Analog computation in theory for critical stability of fluid, F. T. Rogers, Jr., and H. L. Morrison—161(A)
Application of generalization of Heisenberg's model of turbulence to critical Reynolds' numbers, E. N. Parker—161(A)

Comparison between longitudinal and time correlations in turbulent flow, F. N. Frenkiel—1380
Fast jets from collapsing cylinders, F. J. Willig, F. A. Lucy, and R. G. Shreffler—161(A)
Influence of binary collisions on molecular gas flow, J. W. Hiby and M. Pahl—414(L)
Study of impinging liquid jets in liquid stream, George G. Kretschmar and Henry W. Wedaa—161(A)

Fluorescence (see also **Luminescence**)
Internal absorption of fluorescent light in large plastic scintillators, C. N. Chou—167(A)
Scintillators and energy transfer processes, C. Reid—422(L)
Spectral distribution of energy in fluorescence of Na fluorescein, Earl H. Gilmore—174(A)
Wavelength independent photographic dosimeter employing terphenyl intensifying screens, Herman Hoerlin and Frank Kaszuba—174(A)

Gamma-rays (see also **Disintegration and excitation of nucleus; Nuclear spectra; Radioactivity**)
Absorption of 5.3-Mev, 10.3-Mev, and 17.6-Mev γ-rays, E. S. Rosenblum, E. F. Shrader, and R. M. Warner, Jr.—612
Polarized γ-rays from nuclei aligned at low temperatures, G. R. Bishop, J. M. Daniels, G. Goldschmidt, H. Halban, N. Kurti, and F. N. H. Robinson—1432(L)
Precision measurements of nuclear γ-ray wavelengths, David E. Muller, Harry C. Hoyt, David J. Klein, and Jesse W. M. DuMond—775

Gases (see also **Kinetic theory**)
Influence of binary collisions on molecular gas flow, J. W. Hiby and M. Pahl—414(L)
Kinks in gases, George Antonoff—160(A)

Geophysics
Abundances of elements, Harold C. Urey—248
K^{40} radioactive decay: its branching ratio and use in geological age determinations, A. K. Mousuf—150(L)

Gravitation
Gravitation and electrodynamics, Behram Kurşunoğlu—1369

Gyromagnetization (see **Magnetic properties**)

Hall effect
In Ni ferrite, Simon Foner—955(L)
In Zn crystals at low temperatures, John K. Logan and Jules A. Marcus—1234

Heat conduction (see **Thermal conductivity**)

Helium, liquid
Cavitation effect in He II, B. M. Cwilong, J. F. Lees, and F. D. Manchester—138(L)
Heat pulses in He II below 1°K, C. J. Gorter—681(L)
Rayleigh disk measurements in He^3-He^4 mixtures, John R. Pellam and Bernard Weinstock—162(A)
Solidification curve of He II, B. M. Cwilong—135(L); erratum—1435(L)
Vapor pressures of He^3—He^4 mixtures, Raymond A. Nelson and William Band—1431(L)
Vapor pressures of He^3—He^4 mixtures below lambda-point, H. S. Sommers, Jr.—113

Hyperfine structure (see also **Nuclear moments and spin**)
Of H and D, A. G. Prodell and P. Kusch—184
Magnetic hfs in diatomic molecules, R. A. Frosch and H. M. Foley—1337

Instruments (see **Methods and instruments**)

Internal conversion (see **Nuclear spectra**)

Ionization
α-particle ionization in mixtures of noble gases, William P. Jesse and John Sadauskis—417(L)
Average energy loss per ion pair of slow electrons in He C. E. Nielsen, R. H. Frost, and W. J. Choyke—165(A)
Efficiencies, Willard H. Bennett—165(A)
Efficiencies of multiple ionization of Hg, Boyd Harned and Willard H. Bennett—165(A)
Ionization cross sections for metastable atoms, Manfred A. Biondi—660
Ionization loss and straggling of fast electrons, E. L. Goldwasser, F. E. Mills, and A. O. Hanson—1137
Ionization loss at relativistic velocities in nuclear emulsions, Maurice M. Shapiro and Bertram Stiller—169(A)
Production of *E*-layer in oxygen dissociation region in upper atmosphere, D. C. Choudhury—405
Space distribution, G. E. Evans and P. M. Stier—165(A)
Total specific ionization in air, A, and H_2 from 17.5-Mev electrons, J. Ovadia, J. S. Laughlin, J. W. Beattie, and W. J. Henderson—165(A)

Ions
Atmospheric ion monitor, J. D. Graves, W. R. Ketler, and R. I. Condit—157(A)
Local atmospheric ion concentrations as basis for personnel and plant protection, R. I. Condit—158(A)
Method for producing short intense monoenergetic ion pulses, R. C. Mobley—360
Propagation in electron-ion streams, R. Q. Twiss—1392

Ions and electrons, mobility (see also **Semiconductors**)
Drift velocities of ions in Kr and Xe, Robert N. Varney—362
Mobility in high electric fields, E. M. Conwell—1379
Relationship between diffusion constant and mobility of electrons and holes, Transistor Teachers Summer School—1368

Isomers, nuclear (see also **Nuclear spectra; Radioactivity**)
Average electric charge of daughter atoms from β-decay and isomeric transition, Sol Wexler and T. H. Davies—1203(L)
Experiments on Ge^{73} and Ge^{73m}, Alan B. Smith, R. S. Caird, and Allan C. G. Mitchell—150(L)
Isomeric levels in Pb^{201} and Pb^{202}, N. J. Hopkins—680(L)
Mass assignment and γ-radiation of 7-hr Mo isomer, G. E. Boyd and R. A. Charpie—681(L)
Photoproduction of isomeric pair of Br^{80}, Erich M. Harth—170(A)

Isotopes and atomic mass
Abundances of elements, Harold C. Urey—248
Atomic masses from Pd through Xe, Richard E. Halsted—666
Neutron deficient Sr isotopes, Stanley V. Castner and D. H. Templeton—1126
Nuclear mass determinations from disintegration energies: O to S, C. W. Li—1038
K^{40} mass, Walter H. Johnson, Jr.—1213(L)
Variations in relative abundances of isotopes of common Pb, C. B. Collins, R. M. Farquhar, and R. D. Russell—1275

Kinetic theory
Influence of binary collisions on molecular gas flow, J. W. Hiby and M. Pahl—414(L)

Liquids (see also **Hydrodynamics**)
Experimental demonstration of kinks, George Antonoff—177(A)

Low temperature phenomena (see also **Helium, liquid**)
Anomaly in low temperature atomic heat of Ag, P. H. Keesom and N. Pearlman—140(L)
Atomic heat of Si below 100°K, N. Pearlman and P. H. Keesom—397
de Haas-van Alphen effect in enriched Sn isotopes, Ted G. Berlincourt—242

Low temperature phenomena (continued)
Hall effect in Zn crystals at low temperatures, John K. Logan and Jules A. Marcus—1234
Low temperature thermal expansion of U, Henry L. Laquer and Adam F. Schuch—166(A)
Minimum of electrical resistance at low temperatures, D. K. C. MacDonald—148(L)
Optical and infrared reflectivity of metals at low temperatures, T. Holstein—1427(L)
Polarized γ-rays from nuclei aligned at low temperatures, G. R. Bishop, J. M. Daniels, G. Goldschmidt, H. Halban, N. Kurti, and F. N. H. Robinson—1432(L)
Properties of Cr^{+++} ion in paramagnetic alums at low temperatures, Ralph P. Hudson—570
Residual resistance in dilute Cu alloys, D. K. C. MacDonald and W. B. Pearson—149(L)
Resistivity of La, Ce, Pr, and Nd at low temperatures, N. R. James, S. Legvold, and F. H. Spedding—1092
Specific heat of Pb in temperature range 1°K to 75°K, M. Horowitz, A. A. Silvidi, S. F. Malaker, and J. G. Daunt—1182
Spin paramagnetism of Cr^{+++}, Fe^{+++}, and Gd^{+++} at liquid He temperatures and in strong magnetic fields, Warren E. Henry—559

Magnetic properties (see also **Nuclear moments and spin; Crystal structure; Magnetic resonance absorption**)
Anomalous paramagnetism of $CuSO_4 \cdot 5\ H_2O$, W. E. Henry—166(A)
Application of theory of numbers to magnetic properties of free electron gas, M. C. Steele—451
Concept of spin-lattice relaxation in ferromagnetic materials, P. W. Anderson—1214(L)
de Haas-van Alphen effect in enriched Sn isotopes, Ted G. Berlincourt—242
Dielectric constant and permeability of ferrites in microwave region, erratum, Tosihiko Okamura, Tadao Fujimura, and Muneyuki Date—1435(L)
Ferromagnetism at very high frequencies. IV. Temperature dependence of magnetic spectrum of a ferrite, G. T. Rado, R. W. Wright, W. H. Emerson, and A. Terris—909
Gyromagnetic effect in permalloy and iron, S. J. Barnett and Louis A. Giamboni—28
Hall effect in Ni ferrite, Simon Foner—955(L)
Hall effect in Zn crystals at low temperatures, John K. Logan and Jules A. Marcus—1234
Magnetic double refraction at microwave frequencies, M. T. Weiss and A. G. Fox—146(L)
Magnetostriction of single crystals of Co and Ni ferrites, R. M. Bozorth and J. G. Walker—1209(L)
Number theory and magnetic properties of electron gas, M. F. M. Osborne—438
Parallel susceptibility of an antiferromagnet at low temperatures, Jack R. Tessman—1132
Properties of Cr^{+++} ion in paramagnetic alums at low temperatures, Ralph P. Hudson—570
Rotational magnetic moment, magnetic susceptibilities, and electron distribution in H_2, N. J. Harrick and N. F. Ramsey—228
Spherical model of a ferromagnet, H. W. Lewis and G. H. Wannier—682(L)
Spin-lattice relaxation in ferromagnets, Elihu Abrahams and C. Kittel—1200(L)
Spin paramagnetism of Cr^{+++}, Fe^{+++}, and Gd^{+++} at liquid He temperatures and in strong magnetic fields, Warren E. Henry—559
Spontaneous magnetization of triangular Ising lattice, R. B. Potts—352
Spontaneous magnetization of two-dimensional rectangular Ising model, C. H. Chang—1422(L)
Theory of spin waves in ferromagnetic media, erratum, Conyers Herring and Charles Kittel—1435(L)

Magnetic resonance absorption (see also **Nuclear moments and spin**)
Anomalous magnetic moment of the electron, S. H. Koenig, A. G. Prodell, and P. Kusch—191
g-factor of ferrite, Tosihiko Okamura, Yosiharu Torizuka, and Yuzo Kojima—1425(L)
$g_J(^2S_{\frac{1}{2}})$ of K in terms of proton gyromagnetic ratio, Peter Franken and Seymour Koenig—199
Hfs of H and D, A. G. Prodell and P. Kusch—184
Interaction between nuclear spins in HD gas, H. Y. Carr and E. M. Purcell—415(L)
Microwave spin resonance absorption by conduction electrons in metallic Na, T. W. Griswold, A. F. Kip, and C. Kittel—951(L)
Nuclear relaxation time of H_2 gas, Martin E. Packard and Harry E. Weaver—163(A)
Nuclear resonance modulation correction, M. M. Perlman and M. Bloom—1290
Nuclear spin of V^{50} by paramagnetic resonance, C. Kikuchi, M. H. Sirvetz, and V. W. Cohen—142(L)
Paramagnetic resonance in phosphors, W. D. Hershberger and H. N. Leifer—714
Second order effects in nuclear electric quadrupole interaction of Al^{27} in spodumene, H. E. Petch, G. M. Volkoff, and N. G. Cranna—1201(L)
Spin echo measurements of nuclear spin coupling in molecules, E. L. Hahn and D. E. Maxwell—1070
Spin-spin interaction in HD nuclear resonance, B. Smaller, E. L. Yasaitis, E. C. Avery, and D. A. Hutchison—414(L)
Spin-spi relaxation in ferromagnetic resonance, Frederic Keffer 586(L)

Magneto-optical effects
Faraday rotation of guided waves, erratum, H. Suhl and L. R. Walker—1435(L)

Magnetostriction (see **Magnetic properties**)

Mass spectroscopy (see also **Isotopes and atomic mass**)
Rf mass spectrometer, James C. Axtell, Emmett H. Wiley, and S. W. Bass—164(A)

Measurements (see **Methods and instruments**)

Mechanics (see **Dynamics**)

Mechanics, quantum—atomic structure and spectra
Configuration interaction between odd terms in Fe group, Norbert Rosenzweig—580
Iterative procedures and He wave equation, James H. Bartlett—525
Perturbations of atomic g-values, M. Phillips—202
Wave functions and energy levels for Cu^+ as found by Slater approximation to Hartree-Fock equations, George W. Pratt, Jr.—1217

Mechanics, quantum—general
Coulomb functions for heavy nuclear particles, W. D. Barfield and A. A. Broyles—892
Diffraction in time, Marcos Moshinsky—625
Elementary particles at rest, Enrique Bustamante—1179
Equivalent potentials, Res Jost and Walter Kohn—382
Intrinsic parity of elementary particles, G. C. Wick, A. S. Wightman, and E. P. Wigner—101
Lagrangian formulation of quantum theories, Peter G. Bergmann, Ralph Schiller, and James L. Anderson—1216(A)
Variational method for radiationless transitions, B. H. Bransden and A. Dalgarno—148(L)
WKB method, Stanley C. Miller, Jr., and R. H. Good, Jr.—160(A)

Mechanics, quantum—molecular structure and spectra
Convergence of intermolecular force series, Glenn M. Roe—659

Magnetic hfs in diatomic molecules, R. A. Frosch and H. M. Foley—1337
Natural line shape, Francis Low—53
Mechanics, quantum—nuclear
Analysis of energy levels of mirror nuclei, C^{13} and N^{13}, R. G. Thomas—1109
Angular correlations of radiations from deuteron stripping reactions, L. C. Biedenharn, Keith Boyer, and R. A. Charpie—517
Charge independence and multiple pion production, L. Van Hove, R. Marshak, and A. Pais—1211(L)
Coupling constant of nucleon—μ-meson interaction, M. A. Preston and M. F. Duret—1425(L)
Effect of charge symmetry on nuclear reactions, Norman M. Kroll and Leslie L. Foldy—1177
Effect of final state interactions on reaction cross section, Kenneth M. Watson—1163
Evidence of once-forbidden spectra for law of β-decay, H. M. Mahmoud and E. J. Konopinski—1266
Explicit $\gamma-\gamma$ angular correlations. II. Polarization correlations, Stuart P. Lloyd—906
H^3 theory, Robert L. Pease and Herman Feshbach—945
Impulse approximation and field theoretical calculations, John S. Blair and Benjamin Segall—621
Limit on repulsive core from 100-Mev deuteron photoeffect, N. Austern—1207(L)
Neutron capture cross sections, B. Margolis—327
Non-additivity of nucleon moments in heavy nuclei, Marc Ross—935
Nuclear photoprocesses at high energy, J. G. Brennan and R. G. Sachs—824
Photomesons from deuteron, Joseph A. Thie—420(L)
Photon-induced reactions, D. C. Peaslee—812
π^+ to π^- ratio from photon bombardment of D, Malvin A. Ruderman—1427(L)
$p-T$ interaction, J. S. McIntosh, R. L. Gluckstern, and S. Sack—752
Radii of mirror nuclei, Robert R. Wilson—350
Roughness of nuclear energy surface, John A. Eldridge and Richard J. Brundy—163(A)
Stripping and nuclear shell model, S. T. Butler—685(L)
Stripping and pick-up differential cross sections, S. T. Butler and E. E. Salpeter—133(L)
Variational principle for scattering, Herman Feshbach and S. I. Rubinow—484
Very long lifetime of C^{14} β-decay, A. M. L. Messiah—151(L)
Mechanics, quantum—of solid bodies
Concept of spin-lattice relaxation in ferromagnetic materials, P. W. Anderson—1214(L)
Effective mass of electrons in polar crystals, E. P. Gross—153(A)
Electronic states in crystals under large overall perturbations, Paula Feuer—92
Electronic structure of diamond crystal, Frank Herman—1210(L)
Energy states of overlapping impurity carriers in semiconductors, Cavid Erginsoy—893
Motion of slow electrons in polar crystals, Tsung-Dao Lee and David Pines—960(L)
Parallel susceptibility of antiferromagnet at low temperatures, Jack R. Tessman—1132
Spin-lattice relaxation in ferromagnets, Elihu Abrahams and C. Kittel—1200(L)
Spontaneous magnetization of two-dimensional rectangular Ising model, C. H. Chang—1422(L)
Theory of secondary emission, J. F. Marshall—416(L)
Mechanics, statistical
Combinatorial solution of 2-dimensional Ising model, M. Kac and J. C. Ward—1332
Generalized statistical mechanics and Onsager relations, Alice Thomson and Peter G. Bergmann—1216(A)
Of irreversibility, Herbert B. Callen, Murray L. Barasch, and Julius L. Jackson—1382
Meson field theory (see **Field theory**)
Mesons (see also **Cosmic radiation**)
Charge independence and multiple pion production, L. Van Hove, R. Marshak, and A. Pais—1211(L)
Coulomb and nuclear interactions of cosmic-ray mesons and protons in Pb, W. L. Whittemore and R. P. Shutt—1312
Coulomb effects in pion scattering by protons under charge independence hypothesis, Leon Van Hove—1358
Coupling constant of nucleon—μ-meson interaction, M. A. Preston and M. F. Duret—1425(L)
Electronic component at low altitudes produced by π-meson decay, E. D. Palmatier—761
Emulsion cloud-chamber observations on interactions of high energy primary cosmic radiation, M. F. Kaplon and D. M. Ritson—386
Energy loss of cosmic-ray μ-mesons in NaI crystals, Alvin Hudson and Robert Hofstadter—589
Energy spectrum of positrons from decay of the μ-meson, H. J. Bramson, A. M. Seifert, and W. W. Havens, Jr.—304
Excitation function for charged π-meson production in H and C by 345-Mev protons, S. Passman, M. M. Block, and W. W. Havens, Jr.—1247
Interaction mean free path of π-mesons in Pb, Fritz E. Froehlich and Kurt Sitte—169(A)
Lifetimes of μ^- meson stopped in light elements—apparatus, W. E. Bell and E. P. Hincks—168(A); results, E. P. Hincks and W. E. Bell—168(A); 1424(L)
Lifetimes of π^+ and π^- mesons, R. P. Durbin, H. H. Loar, and W. W. Havens, Jr.—179; H. Loar, R. Durbin, and W. W. Havens, Jr.—168(A)
Meson-nucleon scattering and classical strong-coupling theory, David Feldman—890
μ-meson-electron scattering, W. D. Walker—168(A)
Multiple scattering of fast pions in photographic emulsions, Meera Backus and J. J. Lord—169(A); Meera Backus, J. J. Lord, and Marcel Schein—1431(L)
Negative pion activation of Br, T. T. Sugihara and W. F. Libby—587
Neutrons produced in absorption of π^- mesons at rest, V. Cocconi Tongiorgi and D. A. Edwards—145(L)
Nuclear cross section for 37-Mev positive pions in Pb, Kenneth J. Button—956(L)
Photomesons from the deuteron, Joseph A. Thie—420(L)
Photoproduction of mesons in D, Melvin Lax and Herman Feshbach—509
π^+ to π^- ratio from proton bombardment of D, Malvin A. Ruderman—1427(L)
π^0 production cross section for 430-Mev protons on H and Be, J. Marshall, L. Marshall, V. A. Nedzel, and S. D. Warshaw—632
Plural theories for shower component in high energy nuclear disintegrations, H. Messel and R. B. Potts—488
Production cross section and frequency of neutral mesons in cosmic rays, G. Salvini and Y. B. Kim—40
Production of charged photomesons from D and H, R. Stephen White, Mark J. Jakobson, and Alvin G. Schulz—836
Production of charged π-mesons in H, D, C, Cu, and Pb by 381-Mev protons, M. M. Block, S. Passman, and W. W. Havens, Jr.—1239
Production of photomesons in D, James Keck and Raphael Littauer—139(L)
Production of π^0 mesons by γ-rays on H, A. Silverman and M. Stearns—1225

Mesons (continued)
Production of π^0 mesons in H and D by high energy γ-rays, G. Cocconi and A. Silverman—1230
Pseudoscalar mesons with applications to meson-nucleon scattering and photoproduction, S. D. Drell and E. M. Henley—1053
Range distribution of sea level mesons at low geomagnetic latitudes, L. del Rosario and J. Davila-Aponte—998
Ratio of π^+ to π^- meson production from D, J. Carothers and C. G. André—1426(L)
S-wave in pion-nucleon scattering, R. E. Marshak—1208(L)
Scattering of charge symmetric pseudoscalar mesons by nucleons, W. W. Wada—1032
τ-meson decay in flight, M. Annis and N. F. Harmon—1202(L)
V-particle and composite pion, R. J. Finkelstein—555
X-rays from mesic atoms, M. Camac, A. D. McGuire, J. B. Platt, and H. J. Schulte—134(L)
X-rays from π-mesic atom, A. M. L. Messiah and R. E. Marshak—678(L)
Metals (see **Crystalline state**)
Metastable atoms and molecules
Diffusion, de-excitation, and ionization cross sections for metastable atoms, Manfred A. Biondi—660
Meteorology (see also **Atmosphere**)
Pressures, densities, and temperatures in upper atmosphere, Rocket Panel—1027
Wind and temperature measurements above lower isothermal region of atmosphere by acoustic propagation studies, William B. Kennedy—158(A)
Methods and instruments
Atmospheric ion monitor, J. D. Graves, W. R. Ketler, and R. J. Condit—157(A)
Contrast and color in interference fringes, H. W. Wedaa and E. W. Price—174(A)
Deterioration of self-quenching counters, Stephen S. Friedland and Henry S. Katzenstein—168(A)
Direct comparison of Kelvin and electron beam methods of contact potential measurements, Paul A. Anderson—655
Equivalent electrical network of quartz plate used as filter, A. D. Frost, C. R. Mingins, and R. W. Perry—154(A)
High frequency electromechanical filters, C. R. Mingins, S. Bartnoff, and L. A. Howard—154(A)
Instantaneous measurement of transient flame temperatures, George W. Bauserman—174(A)
Internal absorption of fluorescent light in large plastic scintillators, C. N. Chou—167(A)
Low pressure cloud-chamber investigation of range-energy relations, Robert G. Mills—168(A)
Low pressure He diffusion cloud chamber, W. J. Choyke and C. E. Nielsen—167(A)
Method for producing short intense monoenergetic ion pulses, R. C. Mobley—360
Minimum temperature gradient required for formation of tracks in cloud-ion chamber, H. L. Morrison and G. J. Plain—167(A)
Multiple-beam interferometric study of topaz cleavage faces and polished glass surfaces, W. F. Koehler—175(A)
Neutron monochromator crystals, A. W. McReynolds—958(L)
Optical focusing in constant radius accelerators, erratum, David C. dePackh—1434(L)
Precision measurements of nuclear γ-ray wavelengths, David E. Muller, Harry C. Hoyt, David J. Klein, and Jesse W. M. DuMond—775
Probe technique for measuring ion densities in afterglow of pulsed discharge, Morton A. Levine and Winston H. Bostick—153(A)
Radial focusing in linear accelerator, J. P. Blewett—1197
Rf mass spectrometer, James C. Axtell, Emmett H. Wiley, and S. W. Bass—164(A)
Response of organic crystals to neutrons, T. W. Bonner, A. B. Lillie, and H. L. Taylor—162(A)
Scintillators and energy transfer processes, C. Reid—422(L)
Stepped-surface piezoelectric filters, R. R. McDonough, D. W. MacLeod, and G. A. Larson—154(A)
Strong-focusing synchrotron—a new high energy accelerator, Ernest D. Courant, M. Stanley Livingston, and Hartland S. Snyder—1190
Table model computer for Fourier synthesis—160(A)
Temperature effect on counting rate of B neutron counters, Aurel Goodwin, Jr., and Mario Iona—168(A)
Two-plate method of measuring anisotropic fast neutron spectra, John E. Evans—163(A)
Use of radioactive vapor in continuously operating diffusion cloud chamber, G. J. Plain and H. L. Morrison—177(A)
Utah digital computer, D. C. Evans and W. M. Elsasser—160(A)
Wavelength independent photographic dosimeter employing terphenyl intensifying screens, Herman Hoerlin and Frank Kaszuba—174(A)
Microwaves
Magnetic double refraction at microwave frequencies, M. T. Weiss and A. G. Fox—146(L)
Microwave absorption and dielectric relaxation in long-chain esters, P. M. McGeer, A. J. Curtis, G. B. Rathmann, and C. P. Smyth—174(A)
Mobility of ions and electrons (see **Ions and electrons, mobility**)
Molecular beams (see **Atomic and molecular beams**)
Molecular structure and constants (see also **Raman spectra; Spectra, microwave; Spectra, molecular**)
Convergence of intermolecular force series, Glenn M. Roe—659
Rotational magnetic moment, magnetic susceptibilities, and electron distribution in H_3, N. J. Harrick and N. F. Ramsey—228
Moments, nuclear (see **Nuclear moments and spin**)

Neutrino (see also **Radioactivity; Scattering of electrons**)
β-spectrum of T and mass of neutrino, L. M. Langer and R. J. D. Moffat—169(A); 689
Neutron diffraction
Neutron monochromator crystals, Fe_3O_4 and Ge, A. W. McReynolds—958(L)
Neutrons
Activation cross sections for 14-Mev neutrons, Stuart G. Forbes—1309
Differential $n-p$ scattering cross section, G. Guernsey, G. Mott, and B. K. Nelson—15
Diffusion, George Jaffe—603
Electron-neutron interaction as deduced from pseudoscalar meson theory, Burton David Fried—1142
Energy distribution of slow neutrons scattered from solids B. N. Brockhouse and D. G. Hurst—542
Fission to capture cross section ratio, John R. Huizenga and Robert B. Duffield—959(L)
Inelastic collision cross sections for 14-Mev neutrons, D. D. Phillips, R. W. David, and E. R. Graves—600
Mirror measurements of neutron-electron interaction, D. J. Hughes, J. A. Harvey, and N. D. Goldberg—163(A)
Neutron capture cross section, B. Margolis—327
Neutron energy distributions from Be, C, and Pb bombarded by 245-Mev protons, B. K. Nelson, G. Guernsey, and G. Mott—1
Neutron monochromator crystals, Fe_3O_4 and Ge, A. W. McReynolds—958(L)
Neutron optics, Otto Halpern—1003

Neutrons produced in absorption of π^- mesons at rest, V. Cocconi Tongiorgi and D. A. Edwards—145(L)
Response of organic crystals to neutrons, T. W. Bonner, A. B. Lillie, and H. L. Taylor—162(A)
Thermal neutron capture cross section, H. Pomerance—412
Total cross sections for 14-Mev neutrons, J. H. Coon, E. R. Graves, and H. H. Barschall—162(A); 562; Leonard S. Goodman—686(L)
Total neutron cross section of Na, P. H. Stelson and W. M. Preston—1354
Total cross sections of C and H for high energy neutrons, G. R. Mott, G. L. Guernsey, and B. K. Nelson—9
Toral cross sections of heavy nuclei for fast neutrons, D. W. Miller, R. K. Adair, C. K. Bockelman, and S. E. Darden—83

Noise (see **Fluctuation phenomena**)

Nuclear induction (see **Magnetic resonance absorption; Nuclear moments and spin**)

Nuclear moments and spin (see also **Hyperfine structure**)
$g_J(^2S_{\frac{1}{2}})$ of K in terms of proton gyromagnetic ratio, Peter Franken and Seymour Koenig—199
Interaction between nuclear spins in HD gas, H. Y. Carr and E. M. Purcell—415(L)
Non-additivity of nucleon moments in heavy nuclei, Marc Ross—935
Nuclear spin of V^{50} by paramagnetic resonance, C. Kikuchi, M. H. Sirvetz, and V. W. Cohen—142(L)
Relativistic corrections to magnetic moments of nuclear particles, G. Breit and R. M. Thaler—1214(L)
Spin echo measurements of nuclear spin coupling in molecules, E. L. Hahn and D. E. Maxwell—1070
Spin-spin interaction in HD nuclear resonance, B. Smaller, E. L. Yasaitis, E. C. Avery, and D. A. Hutchison—414(L)
Of Ta^{181}, B. M. Brown and D. H. Tomboulian—1158

Nuclear reactions (see **Disintegration and excitation of nucleus**)

Nuclear spectra (see also **Disintegration and excitation of nucleus**)
Al^{25} low-lying levels from $Mg^{24}(d,n)Al^{25}$, E. Goldberg—159(A)
$Al^{27}(d,p)Al^{28}$ magnetic analysis, H. A. Enge, W. W. Buechner, and A. Sperduto—963
Angular correlation in $(d,p\gamma)$ reactions, L. J. Gallaher and W. B. Cheston—684(L)
Angular correlation of γ-rays emitted from excited states of Cd^{114}, Rolf M. Steffen and W. Zobel—170(A)
Angular correlations in $F^{19}(p,\alpha\gamma)O^{16}$, J. Seed and A. P. French—1007
Angular correlations of radiations from deuteron stripping reactions, L. C. Biedenharn, Keith Boyer, and R. A. Charpie—517
Of Sb^{124}, D. R. Hutchinson and M. L. Wiedenbeck—699
As^{76} β-spectrum, E. P. Tomlinson and S. L. Ridgway—170(A)
Of Ba^{131}, M. W. Elliott, L. S. Cheng, J. R. Haskins, and J. D. Kurbatov—263
Be^7, new level, D. M. Thomson—954(L)
β-spectrum of T and mass of neutrino, L. M. Langer and R. J. D. Moffat—169(A); 689
Of Bi^{213}, Pb^{209}, and Tl^{209}, F. Wagner, Jr., M. S. Freedman, D. W. Engelkemeir, and L. B. Magnusson—171(A)
Of Ce^{143}, W. H. Burgus—1129
Of Ce^{144} and Pr^{144}, Fred T. Porter and C. Sharp Cook—170(A)
$Co^{56,\ 57,\ 58}$ β-spectrum, L. S. Cheng, J. L. Dick, and J. D. Kurbatov—887
Co^{60}, Cs^{134}, and Sb^{124} angular and direction-polarization correlation, Robert M. Kloepper, E. S. Lennox, and M. L. Wiedenbeck—695
Dependence of γ-radiation lifetimes on nucleon configurations, R. D. Hill—1428(L)
Energy levels in light nuclei, J. S. Arthur, A. J. Allen, R. S. Bender, H. J. Hausman, and C. J. McDole—1291
Energy levels in Mg, V, Cr, and Mn, H. J. Hausman, A. J. Allen, J. S. Arthur, R. S. Bender, and C. J. McDole—1296
Energy levels in Si^{28} excited by α-particles on Mg^{24}, S. G. Kaufmann, E. Goldberg, L. J. Koester, and F. P. Mooring—673
Evidence of once-forbidden spectra for law of β-decay, H. M. Mahmoud and E. J. Konopinski—1266
Explicit $\gamma-\gamma$ angular correlations. II. Polarization correlations, Stuart P. Lloyd—906
F^{20} β-decay, David E. Alburger—1257
Gd^{153} and Tb^{161}, energy levels associated with radioactive decay, J. M. Cork, J. M. LeBlanc, W. H. Nester, and F. B. Stumpf—685(L)
Geometrical correction in angular correlation measurements, E. L. Church and J. J. Kraushaar—419(L)
Of Ge^{75} and Ge^{75m}, Alan B. Smith, R. S. Caird, and Allan C. G. Mitchell—150(L)
Inherent half-width of K-conversion lines, Hilding Slätis and Gunnar Lindström—1429(L)
Internal conversion of neutron capture γ-rays, C. T. Hibdon and C. O. Muehlhause—943
Of I^{131}, J. R. Haskins and J. D. Kurbatov—884
Fe^{59} disintegration scheme, Franz R. Metzger—1360
Isomeric levels in Pb^{201} and Pb^{203}, N. J. Hopkins—680(L)
K/L internal conversion ratio in $M4$ transitions, G. A. Graves, L. M. Langer, and R. D. Moffat—169(A)
$K/(L+M)$ internal conversion ratios for $M4$ transitions, G. A. Graves, L. M. Langer, and R. D. Moffat—344
$Li^7(\alpha,\gamma)B^{11}$ and states of B^{11}, G. A. Jones and D. H. Wilkinson—423(L)
Mg^{24} internal pair conversion, Stewart D. Bloom—312
Magnetic lens spectrometer measurements of radiations from light nuclear reactions, R. G. Thomas and T. Lauritsen—969
Mass assignment and γ-radiation of 7-hr Mo isomer, G. E. Boyd and R. A. Charpie—681(L)
Neutron capture γ-ray spectra from elements $Z=17$–30 and $Z=45$–57, Bernard Hamermesh and Virginia Hummel—916
N^{14} ground-state parity, D. A. Bromley—565
Nuclear energy levels in 28 neutron shell region, George F. Pieper—1299
Nuclear γ-ray wavelengths of Ir^{192}, Ta^{182}, RaTh, Rn, W^{187}, Cs^{137}, Au^{198}, and annihilation radiation, David E. Muller, Harry C. Hoyt, David J. Klein, and Jesse W. M. DuMond—775
Of Os, J. B. Swan and R. D. Hill—171(A)
Os radioisotopes, J. B. Swan and R. D. Hill—831
Pu^{239} and Pu^{240}, Frank Asaro and I. Perlman—828
Pu^{239} soft radiation, Harvey I. Israel—682(L)
$Pu^{239,240,241}$ β-spectra, Melvin S. Freedman, F. Wagner, Jr., and D. W. Engelkemeir—1155
Polarization correlations of γ-rays of Cs^{134} and of annihilation radiation, Berol L. Robinson and Leon Madansky—1065
Polarization of O^{16} γ-rays, L. W. Fagg and S. S. Hanna—1205(L)
Probability of internal conversion of K-series radiation of Au arising from interaction of L sub-shells, J. W. Mihelich—415(L)
Of Pm^{142}, Pm^{143}, Pm^{145}, Pm^{148}, and Sm^{146}, John K. Long, M. L. Pool, and D. N. Kundu—171(A)
Of Rb^{89} and Ga^{67}, S. C. Fultz, R. J. Nash, R. L. Woodward, and M. L. Pool—170(L)
Of Rb^{109}, David E. Alburger—339

Nuclear spectra (continued)
Of Rb^{85} and Rb^{84}, Charles M. Huddleston and Allan C. G. Mitchell—1350
Of Sc^{45}, J. R. Haskins, J. E. Duval, L. S. Cheng, and J. D. Kurbatov—876
States of light nuclei from *jj*-coupling model, D. Kurath—804
Sr^{88} γ-rays, internal conversion, F. R. Metzger and H. C. Amacher—147(L)
S^{35} β-spectrum, low energy portion, G. J. Plain, H. L. Morrison, and F. T. Rogers, Jr.—170(A)
Tl^{204} decay, using scintillation spectrometer, E. der Mateosian and A. Smith—1186
Sn^{120} γ-rays, C. E. Mandeville, E. Shapiro, R. I. Mendenhall, E. R. Zucker, and G. L. Conklin—554
Ti^{48} excited levels, Maurice M. Miller—516
Total neutron cross section of Na, P. H. Stelson and W. M. Preston—1354
Two-plate method of measuring anisotropic fast neutron spectra, John E. Evans—163(A)
V^{48} disintegration scheme, Paul L. Roggenkamp, Charles H. Pruett, and Roger G. Wilkinson—1262
Very long lifetime of C^{14} β-decay, A. M. L. Messiah—151(L)
Nuclear structure (see also **Disintegration and excitation of nucleus; Nuclear spectra; Radioactivity**)
Coupling constant of nucleon—μ-meson interaction, M. A. Preston and M. F. Duret—1425(L)
Discontinuities in binding energies of neutrons and protons in light nuclei, Martin Redlich—38
Further test of shell model, J. S. King and W. C. Parkinson—141(L)
H^3 theory, Robert L. Pease and Herman Feshbach—945
Limit on repulsive core from 100-Mev deuteron photoeffect, N. Austern—1207(L)
New conception of nuclei and elementary particles, Enos E. Witmer—163(A)
Non-additivity of nucleon moments in heavy nuclei, Marc Ross—935
Nuclear energy levels in 28 neutron shell region, George F. Pieper—1299
Radii of mirror nuclei, Robert R. Wilson—350
Roughness of nuclear energy surface, John A. Eldridge and Richard J. Brundy—163(A)
States of light nuclei from *jj*-coupling model, D. Kurath—804
Stripping and the nuclear shell model, S. T. Butler—685(L)

Optical constants and properties
Of crystalline thoria, O. A. Weinreich and W. E. Danforth—953(L)
Optical instruments (see **Methods and instruments**)

Pair production and annihilation
Annihilation of positrons in flight at 100 and 200 Mev, F. C. Gilbert and Stirling A. Colgate—164(A)
Magnetic quenching of 3-quantum annihilation of positronium, Otto Halpern—164(A)
Pair production by electrons, M. Camac—745
Polarization correlations of γ-rays of Cs^{134} and of annihilation radiation, Berol L. Robinson and Leon Madansky—1065
Precision measurements of wavelength of annihilation radiation, David E. Muller, Harry C. Hoyt, David J. Klein, and Jesse W. M. DuMond—775
Quenching of ortho-positronium decay by magnetic field, John Wheatley and David Halliday—424(L)
Use of annihilation of positrons in flight to give peaked γ-ray spectrum, Stirling A. Colgate—164(A)

Phosphors and phosphorescence (see also **Fluorescence; Luminescence**)
Paramagnetic resonance in phosphors, W. D. Hershberger and H. N. Leifer—714
Response of organic crystals to neutrons, T. W. Bonner, A. B. Lillie, and H. L. Taylor—162(A)
Photoconductivity
In anodic Ta_2O_5, L. Apker and E. A. Taft—58
Field emission from photoconductors, L. Apker and E. Taft—1037
Photodisintegration
Deuteron photodisintegration at high energies, W. S. Gilbert and J. W. Rosengren—901
(γ,pn) reaction in P, J. Halpern, A. K. Mann, and R. Nathans—958(L)
Limit on repulsive core from 100-Mev deuteron photoeffect, N. Austern—1207(L)
$Li^6(\gamma,d)He^4$ reaction at 2.76 Mev, Howard B. Glenn—418(L)
Nuclear photoprocesses at high energy, J. G. Brennan and R. G. Sachs—824
Photomesons from the deuteron, Joseph A. Thie—420(L)
Photon absorption cross sections in Bi and Ta, J. Halpern, R. Nathans, and A. K. Mann—679(L)
Photon-induced reactions, D. C. Peaslee—812
Photoproduction of isomeric pair of Br^{80}, Erich M. Harth—170(A)
Photoproduction of mesons in D, Melvin Lax and Herman Feshbach—509
Photoprotons from heavy elements, W. E. Stephens and M. E. Toms—160(A)
Production of charged photomesons from D and H. I, R. Stephen White, Mark J. Jakobson, and Alvin G. Schulz—836
Production of photomesons in D, James Keck and Raphael Littauer—139(L)
Pseudoscalar mesons with applications to meson-nucleon scattering and photoproduction, S. D. Drell and E. M. Henley—1053
Photoelectric effect and properties; cells
Frequency response of PbS cells, B. D. McMichael and S. Mrozowski—1216(A)
Photons (see **Gamma-rays; Radiation; Scattering of radiation; X-rays**)
Piezoelectric effect
Equivalent electrical network of quartz plate used as filter, A. D. Frost, C. R. Mingins, and R. W. Perry—154(A)
High frequency electromechanical filters, C. R. Mingins, S. Bartnoff, and L. A. Howard—154(A)
Of $ND_4D_2PO_4$, W. P. Mason and T. B. Matthias—477
Stepped-surface piezoelectric filters, R. R. McDonough, D. W. MacLeod, and G. A. Larson—154(A)
Plasticity
Inelastic deformation (cold flow) of certain crystalline materials under flexural stress, Lewis S. Combes, Stanley S. Ballard, and David L. Honkonen—153(A)
Plastic deformation of Ge and Si, C. J. Gallagher—721
Of Si and Ge, Frederick Seitz—722
Polymerization, properties of polymers
Polymer and dimer absorptions in uv spectra of alcohols, Gladys A. Anslow, Irene S. White, and Rika Sarfaty—154(A)
Positrons
Annihilation in flight at 100 and 200 Mev, F. C. Gilbert and Stirling A. Colgate—164(A)
Backscattering of positrons and electrons, H. H. Seliger—408
Energy spectrum from decay of μ-meson, H. J. Bramson, A. M. Seifert, and W. W. Havens, Jr.—304

Magnetic quenching of 3-quantum annihilation of positronium, Otto Halpern—164(A)
Quenching of ortho-positronium decay by magnetic field, John Wheatley and David Halliday—424(L)
Use of annihilation of positrons in flight to give peaked γ-ray spectrum, Stirling A. Colgate—164(A)

Proceedings of the American Physical Society
New England Section Meeting at Tufts College, Medford, Massachusetts, May 24, 1952—153
Summer Meeting at Denver, Colorado, June 30 to July 3, 1952 [Bull. Am. Phys. Soc. **27**, No. 4 (1952)]—155
New York State Section Meeting at Cornell University, Ithaca, New York, October 17 and 18, 1952—1215

Quantum electrodynamics (see also **Field theory**)
Bound states and interaction representation, S. T. Ma—1211(L)
Coulomb scattering of relativistic electrons and positrons by nuclei, Herman Feshbach—295
Current density in quantum electrodynamics, H. C. Corben—677(L)
Fourth order vacuum polarization, M. Baranger, F. J. Dyson, and E. E. Salpeter—680(L)
Interaction between electron and one-dimensional electromagnetic field, erratum, Nathan Rosen—1434(L)
Lower limits for interaction times in photon scattering processes, E. Gora—1212(L)
Relativistic configuration space formulation of multi-electron problem, Marian Günther—1411

Quantum mechanics (see **Mechanics, quantum**)

Quenching of radiation (see **Radiation**)

Radiation (see also **Gamma-rays; Scattering of radiation; Thermal radiation; X-rays**)
Absorption of 5.3-Mev, 10.3-Mev, and 17.6-Mev γ-rays, E. S. Rosenblum, E. F. Shrader, and R. M. Warner, Jr.—612
Diffraction in time, Marcos Moshinsky—625
Penetration and diffusion of x-rays: Calculation of spatial distributions by semi-asymptotic methods, L. V. Spencer—793
Propagation in electron-ion streams, R. Q. Twiss—1392
Radiative transfer and equilibrium associated with far infrared beams in atmosphere, J. I. King—157(A)
Solar "enhanced radiation" and plasma oscillations, Hari K. Sen—816
Variational method for problems of neutron diffusion and of radiative transfer, Su-Shu Huang—50

Radioactivity (see also **Disintegration and excitation of nucleus; Nuclear spectra**)
Of Sb^{124}, D. R. Hutchinson and M. L. Wiedenbeck—699
Average electric charge of daughter atoms from β-decay and isomeric transition, Sol Wexler and T. H. Davies—1203(L)
Ba^{127}, Ba^{128}, and Cs^{128}, M. Lindner and R. N. Osborne—1422(L)
Disintegration of Ce^{144} and Pr^{144}, Fred T. Porter and C. Sharp Cook—170(A)
Evidence of once-forbidden spectra for law of β-decay, H. M. Mahmoud and E. J. Konopinski—1266
F^{20} β-decay, David E. Alburger—1257
Gd^{150} and Tb^{161}, energy levels associated with radioactive decay, J. M. Cork, J. M. LeBlanc, W. H. Nester, and F. B. Stumpf—685(L)
Geiger-Nuttal relation and α-ray spectra, M. L. Chaudhury—137(L)
Fe^{59} disintegration scheme, Franz R. Metzger—1360
Negative pion activation of Br, T. T. Sugihara and W. F. Libby—587
Neutron deficient Sr isotopes, Stanley V. Castner and D. H. Templeton—1126
Of Os, J. B. Swan and R. D. Hill—171(A)
Os radioisotopes, J. B. Swan and R. D. Hill—831
Pu^{239} and Pu^{240} α-spectra, Frank Asaro and I. Perlman—828
$Pu^{239,240,241}$ β-spectra, Melvin S. Freedman, F. Wagner, Jr., and D. W. Engelkemeir—1155
K^{40} radioactive decay: its branching ratio and its use in geological age determinations, A. K. Mousuf—150(L)
Production of P^{32} with thermal neutrons, Torbjorn Westermark—573
Of Pm^{142}, Pm^{143}, Pm^{145}, Pm^{146}, and Sm^{146}, John K. Long, M. L. Pool, and D. N. Kundu—171(A)
Ra α-particles, Frank Asaro and I. Perlman—129
Of Rh^{106}, David E. Alburger—339
Of Sc^{43}, J. R. Haskins, J. E. Duval, L. S. Cheng, and J. D. Kurbatov—876
Specific α-activities and half-lives of U^{234}, U^{235}, and U^{238}, E. H. Fleming, Jr., A. Ghiorso, and B. B. Cunningham—642
Spontaneous fission *vs* α-decay, Arnold Kramish—1201(L)
Three new neutron deficient Xe isotopes, Bruce Dropesky and Edwin E. Wiig—683(L)
V^{48} disintegration scheme, Paul L. Roggenkamp, Charles H. Pruett, and Roger G. Wilkinson—1266
Very long lifetime of C^{14} β-decay, A. M. L. Messiah—151(L)

Range and energy loss of particles
Average energy loss per ion pair of slow electrons in He, C. E. Nielsen, R. H. Frost, and W. J. Choyke—165(A)
Density effect for ionization loss, R. M. Sternheimer—851
Energy loss of cosmic-ray μ-mesons in NaI crystals, Alvin Hudson and Robert Hofstadter—589
Ionization loss and straggling of fast electrons, E. L. Goldwasser, F. E. Mills, and A. O. Hanson—1137
Ionization loss at relativistic velocities in nuclear emulsions, Maurice M. Shapiro and Bertram Stiller—169(A)
Low pressure cloud-chamber investigation of range-energy relations, Robert G. Mills—168(A)
Range-energy relation for heavy ions, P. M. Stier and G. E. Evans—164(A)
Range of α-particles in H_2O, Hervasio de Carvalho and Herman Yagoda—273
Range straggling for heavy particles, David O. Caldwell—131
Stopping power of K-electrons, M. C. Walsk—1283
Total specific ionization in air, A and H_2 from 17.5-Mev electrons, J. Ovadia, J. S. Laughlin, J. W. Beattie, and W. J. Henderson—165(A)

Recombination
In O_2, Joseph Kaplan and Marx Brook—157(A)

Relativity
Gravitation and electrodynamics, Behram Kurşunoğlu—1369
Phase space of nonlocalizable elementary particle, E. J. Schremp—161(A)
Spin and angular momentum in general theory of relativity, Robert Thomson and Peter G. Bergmann—1216(A)

Resistance, electrical (see **Electrical conductivity and resistance**)

Scattering of electrons, mesons, neutrons, protons, deuterons, and ions (see also **Cross section, measurements, theory; Electron diffraction**)
Angular dependence of inelastic scattering of protons on Be^9, K. E. Davis—1433(L)
Atomic electron ejection in large-angle scattering, M. E. Ebel and W. F. Fry—1306
Backscattering of positrons and electrons, H. H. Seliger—408

Scattering of electrons, mesons, neutrons, protons, deuterons, and ions (continued)
Coulomb and nuclear interactions of cosmic-ray mesons and protons in Pb, W. L. Whittemore and R. P. Shutt—1312
Coulomb effects in pion scattering by protons under charge independence hypothesis, Leon Van Hove—1358
$d-d$ elastic scattering at 10.5 Mev, Louis Rosen and J. C. Allred—431
Differential cross-section measurements for scattering of protons by deuterons, R. J. S. Brown, George D. Freier, H. D. Holmgren, W. R. Stratton, and J. L. Yarnell—253
Differential $n-p$ cross section for 220-Mev neutrons, G. L. Guernsey, G. Mott, and B. K. Nelson—15
Elastic scattering of deuterons by tritons, W. R. Stratton, G. D. Freier, G. R. Keepin, D. Rankin, and T. F. Stratton—257
Elastic scattering of 9.7-Mev protons by D and H, J. C. Allred, A. H. Armstrong, R. O. Bondelid, and Louis Rosen—433
Elastic scattering of protons and neutrons by He, D. C. Dodder and J. L. Gammel—520
Elastic scattering of 10-Mev deuterons by H^3 and He^3, J. C. Allred, A. H. Armstrong, A. M. Hudson, R. M. Potter, E. S. Robinson, Louis Rosen, and E. J. Stovall, Jr.—425
Energy distribution of slow neutrons scattered from solids, B. N. Brockhouse and D. G. Hurst—542
High energy electron-electron scattering, erratum, Walter H. Barkas, Robert W. Deutsch, F. C. Gilbert, and Charles E. Violet—1435(L)
High energy $p-p$ scattering and associated polarization effects, L. J. B. Goldfarb and D. Feldman—1099
Impulse approximation and field theoretical calculations, John S. Blair and Benjamin Segall—621
Inelastic collision cross sections for 14-Mev neutrons, D. D. Phillips, R. W. Davis, and E. R. Graves—600
Inelastic scattering of 7.7-Mev protons, J. A. Harvey—162(A)
Interference between Coulomb and nuclear scattering in $p-p$ collisions at 240 Mev, H. P. Noyes and H. G. Camnitz—1206(L)
Meson-nucleon scattering and classical strong-coupling theory, David Feldman—890
μ-meson-electron scattering, W. D. Walker—168(A)
Multiple scattering of fast pions in photographic emulsions, Meera Backus and J. J. Lord—169(A); Meera Backus, J. J. Lord, and Marcel Schein—1431(L)
Multiple scattering of fast protons in photographic emulsions, Martin J. Berger—59
Multiple scattering of neutrons. III. Scattering by spin-dependent forces and polarization phenomena, Otto Halpern—232
$n-p$ scattering using organic crystal scintillation detectors, M. E. Remley, W. K. Jentschke, and P. G. Kruger—162(A)
Nuclear cross section for 37-Mev positive pions in Pb, Kenneth J. Button—956(L)
Paramagnetic neutron scattering cross section of various transition group ions at long neutron wavelengths, R. R. Smith, T. I. Taylor, and W. W. Havens, Jr.—163(A)
$p-d$ scattering at 5.1 Mev and $d-p$ scattering at 10.2 Mev, K. B. Mather—1408
$p-T$ interaction, J. S. McIntosh, R. L. Gluckstern, and S. Sack—752
Pseudoscalar mesons with applications to meson-nucleon scattering and photoproduction, S. D. Drell and E. M. Henley—1053
S-wave in pion-nucleon scattering, R. E. Marshak—1208(L)
Scattering of charge symmetric pseudoscalar mesons by nucleons, W. W. Wada—1032
Scattering of slow neutrons in polycrystalline media, Ronald W. Gurney—466
Scattering of 31.5-Mev protons from several elements, Roy Britten—283
Total cross sections for 14-Mev neutrons, J. H. Coon, E. R. Graves, and H. H. Barschall—162(A); 562; Leonard S. Goodman—686(L)
Total cross sections of heavy nuclei for fast neutrons, D. W. Miller, R. K. Adair, C. K. Bockelman, and S. E. Darden—83
Variational principle for scattering, Herman Feshbach and S. I. Rubinow—484
Scattering of radiation (see also **Raman spectra; X-rays**)
Lower limits for interaction times in photon scattering processes, E. Gora—1212(L)
Scintillation counters (see **Methods and instruments**)
Secondary electrons (see **Electrons, secondary**)
Semiconductors (see also **Electrical conductivity and resistance**)
Acceptors produced in Ge by quenching from high temperatures, Colman Goldberg—920
Activation energy of heat treatment introduced lattice defects in Ge, R. M. Baum and C. S. Hung—134(L)
α-particle bombardment of PbS semiconductors, F. K. Odencrantz—166(A)
Energy states of overlapping impurity carriers in semiconductors, Cavid Erginsoy—893
Grain boundary barriers in Ge, W. E. Taylor, N. H. Odell, and H. Y. Fan—867
Lifetime of injected carriers in Ge, D. Navon, Ralph Bray, and H. Y. Fan—165(A)
Plastic deformation of Ge and Si, C. J. Gallagher—721
$p-n$ junctions produced by growth rate variation, R. N. Hall—139(L)
Shock waves (see also **Explosion phenomena; Supersonics**)
In low pressure spark discharges, Richard G. Fowler, William R. Atkinson, Walter D. Compton, and Robert J. Lee—137(L)
Solid state (see **Crystalline state; Mechanics, quantum—of solid bodies**)
Solutions
Electrical phenomena associated with freezing of dilute aqueous solutions, Marvin E. Backman—165(A)
Sound (see **Acoustics**)
Spallation (see **Disintegration and excitation of nucleus**)
Spark discharge (see **Disintegration and excitation of nucleus**)
Specific heat
Anomaly in low temperature atomic heat of Ag, P. H. Keesom and N. Pearlman—140(L)
Of Pb in temperature range 1°K to 75°K, M. Horowitz, A. A. Silvidi, S. F. Malaker, and J. G. Daunt—1182
Of Si below 100°K, N. Pearlman and P. H. Keesom—397
Spectra, absorption (see also **Absorption of radiation; Spectra, general; Spectra, microwave; Spectra, molecular**)
Atmospheric window, 16 to 24 microns and second fundamental of N_2O, Arthur Adel—128
Confirmation of polymer and dimer absorptions in uv spectra of alcohols, Gladys A. Anslow, Irene S. White, and Rika Sarfaty—154(A)
Induced infrared absorption in H_2 and H_2-foreign gas mixtures at pressures up to 1500 atmos, D. A. Chisholm, J. C. F. MacDonald, M. F. Crawford, and H. L. Welsh—957(L)
Spectra, atomic
Atomic oxygen g-factors, E. B. Rawson and R. Beringer—677(L)
Configuration interaction between odd terms in Fe group, Norbert Rosenzweig—580

Natural line shape, Francis Low—53
Perturbations of atomic g-values, M. Phillips—202
Rydberg constant and atomic mass of the electron, E. Richard Cohen—353
Survey of isotope shift in O I, Lee W. Parker and John R. Holmes—174(A)

Spectra, general
Atmospheric water vapor determination by infrared solar spectroscopy, Robert F. Calfee, David M. Gates, and Byron E. Cohn—157(A)
Non-Rayleigh scattering in very near infrared spectrum of day sky, Romuald Anthony—157(A)
Radiative transfer and equilibrium associated with far infrared bands in atmosphere, J. I. King—157(A)
Spectral solar energy in near infrared, David M. Gates, Robert F. Calfee, and Byron E. Cohn—157(A)

Spectra, microwave
Atomic oxygen g-factors, E. B. Rawson and R. Beringer—677(L)
OCS and N_2O, 6-mm spectra, S. J. Tetenbaum—772

Spectra, molecular
Infrared rotational spectrum of H_2S, E. E. Bell, R. L. Hansler, and R. A. Oetjen—174(A)
Magnetic hfs in diatomic molecules, R. A. Frosch and H. M. Foley—1337
OCS and N_2O, 6-mm spectra, S. J. Tetenbaum—772
Rf spectra of Li^6F^{19} by molecular beam method, J. C. Swartz and J. W. Trischka—1085
Rotational magnetic moment, magnetic susceptibilities, and electron distribution in H_2, N. J. Harrick and N. F. Ramsey—228

Spectra, nuclear (see **Nuclear spectra**)

Spectra, rf
Of Li^6F^{19} by molecular beam methods, J. C. Swartz and J. W. Trischka—1083

Spectroscopy, technique (see **Methods and instruments**)

Spinor fields (see **Field theory**)

Statistical mechanics (see **Mechanics, statistical**)

Superconductivity (see also **Electrical conductivity and resistance; Low temperature phenomena**)
Free energies and phase transition of cylindrical superconductor, Paul M. Marcus—373
Of In-Tl solid solutions, J. W. Stout and Lester Guttman—703
Properties of superconductors below 1°K. III. Zr, Hf, Cd, and Ti, T. S. Smith and J. G. Daunt—1172
Of Re, J. G. Daunt and T. S. Smith—309
Similarity properties of two-fluid model of superconductivity, erratum, E. Maxwell—1434(L)
Superconducting transition in Ta, H. Preston-Thomas—325
Thermal resistivity of superconductors, D. P. Detwiler and Henry A. Fairbank—1049

Thermal conductivity
Of sapphire and rutile as function of temperature, Kathryn A. McCarthy, Stanley S. Ballard, and Edward C. Doerner—153(A)
Of superconductors, D. P. Detwiler and Henry A. Fairbank—1049

Thermal expansion
Of U at low temperatures, Henry L. Laquer and Adam F. Schuch—166(A)

Thermionic emission, emitting surfaces
Electronegativity and work function, William Squire—1216(A)

Thermodynamics
Experimental demonstration of kinks, George Antonoff—177(A)
Kinks in gases, George Antonoff—160(A)
Theorem of irreversible thermodynamics, Richard F. Greene and Herbert B. Callen—1387

Vacuum tubes (see **Electronic tubes**)

Wave mechanics (see **Mechanics, quantum**)

Work function (see also **Photoelectric effect and properties, cells; Thermionic emission**)
Electronegativity and work function, William Squire—1216(A)

X-rays, absorption, diffraction, scattering, reflection, refraction, and polarization
Absorption of high energy x-rays, H. Janzen—653
Penetration and diffusion of x-rays; calculation of spatial distributions by semi-asymptotic methods, L. V. Spencer—793
Small angle x-ray scattering from compact identical particles, K. L. Yudowitch and R. M. Frank—759

X-rays, emission
From mesic atoms, M. Camac, A. D. McGuire, J. B. Platt, and H. J. Schulte—134(L)
From π-mesic atom, A. M. L. Messiah and R. E. Marshak—678(L)

Zeeman effect
Atomic oxygen g-factors, E. B. Rawson and R. Beringer—677(L)